Ecological and Chemical Studies on the Gq-protein Inhibitor FR900359

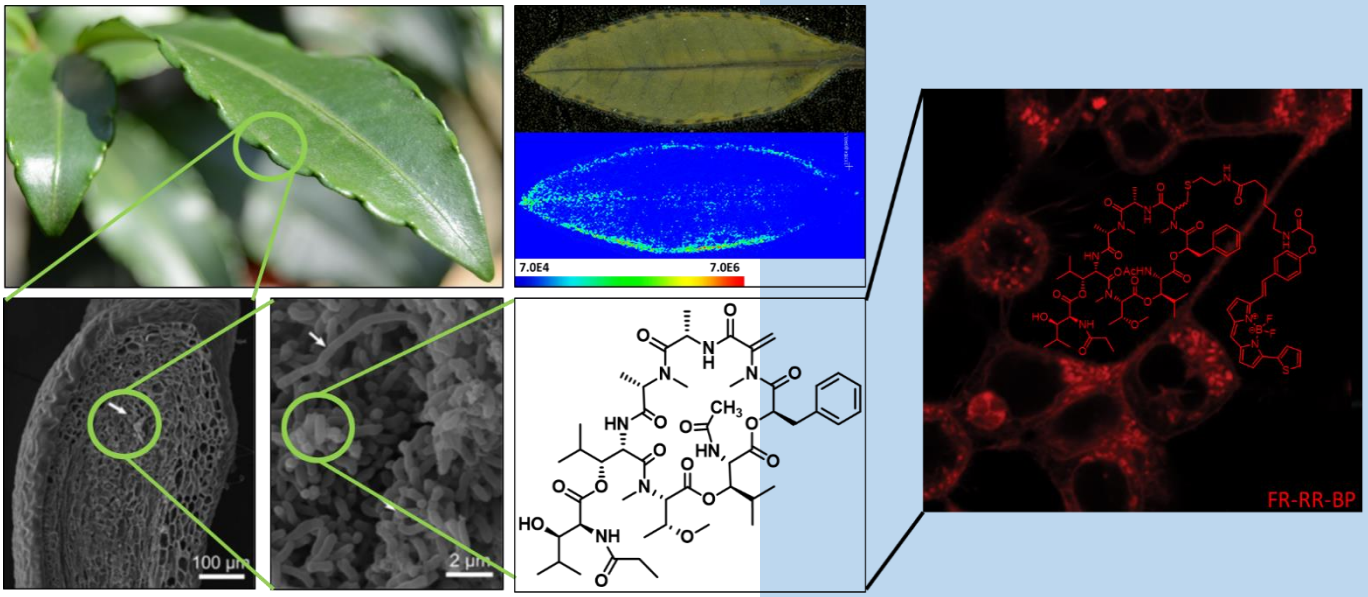

Raphael Reher

Universität Bonn (AK König)

Ecological and Chemical Studies on the Gq-protein Inhibitor FR900359

Dissertation

zur

Erlangung des Doktorgrades (Dr. rer. nat.)

der

Mathematisch-Naturwissenschaftlichen Fakultät

der

Rheinischen Friedrich-Wilhelms-Universität Bonn

vorgelegt von

Raphael Reher

aus

Münster

Bonn 2018

Angefertigt mit Genehmigung der Mathematisch-Naturwissenschaftlichen Fakultät
der Rheinischen Friedrich-Wilhelms-Universität Bonn

1. Gutachter	:	Prof. Dr. G. M. König
2. Gutachter	:	Prof. Dr. E. Kostenis
Tag der Promotion	:	13.09.2018
Erscheinungsjahr	:	2018

Vorveröffentlichungen der Dissertation/ In Advance Publications of the Dissertation

Teilergebnisse aus dieser Arbeit wurden mit Genehmigung der Mathematisch-Naturwissenschaftlichen Fakultät, vertreten durch die Mentorin/Betreuerin der Arbeit, in folgenden Beiträgen vorab veröffentlicht.

Parts of this study have been published in advance by permission of the Mathematisch-Naturwissenschaftliche Fakultät, represented by the supervisor of this study:

Publikationen/Research Papers

Reher R*, Kühl T*, Annala S, Benkel T, Heycke N, Kaufmann D, Nubbemeyer B, Odhiambo JP, Heimer P, Bäuml CA, Kehraus S, Crüsemann M, Kostenis E, Tietze D, Imhof D, and König GM. "Deciphering specificity determinants for Gαq inhibitors derived from YM-254890 and FR900359 based on computational and structure-activity studies." *ACS Chem. Biol.* (submitted).

* These authors contributed equally to this work.

Reher R, Kuschak M, Heycke N, Annala S, Kehraus S, Dai H, Kostenis E, König GM, Crüsemann M. "Applying molecular networking for the detection of new natural sources and analogs of the selective Gq protein inhibitor FR900359." *J. Nat. Prod.* (submitted).

Crüsemann M* and Reher R* … König GM. "Heterologous expression, biosynthetic studies and ecological function of the selective Gq-signaling inhibitor FR900359." *Angew. Chem. Int. Ed*. **2018**. *57*, 836–840.

* These authors contributed equally to this work.

Grundmann M … Reher R, … Kostenis E. "Lack of beta-arrestin signaling in the absence of G protein signaling." *Nat. Commun*. **2018**, *9*, (341).

Carlier A, Fehr L, Pinto M, Schäberle T, Reher R, Dessein S, König GM, Eberl L. "The genome analysis of *Candidatus* Burkholderia crenata reveals that secondary metabolism may be a key function of the *Ardisia crenata* leaf nodule symbiosis." *Environ. Microbiol*. **2015**. *18* (8), 2507-22.

Oral Presentations

Invited talk at the International Association for General and Applied Microbiology (VAAM)-Workshop 2017, Tübingen, Germany. “FR900359 – an endophyte-derived natural product: therapeutic potential, biosynthesis and ecology

Short Talk on the DECHEMA conference 28. Irseer Naturstofftage, Irsee, Germany. “Structural modifications and biosynthesis of the selective Gq protein inhibitor FR900359 from *Ardisia crenata*”.

Invited talk at the Conference of the German Society for Phytotherapy 2015, Rostock, Germany. “Isolierung, Strukturaufklärung und biologische Untersuchung eines neuen zyklischen Depsipeptids der TCM-*Pflanze Ardisia crenata*.“

Poster Presentations

Reher R, Kuschak M, Annala S, Benkel T, Seidinger A, Malfacini D, Kehraus S, Crüsemann M, Wenzel D, Müller, C E, Kostenis E, König GM “Ecological role and SAR studies of the selective Gq protein inhibitor FR900359.” International Symposium on GPCRs and G-Proteins, Bonn.

Benkel T, Annala S, Heycke N, Reher R, Hot B, Schulte G, König GM, Kostenis E “Fluorescent FR900359 for real time imaging of $G\alpha_q$ proteins in living cells.” International Symposium on GPCRs and G-Proteins, Bonn.

Preis P, Simon K, Grundmann M, Merten N, Malfacini D, Reher R, König GM, Inoue A, Gomeza J, Kostenis E “Elucidating G protein-independent signaling functions of GPCRs: do they really signal when G proteins are off?” International Symposium on GPCRs and G-Proteins, Bonn.

Malfacini D, Patt J, Annala S, Tietze D, Reher R, König MG, Kostenis E „FR900359- and YM254890-sensitive $G\alpha_{16}$: a first step towards creation of selective G16 or pan-Gq inhibitors.” International Symposium on GPCRs and G-Proteins, Bonn.

Reher R, Schamari I, Kehraus S, Annala S, Kuschak M, Schäberle TF, Crüsemann M, Müller CE, Carlier A, Eberl L, Kostenis E, König GM “The endophyte *Candidatus*

Burkholderia crenata of the TCM plant *Ardisia crenata* produces the selective Gq-inhibitor FR900359." 9th Joint Natural Products Conference 2016, Copenhagen, Denmark.

Reher R, Schamari I, Kehraus S, Annala S, Kuschak M, Schäberle TF, Crüsemann M, Müller CE, Carlier A, Eberl L, Kostenis E, König GM "The cyclic depsipeptide FR900359 from *Ardisia crenata*: structural insights and biosynthesis of a selective Gq-protein inhibitor." Frontiers in Medicinal Chemistry 2016, Bonn, Germany.

Reher R, Kehraus S, Schäberle TF, König GM "Structural modifications and biosynthesis of the selective Gq-protein inhibitor FR900359 from *Ardisia crenata.*" DECHEMA conference 28. Irseer Naturstofftage 2015, Irsee, Germany

Meiner Mutter

Table of contents

page

1 Introduction 1

1.1 Symbiotic plant-bacterial relationships offer a vast potential for natural product research 2

1.1.1 *Crispardisia-Burkholderia* leaf nodule symbiosis 2

1.2 Nonribosomal peptide biosynthesis using the example of FR 4

1.3 Structural characteristics of the cyclic depsipeptide FR 6

1.4 Plant-derived natural products as pharmacological tools to study GPCR-mediated signaling at different stages 8

1.4.1 Plant-derived tools interfering with GqPCR activation 10

1.4.2 FR900359, a plant-derived tool interfering with Gq protein activation 10

1.4.3 Plant-derived tools interfering with phospholipase Cβ activation 13

1.4.4 Plant-derived tools interfering with inositol 1,4,5-trisphosphate (IP_3)-mediated signaling 13

1.4.5 Plant-derived tools, activating or inhibiting protein kinase C 14

1.4.6 Natural products, interfering with G_iPCR-mediated signaling 14

2 Aim of the study 16

3 Materials and Methods 17

3.1 Materials 17

3.1.1 Plant material 17

3.1.2 Cultivation, Extraction and growth determination of *Chromobacterium vaccinii* MWU205, DSM 25150 18

3.1.3 Chemicals 19

3.1.4 Other materials 20

3.2 Extraction of *Ardisiae crenatae folium* 20

3.3 Chromatographic methods 20

3.3.1 Thin layer chromatography (TLC) 20

3.3.2 Vacuum liquid chromatography (VLC) 21
3.3.3 Size exclusion chromatography (SEC) 21
3.3.4 Flash chromatography 21
3.3.5 Solid phase extraction (SPE) 22
3.3.6 High performance liquid chromatography (HPLC) 22
3.4 Isolation protocols 23
3.4.1 Depsipeptide isolation and purification 23
3.4.2 Isolation of FR and FR analogs (1-4) 23
3.5 Synthetic procedures 24
3.5.1 Synthesis of FR-Hex (11) 24
3.5.2 Synthesis of FR-Cys (12) 25
3.5.3 Synthesis of FR-RR-BP (46) 25
3.5.4 Synthesis of FR-Cys-Boc (47) 26
3.5.5 Synthesis of FR-JK-Boc (48) and FR-JK-BP (49) 26
3.5.6 Synthesis of FR-TAMRA (50) 27
3.5.7 Synthesis of Fmoc-β-HyLeu-OH 27
3.5.8 Peptide synthesis and purification 28
3.5.9 Chemical characterization of FR-analogs 1-22 29
3.6 Structure elucidation 29
3.6.1 Mass spectrometry 29
3.6.1.1 LC-ESI-MS using an HPLC coupled to ..... a quadrupole analyzer (system A) 29
3.6.1.2 High resolution LC-ESI-MS using a UPLC System ..... coupled to Qq-TOF (system B1) 30
3.6.1.3 UPLC/MS of extracts and pure compounds (system B2) 30
3.6.1.4 Tandem mass spectrometry (MS-MS^n), system C 30
3.6.1.5 MALDI-TOF 33
3.6.1.6 MALDI imaging of *A. crenata* leaves 34

3.6.2 Nuclear magnetic resonance spectroscopy 34
3.6.3 Specific rotation 35
3.6.4 Bioinformatic procedures 36
3.6.4.1 Molecular networking 36
3.6.4.2 Structures calculations of YM-254890, FR900359 and their analogs 36
3.6.4.3 Molecular Docking Studies 37
3.6.4.4 Molecular dynamics simulations 37
3.6.4.5 Steered molecular dynamics simulations 37
3.6.5 Life Cell imaging 38
3.7 Biological methods: 38
3.7.1 Resazurin-based Cell viability assay with HEK293-cells 38
3.7.2 Agar Diffusion and Sporulation Assay in Working Group König 39
3.7.3 Agar Diffusion Assay in Working Group Sahl 39
3.7.4 IP1 accumulation assay 40
3.7.4.1 Cell lines and culture conditions 40
3.7.4.2 HTRF-based IP_1 and cAMP assays 40
3.7.4.3 Data evaluation of second messenger HTRF assay 40
3.7.4.4 Wash-out experiments using IP-one HTRF® assay by Cisbio 41
3.7.5 Dynamic mass redistribution (DMR) assay 41
3.7.6 Competition experiments with [^{3}H]PSB-15900 42
3.8 Methods for determination of the ecological role of FR900359 42
3.8.1 Quantification of FR in leaves and nodules of *A. crenata* 42
3.8.2 Feeding experiments of FR and *A. crenata* leaves ..... on *Acheta domesticus* 43
3.8.3 Cloning and transfection of *Bombyx mori* and ..... *Bemisia tabaci* Gq proteins 43

3.8.4 Competition experiments with [³H]PSB-15900 at ..... membrane preparations of Sf9 cells and HEK cells expressing ..... *Bemisia tabaci* and *Bombyx mori* Gq proteins, respectively..... 43

3.8.5 Feeding and effect determination of FR on mice 44

3.8.6 Feeding and effect determination of FR on insects 44

4 Results, Section I: Ecological function, Biosynthesis and ..... Heterologous expression of FR..... 45

4.1 Research towards the ecological role of FR – ..... More than just a tool for pharmacological research designed by nature? . 46

4.1.1 Investigation of the leaf nodule symbiosis of *A. crenata* 46

4.1.2 The putative role of FR as a signaling molecule ..... between host plant and endosymbiont 48

4.1.3 FR shows no antibacterial, antifungal or cytotoxic activity..... 49

4.1.4 FR is orally bioavailable and effective in mice 51

4.1.5 FR as chemical weapon against insect herbivores 52

4.1.5.1 Antifeedant effects of *A. crenatae folium* on *Acheta domesticus* 52

4.1.5.2 Feeding experiments with FR on *A. domesticus* 52

4.1.5.3 Sequence alignment of Gα subunits of different metazoans ..... around the YM binding site 53

4.1.5.4 Affinity of FR to pest insect G proteins 54

4.1.5.5 Feeding experiments with FR on bean bug larvae 55

4.2 Bioinformatics and *in vitro* enzymatic studies on FR biosynthesis..... 57

4.3 Heterologous expression of FR in *E. coli* 61

5 Results, Section II: Detection, Isolation and Structure Activity Relationship ..... studies of new FR analogs 64

5.1 Discovery of new FR analogs and further natural sources of FR..... 66

5.1.1 New FR analogs derived from *A. crenata* assisted by ..... bioactivity-guided fractionation 66

5.1.1.1 Structure Elucidation of **1** (FR-1) 68

5.1.1.2 Structure elucidation of **2** (FR-2) 71

5.1.2 New FR analogs derived from *A. crenata* detected via ..... MS-based molecular networking 74

5.1.3 Synergistic effects of *Ardisia crenata* fractions ..... towards FR activity 85

5.1.4 Detection of FR by molecular networking ..... in several *Ardisia* species 85

5.1.5 Isolation of FR from the cultivable *Chromobacterium vaccinii* ..... MWU205, DSM 25150 88

5.2 Towards the pharmacophore of FR – Structure-Activity Relationship ..... studies of all currently known Gq inhibitors 92

5.2.1 Bioactivity of FR analogs derived from *A. crenata* 93

5.2.2 Semisynthetic modification of FR 94

5.2.2.1 Synthesis and analysis of FR-Hex (**11**) and FR-Cys (**12**) 95

5.2.2.2 Biological evaluation of FR-Hex (**11**) and FR-Cys (**12**) 102

5.2.3 YM-254890 and FR900359 – ..... the ultimate Gq inhibitors designed by nature 103

6 Results, Section III: Development of the ..... first fluorescent Gq protein inhibitor 121

6.1 Synthesis and biological evaluation of the ..... first fluorescent Gq protein inhibitor FR-RR-BP 122

6.1.1 Synthesis of FR-RR-BP (46) 122

6.1.2 Analysis of FR-RR-BP (46) 123

6.1.3 Bioactivity of FR-RR-BP 124

6.1.3.1 Molecular modelling studies of compounds **12** and **46** 125

6.1.3.2 Synthesis of FR-Cys-Boc (**47**) 129

6.1.4 Application of FR-RR-BP (46) 130

6.2 Development of a fluorescent FR probe with reduced hydrophobicity ... 132

6.2.1 Syntheses of FR-JK-Boc (48) and FR-JK-BP (49) 134

6.2.2 Analysis of FR-JK-BP (49) 135

6.2.3 Application of FR-JK-BP (49) 136

6.3 Development of FR probes with different fluorophores 136

6.3.1 Analysis of FR-TAMRA (50) 137

6.3.2 Semisynthetic approach towards a coumarin-containing fluorophore 138

6.4 Alternative synthetic approach towards a fluorescent FR probe 139

7 Discussion 141

7.1 Ecological considerations concerning the leaf nodule symbiosis and FR900359 141

7.1.1 Burkholderia symbioses with plants and insects: Considerations about the origin of the leaf nodule symbiosis 141

7.1.1.1 Endosymbiotic *Burkholderia* – double agents, switching hosts between plants and insects and *vice versa*? 142

7.1.1.2 *Burkholderia-Ardisia lucida*: A pre-form of leaf nodule symbiosis? 143

7.1.2 Ecological function of leaf nodule symbiosis 145

7.1.2.1 Insecticidal properties of FR via inhibition of insect GqPCR signaling ... 147

7.1.2.2 Potential of FR as crop protection chemical 148

7.1.2.3 Discovery of putatively FR-resistant scale insects on *A. crenata* 148

7.1.2.4 General considerations about symbiotic relationships between bacteria of the genus *Burkholderia*, - plants, - and insects 150

7.2 Biosynthetic considerations concerning FR and its analogs 151

7.2.1 Generation of new FR analogs via molecular biology-based approaches 151

7.2.1.1 Generation of new FR analogs by genetic engineering – a glimpse to future studies 151

7.2.1.2 Optimization of FR production in *Chromobacterium vaccinii* 152

7.2.1.3 Generation of new FR analogs by feeding experiments of *Chromobacterium vaccinii* 153

7.2.1.4 Generation of new FR analogs by chemoenzymatic assays 154

7.3 Structure-activity considerations of FR and analogs 154

7.3.1 Conformational analysis of FR with emphasis on the influence ..... of *N*-methylation and *cis-trans* isomerization 154

7.3.1.1 FR and analogs adopt different conformations ..... in aqueous medium compared to $CDCl_3$ 157

7.3.2 Implications of the *N*-methyldehydroalanine moiety of FR 157

7.4 Application of FR and its derivatives as tools to study ..... Gq-signaling and as therapeutic agents 160

7.4.1 Application of FR as tool to study Gq-signaling 160

7.4.1.1 Application of different attachment points of the fluorophore ..... (fluorescent analogs of FR-1) 161

7.4.1.2 Application of regioselective reactions followed by Click-Chemistry 162

7.4.1.3 Application of click chemistry as proof of principle ..... for BRET assays between Gq- NanoLuc® and FR-binding pocket 163

7.4.2 Applications of FR as potential drug lead 163

7.4.2.1 Targeted inhibition of Gq with FR for the ..... treatment of pulmonary diseases 164

7.4.2.2 FR has potential as first-in-class agent treatment of ..... GNAQ/11-driven cancers 164

8 Summary 166

9 References 170

10 Appendix 189

11 Abbreviations and Units .....

12 Acknowledgements .....

1 Introduction

Ardisia, formerly the largest genus in the family Myrsinaceae contains approximately 500 species and was included in the expanded family of Primulaceae with the implementation of APG III system (2009), the third version of a modern, mostly molecular-based system of plant taxonomy and its successor APG IV (2016).[1,2] At least 70 species have been assigned to *Crispardisia*, the subgenus characterized by leaf nodules (see definition in **Chapter 1.1**).[3] The most investigated species from *Crispardisia*, the coral berry *Ardisia crenata* SIMS, is a low-growing evergreen shrub widely dispersed in south-eastern subtropical and tropical regions of Asia and invasive in Florida (USA) and La Réunion.[4] In the Chinese Pharmacopeia its roots are listed as traditional Chinese medicine (TCM) for the treatment of several diseases, especially of the respiratory tract.[5,6] While the Bacterial Leaf Nodule symbiosis between *Crispardisia* and their respective endophytes has been investigated for a century, the reason for the development of this close and obligate relationship remains controversial.[7] The cyclic depsipeptide FR900359 (FR) from *Ardisia crenata* was not the key aspect of reported research until recently, in spite of FRs enormous potential as pharmacological tool and drug candidate. For this reason, the focus of the presented work is put on cyclic peptides, *e.g.* FR and analogs, from the vascular plant *A. crenata* SIMS and other *Crispardisia*. Furthermore, the question will be addressed, whether symbiont-produced FR is important for the host plant, thus we investigate the ecological role of FR for the first time.

Figure 1-1: (**A**) Cultivation of *A. crenata* in the green house of the Univ. of Bonn, Germany. (**B**) Close-up picture displaying leaves, flowers, and berries of *A. crenata*. Diameter of berries ca. 1cm.

1.1 Symbiotic plant-bacterial relationships offer a vast potential for natural product research

Endophytes, by definition, are commonly bacteria or fungi, which reside inside the tissues of plants beneath the epidermal cell layers and cause no apparent harm to the host.[8] Strobel and Daisy claim that of the estimated 300,000 plant species existing on earth, at least all angiosperms accommodate endophytes.[9] This opens a complete new perspective on phytochemical research. Although many plants have been extensively studied, the corresponding endophytes are barely examined. The investigation of plants' endophytes can lead to a vast range of new microorganisms when considering plants in different settings and ecosystems. It is believed that plants benefit of the bioactive metabolites of their endophytes, *e.g.* antimicrobial, antifungal, and insecticidal substances to prevent any damage from plant pathogens. Such compounds could be of great pharmaceutical and agricultural value in order to fight the problem of ongoing resistance development towards antibiotics and insecticides.[10–12]

1.1.1 *Crispardisia-Burkholderia* leaf nodule symbiosis

A system of plant-endophyte symbiosis little investigated is the Bacterial Leaf Symbiosis, *e.g.* found in the subgenus of *Ardisia*, called *Crispardisia*, consisting of 70 species. All of these are characterized by leaf nodules that are vascularized bumps on the leaf margins open to the exterior by way of stomatal pores only in early stages of the nodule development (**Figure 1-1**).[13,14] To uncover the identity of the bacterial symbionts, Lemaire *et al.* used a molecular phylogenetic approach to investigate nodulated species of *Ardisia* and concluded that the symbionts belong to the genus *Burkholderia*.[15] The vertical transmission was first postulated by Miller and is supported by several investigations.[16,17] PCR detection showed that the same bacteria occur not only in leaf nodules but also in shoot apices and reproductive organs, suggesting vertical transmission of these symbionts. Further evidence was provided by the sequence similarity of the symbionts harbored by different hosts of the same *Crispardisia* species, irrespective of their geographic origins, as well as by cophylogenetic analysis.[3] Within *Ardisia*, the subgenus *Crispardisia* appears to be monophyletic. The same is true for its

symbionts, implying the *Ardisia-Burkholderia* leaf-nodule symbiosis to have a single origin.[3,15]

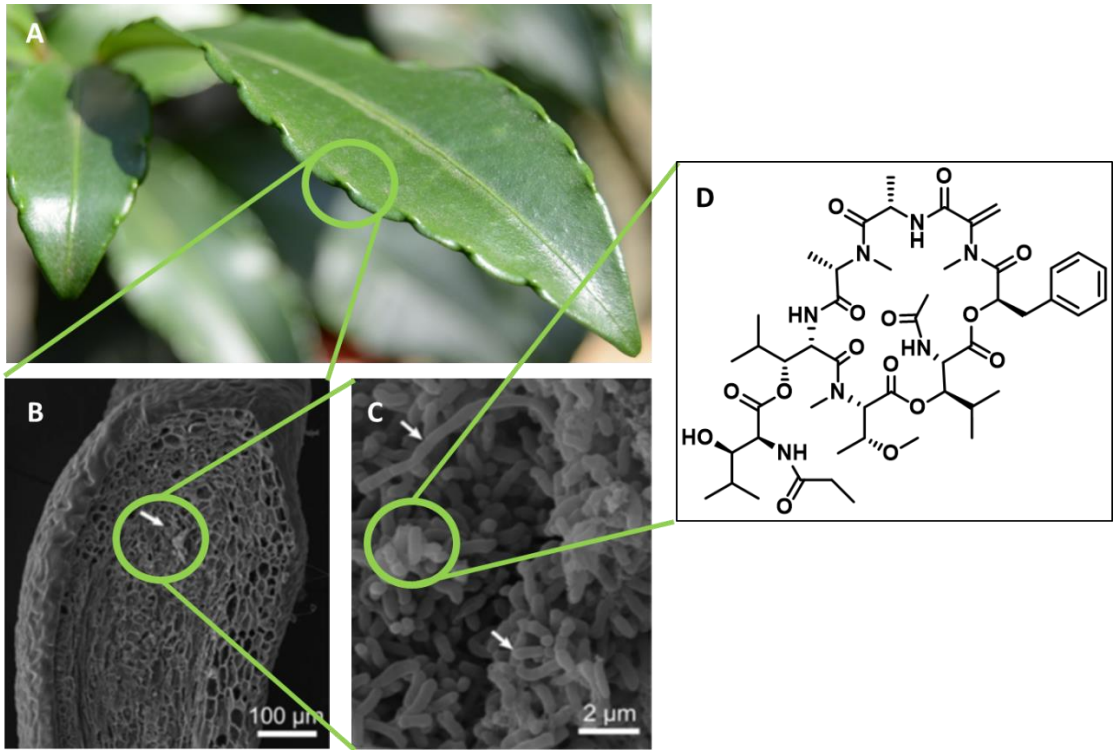

Figure 1-2: (**A**) Leaves from *Ardisia crenata* with nodules (green circle), (**B**) Cross-section of a bacterial nodule from a *Crispardisia*. (**C**) Bacterial symbionts of a *Crispardisia*. (B and C are taken from Ku & Hu[3]), (**D**) Structure of endophyte-derived natural product FR900359.

The genus *Burkholderia* consists of more than 100 species known for their widespread occurrence in diverse ecological niches: It includes (human and plant) pathogens, symbionts, nonpathogenic soil bacteria, and plant-growth-promoting bacteria.[18,19] There appears to be a tremendous variation in genome size ranging from 2.4 Mb to more than 9 Mb[19] among these phylogenetically closely related organisms, which can explain the broad metabolic diversity of *Burkholderia*. Plasticity of the genomes and horizontal gene transfer between *Burkholderia* and other Proteobacteria also contribute to this.[20,21] Ku and Hu showed for other *Crispardisia* species that the nodules are filled with endosymbiotic *Burkholderia*. Accordingly, the corresponding endosymbiotic *Burkholderia* within the nodules of *A. crenata* are most probably the true FR producer.(**Figure 1-2**).[3] The taxonomy of the genus *Burkholderia* is currently being revised, with some species transferred to the genera *Caballeronia* and *Paraburkholderia*. For the sake of simplicity, we adhere in this study to the outdated, yet still valid nomenclature.

To confirm the link between FR and the symbiotic bacteria, we quantified the concentration of FR in methanolic extracts of leaf tissue of *A. crenata* in a former study, serving as basis for deeper investigation of the symbiont-host relationship.[22] The concentration of FR in crude extracts of dissected leaf nodules was 247.0 ± 22.3 µg mg^{-1}, *i.e.* more than 36 times higher than

in leaves where the margins containing the nodules had been cut out (6.7 ± 1.6 μg mg^{-1}).[22] This gives a clear indication that synthesis of FR is concentrated in the leaf nodules and that the endosymbiont is responsible for the synthesis of FR. In that study, we further sequenced the genome of the bacterial leaf symbiont from *A. crenata* and designated it as "*Candidatus* Burkholderia crenata" (*Ca*. B. crenata).[22] Analysis of the only 2.85Mb sized genome sequence revealed essential pathways to be malfunctioned, highlighting the advanced evolutionary stage of this plant-bacterium symbiosis and ongoing genome reductive evolution. Additionally, the putative FR biosynthetic gene cluster *frs* (**Figure 1-4**), encoding two nonribosomal peptide synthetases (NRPSs), was identified on an extrachromosomal plasmid. This further strengthens our assumption that the endophyte *Ca*. B. crenata is the true FR producer.

1.2 Nonribosomal peptide biosynthesis using the example of FR

The biosynthesis of cyclic depsipeptides in microorganisms is well investigated. Many of them are synthesized by giant multi-domain nonribosomal peptide synthetases (NRPSs), following the so-called thiol template mechanism, which features the domain organization seen in **Figure 1-3**.[23] The structural diversity of non-ribosomal peptides (NRPs) exceeds by far that of ribosomally synthesized peptides. This is achieved by the incorporation of proteinogenic and more than 500 presently reported non-proteinogenic amino acids, as well as α-hydroxy and other carboxylic acids. Further modifications such as *N*-, *C*- and *O*-methylation, acylation, glycosylation, heterocyclic ring formation, dehydration, and conversion of the building blocks into their stereoisomers can be conducted by the corresponding enzymes, located on specialized domains of those peptide synthetases.[24]

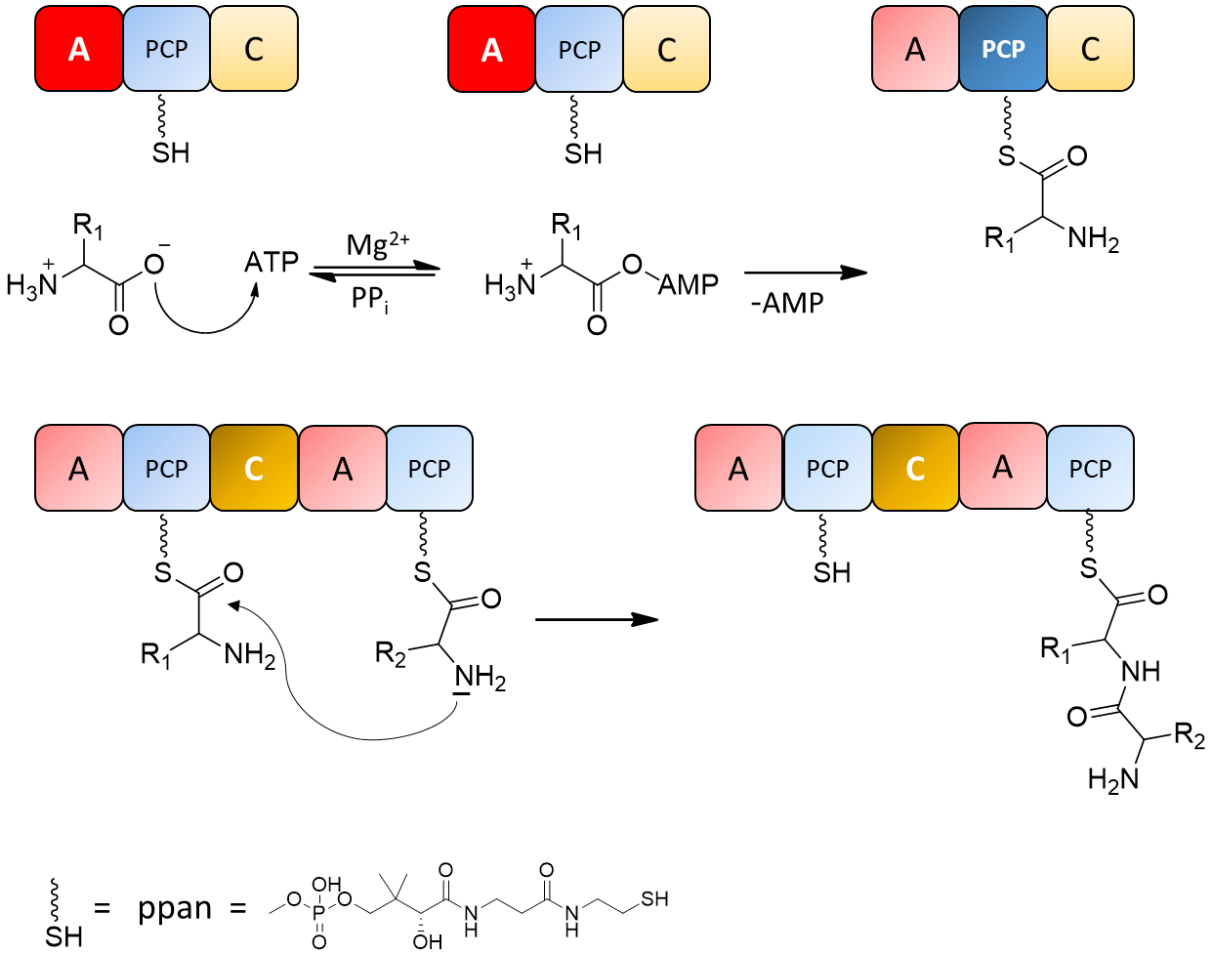

Figure 1-3: Chemical reactions catalyzed by NRPS core domains. A = adenylation-domain, PCP = peptidyl carrier protein (thiolation-domain), C = condensation-domain. Domains in action are drawn dark colored with white & bold letters. The peptide assembly starts with the selection and activation (by adenylation) of a specific amino acid by the A-domain. The activated amino acid is loaded onto the (nucleophilic) thiol moiety of the T-bound cofactor 4´-phosphopantetheine (ppan). The C-domain catalyzes the C-N bond formation between the amino group of the downstream loaded amino acid and the upstream loaded amino acid or peptide (modified after[25]).

Due to the eroded genome, cultivation of *Candidatus* Burkholderia crenata (see **Chapter 1.1**) seems unlikely, and indeed numerous cultivation attempts failed, making FR supply dependent on cultivating and extracting of *A. crenata* leaves. By defining all genes necessary for FR biosynthesis, we draw a plausible biosynthetic hypothesis for this complex metabolite, supported by bioinformatics, *in vitro* characterizations of biosynthetic enzymes and characterization of FR analogs (for detailed information see also **Chapter 4.2**). Unexpectedly, bioinformatics of the *frs* genes showed the presence of two thioesterase (TE) domains, representing two NRPS machineries, which together display a clear colinearity between module and domain architecture and FR structure (**Figure 1-4**).

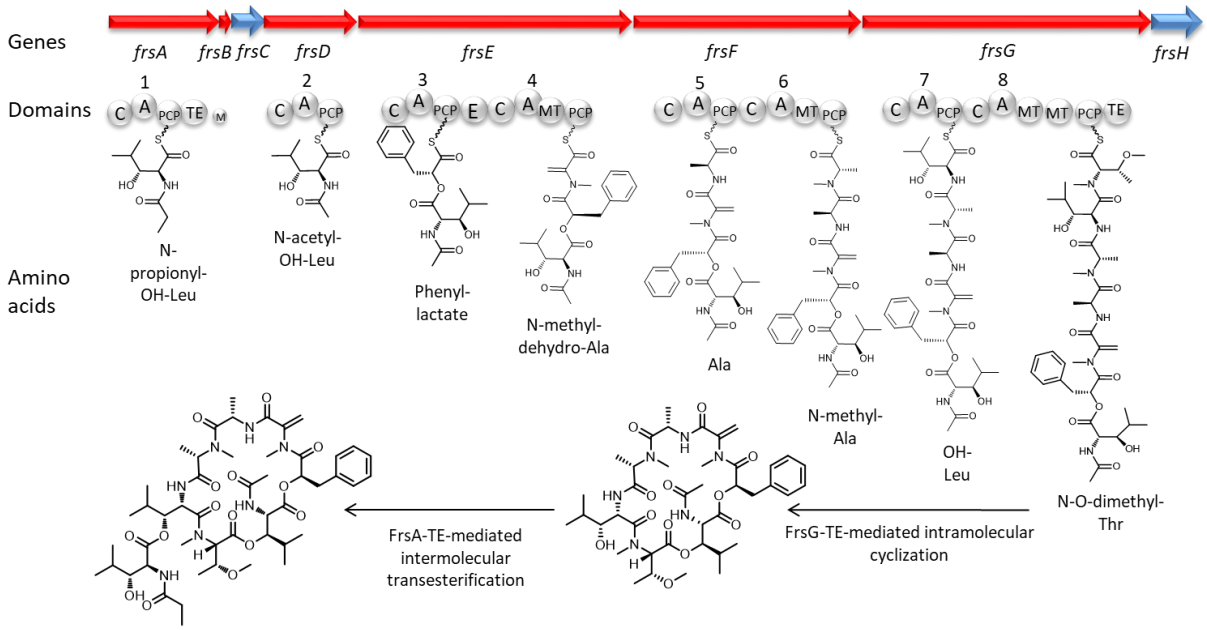

Figure 1-4: Scheme of the putative FR biosynthesis deduced from bioinformatics and *in vitro* experiments. The NRPS genes, the catalytic domains they encode, and the amino acids incorporated by the respective modules are displayed. The peptide formation on the FrsA-G NRPS machineries, including release and transesterification by FrsA-TE is shown. Domains: A, adenylation; C, condensation; MT, methylation (of phenylalanine); PCP, peptidyl carrier protein; E, epimerization and TE, thioesterase (Ile-Thr ring closure). Figure was modified after Crüsemann and Reher *et al.*[10]

In order to confirm the completeness of the FR biosynthetic gene cluster, we next aimed to transfer the *frs* genes to a cultivable bacterium for heterologous FR production. In future, production of FR by fermentation would alleviate the current laborious extraction and isolation process from *Ardisia* plants. Total synthesis of FR was recently achieved, however with low yields and high expenses.[26] Heterologous expression would also be a key step to establish an *in vivo* platform to further investigate FR biosynthesis and to generate analogs for pharmacological evaluation by mutasynthesis or biosynthetic engineering (see **Chapter 4.3**).

1.3 Structural characteristics of the cyclic depsipeptide FR

Symbiotic life forms are widespread in nature and include complex biochemical interactions to the benefit of each partner. Obligatory plant-bacteria associations, as observed in the case of the nodulated *A. crenata*, pose a fascinating ecological system.[22] From *A. crenata*, the cyclic depsipeptide FR was already characterized in 1986[27] and exhibits remarkable structural features such as two adjacent ester bonds, and the rare amino acid building blocks *N*-methyldehydroalanine and *N*-,*O*-dimethylthreonine. The latter is uniquely found in FR, and the structurally related natural products YM-254890 (YM) and sameuramide (SA) (**Scheme 1-1**).[28,29] Structural studies including X-ray crystallography, revealed two *cis*-peptide bonds in the

structure of FR.[30] This is exceptional, because generally the *trans* conformation of amides is favored for thermodynamic reasons.

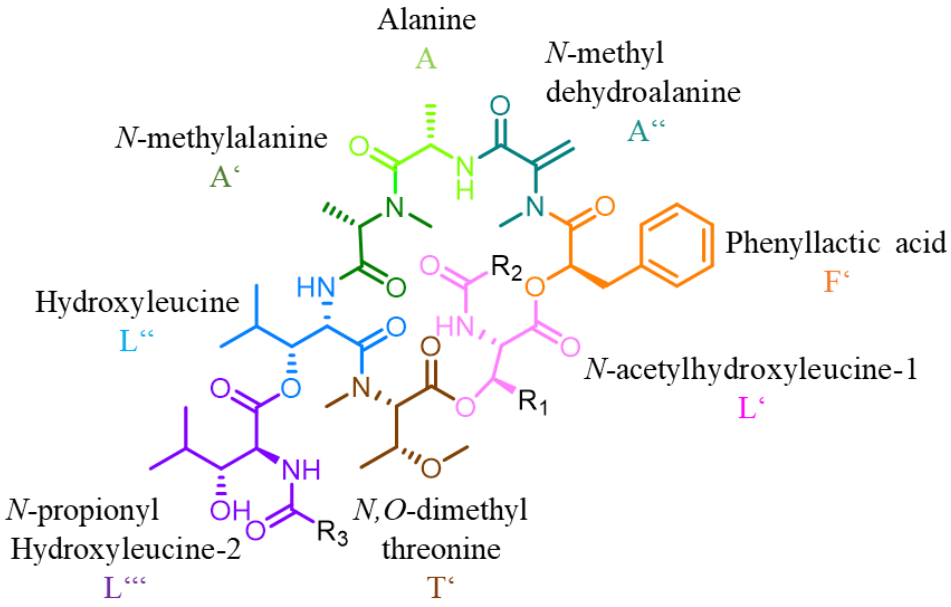

FR	R_1 = -$CH(CH_3)_2$	R_2 = CH_3	R_3 = CH_2CH_3
YM	R_1 = CH_3	R_2 = CH_3	R_3 = CH_3
SA	R_1 = -$CH(CH_3)_2$	R_2 = CH_2CH_3	R_3 = CH_2CH_3

Scheme 1-1: Structures of FR900359 (FR), Sameuramide (SA), and YM-254890 (YM). (Non-proteinogenic) amino acid building blocks colored and annotated for FR, including one-letter code.

Peptides are usually not considered to be promising drug candidates, even though almost all pharmacological targets, *e.g.* receptors, ion channels, enzymes are composed of amino acids. However, the problem with linear peptides is that they are digested by proteolytic enzymes before they can operate, and cyclic peptides often violate several of Lipinski's rules *i.e.* a molecular weight less than 500 Da, no more than 5 H-bond donors, and no more than 10 H-bond acceptors atoms. These rules are an attempt to improve the predictions of druglikeness of small molecules, but Lipinski *et al*. partially revised their applicability for natural products, whose biosynthesis is based on evolutionary selection.[31–34] Cyclic depsipeptides like FR overcome the issue of proteolytic digestion, because they do not possess a terminal amino or carboxylic functionality and furthermore the ester bonds are not accessible for the enzymes. In addition, *N*-methylation of peptide bonds prevent enzymatic degradation, *e.g.* by chymotrypsin, resulting in increasing biological half-life.[35] Beside enzymatic stability, *N*-methylated peptides

offer numerous additional advantages regarding pharmacodynamics and -kinetics. Multiple *N* -and *O*-methylations increase the lipophilicity of molecules, resulting in higher intestine absorption rates and thus higher bioavailabilities.[36,37] Finally, *N*-methylation decreases the number of possible intramolecular and intermolecular hydrogen bonds, offering less aggregation potential, and leading along with the cyclic nature of FR to conformational restriction. The latter can contribute to increased receptor selectivity and altered potency.[38,39]

1.4 Plant-derived natural products as pharmacological tools to study GPCR-mediated signaling at different stages

Structurally complex natural products are often derived from the plant kingdom, and plants have been demonstrated to be a fruitful source of bioactive metabolites. It is assumed that plant secondary metabolites help the producer organisms to survive in their environment, *i.e.* by interaction with competitors or herbivores.[40–42] Therefore, production of such compounds is considered to allow occupation of special ecological niches or to provide competitive advantages against contenders. Many secondary metabolites from plants but also microorganisms are used in medicine, due to their prominent bioactivities and are helpful for a vast range of indications (*e.g.* paclitaxel in cancer, colchicine in gout, morphine for pain).

Often neglected however, is the application as selective, mostly cell-permeable tools in pharmacology. Prominent examples of mainly plant-derived natural products and their molecular targets are illustrated in **Figure 1-5**. As this thesis focusses on the investigation of the plant-derived, selective $G\alpha_{q/11/14}$ protein inhibitor FR, special emphasis in **Figure 1-5** is put on plant-derived natural products and their abilities to interact with activated $G\alpha_q$ (Gq) protein coupled receptors (GqPCRs) signaling at different stages. Upstream of G proteins, GPCRs are situated comprising around 800 members and represent ≈3% of the human genome. They are involved in a wide variety of physiological processes by detecting molecules outside the cell and activating internal signal transduction pathways and, ultimately, cellular responses.[43] Thus not surprisingly, currently about 36% of all available medications target GPCRs, which renders them as the most important class of drug targets.[44]

To exemplify the potential of plant-derived natural products able of interacting with GPCRs and their signaling, the human muscarinic acetylcholine receptor M1 was chosen, because it couples predominantly to Gq, but to less extent also to $G\alpha_s$ (Gs) and $G\alpha_i$ (Gi).[45]

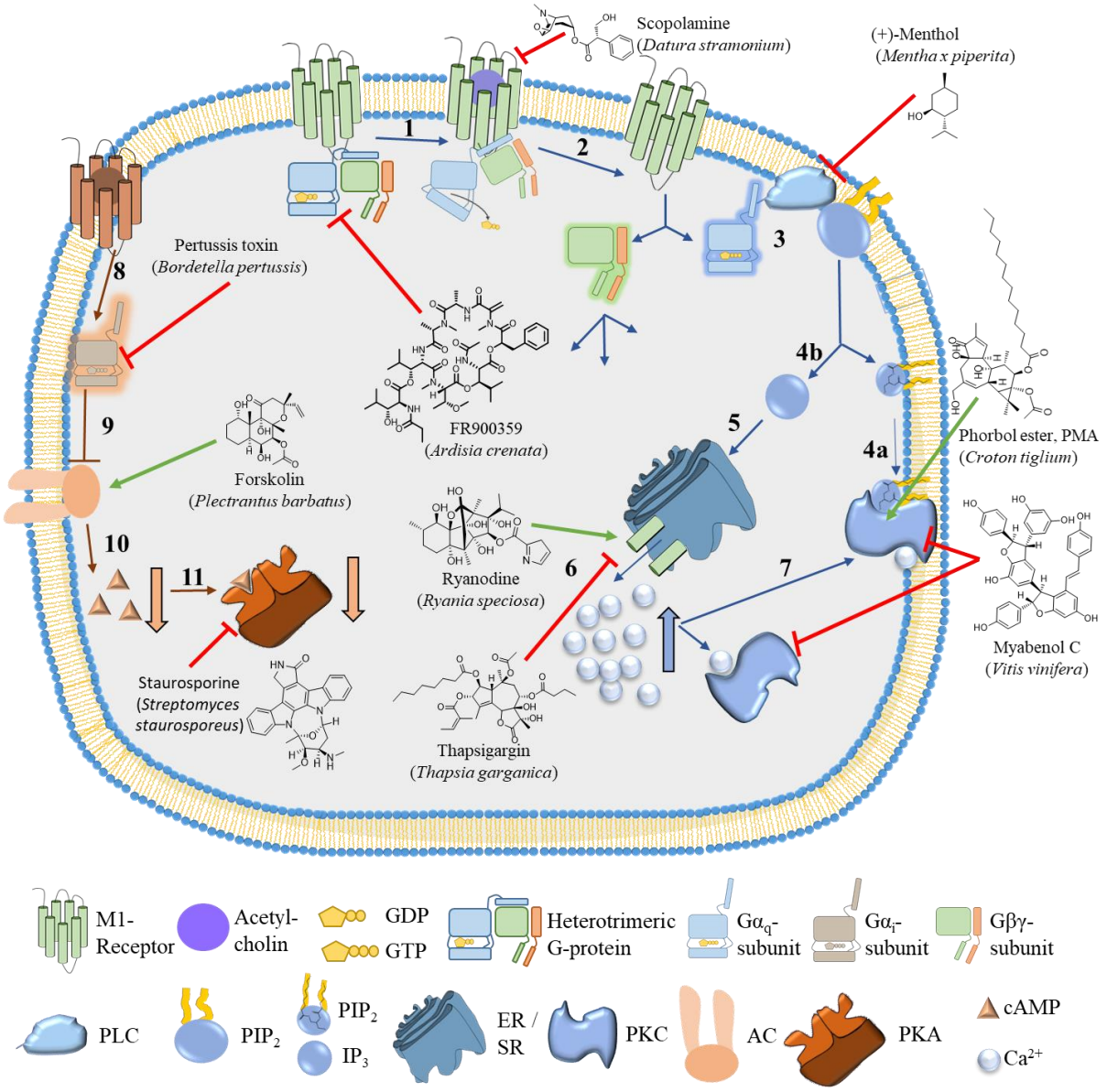

Figure 1-5: Natural products and their molecular targets with emphasis on GqPCR-mediated signaling in mammalian cells. Natural products that are widely applied as pharmacological tools are shown with their respective trivial name, structure, and source. Green arrows display activation and red arrows display the inhibition of target structure. The signaling cascade upon GqPCR activation is shown with blue arrows. (**1**) In its inactive state the muscarinic M1-receptor, a G protein–coupled receptor (GPCR), is bound to a heterotrimeric G protein. M1-receptors are known to predominantly bind $G_{q/11}$ proteins, which in turn bind guanosine diphosphate (GDP), when inactive. (**2**) M1-receptor is activated *e.g.* by the endogenous ligand acetylcholine, leading to a conformational change of the receptor and subsequent G protein activation. (**3**) Active Gq protein heterotrimer dissociates into Gα and Gβ,γ subunits (activated state highlighted by light effect), which each contribute to downstream signaling. (**4**) Gαq subunit activates phospholipase Cβ (PLCβ). PLCβ catalyzes the hydrolysis of phosphatidylinositol 4,5-bisphosphate (PIP_2) to inositol 1,4,5-trisphosphate (IP_3, **4b**) and diacyl glycerol (DAG). (**4a**) DAG activates membrane-bound protein kinase C (PKC) and facilitates translocation of PKC. (**5**) Soluble IP_3 diffuses to endoplasmic or sarcoplasmic reticulum (ER or SR respectively) and binds to a ligand-gated Ca^{2+} channel leading to Ca^{2+} release into the cytoplasm. (**6**) Elevated Ca^{2+} levels have multiple effects, *e.g.* (**7**) activation of calcium-dependent PKC. To a less extent M1-receptors are also reported to bind Gi in certain tissues.[46] (**8**) Gi protein-mediated signaling is shown on the left side (brown arrows). (**9**) Activated $G\alpha_i$ binds and inhibits adenylyl cyclase (AC). (**10**) Thus, AC decreases the production of cAMP from ATP, which, in turn, (**11**) results in decreased activity of cAMP-dependent protein kinase (PKA). For details please refer to the text.

1.4.1 Plant-derived tools interfering with GqPCR activation

In the first step of the M1 receptor signaling cascade the endogenous ligand acetylcholine binds to the receptor and activates it. Binding to the receptor can be prevented by addition of non-covalent competitive antagonist such as the non-selective natural product atropine from *Atropa belladonna* or the M1-selective scopolamine (Hyoscine) derived *e.g.* from *Datura stramonium* (**Figure 1-5**).[47] Scopolamine has been used as a research tool to study the involvement of acetylcholine in cognition. Results in primates suggest that acetylcholine is involved in the encoding of new information into long term memory.[48,49] Furthermore, scopolamine has been investigated as an antidepressant with a number of small studies finding positive results.[50]

1.4.2 FR900359, a plant-derived tool interfering with Gq protein activation

Binding of acetylcholine to the M1 receptor activates the latter, resulting in a conformational change in the receptor that is transmitted to the bound $G\alpha_q$ subunit of the heterotrimeric Gq protein via protein domain dynamics.[51] The activated $G\alpha_q$ subunit exchanges GTP with GDP which in turn triggers the dissociation of $G\alpha_q$ subunit from the $G\beta\gamma$ dimer and from the receptor (see **Figures 1-5** and **1-6**).[51] The latter can be prevented, *e.g.* by guanine nucleotide dissociation inhibitors (GDI).

Of the few inhibitors for G protein signaling, mechanistic details on the structural level are only available for the $G\alpha_{q/11/14}$-selective YM, discovered and isolated from *Chromobacterium* sp. QS3666.[28,52] Its binding mode, as elucidated by means of mutagenesis and structural data, provides a plausible mechanism for inhibition of GDP release.[53] Nishimura *et al.* propose that YM forms a cone-like structure with its phenyl group at the head, and is stuck deeply in the cleft between both interdomain linkers, thus acting as GDI (see **Figure 1-7**). The cyclic depsipeptide FR from *A. crenata* supposedly share this mode of action as GDI, which will be discussed in detail in this thesis. FR also selectively blocks heterotrimeric G proteins of the Gq family ($G\alpha_{q/11/14}$) which relay signals from activated GqPCRs to the cell interior, just as the bacterial metabolite YM. Docking experiments with FR and Gq suggest this similarity in the mode of action between FR and YM (see **Figure 1-7**).[54] FR and YM are unique in that they are the only chemicals competent to interdict Gq signaling with high selectivity and potency.[54]

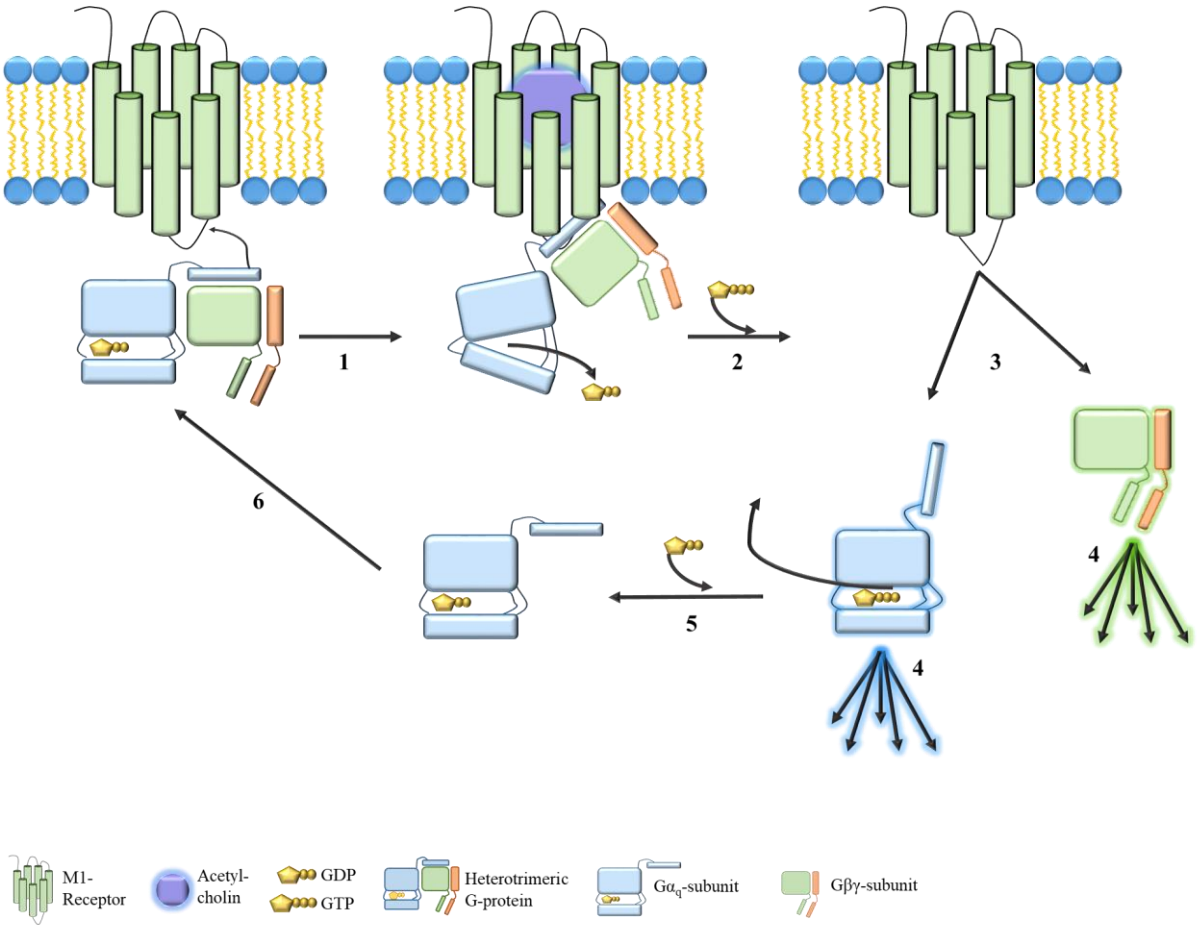

Figure 1-6: Mechanism of the G protein activation cycle. (**1**) In the inactive state, the heterotrimeric G protein rests in the GDP-bound form. (**2**) Upon activation, *e.g.* by acetylcholine-mediated M1-receptor activation or guanine nucleotide exchange factor (GEF), a conformational change within the G protein induces the release of GDP and the binding of GTP to the α-subunit. (**3**) This triggers the dissociation of α- and βγ-subunit, (**4**) both of which in turn can interact with signaling effectors. (**5**) GTPase-activating proteins (GAPs) enhance the intrinsic GTPase activity of the α-subunit and thus allow the βγ-subunit to re-associate with the GDP-bound α-subunit (**6**) to form an inactive heterotrimeric G protein again.

FR is thus essential for studies that aim to unravel the contribution of Gq to complex cellular signaling processes.[55–59] Gq-mediated signaling pathways regulate a large number of essential processes in eukaryotic cells.[60] By blunting signal transduction of many GqPCRs simultaneously, FR may be decisively advantageous as therapeutic to treat conditions where multiple GqPCRs contribute to pathology.[61–63] Also YM is applied as molecular tool for investigations of complex signaling cascades mediated by the Gq pathway. In the field of neurosciences, several investigators used YM. In this way Matsuo *et al.*[64] identified a novel Gq coupled orphan GPCR, termed GPRg1and Morishita *et al.*[65] applied YM for investigating the involvement of $G\alpha_{q/11}$ signaling mediated via the endothelin-B receptor in neural progenitor proliferation. On the basis of this mode of action, YM demonstrated a series of pharmacological effects, *e.g.* platelet aggregation inhibition, inhibition of neointima formation, decreasing of systemic blood pressure and vasorelaxant effects in rats.[66,67]

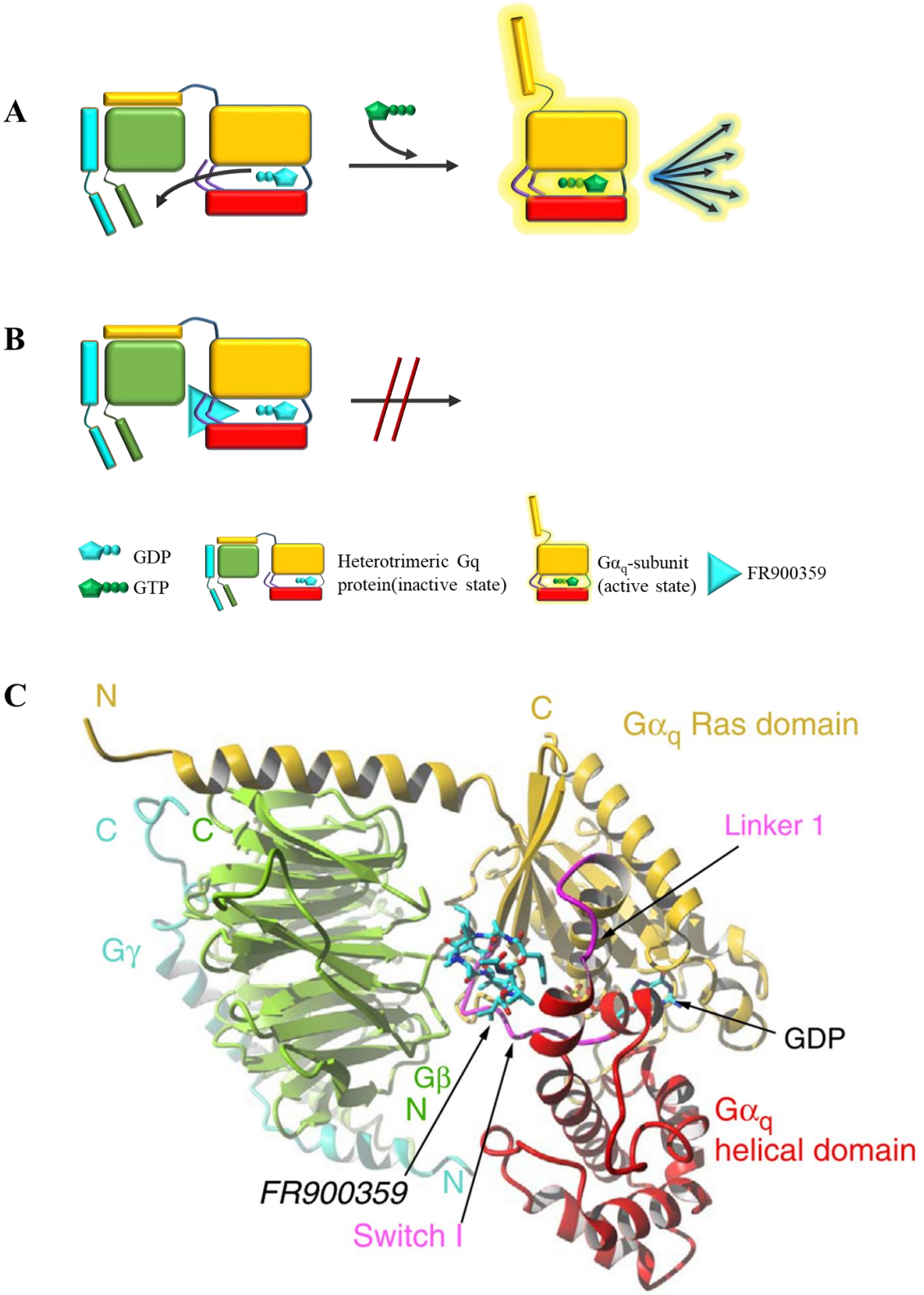

Figure 1-7: FR inhibits Gq-signaling by acting as guanine nucleotide dissociation inhibitor (GDI). (**A**) Schematic representation of Gq protein activation. Upon activation, a conformational change within the Gq protein induces the release of GDP and the binding of GTP to the α-subunit. This triggers the dissociation of α- and βγ-subunit, both of which in turn can interact with several signaling effectors. $G\alpha_q$ subunits and domains are color coded: $G\alpha_q$ Ras domain: yellow, helical domain: red, Gβ: green, Gγ: cyan. (**B**) Schematic representation of the mechanism of action of FR that is acting as guanine nucleotide dissociation inhibitor (GDI) and thus keeping the Gq protein in its inactive state. (**C**) Zoomed-out view of the heterotrimeric Gq protein bound to FR900359 derived from docking **(**taken from Schrage *et al.*[54]).

1.4.3 Plant-derived tools interfering with phospholipase Cβ activation

After dissociation of the heterotrimeric G proteins into $G\alpha_q$ and Gβ,γ subunits each contribute to downstream signaling. The $G\alpha_q$ subunit activates phospholipase Cβ (PLCβ). PLCβ catalyzes the hydrolysis of phosphatidylinositol 4,5-bisphosphate (PIP_2) to inositol 1,4,5-trisphosphate (IP_3) and diacyl glycerol (DAG). While the currently most valuable tool for studying PLCβ is the small molecule inhibitor U-73122 and analogs thereof[68,69], intriguingly also menthol from *Mentha x piperita* previously known to chemically trigger the cold-sensitive Transient receptor potential cation channel subfamily M member 8 (TRPM8) and Transient receptor potential cation channel, subfamily V, member 3 (TRPV3) in the skin,[70] shows an inhibitory effect on the PLC pathway.[71]

1.4.4 Plant-derived tools interfering with inositol 1,4,5-trisphosphate (IP_3)-mediated signaling

Subsequent to the cleavage of PIP_2 to DAG and IP_3, the soluble IP_3 diffuses to the endoplasmic or sarcoplasmic reticulum (ER or SR respectively) and binds to a ligand-gated Ca^{2+} channel, leading to Ca^{2+} release into the cytoplasm. Thapsigargin is a potent and selective non-competitive inhibitor of a class of enzymes known by the acronym SERCA, (sarco / endoplasmic reticulum Ca^{2+} ATPase) in the sub-nanomolar range.[72] Thus, thapsigargin is useful in experimentation, examining the impacts of calcium homeostasis. Structurally, thapsigargin is classified as a sesquiterpene lactone of the guaianolide-type, and is isolated from the plant *Thapsia garganica*. Because its mechanism of action provokes apoptosis very effectively, a semisynthetic peptide-drug-conjugate (mipsagargin) was tested in a human phase I clinical study against androgen-independent metastatic prostate cancer, for which no drug is approved at present. It was found to be effective, to have acceptable tolerability and displaying a favorable pharmacokinetic profile in patients with solid tumors.[73,74] Astonishing in this context, is however another study that showed tumor promoting properties of thapsigargin in mammalian cells.[75] Further effects of thapsigargin are the specific inhibition of the fusion of autophagosomes with lysosomes, the last step in the autophagic process.[76]

Another natural product used as tool is known to deplete intracellular Ca^{2+} stores. Ryanodine is a diterpenoid from *Ryania speciosa*. At nanomolar concentrations, ryanodine locks the ryanodine receptors (RYR-1, RYR-2, RYR-3) in a half-open state causing Ca^{2+} release from Ca^{2+} stores of the sarcoplasmic reticulum into the cytoplasm, resulting in massive muscle contractions, whereas it fully closes the receptor at micromolar concentration, leading to

paralysis.[77,78] The vast number of applications for compounds interacting with Ca^{2+} signaling for basic research and in therapy was investigated in detail by Stutzmann and Mattson.[79]

1.4.5 Plant-derived tools, activating or inhibiting protein kinase C

In terms of GPCR-mediated signaling, elevated Ca^{2+} as well as DAG levels, have multiple effects, *e.g.* activation of calcium-dependent protein kinase C (PKC), which in turn is involved in controlling the function of other proteins via the phosphorylation of serine and threonine residues of these proteins.[80] There are several natural products reported to inhibit or enhance PKC activity such as gossypol, chelerythrine, phorbol esters, and myabenol C.[81–84] The latter is a stilbenoid resveratrol trimer found in *Vitis vinifera* with moderate and unselective PKC inhibitory activity. Chelerythrine, a benzophenanthridine alkaloid present in the plant *Chelidonium majus* is marketed as a potent, selective, and cell-permeable PKC inhibitor. This effect, however, is debunked by many investigators and critically summarized by Wu-Zhang and Newton.[82]

The latter example demonstrates the potential risks of ever-growing tool boxes without robust and high-quality suitability tests. According to the authors[82] the continued marketing of chelerythrine as a specific PKC inhibitor has resulted in the inappropriate attribution of numerous and wide-ranging biological effects to PKC activity.

Prominent examples of PKC activators are phorbol esters, derived from Euphorbiaceae, *i.e. Croton tiglium*, one of the 50 fundamental herbs used in traditional Chinese medicine. 12-O-Tetradecanoylphorbol-13-acetate (TPA), also commonly known as phorbol 12-myristate 13-acetate (PMA) is a diester of phorbol and a potent tumor promoter often employed as a tool in biomedical research in models of carcinogenesis.[85,86] A structurally related compound, ingenol mebutate found in the sap of the plant *Euphorbia peplus* is applied as drug for the topical treatment of actinic keratosis.[87] Further it has been found to reactivate latent HIV, thus together with anti-retroviral drugs it potentially provides a permanent cure for HIV infection.[88]

1.4.6 Natural products, interfering with G_iPCR-mediated signaling

In a lesser extent, M1-receptors are also reported to bind Gi proteins.[46] Gi protein-mediated signaling is shown in **Figure 1-5** (on the left side, brown arrows). Similar to FR for Gq, pertussis toxin (PTX) from *Bordetella pertussi*s locks the $G\alpha_i$ subunit in its GDP-bound, inactive state. The mechanism of action differs from that of the Gq inhibitor FR in that PTX catalyzes the ADP-ribosylation of the α_i subunits of the heterotrimeric Gi protein, preventing the interaction

of Gi proteins with their respective GPCRs.[89] The value of PTX as a tool to study Gi-related processes is undeniable (2928 entries of "pertussis toxin" in titles of scientific publications, 162 of these have >100 citations each, 04-22-2018, web of science, https://apps.webofknowledge.com/WOS_GeneralSearch_input.do?product=WOS&search_mode=GeneralSearch&SID=C3sdzHxS5d7xiIivO1J&preferencesSaved=).[90–92]

Further downstream, activated and dissociated $G\alpha_i$ binds and inhibits adenylyl cyclase (AC). Thus, AC decreases the production of 3',5'-cyclic adenosine monophosphate (cAMP) from ATP, which, in turn, results in decreased activity of cAMP-dependent protein kinase (PKA). Forskolin, occurring in *Plectranthus barbatus*, belongs to the group of labdane diterpenes. In human and animal organisms, forskolin, acts as direct stimulator of the enzyme AC, responsible for cAMP production, and thus has pleiotropic effects. Cyclic adenosine monophosphate acts as second messenger, thus as mediator for Gs/Gi coupled signal transduction. Therefore, beside its potential for the treatment of glaucoma[93,94] forskolin is of particular value as tool in biochemistry and pharmacological research on Gi/sPCRs.

In conclusion it was demonstrated that natural products (especially FR) have tremendous potential as lead structures for the development of new drugs[95] as well as selective pharmacological tools unraveling complex biological processes in physiology and pathophysiology.[96]

2 Aim of the study

The cyclic depsipeptide FR900359 (FR) is a selective inhibitor of $G\alpha_{q/11/14}$-protein mediated signaling of GPCRs and thus extremely useful as a pharmacological tool. This natural product is in the center of the DFG-funded research unit 2372. FR is present in the higher plant *Ardisia crenata*, which is known to harbor symbiotic bacteria that we designated as *Candidatus* Burkholderia crenata.

Within this thesis the ecological function of FR in the plant/symbiont association, which is not known to date, shall be investigated. To shed light on the biosynthesis of FR we sequenced the genes for a putative nonribosomal peptide synthetase from the endophytic *Burkholderia*, which shall serve as a basis for the heterologous expression and genetic engineering of FR derivatives. The sequence of the biosynthetic gene cluster for FR production will also be employed for mining publicly available bacterial genomes for bacterial strains, being able to produce FR or related compounds.

To understand the mechanism of action of FR on the molecular level it is necessary to examine the structural elements of the depsipeptide FR, responsible for the biological activity. In this way the pharmacophore of FR shall be derived. In order to achieve this, structural variants of FR shall be obtained by semisynthetic modification of FR, including the development of fluorescent FR analogs as molecular tools to study kinetics and the mechanism of cellular uptake of FR. Further, FR analogs shall be derived by isolating minor depsipeptide-metabolites from *A. crenata* as well as other *Crispardisia* known to have related bacterial symbionts. All FR derivatives will be assessed in comparison to FR for their bioactivity and will give deep insights into structure-activity relationships.

3 Materials and Methods

3.1 Materials

3.1.1 Plant material

Ardisia crenata was purchased commercially and afterwards cultivated in the "Nutzpflanzengarten" of the Institute for Pharmaceutical Biology of the University of Bonn. *A. lucida* leaves were provided by the Botanical Garden Bonn. A herbarium specimen is located at the Institute for Pharmaceutical Biology of the University of Bonn. The *Ardisia villosa*, *mamillata*, *hanceana* samples were collected in January/2016 at a height of 800 m by excursion near Bawang Mountain in Changjiang County, Heinan, China. The specimen were dried at 25 °C until extraction.

Figure 3-1: Cultivation of *Ardisia crenata* in the green house of the Univ. of Bonn.

Botanical plant name	**Drug designation**	**Origin**
Ardisia crenata SIMS	*Ardisiae crenatae folium*	Botanical Garden Bonn

Ardisia hanceana	*Ardisiae hanceanae folium*	Hao-Fu Dai, Hainan China
Ardisia lucida	*Ardisiae lucidae folium*	Botanical Garden Bonn
Ardisia mamillata	*Ardisiae mamillatae folium*	Hao-Fu Dai, Hainan China
Ardisia polycephala	*Ardisiae policephalae folium*	Botanical Garden Bonn
Ardisia villosa	*Ardisiae villosae folium*	Hao-Fu Dai, Hainan China

3.1.2 Cultivation, Extraction and growth determination of *Chromobacterium vaccinii* MWU205, DSM 25150

Chromobacterium vaccinii from a glycerol stock was fermented in Luria-Bertani Medium (containing 10 g NaCl, 5 g yeast extract and 10 g tryptone solved in 1 L Milli Q Water and adjusted the pH to 7.5 with 5 M NaOH) with carbenicillin (stock concentration: 50 mg/mL; final concentration: 0,05 mg/mL) on a rotary shaker at 200 rpm and 25 °C for 24 h. Afterwards 1% (v/v) of final volume was taken of the pre-culture to inoculate the final cultivation volume necessary for the experiment, *e.g.* 100 mL medium were inoculated with 1 mL medium pre-culture. Cultivation was also performed by Emilie Goralski and Wiebke Hanke, Institute for Pharmaceutical Biology, Univ. of Bonn.

For growth determination the optical density was measured at 600 nm and 764 nm. Measurement was performed once of a sample directly taken out of the culture and once with the sample from the culture being centrifuged for 1 minute at 13,300 rpm. The supernatant was removed and the pellet was resuspended in 1 mL LB medium. The sample was diluted if necessary so that the optical density was around 0.0-0.8.

Extraction for the production curve of FR and derivatives was done every 12 hours with 40 mL butanol for 40 ml culture. After 24 hours the extraction mixture was filled in tubes and centrifuged at 4000 rpm for 5 minutes. The organic phase was collected. Afterwards, 40 mL butanol was added, mixed, directly centrifuged and again the organic phase was taken. The phases were united and evaporated. LCMS measurements of every sample were conducted. Experiments were performed by Wiebke Hanke, Institute for Pharmaceutical Biology, Univ. of Bonn.

Chemicals were purchased from Carl Roth and Hedinger.

3.1.3 **Chemicals**

- *Chemicals:*

- 2-Aminoethanethiol hydrochloride	Sigma-Aldrich (Steinheim, Germany)
- Acetic anhydride (99.6%)	VWR International (France)
- Acetone-*d6*	Deutero GmbH (Kastellaun, Germany)
- Acetonitrile HPLC grade)	VWR International (France)
- Acetonitril-*d3*	Deutero GmbH (Kastellaun, Germany)
- Acetyl Chloride	Sigma-Aldrich (Steinheim, Germany)
- *N*-Boc-2-aminoethanethiol	Sigma-Aldrich (Steinheim, Germany)
- BODIPY-630/650-X-SE	ThermoFisher Scientific (Hennef, Germany)
- *n*-Butanol	Roth (Karlsruhe, Germany)
- Chloroform	Roth (Karlsruhe, Germany)
- Chloroform-*d1*	Deutero GmbH (Kastellaun, Germany)
- Deuteriumoxide	Deutero GmbH (Kastellaun, Germany)
- DCM (pure, anhydrous)	Roth (Karlsruhe, Germany)
- DMAP	Roth (Karlsruhe, Germany)
- DMSO-d6	Deutero GmbH (Kastellaun, Germany)
- Hexanoic anhydride	Sigma-Aldrich (Steinheim, Germany)
- HPLC- grade water	
- Methanol-*d4* (99.8 %)	Deutero GmbH (Kastellaun, Germany)
- Methanol (hypergrade for LC/MS)	Merck (Darmstadt, Germany)
- Methanol (HPLC gradient grade)	Avantor (Deventer, Netherlands)
- Potassium hydrogen sulfate	Roth (Karlsruhe, Germany)
- Pyridine (99%)	Roth (Karlsruhe, Germany)
- Sodium chloride	Roth (Karlsruhe, Germany)
- Sodium dodecyl sulfate	Sigma-Aldrich (Steinheim, Germany)
- Sodium hydrogen carbonate	Sigma-Aldrich (Steinheim, Germany)
- Sodium sulfate	Sigma-Aldrich (Steinheim, Germany)
- TAMRA-Thiol	BioActs (South Corea)
- TPGS-750-M	Sigma-Aldrich (Steinheim, Germany)
- Triethylamine	Roth (Karlsruhe, Germany)
- Trifluoroacetic acid (TFA) 99.9%	Roth (Karlsruhe, Germany)

Solvents used for chromatography were distilled before application, especially acetone, ethyl acetate, methanol and dichloromethane. Water for HPLC purification was taken from „Milli-Q Reagenzwasser“-system (Millipore, Eschborn, Germany). Reagents for chemical derivatization of FR were purchased from commercial sources and were used without further purification. Oxygen- or water-sensitive reactions were performed under argon atmosphere. Standard coupling reagents (HBTU, HOBt, TFFH, PyBOP), resins and amino acid derivatives used for

solid phase synthesis of analogs were purchased from Orpegen Peptide Chemicals GmbH (Heidelberg, Germany), Novabiochem and IRIS Biotech (Marktredwitz, Germany), respectively. Peptide synthesis reagents (piperidine, DIEA, trifluoroacetic acid, BTSA) and solvents (*N*,*N*-dimethylformamide, and dichloromethane) were of reagent grade, and solvents for chromatography (acetonitrile, water, and methanol) were of analytical grade obtained from VWR International (Dresden, Germany). Cell culture reagents were purchased from Invitrogen. All other reagents were from Merck (Darmstadt, Germany), Fluka (Buchs, Switzerland), Sigma-Aldrich (Steinheim, Germany) and Roth (Karlsruhe, Germany).

3.1.4 Other materials

- Hamilton syringe 100µl	Sigma-Aldrich (Steinheim, Germany)
- Pasteur pipettes	Roth (Karlsruhe, Germany)
- Pipette tips 200µl, 1000µl Tip One ®	Starlab GmbH (Hamburg, Germany)

3.2 Extraction of *Ardisiae crenatae folium*

After harvesting and drying 150g leaves of *Ardisia crenata*, the dried leaves were crushed and extracted three times with 800ml MeOH each. The methanol crude extract, about 40 g, was suspended in 1000ml distilled water and extracted with three times 400ml BuOH in a separation funnel to yield about 20 g BuOH-extract.

3.3 Chromatographic methods

3.3.1 Thin layer chromatography (TLC)

Thin layer chromatography was used to get information about the running performance of FR and its derivatives in several solution systems and to determine their purity. TLC was carried out using either TLC aluminum sheets (20 x 20 cm) silica gel 60 F_{254} (Merck 1-05554) or TLC aluminum sheets (20 x 20 cm) RP-18 F_{254} (Merck 1-05559) as stationary phase. Standard chromatograms of plant extracts and fractions were prepared by applying 20 µL of solution (1 mg/mL) to a TLC plate and using $CHCl_3$/MeOH/H_2O = 26:15:3 as mobile phase under chamber saturated conditions. Developed chromatograms were detected under UV light at λ = 254 nm (fluorescence quenching) and λ = 366 nm (intrinsic fluorescence). Afterwards they were

sprayed with vanillin-sulphuric acid reagent (0.5 g vanillin dissolved in a mixture of 85 ml methanol, 10 mL acetic acid and 5 sulphuric acid, TLC plate heated at 110°C after spraying) giving colored spots on a white plate and subsequently analyzed. For reaction control of the synthesis of compound **12**, the plates were sprayed with ninhydrin.

3.3.2 Vacuum liquid chromatography (VLC)

VLC is a method to separate both large and small quantities of mixtures efficiently, rapidly, and inexpensively. Basically, it is a column chromatography accelerated by vacuum.[97,98]

Fractionation of crude extracts (BuOH) was performed with VLC. Depending on the amount of extract, columns with 4 cm diameter (500 mg to 2 g), 6.5 cm diameter (2 to 4 g) or 10 cm (> 4 g) were used. Vacuum liquid chromatography was carried out using Polygoprep 60-50 RP18 (Macherey-Nagel, Düren, Germany). Sorbent was poured as a suspension into the column and compressed under vacuum for accelerating the separation. Afterwards, the system was equilibrated with 200 mL of the first solvent ($MeOH/H_2O$ = 30/70). The sample was dissolved in low volume of the same solvent mixture and applied on the surface. For RP separation water/methanol mixtures with various ratios were used ($MeOH/H_2O$ = 30/70 → $MeOH/H_2O$ = 100/0). Each fraction contained 200mL solvent when a 10 cm column was used.

3.3.3 Size exclusion chromatography (SEC)

After pre-fractionizing via VLC, based on polarity the following size exclusion chromatography (SEC) procedure helped to separate FR from other substances with similar polarity but varying size. Therefore, the FR-containing VLC-fraction (Fraction 7) diluted in a minimal amount of MeOH was put onto the 100cm in height and 2cm in diameter column, filled with Sephadex LH-20 material dispersed in MeOH. After sample loading, the column was eluted with MeOH by gravity and eight fractions with 20ml each were collected after the first 100ml were discarded (dead volume). About ninety percent of FR elute in Fraction 7.3 and lower quantities of FR are situated in fraction 7.4 together with high amounts of contaminants.

3.3.4 Flash chromatography

A Reveleris X2 Flash Chromatography System with UV-detector and ELSD was used. Software: Navigator. For sample preparation 3 g-, 12 g- or 40 g-solid loader was applied. Packing of the solid loaders was achieved through adsorption of the sample onto silica gel 60 (0.063-0.200 mm, Merck) or Polygoprep 60 C_{18} (0.05 mm, Machery-Nagel), respectively. The

dried material was then filled into the solid loader. Reveleris® flash cartridges, prefilled with 4 g, 12 g, 40 g, 120g or 220 g of C_{18}-silica, were used (with 40 µm particle size).

3.3.5 **Solid phase extraction (SPE)**

For solid phase extraction, a Bakerbond C18 column (2000 mg/6mL) was used. Separations were performed using water-methanol mixtures with decreasing polarity and accelerated by a membrane vacuum pump. Column was equilibrated with the first designated eluent.

3.3.6 **High performance liquid chromatography (HPLC)**

HPLC is a sort of column chromatography, pressing liquid solvent assisted by pumps through a column filled with a solid adsorbent material.[99] HPLC is the method of choice for analysis of substance mixtures for qualitatively and quantitatively purposes.

Following systems containing an interface, a pump, an injector, a detector, and a fraction collector were used for HPLC purification of extracts and compounds:

System A: Waters system, controlled by Millenium software, equipped with a 600 Controller pump, a 717 plus autosampler with in-line Degasser AF and a 996 photodiode array detector and fractionizer.

System B: Waters 1525µ binary pump with Waters 2998 diode array detector (DAD).

Software: Breeze 2 (© 2008 Waters C.)

System C: Waters HPLC system equipped with a 2695 separation module, a 996 DAD and QuickStart Empower 2 software (© 2005 Waters Co.).

Following columns were used:

Column A: YMC Hydrosphere C_{18}, 3µm, 250x4.6 mm, analytical column (raw peptide isolation)
Column B: Nucleodur RP_{18} plus column, 5 µm, 250 x 8 mm, semi-preparative column (raw peptide isolation)
Column C: Nucleoshell RP_{18} plus column 5 µm, 250 x 4.6 mm, analytical column (pure FR900359 isolation)
Column D: Kinetex C_{18} column 5 µm, 250 x 4.6 mm, analytical column

As solvent for RP columns, usually methanol/water mixtures with ratios between 70/30 and 100/0 were used. If a degasser was not part of the instruments, the solvent was degassed under reduced pressure via water jet pump. For optimization of FR900359 isolation on a RP18 column the following modifier were added to the methanol/water solvent: trifluoroacetate (0.05 %). Analytical columns were used with a flow of 0.70 to 1 mL/min. 25 µL of an extract, which was

adjusted to a concentration of 10-20 mg/mL were injected. Separation was monitored with UV-detector systems.

3.4 Isolation protocols

3.4.1 Depsipeptide isolation and purification

Bioassay, LC-MS and ^{1}H NMR guided fractionation of the crude extracts obtained from the plant *Ardisia crenata*, yielded the cyclic depsipeptide FR. The investigated plant material was cultivated in the green house of the Botanical Garden Bonn.
200 g of dried plant leaves were coarsely crashed and extracted with methanol. Further purification steps included liquid-liquid extraction, RP-18 vacuum liquid chromatography and size exclusion chromatography.

3.4.2 Isolation of FR and FR analogs (1-4)

Final purification was done by HPLC with a semi-preparative YMC Hydrosphere RP-18 column (250 x 4.6 mm, 3µm). The elution system was water (eluent C) and methanol (eluent D). The crude peptide was derived with isocratic conditions (80% eluent D for 35 minutes). The separation of FR from its analogs was achieved using a Nucleoshell RP_{18+} column (250 x 8 mm, 5 µm) with isocratic 75% eluent D for 20 minutes, followed by a linear gradient to 100% eluent D in 35 minutes. Pure FR was isolated as a white powder t_R: 28.2 min (10 mg from 200 g dried leaves). The isolation scheme is shown in **Scheme 5-1**.
Compound **1** was isolated as described by Crüsemann & Reher *et al.*[10] A shoulder of the FR peak eluting prior to FR was collected. This fraction included a peptide mix of FR and another similar peptide as judged from LC-MS data. HPLC conditions had to be adjusted to separate the new peptide quantitatively from FR. The composition of the mobile phase was changed from isocratic 80% methanol to 75% methanol and a Nucleoshell $RP18^{+}$ column 5 µm, 250 x 8 mm was applied. The new cyclic depsipeptide, FR-1 (**1**)) was obtained as white powder (tR: 23.0 min, 0.7 mg from 200 g dried leaves). The isolation process was repeated until 2.8 mg of AC-1 were collected for structure elucidation.

Compound **2** had only slightly different retention times compared to **1** (for the complete isolation scheme refer to **Scheme 5-1**). The composition of the mobile phase was changed from isocratic 80% eluent D to 75 % eluent D applying a 75:25 Nucleoshell RP_{18+} column (250 x 8 mm, 5 µm) for 20 minutes followed by a linear gradient from 75–100% eluent D within 15

minutes. The new cyclic depsipeptide, **2**, was obtained as white powder (about 0.2 mg from 200 g dried leaves, t_R = 23.7 min). The isolation process was repeated until 1.6 mg of **2** were collected for structure elucidation.

Further, a shoulder of the FR peak eluting after FR was collected. This fraction included a peptide mix of FR-3 (**3**) and FR-4 (**4**) as judged from LC-MS data. HPLC conditions had to be adjusted to separate the new peptides from each other. The composition of the mobile phase was changed from isocratic 80% methanol to 75% methanol and a Nucleoshell RP18$^+$ column 5 µm, 250 x 8 mm was applied. The new cyclic depsipeptides, FR-3/FR-4 = 3:1 were obtained as white powder (tR: 30 min, 0.2 mg from 200 g dried leaves). The isolation process was repeated until 0.8 mg of FR-3/FR-4 was collected for structure elucidation. Compound **3/4** (FR-3/FR-4): <0.5mg/kg dried plant material (predominantly leaves).

3.5 Synthetic procedures

Reagents were purchased from commercial sources and were used without further purification. Oxygen- or water-sensitive reactions were performed under argon atmosphere. The synthesized compounds were analyzed by uHPLC-MS/MS on a micrOTOF-Q mass spectrometer (Bruker) with ESI-source coupled with an HPLC Dionex Ultimate 3000 (Thermo Scientific) using a Zorbax Eclipse Plus C_{18} 1.8 µm column, 2.1x50 mm (Agilent). The column temperature was 45 °C. MS data were acquired over a range from 100–3000 m/z in positive mode. Auto MS/MS fragmentation was achieved with increasing collision energy (35–50 keV over a gradient from 500–2000 *m/z*) with a frequency of 4 Hz for all ions over a threshold of 100. UPLC begins with 90% H_2O containing 0.1% acetic acid. The gradient starts after 0.5 min to 100% acetonitrile (0.1% acetic acid) in 4 min. 2 µL of sample solution was injected to a flow of 0.8 mL/min.

3.5.1 Synthesis of FR-Hex (11)

Compound **11**: (2S,3R)-1-((1R)-1-((6S,9S,12S,18R,21S,22R)-21-acetamido-18-benzyl-22-isopropyl-3-((R)-1-methoxyethyl)-4,9,10,12,16-pentamethyl-15-methylene-2,5,8,11,14,17,20-heptaoxo-1,19-dioxa-4,7,10,13,16-pentaazacyclodocosan-6-yl)-2-methylpropoxy)-4-methyl-1-oxo-2-propionamidopentan-3-yl hexanoate

FR (20 mg, 19.96 µmol) was dissolved in pyridine (1 mL) and stirred at room temperature under argon atmosphere. DMAP (12.2 mg, 99.8 µmol) and hexanoic anhydride (21.4 mg, 99.8 µmol) was added. After 2 h the reaction mixture was heated to 50 °C and stirred. After 16 h at

50 °C the reaction was stopped by diluting with 5 mL water and the reaction mixture was extracted with CH_2Cl_2 (3 mL x 3). The combined organic layers were washed with solutions of $NaHCO_3$ (pH 9), $KHSO_4$ (pH 2) and saturated NaCl and afterwards dried over Na_2SO_4 and concentrated in vacuo. Crude peptide was purified by HPLC, YMC Hydrosphere C18 column (250 x 4.6 mm, 3 µm). The elution system was 0.05% TFA in water (eluent E) and 0.05% TFA in acetonitrile (eluent F). A linear gradient was applied from 70% eluent F to 100% eluent F in 30 minutes. **11** eluted at t_R = 13.1 min and after solvent evaporation appeared as white-yellow powder (2.6 mg).

3.5.2 **Synthesis of FR-Cys (12)**

Compound **12**: (2S,3R)-(1R)-1-((6S,9S,12S,18R,21S,22R)-21-acetamido-15-(((2-aminoethyl)thio)methyl)-18-benzyl-22-isopropyl-3-((R)-1-methoxyethyl)-4,9,10,12,16-pentamethyl-2,5,8,11,14,17,20-heptaoxo-1,19-dioxa-4,7,10,13,16-pentaazacyclodocosan-6-yl)-2-methylpropyl 3-hydroxy-4-methyl-2-propionamidopentanoate

To a micellar solution of SDS (1 mL), at the critical micelle concentration (CMC) = 8.1 x 10^{-3} M), was added FR (20 mg, 19.96 µmol), 2-aminoethanethiol hydrochloride (26.7 mg, 199.6 µmol) at room temperature. The mixture was stirred vigorously (800 rpm) and monitored by TLC until the starting material had been consumed after 12 h. Then the mixture was extracted with butanol (3 mL x 3). The combined organic layer was dried over Na_2SO_4 and concentrated in vacuo. The crude peptide mixture was purified by HPLC, Nucleoshell RP^{18+}column (250 x 4.6 mm, 5 µm). The elution system was water (eluent C) and methanol (eluent D). **12** elutes at t_R = 27.2 minutes using isocratic conditions (57% eluent D for 35 minutes) and and appears as transparent film (6 mg) after solvent evaporation.

3.5.3 **Synthesis of FR-RR-BP (46)**

20 mg of FR were reacted with 10 eq cysteamine hydrochloride, using DL-α-Tocopherol methoxypolyethylene glycol succinate (TPGS-750-M, 2 wt %) in aqueous media to obtain 7.5 mg of compound **12** (25%). The reaction was performed under argon atmosphere to avoid cysteamine oxidation to the corresponding disulfide.

7.5 mg (1 eq) of compund **12** was dissolved in 500 µL DMSO, 10µL of 100 mM triethylamine was added to the reaction solution to ensure amine deprotonation. Next, the amine-reactive dye BODIPY630/650-X-NHS (5 mg, about 1.1 eq) was added to the reaction solution. The reaction mixture was stirred at room temperature for 4 hours, protected from light. Subsequently to

freeze-drying, the conjugate was purified via HPLC and the desired conjugated FR-RR-BP (**46**) was obtained in moderate yields (3 mg from 7.5 mg **12**, 40%).

3.5.4 **Synthesis of FR-Cys-Boc (47)**

In general we applied the protocol from the synthesis of compound **47** (see **Chapter 6.2**) with small changes. We reacted 35 mg of FR with 20 eq *N*-Boc-cysteamine under argon atmosphere in 1 mL hypergrade methanol containing 10 % milli-Q water; deprotonation of the thiol was achieved by addition of 20 eq TEA. The reaction was stirred vigorous for 2.5 h at 40 °C. Then we added 10 ml milli-Q water and extracted three times with 15 mL butanol each. Afterwards the raw product was purified by flash chromatography (Appendix **Figure 10-3**) and HPLC to yield 27 mg of compound **50** (FR-Cys-Boc) again as mixture of oxidized and unoxidized product (**Scheme 6-2**).

3.5.5 **Synthesis of FR-JK-Boc (48) and FR-JK-BP (49)**

LinkerJK was synthesized and provided by Jim Küppers (Gütschow lab, Institute for Pharmaceutical Chemistry I, Univ. of Bonn) and contained two ethylene glycole units with a terminal tert-butyloxycarbonyl (=Boc)-protected amine on the one side and a free terminal thiol group on the other side (**Scheme 6-2**). In general the synthesis protocol of compound **12** was applied with small changes. 40 mg of FR (about 40 µM) and 120 mg LinkerJK (370 µM) were dissolved in 1 mL hypergrade methanol containing 10 % milli-Q water under argon atmosphere; pH was adjusted to 9.1 with Na_2CO_3/$NaHCO_3$ buffer. The reaction was stirred vigorously overnight. Next morning, the reaction mixture was heated for 2 h to 45 °C. Afterwards 10 ml milli-Q water were added to stop the reaction and extracted three times with 15 mL butanol each. The organic phase was dried over Na_2SO_4 and concentrated *in vacuo*. Afterwards the crude product was purified by flash chromatography (Appendix **Figure 10-1**) to yield 15 mg of the desired FR-Linker conjugate (FR-JK-Boc, **48**). The acid-labile Boc group of compound **48** was then cleaved with a mixture of DCM/TFA = 5/1 and subsequently carefully evaporated under reduced pressure. To prevent concentration of TFA we added DCM several times, before evaporating to dryness. This procedure was repeated ten times and the outcome controlled by thin layer chromatography (TLC) sprayed with ninhydrin to detect the primary amine of compound **48**. After removal of final TFA residues we carried out the last step of the synthesis, adding BODIPY630/650-X-NHS ester in DMSO and trimethylamine as catalyst. The reaction

was stirred over night at room temperature and protected from light. After HPLC purification of the 10 mg raw product we finally yielded 1.4 mg of the desired product FR-JK-BP (**49**).

3.5.6 **Synthesis of FR-TAMRA (50)**

In general, we applied the synthesis protocol of compound **47** (see **Chapter 3.5.4**) with small changes. We reacted 25 mg of FR with 25 mg TAMRA-thiol (2 eq) under argon atmosphere in 1 mL hypergrade methanol containing 10 % milli-Q water; deprotonation of the thiol was achieved by addition of 2 eq TEA. The reaction was stirred vigorous for 2.5 h at 40 °C protected from light. Then we added 10 ml milli-Q water and extracted three times with 15 mL butanol each. Afterwards the raw product was purified by flash chromatography (Appendix **Figure 10-2**) and HPLC to yield 1.1 mg of compound **50** (FR-TAMRA).

3.5.7 **Synthesis of Fmoc-β-HyLeu-OH**

For the preparation of Fmoc-β-HyLeu-OH, a mixture of H-β-HyLeu-OH (1 equiv.) in DCM was stirred while bis(trimethylsilyl)acetamide (6 equiv.) was added dropwise over a duration of 15 min at room temperature until complete dissolution and allowed to stir for further 2 h. The solution was cooled to 0 °C and DIEA (1.25 equiv.) added at once. Under vigorous stirring Fmoc-Cl (1.25 equiv.) was added in portions for a duration of 30 min while stirring at 0 °C. This was continued for 1 h on ice and further 4 h at room temperature. The solvent was removed and the crude product (oil) was dissolved in ethyl acetate and washed with salt solutions of 5% $KHSO_4$, saturated NaCl (brine), saturated $NaHCO_3$, and again with brine. The ethyl acetate was dried with sodium sulphate (anhydrous) and then filtered. The solvent was removed and the product redissolved in 80% t-BuOH. Subsequent freeze-drying gave Fmoc-β-HyLeu-OH (48%) as a white powder. Purity was confirmed by analytical HPLC using a Vydac 218TP54 column (C18, 5 µm particle size, 300 Å pore size, 4.6 mm × 25 mm) and a gradient of 20% to 80% acetonitrile in water with 0.1% TFA in one hour (t_R = 29.86 min). Further Characterization of the product was performed by mass spectrometry, NMR spectroscopy and thin layer chromatography (TLC).

MS (ESI): mass calculated for $C_{21}H_{23}NO_5$, 369.2; *m/z* found, 370.2 $[M+H]^+$. ^{1}H NMR (600 MHz, $CDCl_3$) δ ppm 0.92 (d, J = 6.6 Hz, 3H), 1.02 (d, J = 6.6 Hz, 3H), 1.80–1.71 (m, 1H), 3.82 (dd, J = 9.2, 1.1 Hz, 1H), 4.19 (t, J = 7.2 Hz, 1H), 4.36 (dd, J = 7.2, 4.7 Hz, 2H), 4.58 (dd, J = 9.4, 1.2 Hz, 1H), 4.84 (br s, 1H), 5.94 (d, J = 9.4 Hz, 1H), 7.27 (dd, J = 7.4, 7.4 Hz, 2H), 7.40–7.33 (m, 2H), 7.57 (dd, J = 11.7, 7.5 Hz, 2H), 7.73 (dd, J = 7.5, 2.3 Hz, 2H). ^{13}C NMR (151 MHz, $CDCl_3$, T = 298 K) δ ppm 19.0, 19.3, 30.9, 47.2, 56.3, 67.5, 77.5, 120.1 (2C), 125.3,

125.3, 127.2 (2C), 127.8 (2C), 141.4 (2C), 143.7, 144.0, 157.2, 175.7. TLC was performed using glass plates impregnated with silica gel 60 F254, 10 x 20 cm. The applied solvent system was chloroform/methanol (9:1). Detection was done by UV at a wavelength of 254 nm. The observed R_f value was 0.83.

3.5.8 **Peptide synthesis and purification**

Peptides **13-22** were synthesized by Dr. Toni Kühl Britta Nubbemeyer, Justin Patrick Odhiambo, Pascal Heimer and Charlotte Anneke Bäuml, Institute for Pharmaceutical Chemistry, Univ. of Bonn). The linear precursor peptides of **15**, **16**, **19**, and **20** were synthesized on an automated peptide synthesizer EPS 221 (Intavis Bioanalytical Instruments AG, Cologne, Germany) according to a standard Fmoc-protocol. Peptides **13**, **14**, **17**, **18**, **21**, and **22** were synthesized manually. The polymer support was 2-chlorotrityl chloride resin with a loading capacity of 2.1 mmol/g (Advanced ChemTech 5609 Fern Valley Road, Louisville KY, USA) for manual peptide synthesis or alanine-loaded 2-chlorotrityl chloride resin with a loading capacity of 0.67 mmol/g (Iris Biotech GmbH, Marktredwitz, Germany) for automated peptide synthesis. Amino acid derivatives used were as follows: Fmoc-*N*-Me-Thr(tBu)-OH; Ac-Thr-OH; Fmoc-*N*-Me-Ala-OH; Fmoc-Lys(Ac)-OH and Fmoc-Thr(Ac)-OH, Fmoc-*N*-Me-D-Phe-OH, Fmoc-6-Ahx-OH, Boc-Dap(Fmoc)-OH and Fmoc-Leu-OH, Fmoc-β-HyLeu-OH.

For manual peptide synthesis, coupling reactions were performed as double couplings using Fmoc-amino acids (4 equiv.) activated with TFFH (4 equiv.) for 12 min, in the presence of DMF and DIPEA (8 equiv.). Fmoc removal was carried out by treating the resin twice with 20% of piperidine in DMF for 5 and 15 min, respectively. All deprotection and coupling steps were followed by intensive washings using DMF and DCM alternately. Peptide cleavage and deprotection was accomplished with 5% TIPS in 95% TFA/H_2O for peptides **13**–**22** for 3 h at room temperature. The crude peptides were precipitated in cold diethyl ether, centrifuged and washed with diethyl ether several times. Linear peptides were of sufficient purity and subsequently used without prior purification for the following steps. The peptide cyclization was performed using PyBOP (6 equiv.) and DIEA (12 equiv.) in DMF (final concentration of peptides: 320 µM) for 6 h at room temperature.

The crude peptides were evaporated and then purified by semi-preparative reversed-phase HPLC using a Shimadzu LC-8A system (Duisburg, Germany) equipped with a C18 column (250 × 32 mm, Knauer Eurospher 100, Berlin, Germany). The gradient elution system was 0.1% TFA in water (eluent A) and 0.1% TFA in acetonitrile/water (9:1) (eluent B). The peptides were eluted with varying gradients of eluent B in eluent A in 120 min as depicted in Table S2 and a

flow rate of 10 mL/min. The peaks were detected at 220 nm. Collected fractions were combined, freeze-dried and stored at −20 ºC. Purity of the peptides was confirmed by analytical reversed-phase HPLC on a Shimadzu LC-10AT chromatograph (Duisburg, Germany) equipped with a Vydac 218TP54 column (C18, 5 µm particle size, 300 Å pore size, 4.6 mm × 25 mm). The peptides were eluted with varying gradients as noted in Table S2. The flow rate was 1 mL/min with eluent A: 0.1% TFA in water and eluent B: 0.1% TFA in acetonitrile; detection was at 220 nm. All peptides used for biological assays were of >95% HPLC purity.

3.5.9 **Chemical characterization of FR-analogs 1-22**

Peptides were characterized by analytical HPLC (see above), amino acid analysis, and mass spectrometry. For amino acid analysis, samples (0.5–1 mg) were hydrolyzed in 6 N HCl at 110 °C for 24 h, dried and used for analysis in sample dilution buffer (Onken Laboratories, Hamburg, Germany) on an Eppendorf Biotronik Amino Acid Analyzer LC3000. The molecular weight of crude and purified peptides **13**–**22** was confirmed by mass spectrometry on an ESI micrOTOFQ III system (Bruker Daltonics GmbH, Bremen, Germany).

TLC characterization was performed using glass plates impregnated with silica gel 60 F254, 10 x 20 cm. Two solvent systems were applied, which were; system A: *n*-butanol/acetic acid/water (48:18:24) and system B: *n*-propanol/ 25% NH_3 (7:3). Detection methods used were UV at a wavelength of 254 nm and KI-containing acetic *o*-tolidin solution.

The chemical characterization of FR analogs **1-12** is explained in detail in chapters **5.1** and **5.2**.

3.6 Structure elucidation

3.6.1 **Mass spectrometry**

Mass spectrometry was performed on the following systems:

3.6.1.1 LC-ESI-MS using an HPLC coupled to a quadrupole analyzer (system A)

Samples were adjusted with hypergrade methanol for LC/MS to a concentration of 1 mg/mL. 500 µL of the extract samples were given to LC/MS analysis or 100 µL of pure compound samples. Ms. E. Egereva (Institute for Pharmaceutical Biology, University of Bonn, Germany) performed the measurements using an Agilent 1100 system including a diode array detector (DAD) and an API 2000 Triple Quadrupole LC/MS/MS with ESI source (Applied Biosystems/MDS Sciex, Analyst software). An RP-18 column (Machery-Nagel Nucleodur 100, 125 x 2 mm, 5 µm) served as stationary phase. Gradient elution was used with following

parameters: It started at MeOH/H_2O (10/90) and was ramped up to 100% MeOH in 20 min, followed by isocratic elution with 100% MeOH, NH4OAc was added as a buffer (c = 2 mM); flow rate: 0.25mL/min. Experiments were recorded only in positive ode using a declustering of either 30 V (experiment 1) or 70 V (experiment 2).

3.6.1.2 High resolution LC-ESI-MS using a UPLC System coupled to Qq-TOF (system B1)

Spectra were recorded by Dr. Max Crüsemann (Institute for Pharmaceutical Biology, University of Bonn, Germany). A micrOTOF-Q mass spectrometer (Bruker) with ESI-source coupled to a HPLC Dionex Ultimate 3000 (Thermo Scientific) and a EC10/2 Nucleoshell C_{18}, 2.7 µm column (Machery-Nagel) was used. The column temperature was set to 25°C.

MS data were acquired over a range from 100-3000 *m/z* in positive mode. Auto MS/MS fragmentation was achieved with rising collision energy (35-50 keV over a gradient from 500-2000 *m/z*) with a frequency of 4 Hz for all ions over a threshold of 100.

HPLC started with 90 % H_2O containing 0.1 % acetic acid. The gradient starts after 1 min ending up with 100 % CAN (0.1 % acetic acid) in 20 min. The flow was set to 0.3 mL/min. 5 µL per sample solution (0.5 mg/mL) was injected for each run.

3.6.1.3 UPLC/MS of extracts and pure compounds (system B2)

Fractions from *A. crenata* were analyzed by UPLC-MS/MS on a micrOTOF-Q mass spectrometer (Bruker) with ESI-source coupled with a HPLC Dionex Ultimate 3000 (Thermo Scientific) using a Zorbax Eclipse Plus C18 1.8 µm column, 2.1x50 mm (Agilent). The column temperature was 45 °C. MS data were acquired over a range from 100-3000 m/z in positive mode. Auto MS/MS fragmentation was achieved with rising collision energy (35-50 keV over a gradient from 500-2000 m/z) with a frequency of 4 Hz for all ions over a threshold of 100. uHPLC begins with 90 % H_2O containing 0.1% acetic acid. The gradient starts after 0.5 min to 100% acetonitrile (0.1% acetic acid) in 4 min. 2 uL of sample solution was injected to a flow of 0.8 mL/min.

3.6.1.4 Tandem mass spectrometry (MS-MS^n), system C

Spectra were recorded by Dr. Marc Sylvester (Institute for Biochemistry and Molecular Biology, Univ. of Bonn). The dried samples were dissolved in 50 µL ACN/H_2O (70/30) per vial. 2 µL of this solution was then diluted in an Eppendorf vial using 18 µL of 0.1& formic acid. The resulting solution was centrifuged for several minutes at 12,000 g to separate precipitates.

2 µL (=0.4% of the original sample) were injected onto a C_{18} trap column (20 mm length, 100 µm inner diameter) coupled to a C_{18} analytical column (200 mm length, 75 µm inner diameter), made in house with 1.9 µm ReproSIl-Pur 120 C_{18}-AQ particles (Dr. Maisch, Ammerbuch, Germany). Solvent A was 0.1% formic acid. Analytes were separated during a linear gradient from 1% to 35% solvent B (90% ACN, 0.1% formic acid) within 40 min and 35% to 50% within 7 min at a flow rate of 320 nL/min.

The nanoHPLC was coupled online to an LTQ Orbitrap Velos mass spectrometer using a nanoESI ion source (Thermo Fisher Scientific, Bremen, Germany). Precursor ions between 800 and 1200 *m/z* were scanned in the Orbitrap detector with a resolution of 30,000 (maximum fill time 400 ms, AGC target 10^6, lock mass 1002.53939 Da (for FR)). The 10 most intense precursor ions (threshold intensity 5000) were subjected to collision induced dissociation and fragments also analyzed in the linear ion trap. Fragmented ions were excluded from repeat analysis for 15 s.

The term MS/MS^n (also known as tandem mass spectroscopy) refers to instruments in which two independent stages of m/z analysis are used. This type of analysis helps to establish the relationships between ions in a mass spectrum, for example what ions are formed when the $M^{+\cdot}$ or other ions in the spectrum undergo fragmentation. This, in turn, helps to elucidate fragmentation pathways for the molecule being studied and finally leads to structure determination.[100]

Peptide fragment ions are labeled according to a nomenclature system developed by Ngoka *et al.*[101] based on Biemanns modifications[102] of Roepstorffs nomenclature[103]. **Scheme 3-1** serves as an example for the initial step of FR fragmentation and illustrates the nomenclature. The system makes use of the general formula x_{nJZ} where "x" is the designation for the general type of ion series. Thus, after peptides fragment in MS/MS^n experiments, they form acylium ions, *i.e.* "b" series, ammonium ions, *i.e.* "y" series, and if carbon monoxide (CO) is cleaved from "b" ions, "a" ions are produced. These types of ions ("a", "b", "y") are usually given, including the number (n) of amino acids as a suffix, *i.e.* "b_7" means that an acylium ion is composed of seven amino acids. In cyclic peptides breakage of the amide (or ester bond) lead to the formation of a linear peptide with a C-terminal oxazolone ring. "J" and "Z" are the one-letter codes for the two amino acid residues, which were connected via the former backbone amide or ester bond, *i.e.* "J" is the N-terminal amino acid residue and "Z" the novel C-terminal oxazolone of the linearized peptide. If non-proteinogenic amino acids occur in the peptide, nomenclature is

modified, for example *N*-acetyl-hydroxyleucine is designed as L' instead of L. When a fragment ion is sodiated, sodium is omitted from the label for simplicity, and the fragment is designated by a superscript asterisk, for example $b^*_{nJZ} = [b_{nJZ} - H + Na]^+$. Although peptide backbone cleavage is the most useful for sequencing and peptide identification, other fragment ions may be observed under high-energy dissociation conditions. These include the side chain loss ions d, v, w and immonium ions.[104]

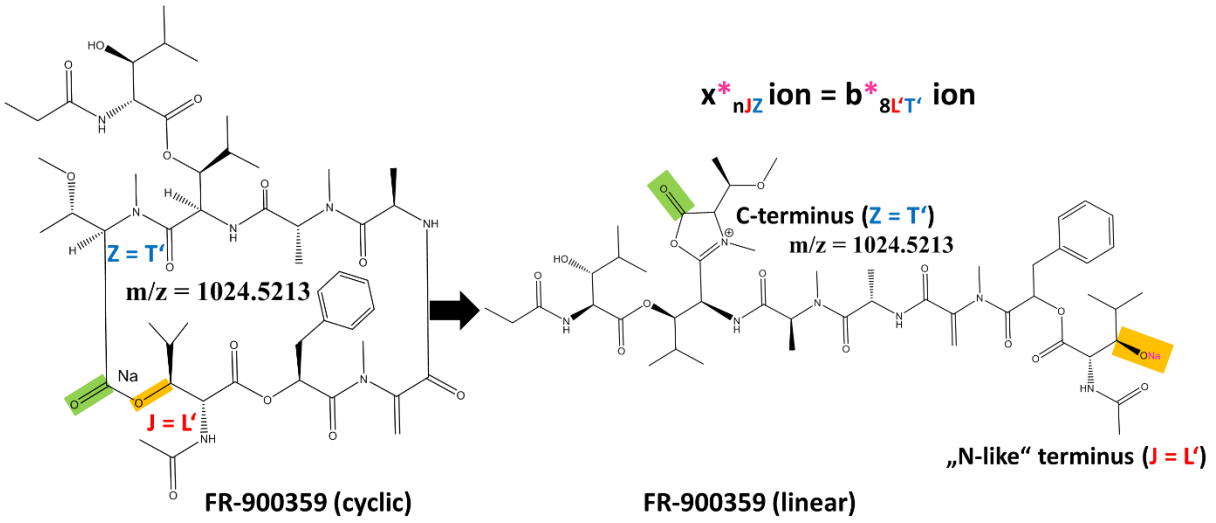

Scheme 3-1: Initial cleavage of the cyclic backbone of FR, producing the linear acylium ion $b^*_{8L'T'}$. $_x$ = type of ion = acylium ion (oxazolone) = b, n = number of amino acid residues of which the ion consists of = 8, J = "N-like" terminus = "N-like", because in depsipeptides the amino terminus does not exists but a terminal hydroxyl group = L' (*N*-acetyl-hydroxyleucine), Z = C-terminus = in cyclic peptides often as oxazolone ring, for reasons of charge delocalization = T' (*N*,*O*-dimethyl-threonine).

A schematic diagram of MS/MS instrumentation and workflow is illustrated in **Scheme 3-2**. The MS/MS spectra in the current study were recorded on Thermo Dionex UltiMate 3000 with splitted nanoflow via UltiMate 3000 RSLCnano connected to Thermo LTQ Orbitrap Velos (mass analyzer). Dr. M. Sylvester, scientific officer, Institute of Biochemistry and Molecular Biology (IBMB), Bonn, Germany, performed all experiments.

After sample injection into the Advion TriVersa NanoMate the analyte is ionized by chip-based nano-ESI[105] and the ions are conveyed to the first analyzer, a linear ion trap (MS^1 spectrum). There, ions of certain *m/z*-values are selected and directed to the collision chamber. The molecular ions are allowed to collide with neutral molecules, *i.e.* helium gas. The technique is called Collision-induced dissociation (CID), also known as collisionally activated dissociation (CAD).[106] In the collision cell, some of the kinetic energy is converted into internal energy, which results in bond breakage and fragmentation of the molecular ion into smaller fragments.

Afterwards the fragment-ions are collected and collisionally cooled in a C-Trap, situated in an electromagnetic field. Cooled ions are injected with high energy and precise trajectory into the orbitrap mass analyzer. They oscillate axially across the trap at frequency proportional to $(z/m)^{1/2}$. The movement of every ion species (*m/z*) induces a detectable alternating current, so-called "image current". Its frequency is dependent on the *m/z*-ratio and decreases exponentially after shutdown of the excitation current. The FID (free induction decay) is detected by electrodes and transformed to the mass spectrum by Fourier Transform (MS^2). This is how specific ions with certain *m/z*-values can be isolated.[107] The received spectra can be processed with the Thermo Scientific software Xcalibur™ resulting in partial or complete structural determination of the analyte.

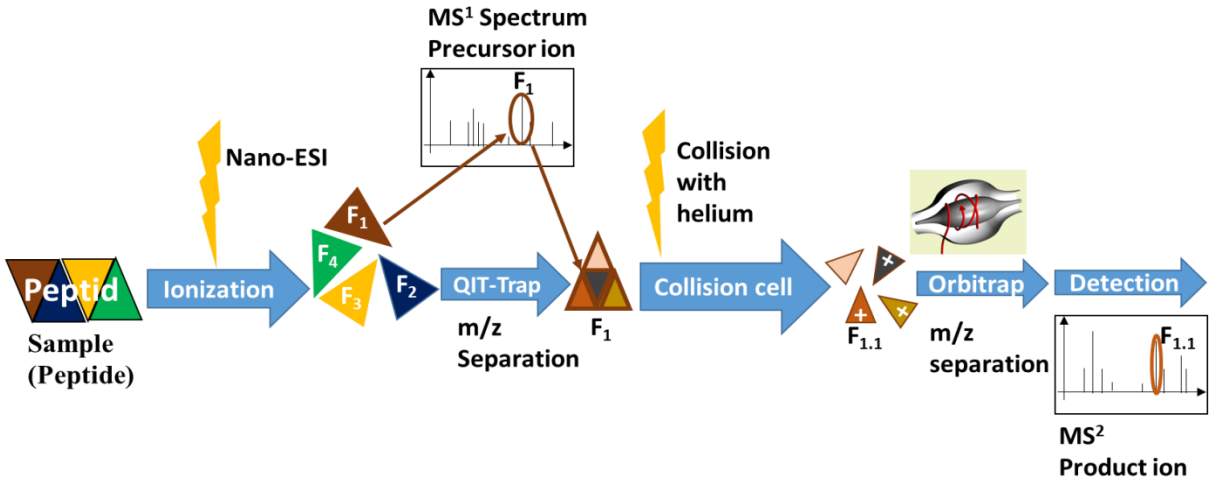

Scheme 3-2: Schematic of tandem mass spectrometry. QIT = quadrupole ion storage trap. For explanation see text.

Beside its higher speed, the major advantage for tandem mass spectrometry is that it enables the structural characterization of cyclic peptides produced in such low quantities that normally prohibit the use of other structural methods such as NMR.[108,109]

3.6.1.5 MALDI-TOF

Spectra were recorded by Dr. Marc Sylvester and Mr. Bernd Gehrig (Institute for Biochemistry and Molecular Biology, Univ. of Bonn). The matrix-assisted laser desorption ionization (MALDI) combined with a time-of-flight (TOF) mass analyzer is routinely used for the mass assignment of peptides and proteins up to a molecular weight of about 10^5 Da.[110] The sample is mixed with matrix material in a ratio of 1 to 10000. The matrix has the following functions: First of all, it dilutes the sample, preventing interaction of sample molecules with each other, secondly it absorbs the laser energy and desorption energy to the sample, and it lastly protects

the sample from photolytic disintegration. Also, it supplies the required protons for the ionization. For rather hydrophobic peptides like FR, α-cyano-4-hydroxycinnamic acid is the matrix of choice. After sample preparation it is irradiated with a laser pulse (nitrogen laser, 337nm), which lies within the absorption maxima of the matrix. Because of that, it absorbs the energy, transfers or takes over protons of the sample and provides the energy needed for desorption. Mainly $[M+H]^+$ -and $[M + \text{alkaline metal}]^+$ ions are formed. For recording a measurement, 100µg of FR or analog was used and several pulses (about 100) were directed towards the sample to improve the signal-to-noise ratio.

3.6.1.6 MALDI imaging of *A. crenata* leaves

Spectra were recorded under supervision of Dr. Alexander Brachmann (Institute of Microbiology, ETH Zurich). A young leaf of *A. crenata* was immersed in dichloromethane for 1 min to thin out wax layers of the thick cuticle.[111] The leaf was fixed on a conductive carbon tape mounted on a stainless steel slide making the leaf underside accessible for MALDI matrix. A MALDI matrix spotter (SunChrom SunCollect) was used to coat the leaf uniformly with 7-8 layers of MALDI matrix (1:1 mixture of α-cyano-4-hydroxycinnamic acid and 2,5-dihydroxybenzoic acid (Sigma-Aldrich); 30 mg/mL in methanol and 0.1% TFA). MALDI imaging was performed on a LTQ Orbitrap XL (Thermo Scientific™) equipped with a nitrogen laser (wavelength 337 nm). MALDI FTMS spectra were acquired in positive mode for a mass range between 800 and 1200 m/z, a laser energy of 55 µJ, two microscans per step, a resolution of R = 60,000 and mass tolerance of 0.01 amu. The leaf was measured at 100 µm pixel size, yielding 31,050 pixels in total. Spectra were extracted for the potassium adduct ion of FR $[M+K]^+$ = 1040.49 m/z using Image Quest software (Thermo Scientific™). The resulting 2D image was displayed in rainbow color scheme and linear scaling type from 7.00E4 to 7.00E6 showing the abundancies of FR ions in different colors.

3.6.2 **Nuclear magnetic resonance spectroscopy**

NMR spectra of crude extracts and pure compounds were recorded on a Bruker Avance 300 DPX operating at 300 MHz (^{1}H) and 75 MHz (^{13}C) at room temperature. Compounds, which were isolated in low amounts and two dimensional measurements, were guided on a Bruker Ascend 600 spectrometer operating at 600 MHz (^{1}H) and 150 MHz (^{13}C) in the Institute for Pharmaceutical Chemistry, University of Bonn, Germany by Dr. S. Kehraus (Institute for Pharmaceutical Biology, University of Bonn, Germany). NMR spectra were processed using Bruker XWIN-NMR Version 3.5 software and MestReNova 8.0.1. Spectra were referenced to

residual solvent signals with resonances at $\delta_{H/C}$ 7.26/77.0 in the case of $CDCl_3$. The multiplicity of the carbons was deduced by DEPT experiments. Structural assignments were based on spectra resulting from one or more of the following NMR experiments: ^{1}H, ^{13}C, DEPT-135, ^{1}H-^{1}H COSY, ^{1}H-^{13}C direct correlation (HSQC), ^{1}H-^{13}C long-range correlation (HMBC), ^{1}H-^{1}H ROESY. Chemical shifts of the signals of a compound were compared to calculated values using Advanced Chemistry Development (ACD/Labs) Software V11.02 (® 2012 ACD/Labs).

For structure-activity relationship studies described in **Chapter 5.2** NMR spectra of FR, **1**, **13**, and **22** were recorded in 90% H_2O/10% D_2O, using the freeze-dried solid compound at 298 K on a Bruker Avance III or Avance HD spectrometers at proton frequencies of 600 or 500 MHz. In all NMR spectra, the ^{1}H peak from water was used as a chemical shift reference by setting its frequency at 4.7 ppm. All NMR data were processed and analyzed using TopSpin 3.1 (Bruker) and CcpNMR Analysis.[112] The proton resonance assignment was performed by a combination of 2D [^{1}H,^{1}H]-DQF-COSY, [^{1}H,^{1}H]-TOCSY, [^{1}H,^{1}H]-NOESY and/or [^{1}H,^{1}H]-ROESY and [^{1}H,^{13}C]-HSQC. Distance constraints were extracted from [^{1}H,^{1}H]-NOESY (**22** and FR) or [^{1}H,^{1}H]-EASY ROESY (**13**) spectra acquired with a mixing time of 120 ms and a recycle delay time of 1.5 s. Upper limit distance constraints were calibrated according to their intensity in the NOESY spectrum and the intensity of geminal protons was used for peak intensity calibration. Torsion angle constraints for FR, **13** and **22** were obtained from ^{1}H and ^{13}C chemical shift analysis using DANGLE and $^{3}J_{NHHa}$-coupling constants.[113] Structure calculations and refinements were performed with YASARA structure.[114–116] The 10 structures with the lowest energy were selected to represent the NMR solution structures. Additionally, a set of NMR spectra of FR and **1** in $CDCl_3$[10] and MeOH/H_2O/D_2O (v:v:v/ 1:1:0.2) was obtained.

3.6.3 **Specific rotation**

Optical rotation measurements were conducted on a Jasco model DIP140 polarimeter (1 dm, 1 cm3 cell) operating at the wavelength λ=589 nm corresponding to the sodium D line at room temperature. The specific optical rotation $[\alpha]_D^T$ was calculated pursuant to:

$$[\alpha]_D^T = \frac{100 \times \alpha}{c \times l}$$

T = temperature [ºC]

D = sodium D line at λ=589 nm

c = concentration [g/100 mL]

l = cell length [dm]

The compounds were dissolved in an appropriate organic solvent (*e.g.*, MeOH). The rotation angles α were determined as an average value based on at least 10 measurements.

3.6.4 **Bioinformatic procedures**

3.6.4.1 Molecular networking

The MeOH extract from *A. crenata l*eaves and fractions thereof were analyzed with UPLC-MS/MS. Data files were exported to .mzxml format, and then uploaded to CCMS (ccms.ucsd.edu). A molecular network was created using the online workflow at GNPS (gnps.ucsd.edu). The data was filtered by removing all MS/MS peaks within +/- 17 Da of the precursor *m/z*. MS/MS spectra were window filtered by choosing only the top 6 peaks in the +/- 50 Da window throughout the spectrum. The data was then clustered with MS-Cluster with a parent mass tolerance of 0.02 Da and a MS/MS fragment ion tolerance of 0.02 Da to create consensus spectra. Further, consensus spectra that contained less than 2 spectra were discarded. A network was then created where edges were filtered to have a cosine score above 0.7 and more than 6 matched peaks. Further edges between two nodes were kept in the network if and only if each of the nodes appeared in each other's respective top 10 most similar nodes. The spectra in the network were then searched against GNPS' spectral libraries. The library spectra were filtered in the same manner as the input data. All matches kept between network spectra and library spectra were required to have a score above 0.7 and at least 6 matched peaks. Results were visualized in Cytoscape 3.4.0 (www.cytoscape.org).

3.6.4.2 Structures calculations of YM-254890, FR900359 and their analogs

Molecular structures of the YM and FR derivatives were constructed with the Yasara molecular modeling program[114,115] employing the crystal structure of Gq-bound YM.[53] The resulting molecules were geometry optimized with the Yasara YAPAC module using semi-empirical quantum chemical methods followed by an energy minimization step in explicit water, using the PME method[117] and a cut-off distance of 8 Å to describe long-range electrostatics and the Yasara2[118] force field (0.9% NaCl, 298 K, pH 7.4[119]). Additionally, selected structures were equilibrated through a 100 ns molecular dynamics simulation to probe for their conformational

integrity. The final structure was derived from the simulation period suggesting a stable conformation as indicated by the Cα RMSD, again followed by an energy minimization. Structure calculation experiments were performed by Dr. Daniel Tietze, TU Darmstadt.

3.6.4.3 Molecular Docking Studies

The Gαq target structure was derived from PDB ID 3AH8.[53] Docking was performed using VINA[120] (default parameters). The setup was done with the YASARA molecular modeling program,[114,115] and the best scoring result of 32 independent docking runs was subjected to further analysis. To guide the docking runs the docking cell was placed around the YM binding epitope revealed by Nishimura *et al.*[53]Ligands and receptor residues were kept flexible during the docking runs. Molecular Docking studies were performed by Dr. Daniel Tietze, TU Darmstadt.

3.6.4.4 Molecular dynamics simulations

Energy minimization was carried out for best scoring structures from the docking runs before subsequent analysis of Gαq-inhibitor interactions. The energy minimization was achieved by a steepest-descent minimization followed by a simulated annealing minimization until convergence (<0.05 kJ/mol/200/steps). Charged amino acids were assigned according to the predicted pK_a of the amino acid side chains by Ewald summation[119] and were neutralized by adding counter ions (NaCl). Force field parameters for the ligands were assigned by Yasara's AutoSMILES approach.[121,122]

To gain performance, a multiple time step algorithm together with a simulation time step interval of 2.5 fs was chosen.[115,123] Unless otherwise stated TIP3P water model and the Amber14 force field was used for energy minimization and molecular dynamics simulations[124,125] employing the PME method[117] to describe long-range electrostatics at a cut-off distance of 8 Å at physiological conditions (0.9% NaCl, 298 K, pH 7.4[119]).

Molecular graphics were created with YASARA (www.yasara.org) and POVRay (www.povray.org). Molecular dynamics simulations were performed by Dr. Daniel Tietze, TU Darmstadt.

3.6.4.5 Steered molecular dynamics simulations

Steered molecular dynamics simulations with constant acceleration were performed taking a snapshot from the initial period of the MD run after the structure of the docked protein-inhibitor complex was equilibrated and the inhibitor position was stable for some time. Steering was achieved by constant acceleration of the center of mass of the α-domain of Gq and the inhibitor.

The steering path was set along the direction vector connecting the center of mass of the receptor (Gαq) and the center of mass of the FR core structure excluding BODIPY and complete ligand unbinding was assumed, when a distance > 30 Å was reached. Accelerations were as follow: 750, 1250, 1750, 2250, and 2750 pm/ps^2. Integration time steps for intra-molecular and inter-molecular forces were 1.25 fs and 2.5 fs. All other simulation parameters were identical to the regular MD simulations. Experiments were performed by Dr. Daniel Tietze, TU Darmstadt.

3.6.5 **Life Cell imaging**

Life cell images of compound **46** (FR-RR-BP) on HEK293 cell (wt or Gq/Ko, respectively) were taken at a Axiovert 200 M with Reflektor 50 Cy-5 and a Plan-Apochromat 63x/1.40 oil Ph 3 objective of a AxioCamMR3 (all Zeiss). Living cells were moistened at 37 °C and measured in 300 µL Locke. Experiments were performed by Dr. Thomas Sorkalla, Dr. Sebastian Franken, Stefan Aatz, Häberlein lab (Institute for Biochemistry and Molecular Biology, Univ. of Bonn).

3.7 **Biological methods:**

3.7.1 **Resazurin-based Cell viability assay with HEK293-cells**

This assay was carried out by Dr. Nicole Merten (Kostenis lab, Institute for Pharmaceutical Biology, Univ. of Bonn). Data was generally obtained from three independent experiments, performed in triplicates. Cell viability was assessed using a fluorimetric detection of resorufin (CellTiter-Blue Cell viability Assay, Promega). HEK293 cells were seeded at a density of 25,000 cells per well into black 96-well poly-D-lysine-coated plates with clear bottom. 4 h after seeding cells were treated with 0.3 % dimethylsulfoxide (DMSO) or 20 µL of compound or the respective solvent and incubated for 24 hours at 37 °C and 5% CO_2. The next day, 20 µL of CellTiter-Blue reagent was added to each well and cells were incubated for 1 h according to the manufacturer's instructions. To detect cell viability, fluorescence (excitation 560 nm, emission 590 nm) was measured using a FlexStation 3 Benchtop Multimode Plate Reader and data were expressed as percentage of cell viability relative to DMSO control (The cytotoxic anticancer drug etoposide was used as a positive control).

3.7.2 Agar Diffusion and Sporulation Assay in Working Group König

Antimicrobial tests of extracts and isolated pure compounds were performed by Emilie Goralski and Ekaterina Egereva (Institute for Pharmaceutical Biology, University of Bonn) following the method described by Schulz *et al*.[126] The bacteria *Bacillus megaterium* de Bary (Gram positive) and *Escherichia coli* (Migula) Castellani & Chambers (gram negative), the fungi Microbotryum violaceum (Pers.) Roussel (Ustomycetes), Eurotium rubrum (formerly E. repens) König, Spieckermann & Bremer (Ascomycetes) (all from DSMZ; Braunschweig, Germany), and Mycotypha microspora Fenner (Zygomycetes kindly provided by B. Schulz, Institute of Microbiology, University of Braunschweig, Germany) were used as test organisms. Sample solutions contained 1 mg/mL per test sample. 50 µL (equivalent to 50 µg) of each solution were pipetted onto a sterile antibiotic filter disk (Schleicher & Schuell 2668®), which was then placed onto the appropriate agar medium and sprayed with a suspension of the test organism. Growth media, preparation of spraying suspensions, and conditions of incubation were carried out according to Schulz *et al*.[126] Growth inhibition was defined as follows: growth of the appropriate test organism was significantly inhibited compared to a negative control; total inhibition: no growth at all in the appropriate zone. Benzyl penicillin (1 mg/mL MeOH), streptomycin (1 mg/mL MeOH) and miconazole (1 mg/2 mL DCM) were used as positive controls.

In a similar manner sporulation experiments were performed with *Cryphonectria parasitica* and *Microbotrium violaceum*, but agar plates with these fungi were not treated with antibiotics or fungicides, but with FR (0.5 mg/mL MeOH). Sporulation were investigated under the microscope.

3.7.3 Agar Diffusion Assay in Working Group Sahl

Antimicrobial tests of extracts and isolated pure compounds were performed by Michaele Josten (Institute for Medical Microbiology, University of Bonn). Culture plates (5% sheep blood Columbia agar, BD) were overlaid with 3 ml Tryptic soy soft agar, inoculated with TSB (Tryptic soy broth, Oxoid) growth suspension of the bacteria to be tested. Compounds were diluted to a concentration of 1mg/ml (Syringomycin 0,5mg/ml) with DMSO and 3 µl of this dilution were placed on the surface of the agar. Compounds diffuse into the agar and the size of the inhibition zone was measured after 24 hours incubation at 37 °C.

3.7.4 **IP1 accumulation assay**

3.7.4.1 Cell lines and culture conditions

CHO and HEK293 cells stably transfected with the muscarinic M1 receptor[127] were obtained from the American Type Culture Collection (ATCC). CHO cells were cultivated in Ham´s F12 Nutrient Mix (Ham´s F12) supplemented with GlutaMax, 10% fetal bovine serum (PAN biotech, Germany), 100 U mL^{-1} Penicillin, 100 mg mL^{-1} Streptomycin (Invitrogen). For CHO-M1 cells, 0.2 mg mL^{-1} G418 was added to the medium. Cells were maintained in humidified atmosphere at 37 °C and 5% CO_2. HEK293 cells were cultured in Dulbecco´s Modified Eagle´s Medium (DMEM, Invitrogen). All cell lines were tested negative by PCR for mycoplasma contamination.

3.7.4.2 HTRF-based IP_1 and cAMP assays

All homogenous time-resolved fluorescence (HTRF)-based assays were carried out according to manufacturer's instructions (Cisbio GmbH, Berlin). In brief, for the IP_1/cAMP assay, 50,000cells/well were suspended in the respective assay buffers containing 10 mM LiCl (for IP_1) or 1 mm 3-isobutyl-1-methylxanthine (IBMX, for cAMP), respectively, and incubated in a 384-well, white microtiter plate for 15 minutes. To determine inhibitory effects of compounds cells were pre-incubated with ligands or solvent for 2 hours prior to stimulation with the stated agonists for further 30–35 minutes (100 µM carbachol for IP_1, Gq; 1 µM Iperoxo for cAMP, Gi; 100 µM Iper-6-phth for cAMP, Gs). Reactions were terminated by addition of lysis buffer containing the HTRF® reagents. All incubation steps were carried out at 37 °C and 5% CO_2. After incubation for at least 1 hour at room temperature HTRF ratios were measured using the Mithras LB 940 multimode reader (Berthold technologies) at 665 nm and 620 nm.

All of the bioassays were performed by Nina Heycke, Suvi Annala, Tobias Benkel or Dr. Davide Malfacini (Institute for Pharmaceutical Biology, University of Bonn). The measurement of intracellular IP1 was executed as described below. Inhibition of Gq-signaling was determined in CHO cells stably expressing the m_1-receptor subtype using a competitive immuno-assay for IP1 quantification. Data was generally obtained from three independent experiments, performed in triplicates.

3.7.4.3 Data evaluation of second messenger HTRF assay

Results were calculated from the ratio of absorbance at 665 nm/620 nm. Obtained ratio values were corrected by a negative control, consisting of buffer and europium cryptate. Calculations were performed according to following formula:

Delta F = [$Ratio_{sample}$ - $Ratio_{neg}$/ $Ratio_{neg}$] x 100

Because of the inverse relationship between signal and IP1 concentration, accumulation of IP1 resulted in a decreased signal. Data were analyzed using GraphPad Prism 5.04 (Graph Pad). Levels of IP1 were normalized to the maximum amount of IP1 generated by ligand-induced GPCR activation. In some analyses, data were presented as arbitrary units, meaning amount of IP1 related to the examined basal levels ((buffer HTRF ratio subtracted by agonist-induced HTRF ratio) +buffer HTRF ratio).

3.7.4.4 Wash-out experiments using IP-one HTRF® assay by Cisbio

To determine the affinity for the $G_{\alpha q}$-protein, we investigated wash-out Assays using an IP-one HTRF® assay by Cisbio: Cells have been resuspended using an alloy of 1x Stimm-buffer and the respective substance (FR [1µM] and AC1 [30 µM]) and incubated for 2h at 37°C, followed by a repetitive (6x) wash-out using PBS, either 1x Stimm-buffer or Carbachol [100µM] (Agonist at M1) have been added and incubated for 35min. Subsequently, we added an IP1 analog coupled to a d2 fluorophore (acceptor) and an anti-IP1 monoclonal antibody labeled with Eu Cryptate (donor). Being a competitive immunoassay the read-out, using Mithras LB 940 by Berthold Technologies, is inversely proportional to the resulting signal. The buffer solution contains LiCl to avoid IP1 degradation. Subsequent data analysis has been performed using GraphPad Prism 6. All experiments were performed by Nina Heycke and Tobias Benkel (Institute for Pharmaceutical Biology, Univ. of Bonn).

3.7.5 **Dynamic mass redistribution (DMR) assay**

Dynamic mass redistribution assays were conducted as described previously in detail.[128] Briefly, cells were seeded and grown overnight to confluence in 384 well EPIC biosensor plates (Corning). On the next day, cells were washed twice with HBSS containing 20 mM HEPES adjusted for DMSO and incubated for at least 2 h at 37 °C in the EPIC reader (Corning). FR or other potentially Gq-inhibiting compound was added 2 h before the measurement in HBSS (+HEPES) at a final concentration of 1 µM. At least 3 min of baseline read were recorded when cells were equilibrated (no change in basal DMR) and carbachol was added with a liquid handling robotic (Selma, CyBio). DMR changes were monitored for at least 2 h at 37 °C. Raw data were processed using the microplate analyzer MS-Excel macro (Corning) and subsequently analyzed in GraphPad Prism. Real-time DMR records are depicted as representative experiments (mean + s.e.m.) with each trace reflecting the average of three technical replicates. Each experiment was repeated at least three times to obtain three

independent biological replicates and performed by Tobias Benkel, Nina Heycke, Suvi Annala or Dr. Davide Malfacini, Institute for Pharmaceutical Biology, Univ. of Bonn.

3.7.6 Competition experiments with [^{3}H]PSB-15900

Competition experiments with [^{3}H] PSB-15900 at membrane preparations of platelets. Membrane preparations were performed by Markus Kuschak (Institute for Pharmaceutical Chemistry I, Univ. of Bonn) as previously described.[129,130] Competition experiments were performed for FR900359 or FR analogs versus [^{3}H]PSB-15900 on platelet cell membrane preparations using 9 different concentrations of FR900359 or FR analogs ranging from 0.1 nM to 100 µM. Three separate experiments were performed and data were analyzed with GraphPad Prism, Version 6.01 (GraphPad Inc., La Jolla, CA). [^{3}H]PSB-15900 was obtained by tritiation of FR900359 with tritium gas in analogy to the procedure described by Schrage et al. for the preparation of its non-radioactive analog.[54]

3.8 Methods for determination of the ecological role of FR900359

3.8.1 Quantification of FR in leaves and nodules of *A. crenata*

Air-dried plant material (dissected nodules, whole leaves or leaf lamina without nodules) was manually ground to a powder and extracted with methanol. The resulting crude extract was dried in a rotary evaporator and dissolved in methanol to give a concentration of 1 mg dried residue per millilitre. HPLC separation was carried out using a reversed phase C18 column (Machery-Nagel Nucleodur 100, 125 mm × 2 mm, 5 µm) with a gradient elution (from methanol/H_2O 10/90 to methanol 100% in 20 min, followed by isocratic conditions for 10 min as washing step. The mobile phase was buffered with ammonium acetate 2 mM at a flow rate of 0.25 ml x min^{-1}. The HPLC-MS (ESI) measurements were performed on an Agilent 1100 Series HPLC including DAD (250 nm) coupled with an API of 2000, Triple Quadrupole, LC/MS/MS, Applied Biosystems/MDS Sciex and ESI source. The concentration of FR900359 in the samples was calculated by linear regression against known concentrations of FR900359 purified as described by Fujioka and colleagues (1988) (concentrations applied: 100, 300, 1000 µg x ml^{-1}). Measurements were performed at least in triplicate, and the mean value and the standard deviation are given.

3.8.2 Feeding experiments of FR and *A. crenata* leaves on *Acheta domesticus*

In a collaboration with Timo Hartmann from the Museum for Natural History Alexander Koenig, Bonn we fed the leaves (dried and fresh) of *A. crenata* as sole nutrition to house crickets (*Acheta domesticus*) for two days.

In a further experimental setting, we prepared 0.5cm² pieces of the favorite diet (carrots) of house crickets in different geometries: untreated (pentagon), treated with acetone (hexagon), or treated with 10µl FR 1µM, 10µM, 100µM, 1mM respectively, dissolved in acetone (square). Before the experiment started the crickets hungered for two days. Six crickets only obtained untreated carrots, 6 crickets carrots treated with acetone as negative control, 6 crickets each (30 in total) got 1µM-1mM FR-treated carrots. Furthermore, 6 crickets each (30 in total) could choose between untreated, acetone-treated and FR-treated (1µM-1mM) carrots to examine, if the insects are able to sense FR and thus avoid feeding on it, when alternatives were provided. After three days all carrots had been consumed by the crickets.

3.8.3 Cloning and transfection of *Bombyx mori* and *Bemisia tabaci* Gq proteins

Bemisia tabaci Gq isoform X1 and *Bombyx mori* Gq isoform 1 sequences were kindly provided by Misty Attwood and Helgi Schiöth (Uppsala University, Sweden). DNA samples were generated by GeneCust Europe (Ellange, Luxembourg) and cloned in pcDNA3.1(+). *E. coli* DH5-α was used to amplify the two plasmid DNA. HEK293 cells CRISPR-Cas9 knock out for Gq/11 Gα protein subunits were obtained as described previously[54] and kindly provided by Asuka Inoue (Tohoku University, Japan). HEK293 Gq/11 knock out were transiently transfected with 180 ng/cm² DNA of *Bemisia tabaci* Gq isoform X1 or *Bombyx mori* Gq isoform 1 by using the calcium phosphate co-precipitation method.

3.8.4 Competition experiments with [³H]PSB-15900 at membrane preparations of Sf9 cells and HEK cells expressing *Bemisia tabaci* and *Bombyx mori* Gq proteins, respectively

Membrane preparations were performed as previously described.[129,130] Competition experiments were performed for FR versus its tritiated derivative [^{3}H]PSB-15900 (manuscript in preparation) on *Spodoptera frugiperda* (Sf9) cell membrane preparations using 9 different concentrations of FR ranging from 0.1 nM to 3 µM. Three separate experiments were performed and data were analyzed with GraphPad Prism, Version 6.01 (GraphPad Inc., La Jolla, CA).

[^{3}H]PSB-15900 was obtained by tritiation of FR with tritium gas in analogy to the procedure described by Schrage et al. for the preparation of its non-radioactive analog.[54]

3.8.5 Feeding and effect determination of FR on mice

All animal experiments were carried out according to the guidelines of the German law of protection of animal life with approval of the local authorities (LANUV, NRW, Germany). The solvent as control or FR were applied orally via gavage in female 10 weeks old CD1 wildtype mice. Therefore, 0.2 mg FR was administered in 200 µL (1:10 DMSO in 0.9% NaCl) by a stomach tube. After 1 hour blood pressure was determined by a Millar catheter as described before.[131,132] Briefly, for analgesia ketamine 50 mg/kg and xylazine 5 mg/kg were injected *i.p.* Then, mice were anesthetized by 1.5% isoflurane via a face mask. A small pressure catheter was inserted via the right carotid artery into the aorta and systemic pressure was recorded using the Millar Aria 1 system (Millar, Houston, TX, USA). For analysis systolic arterial pressure (SAP) in mice that had received the solvent or FR was compared exactly 1 hour after drug application. After the experiment, the mice were sacrificed by cervical dislocation. Experiments were performed by Alexander Seidinger, UKM, Bonn.

3.8.6 Feeding and effect determination of FR on insects

A small cotton particle soaked with 500µl of FR-containing water was served to first instar nymphs of a stinkbug (*Riptortus pedestris*) so that the insects orally take FR. FR was dissolved in 100% methanol, diluted with water to 0.2, 0.04, and 0.02 µg/µl concentrations, and tested. As a control, distilled water containing methanol (2%) was used. For each experiment, 20 individuals of the stinkbug were used. Insects were reared in a moisture chamber at 25 ºC under a long day regimen (16 h light, 8 h dark), supplied with dried soybean seeds. The FR-containing water was exchanged every three days, and survival rate was monitored every day at the same time for nine days. Experiments were performed by Dr. T. Ohbayashi, CNRS, Paris.

4 Results, Section I: Ecological function, Biosynthesis and Heterologous expression of FR

The cyclic depsipeptide FR900359 (FR), isolated from the tropical plant *Ardisia crenata*, displays a strong and selective inhibition of Gq proteins. Therefore, FR is an indispensable pharmacological tool to study Gq-related processes, as well as a promising drug candidate. It is assumed that FR is the product of the bacterial symbionts of *A. crenata* that we designated as *Candidatus* Burkholderia crenata.[22] Due to structural features of FR it is considered that the cyclic depsipeptide is assembled by a NRPS biosynthetic machinery. The detailed knowledge of the biosynthetic process will help to develop systems for manipulating the biosynthesis by bioengineering, and thus allowed us to create structural derivatives. Our preliminary investigations enabled us to identify a NRPS encoded on a plasmid of the *Burkholderia* symbiont, putatively responsible for FR biosynthesis. This would affirm our hypothesis that FR is biosynthetically rather derived from the symbiont than the plant.

The following questions shall be addressed in Section I:

1. What is the ecological function of FR (**Chapter 4.1**)?

2. Is the approx. 34 kb large sequence information *frsA-H* indeed encoding the biosynthetic enzymes for FR production and what is the function of its specific domains (**Chapter 4.2**)?

3. How would a heterologous expression system for FR900359 be constructed (**Chapter 4.3**)?

4.1 Research towards the ecological role of FR – More than just a tool for pharmacological research designed by nature?

Plants are one of the major sources for therapeutically applied compounds, *e.g*. paclitaxel[133], vinca-alkaloids[134,135], camptothecin.[136] In most cases the higher plants themselves are the producers of these metabolites. However, all of the about 300.000 higher plants are suspected to contain endosymbiotic organisms, which were largely neglected by researchers until recently.[7,9,137] Thus, endophytes open up a new research field in terms of new natural products for medical use and also for investigations of the chemical ecology and evolutionary aspects of symbioses. In general, it is believed that symbiotic microbes function as biological defense for the host plant to combat phytopathogens. The protection mechanism of the endophytes are exerted directly by releasing metabolites to attack any antagonists, and indirectly, by either inducing host defense mechanisms or promoting growth.[11,12,138] Carlier *et al.* provided evidence in this regard for the specialized leaf nodule symbiosis, occurring between the genus *Burkholderia* and plants of Primulaceae, *e.g*. *A. crenata* and Rubiaceae, *e.g*. *Psychotria* spp. This leaf nodule symbiosis (see **Chapter 1.1**) is considered to be obligate[139], because neither the host nor the endosymbiont can survive outside the symbiotic interaction.[15,140–142]

4.1.1 Investigation of the leaf nodule symbiosis of *A. crenata*

In this study we started the investigation of the endosymbiont-host relationship in *Crispardisia*. Nakahashi *et al*. have previously reported that it had no detrimental effect on the plant when they clipped the nodules from mature seedlings of *A. crenata*.[143] They hypothesized that the benefit, provided by the bacteria could be limited to another life stage. A similar approach was used by Yamada *et al*. to investigate effects after removal of endosymbiotic bacteria. They discovered, that antibiotic treatment of *A. crispa* and A. *punctata* seeds with streptomycin led *inter alia* to the development of non-leaf-nodulated plants.[144] We applied the same procedure for *A. crenata* and immersed the seeds in streptomycin (1 mg/mL) solution in sterilized dishes for seven days, sowed them in flower-pots and cultivated the plants for nine month in a green house under controlled conditions. In parallel, we also grew non-treated plants for comparison. After nine months, no difference could be observed between treated and non-treated plants. Both groups developed well and also all of them contained leaf nodules. In order to investigate whether the nodules of the treated plants harbor bacteria or not we harvested the leaves and examined them under the microscope. Cross-sections of the nodules revealed that they were filled with rod-shaped bacteria (**Figure 4-1**) and also PCR results were positive for

Burkholderia sp. (data not shown). The unsuccessful eradication of *Burkholderia* symbionts despite our antibiotic treatment corroborates the assumption for the vertical transmission of the endosymbionts. In order to eradicate the endosymbiotic bacteria in further experiments completely, we suggest an extended antibiotic treatment and, *e. g*. the addition of antibiotics also to the applied fertilizer.

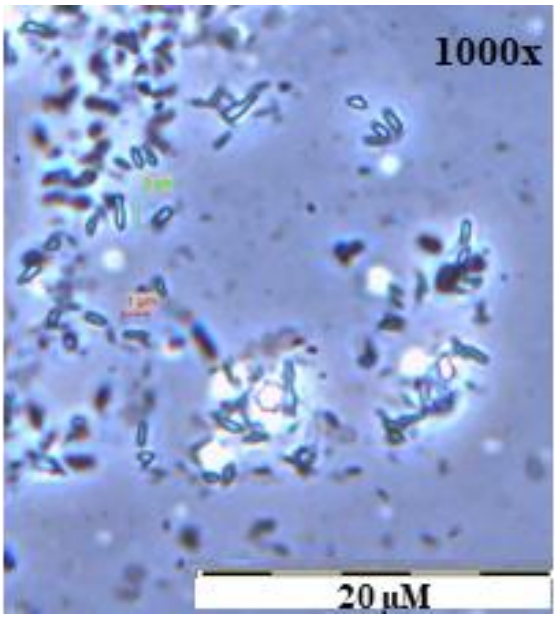

Figure 4-1: Bacterial Leaf Nodule of *A. crenata* was cut off the leaf rim and crushed, Nodules are filled with bacteria. Magnification 100x (left), magnification 1000x (right), reveals 1-2µM rod-shaped bacteria.

Based on genome analysis of the leaf symbiont of the plant *Psychotria kirkii* (Rubiaceae), *Candidatus* Burkholderia kirkii, it was proven by Sieber *et al*. that the endophytic bacteria produce secondary metabolites of the C_7N aminocyclitol family (known for antifungal, antibacterial, insecticidal activities).[145] These metabolites could bestow a fitness advantage upon the host plant, which may provide sufficient selective pressure to maintain the vertically-transmitted symbionts.[146] This emphasizes that genome reduction does not necessarily lead to a complete loss of the potential to produce secondary metabolites.[147]

In the here investigated case of *A. crenata* the symbiont, *Candidatus* Burkholderia crenata (*Ca.* B. crenata) was found to harbor the second smallest *Burkholderia* genome (2.85Mb) to date.[22] FR is due to its structural features obviously not a typical plant metabolite. For that reason, the presence of *Ca.* B. crenata would explain how and might give an indication where FR is produced. We determined the concentration of FR via HPLC-MS in crude extracts of dissected leaf nodules to be 247.0 ± 22.3 µg mg^{-1}, *i.e.* more than 36 times higher (Appendix **Figure 10-4**) than in leaves where the margins containing the nodules had been cut out (6.7 ± 1.6 µg mg^{-1}).[22] To confirm this result we directly tracked FR in a young *A. crenat*a leaf via MALDI imaging in the laboratory of Prof. Piel, ETH Zurich under the supervision of Dr. Alexander

Brachmann. In that way, we could clearly demonstrate and visualize the co-localization of the bacterial leaf nodules, *i.e*. endosymbiotic *Ca.* B. crenata and FR (**Figures 4-2**).

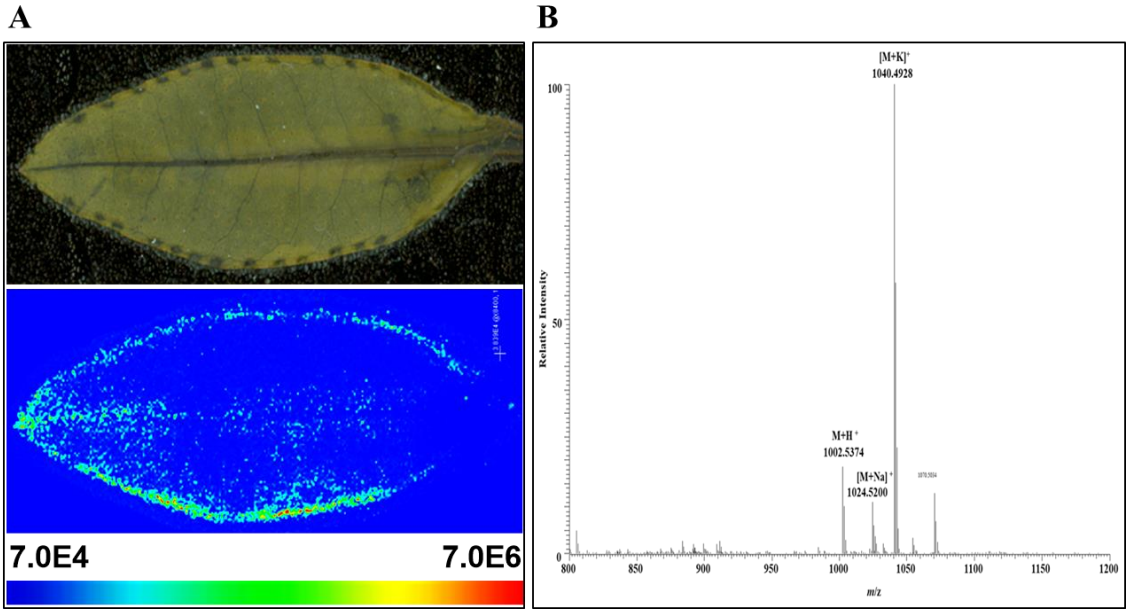

Figure 4-2: (**A**) **MALDI imaging mass spectrometry of an *Ardisia crenata* leaf**. Direct detection of potassium adduct of FR (mass tolerance: 0.001 Da) reveal FR to be concentrated at the leaf rim. (**B**) MALDI MS spectrum of a nodulated spot of a young *Ardisia crenata* leaf. Molecular ion, sodium and potassium adducts of FR are labeled and dominate the spectrum. Experiments performed under the supervision of Dr. Alexander Brachmann, Piel lab, ETH Zurich.

4.1.2 The putative role of FR as a signaling molecule between host plant and endosymbiont

In beneficial bacterial endophyte-plant interactions the production and modulation of phytohormones by endophytes play an essential role in plant development and stress tolerance. Furthermore, metabolites are reported to act as signals for communication between bacterial symbiont and plant, and that host-specific signal exchange may occur.[147]

FR is known for the inhibition of $G\alpha_q$-signaling in mammalian cells, and it is produced by *Ca.* B. crenata (see below, **Chapters 4.2, 4.3**) living in obligate symbiosis with *A. crenata*. Hence, we asked the question whether *A. crenata* utilizes this molecule to regulate its own G protein signaling. This idea is supported by the structural similarity of mammalian G proteins to the plant G protein AtGPA1 from *Arabidopsis thaliana*. The root mean square deviation (RMSD) between the backbones of the superimposed structures of AtGPA1 and $G\alpha_{i1}$ and transducin was only1.8 Å.[148] However, plant G proteins differ from mammalian G proteins in protein dynamics. They are self-activating, which means that they do not need GPCRs to promote GDP-GTP exchange. Therefore, regulation of G protein activation in plants occurs at the deactivation step.[149,150] Nevertheless, plants may also utilize a GDP dissociation inhibitor (GDI) like FR,

which may slow down nucleotide exchange. This question was examined by the Kostenis lab (Univ. of Bonn) in collaboration with the Dohlmann lab (Chapel Hill, NC). They found out that AtGPA1 was insensitive towards FR (**Figure 4-3**), contradicting our assumption at least for *A. thaliana*.

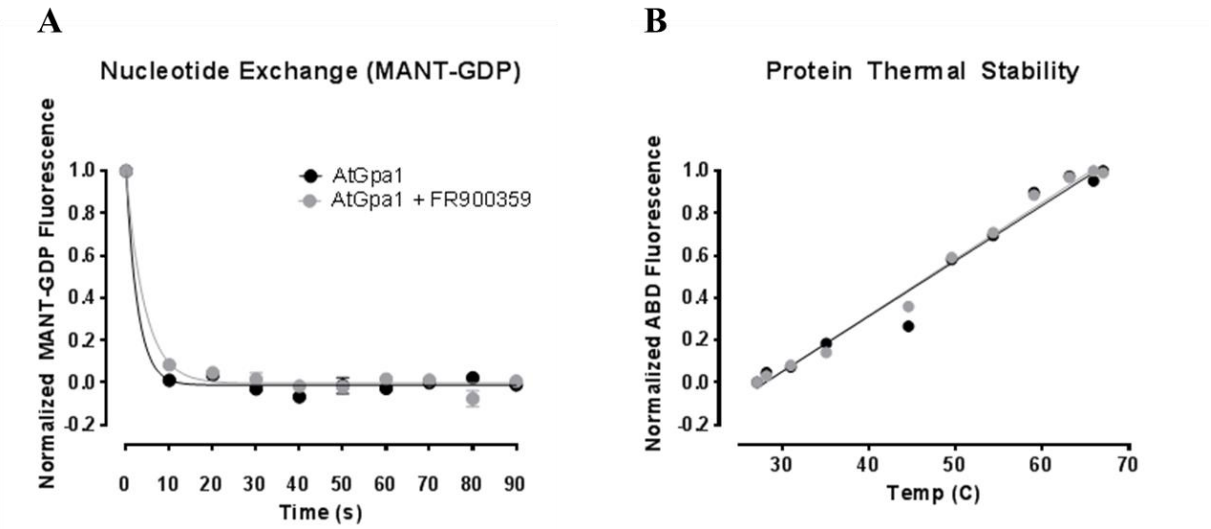

Figure 4-3: (A) FR does not interfere with AtGpa1 nucleotide exchange. Measurement of the effect of FR on nucleotide exchange of plant AtGpa1 (*Arabidopsis thaliana* Gpa1) using the fluorescent GDP analog MANT-GDP. Data are mean ± SEM of three independent experiments and curve fit was based on a one-phase exponential decay. w/o, without FR. (**B**) FR does not impair the stability of plant AtGpa1. Analysis of AtGpa1 protein thermal stability in absence or presence of 10 µM FR measured by fast quantitative cysteine reactivity (fQCR). Shown are data of a representative experiment. ABD, paminobenzamidine. w/o, without FR. (**A**) + (**B**) modified after Schrage *et al.*[54] and experiments were performed in the Henrik Dohlmann lab, Chapel Hill, NC, USA**.**

4.1.3 FR shows no antibacterial, antifungal or cytotoxic activity

Inspired by the antimicrobial secondary metabolites from *Candidatus* Burkholderia kirkii, we intended to study the antibacterial activity of FR, which also serves as unspecific toxicity test for FR, because bacteria are not known to have G proteins (**Table 4-1**).

Table 4-1: Agar diffusion assay. FR900359 dissolved in DMSO (1 mg/ml). 3µl of this solution were applied to agar plates grown with 28 bacterial strains and two yeasts (*Candida*). DMSO was used as negative control. Values in millimeter inhibition zone. Experiments performed by Michaele Josten, Institute for Medical Microbiology, Bonn.

	strain	no.	DMSO	FR900359
1	MSSA	5185	0	0
2	MSSA	I-11574	0	0
3	MRSA	LT-1334	0	0
4	MRSA	LT-1338	0	0
5	MRSE	LT-1324	0	0
6	*Candida albicans*	I-11301	0	0
7	*Candida albicans*	I-11134	0	0

8	*Citrobacter freundii*	I-11090	0	0
9	*Klebsiella pneumoniae subsp. ozeanae*	I-10910	0	0
10	*Enterococcus faecium*	I-11305b	0	0
11	*Enterococcus faecium*	I-11054	0	0
12	*Escherichia coli*	I-11276b	0	0
13	*Escherichia coli*	O-19592	0	0
14	*Stenotrophomonas maltophilia*	O-16451	0	0
15	*Stenotrophomonas maltophilia*	I-10717	0	0
16	*Pseudomonas aeruginosa*	I-10968	0	0
17	KNS	I-10925	0	0
18	*Staphylococcus simulans*	22	0	0
19	*Micrococcus luteus*	ATCC 4698	0	0
20	*Mycobacterium smegmatis*	ATCC 70084	0	0
21	*Bacillus subtilis*	168	0	0
22	*Arthrobacter crystallopoietes*	DSM 20117	0	0
23	*Listeria welchimeri*	DSM 20650	0	0
24	*Staphylococcus aureus*	133	0	0

MSSA = methicillin-sensitive *Staphlococcus aureus*, MRSA = methicillin-resistant *S. aureus*, MRSE = methicillin-resistant *S. epidermis*, KNS = coagulase-negative *Staphylococci*.

We tested FR against a panel of Gram positive and Gram negative bacteria, as well as fungi. None of the tested organisms were harmed by FR. Thus, we concluded that FR displays no antimicrobial effects. FR is also not cytotoxic, since 1 µM (FR completely blunts Gq-signaling at 1 µM) showed no detectable cytotoxicity towards HEK293 cells (data not shown) and no change in cell phenotype (**Figure 4-4**).

G proteins in fungi have been only scarcely investigated, yet. So far the Gi protein of mammals is 55% identical with GNA1 of fungi, but the Gq sequence is more distinct.[151] Gq-like proteins in fungi are critical for virulence, morphology, and sporulation.[152–160] Consequently, sporulation is considered as a fungal process, which would be likely affected by a fungal Gq-like protein interaction and could be easily monitored by a phenotypic change. Therefore we examined the effect of FR (1 mg/mL) towards the fungi *Microbotrium violaceum* and *Cryphonectria parasitica* (cultivation performed together with Ekaterina Egereva, Univ. of Bonn). However no phenotypic difference could be detected between the positive control group (treated with 100 µL of a 1 mM solution FR) and the negative control group (untreated, no FR supplementation). Both tested fungal species sporulated well despite the treatment with a high concentrated dosage with a very potent Gq inhibitor. This indicated that FR does not influence signaling of fungal Gq-like proteins.

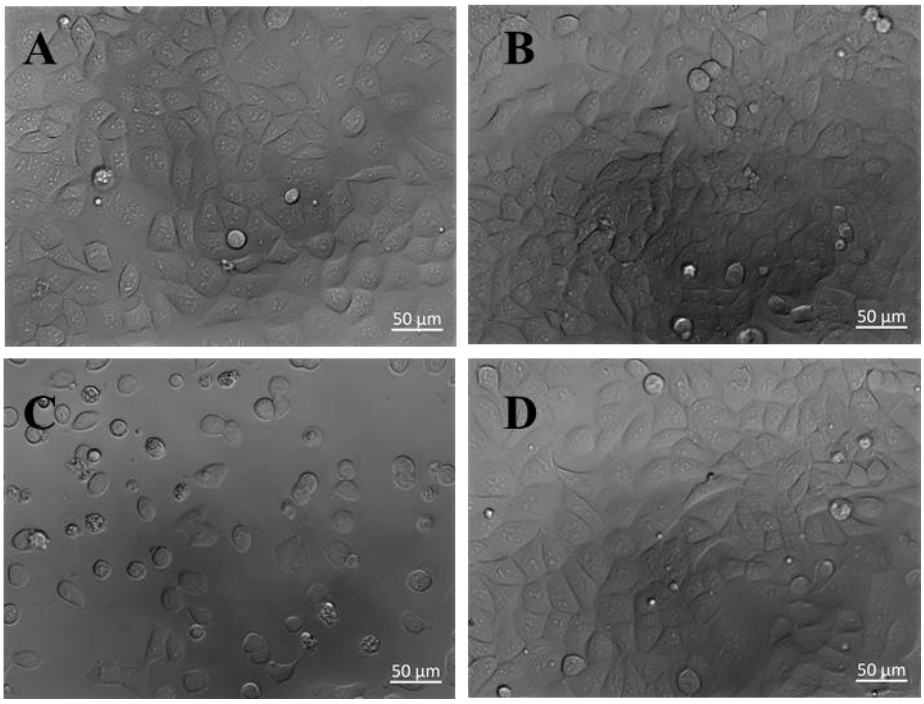

Figure 4-4: Cell viability assay with HEK293 cells (**A**) w/o any treatment (**B**) 0.3% DMSO, (**C**) Etoposide 50 µM as positive control (**D**) FR 1 µM dissolved in 0.3 % DMSO. Experiments performed by Dr. Nicole Merten, Kostenis lab, Univ. of Bonn.

4.1.4 FR is orally bioavailable and effective in mice

Gq proteins are not exclusively expressed in humans, but are highly conserved in the evolution of metazoans.[161] A pan-Gq inhibitor, would thus impact any organism with homologous Gq proteins, like other mammals than humans or insects, pointing towards the ecological function of FR. Oral application of FR to mice (comparable to the situation in the field where mammals may prey on *A. crenata*), which have Gq proteins 100 % homologous to human Gq should thus affect the animals, if FR is orally bioavailable. Indeed, oral FR application, resulted in uptake of the compound and significant reduction of blood pressure (**Figure 4-5**, experiment performed by Alexander Seidinger, Wenzel lab, University clinic, Bonn). When we compared systolic arterial pressure (SAP) after oral application of the solvent (without FR) and with FR by a Millar catheter in the aorta, we found a pressure of 79.3±2.0 mmHg, in mice that had received the solvent and a strongly reduced pressure of 57.5±3.5 mmHg, in animals after oral FR application.

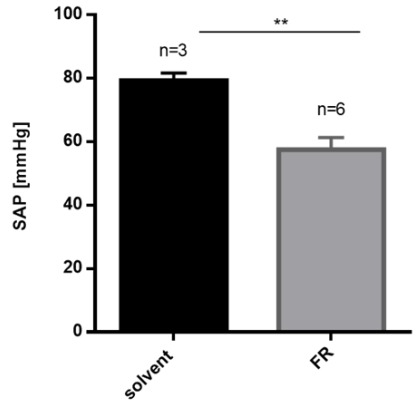

Figure 4-5: Statistical analysis of in vivo blood pressure recordings in mice revealed a strong reduction of systolic arterial pressure (SAP) in the aorta 1 hour after oral FR application (0.2 mg per mouse, $p<0.01$). Experiment performed by Alexander Seidinger (Wenzel lab, University clinic Bonn, Germany).

4.1.5 FR as chemical weapon against insect herbivores

4.1.5.1 Antifeedant effects of *A. crenatae folium* on *Acheta domesticus*

Insects are a major threat for plants. In a collaboration with Timo Hartmann from the Museum for Natural History Alexander Koenig, Bonn we fed the leaves (dried and fresh) of *A. crenata* as sole nutrition to house crickets (*Acheta domesticus*) for 5 days. The insects ignored the leaves and rather hungered to death than feeding on them. The antifeedant effect of methanolic *A. crenata* leaf extract was also reported from Sandoval-Mojica *et al*.[162] They had examined the extract against nymphs of *Schistocerca americana* (Orthoptera: Acrididae) and adult *Diaprepes abbreviatus* (Coleoptera: Curculionidae), two serious pests of citrus crops in Florida.

4.1.5.2 Feeding experiments with FR on *A. domesticus*

Next, we prepared the favorite diet (carrots) of house crickets and treated the carrots with an acetonic solution of FR in different concentrations (n=6 for each concentration, 1µM-1mM, and untreated carrots, **Chapter 3.8.2**). Furthermore, crickets were offered untreated, acetone-treated and FR-treated (1µM-1mM) carrots at the same time, to examine, if the insects are able to sense FR and thus avoid feeding on it, when alternatives were provided (**Figure 4-6**). In this respect, it is worthy to mention that insect G proteins are reported to be involved in tasting, odor sensing, but also in metamorphosis.[163–168]

Figure 4-6: Feeding experiments on *Acheta domesticus* with FR-treated carrots in concentrations from 1µM - 1mM displayed no detrimental effects for the insects.

After three days all of the carrots were consumed, and no abnormal behavior of the crickets or any toxic effects could be observed. We concluded that FR has no direct toxicity on crickets and thus is not the reason for the strong deterrent effect of *A. crenata* leaves. *A. crenata* leaves possess high concentrations of triterpenoid saponins, which could be responsible for the deterrency.[169] In this experiment however, the duration was possibly too short to observe long term effects. Of course it may also be speculated that Gq proteins of crickets are not sensitive to FR.

4.1.5.3 Sequence alignment of Gα subunits of different metazoans around the YM binding site

In further studies to unravel the interaction of FR with insect Gq, we changed our strategy towards a more rational approach. Only recently the crystal structure of YM (a close structural analog of FR, see **Chapter 1.4**) bound to chimeric Gq/i protein was published.[53] This study included mutations in the $G\alpha_q$ protein and their impact on Gq signaling probed by using YM.

With this knowledge in mind and the high degree of conservation of Gq proteins of various organism an alignment of Gq proteins from several metazoans were done to predict putative YM-sensitivity of the respective animals, especially insects. We intended to combine the information from Nishimura *et al.* with the Gαq-subunits from different species sequenced by Krishnan *et al.*[161](**Figure 4-7**). The sequence alignment of G protein α subunits of various metazoans around the YM binding site reveals that besides *Drosophila melanogaster*, many insects are suggested to be sensitive to YM as they do not contain mutations in the binding motif of YM. Due to the structural similarity of YM and FR we assume identical binding properties of both compounds.

As YM was not commercially available at that point of the study, only the putative influence of FR on different organisms will be discussed.

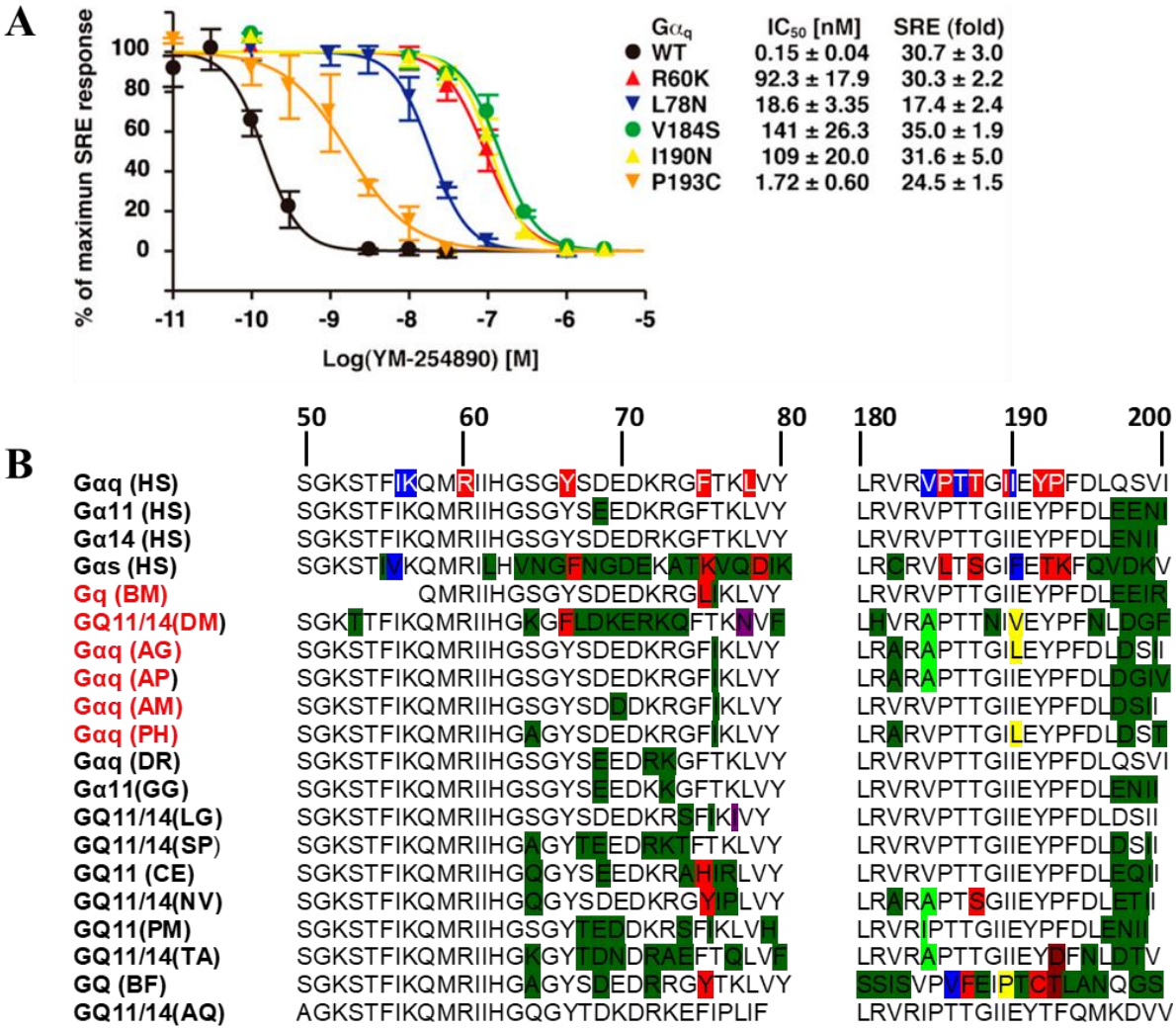

Figure 4-7: (A): Mutational analysis of Gαq residues that appear to directly interact with YM-254890, taken from[53]. YM-254890 sensitivity of each Gαq mutant was evaluated by serum response element (SRE) activation. The calculated IC_{50} values of YM-254890 for each $G\alpha_q$ mutant and SRE activity of each $G\alpha_q$ mutant are shown. Each value represents the mean ± S.D. from three independent experiments performed in duplicate. Mutant protein samples were confirmed to retain proper conformations by the trypsin protection assay. (**B**) Sequence alignment of G protein α subunits of various metazoans around the YM-254890 binding site based on the mutational analysis described in (**A**) using the same color code. The residues that appear to directly interact with YM-254890 are shown on a red background. In particular, the residues that form the hydrophobic pocket, which would bind to the phenyl group of YM-254890, are marked with a blue background. Organisms belonging to the class of insects are labeled in red. HS = *Homo sapiens*, BM = *Bombyx mori*, DR = *Danio rerio*, PM = *Petromyzon marinus*, CI = *Ciona intestinalis*, BF = *Branchiostoma floridae*, SP= *Strongylocentrotus purpuratus*, SK = *Saccoglossus kowalevskii*, CE = *Caenorhabditis elegans*, SM = *Schistosoma mansoni*, NV = *Nematostella vectensis*, TA = *Trichoplax adhaerens*, AQ = *Amphimedon queenslandica*, GG = *Gallus gallus*, LG = *Lottia gigantean*, AG = *Anopheles gambiae*, AP = *Acyrthosiphon pisum*, AM = *Apis mellifera*, PH = *Pediculus humanus*. Sequences were provided by Misty M. Attwood, Schiöth lab, University of Upsalla.

4.1.5.4 Affinity of FR to pest insect G proteins

Using a competitive radioligand binding assay, applying the tritiated FR radioligand [^{3}H]PSB-15900, affinity of FR to G proteins of distinct pest insects (*Bombyx mori* , *Spodoptera frugiperda, Bemisia tabaci)* was assessed (Assays performed by Markus Kuschak, Müller lab, Univ. of Bonn).

B. mori and *B. tabaci* (silverleaf whitefly) are native insects to subtropical and tropical Asia, the geographical origin of *A. crenata*. Membrane preparations of both species were provided by Dr. Davide Malfacini, Kostenis lab, Univ. of Bonn). Further on we investigated Gq proteins, endogenously expressed in the Sf9 cell line developed from ovaries of *S. frugiperda*, which is found in the Americas. It is the larval stage (caterpillar) of the fall armyworm moth. These insects can damage crops, mainly maize, eating up the entire crop before moving to another plantation.

Membrane preparations, which contained G proteins of Sf9, *B. mori*, or *B. tabaci* were used; the radioligand concentration was 5 nM. Non-specific binding of the radioligand [^{3}H]PSB-15900 was determined in the presence of 5 µM FR. FR showed a pIC_{50} value of 8.13 ± 0.06 at SF9 membrane preparations, 8.98 ± 0.05 at *B. mori* membrane preparations and 9.27 ± 0.10 at *B. tabaci* membrane preparations (see **Figure 4-8**). This indicates that FR displays very high affinity for Gq proteins expressed in insect cells, even surpassing affinity for mammalian Gq proteins.

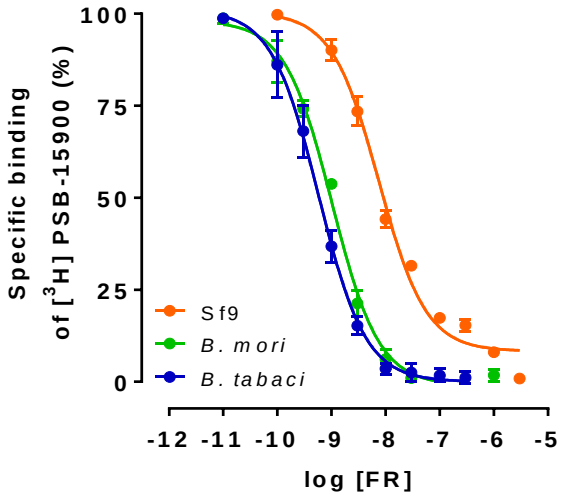

Figure 4-8: Competition binding study of FR versus [^{3}H]PSB-15900 (5 nm), the tritiated derivative of FR, at Sf9 insect cell membranes, and at Gq proteins of *Bombyx mori* and *Bemisia tabaci* expressed in Gq-knockout HEK cell membrane preparations. Values represent means: SEM of three independent experiments. pIC_{50} values of 8.13–9.27 were determined. Experiments were performed by Markus Kuschak, Müller lab, University of Bonn, Germany.

4.1.5.5 Feeding experiments with FR on bean bug larvae

The bean bug *Riptortus pedestris* is a sucking pest of soybean, common beans and various other crops that is found in eastern Asia. Both adults and nymphs feed on the soybean pods.[170] Toxicity of FR towards these insects was assessed, showing killing and preventing of molting

of bean bug nymphs by Dr. Tsubasa Ohbayashi, CNRS, Université Paris, France (**Figure 4-9**). After seven days, all of the *R. pedestris* nymphs were dead when exposed to FR at concentration of 0.2 and 0.04 µg/µl (see Figure 1D). Additionally, 18 of 20 insects could not molt to 2nd instar with 0.04 µg/µl FR and no insects could molt to 2nd instar when exposed to 0.2 µg/µl FR. Thus, FR was demonstrated to have insecticidal and molting-inhibiting activity, but did not display acute toxic effects towards *R. pedestris* in a concentration-dependent manner.

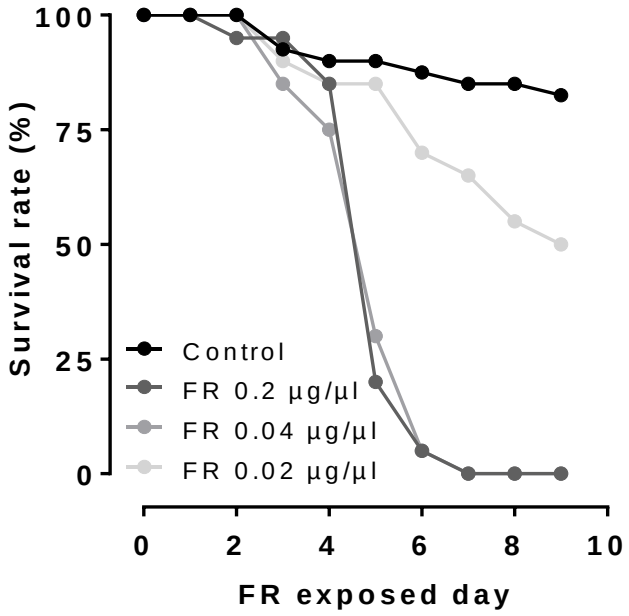

Figure 4-9: Exposure of nymphs of a bean bug (*Riptortus pedestris*) to different concentrations of FR; the survival rate was measured. Experiments were performed by Dr. Tsubasa Ohbayashi, CNRS, Université Paris, France.

An ecological role of FR as defense chemical for the host plant has been discussed before.[22] The results of **Chapter 4.1.5** add further evidence to this assumption. First of all, bioinformatics predicted for several insect Gq proteins to be FR-sensitive, which could be affirmed using binding assays of Gq proteins from distinct pest insects. Finally, feeding experiments on *R. pedestris* confirmed potent effects of FR towards a specific insect species. Altogether this suggests a protective role of FR for the host plant against herbivores.

4.2 Bioinformatics and *in vitro* enzymatic studies on FR biosynthesis

As described in **Chapter 1.1**, we sequenced the genome of the bacterial leaf symbiont *Ca*. B. crenata from *A. crenata*.[22] Analysis of the genome sequence revealed essential pathways to be malfunctional, highlighting the advanced evolutionary stage of this plant-bacterium symbiosis and ongoing genome reductive evolution. In that study, the putative FR biosynthetic gene cluster *frs* (**Figure 4-10**), encoding a nonribosomal peptide synthetase (NRPS), was identified on an extrachromosomal plasmid. Due to the eroded genome, cultivation of *Ca*. B. crenata seemed unlikely, and indeed numerous cultivation attempts failed, making FR supply dependent on cultivating and extracting *A. crenata* leaves. By defining all genes necessary for FR biosynthesis, we draw a plausible biosynthetic hypothesis for this complex metabolite, supported by bioinformatics, *in vitro* characterizations of biosynthetic enzymes and characterization of FR analogs. This now paves the way for a biotechnological production of FR. The following experiments were conducted by Dr. Max Crüsemann (Institute for Pharmaceutical Biology, Univ. of Bonn) and coworkers.

Unexpectedly, bioinformatics of the *frs* genes showed the presence of two thioesterase (TE) domains, representing two NRPS machineries, which together display a clear colinearity between module and domain architecture and FR structure (**Figure 4-10**).[10,22]

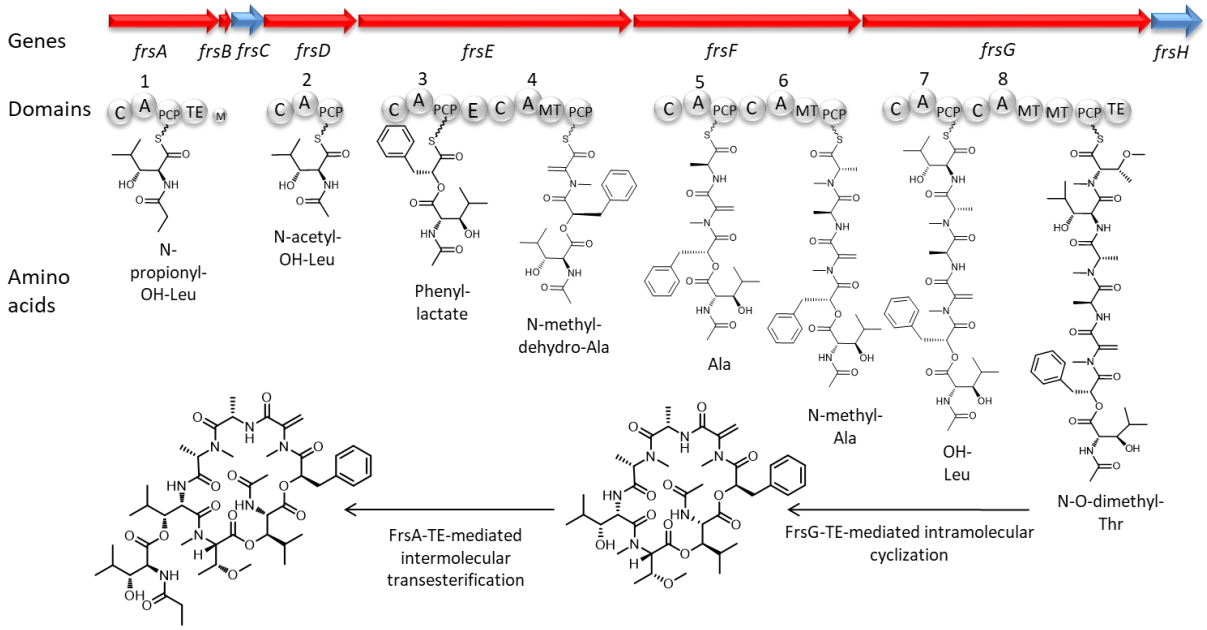

Figure 4-10: Scheme of the putative FR biosynthesis deduced from bioinformatics and in vitro experiments. The NRPS genes, the catalytic domains they encode, and the amino acids incorporated by the respective modules are displayed. The peptide formation on the FrsA-G NRPS machineries, including release and transesterification by FrsA-TE is shown. Domains: A, adenylation; C, condensation; MT, methylation; PCP, peptidyl carrier protein; E, epimerization and TE, thioesterase (Ile-Thr ring closure). Figure was modified after[10].

To further analyze the FR-NRPS, we first investigated the Frs condensation (C) domains bioinformatically. This is done to classify C domains by function such as epimerization, and acceptance of acyl groups, L or D amino acids.[171] We aligned the C domain sequences with available sequences based on the NaPDoS database[172] to construct a phylogenetic tree (**Figure 4-11**), which confirmed most of the proposed features such as transfer of acyl units for FrsA and FrsD C domains.

In FR the acyl residues transferred by FrsA and FrsD C domains are propionic and acetic acid. These C domains however, have somewhat flexible substrate specificity. This is illustrated by an unusual FR derivative, *i.e.* FR-1 (**1**), that we isolated from dried *A. crenata* leaves. In **1** the acetate unit of FR is replaced by a 3-hydroxypropionate moiety, the latter being a most uncommon acyl residue for bacterial natural products. The structure of **1** was unambiguously established from NMR data (**Chapter 5.1.1**, **Table 5-1**, Appendix **Figures 10-14 – 10-20, Scheme 10-1**), especially in comparison to those of FR (Appendix **Figures 10-5 – 10-13, Scheme 10-1, Table 10-1**).

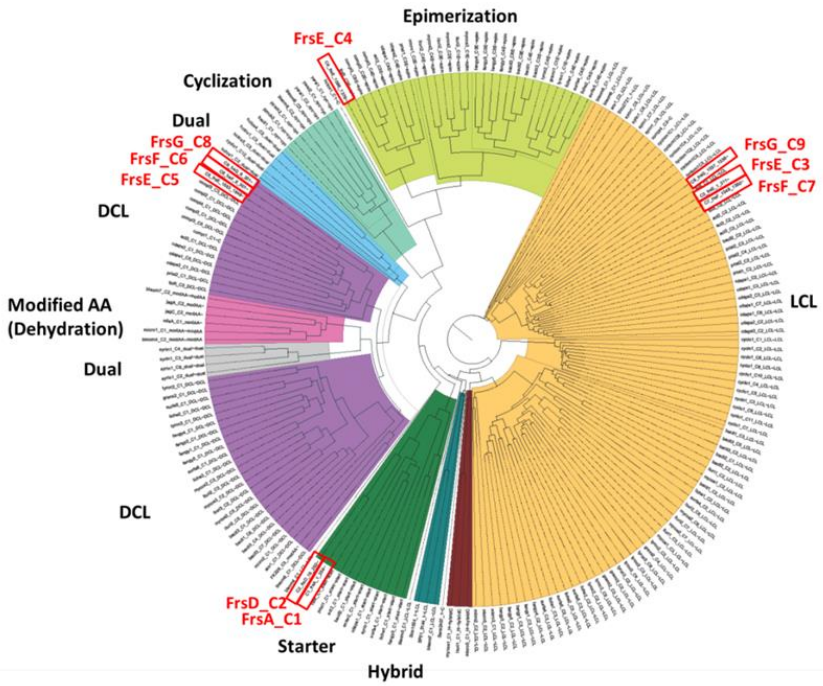

Figure 4-11: Phylogenetic tree of condensation domains in the *frs* gene cluster taken from[10]. The C domain phylogenetic tree C_{DH} confirms most of the proposed features such as transfer of acyl units for FrsA and FrsD C domains (starter C domains C1 and C2). Furthermore, that the three determined $^{L}C_{L}$ C domains, catalyzing bonds between two L-amino acids in modules 3, 6, and 8 (C3,C7 and C9), clade as expected, as well as the epimerase domain and D-phenyllactate-accepting domain in module 4 (C4 and C5). Curiously, the C domains in modules 5 and 7 (C6 and C8), connecting the L-configured *N*-methyldehydroalanine and –alanine with L-alanine and L-OH-leucine, cluster with the $^{D}C_{L}$ domains, usually linking D- with L-amino acids.

Our classification of C domains showed furthermore, that the three determined $^{L}C_{L}$ C domains, catalyzing bonds between two L-amino acids in modules 3, 6, and 8, clade as expected, as well as the D-phenyllactate-accepting domain in module 4. Curiously, the C domains in modules 5 and 7, connecting the L-configured *N*-methyldehydroalanine and *N*-methylalanine with L-alanine and L-OH-leucine, cluster with the DCL domains (**Scheme 4-1**), usually linking D- with L-amino acids.

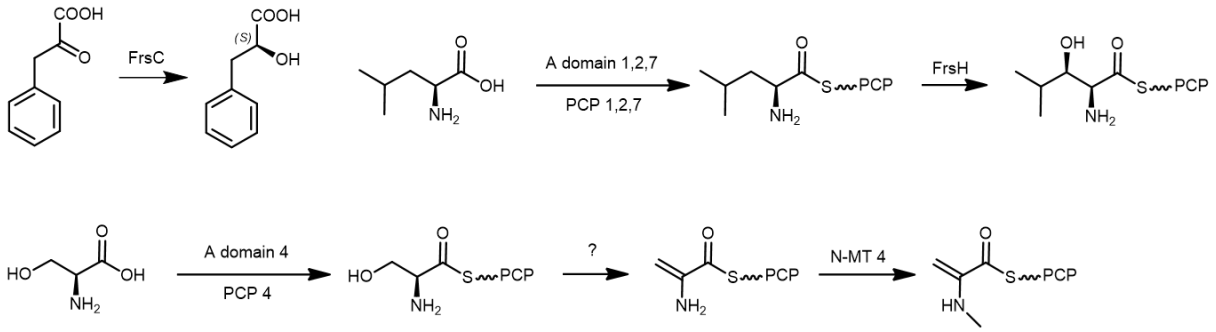

Scheme 4-1: Proposed biosynthesis of non-proteinogenic building blocks.

The monomodular NRPS FrsA, responsible for the synthesis of *N*-propionylhydroxyleucine, contains a TE that likely transfers this building block onto the cyclic peptidic substrate. We thus hypothesize that FR biosynthesis proceeds first by the generation of a TE bound heptapeptide by FrsD-G (**Figure 4-10**). The FrsG TE then catalyzes offloading and intramolecular cyclization of the intermediate. Finally, the FrsA TE is predicted to perform an intermolecular transesterification by transferring *N*-propionylhydroxyleucine onto the free β-hydroxyl moiety of the cycloheptapeptide. A similar mechanism has, to our knowledge, so far only been observed in the biosynthesis of the salinamides, nonribosomal peptides from a marine streptomycete.[173] MS/MS molecular networking[174] was applied to detect minor biosynthetic intermediates confirming our hypothesis (for detailed workflow see **Chapter 5.1.2**). Indeed, a molecular ion with *m/z* 817 strongly suggested the presence of only the FR macrocycle without the *N*-propionylhydroxyleucine side chain (see **Chapter 5.1.2, Scheme 5-5**). Interestingly, a similar congener of the structurally related YM was characterized, pointing to an analogous biosynthetic route.[52]

Although 7 of 8 building blocks of FR are non-proteinogenic, remarkably the *frs* gene cluster contains only two putative tailoring genes, *i.e. frsC* and *frsH*. Bioinformatic analysis of FrsC revealed high sequence similarity to malate dehydrogenases (MDH)[175,176] and L-lactate dehydrogenases (L-LDH) with all conserved residues necessary for the reduction of a keto function in the substrate (see Crüsemann & Reher *et al.*[10]). Thus, we propose, that FrsC

catalyzes the reductive formation of L-phenyllactate from phenylpyruvate, an intermediate from phenylalanine metabolism. The epimerization domain encoded in FrsE, which is functional based on bioinformatics (see Crüsemann & Reher *et al.*[10]), then catalyzes the formation of D-phenyllactate.

The other encoded modifying enzyme in the *frs* genes, FrsH, did not exhibit high sequence homology to any other characterized protein. However, a more detailed bioinformatics search revealed homologies in the active center to CmlA, a non-heme iron-dependent β-hydroxylase from chloramphenicol biosynthesis (see Crüsemann & Reher *et al.*[10]). CmlA catalyzes the hydroxylation of *para*-aminophenylalanine, when bound to the peptidyl carrier protein (PCP).[177,178] A structural model of FrsH generated by Dr. Max Crüsemann (Institute for Pharmaceutical Biology, Univ. of Bonn) supports the anticipated similarity of FrsH and CmlA (**Figure 4-12**).

Figure 4-12: Structural model of FrsH, generated by I-TASSER based on CmlA taken from[10]. (A) Structure of CmlA, taken from PSB (Accession number: 4JO0). (B) Structural model of FrsH, generated by I-TASSER[179], based on CmlA (Estimated RMSD: 3.2±2.2 Å). (C) Overlay of both structures.

Analogous to chloramphenicol biosynthesis, we reasoned that hydroxylation of leucines in FR could take place on the leucinyl-PCP of modules 1, 2, and 7. To investigate this hypothesis, *frsA* and *frsD* adenylation (A) domain-encoding regions (modules 1 and 2) were cloned into pET28 and expressed in *E. coli* with or without the MbtH-like protein (MLP) FrsB (see Crüsemann & Reher *et al.*[10]). MLPs are small, highly conserved proteins that are frequently associated with bacterial NRPSs and are in many but not all cases crucial for A domain activity.[180] However, SDS gels of single expression and coexpression experiments showed that the A domains of FrsA and FrsD do not bind to FrsB during purification. An $^{18}O_4$-ATP exchange assay[181] could detect adenylating activity for both A domains without the presence of FrsB. Interestingly, leucine was preferentially activated by both domains, while 3-OH-leucine

was accepted to a much lower extent (see Crüsemann & Reher *et al.*[10]). This result strongly supports loading of leucine, followed by a hydroxylation of leucinyl-PCP by FrsH in three different modules.

Since there is no obvious candidate for dehydroalanine formation in the *frs* genes, we hypothesize that the dehydrating activity is embedded in a C domain as it was speculated for microcystin biosynthesis.[182] In a phylogenetic analysis, the McyA C domain forms a separate clade with other domains that are hypothesized to perform dehydrations.[172] However, our phylogenetic analysis points to a different dehydration mechanism in FR biosynthesis, since the C domain in module 5 is not clustering with the above mentioned domains (**Figure 4-11**).

4.3 Heterologous expression of FR in *E. coli*

In order to confirm the completeness of the FR biosynthetic gene cluster, we next aimed to transfer the *frs* genes to a cultivable bacterium for heterologous FR production. In future, production of FR by fermentation would alleviate the current laborious extraction and isolation process from *Ardisia* plants. Total synthesis of FR was recently achieved, however with low yields and high expenses.[26] Heterologous expression would also be a key step to establish an *in vivo* platform to further investigate FR biosynthesis and to generate analogs for pharmacological evaluation by mutasynthesis or biosynthetic engineering. The following experiments were conducted by Dr. Max Crüsemann (Institute for Pharmaceutical Biology, Univ. of Bonn) and coworkers.

Clone I9E from our BAC library[22] kindly provided by Dr. Aurelièn Carlier (Univ. Of Zurich/Ghent) contained all *frs* genes. However, cultivation of *E. coli* strains with I9E did not lead to FR production. To switch on FR production, the constitutive promoter pS7[183] was cloned upstream of *frsA* via PCR-based recombineering, yielding pMC1 (**Figure 4-13A**). First attempts to cultivate *E. coli* strains carrying pMC1 under various different conditions still yielded no FR. One reason for the lack of FR production could be due to protein insolubility. Thus, we sought to co-express the FR biosynthesis genes with chaperones. Constitutively high concentrations of molecular chaperones are regarded as essential for protein stability in obligate symbionts with reduced genomes,[184] a phenomenon that was also observed in other leaf nodule symbioses.[185] To ensure co-expression from both plasmids, we exchanged the resistance cassette for chloramphenicol against one for kanamycin in pMC1 to maintain the chloramphenicol-resistant chaperone plasmids in the expression strains. This was again achieved using PCR-based recombineering, yielding pMC2, that was subsequently co-

transformed with either of the five available chaperone plasmids in both *E. coli* BAP1 and BL21. All 10 resulting expression strains were then cultivated in LB and M9 minimal media at temperatures of 16, 30 and 37 ˚C. Of the 60 conditions tested, we could only detect FR (1 µg/L) in n-butanol extracts of cultures of *E. coli* BL21 or BAP1 co-expressing pMC2 and pG-KJE8 (encoding the *E. coli* chaperones DnaK, DnaJ, GrpE, GroES and GroEL) grown in M9 medium at 16 °C (**Figure 4-13B**). The exact mass of all FR adducts as well as retention time and MS^2 spectrum correspond to an authentic FR standard (**Figure 4-13C1-C2**), confirming FR production in the heterologous host.

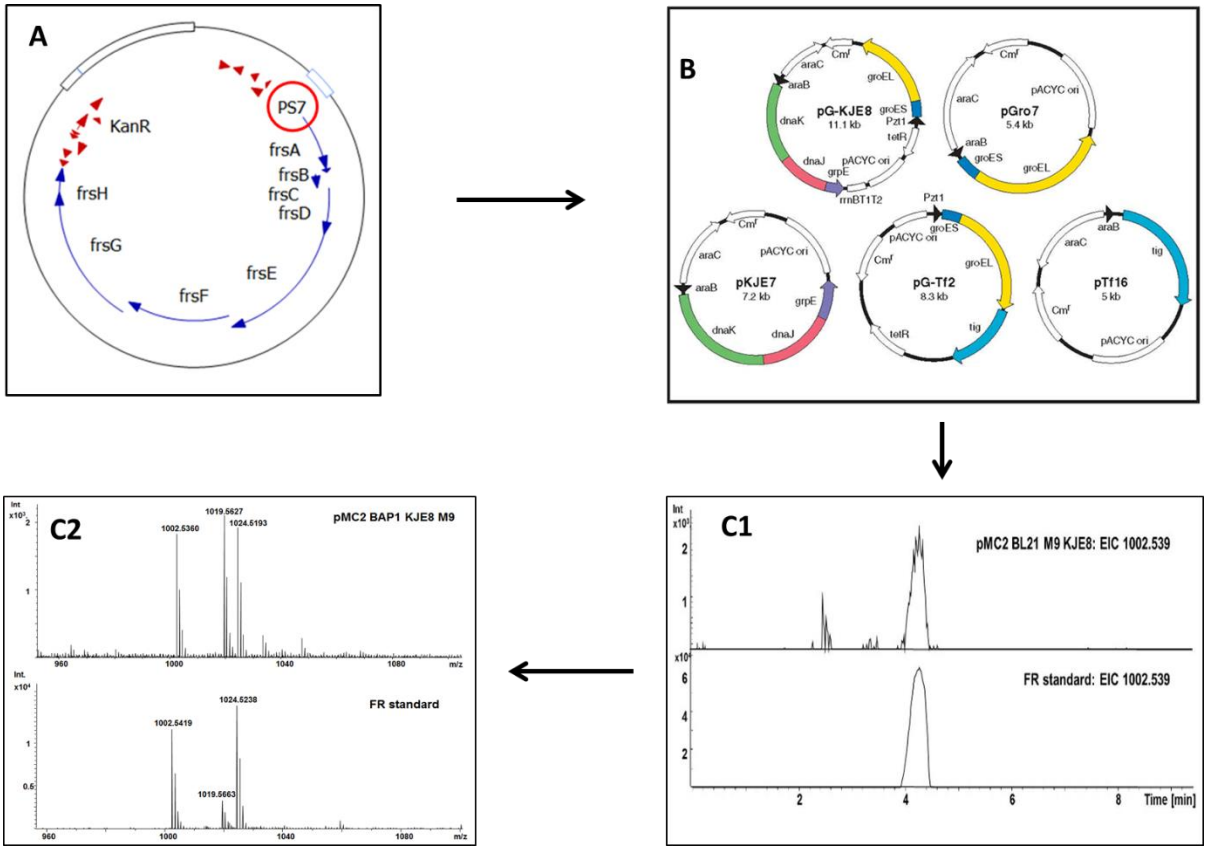

Figure 4-13: Heterologous expression of FR900359 modified after Crüsemann and Reher *et al.*[10] (**A**) BAC library clone I9E (55 kbp), pSMART (from Dr. A. Carlier, Univ. Zurich). (**B**) Co-transformation with 5 chaperone-containing plasmids into *E.coli* BL21(DE3) *E.coli* BAP1, cultivation for three days at 16 °C and subsequent n-butanol extraction. C: UPLC-MS/MS analysis. (**C1**) Extracted ion chromatogram of *m/z* 1002.539. Comparison of FR standard with extract gained from *E.coli* BL21(DE3). (**C2**): MS spectrum of FR standard and extract gained from *E.coli* BL21(DE3). Experiments performed by Dr. Max Crüsemann, Univ. Bonn.

Conclusion Section I

Gq inhibition is a novel mode of action for defense chemicals, and targeting Gq seems crucial for the ecological function of FR, as shown by *in vivo* experiments on mice, affinity to insect Gq proteins and insect toxicity studies. Interestingly, FR is produced by the bacterial symbiont of *A. crenata*. This uncultured endosymbiont, *i.e. Candidatus* Burkholderia crenata was sequenced and revealed the FR nonribosomal peptide synthetase (*frs*) gene cluster. FR biosynthesis was finally proven by expression of the *frs* genes in *E. coli*, which led to heterologous FR production in a cultivable, bacterial host for the first time. Heterologous expression of a natural product from an uncultivated endosymbiotic to our knowledge, has rarely been achieved.[186,187] Our results lay the foundation for future production of FR, independent from time- and work-intensive plant cultivation, harvesting and extraction.

5 Results, Section II: Detection, Isolation and Structure Activity Relationship studies of new FR analogs

Chapter 5.1:

GPCR signaling is considered as a highly important research field as 36% of all available medicinal drugs target GPCRs.[44] The natural product FR has proven to be a most valuable tool to study GqPCRs (see **Chapter 1.4**). Compared to the structural analog YM, FR contains an acetylated β-hydroxyleucine residue instead of an acetylated threonine in the cyclic part of the molecule, and a propionate unit replaces an acetate acyl residue located at the side chain (**Scheme 1-1**). Such depsipeptides are typically produced by non-ribosomal peptide synthetases, biosynthetic machineries, which are known to produce - apart from their major product (here FR, YM) - also minor compounds, due to some promiscuity of the biosynthetic enzymes (see **Chapter 1-2**, **Chapter 4-2**).[10,188] Indeed, Taniguchi *et al*. were able to isolate further YM derivatives from the culture broth of *Chromobacterium* sp. QS3666.[52] These small structural changes, *e.g.* propionyl instead of acetyl residues, isoleucine instead of leucine, originate from biosynthetic enzymes, accepting to a certain extent structurally related building blocks.

It could thus be considered very likely that extracts of *A. crenata* also contain further FR analogs. Furthermore, it is known that *Ardisia* species, other than *A. crenata* from the subgenus *Crispardisia*, also harbor symbiotic bacteria, of the genus *Burkholderia*, and are thus of special interest for our research.[15] Indeed, these plants were expected to be a further source of FR analogs. Finally, in our attempt to detect and isolate further FR derivatives, genome mining of publicly available bacterial genomes was thought to lead to the detection of biosynthetic genes related to those for FR and thus reveal further bacterial sources that could be exploited.

The following questions are addressed in Chapter 5.1:

1. Can we obtain further FR derivatives from *A. cre*nata and what is their structure?

→ Chapter 5.1.1 and 5.1.2

2. Do other *Ardisia* species also contain similar cyclic depsipeptides?

→ Chapter 5.1.3 and 5.1.4

3. Can we obtain culturable bacteria from culture collections, which harbor biosynthetic genes for depsipeptides identical or similar to those for FR and do they produce compounds under laboratory conditions?

→ Chapter 5.1.5

5.1 Discovery of new FR analogs and further natural sources of FR

Natural products mostly occur as a mixture of closely related metabolites. Often a major metabolite is accompanied by much smaller quantities of derivatives as described by Taniguchi et al. for YM.[52] Taniguchi *et al.* were able to work with a cultivable bacterium in a pharmaceutical industry framework (Yamanouchi Pharmaceutical Co) using an industrial scale fermenter. From the fermentation broth (80 L) they were able to isolate 1.2 g YM. Hence, the minor metabolites could still be isolated in yields > 30 mg, *i.e.* 35 mg for YM-280193, which facilitated their structure elucidation via NMR.[52]

In contrast, we were dependent on the material from a slow growing plant source in form of the perennial shrub of *A. crenata*, with rather demanding growing conditions (green house planting, humidity adapted, limited temperature range), which provided lower yields. One extraction cycle, which consisted of 200 g of dry leaf material provided about 10 mg of the major metabolite FR. Assuming quantities for FR analogs of about 3% of the FR amounts or lower, we expected less than 0.5 mg of putative FR analogs per extraction cycle, making structure elucidation via NMR experiments very difficult or in some cases even not feasible. Therefore, in some cases we applied different approaches allowing us to deduce merely putative structures. Derivatives present in higher amounts were obtained using activity-guided fractionation of *Ardisia* extracts, whereas mass spectrometry-based Global Natural Products Molecular Networking (GNPS) was used to detect new and very minor FR analogs. $LCMS^2$ based structural assignment was used to determine the putative structures of the latter.[174]

5.1.1 New FR analogs derived from *A. crenata* assisted by bioactivity-guided fractionation

NRPS machineries are often known for producing one major metabolite, and to a smaller extent also derivatives due to the "erroneous" loading of substrates. To obtain these minor metabolites we started an activity-guided isolation approach towards dried A. *crenata* leaves.

Dried plant leaves were coarsely grinded and extracted with methanol. Further purification steps included liquid-liquid extraction, RP-18 vacuum liquid chromatography and size exclusion chromatography. Final purification was done by HPLC with a semi-preparative RP-18 column. The elution system was water (eluent A) and methanol (eluent B). The crude peptide mixture (including FR and its analogs FR-1, FR-2, FR-3/FR-4) was derived with isocratic conditions (80% eluent B for 35 minutes). The separation of FR from its putative analogs was

achieved applying different further HPLC purification steps for each of the analogs. The isolation scheme is shown in **Scheme 5-1**.

FR-1 (**1**, formerly called AC-1) was isolated as described by Crüsemann & Reher *et al* (for 1D and 2D NMR data refer to Appendix **Figures 10-14 to 10-20, Scheme 10-2**).[10] In short, from 200 g of dried *A. crenata* leaves we obtained 0.7 mg of compound **1**.

HPLC conditions had to be adjusted to separate FR-2 (**2**, formerly called AC-0, manuscript including structure elucidation submitted) from **1** (for the complete isolation scheme refer to **Scheme 5-1, Chapter 3.4**, and Appendix **Figures 10-21 to 10-26, Scheme 10-3**). The composition of the mobile phase was changed from isocratic 80% eluent B to 75 % eluent B applying a 75:25 Nucleoshell RP^{18+} column (250 x 8 mm, 5 µm) for 20 minutes followed by a linear gradient from 75–100% eluent B within 15 minutes. The new cyclic depsipeptide, **2**, was obtained as white powder (about 0.2 mg from 200 g dried leaves, t_R = 23.7 min). The isolation process was repeated until 1.6 mg of **2** were collected for structure elucidation.

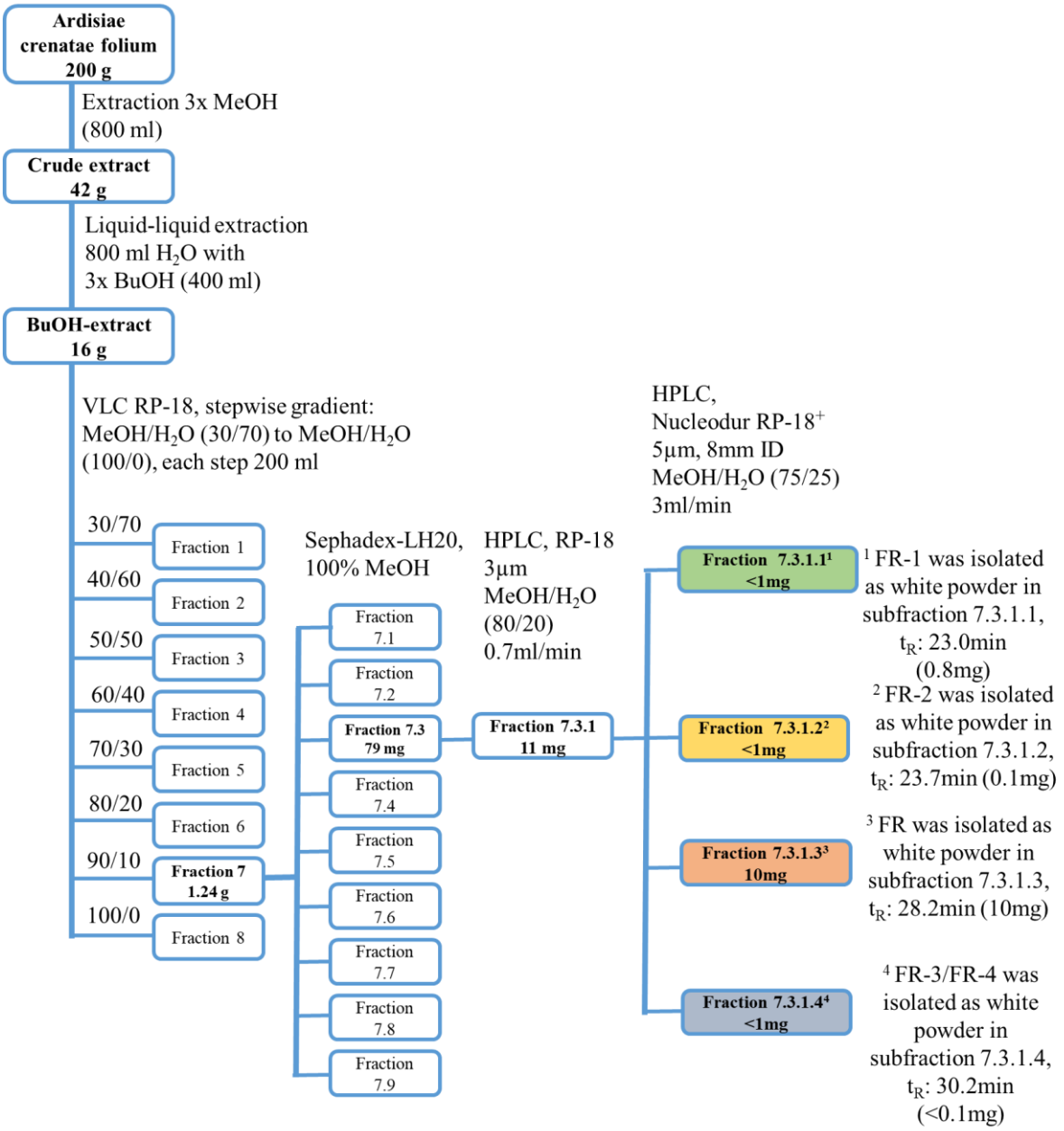

Scheme 5-1: Workflow chart for the extraction of FR- and analogs from dried leaves of the plant *A. crenata.*

5.1.1.1 Structure Elucidation of **1** (FR-1)

The molecular formula of **1** (FR-1) was determined to be $C_{50}H_{77}N_7O_{16}$, based on HR-FTICR mass spectral measurements (calcd. 1032.5500; obsd. 1032.5533) for $[M+H]^+$. Sequential fragmentation of the depsipeptide via collision induced dissociation demonstrated the structural similarities between FR and **1**, and further indicated that **1** differs from FR regarding the acyl residue of the respective *N*-acetylhydroxyleucine-1 (L') of FR (**Figure 5-2**). From extensive NMR spectral data analysis (^{1}H, ^{13}C, ^{1}H-^{1}H-COSY, ^{1}H-^{13}C-HSQC, ^{1}H-^{13}C-HMBC, ^{1}H-^{1}H-ROESY) we concluded for **1** that 3-hydroxypropionic acid is placed at this L' residue instead of acetic acid (as in FR, **Scheme 1-1, Scheme 5-2**) that we label as L* in the following.

Evidence was provided from (i) the lacking NMR signals for an acetate moiety at δ_H 2.23 / δ_C 22.6 as observed for FR, (ii) the additional NMR signals for the methylene groups CH_2-24 and CH_2-25 of which C-25 had to be substituted with oxygen, resulting in resonances at δ_H 2.80 / δ_C 37.3 and δ_H 3.93 / δ_C 59.5, respectively (1D-NMR and HSQC spectral data), as well as (iii) the COSY correlations of resonances for H_2-24 and H_2-25 to each other and HMBC correlations of both methylene group resonances to the neighboring amide carbonyl group (C-23, δ_C 174.1 ppm). For the complete assignment, please refer to **Table 5-1** and **Appendix Figures 10-14 to 10-21**. The position of the hydroxypropionyl moiety at NH-18 was also verified from the results of $LCMS^2$ experiments (**Figure 5-2**).

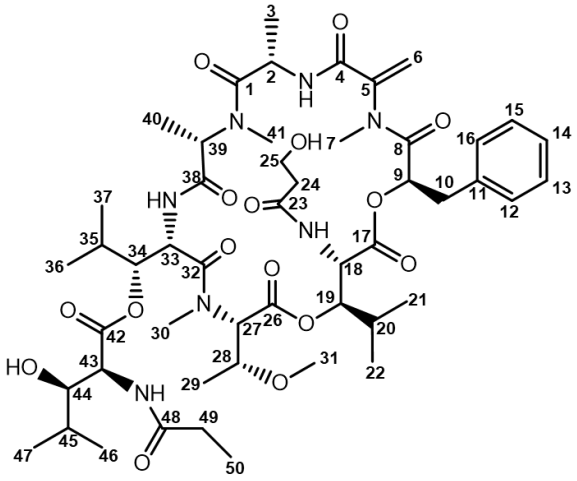

Scheme 5-2: Structure and numbering of C-atoms of **1** (FR-1).

Compound **1** (FR-1): 5 mg/kg dried plant material (predominantly leaves), $C_{50}H_{77}N_7O_{16}$, HR-FTICR (calcd. 1032.5500; obsd. 1032.5533) for $[M+H]^+$, $[\alpha]_D^{20}$=-35.4°·ml·dm^{-1}·g^{-1} (*c*=0.72g/ml in methanol), NMR data see **Table 5-1**.

Table 5-1: ^{1}H and ^{13}C NMR spectroscopic data of **1** (FR-1) in $CDCl_3$ (^{1}H: 600 MHz; ^{13}C: 150 MHz).

Residue[c]	**No C/H[b]**	**δ_C[a], mult**	**δ_H[a] (mult, *J* in Hz)**
Ala	1	172.5, C	–
	2	45.7, CH	4.91 (dq, 9.1, 6.6)
	2-NH	–	8.50 (d, 9.1)
	3	18.0, CH_3	1.39 (d, 6.6)
N-Me-Dha	4	163.8, C	–
	5	145.3, C	–
	6	107.2, CH_2	a: 5.34 (d, 2.2)
			b: 5.09 (d, 2.2)
	7	36.4, CH_3	3.18 (s)
Pla	8	167.9, C	–
	9	72.8, CH	5.22 (dd, 3.9, 8.9)
	10	36.7, CH_2	a: 3.12 (dd, 3.9, 14.9)
			b: 2.97 (dd, 8.9, 14.9)
	11	136.0, C	–
	12/16	129.5, CH	7.24 (d, 7.7)
	13/15	128.6, CH	7.30 (t, 7.7)
	14	127.0, CH	7.24 (t, 7.7)
N-(3-hydroxypropionyl)-β-HyLeu-1	17	169.0, C	–
	18	50.3, CH	5.25 (dd, 1.8, 10.0)
	18-NH	–	7.62 (d, 10.0)
	19	77.5, CH	5.14 (dd, 1.8, 10.0)
	20	29.0, CH	1.89 (m)
	21	18.86, CH_3	1.01 (d, 6.6)
	22	18.5, CH_3	0.86 (d, 6.6)
	23	174.1, C	–
	24	37.3, CH_2	2.80 (brt, 5.5)
	25	59.5, CH_2	3.93 (t, 5.5)
	25-OH	–	n.d. [d]
N,*O*-Me_2-Thr	26	166.4, C	–
	27	64.5, CH	4.06 (d, 9.9)
	28	72.4, CH	3.76 (m)
	29	16.3, CH_3	1.18 (d, 5.8)
	30	28.8, CH_3	2.70 (s)
	31	57.2, CH_3	3.41 (s)
β-HyLeu	32	171.1, C	–
	33	46.7, CH	5.34 (m)
	33-NH	–	6.78 (d, 10.0)
	34	77.0, CH	5.32 (m)
	35	30.5, CH	1.71 (m)
	36	19.4, CH_3	1.09 (d, 6.6)

	37	18.2, CH_3	0.83 (d, 6.6)
N-Me-Ala	38	170.1, C	–
	39	56.4, CH	4.69 (q, 6.6)
	40	14.3, CH_3	1.40 (d, 6.6)
	41	31.4, CH_3	2.88 (s)
N-Pr-*β*-HyLeu-2	42	170.2, C	–
	43	56.9, CH	4.56 (dd, 2.0, 7.8)
	43-NH	–	7.17 (d, 7.8)
	44	78.3, CH	3.73 (m)
	44-OH	–	6.84 (d, 4.4)
	45	30.0, CH	1.98 (m)
	46	20.5, CH_3	1.17 (d, 6.6)
	47	18.92, CH_3	0.88 (d, 6.6)
	48	174.8, C	–
	49	28.7, CH_2	a: 2.58 (dq, 14.8, 7.7)
			b: 2.49 (dq, 14.8, 7.7)
	50	10.0, CH_3	1.19 (t, 7.7)

[a] Assignments are based on extensive 1D and 2D NMR measurements (HMBC, HSQC, COSY). See also SI. [**b**] Numbers according to Scheme S2. [**c**] Residues: Ala = alanine, *N*-Me-Dha = *N*-methyldehydroalanine, Pla = 3-phenyllactic acid, *N*-(3-hydroxypropionyl)-Hle-1 = *N*-3-hydroxypropionylhydroxyleucine-1, *N*,*O*-Me2-Thr = *N*,*O*-dimethylthreonine, *β*-HyLeu = hydroxyleucine, *N*-Me-Ala = *N*-methylalanine, *N*-Pr-*β*-HyLeu 2= *N*-propionylhydroxyleucine-2**.** [d] n.d. = not determined.

5.1.1.2 Structure elucidation of **2** (FR-2)

The molecular formula of **2** was determined to be $C_{48}H_{73}N_7O_{15}$, based on HR-FTICR mass measurements (calcd. 988.5237; obsd. 988.5236) for $[M+H]^+$. Compared with FR, compound **2** thus had a molecular mass 14.01 Da lower, which indicated that compound **2** contains one methylene group less in its structure. Sequential fragmentation of the depsipeptide **2** via collision induced dissociation demonstrated close structural similarities between FR and **2**, and further indicated that **2** differs from FR regarding the acyl residue of *N*-propionylhydroxyleucine-2 (L’’’) of FR (**Figure 5-2**). In general, FR, **1**, and **2** have similar MS fragmentation patterns. The compounds can be distinguished by characteristic *Δm/z* values resulting from the different composition and incorporation of amino acids into the cyclic peptide backbone. In the first fragmentation step compound **2** loses the side chain, which can be seen in the MS spectra as a 171.10 Da fragment (*N*-acetylhydroxyleucine-2 = L^). Instead, for FR a *m/z* 185.11 Da fragment, *i.e*. *N*-propionylhydroxyleucine-2 is cleaved off. Comparison of further fragments also proved that in compound **2** the *N*-acyl residue at C-42 is different (see also **Scheme 5-3**). These MS data together with extensive NMR spectral data analysis (^{1}H, ^{13}C, ^{1}H-^{1}H-COSY, ^{1}H-^{13}C-HSQC, ^{1}H-^{13}C-HMBC) lead us conclude that in **2** an acetic acid moiety is placed at the side chain hydroxyleucine residue instead of the propionic acid, which is present at the analogous position of FR.

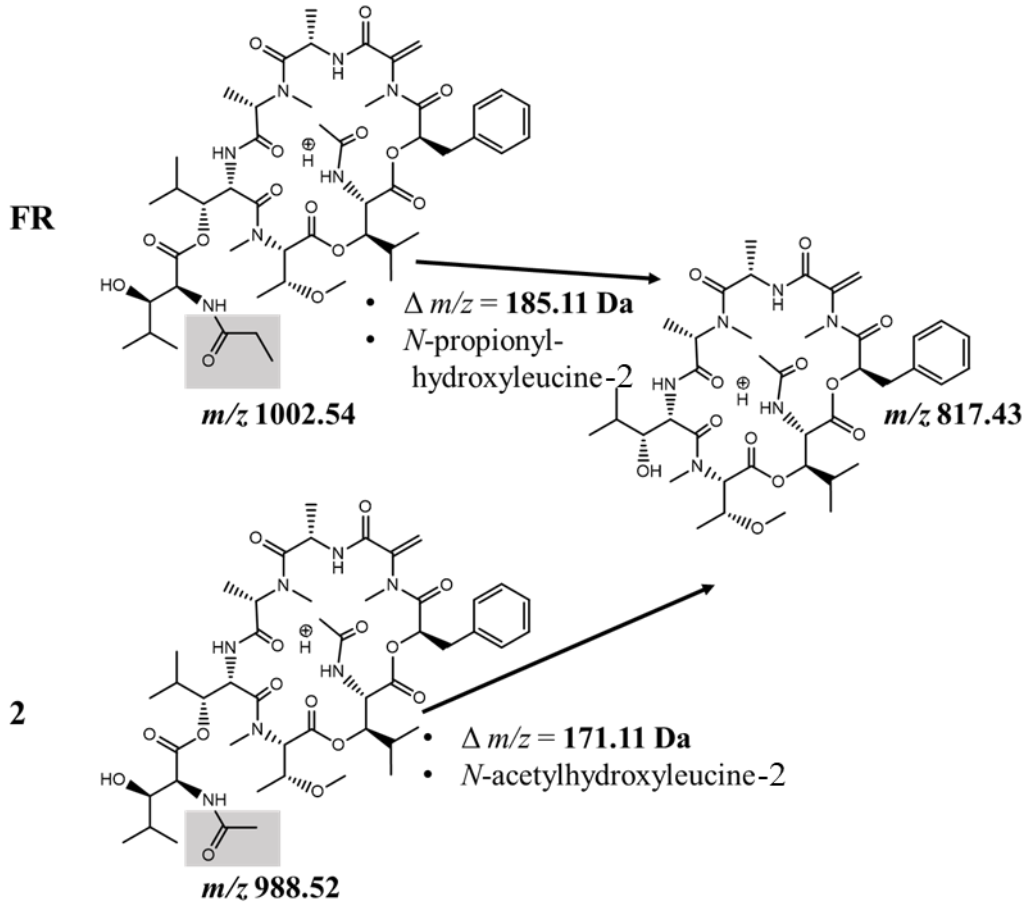

Scheme 5-3: Fragmentation pathways of first-generation (MS^2) product ions obtained from FR and compound 2 (FR-2). *m/z* 1002.54 (FR) or rather *m/z* 988.52 (**2**) lose their distinctive side-chain amino acid *N*-propionylhydroxyleucine-2 (FR) or *N*-acetylhydroxyleucine-2 = L^ (**2**), resulting in the formation of the same fragment, *i.e*. *m/z* 817.43 for both compounds.

Evidence was provided from (i) the lacking NMR signals for a propionate methylene CH_2-48, at δ_H 2.57 and δ_H 2.50 / δ_C 28.2 and a methyl moiety CH_3-49 at δ_H 1.19 / δ_C 10.1, respectively (as compared to FR (Appendix **Figures 10-21 to 10-26**), (ii) the additional NMR signals for the acetate methyl group CH_3-48 at δ_H 2.24 / δ_C 22.7, (1D-NMR and HSQC spectral data of **2**), as well as (iii) the HMBC correlation of methyl group resonance CH_3-48 to that of the neighboring amide carbonyl group (C-47, δ_C 171.4, **Table 5-2,** Appendix**, Figures 10-21 to 10-26**). The position of the acetate moiety at NH-42 was evident from HMBC correlations between the resonance for NH-42 (δ_H 7.27) and that of C-47 (δ_C 171.4). Further evidence for the site of modification of **2** as compared to FR came from $LCMS^2$ experiments (**Figure 5-2**).

Compound **2** (FR-2): 1mg/kg dried plant material (predominantly leaves), $C_{48}H_{73}N_7O_{15}$, HR-FTICR (calcd. 988.5237; obsd. 988.5236) for $[M+H]^+$, $[\alpha]_D^{20}$=-70.2°·ml·dm^{-1}·g^{-1} (*c*=0.58g/ml in methanol), NMR data see **Table 5-2**.

Table 5-2: ^{1}H and ^{13}C NMR spectroscopic data of **2** (FR-2) in $CDCl_3$ (^{1}H: 300 MHz; ^{13}C: 75 MHz).

Residue[c]	**No C/H[b]**	**δ_C[a], mult**	**δ_H[a] (mult, *J* in Hz)**
Ala	1	172.8, C	–
	2	45.9, CH	4.90 (m)
	2-NH	–	8.53 (d, 9.2)
	3	18.1, CH_3	1.39 (d, 6.8)
N-Me-Dha	4	164.0, C	–
	5	145.4, C	–
	6a	106.9, CH_2	a 5.32 (d, 2.0)
	6b	–	b 5.07 (d, 2.0)
	7	36.3, CH_3	3.15 (s)
Pla	8	167.9, C	–
	9	72.8, CH	5.21 (dd, 4.1, 8.2)
	10a	36.8, CH_2	a 3.11 (dd, 4.1, 14.8)
	10b	–	b 2.98 (dd, 8.2, 14.8)
	11	136.1, C	–
	12/16	129.7, CH	7.26[d]
	13/15	128.7, CH	7.29[d]
	14	127.1, CH	7.23[d]
N-Ac-*β*-HyLeu-1	17	169.4, C	–
	18	50.5, CH	5.26 (brd, 10.0)
	18-NH	–	7.54, (d, 10,0)
	19	77.8, CH	5.11 (brd, 10.0)
	20	29.0, CH	1.91 (m)
	21	19.1, CH_3	1.01 (d, 6.5)
	22	19.0, CH_3	0.85 (d, 6.6)
	23	171.6, C	–
	24	22.6, CH_3	2.23 (s)
N,*O*-Me_2-Thr	25	166.6, C	–
	26	64.6, CH	4.07 (d, 9.8)
	27	72.5, CH	3.74 (m)
	28	16.4, CH_3	1.17 (d, 5.8)
	29	28.9, CH_3	2.69 (s)
	30	57.3, CH_3	3.40 (s)
β-HyLeu	31	171.2, C	–
	32	46.8, CH	5.35 (d, 10.0)
	32-NH		6.73, (d, 10.0)
	33	77.4, CH	5.31 (m)
	34	30.7, CH	1.71 (m)
	35	19.5, CH_3	1.09 (d, 6.6)
	36	18.4, CH_3	0.83 (d, 6.6)
N-Me-Ala	37	170.1, C	–

	38	56.6, CH	4.71 (q, 7.0)
	39	14.4, CH_3	1.39 (d, 7.0)
	40	31.5, CH_3	2.88 (s)
N-Ac-*β*-HyLeu-2	41	170.3, C	–
	42	57.1, CH	4.53 (dd, 1.3, 7.6)
	42-NH	–	7.27 (m)
	43	78.3, CH	3.73 (m)
	43-OH	–	6.88 (d, 4.5)
	44	30.2, CH	1.98 (m)
	45	20.6, CH_3	1.17 (d, 6.6)
	46	18.7, CH_3	0.88 (d, 6.8)
	47	171.4, C	–
	48	22.7, CH_3	2.24 (s)

[a] Assignments are based on extensive 1D and 2D NMR measurements (HMBC, HSQC, COSY).. [**b**] Numbers according to Scheme S3. [**c**] Residues: Ala = alanine, *N*-Me-Dha = *N*-methyldehydroalanine, Pla = 3-phenyllactic acid, *N*-Ac-*β*-HyLeu1 = *N*-acetylhydroxyleucine-1, *N*,*O*-Me2-Thr = *N*,*O*-dimethylthreonine, *β*-HyLeu = hydroxyleucine, *N*-Me-Ala = *N*-methylalanine**.** , *N*-Ac-*β*-HyLeu2 = *N*-acetylhydroxyleucine-2. [**d**] overlaying resonances.

Structure activity relationship studies of **1** and **2** are described in **Chapter 5.2**.

5.1.2 New FR analogs derived from *A. crenata* detected via MS-based molecular networking

Wang *et al*. and Yang *et al*. demonstrated that global natural product social molecular networking (GNPS), an approach that organizes MS/MS data based on chemical similarity, is powerful to identify known and new natural products in a complex matrix.[174,189] This MS^2-based approach allows comparisons of fragmentation patterns of molecular ions leading to clustering of structurally similar compounds and their visualization in a molecular network. Here, molecular ions represent nodes, which are connected by edges, highlighting the structural relationships and similarities of the molecules. Molecular networking has been successfully applied to dereplicate natural products from complex extracts,[183] to compare the metabolomes of various natural product producers[190] and to improve and accelerate natural product isolation and structure elucidation workflows.[191–194] Further, molecular networking should not only dereplicate known molecules from complex mixtures, but also capture related analogs, making it most valuable this study.

We integrated molecular networking in our study applying the following workflow. First, *A. crenata* leaves were extracted with methanol and after liquid-liquid distribution, a butanolic extract was obtained. Subsequently, the butanol phase was further fractionated using vacuum liquid chromatography and size exclusion chromatography on Sephadex LH-20 and monitored by bioactivity (IP1 accumulation assay, **Chapter 3.7.4**). This depsipeptide containing fraction

was investigated applying MS²-based GNPS molecular networking to visualize the FR molecular family (**Figure 5-1**).

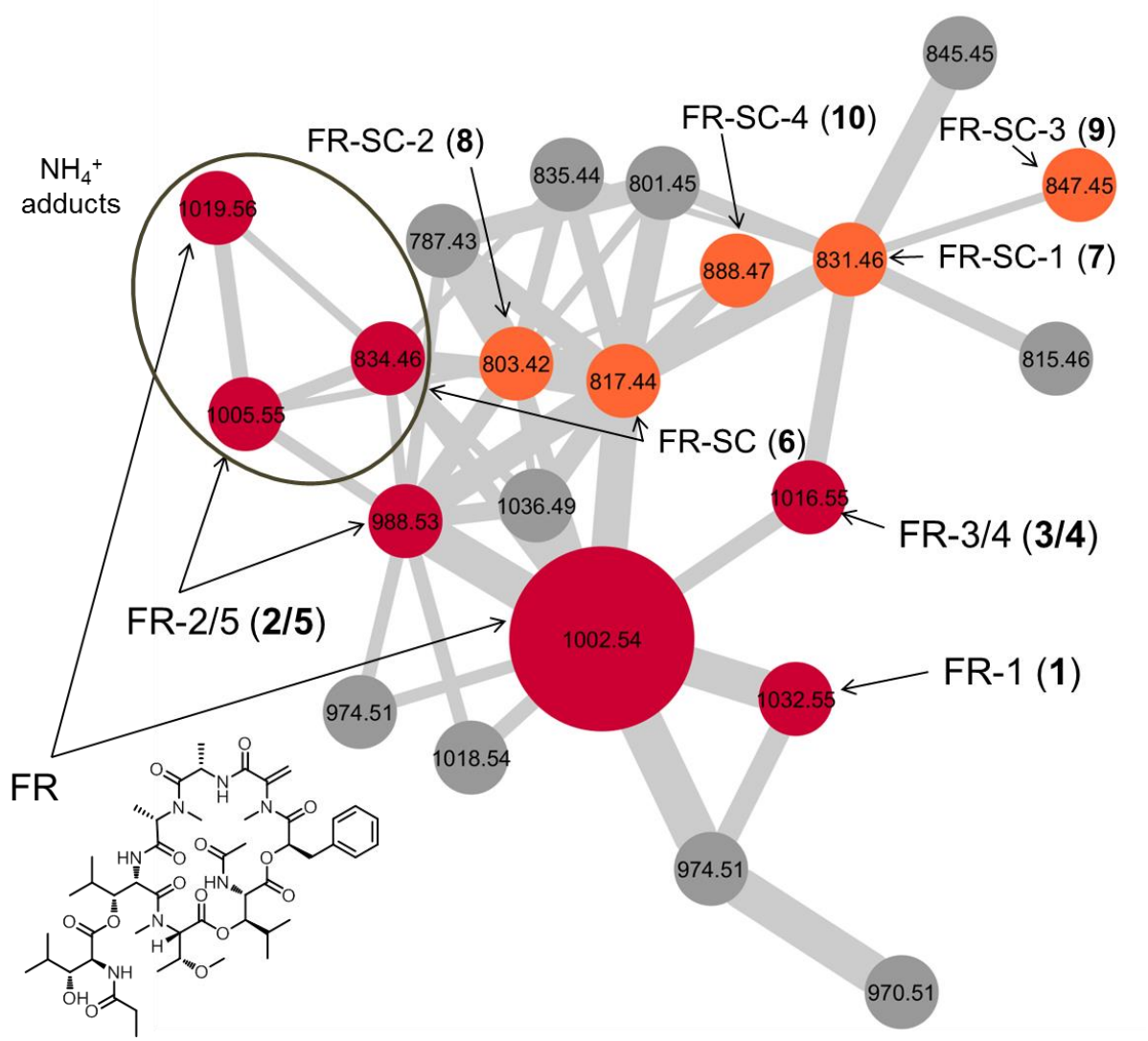

Figure 5-1: Molecular network of the FR molecular family from *Ardisia* leaves (Sephadex fraction 7-3). Nodes display distinct *m/z* features, corresponding to their parent mass. Width of edges is proportional to cosine. Sizes of the nodes correspond to extraction number of species (small nodes all originate from *A. crenata* extract, *m/z* 1002.54 and 1019.56 were also detected in *A. hanceana*, *A. villosa*, and *A. lucida*). Highlighted in red are FR and the structural-related derivatives FR-1 to FR-5 (**1-5)**. Orange-labeled nodes display putative FR analogs **6-10**, lacking the side chain *N*-propionylhydroxyleucine2. For (putative) structures of **1-10**, see **Schemes 5-5 and 5-6**.

The molecular network of the FR family (**Figure 5-1**) shows 22 nodes. The protonated FR (*m/z* 1002.54) molecular ion clusters with those of **1** (*m/z* 1032.55)[10] and **2** (*m/z* 988.53), described in **Chapter 5-1** , and additionally with those of analogous peptides, *e.g. m/z* 974.51, 1016.55, and 817.44.

In order to deduce putative structures of to date unknown FR derivatives, one characteristic MS fragmentation pathway, observed for proton adducts of FR and presumably all putative FR analogs, was thoroughly analyzed and is shown in **Scheme 5-4**. In a first step, the core structure

is cleaved between alanine and *N*-methylalanine and linearized. In cyclic peptides breakage of the amide (or ester bond for depsipeptides, respectively) is reported to lead to the formation of a linear peptide with a C-terminal oxazolone ring[195], which sequentially loses amino acids. This is clearly evident when LCMS² spectra of FR are compared with those of the known and structurally proven analogs **1**[10] and **2**. The different acylations in **1** and **2** lead to a characteristic change in the mass of the respective fragments (**Scheme 5-4**).

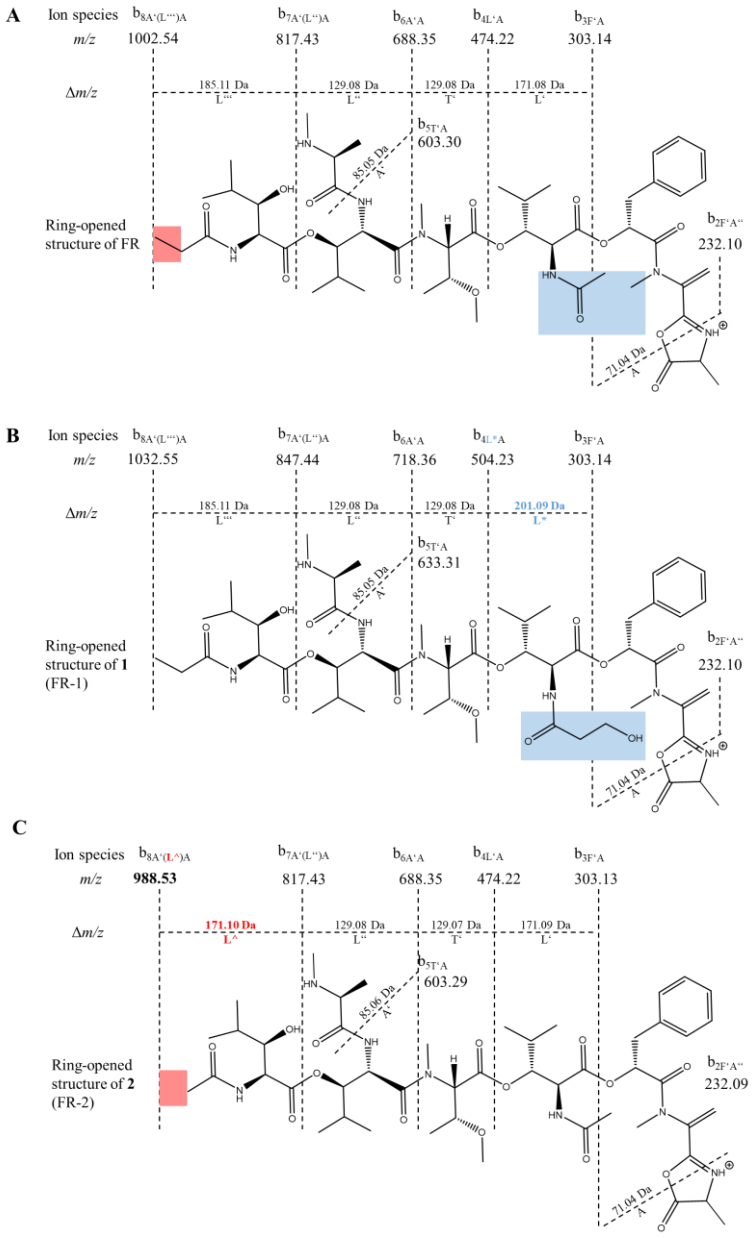

Scheme 5-4: (**A**) Fragmentation pathway of FR900359 (FR). FR ring structure is first cleaved, followed by sequential loss of amino acids see also **Scheme 1-1** (*m/z* 1002.54 → (-L''') *m/z* 817.44 → (-L'') *m/z* 688.35 →(-A') *m/z* 603.30 → (-T') *m/z* 474.22 → (-L') *m/z* 303.14 →(-A) *m/z* 232.10). Peptide fragment ions are labeled in one-letter amino acid code, according to a nomenclature system described in **Chapter 3.4.1.3**. L''' = *N*-propionylhydroxyleucine-2, L'' = hydroxyleucine, A' = *N*-methylalanine, T' = *N,O*-dimethylthreonine, L' = *N*-acetylhydroxyleucine-1, A = alanine, F' = phenyllactic acid, A'' = *N*-methyldehydroalanine. (**B**) Fragmentation pathway of **1** (FR-1). L* = *N*-3-hydroxypropionylhydroxyleucine-1. (**C**) Fragmentation pathway of **2** (FR-2). L^ = *N*-acetylhydroxyleucine-2.

Knowledge on the typical MS fragmentation pattern of FR and related compounds, now allowed to search MS data for the presences of further derivatives. In-depth analysis of the LCMS² data revealed next to the compound peak of compound **2** a peak of compound **5**. Both compounds share the same *m/z* feature of 988.53 for the molecular ion at, but display different fragmentation patterns and retention times. Whereas compound **2** elutes at t_R 4.0 minutes (HPLC conditions see **Chapter 3.6.1.3**), the isomer (**5**) elutes slightly earlier (t_R = 3.7 minutes). We compared the MS² spectra of **5**, **2** and of FR. According to **Scheme 5-4**, the first fragmentation step is the cleavage of the side-chain (for FR *N*-propionylhydroxyleucine-2 = L'''). As **2** differs from FR in the side chain, the loss of the latter leads to the same *m/z* 817.44 for FR and **2** (**Figure 5-2**). In contrast, **5** must have the same side chain as FR, as after cleaving of L''', **5** displays *m/z* 803.42, which is equivalent to the fragment of FR (*m/z* 817.44), except that it has a 14.01 Da lower mass. The subsequent three fragmentation steps also result in equivalent fragment ions for **5** and FR, again with a 14.01 Da lower mass for the ions of **5**. The fourth fragmentation step finally allowed to distinguish between FR and **5**. While a Δ*m/z* 129.08 (*N,O*-dimethylthreonine = T') loss from the *m/z* 603.30 ion of FR resulted in the *m/z* 474.22 ion, for **5** a Δ*m/z* 115.07 loss of the corresponding *m/z* 589.29 ion lead to the same *m/z* 474.22 ion. Thus, we concluded that **5** differs from FR in the T' building block (T° for **5**), which was further supported by other fragmentation pathways. Based on the NRPS origin of FR and its analogs, for T° three possible and reasonable structures remain, *i.e. N*-methylthreonine, *O*-methylthreonine and *N,O*-dimethylserine (Appendix **Scheme 10-4**). So, LCMS² analysis enabled us to reduce the number of possible structures for **5** from several hundred to three. Compound **5** is only present in minute amounts in the extract and could not be isolated yet.

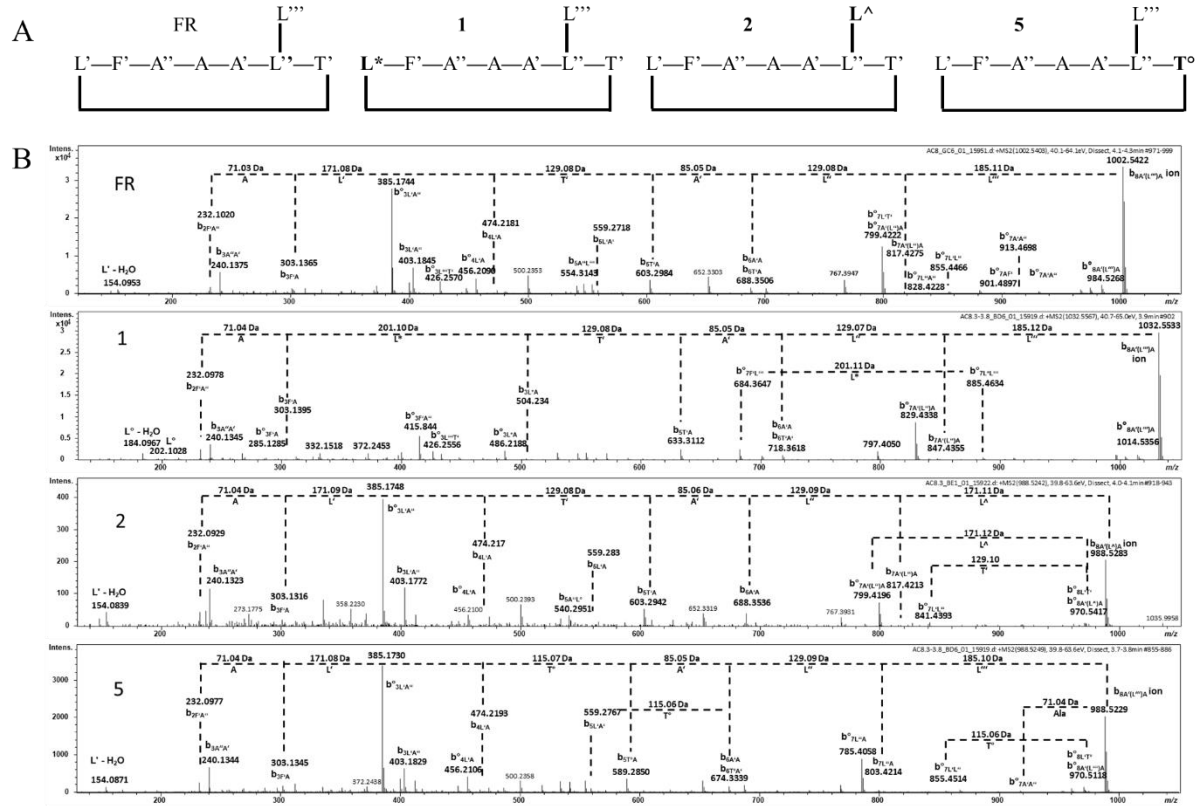

Figure 5-2: (**A**) Schematic structure of FR900359 (FR), FR-1 (**1**), FR-2 (**2**), and putative FR-5 (**5**). Peptide fragment ions are labeled in one-letter amino acid code, according to a nomenclature system described in Chapter 3.4.1.3. b° = b-ion with loss of water. L' = *N*-acetylhydroxyleucine-1, L* = *N*-3-hydroxypropionyl-hydroxyleucine-1, F' = phenyllactic acid, A'' = *N*-methyldehydroalanine, A = alanine, A' = *N*-methylalanine, L'' = hydroxyleucine, T' = = *N*,*O*-dimethylthreonine, L''' = *N*-propionylhydroxyleucine-2, L^ = *N*-acetylhydroxyleucine-2, T° = three possibilities, *i.e.* *N*-methylthreonine, *O*-methylthreonine and *N*,*O*-dimethylserine (please also refer to Scheme S2. (**B**) Comparison of first-generation, product-ion spectra of FR, **1**, **2**, and **5**; $[M+H]^+$. **1** has a different acylation residue at L'; instead of an acetate residue (L' in FR), **1** contains of a 3-hydroxypropionate residue (L*). **2** has a different acylation residue at L'''; instead of an propionate residue (L''' in FR), **2** contains of an acetate residue (L^). **5** differs from FR in the amino acid *N*,*O*-dimethylthreonine (T'). **5** cannot be assigned unambiguously based on LCMS² analysis only.

In a former study we assigned *m/z* 817.44 as putative biosynthetic FR-precursor FR-SC (**6**), standing for FR without the *N*-propionylhydroxyleucine-2 side-chain.[10] Interestingly, a similar congener of the structurally related YM (YM lacking the side chain = YM-280193) was characterized, pointing to an analogous biosynthetic route.[196] Apart from compound **6** (*m/z* 817.44) further compounds having only the cyclic part of FR, but with subtle differences were observed. Analysis of fragments at *m/z* 831.46 (**7**, FR-SC1), *m/z* 803.43 (**8**, FR-SC2), *m/z* 847.45 (**9**, FR-SC3), and *m/z* 888.47 (**10**, FR-SC4), clustering with *m/z* 817.44 evidenced this assumption and suggested that there are a multitude of further FR derivatives differing from the major metabolite by lacking the side chain and some features of the cyclic part of FR (**Figure 5-3**).

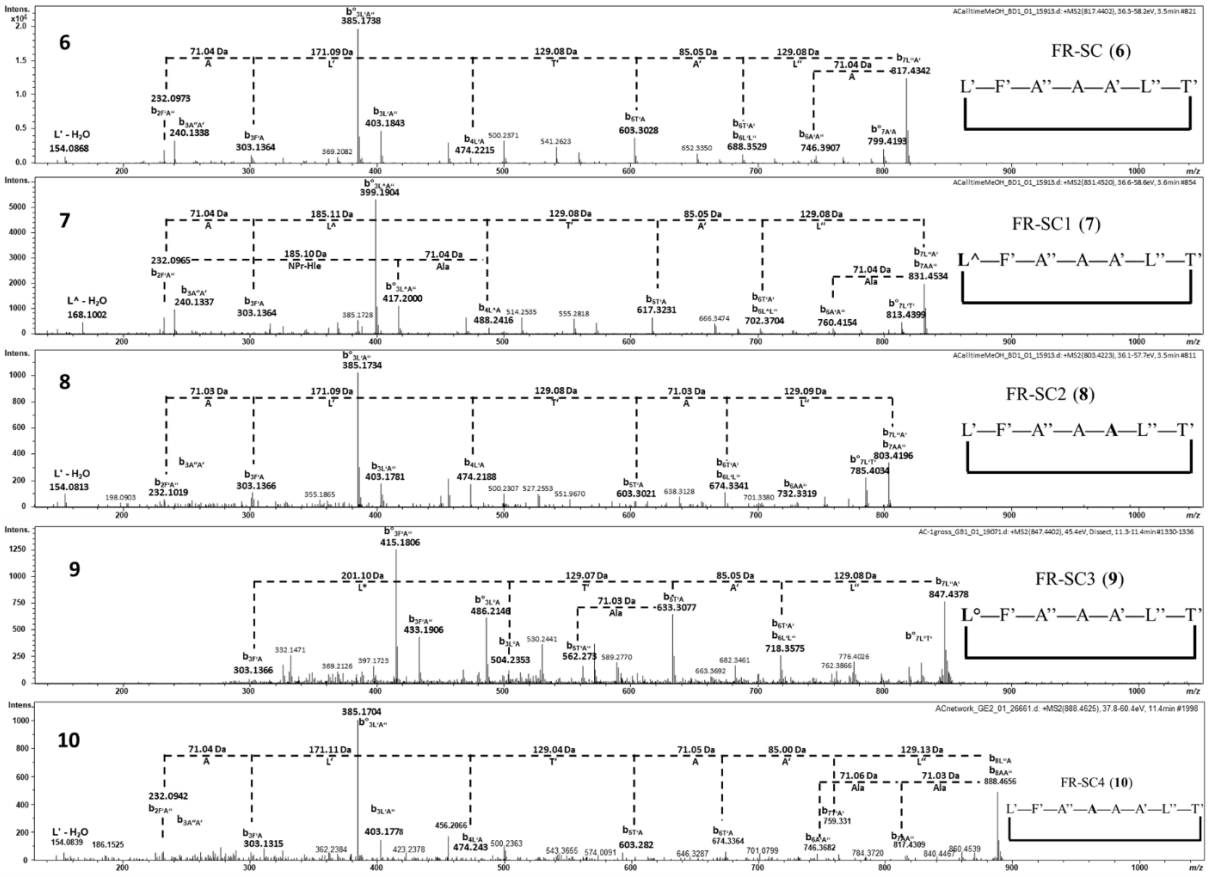

Figure 5-3: Schematic structure of FR-SC (**6**), and derivatives thereof **7**, **8**, **9**, and **10** on the right side. FR derivatives **6-10** are all lacking the side chain L''' = *N*-propionylhydroxyleucine-2. Peptide fragment ions are labeled in one-letter amino acid code, according to a nomenclature system described in **Chapter 3.4.1.3**. b° = b-ion with loss of water. L' = *N*-acetylhydroxyleucine-1, F' = phenyllactic acid, A'' = *N*-methyldehydroalanine, A = alanine, A' = *N*-methylalanine, L'' = hydroxyleucine, T' = *N,O*-dimethylthreonine, L^ = *N*-propionylhydroxyleucine-1, L° = N-3HPr-Hle = *N*-3hydroxypropionylhydroxyleucine-1. (**B**) Comparison of first-generation product-ion spectra of **6-9**; $[M+H]^+$. **6**, **7**, and **9** have different acylation residues at L'; instead of an acetate residue (L' in **6**), **7** contains of a propionate residue (L^) and **9** contains of a 3-hydroxypropionate residue (L°). **8** differs from **6** in the amino acid *N*-methylalanine (A'). A' is substituted in **8** by alanine (A).

In that way we assigned **7** to be the cyclic part of **3** (for structure elucidation refer to following pages) with an *N*-propionylhydroxyleucine-1 instead of *N*-acetylhydroxyleucine-1, **8** to be the cyclic part of **5** with a modified *N,O*-dimethyl-threonine residue lacking one methylene group, **9** to be the precursor of **1** thus harboring *N*-3-hydroxypropionylhydroxyleucine-1 instead of *N*-acetylhydroxyleucine-1, and most interestingly **10** to be an analog of **6** with an additional alanine moiety in its cyclic backbone (**Scheme 5-5**). These putative derivatives suggest that the trans-esterification step, which attaches the side chain to the cyclic core peptide is the last step in the biosynthesis. Compound **10** also demonstrates unexpected flexibility of the FR-NRPS, as apparently module 5 has to be used twice to incorporate an additional alanine unit.

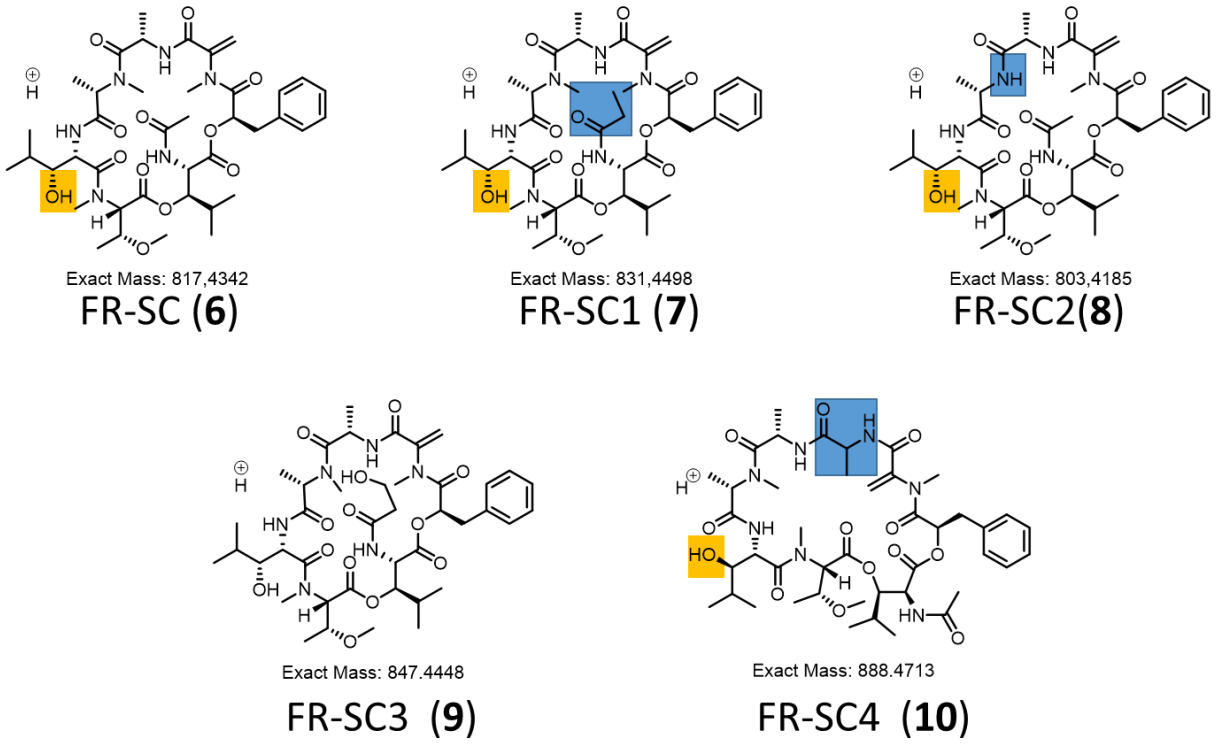

Scheme 5-5: Putative structures of **6**, **7**, **8**, **9**, and **10**. All FR derivatives shown lack the *N*-propionylhydroxyleucine2 side chain (yellow box, Scheme S1). Putative structural differences from **6** are highlighted (blue box).

These results encouraged us to analyze further FR analogs clustering with FR in the MS²-based network, *i.e.*, compounds **3** and **4**. From the molecular network an ion with *m/z* 1016.55 (**Figure 5-1**) attracted our attention, because it directly clustered with the FR ion (*m/z* 1002.54). Investigation of the extracted ion chromatogram of the LCMS measurement for *m/z* 1016.55 of the isolated sample indicated, that it was not a single compound, but consisted of two isomeric compounds as evident from slightly different retention times (Δt_R 0.2 min). We named these compounds FR-3 (**3**) and FR-4 (**4**). ^{1}H-NMR spectroscopy revealed that the compounds were present in in a 1:1 mixture (Appendix **Figures 10-27 to 10-31**) making an assignment of resonances impossible at this stage. The molecular formulae of **3** and **4** were determined to be $C_{50}H_{77}N_7O_{15}$ (calcd. 1016.5550; obsd. 1016.5544 (**3**) and 1016.5553 (**4**), respectively) for $[M+H]^+$. These results showed a mass difference of 14.01 Da between FR and compounds **3** and **4**, and suggested an additional methylene group in the structures of **3** and **4**. In-depth MS² analysis allowed us to analyze **3** and **4** separately. It revealed that FR, **3** and **4** can be distinguished by different *Δm/z* values resulting from differently modified amino acids that were sequentially lost, similar as above described for **2** and **5** (**Figure 5-4**). In the fifth fragmentation step, the *m/z* 474.22 of FR loses *N*-acetyl-hydroxyleucine1 (L', *Δm/z* 171.08 Da)

to yield the *m/z* 303.14 ion. The corresponding *m/z* 488.24 ion of **3** loses *Δm/z* 185.10 Da fragment to give the same *m/z* 303.14 ion. Thus, together with further evidence from other fragmentation pathways, we conclude that **3** has a modified L' residue, designated as L° in the following. Taking biosynthetic considerations into account reduced the possible structures of L° to either *N*-propionylhydroxyleucine-1 or *N*-acetyl-hydroxyhomoleucine-1.

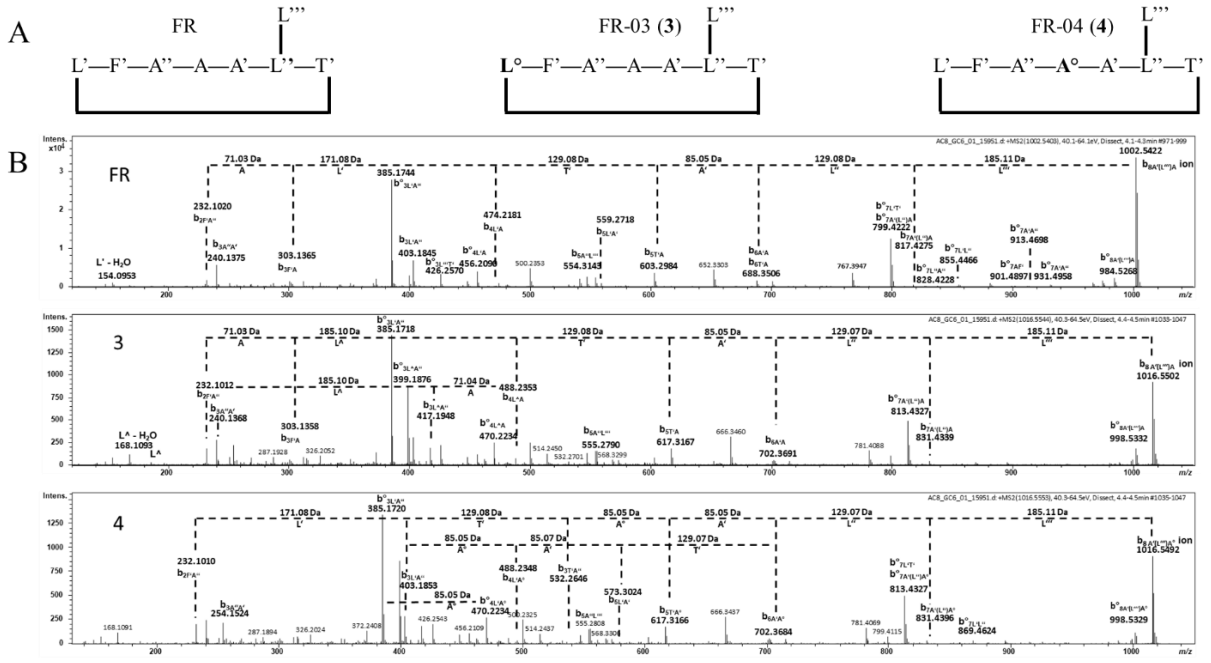

Figure 5-4: (**A**) Schematic structure of FR, FR-3 (**3**), and FR-4 (**4**). Peptide fragment ions are labeled in one-letter amino acid code, according to a nomenclature system described in **Chapter 3.4.1.3.** b° = b-ion with loss of water. L' = *N*-acetylhydroxyleucine-1, L° = *N*-propionylhydroxyleucine-1, F' = phenyllactic acid, A'' = *N*-methyldehydroalanine, A° = homoalanine, A = alanine, A' = *N*-methylalanine, L'' = hydroxyleucine, T' = *N,O*-dimethylthreonine, L''' = *N*-propionylhydroxyleucine-2. (**B**) Comparison of first-generation, product-ion spectra of FR, **3**, and **4**; $[M+H]^+$. Compared to FR, **3** has a different acylation residue at L'; instead of an acetate residue (L' in FR), **3** contains of a propionate residue (L°). **4** differs from FR in the amino acid alanine (A). A is substituted in **4** by homoalanine (A°).

Compound **4** differs from FR concerning the alanine residue (A) (R_3 in **Scheme 5-6**). Instead of alanine, **4** contains a residue with a 14.01 Da higher mass, *i.e.* homoalanine or alternatively a *N*-methylalanine building block, as revealed from the $LCMS^2$ data **(Supporting information**). This was again evident from different *Δm/z* values resulting from sequential loss of amino acids. Compound **4**, but not FR produced a fragment with *m/z* 470.22. Instead of a *Δm/z* 71.03 Da (alanine) loss as for FR, **4** loses a *Δm/z* 85.05 Da fragment (A° = homoalanine or *N*-methylalanine) leading to the same *m/z* 385.17 fragment. Analysis of further fragmentation pathways supported this assumption (see also **Figure 5-4**). Therefore we could reduce the number of possible structures for **3** and **4** to two reasonable structures for each compound.

Applying a further HPLC purification step we were finally able to isolate **3** as white powder only containing minor amounts of **4** (ratio **3** / **4** = 3 / 1). After recording ^{1}H NMR and ^{1}H-^{13}C-HSQC spectra, we were able to unambiguously assign the structures of **3** and **4** (**Table 5-3,** Appendix **Scheme 10-5**).

Table 5-3: ^{1}H and ^{13}C NMR spectroscopic data of **3** (FR-3) and **4** (FR-4) in $CDCl_3$ (^{1}H: 600 MHz; ^{13}C: 150 MHz).

	FR-3 (**3**)				FR-4 (**4**)		
Residue[c]	**No C/H[b]**	**δ_C[a], mult**	**δ_H[a] (*J* [Hz])**	**Residue[c]**	**No C/H[b]**	**δC[a], mult**	**δH[a] (*J* [Hz])**
Ala	1	172.6, C	–	Homo-Ala	1	172.2, C	–
	2	45.6, CH	4.91 (dq, 9.1, 6.7)		2	51.4, CH	4.69 (m)
	2-NH	–	8.52 (d, 9.1)		2-NH	–	8.49 (d, 9.1)
	3	18.0, CH_3	1.41 (d, 6.7)		3a	26.4, CH_2	a 1.78, m
N-Me-Dha	4	164.0, C	–		3b		b 2.00, m
	5	145.5, C	–		4	10.3, CH_3	0.97 (t, 7.2)
	6a	106.9, CH_2	a 5.32 (d, 2.2)	*N*-Me-Dha	5	164.4, C	–
	6b	–	b 5.07 (d, 2.2)		6	145.5, C	–
	7	36.3, CH_3	3.16 (s)		7a	106.9, CH_2	a 5.37 (d, 2.2)
Pla	8	167.9, C	–		7b	–	b 5.09 (d, 2.2)
	9	72.8, CH	5.19 (dd, 4.1, 8.3)		8	36.3, CH_3	3.20 (s)
	10a	36.8, CH_2	a 3.11 (dd, 4.1, 14.8)	Pla	9	167.9, C	–
	10b	–	b 2.98 (dd, 8.3, 14.8)		10	72.7, CH	5.21 (dd, 4.1, 8.3)
	11	136.1, C	–		11a	36.8, CH_2	a 3.11 (dd, 4.1, 14.8)
	12/16	129.4, CH	7.26[d]		11b	–	b 2.98 (dd, 8.3, 14.8)
	13/15	128.8, CH	7.32[d]		12	136.1, C	–
	14	127.2, CH	7.25[d]		13/17	129.7, CH	7.26[d]
N-Pr-*β*-HyLeu-1	17	169.4, C	–		14/16	128.7, CH	7.29[d]
	18	50.3, CH	5.30 (dd, 1.3, 10.0)		15	127.1, CH	7.23[d]
	18-NH	–	7.45, (d, 10,0)	*N*-Ac-*β*-HyLeu-1	18	169.4, C	–
	19	77.8, CH	5.12 (dd, 1.3, 10.0)		19	50.5, CH	5.26 (dd, 1.3, 10.0)
	20	29.1, CH	1.91 (m)		19-NH	–	7.55, (d, 10,0)
	21	18.9, CH_3	1.01 (d, 6.8)		20	77.8, CH	5.12 (dd, 1.3, 10.0)
	22	18.8, CH_3	0.85 (d, 6.8)		21	29.0, CH	1.89 (m)
	23	175.6, C	–		22	19.1, CH_3	1.01 (d, 6.8)
	24a	28.7, CH_2	2.59 (m)		23	19.0, CH_3	0.85 (d, 6.8)
	24b		2.53 (m		24	171.6, C	–
	25	10.3, CH_3	1.24 (m)		25	22.6, CH_3	2.26 (s)
N,*O*-Me_2-Thr	26	166.6, C	–	*N*,*O*-Me_2-Thr	26	166.6, C	–
	27	64.4, CH	4.08 (d, 9.8)		27	64.6, CH	4.07 (d, 9.8)
	28	72.3, CH	3.76 (m)		28	72.5, CH	3.75 (m)
	29	16.2, CH_3	1.18 (d, 4.8)		29	16.2, CH_3	1.23, (d, 4.8)

	30	28.8, CH_3	2.70 (s)		30	28.9, CH_3	2.70 (s)
	31	57.0, CH_3	3.41 (s)		31	57.3, CH_3	3.41 (s)
β-HyLeu	32	171.4, C	–	*β*-HyLeu	32	171.4, C	–
	33	46.9, CH	5.36 (d, 9.9)		33	46.8, CH	5.38 (d, 9.9)
	33-NH		6.75, (d, 9.9)		33-NH		6.70, (d, 9.9)
	34	77.1, CH	5.31 (m)		34	77.1, CH	5.31 (m)
	35	30.4, CH	1.75 (m)		35	30.7, CH	1.72 (m)
	36	19.3, CH_3	1.10 (d, 6.7)		36	19.5, CH_3	1.10 (d, 6.7)
	37	18.3, CH_3	0.83 (d, 6.7)		37	18.3, CH_3	0.83 (d, 6.7)
N-Me-Ala	38	170.1, C	–	*N*-Me-Ala	38	170.1, C	–
	39	56.5, CH	4.71 (q, 6.8)		39	56.4, CH	4.69 (q, 6.8)
	40	14.2, CH_3	1.41 (d, 6.8)		40	14.4, CH_3	1.41 (d, 6.8)
	41	31.3, CH_3	2.90 (s)		41	31.5, CH_3	2.88 (s)
N-Pr-*β*-HyLeu-2	42	170.4, C	–	*N*-Pr-*β*-HyLeu-2	42	170.4, C	–
	43	56.8, CH	4.57 (dd, 1.8, 7.8)		43	57.0, CH	4.55 (m)
	43-NH	–	7.25 (d, 7.8)		43-NH	–	7.17 (d, 7.8)
	44	78.3, CH	3.73 (m)		44	78.4, CH	3.73 (m)
	44-OH	–	6.87 (d, 4.2)		44-OH	–	6.81 (d, 4.3)
	45	30.0, CH	1.99 (m)		45	30.1, CH	1.98 (m)
	46	20.3, CH_3	1.17 (6.7)		46	20.6, CH_3	1.17 (6.7)
	47	18.7, CH_3	0.89 (6.7)		47	18.7, CH_3	0.88 (6.7)
	48	174.9, C	–		48	174.9, C	–
	49a	28.8, CH_2	a 2.57 (dq, 14.9, 7.5)		49a	28.8, CH_2	2.57 (dq, 14.9, 7.5)
	49b		b 2.50 (dq, 14.9, 7.5)		49b		2.50 (dq, 14.9, 7.5)
	50	10.0, CH_3	1.19 (t, 7.5)		50	10.1, CH_3	1.19 (t, 7.5)

[**a**] Assignments are based on extensive 1D and 2D NMR measurements (HMBC, HSQC, COSY). ^{13}C-NMR spectra were recorded at 150 MHz. [**b**] Numbers according to Scheme S1. [**c**] Residues: Ala = alanine, Homo-Ala = homoalanine *N*-Me-Dha = *N*-methyldehydroalanine, Pla = 3-phenyllactic acid, *N*-Ac-*β*-HyLeu-1= *N*-acetylhydroxyleucine-1, *N*-Pr-*β*-HyLeu-1= *N*-propionylhydroxyleucine-1 *N*,*O*-Me2-Thr = *N*,*O*-dimethylthreonine, *β*-HyLeu = hydroxyleucine, *N*-Me-Ala = *N*-methylalanine, *N*-Pr-*β*-HyLeu-2 = *N*-propionylhydroxyleucine-2.[d] overlaying resonances.

Evidence for the structure of **3** was provided from (i) the lacking NMR signals for an acetate moiety at δ_H 2.23 / δ_C 22.6 as observed for FR, (ii) the additional NMR signals for the methylene group CH_2-24 and methyl group CH_3-25, resulting in resonances at δ_H 2.55 / δ_C 28.7 and δ_H 1.24 / δ_C 10.1, respectively (**Table 5-3**), as also, (iii) the COSY correlations of H_2-24 and H_2-25 (Appendix **Figure 10-29**) and HMBC correlations (Appendix **Figure 10-31**) of H_2-24 and H_2-25 to the neighboring amide carbonyl group (C-23, δ_C 175.6 ppm). Thus, we finally concluded that compound **3** contains a *N*-propionylhydroxyleucine-1 (L°) instead of *N*-acetylhydroxyleucine-1 (L') in the cyclic backbone. Interestingly this means that FR-3 (**3**) would have the same planar structure as sameuramide, a compound previously isolated from a marine ascidian.[29] After the assignment of **3**, we could assign **4** from the NMR spectra of the 1:1 mixture (Appendix **Figures 10-32, 10-33**).

Evidence for the homoalanine residue of **4** was provided from (i) the shifted methine αCH-2 δ_H 4.69 / δ_C 51.4 as compared to δ_H 4.90 / δ_C 45.9 for FR (ii) the additional NMR signals for the methylene group CH_2-3a/3b (δ_{Ha} 1.78 / δ_{Hb} 2.00 / δ_C 26.4) and methyl group CH_3-4 (δ_H 0.97 / δ_C 10.3), respectively (**Table 5-3**), as well as (iii) the COSY correlations of H-2 to H_2-3 and H_2-3 and H_3-4, and HMBC correlations of H_2-4 to the neighboring methine αCH-2 (δ_H 4.69 / δ_C 51.4). Thus, we concluded for **4** to contain homoalanine (A°) instead of alanine (A) (**Scheme 5-6**).

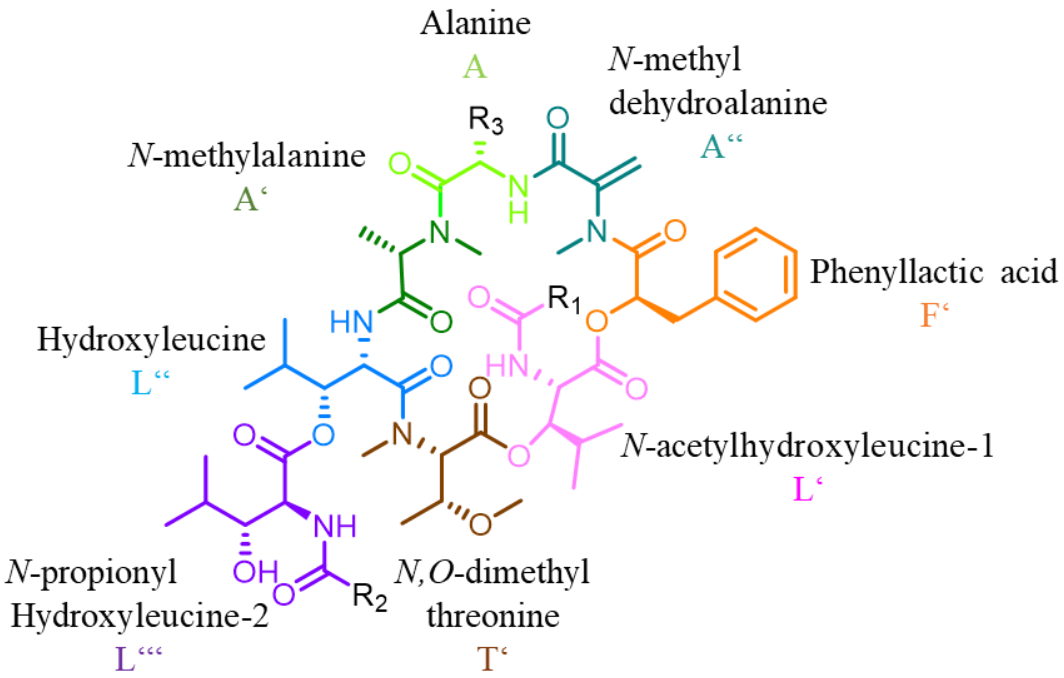

FR900359	$R_1 = CH_3$	$R_2 = CH_2CH_3$	$R_3 = CH_3$
FR-1 (**1**)	$R_1 = CH_2CH_2OH$	$R_2 = CH_2CH_3$	$R_3 = CH_3$
FR-2 (**2**)	$R_1 = CH_3$	$R_2 = CH_3$	$R_3 = CH_3$
FR-3 (**3**)	$R_1 = CH_2CH_3$	$R_2 = CH_2CH_3$	$R_3 = CH_3$
FR-4 (**4**)	$R_1 = CH_3$	$R_2 = CH_2CH_3$	$R_3 = CH_2CH_3$

Scheme 5-6: Structures of FR and isolated FR analogs **1-4** from *Ardisia crenata*. (Non-proteinogenic) amino acid building blocks colored and annotated for FR, including one-letter code.

5.1.3 Synergistic effects of *Ardisia crenata* fractions towards FR activity

Despite the activity of FR to perturb $G\alpha_q$ signaling, further *Ardisia* plant derived products may excert activity and/or interact with the bioactivity of FR. We (Tobias Benkel, MSc student, Kostenis lab) thus aimed to evaluate potential effects of other components in *Ardisia* leaves regarding the capability to blunt $G\alpha_q$ signaling and to interact with the activity of FR. For this purpose, we isolated and purified FR from dried leaves of *A. crenata* and collected all fractions received during the different extraction steps (**Scheme 5-1**). To confirm the potency of the isolated FR we applied the previously described functional assay (IP1 accumulation assay, **Chapter 3.7.4**). Agonist activation was completely inhibited by pre-incubation with isolated FR in a concentration-depended manner. The calculated $LogIC_{50}$ values are in line with former reported potency of FR, which hereafter forms the basis of the following synergism trails.

To determine the synergistic effects on FR we also applied the IP1 accumulation assay. All collected fractions have been tested in absence and presence of a non-active concentration of FR (10^{-7} M). All compounds have been tested once (n = 1) at first and repeated in case of any conspicuities (n = 2). For none of the tested compounds a synergistic effect on the potential to perturb the Carbachol induced IP1 production could be observed. Nonetheless, some Fractions (VLC 4, 5, 6 and S1, 5) revealed inhibitory potential on their own (Appendix **Figures 10-34 to 10-37**).

This should be further evaluated and might ultimately lead to novel compounds which could be superior to FR.

5.1.4 Detection of FR by molecular networking in several *Ardisia* species

Ardisia is one of the largest genera within the family Primulaceae and comprises approximately 500 species.[197] Especially the subgenus *Crispardisia* is of interest, because all of these plants (*e.g. A. crispa, A. hanceana, A. mamillata,* and *A. villosa*) are known to have bacterial nodules that harbor endosymbiotic bacteria.[3]

Leaves of several species belonging to *Crispardisia*, *i.e. A. hanceana, A. villosa*, and *A. mamillata* were collected in 2016 from tropical forest habitats in Hainan, China. Additionally, plants of *A. crispa*, and the non-nodulated species *A. lucida* and *A. polycephala* were cultivated in the Botanical Garden Bonn, Germany. In the butanolic extracts (derived from liquid-liquid separation of the methanolic extract with water) of *A. crispa*, *A. hanceana, A. villosa and A.*

mamillata, an ion with the same mass and retention time as FR was detected, although the respective concentration was significantly lower than in *A. crenata*.

In *A. lucida*, and *A. polycephal*a we could initially not detect such an ion. Thus, we further fractionated the butanolic extracts and could detect the signal in a subfraction of the *A.lucida* extract (Sephadex fraction AL-8-3-2) (**Figure 5-5**), but not in *A. polycephala*.

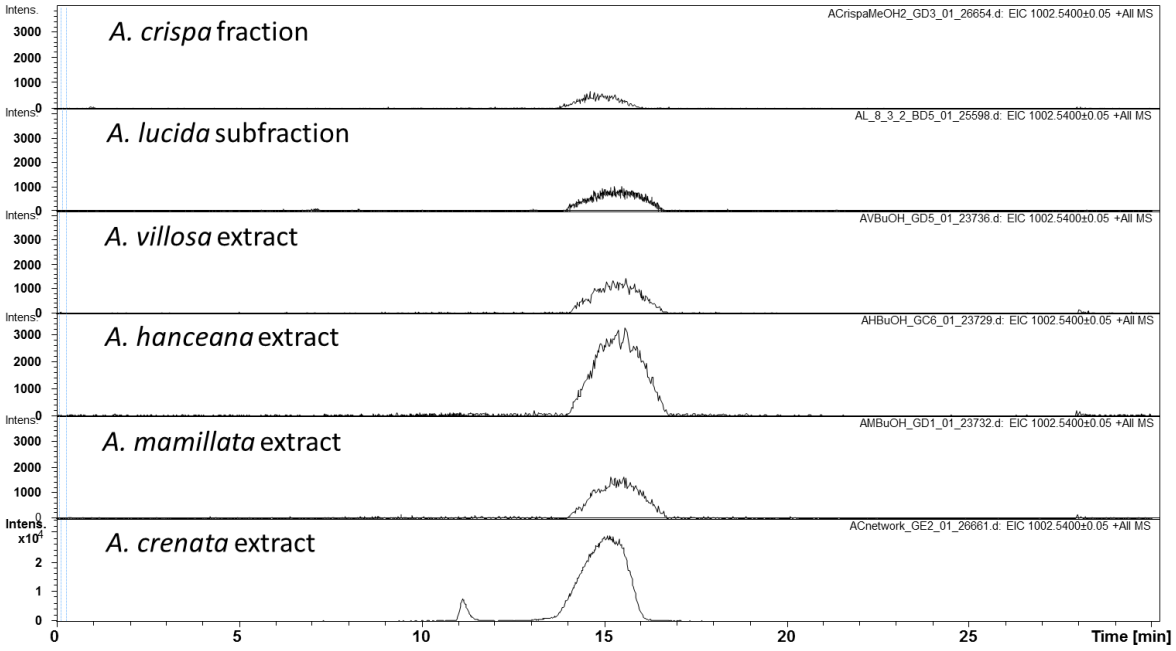

Figure 5-5: Extracted ion chromatograms *m/z* 1002.54 ± 0.05 Da of extracts/fractions from different *Ardisia* species.

The FR-containing samples were networked with the *A.crenata* extract to confirm the identity of FR by MS^2 comparison and matching with an authentic FR standard uploaded to the GNPS database (**Figure 5-1, 5-6**).

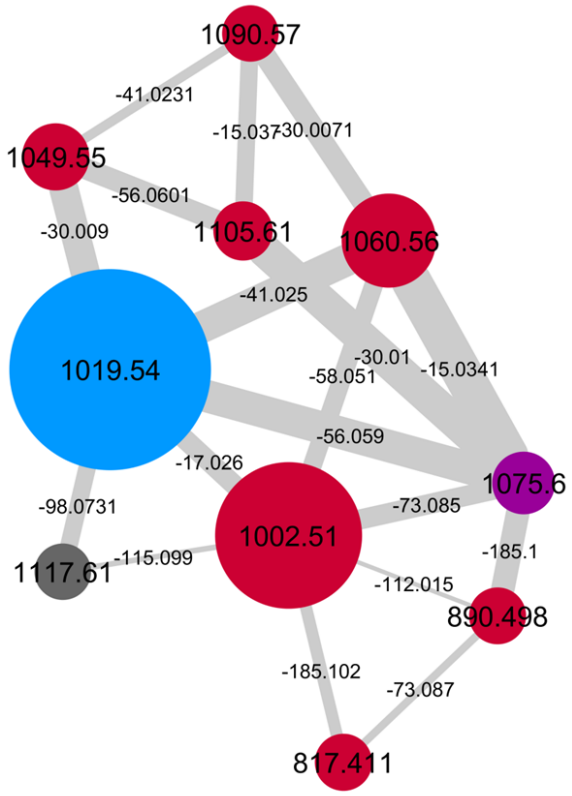

Figure 5-6: Molecular network of the fractions from *A. hanceana*, *A. lucida,* and *A. villosa* leaves. Nodes display distinct *m/z* features, displaying their parent mass. Width of edges is proportional to cosine, labeled with delta *m/z* values. Sizes of the nodes correspond to sum of precursor intensities. Highlighted are nodes occurring only in *A. hanceana* (red), *in A. hanceana* and *A. lucida* (purple) and in all three species (blue). All *m/z* values display 0.03 Da lower masses due to calibration error.

The detection of FR in the non-nodulated *A. lucida* suggests the presence of an endosymbiont that is not located in the usual nodules, and may thus represent the very early stage of a plant-bacterial symbiosis. Overall our results point toward a much broader distribution of FR in the genus *Ardisia*, than previously known, since all six analyzed *Ardisia* species do contain FR. Additionally, it is worthwhile to mention, that FR derivatives like YM-254890 and sameuramide were found in a in a soil bacterium[28] and even a marine tunicate[29], respectively. This again points to an even broader distribution of this molecule as currently anticipated.

5.1.5 Isolation of FR from the cultivable *Chromobacterium vaccinii* MWU205, DSM 25150

The fact that YM analogs have before been found in free living bacteria, *i.e. Chromobacterium* sp. QS3666[28] makes it rather likely that biosynthetic genes for such molecules like YM and FR are present in other bacterial genomes. At this point it also has to be noted that up- and downstream of the *frs* cluster sequences for transposons were detected, and that the G/C content of the cluster is markedly different from that of the surrounding sequences. Horizontal gene transfer of the *frs* cluster is thus likely. Hence, it can be assumed that the ability to produce FR-type molecules can be found in other bacteria as well. Under application of state-of-the-art similarity search algorithms, the multitude of bacterial genome sequences available were searched for biosynthetic genes related to the *frs* sequences.

Using the BLAST similarity search tool,[198] we took notice of *Chromobacterium vaccinii* MWU205, DSM 25150[199,200], because the draft genome sequence apparently contains several small fragments of the *frs* gene cluster (>70% identity). This strain has been patented as potential biocontrol agent against mosquito (*Aedes aegypti*) larvae before[199]. As we already demonstrated the insecticidal properties of FR (**Chapter 4.1.5**), this fact made it an even more likely candidate for FR production.[10] *C. vaccinii* had been isolated from soil and roots of *Vaccinium macrocarpon* (cranberry) in Massachusetts, USA and is a producer of violacein, a pigment with antibiotic properties.[200] The putative chromobacterial *frs* gene cluster sequence was scattered on 11 contigs and incomplete and while we tried to close the gaps by resequencing of the strain and manual filling of the sequence gaps by PCR (performed by Dr. René Richarz, Institute for Pharmaceutical Biology, Univ. of Bonn), we planned to find direct evidence for FR production by cultivation and isolation procedures.

We obtained *C. vaccinii* MWU205, DSM 25150 from the DSZM strain collection, grew it on liquid medium. After five days, we extracted the culture with butanol. LCMS measurements indicated the presence of FR and FR-2 (**2**) in almost equal quantities (**Figure 5-7**), but interestingly no FR-1 (**1**), being the most abundant FR analog in *A. crenata* extracts, could be detected. Subsequent purification via VLC, SEC and HPLC yielded pure white powders of FR (2.0 mg, 6.1 mg/L) and **2** (1.3 mg. 4.3 mg/L). Structures were confirmed by ^{1}H NMR (**Figure 5-7**). As both isolated compounds displayed the same bioactivity profiles in the IP1 accumulation assay as FR and FR-2 isolated from *A. crenata*, it was unequivocally shown that

the plants and *C. vaccinii* produce the same bioactive compounds, albeit in different ratios (Appendix **Figure 10-38**).

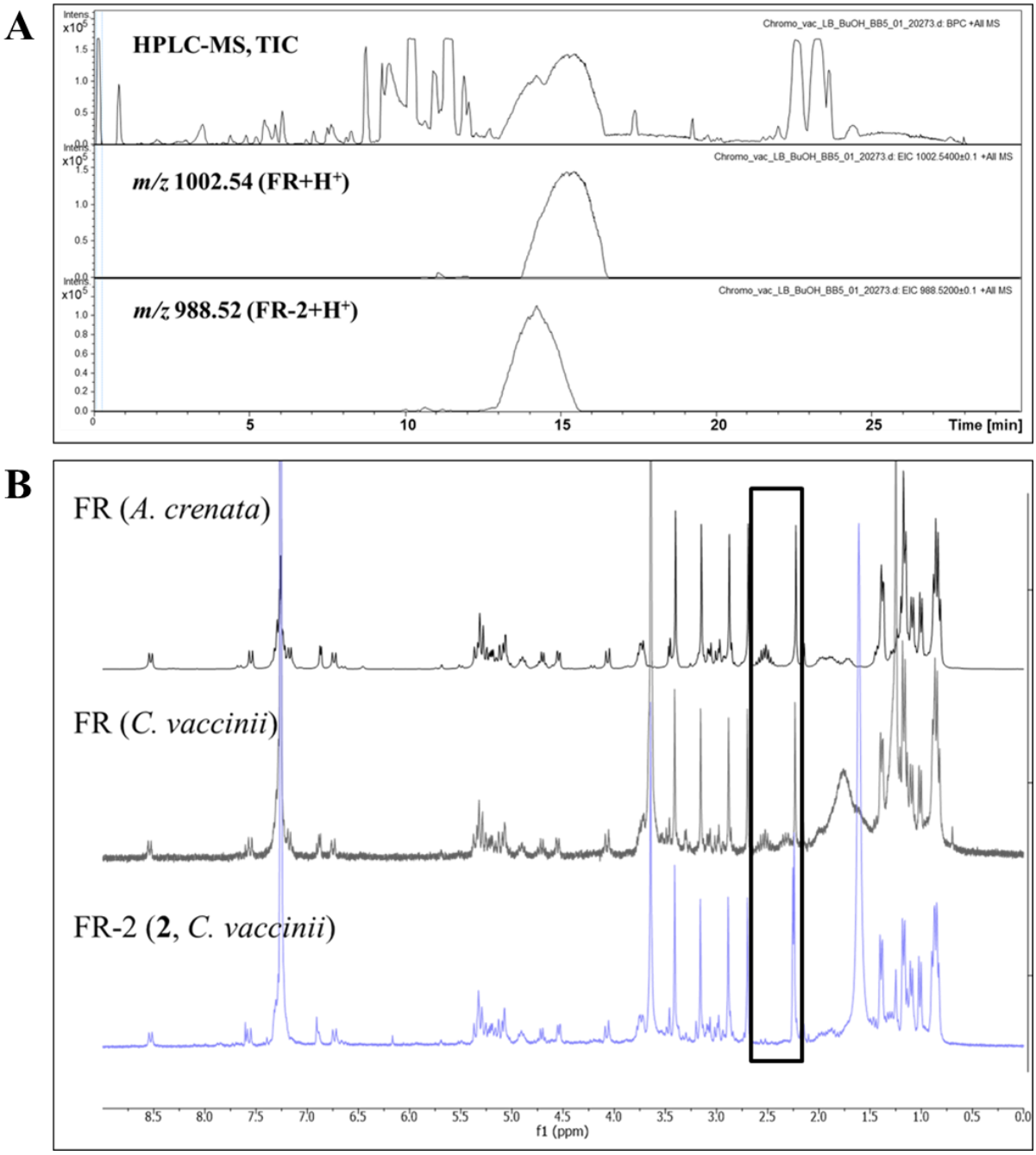

Figure 5-7: (**A**) Extracted ion chromatograms of FR *m/z* 1002.54 ± 0.01 Da and FR-2 (**2**) *m/z* 988.52 ± 0.01 Da of butanolic extract from *Chromobacterium vaccinii MWU205, DSM 25150*. (**B**) Comparison of ^{1}H NMR spectra (300 MHz $CDCl_3$) of FR from *A. crenata*, FR from *C. vaccinii* and **2** from *C. vaccinii*. Spectral range of 2.7-2.2 ppm is highlighted by black rectangle to demonstrate the differences between FR and **2.** For **2** this is in essence the lacking resonances for a CH_2 multiplet at 2.55 ppm and an additional resonance for a second acetate-CH_3 singulet at 2.24 ppm.

Altogether we can state that *C. vaccinii* contains the FR gene cluster *frs* and is cultivable. FR was produced at a rate of 6.1mg/L and compound 2 amounted to 4.3mg/L. In comparison, isolation from *A. crenata* supplies about 50 mg/kg dried leaves after about 6 month of plant cultivation.

In order to investigate the biosynthetic production of FR and its analogs we acquired the growth curves of *C. vaccinii* via optical density measurements (**Chapter 3.1.2**, experiments performed by Wiebke Hanke, Institute for Pharmaceutical Biology, Univ. of Bonn). The stationary phase was reached after 36 hours. In parallel to the optical density measurements we also monitored the FR production via LCMS. The FR concentration peaked after 36 hours, thus upon transition from log- to stationary phase of bacterial growth. Interestingly, after 36-48 hours the FR concentration decreased possibly due to degradation and reached the level it has had during the lag phase after 228 hours. At the same time a molecular ion with the same *m/z* as FR increases at much lower retention times, possibly caused by ring-opening and re-esterification with the sidechain secondary alcohol of FR, altering the global conformation of FR. For determination of the conformation we need to isolate this degradation product and analyze it via NMR spectroscopy in future attempts.

Conclusion Chapter 5.1

We demonstrated the usefulness of MS-based GNPS molecular networking for the detection of a family of FR derivatives in *A. crenata*. Based on the molecular network we were able to isolate and elucidate two new FR analogs, FR-3 (**3**) and FR-4 (**4**). The evaluation of these newly identified FR analogs and of the previously discovered FR-1 (**1**) and FR-2 (**2**) regarding their affinities to the Gq protein and their potential to inhibit Gq-mediated signaling will be described in **Chapter 5.2.1**.

Based on our 1D and 2D NMR spectroscopic data analysis we conclude that small structural alterations of the acylation chains of L' and L''' as observed for **1**-**3** have only marginal influence on the global conformation of the molecule. The same is true for the replacement of homoalanine for alanine in **4**.

Additionally, we were able to discover previously unknown FR producers, namely the nodulated *A. crispa*, *A. hanceana*, *A. mamillata*, and *A. villosa* and surprisingly also the non-nodulated *A. lucida*. This finding together the newly discovered FR-producer *Chromobacterium vaccinii* MWU205, DSM 25150, and in conjunction with reports on the FR related compounds YM and sameuramide found in soil bacteria[28] and a marine tunicate[29], respectively, suggest an unexpected broad distribution of the FR molecular family in nature. This may implicate an important ecological role of the FR molecular family in nature, not only for *Ardisia* plants, but also in several other contexts.

5.2 Towards the pharmacophore of FR – Structure-Activity Relationship studies of all currently known Gq inhibitors

Direct targeting of intracellular Gα subunits is a challenging task in terms of finding chemical tools for mechanistic pharmacological studies and for developing novel therapeutic approaches. To date, the depsipeptides FR and YM have been established as Gq inhibitors, and it can be suggested that their activity correlates with a certain conformation, *i.e.* 3D shape.

FR is a large molecule (MW 1002.17 Da), which adopts multiple conformations, as can easily be detected in NMR spectra showing resonances for major and minor conformers. Of special interest for the 3D shape of the molecule are *cis* amide bonds in the cyclic structure between alanine and *N*-methylalanine, as well as between hydroxyleucine and *N,O*-dimethylthreonine, as evidenced in an X-ray study[30] and deduced from NOE data (see **Figure 7-6**). This applies to the major conformer, whereas the minor conformer may – according to our ROESY and ^{13}C NMR data – has an additional *cis* amide bond between *N*-methyldehydroalanine and phenyllactic acid (see **Table 5-5**). Such *cis* amide bonds are generally energetically less favored (as compared to *trans*) and occur rather rarely. They clearly, however play a major role concerning the bioactivity of FR. To date, the 3D shape of FR may be envisaged as a wedge, where the phenyl ring of phenyllactic acid is forming the tip and dives deeply inside the G-Protein/GDP complex.

According to molecular modelling experiments many changes in the structure of FR seems to diminish its activity towards GDP-bound $G\alpha_q$. X-ray studies of the $G\alpha_q$/GDP/YM complex showed that especially the residues of YM (and in our case FR) targeting the linker 1 region of the protein may be important for the selectivity toward certain G-protein isoforms.[53]

Thus, subsequent to the isolation and structure elucidation of new FR analogs from the above mentioned sources these compounds were analyzed in bioactivity assays such as IP_1 and cAMP accumulation assays for determining their capabilities of interfering with Gq,- Gs,- and Gi-mediated signaling, respectively. Additionally, analogs, which inhibited Gq-mediated signaling were assayed for their affinity to Gq proteins by competitive radioligand binding assays against tritiated FR, [^{3}H]PSB-15900. Finally, in-depth analysis of the interaction of (i) simplified YM analogs provided by the Imhof lab (Pharmaceutical Chemistry I, Univ. of Bonn), (ii) molecular modelling studies by Dr. Daniel Tietze (TU Darmstadt) of all analogs provided (iii) and

molecular modelling of all so far described YM analogs in literature, were included in the present study in order to derive key molecular properties for binding to and inhibition of Gq.

Altogether, these experiments should enable us to understand the relationship between the 3D shape of the molecule and its activity. The following questions shall be answered in **Chapter 5-2**:

1. Which influence do small structural changes of FR have on its 3D structure (*i.e.* conformation)?

2. How does this correlate with its biological effects?

3. Based on the results of 1) and 2): Can we derive the pharmacophore of FR and use the FR skeleton to develop inhibitors for other Gα subunits?

5.2.1 **Bioactivity of FR analogs derived from *A. crenata***

FR is characterized by its ability to inhibit Gq proteins and in this way the signal transduction of many GPCRs. In the context of the current study we wanted to assess whether in **Chapter 5.1** described, newly isolated FR analogs **1** - **4** (FR-1 to FR-4) differ in their affinity towards, and their effect on the downstream signaling of Gq proteins. For this reason, competitive radioligand binding studies (Markus Kuschak Pharmaceutical Chemistry I, Univ. of Bonn, **Chapter 3.7.6**) and IP1 accumulation assays (Nina Heycke, Suvi Annala, Tobias Benkel, Pharmaceutical Biology, Univ. of Bonn) were performed (**Chapter 3.7.4**).

Due to the minute amounts of the 3:1 mixture (approx. 500 µg from 2 kg of leaves) of compounds **3** and **4**, we decided to biologically evaluate the mixture without further purification. Intriguingly, while most of the synthetic FR analogs published so far[26,201] showed a dramatic decrease in potency, the here discovered FR analogs **1**, **2**, and **3/4** (3/1) are almost equipotent to FR in terms of inhibiting Gq-signaling as determined by IP1 accumulation assay (pIC_{50} ± SEM: FR = 6.10 ± 0.05, compound **1** = 5.97 ± 0.05, compound **2** = 5.63 ± 0.05, compounds **3/4** (3/1 = 5.96 ± 0.07, **Figure 5-8A**).
Competitive binding assays, applying the tritiated FR-radioligand ([^{3}H]PSB-15900) and purified membrane preparations of platelets allowed the comparison of affinities of FR, **1**, **2**, and **3/4** (3/1) towards the Gq protein (**Figure 5-8B**).[54] All of the tested compounds show K_i and IC_{50} values in the low nanomolar range with the new discovered **3/4** (3/1) being the most Gq-affine compounds so far discovered (K_i ± SEM =1.24 ± 0.06 nM).

In terms of Gq inhibition, no compound surpassed the activity of the parent substance FR. With data on Gq affinity and Gq mediated signaling of all three, respectively four (mixture **3/4** (3/1)), naturally produced compounds (**1**, **2**, and **3/4** (3/1)) in hand, it can be concluded that alterations in the length of the acylation chains at L' and L''' as well as a substitution of alanine for homoalanine hardly affect Gq binding and inhibiting of downstream signaling. So, in contrast to most of the synthetically derived Gq-inhibitors[26,201], all of the analogs provided by nature (**1**, **2**, and **3/4** (3/1)) are potent and efficacious.

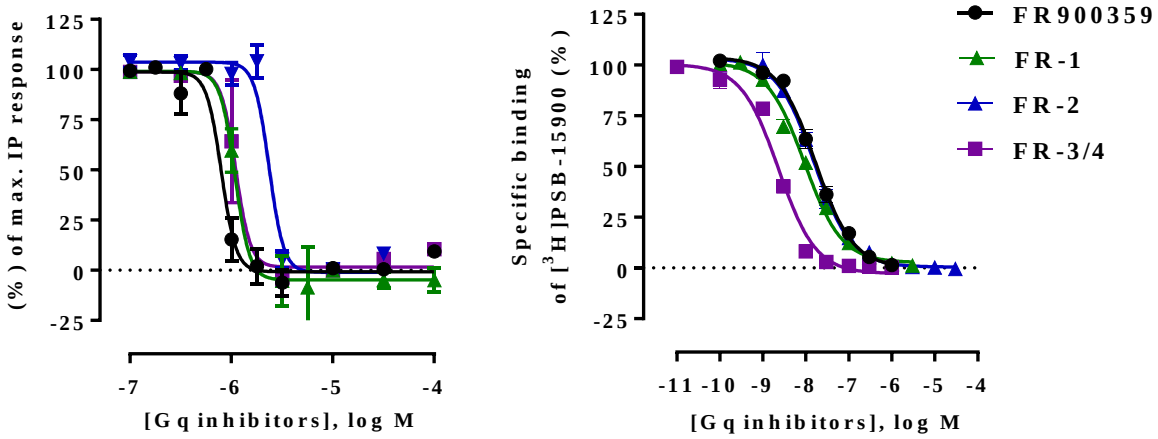

Figure 5-8: **Bioactivity of FR, 1, 2, 3/4** (3:1 ratio). (**A**) Inhibition of agonist-induced second messenger production in CHO cells expressing the Gq-sensitive muscarinic M1 receptor. Indicated analogs were evaluated against the muscarinic agonist Carbachol at its EC_{80}. pIC_{50} ± SEM: FR = 6.10 ± 0.05, **1** = 5.97 ± 0.05, **2**, = 5.63 ± 0.05, **3/4** (3/1 = 5.96 ± 0.07. (**B**) Competition binding study of FR, **1**, **2** and **3/4** (3:1 ratio) versus [^{3}H]PSB-15900 (5 nM), the tritiated derivative of FR, at cell membrane preparations of platelets. Values represent means ± SEM of three independent experiments. pIC_{50} values ranging from 7.79 to 8.64 were determined.

5.2.2 **Semisynthetic modification of FR**

As the so far isolated FR analogs demonstrated that there are several residues on the FR scaffold that can be altered without causing detrimental effects regarding inhibitory activity towards Gq (**Figure 5-8**) semisynthetic modification of FR was envisaged. Inspection of the FR structure reveals that it offers only few residues susceptible to modification, a secondary alcohol on the side chain L''' and a Michael acceptor, *i.e.* an exomethylene group in conjugation with a carbonyl group at A''.

5.2.2.1 Synthesis and analysis of FR-Hex (**11**) and FR-Cys (**12**)

Synthesis of FR-Hex (**11**)

The first residue we planned to modify was the secondary alcohol on the L''' side chain of FR (**Scheme 5-6**). Because this reaction proved to be sterically demanding, we applied a modified Steglich esterification[202] with glacial acetic acid, pretreated with *N*-ethyl-*N*'-(3-dimethylaminopropyl)carbodiimide (EDC), an water-soluble-byproduct-forming analog of *N,N*'-dicyclohexylcarbodiimide (DCC), and catalytic amounts of 4-dimethylaminopyridine (DMAP).[203] Unfortunately, no detectable turnover rates towards the corresponding FR-acetate product were detected. Also the reaction with acetylchloride failed, but the reaction with acetic anhydride and catalytic amounts of DMAP, did lead to the formation of the desired product, according to LCMS measurements. However, we were not able to separate the assumed product from the educt FR, despite much effort. Consequently, we intended to couple a larger and more lipophilic residue to FR with the aim to improve the chromatographic separation of educt and product: The successful esterification of FR with hexanoic anhydride to the corresponding FR-Hex (**11**, **Scheme 5-7**) is described in **Chapter 3.5.1** in detail and was verified by MALDI-TOF (Appendix **Figure 10-39**), MS^n (**Figure 5-9**) and $LCMS^2$ analysis (**Figure 5-10**) as previously described in **Chapter 5.1.2**.

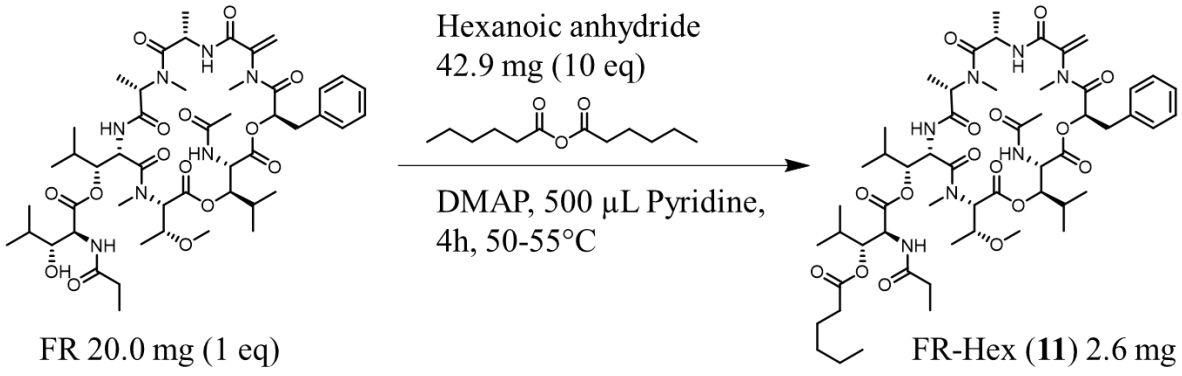

Scheme 5-7: Reaction scheme of the synthesis of FR-Hex (11).

Structural analysis of FR-Hex (**11**)

The molecular formula of **11** was determined to be $C_{55}H_{85}N_7O_{16}$ (calcd. 1122.5945; obsd. 1122.5952) for $[M+Na]^+$. This result from an accurate mass measurement, which showed a mass difference of 98 Da between FR and compound **11**, suggests the successful esterification of the secondary alcohol of the *N*-propionylhydroxyleucine2 (L''') residue of FR with hexanoic anhydride to the corresponding L^+ = *N*-propionyl-(2S,3R)-3-(hexanoyloxy)-hydroxyleucine2 moiety of **11**. Mass spectrometric analysis, especially when comparing fragments from sequential fragmentation via collision induced dissociation of the depsipeptides FR and **11** demonstrated that **11** differs from FR regarding the L''' moiety of FR, as expected. Indeed, the compounds can be distinguished by different *Δm/z* values of the modified amino acids. For **11** this is evident from the second-generation mass spectra (MS^3) of *m/z* 993.51 compared with the 98 Da lower weight *m/z* 895.45 for FR. Loss of the side chain L''' (FR, *Δm/z* 185.11 Da) or L^+ (**11**, *Δm/z* 283.17 Da), respectively leads for both compounds to the same fragment, *i.e m/z* 710.34 Da (**Figure 5-9, 5-10**).

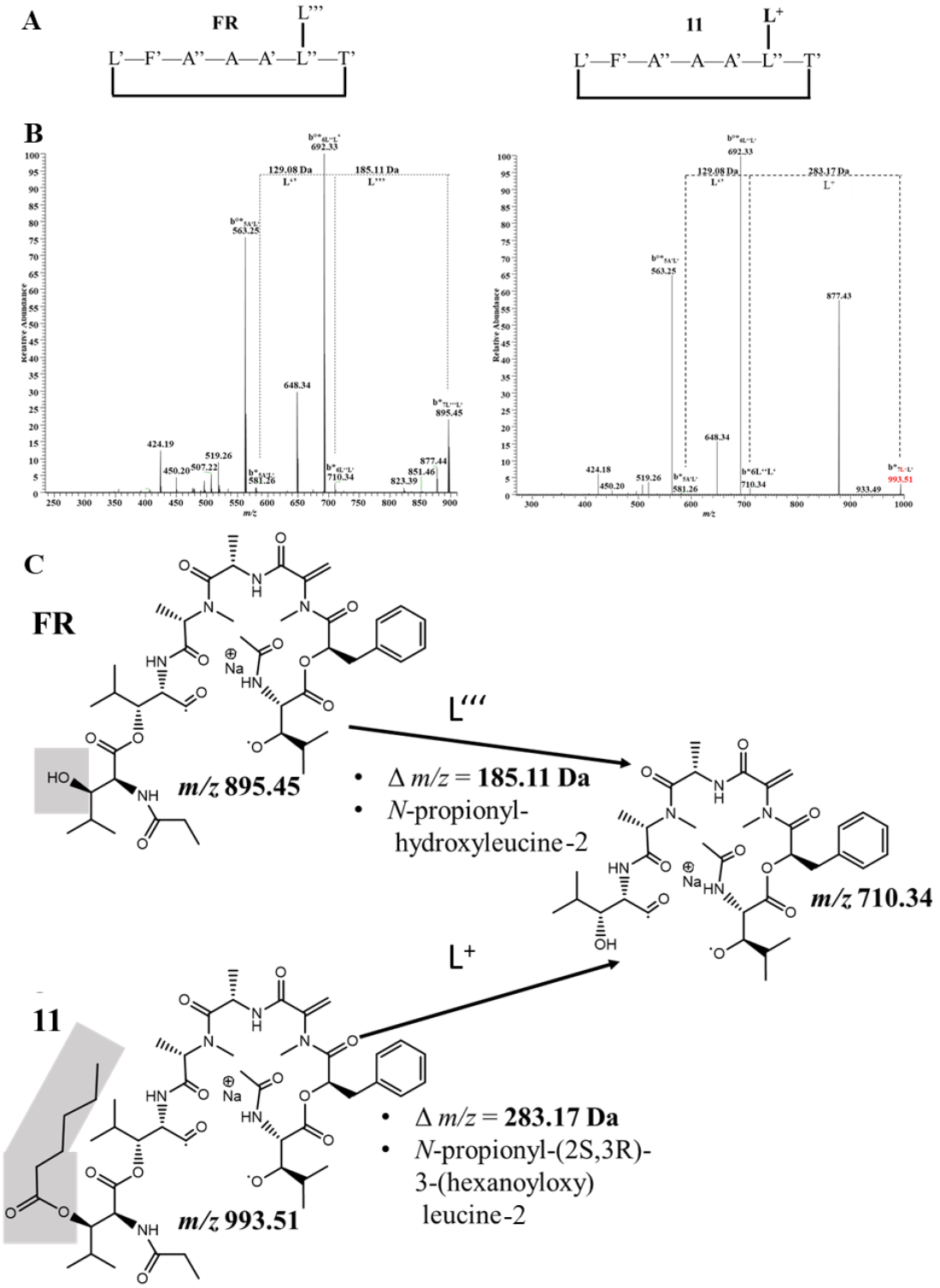

Figure 5-9: (**A**) Schematic structure of FR and **11** in one-letter amino acid code. L' = *N*-acetylhydroxyleucine-1, F' = phenyllactic acid, A'' = *N*-methyldehydroalanine, A = alanine, A' = *N*-methylalanine, L'' = hydroxyleucine, T' = *N,O*-dimethylthreonine, L''' = *N*-propionylhydroxyleucine-2, L^+ = *N*-propionyl-(2S,3R)-3-(hexanoyloxy)leucine2. (**B**) Comparison of second-generation (MS^3), product-ion spectra of FR and **11**; $[M+Na]^+$. Comparison of the MS^3 spectra of FR and **11** reveals the same pattern of signals and intensities for both compounds, except that all signals from **11**, containing the hexanoate residue with a 98 Da higher *m/z*. Loss of the sidechain L''' (FR, Δ *m/z* 185.11 Da) or L^+ (**11**, Δ *m/z* 283.17 Da), respectively leads for both compounds to the same fragment *m/z* 710.34 Da. (**C**) Fragmentation pathways of second-generation (MS^3) product ions obtained from FR and **11**. *m/z* 895.45 (FR) or rather *m/z* 993.51 (**11**) lose their distinctive side-chain amino acid *N*-propionylhydroxyleucine-2 (FR) or *N*-propionyl-(2S,3R)-3-(hexanoyloxy)leucine-2 = L^+ (**11**), resulting in the formation of the same fragment *m/z* 710.34 for both compounds.

Similar reactions with more bulky residues such as 1,8-naphthalic anhydride failed, most likely because of the steric hindrance of the secondary alcohol.

Antibacterial activity of compound **11**

For analogs of the antibiotic drug and cyclic lipodepsipeptide daptomycin, it was evaluated that *in vitro* antibacterial activity increased with acyl chain length up to C-12 to C-13.[204] *Müller et al*. proposed that the fatty acid tail of daptomycin inserts between the fatty acyl chains of the cell membrane bilayer und thus initiates its cellular uptake.[205] To investigate whether this mechanism can be transferred to FR-related compounds we tested compound **11** for antibacterial activity, because it contains a hexanoate residue. However, neither FR, nor compound **11** showed any bactericidal effects on *Arthrobacter* assay (data not shown, Assay performed by Nils Böhringer, Univ. of Bonn). Possibly the C_6-chain is too short to act as anchor into the cell membrane and the experiment should be repeated with a longer acyl residue such as decanoate.

Synthesis of FR-Cys (**12**)

The second reactive moiety on the FR scaffold is the exomethylene group of the *N*-methyldehydroalanine moiety in conjugation to the peptide carbonyl group, which is a Michael acceptor with an expected reduced nucleophilicity due to the flanking amides. It is generally known that nucleophiles may attack α,β-unsaturated carbonyl groups via Michael addition. Before the synthesis of **12** was considered the reactivity of such a functional group in natural products was researched. In general, dehydroalanine moieties are common among peptidic natural products, especially for ribosomally synthesized lantibiotics.[206] In contrast, the amino acid *N*-methyldehydroalanine is besides FR (and FR-related YM-254890, sameuramide) only known from the streptomycete-derived BE-22179[207,208] and cyclic depsipeptides of several cyanobacterial genera, *e.g. Microcystis aeruginosa*. The latter produces numerous structurally diverse hepatotoxic microcystins.[209] The mechanism of action of microcystins was reported to be a covalent linkage via Michael addition of the *N*-methyldehydroalanine to a cysteine (Cys273) residue and hence irreversible inhibition of human protein phosphatase 1 (PP1).[210] PP1 plays a crucial role in the regulation of blood-glucose levels in the liver and glycogen metabolism.[211] On the other hand, microcystins immobilized to a sepharose bead through an aminoethanethiol (cysteamine) adduct retained inhibitory activity.[211] These results imply that

the *N*-methyldehydroalanine residue probably does not play a role in early enzyme–inhibitor interactions. Mechanistic studies by Craig and co-workers[212] confirmed a two-step mechanism for irreversible inhibition by microcystins. In the first step, the rapid noncovalent binding and inhibition occurs, and then the slower covalent modification of a cysteine residue occurs over the course of hours.[213] Notably, such adducts might not be resistant toward retro-Michael reaction *in vivo*, and reversible adduct formation may explain the observed biological activity. To test whether *N*-methyldehydroalanine is essential for $G\alpha_{q/11}$ inhibitory activity of FR, the reactive moiety was removed by catalytic hydrogenation, complying with the procedure published for the hydrogenation of YM.[52] For YM, Taniguchi *et al*. discovered that one of the two resulting diastereomers (epimers), YM-385781 (R)-epimer, was active, while the other one, YM-385780 (S-epimer), showed a 40-fold decrease in activity. These findings contradict a crucial role for *N*-methyldehydroalanine for the biological effect of YM by covalent binding to the $G\alpha_{q/11}$ protein. The fact that the inactive (S)-epimer YM-385780 differs in its conformation from the active (R)-epimer YM-385781 and YM, emphasizes the dependence of the biological effect from the spatial arrangement of the molecules. Similar results were experienced for hydrogenated FR.[54]

In general the Michael addition reaction is a versatile synthetic methodology for the efficient coupling of electron poor olefins with a vast array of nucleophiles. Due to the limited amount of FR available for reactions due time- and resource consuming planting, isolation and purification, literature was thoroughly screened for determination of optimal mild conditions, regarding base (strength), solvent, catalysts and also type of Michael reaction (carbon Michael addition vs aza- or thio-Michael additions). Besides solvent-free protocols[214], the focus was put on reactions using model substrates similar to FR such as dehydropeptide derivatives[215] and the previously mentioned microcystins.[216] Naidu *et al*. reported on Michael addition reactions of several amines and thiols with triethylamine to dehydroalanine amides being significantly accelerated by water.[217] Because of the excellent yields and the faster reactions we decided to perform a thio-Michael addition. As substrate 2-aminoethanethiol hydrochloride (cysteamine) was chosen. Hetero-Michael reactions usually require catalytic amounts of a strong base or a Lewis acid, resulting in many side reactions, apart from including toxic chemicals and hydrolysis may occur. Further the differential solubility of cysteamine and FR was a challenge to overcome. While cysteamine is a water-soluble salt, FR is only poorly soluble in aqueous media. Firouzabadi *et al.* published a procedure overcoming all these issues by using sodium dodecyl sulfate (SDS) in the critical micellar concentration.[218] The protocol of Firouzabadi *et*

al. was demonstrated to be an effective method for the addition of thiols to α,β-unsaturated ketones under mild and neutral conditions.[218] The accelerating effect of the SDS micelles was related to the concentrating of the hydrophobic species (in our case FR) into the micellar core (**Scheme 5-8**).[218] We decided to generally follow the protocol of Firouzabadi *et al*. with slight modifications and successfully obtained 6 mg of the desired product FR-Cys (**12**) from 20 mg of FR. The reaction was performed under argon atmosphere to avoid cysteamine oxidation to the corresponding disulfide.

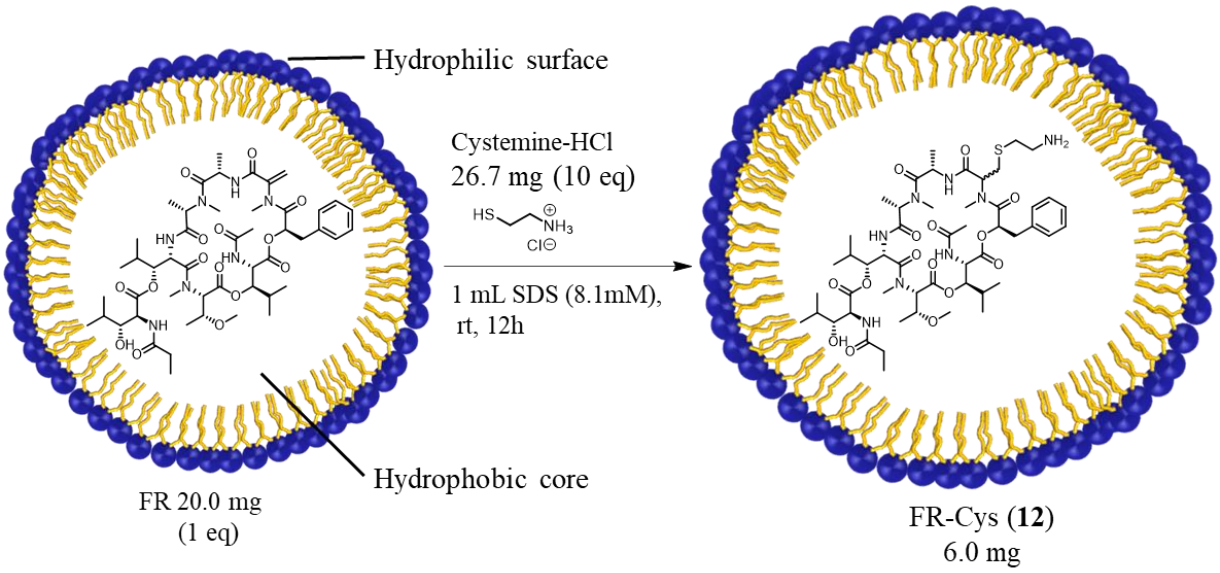

Scheme 5-8: Reaction scheme of the synthesis of FR-Cys (12). The reaction is assumed to occur in the hydrophobic core of the sodium dodecyl sulfate (SDS) micellar droplets.

Structural analysis of FR-Cys (**12**)

The molecular formula of **12** was determined to be $C_{51}H_{82}N_8O_{15}S$ (calcd. 1079.5693; obsd. 1079.5844) for $[M+H]^+$. This result from an accurate mass measurement, which showed a mass difference of 77.03 Da between the molecular ions of FR and compound **5**, suggested the successful addition of 2-aminoethanethiol to the *N*-methyldehydroalanine (A'') moiety of FR. Mass spectrometric analysis, especially when comparing fragments from sequential fragmentation via collision induced dissociation of the depsipeptides FR and **12** indeed demonstrated that **12** differs from FR regarding the *N*-methyldehydroalanine (A'') moiety, as expected (Appendix **Scheme 10-6**). Instead of the latter, compound **12** contains a *N*-methyl-3-((2-aminoethyl)thio)-2-alanine moiety, which was revealed from comparison of the $LCMS^2$ data (**Figure 5-10**) of FR and **12**.

For compound **12** a loss of *Δm/z* 77.03 Da referring to a 2-aminoethanethiol moiety is observed, *e.g.* fragmentation of the ion at *m/z* 309.13 (only occurring in **12**) results in a loss of 77.03 Da to yield *m/z* 232.10. The latter represents the A''-F'-dipeptide occurring in **12** and FR. Comparison of further MS fragments strengthened this assumption (**Figure 5-10**).

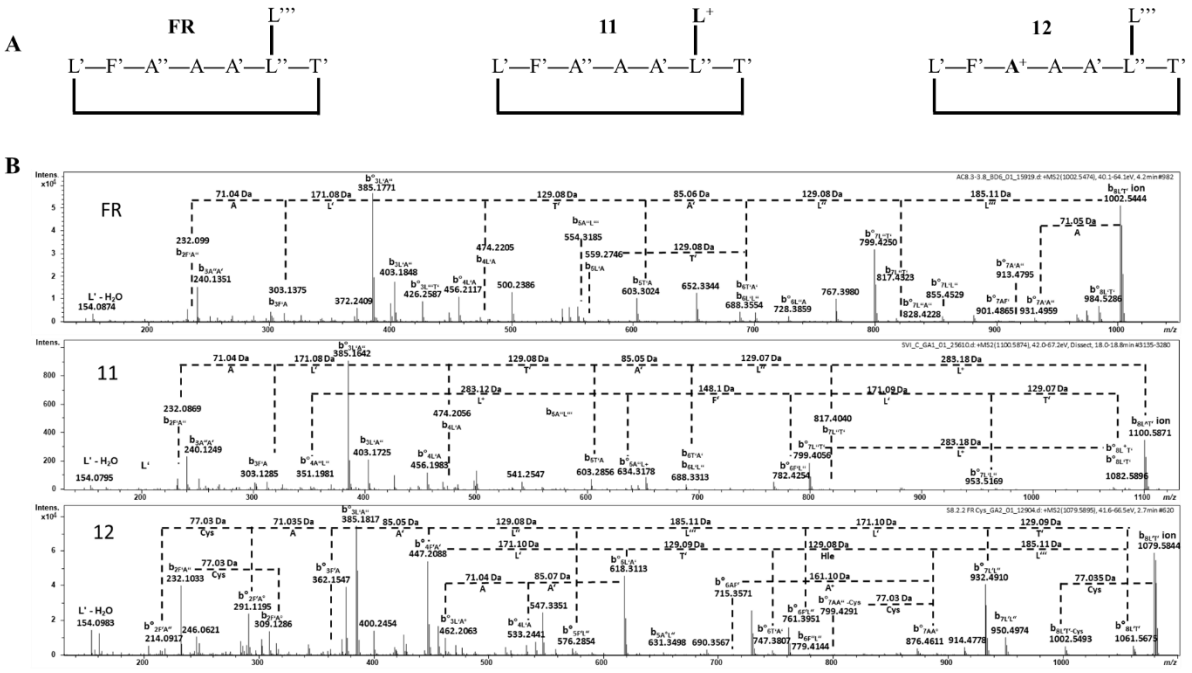

Figure 5-10: (**A**) Schematic structure of FR, **11**, and **12** in one-letter amino acid code. L' = *N*-acetylhydroxyleucine-1, F' = phenyllactic acid, A'' = *N*-methyldehydroalanine, A^+ = 3-((2-aminoethyl)thio)-2-alanine, A = alanine, A' = *N*-methylalanine, L'' = hydroxyleucine, T' = *N,O*-dimethylthreonine, L''' = *N*-propionylhydroxyleucine-2, L^+ = N-propionyl-(2S,3R)-3-(hexanoyloxy)leucine-2. (**B**) Comparison of first-generation, product-ion spectra of FR, **11**, and **12**; $[M+H]^+$. Nomenclature was used according to Chapter 3.4.1.3. Compared to FR, **11** has a different side chain; instead of L''' in FR, **11** contains after esterification with hexanoic anhydride L^+. **12** differs from FR in the A'' moiety. Via Michael addition a 2-aminoethanethiol moiety was added to the Michael acceptor functionality of A'' leading to A^+. This residue is evident from the 77.03 higher mass of the molecule ion of **12** and characteristic losses of this moiety, e.g. *m/z* 309.1286 (only occurring in 12) loses 77.03 Da to yield *m/z* 232.10, which represents the A''-F'-dipeptide.

The conjugation of 2-aminoethanethiol to FR seems to give stereospecifically one epimer of the conjugate, deduced from of a single peak in the extracted ion HPLC chromatogram (**Figure 5-11**), but the configuration at C-5 of compound **12** was not determined. The stereospecificity of Michael reactions were also described by similar conjugation reactions of *N*-methyldehydroalanine moieties of microcystins.[216,219,220] Miles *et al*. explained the stereoselectivity of the reaction with the steric effect of the *N*-methyl group of *N*-methyldehydroalanine, which prohibits the attack of C-5 from two sides. Interestingly, LCMS data indicated that cysteamine was sensitive to oxidation and formed the corresponding disulfide. The primary amine of this disulfide was also able to react via aza-Michael addition to FR as revealed from the *m/z* 1154.58 molecular ion (Appendix **Figure 10-40**).

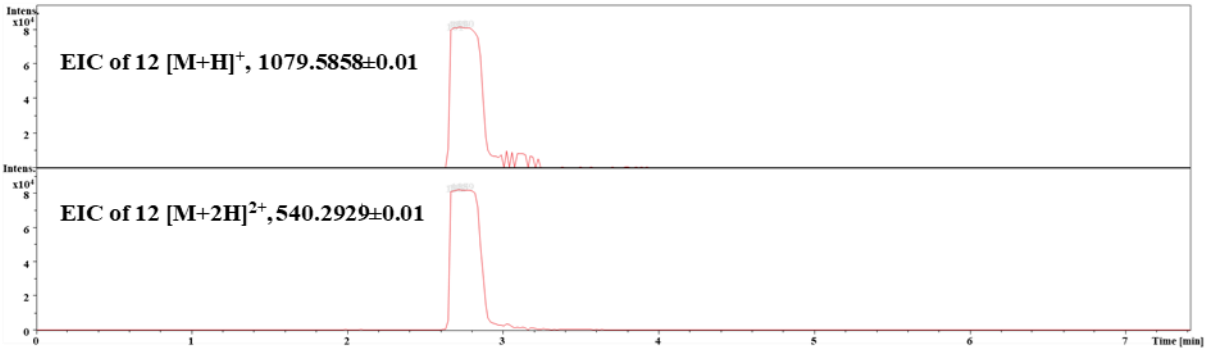

Figure 5-11: Extracted ion chromatograms of $[M+H]^+$ and $[M+2H]^{2+}$ of **12**, demonstrating that only one epimer of the conjugate product of FR and 2-aminoethanethiol was formed.

5.2.2.2 Biological evaluation of FR-Hex (**11**) and FR-Cys (**12**)

The depsipeptides **11** and **12** were tested for their inhibitory activity on second messenger-generating Gq, Gs, and Gi signaling pathways, respectively (**Figure 5-12**).

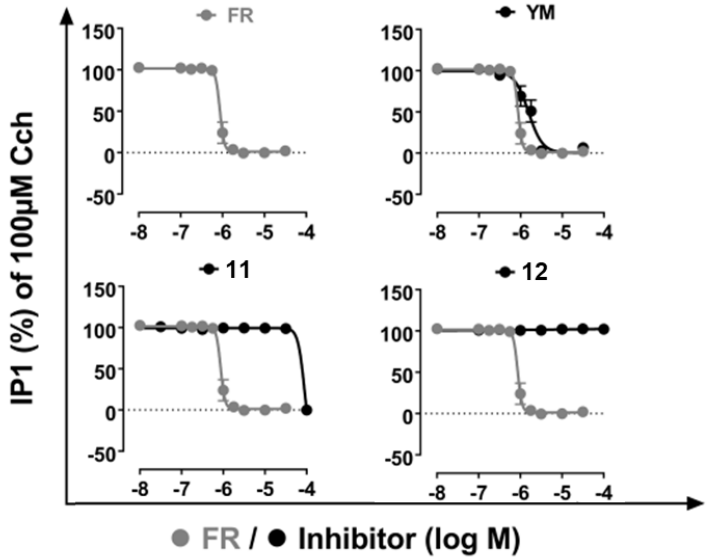

Figure 5-12: Carbachol-induced IP_1 accumulation in CHO M1 stable cell line preincubated with or without potential Gq inhibitors FR, YM, 11, 12). Assays performed by Suvi Annala, Tobias Benkel and Nina Heycke Univ. of Bonn.

Depsipeptide **11** only revealed an IC_{50} value of ~90 µM, while compound **12** was inactive at Gq. Exactly the same picture could be drawn from competitive radioligand binding studies (**Figure 5-13**), *i.e* both compounds showed only low affinity (**11**) or even no affinity (**12**) to Gq, respectively. In case of **11** this result was somehow expected, because the secondary alcohol of FR was reported to be involved in the complex hydrogen bond network of the

molecule. The crystal structure of FR had revealed this OH group to take part in three intramolecular hydrogen bonds, crucial for the conformation of FR.[30] Further, according to the mode of action described for YM by Nishimura *et al*.[53] the same OH group is responsible for refolding of the molecule upon target interaction with Gq, developing a new hydrogen bond to Glu 196 residue of the helicale domain of Gq. Regarding **12**, the inactivity of the molecule was somehow unexpected and points towards having isolated the (S)-epimer (= (D)-epimer, because of the higher priority of the sulfur atom) corresponding to the (S)-epimer (= (L)-epimer) of YM-385780, which was also shown to be inactive.[26,52] Due to the stereoselectivity of the reaction we were not able to confirm this hypothesis, by testing the putatively active (R)-epimer. This hypothesis was supported by docking experiments (**Chapter 6.1.3**).

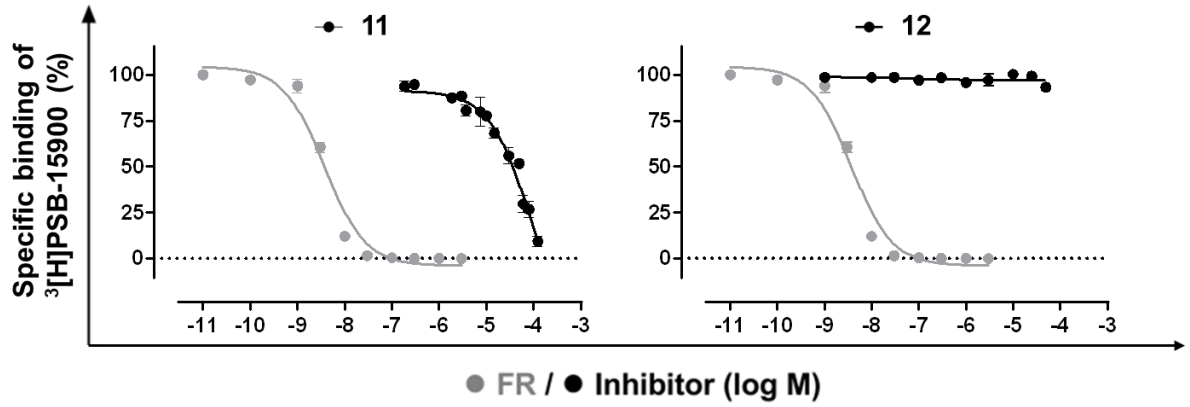

Figure 5-13: Competition binding study of FR, **11**, and **12** versus [^{3}H]PSB-15900 (5 nM), the tritiated derivative of FR, at cell membrane preparations of platelets. Values represent means ± SEM of three independent experiments. Assay was performed by Markus Kuschak, Univ. of Bonn.

In contrast to the natural FR derivatives **1-4** (**Chapter 5.2.1**), semisynthetic FR analogs **11** and **12** were less active or devoid of activity, respectively.

5.2.3 **YM-254890 and FR900359 – the ultimate Gq inhibitors designed by nature**

The natural FR analogs **1-4** and semisynthetically derived analogs **11** and **12** described in **Chapters 5.1**, **5.2.1** and **5.2.2** allowed for first structure-activity insights, though they do not suffice to determine the complete pharmacophore of FR. That is why we introduce a holistic approach, including the aforementioned FR analogs, but also YM analogs synthesized by us (Imhof lab, Univ. of Bonn) and others[26,196,201,221] to devise a strategy for the elucidation of characteristics that determine interaction with Gq. Although a small number of analogs such as WU-07047,[221] YM-280193,[196] and YM1-YM18[26,201] (**Scheme 5-9**) were reported earlier, a

detailed analysis of the SAR of these compounds with respect to Gq and other G proteins was still missing. The major reason for this is the lack of NMR structural analysis of suitable compounds together with a detailed *in-silico* analysis which enables the visualization of the recognition mode of ligand-Gq protein interaction. Here we report an in-depth analysis of the interaction of differentially active and inactive analogs of YM and FR.

Therefore, we first grouped all 23 already published and further 14 new FR- and YM-derived compounds according to their potency, to identify tolerated, partially tolerated, non-tolerated minor, and non-tolerated major modifications in the original sequence(s) (**Scheme 5-9, Table 5-4**). As we have **3** and **4** as mixture and only putative structure proposals for **5**-**10**, these were not included in our study. Peptides **13-22** were synthesized in the Imhof lab, Univ. of Bonn (see **Chapter 3.5.7-3.5.9, Appendix Table 10-3**). These peptides were synthesized according to standard Fmoc-protocol on a solid support and cyclized by head-to-tail cyclization in solution using PyBOP as coupling reagent.[222] Complexity and low yields of depsipeptide syntheses encouraged several other groups to provide simplified and more easily accessible analogs of YM or FR, which can be exemplified with WU-07047 (**45**),[221] YM-280193 (**36**),[196] and the recently reported 18 YM-analogs (**23**, **26**–**35**, **38**–**44**, **Scheme 5-9**).[26,201] Biological activities for YM, FR and compounds **23**–**45** (**Scheme 5-9**) vary somewhat due to different methods used for determining biological activity in various laboratories. It is thus only referred to the herein determined values (**Figure 5-14**, **Table 5-4**).[223]

A one letter amino acid code as shown in **Scheme 5-9** is used in the following SAR studies.

T'' = *N*-acetylthreonine-1	(YM)
L' = *N*-acetylhydroxyleucine-1	(FR)
L* = *N*-3-hydroxypropionyl-hydroxyleucine-1	(**1** = FR-1)
F' = phenyllactic acid	
A'' = *N*-methyldehydroalanine	
A^+ = 3-((2-aminoethyl)thio)-2-alanine	(**12** = FR-Cys)
A = alanine	
A' = *N*-methylalanine,	
L'' = hydroxyleucine	
T' = = *N*,*O*-dimethylthreonine,	
L''' = *N*-propionylhydroxyleucine-2	(FR)
L^ = *N*-acetylhydroxyleucine-2	(**2** = FR-2 + YM)
L^+ = *N*-propionyl-(2S,3R)-3-(hexanoyloxy)leucine-2	(**11**, FR-Hex)

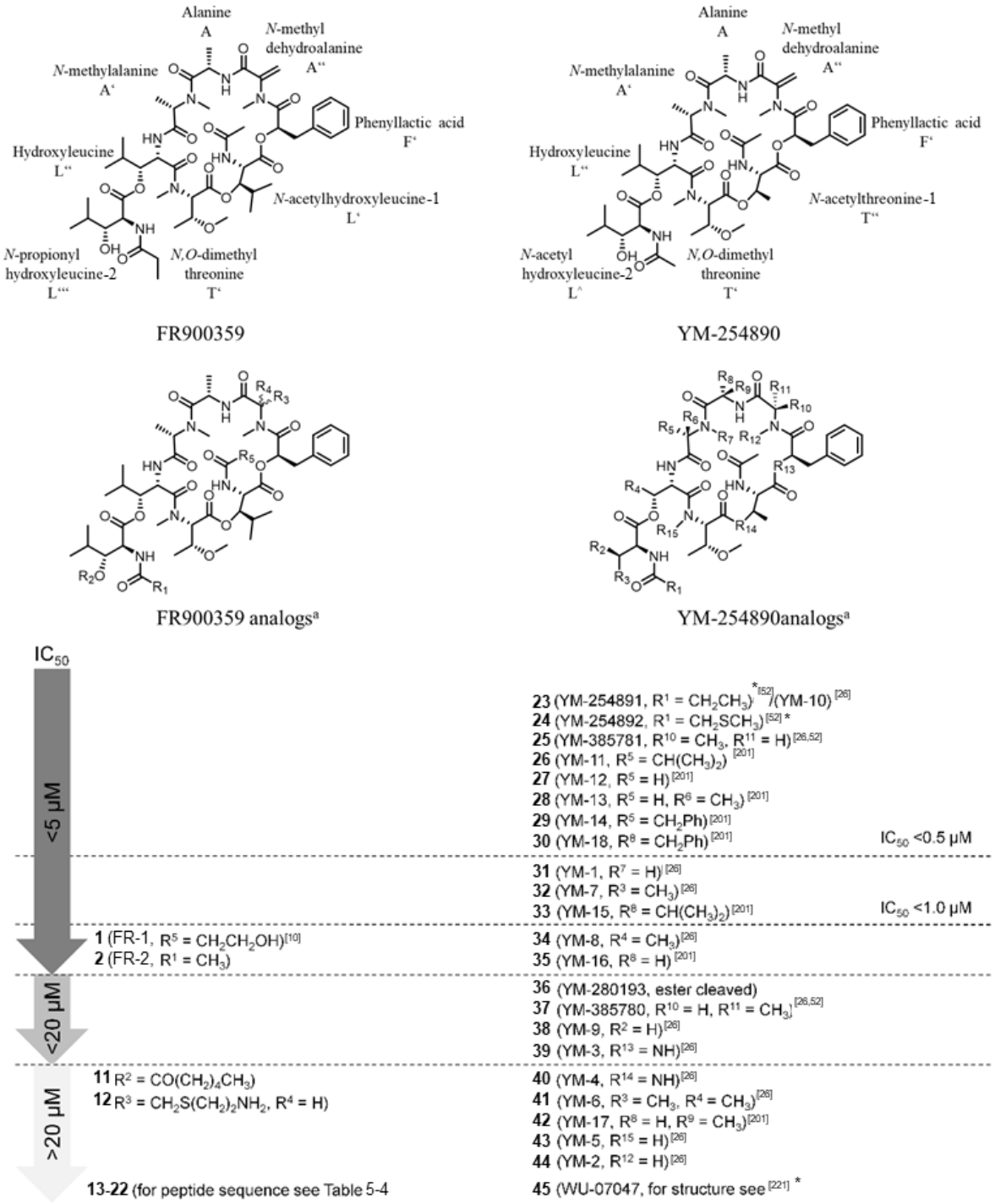

Scheme 5-9: Compounds are listed based on their reported IC_{50} values determined by inhibition of carbachol-induced IP1 production where available (Compounds measured with other assays are marked with an asterisk). [a]Chemical modifications relative to FR and YM are given in brackets (R_1–R_{15}) for the corresponding compound.

SAR of natural and semisynthetic FR900359 analogs

Compounds **1** (FR-1) and **2** (FR-0) differ from native FR with respect to their acylation pattern (for structure elucidation refer to **Chapter 5.1**).[10] Semisynthesis yielded FR analogs **11** and **12** (for structure elucidation refer to **Chapter 5.2.1**), in which the secondary alcohol of L''' was esterified with hexanoic acid (**11**) or Michael addition of cysteamine to the α,β-unsaturated double bond of FR (**12**).

Table 5-4: Sequences of test compounds including FR900359, YM-254890 and analogs (FR analogs **1**, **2**, **11**, **12**) prepared in this study and their Gα inhibitory activity.

No.	Peptide sequence or name	$G\alpha_q$ IC_{50} (µM)	$G\alpha_i$ IC_{50} (µM)	$G\alpha_s$ IC_{50} (µM)
	FR900359	0.87	>100	>100
	YM-254890	1.55	>100	>100
1	cyclo-[L*-F'-A''-A-A'-L''(L''')-*T'*]	1.04	>100	>100
2	cyclo-[L'-F'-A''-A-A'-L''(L^)-*T'*]	1.79	>100	>100
11	cyclo-[L'-F'-A''-A-A'-L''(L^+)-*T'*]	90	>100	>100
12	cyclo-[L'-F'-A^+-A-A'-L''(L''')-*T'*]	>100	>100	>100
13	cyclo-[A6-A'7-Lys(Ac)-Thr(*O*Me)-Thr(*O*Me)-D-Phe-A'5]	>100	>100	>100
14	cyclo-[A-A'-Lys(Ac)-Thr(*O*Me)-Thr(*O*Me)-F-A'5]	>100	>100	>100
15	cyclo-[A-A-Lys(Ac)-Thr(*O*Me)-Thr(*O*Me)-DF-A5]	>100	>100	>100
16	cyclo-[A-A-Lys(Ac)-Thr(*O*Me)-Thr(*O*Me)-F-A5]	>100	>100	>100
17	cyclo-[A-A'-L-Thr(*O*Me)-Thr(*O*Me)-DF-A'5]	>100	>100	>100
18	cyclo-[A-A'-L-Thr(*O*Me)-Thr(*O*Me)-F-A'5]	>100	>100	>100
19	cyclo-[A-A-L-Thr(*O*Me)-Thr(*O*Me)-DF-A5]	>100	>100	>100
20	cyclo-[A-A-L-Thr(*O*Me)-Thr(*O*Me)-F-A5]	>100	>100	>100
21	cyclo-[Ahx-DF'-Ado-Dap(T'')]	>100	>100	>100
22	cyclo-[Ahx-DF'-Ado-β-HyLeu]	>100	>100	>100

DF, D-phenylalanine; DF', *N*-methyl-D-phenylalanine; Thr(OMe), *O*-methylthreonine; Lys (Ac), *N*-acetyllysine; Dha, dehydroalanine; Pla, phenyllactic acid; Ahx, 6-aminohexanoic acid; Ado, 8-amino-3,6-dioxaoctanoic acid; Dap, 2,3-diaminopropionic acid

Inhibitory activity of FR900359-derived analogs and peptides

The depsipeptides **1**, **2**, **11**, **12** and peptides **13**–**22** were tested for their inhibitory activity on second messenger-generating Gq, Gs, and Gi signaling pathways, respectively (**Figure 5-14**, **5-15**). As described in **Chapters 5.2.1** and **5.2.2** FR analogs **1** and **2** were in the same activity range as the lead compounds (**Table 5-4**, **Figure 5-14**), while surprisingly, depsipeptide **11** only revealed an IC_{50} value of ~90 µM, and compound **12** was inactive. Also peptides **13**–**22** (**Figure 5-15**) were devoid of activity towards Gq inhibition. In addition, no Gs or Gi activity was observed as determined in second messenger cAMP accumulation assays for all compounds (**1, 2, 11-22**).

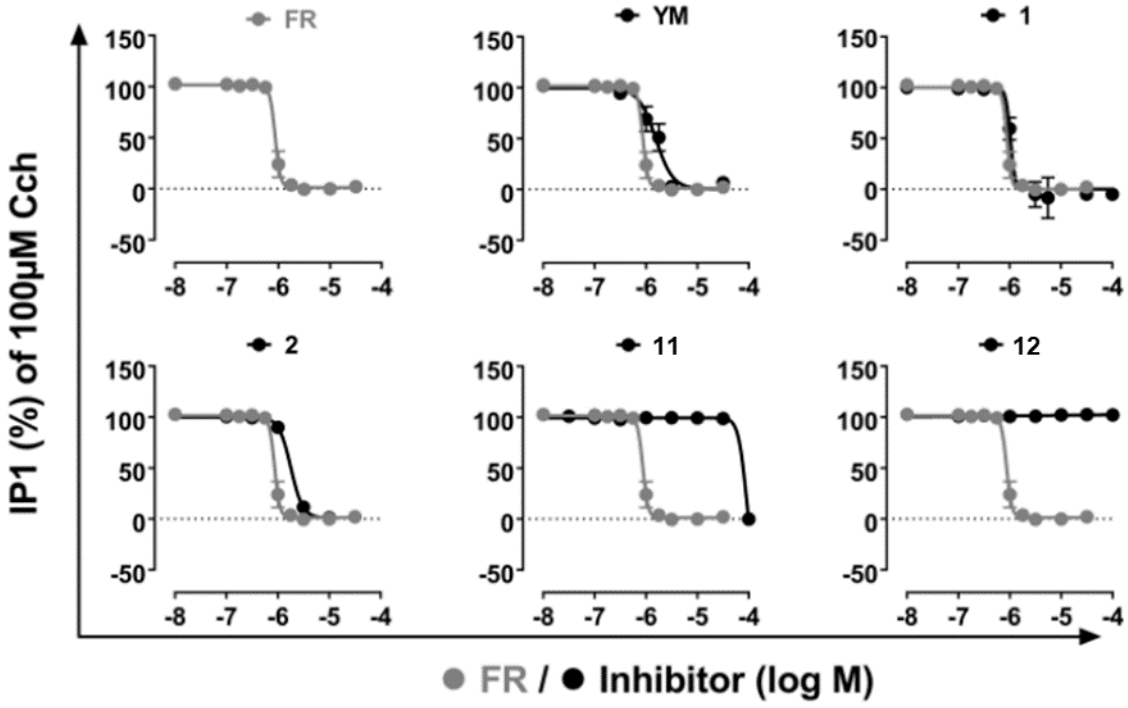

Figure 5-14: Carbachol-induced IP1 accumulation in CHO M1 stable cell line preincubated with or without potential Gq inhibitors. Assays performed by Suvi Annala, Tobias Benkel and Nina Heycke Univ. of Bonn.

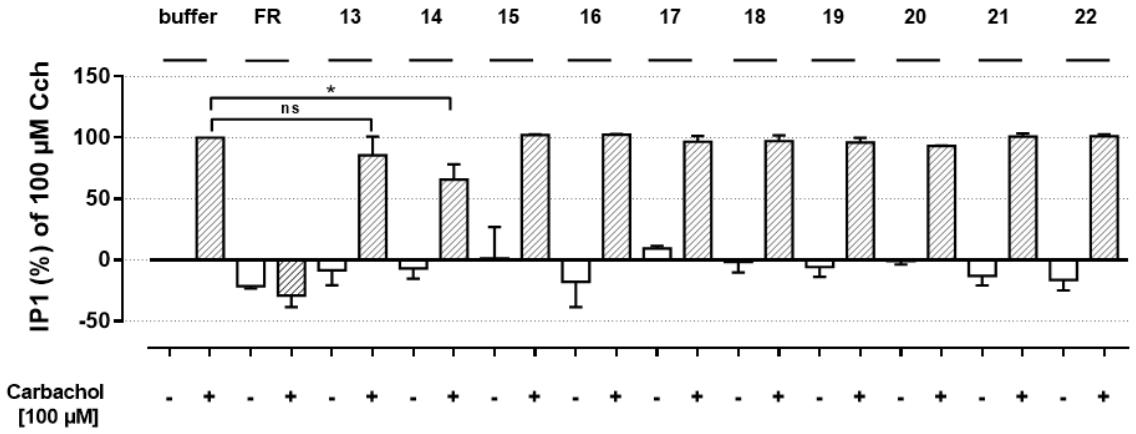

Figure 5-15: Carbachol induced IP1 accumulation in CHO M1 stable cell line preincubated with or without potential Gq inhibitors. Assays performed by Suvi Annala, Tobias Benkel and Nina Heycke Univ. of Bonn.

Structural studies on FR and analogs by NMR spectroscopy

In order to explain the differential activity of Gq inhibitors, ^{1}H NMR-based characterization of the conformation of FR, FR analogs **1**, and **2**, and YM-inspired peptides **13** and **22** was accomplished in various solvents and temperatures (water, chloroform, and methanol/water). Additionally, solution structures were calculated from NOE intensities in water for FR and peptides **13** and **22** (**Figure 5-17, Table 5-5,** Appendix **Table 10-3**). Similar to YM, chloroform ^{1}H NMR spectra of FR showed two resolved sets of NMR signals, indicating a major and a minor conformation at a ratio of 10:1 at 293 K (**Table 5-5**).[52] These two conformations are most likely caused by a *cis/trans* isomerization of the amide bond between A'' and F' with the major conformer exhibiting the *trans* amide bond. Apart from the major isomer, a large chemical shift separation of the two Hβ protons of A'' (5.69; 3.73 ppm vs. 5.32; 5.07 ppm, $CDCl_3$, **Table 5-5**) was observed which is presumably due to the ring current effect of the nearby phenyl ring of F' accounting for a *cis* amide bond.

Table 5-5: ^{1}H and ^{13}C NMR spectroscopic data of FR900359 in $CDCl_3$ (^{1}H: 600 MHz; ^{13}C: 150 MHz), H_2O/D_2O (v:v/ 9:1, ^{1}H: 500 MHz), $MeOH/H_2O/D_2O$ (v:v:v/ 1:1:0.2, ^{1}H: 500 MHz).

Isomer		**major**		**minor**	**Major**	**major**
			$CDCl_3$		**H_2O/D_2O**	**MeOH /H_2O/ D_2O**
Residue[c]	**No C/H[b]**	**δ_C[a], mult**	**δ_H[a] (mult, J in Hz)**	**δ_H[a] (mult, J in Hz)**	**δ_H**	**δ_H**
A	1	172.6, C	–	–		
	2	45.9, CH	4.90 (m)	5.05 (m)	4.82	5.03
	2-NH	–	8.51 (d, 9.1)	7.65 (d, 9.5)	7.06	7.24
	3	18.1, CH_3	1.39 (d, 6.7)	1.29 (d, 6.5)	0.82	1.02
A''	4	164.0, C	–	–		
	5	145.5, C	–	–		
	6a	106.9, CH_2	a 5.32 (d, 2.2)	5.69 (d, 1.7) [e]	5.73	5.87
	6b	–	b 5.07 (d, 2.2)	3.73 (m)	3.43	3.58
N-Me	7	36.3, CH_3	3.15 (s)	2.97 (s)	2.64	
F'	8	167.9, C	–	–		
	9	72.7, CH	5.21 (dd, 4.1, 8.3)	5.07 (dd, 9.0, 3.9)	5.42	5.61
	10a	36.8, CH_2	a 3.11 (dd, 4.1, 14.8)	3.41	2.91	3.11
	10b	–	b 2.98 (dd, 8.3, 14.8)	2.74 (dd, 12.6, 4.4)	2.83	2.99
	11	136.1, C	–	–		
	12/16	129.7, CH	7.26[d]	7.15 (m)	7.06	7.07
	13/15	128.7, CH	7.29[d]	n.d.	6.91	7.18
	14	127.1, CH	7.23[d]	7.28 (m)		
L'	17	169.4, C	–	–		
	18	50.5, CH	5.27 (dd, 1.3, 10.0)	5.17	4.68	4.89
	18-NH	–	7.55, (d, 10,0)	7.33 (d, 9.4)	8.81	8.63
	19	77.8, CH	5.12 (dd, 1.3, 10.0)	5.15 (m)	5.22	5.38
	20	29.0, CH	1.89 (m)	1.72 (m)	1.56	1.72
	21	19.1, CH_3	1.01 (d, 6.8)	1.14 (6.8)	0.55	0.75
	22	19.0, CH_3	0.85 (d, 6.8)	1.07	0.55	0.75
Ac	23	171.6, C	–	–		
	24	22.6, CH_3	2.23 (s)	2.15 (s)	1.80	1.96
T'	25	166.6, C	–	–		

	26	64.6, CH	4.07 (d, 9.8)	4.22 (d, 9.8)	3.72	3.81
	27	72.5, CH	3.76 (m)	3.87 (m)	3.63	3.65
	28	16.5, CH_3	1.18 (d, 5.8)	1.23 (d, 6.1)	1.01	1.18
N-Me	29	28.9, CH_3	2.70 (s)	3.05 (s)	3.01	3.11
O-Me	30	57.3, CH_3	3.41 (s)	3.46 (s)	2.93	
L''	31	171.4, C	–	–		
	32	46.8, CH	5.36 (d, 9.9)	5.51 (d, 9.8)	4.92	5.13
	32-NH		6.74, (d, 9.9)	6.65 (d, 9.8)	6.79	6.96
	33	77.1, CH	5.31	5.04	4.66	4.84
	34	30.7, CH	1.72 (m)	ca. 1.90	1.82	1.61
	35	19.5, CH_3	1.09 (d, 6.7)	1.12 (d, 6.7)	0.71	0.95
	36	18.3, CH_3	0.83 (d, 6.7)	0.83 (d, 6.7)	0.67	0.66
A'	37	170.1, C	–	–		
	38	56.6, CH	4.71 (q, 6.8)	4.76 (q, 6.8)	3.31	3.51
	39	14.4, CH_3	1.38 (d, 6.8)	1.45 (d, 6.8)	1.06	1.27
N-Me	40	31.5, CH_3	2.88 (s)	2.86 (s)	2.82	3.02
L'''	41	170.4, C	–	–		
	42	57.0, CH	4.55 (dd, 1.4, 7.8)	4.60 (dd, 8.1, 1.3)	4.86	4.94
	42-NH	–	7.17 (d, 7.8)	7.27	7.86	7.77
	43	78.4, CH	3.73 (m)	3.73 (m)	3.60	3.82
β-OH	43-OH	–	6.85 (d, 4.2)	6.43		
	44	30.1, CH	1.98 (m)	1.95 (m)	1.29	1.47
	45	20.6, CH_3	1.17 (6.7)	1.07 (d, 6.7)	0.66	0.84
	46	18.7, CH_3	0.88 (6.7)	0.92 (6.6)	0.66	0.81
Pr	47	174.9, C	–	–		
	48a	28.8, CH_2	2.57 (dq, 14.9, 7.5)	2.35 (m)	2.06	2.24
	48b		2.50 (dq, 14.9, 7.5)	2.35 (m)	2.06	2.24
	49	10.1, CH_3	1.19 (t, 7.5)	1.19 (t, 7.5)	1.26	1.44

[**a**] Assignments are based on extensive 1D and 2D NMR measurements (HMBC, HSQC, COSY). ^{13}C-NMR spectra were recorded at 150 MHz. [**b**] Numbers according to Scheme S1. [**c**] Residues: Ala = alanine, *N*-MeDha = *N*-methyldehydroalanine, D-Pla = D-3-phenyllactic acid, *N*-Ac-β-HyLeu= *N*-acetylhydroxyleucine, *N*-MeThr(*O*Me) = *N*,*O*-dimethylthreonine, β-HyLeu = β-hydroxyleucine, *N*-MeAla = *N*-methylalanine, *N*-Pr-β-HyLeu = *N*-propionyl-β-hydroxyleucine.[d] overlaying resonances

In contrast to the above observations, the minor conformer appears to be the major conformer in aqueous media as revealed by a series of ^{1}H-NMR spectra at different temperatures in a water/methanol mixture (**Figure 5-16**). Moreover, this isomer was the only observable species at 275 K, while multiple minor conformations emerged with increasing temperature as concluded from the appearance of multiple additional signals in the ^{1}H chemical shift region of 6 to 9 ppm (**Figure 5-16,** Appendix **Table 10-4**).

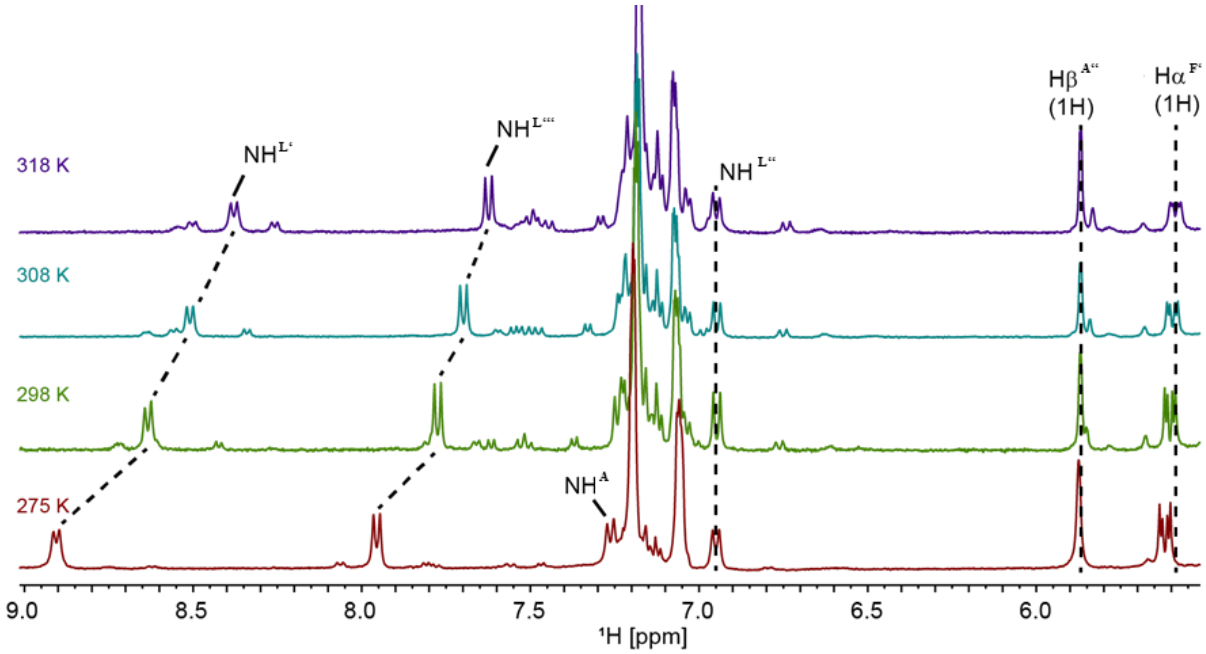

Figure 5-16:. ^{1}H spectra of the aromatic region of FR in MeOH/H_2O/D_2O (v:v:v/ 1:1:0.2, ^{1}H: 500 MHz) at different temperatures.

Finally, NMR structure calculations clearly confirmed that FR exclusively exists in a well-defined global conformation (ensemble heavy atom RMSD 0.48 Å, **Figure 5-17D**) in aqueous solution, which indeed revealed a *cis* amide bond between F' and A''.

All other amide bonds were identified to be in a *trans* conformation. In contrast, earlier NMR studies on YM-254890 in various organic solvents[28] indicated *cis* amide bonds between T'/L'', A'/A based on the presence of $H\alpha_i/H\alpha_{i+1}$ NOE crosspeaks, which were clearly missing in FR. Even though this amide bond was found to be in a *trans* conformation in Gq-bound YM (PDB ID 3AH8),[53] the global backbone fold of the cyclic FR-core remained fairly similar. In contrast, the L'''/L'' tail was found to be in a different orientation and rotated along the L'''/L'' ester bond by approx. 150° (**Figure 5-17D**).

In contrast to FR, analog **13** forms a rather flat cycle (ensemble heavy atom RMSD 0.83 Å, **Figure 5-17B**) folding into two equally populated conformations showing *cis/trans* isomerism between A'5 and A6. A second stable *cis* peptide bond was observed between A6 and A'7. In addition, although distinct parts of the structure of **13** (A'5, A6, A'7, and Ac-Lys1) are in good agreement with FR (A'', A, A'), it deviates to some extent from the solution structure of FR (RMSD 7.1 Å, **Figure 5-17E**). Similarly, **22** also folds into a flat cyclic structure (ensemble heavy atom RMSD 0.71 Å, **Figure 5-17C**), which appears to be more flexible compared to **13** (**Figure 5-17B**, **C**). The structural deviation of **22** from the global conformation of FR, however, is significant (RMSD 8.7 Å, **Figure 5-17F**). Thus, **13** and **22** do not reproduce the global fold of FR, which most likely accounts for their lack of biological activity.

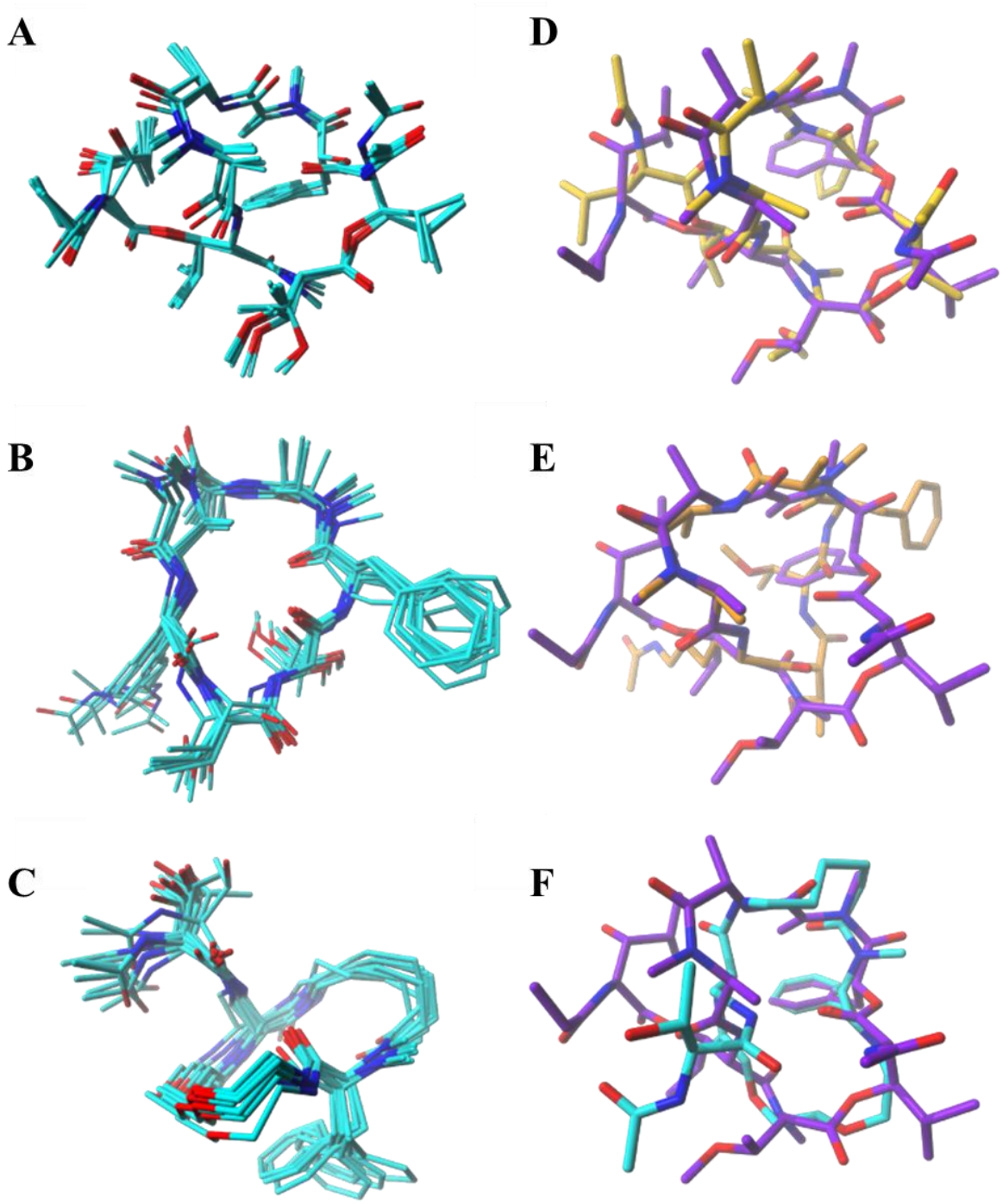

Figure 5-17: Solution NMR structures of FR (**A**) and its analogs **13** (**B**) and **22** (**C**) (presented as ensembles of 10 lowest energy structures (coloring scheme: carbon - cyan, nitrogen - blue, oxygen - red). Superposition of the NMR solution structure of FR (carbon - purple) with (**D**) YM (PDB ID 3AH8,[14] all atom RMSD 2.41 Å, carbon - yellow), (**E**) **13** (all atom RMSD 7.14 Å, carbon - orange), and (**F**) **22** (all atom RMSD 8.67 Å, carbon - cyan).

Molecular modeling and docking studies

Molecular modeling and docking studies were performed by Dr. Daniel Tietze, TU Darmstadt, Germany and applied to provide in-depth insight into inhibitor-Gq interactions and to characterize the binding mode of the most potent inhibitors. The YM-derived analogs **23**, **26**–**36**, and **39**–**45**, investigated herein were constructed from the Gq-bound conformation of YM-254890 (PDB ID 3AH8).[53,224] For FR-derived analogs **1, 2 11, 12**, two conformations were built employing the solution NMR structure of FR and the Gq-bound conformation of YM. The structures obtained were then docked to the heterotrimeric Gq protein in the original conformation. Except of **31**, which carries a backbone modification (A' to A), these analogs contain side chain modifications at A', A, L'''/ Leu'' or at the acetyl group of T'' (YM)/L' (FR). A closer look at the target-bound conformation of these analogs obtained from the docking runs revealed only minor alterations of the global fold of the inhibitor molecules retaining the intramolecular hydrogen bonds as observed in YM/FR (**Figure 5-18**). Consequently, the high-affinity analogs **1**, **2**, and **23**–**31** (**Scheme 5-9**) also share a similar orientation in the Gq binding pocket resulting in almost identical hydrogen bond interactions with Gq (**Figure 5-18A+B**). Moreover, similar orientations within the Gq binding pocket in comparison to the orientation of YM were observed when the alternative NMR-derived structures for FR and **1** (named FR *cis* and **1** *cis* thereafter) were employed in the docking experiments (**Figure 5-19A-C**). A marginally different Gq-bound orientation was found for the NMR derived structure of **2** (named **2** *cis* thereafter, **Figure 5-19D**).

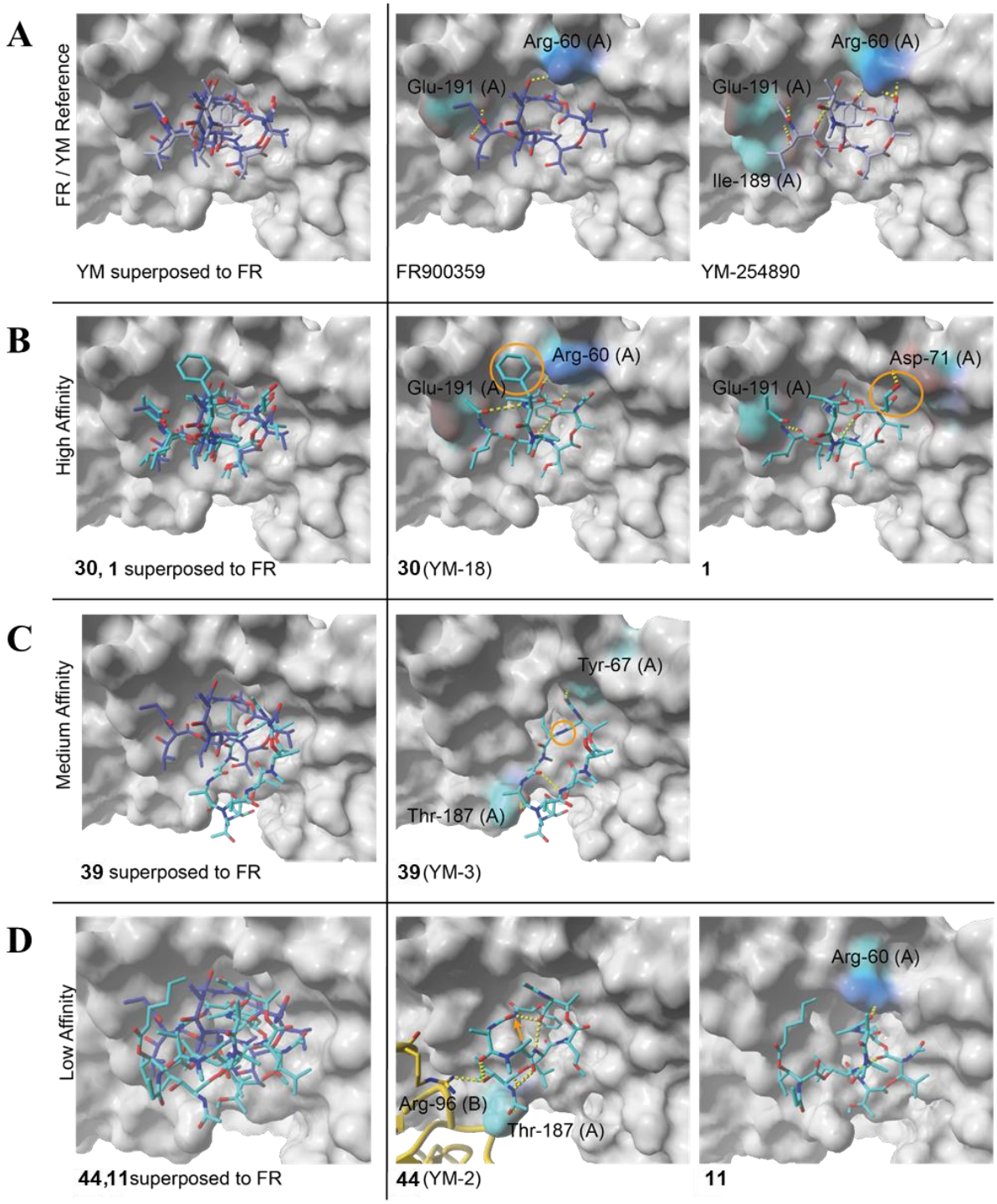

Figure 5-18: **Docking results** (a) Superposition of reference structures YM-254890 (PDB ID 3AH8, carbon - purple) and FR900359,[54] carbon - navy blue) on the left, separate views of their individual binding modes on the right (coloring scheme: nitrogen - blue, oxygen - red, hydrogens are omitted for clarity, hydrogen bonds are shown as yellow dashed lines; Gαq surface - gray, hydrogen bond interacting residues - labeled and highlighted by element color, Gβ - dark yellow). (b) Superposition of FR900359 (carbon - navy blue) with the docked conformation of two selected high-affinity analogs **30** (YM-18) and **1** (carbon - cyan) (left) as well as separate views of their individual resulting binding modes (right); particular modifications are tagged by orange circles or arrows. (c) Superposition of FR900359 (carbon - navy blue) and the docked conformation of the selected medium-affinity analog **39** (YM-3) (carbon - cyan) (left) as well as separate view of its individual binding mode (right) (d) Superposition of FR900359 (carbon - navy blue) and the docked conformation of two selected low-affinity analogs **44** (YM-2) and **11** (carbon - cyan) (left) as well as separate views of their individual binding modes (right).

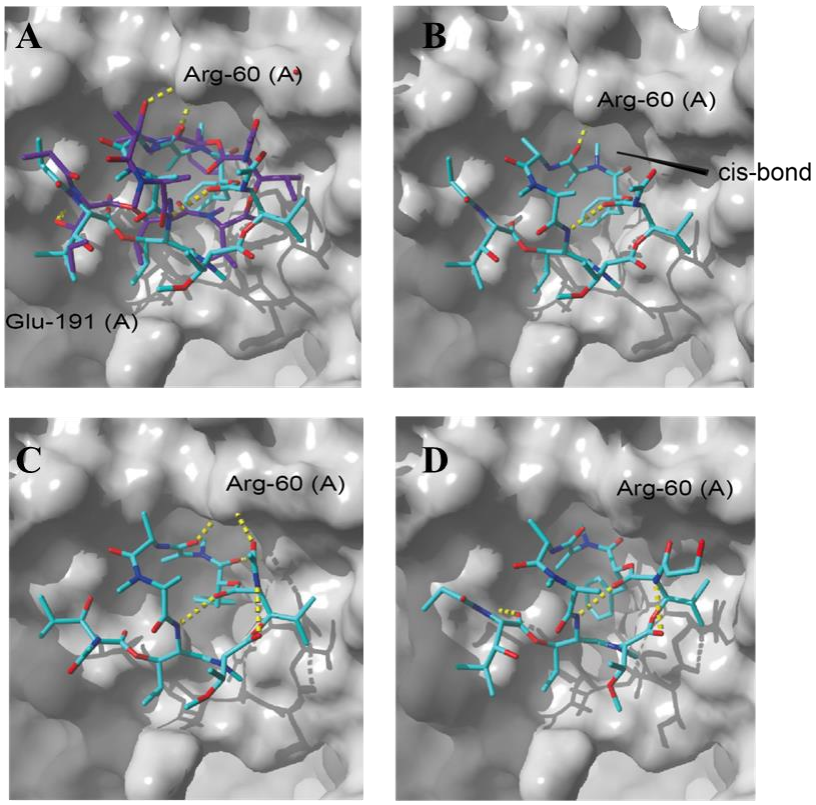

Figure 5-19: (**A**) Superposition of FR and cis FR bound to Gq as revealed from the docking studies. Orientation of (**B**) *cis* FR (**C**) *cis* 1 and (**D**) *cis* 2 bound to the Gq-YM binding pocket.

In conclusion, this strong orientation towards linker 1 and β sheet 2 of the Gα subunit, mainly represented by the hydrogen bonds to Arg60 and Glu191 and hydrophobic interactions towards segments α1 (I56, K57), αA (F75), switch I (V184), and β sheet 2 (I190, Y192, P193), complement intrinsic features of powerful Gq inhibitors (**Figure 5-20**).

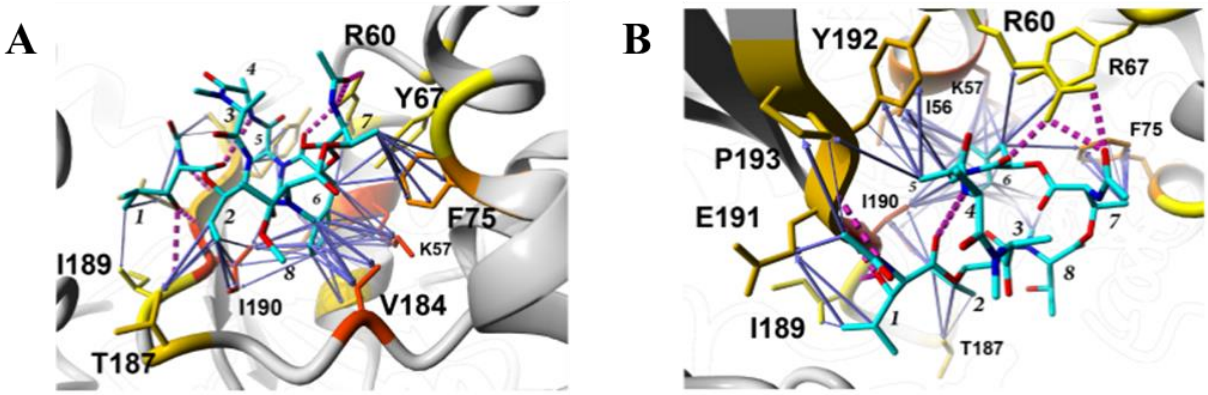

Figure 5-20: (**A**) and (**B**) Illustration of key interactions of high affinity inhibitors with Gq (residue numbers – regular, bold), exemplarily shown for YM (residue numbers – italic, coloring scheme: carbon - cyan, nitrogen - blue, oxygen – red). Hydrogen bonds are indicated by magenta dotted lines. Hydrophobic interactions between Gq and YM are indicated by blue arrows between the interacting atom pairs (thickness of arrow indicates interaction strength). Gq residues are colored according to the sum of their hydrophobic interaction energy with YM, ranging from yellow (1 kJ/mol - weak) to red (10 kJ/mol - strong).

In case of the medium-affinity analogs **36**–**39**, each compound appears to be conformational more flexible compared to YM/FR as revealed by our MD simulations (**Figure 5-21**). Thus, these would result in different global conformations compared to the original conformation (**Figure 5-18C**) and, in turn, in different orientations in the Gq binding pocket compared to YM (**Figure 5-18C**).

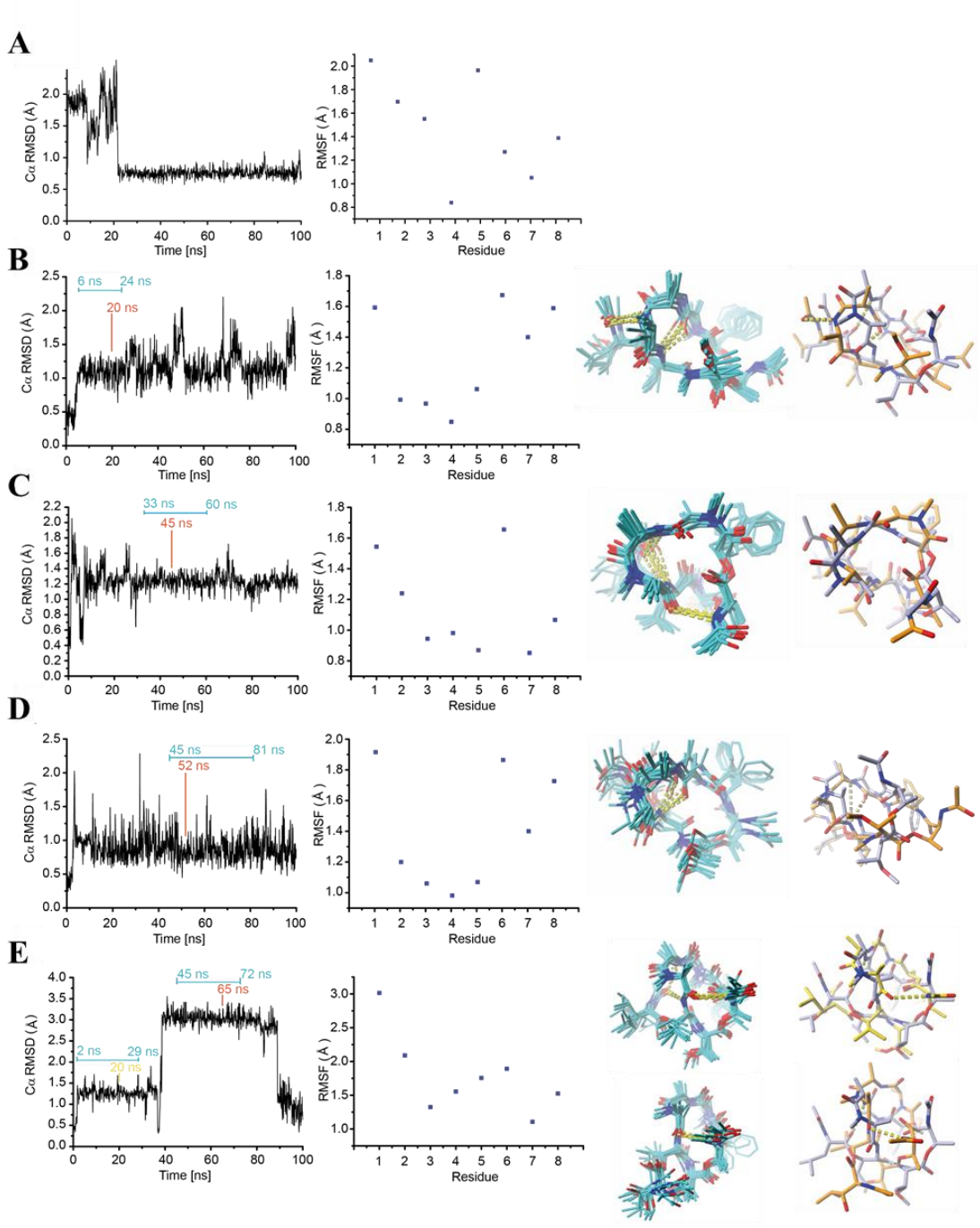

Figure 5-21: Overview of MD simulations of (**A**) YM, (**B**) **31** (YM-1), (**C**) **38** (YM-9), (**D**) **39** (YM-3) and (**E**) **37** (YM-385780). RMSD time trace of Cα atoms and per residue RMSF (first two panels from left) and structural ensemble (third panel, 10 structures, coloring scheme: carbon - cyan, nitrogen - blue, oxygen - red, hydrogens are omitted for clarity, hydrogen bonds are shown as yellow dashed lines) derived from the time interval indicated (blue line) at the Cα RMSD-time trace. Fourth panel: Superposition of YM-254890 (carbon – light purple) and energy-minimized representative structure (carbon – orange/yellow) extracted from the simulation after a certain time, which is indicated by yellow/orange label at the Cα RMSD-time trace and which was used for docking.

Regarding the low-affinity or inactive compounds **11**–**22** and **40**–**44** an increased structural flexibility as assessed by NMR analysis and MD simulation (except of **11** and **12** significantly altered the global conformation, resulting in highly dissimilar structures compared to YM/FR (**Figure 5-22**). Taking a closer look at the orientation of the low-affinity compounds in the Gq binding pocket, except of **43**, the phenyl ring of F' resides in the hydrophobic cleft as already observed for the high- and medium-affinity YM/FR analogs. Another common feature among this group of YM analogs is the tendency of hydrogen bond formation with the switch I region or residues of the Gβ subunit as shown for **11** and **44** in **Figure 5-18D**. However, with the exception of **11** and **40**, Arg60 was no longer linked via hydrogen bonding by any of these analogs. Instead, Arg96 of the Gβ subunit became a major hydrogen bonding partner. In any case, the modifications introduced into the low-affinity YM/FR analogs significantly altered the conformation of the inhibitor molecule and thus the ability to correctly access the rather deep binding pocket. This interpretation becomes even more valid with respect to the different conformations of the inactive peptides (**13**–**22**).

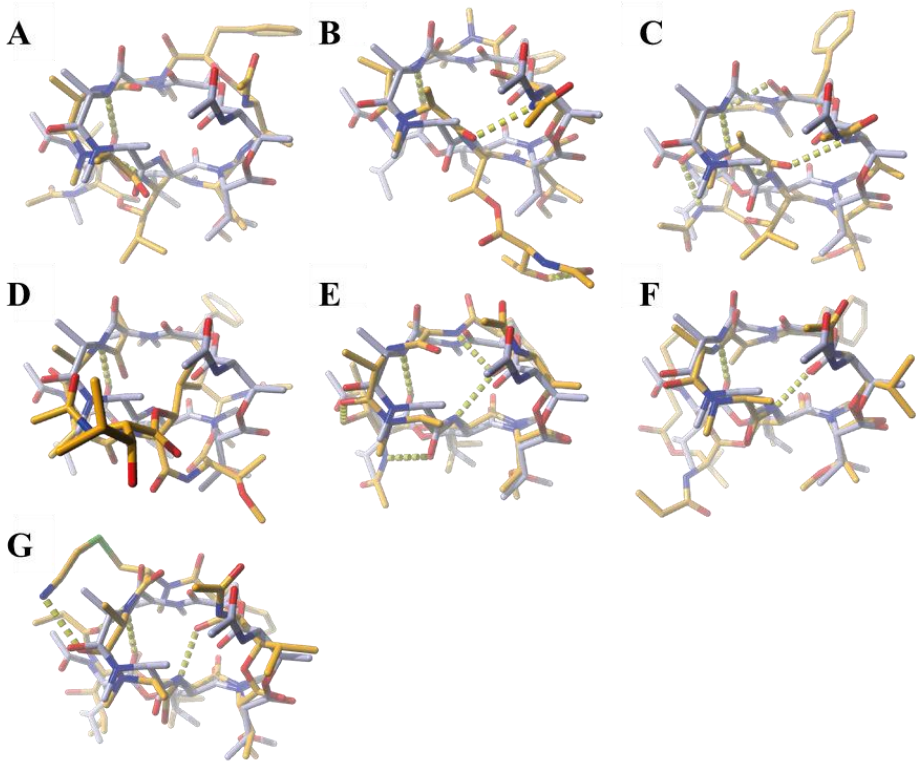

Figure 5-22: Superposition of the protein-bound conformation of YM (color scheme: carbon - light purple, nitrogen - blue, oxygen - red, PDB ID 3AH8) with the conformation of the protein-bound YM/FR analog (carbon - yellow) (**A**) **40**, (**B**) **41**, (**C**) **42** (**D**) **43** (**E**) **44** (**F**) **11**, and (**G**) **12** as revealed by the docking experiments.

Deviation of recognition determinants for inhibitor binding to $G\alpha_q$

FR and YM represent small to medium-sized compounds with a high degree of chemical complexity, specific three-dimensional conformations, and consequently precise orientation of backbone and side chain atoms through intrinsic rigidity. Our attempt focused on characterizing features accounting for the high inhibitory activity of YM/FR towards Gq and on sampling chemical space to identify possible sites for further optimization. This analysis revealed how changes in three distinct categories affect inhibitory potency compared to the lead compounds, namely I) backbone conformation, II) backbone conformation influencing the intramolecular hydrogen bond network, and III) side chain constitution and orientation (**Scheme 5-10**). In analogs belonging to categories I and II, which are based mainly on backbone modifications, most drastic effects or even complete loss of activity were observed in derivatives **44**, **43**, **42**, and **40**, in which only single atoms or small groups were changed at T', (T'' in YM), (A''), or (A) relative to YM/FR (**Scheme 5-9, 5-10**). Considering structural alterations within backbone modifications, two different types need to be taken into account: a) sole conformational changes (category I), e.g. evoked by inversion of configuration as in **42**, and b) functional impairment of intramolecular hydrogen bonding (category II), as occurring in **40**, **43**, and **44** (**Figure 5-22**). Exploring their individual binding modes revealed perturbations on the individual molecule's integrity with respect to YM/FR and their binding behavior. Substitution of an ester by an amide bond as in **40** was also introduced in a further compound (**39**) at a different position (F' to *DF*), which turned out to result in a moderately active derivative compared to the inactive **40**, **42**–**44**. This demonstrates that the ester bond linking T' and L' (or T'' for YM respectively) is more important concerning the macrocycle's bioactive conformation than the bond between L' (T'') and F'. There was one further modification in the backbone associated with a change in the hydrogen bond network, namely compound **31** (A' to A), which, however, did not significantly change the inhibitory activity compared to YM/FR (**Scheme 5-10A**). Finally, concerning backbone modifications only the reduction of A'' to A' led to a strong effect on activity, which induced stronger changes to the backbone conformation than the *N*-Me-D-Ala substitution. All further alterations as found in **35**, **31**, **28**, **27**, and **25**, including changes such as an increase in flexibility (*e.g.* A to G, **35**) or the inversion of configuration (A' to *N*-Me-D-Ala, **28**), were tolerated (**Scheme 5-10A**).

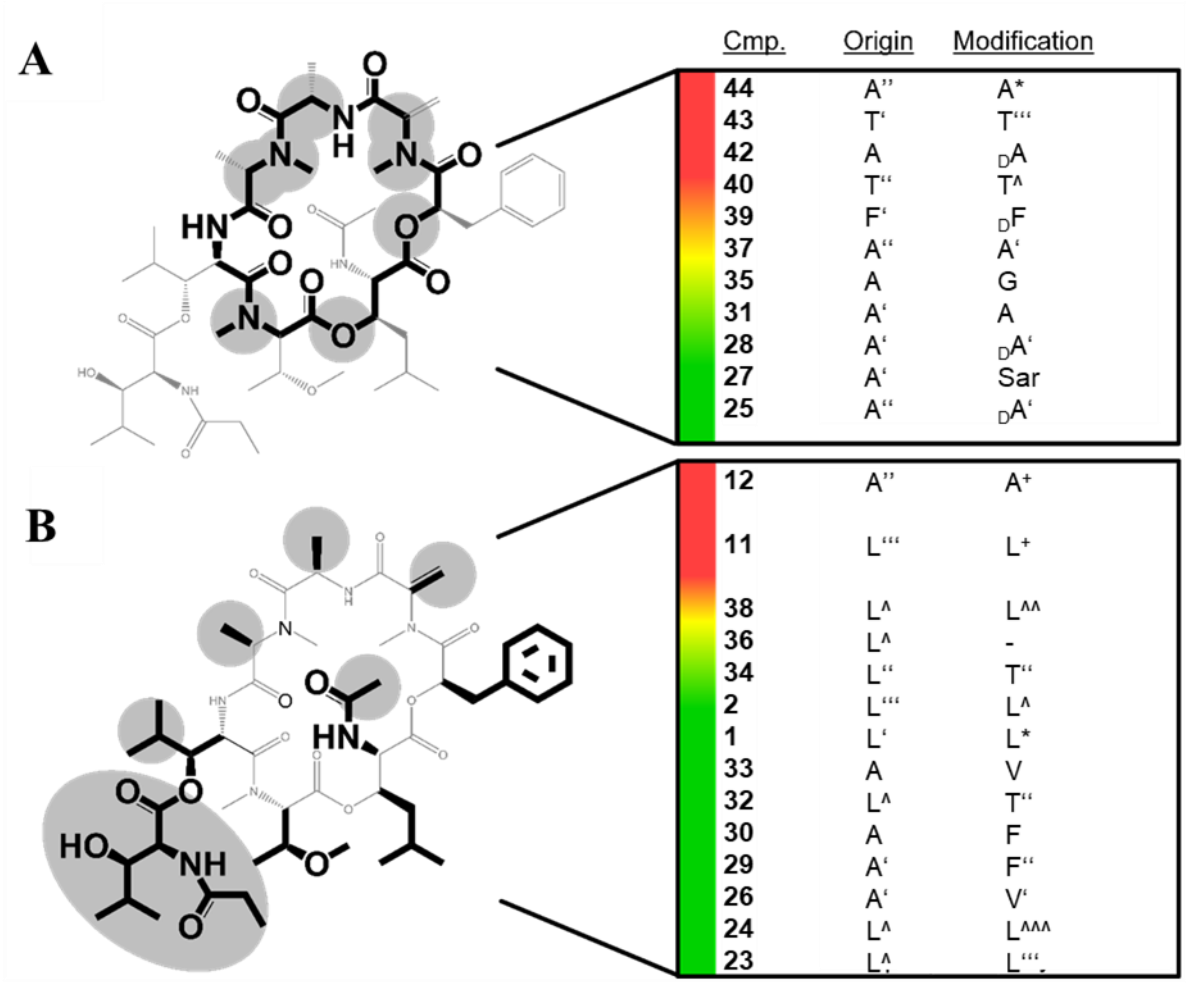

Scheme 5-10: Structural classification of compounds with modifications at one side of FR and/or YM according to their impact on (**A**) backbone and intramolecular hydrogen bonds and (**B**) side-chain modifications. Colored bars next to compounds indicate acceptance of modifications (red - inactive compounds with minor, non-tolerated substitutions, yellow - moderately active compounds with partially tolerated substitutions, green - active compounds with tolerated substitutions). *Nomenclature refers to YM-254890. A*, dehydroalanine; T'', *N*-acetylthreonine; T^, 2,3-diaminobutyric acid; T''', *O*-methylthreonine; $_D$A, D-alanine; $_D$A', *N*-methyl-D-alanine; $_D$F, D-phenylalanine; F'', *N*-methylphenylalanine; L^^, *N*-acetylleucine; L^^^, *N*-methylthioacetylhydroxyleucine[52]; Sar, sarcosine; V', *N*-methylvaline.

Thus, it is obvious that the surface region of the YM/FR molecule comprising residues A' and A accepts such changes, whereas in the region between A'' to T' not even marginal modifications are tolerated, most likely due to their direct interaction with the protein surface.

A more detailed analysis of category III comprising primarily side chain modifications and functionalities apart from the backbone atoms revealed a rather different picture. While molecules with acyl-modifications in the side-chain, *e.g.* such which occur in natural YM analogs **23**, **24**, and natural FR analog **2**, displayed equivalent potency compared to YM and FR, respectively, the $G\alpha_{q/11}$ protein did not tolerate a complete absence of an acylated side chain.[26,52] This observation was confirmed by Kaur *et al.*, who succeeded in the total synthesis of YM-280193, a YM analog lacking of the previously mentioned side-chain.[196] The corresponding FR analog, compound **6**, isolated from *A. crenata* and also detected in *C.*

vaccinii, was introduced in Chapter **5.1**. First biological data revealed also significant reduced potency towards Gq-inhibition (IC_{50} about 20 µM, data not shown). Acylation of the secondary alcohol, performed in our laboratory, caused a dramatic loss of biological activity, probably by destroying the intramolecular hydrogen network, resulting in conformational change (**11** = FR-Hex, **Chapter 5.2**). Further the side-chain seems to be important for the stabilization of the biologically active conformation of FR. **Figure 7-6** shows that the side chain is closely bound to the cyclic backbone of FR, and ^{1}H-NMR spectroscopic data of compound **6** (= FRSC, FR lacking the side chain) shows that much more conformations appear, if the side chain is missing. The equipotency of compounds **1**, **2**, **23**, and **24** can be attributed primarily to the fact that the aforementioned backbone-related criteria are retained in these analogs.

In addition, regarding the protein-facing side in YM/FR no alterations were made or identified at F', L' (T''), T', whereas at both ends spanning the sequence between residues A'') and L''', L'' modifications maybe critical as can be proven with compounds **11**, **12**, **36**, and **38** (**Scheme 5-10**). For **11**, **36** and **38**, important hydrogen bond interactions between the hydroxyl function of L^{+} (or L^) and the Gq backbone at Ile190 and Glu191 are missing, while in case of **12** the bulkiness of semisynthetically prolonged A'' to A^{+} avoids interactions at the binding site of F'. If more than one amino acid substitution was introduced at the same time, effects were even more striking. In case of **41**, simultaneous exchange of L^ and L'' for T'' led to complete loss of activity at Gq most likely due to their smaller size. With respect to our simulations, this would allow for a reorientation of the two tail residues towards Arg96 at the Gβ subunit not only resulting in the loss of hydrogen bond interaction with Ile190 and Glu191 similar to compounds **11**, **36** and **38** but also loosing hydrophobic contacts in this region. In case of **32** and **34**, in which each of the L'' residues was mutated to T'' independently, the steric reductions were not sufficient to allow for such reorientations, thus preserving the hydrogen bond interactions with the protein.

Conclusions Chapter 5.2

Together with the analysis of the backbone (categories I and II) it becomes apparent that except of two residues, *N*-Me-Ala and Ala, the remaining part of the YM/FR molecule represents the "pharmacophore" for this specific Gq binding pocket (**Figure 5-18**). In addition, both molecules obviously represent optimal, highly efficient and specific compounds for Gq inhibition, since none of the natural as well as the artificial modifications yielded more potent analogs so far.

It is known that natural products represent structures validated from millions of years of coevolution with their specific target exploiting precision in complementary chemical design.[225–227] Hence, it seems unlikely that a significant improvement regarding Gq-inhibitors can be obtained with the limited opportunities provided by the YM/FR template(s). Also, there was no effect detected at Gi and Gs proteins for the compounds analyzed herein. These observations for artificial YM-analogs together with our results on the native derivatives of FR (**1**, **2**) strongly indicate that the lead molecules already seem to be optimized for Gq inhibition. In terms of perspective, one conceivable task thus could be the implementation of strategies to target other Gα protein subunits based on the YM/FR template(s).

6 Results, Section III: Development of the first fluorescent Gq protein inhibitor

In **Chapter 5** SAR of FR and its derivatives in the context of Gq inhibition were extensively studied. The gained insights are considered also as useful to assist in the development of a fluorescent FR probe. Such a probe would possibly allow monitoring of trajectories of individual fluorescently labelled receptors and thus would provide additional information concerning the molecular receptor dynamic and interaction with FR, given that fluorescence-labeling does not perturb its biological activity. These experiments could help to get deeper insights into the interaction of FR and Gq on a molecular basis and enlighten the mechanism of action. For technical reasons, many of the ligand-receptor affinities published in the literature have been derived using purified cell membranes assayed at 4 °C.[228] Conclusions from such experiments, however refer to receptors in live cells at 37 °C.[228] This may be problematic. A fluorescent FR analog could be applied for real-time imaging in living cells to study, e.g. the mechanism of cell membrane permeation of FR. Furthermore, BRET assays were envisaged to characterize binding kinetics of cold (non-fluorescent) ligands.

According to the gained SAR insights (**Chapter 5.2**), *N*-Me-Ala and Ala are the residues of choice for derivatization as also suggested by Zhang *et al*.[201] However, these residues are only accessible in total synthesis approaches. Alternatively, we put our main focus on the development of fluorescent probes via isolation of FR and subsequent semisynthetic modification. Hence, we planned to utilize the exomethylene group of FR to add further substituents, since this part of the molecule interacts with the linker 1 region and is chemically feasible for reactions (compare **Chapter 5.2**). Thus, it was planned to use thiols to perform hetero-Michael additions,[220] *e.g*. using cysteamine as substrate (described for **12** in **Chapter 5.2.2**, which after addition to the exomethylene residue will yield a thioether with a primary amine. The latter can be further derivatized to obtain a fluorescent molecule. This approach is regarded as very versatile, since other thiols could be applied like cysteine or glutathione. This was successfully done for *N*-methyldehydroalanine containing microcystins. These microcystin-conjugates showed comparable properties to unconjugated microcystins, regarding conformation and toxicity, but the formation of epimers has to be taken into account.[216,219] In the case of microcystins, the exomethylene group was also taken for the addition of a fluorophore, *e.g*. first cysteine was attached and subsequently fluorescein (FITC) via its isothiocyanate group.[229]

As a fluorophore BODIPY630/650-X-NHS was envisaged due to its relatively low molecular weight, high fluorescent intensity, and its low photobleaching rate. A further advantage of BODIPY fluorophore-linked fluorescent ligands is the fact that they are heavily quenched in aqueous solution and are brighter in a non-aqueous environment, that is, when receptor bound.[230] These was desired by us as G proteins signal via membrane-bound GPCRs. BODIPY630/650-X-NHS contains a seven-atom aminohexanoyl ("X") spacer between the fluorophore and the NHS ester group. This spacer helps to separate the fluorophore from its point of attachment, potentially reducing the interaction of the fluorophore with FR or Gq respectively.

The main focus of **Chapter 6** is addressed to answer the following questions (taking account on the results of Section II):

1. Can we modify FR toward a fluorescent probe?

2. If so, is the fluorescent FR analog still able to inhibit Gq signaling?

3. If so, can we apply the fluorescent probe for, *e.g*. real-time imaging in living cells?

6.1 Synthesis and biological evaluation of the first fluorescent Gq protein inhibitor FR-RR-BP

6.1.1 Synthesis of FR-RR-BP (46)

A first fluorescent FR analog was synthesized in a two-step process. In the first step FR-Cys (**12**, see **Chapter 5.2.2**) was made to introduce a primary amine into the molecule. In a second step served to couple the primary amine to commercially available *N*-hydroxysuccinimide (NHS) ester containing fluorophores.

Regarding the first step, *i.e*. thio Michael addition of cysteamine to FR in micellar media, an increase in yields as compared to the procedure of compound **12** synthesis was attempted by using DL-α-tocopherol methoxypolyethylene glycol succinate (TPGS-750-M), a 2nd generation designer surfactant developed by the Lipshutz Group (**Scheme 6-1**).[231] TPGS-750-M was reported to have superior properties compared to SDS like (i) it is nonionic, (ii) the stabile ester residues make it relatively inert, (iii) it was designed to produce optimal sized nanomicelles, (iv) it was engineered to be water-soluble such that it cannot be extracted with most organic solvents (anything except chlorinated solvents) and (v) it is non-frothing. However, in our hands

the reaction using TPGS-750-M (2 wt %) in aqueous media led to even lower production yields of **12** (7.5 mg from 30 mg FR, 25%) as compared to using SDS (6 mg from 20 mg FR, 30%), *inter alia* due to laborious work-up procedure for TPGS-750-M (similar retention times like FR under standard conditions). The reaction was performed under argon atmosphere to avoid cysteamine oxidation to the corresponding disulfide.

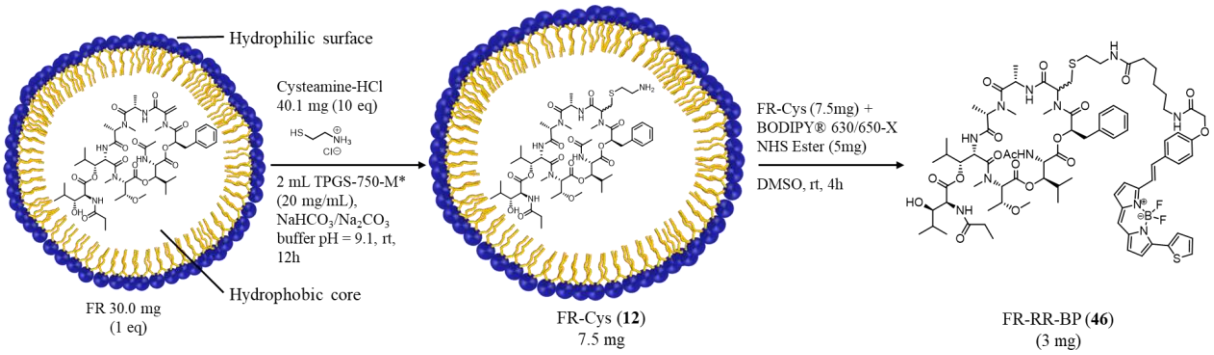

Scheme 6-1: Reaction scheme of FR-RR-BP synthesis.

In general, the second step of the reaction was performed according to the manufacturer's instructions (http://www.thermofisher.com/order/catalog/product/D10000). 7.5 mg (1 eq) of compound **12** were dissolved in DMSO and trimethylamine was added to ensure that the amine was deprotonated. Next, the amine-reactive dye BODIPY630/650-X-NHS (5 mg, about 1.1 eq) was added to the reaction mixture. The mixture was stirred at room temperature for 4 hours, protected from light. Subsequently to freeze-drying and purifying the conjugate via HPLC the desired conjugated FR-RR-BP (**46**) was obtained in moderate yields (3 mg from 7.5 mg **12**, 40%).

6.1.2 Analysis of FR-RR-BP (46)

The molecular formula of compound **46** was determined to be $C_{80}H_{108}BF_2N_{11}O_{18}S_2$ (calcd. 1624.7449; obsd. 1624.7438) for $[M+H]^+$. This result from an accurate mass measurement suggests the successful conjugation between BODIPY630/650-X and compound **12** (**Figure 6-2**). Interestingly, when comparing the LCMS² data of FR, **12** and **46**, for compound **46** a molecular ion *m/z* 1640.7 was much more abundant than the expected $[M+H]^+$ =1624.7 and pointing to an oxidation of the thioether to the sulfoxide catalyzed by DMSO. Oxidation of thioethers (sulfides) of various amino acids, peptides and proteins by DMSO have been reported earlier[232,233], however required acidic conditions. Lushington *et al*. speculated these reactions to occur also under physiological conditions *in vivo*.[234,235] In contrast to an achiral thioether sulfur atom that can be described as sp^3 -hybridized, with two lone electron pairs and two alkyl

groups occupying points of a distorted tetrahedron, the pyramidal sulfur center of a sulfoxide, with an oxygen atom replacing one of the lone pairs of electrons of the thioether is chiral, when the two organic residues are dissimilar as in compound **46**. The additional chiral center complicates analysis and made clear assignment of NMR resonances unfeasible.

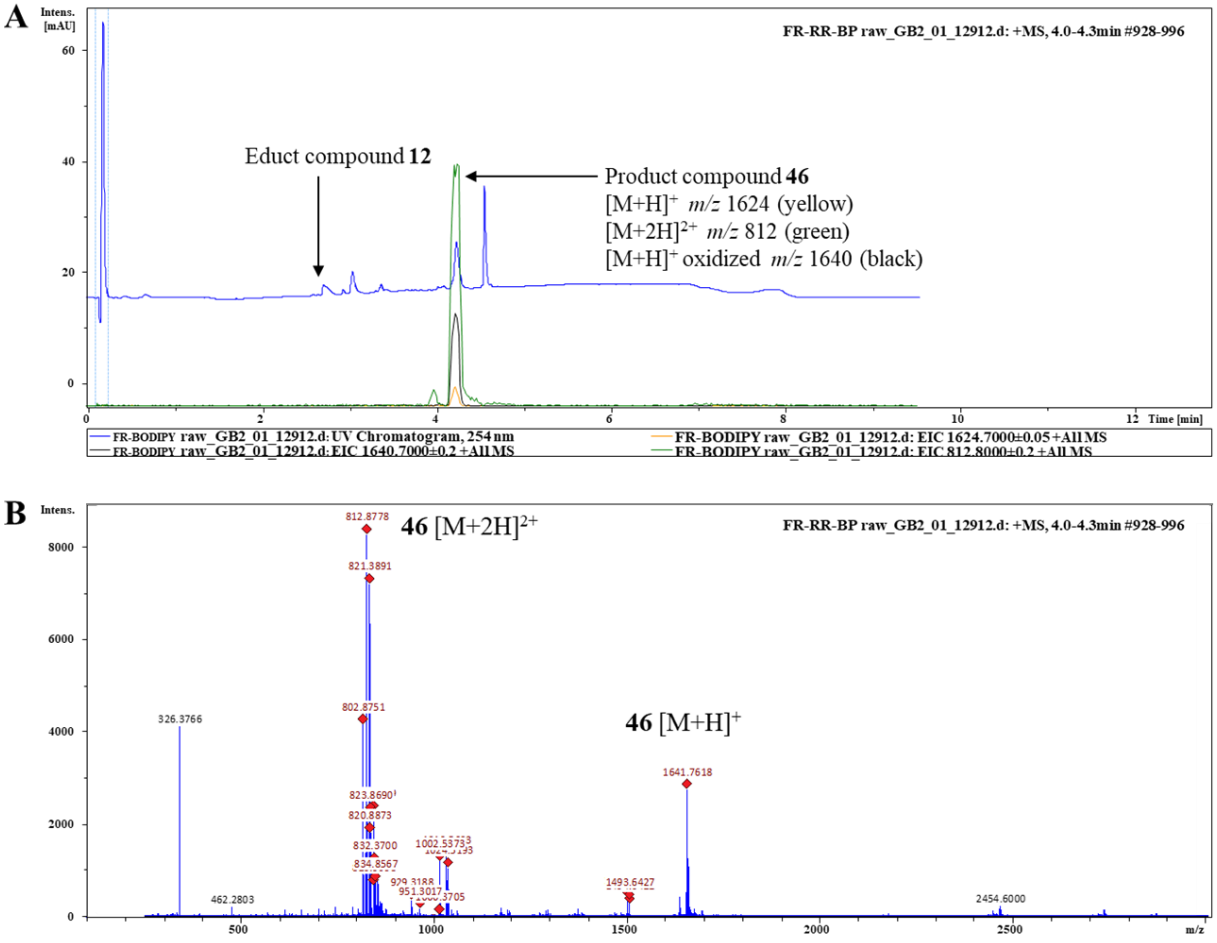

Figure 6-1: LCMS analysis of FR-RR-BP reaction mixture after 4h. (A) UV spectrum at 254 nm and extracted ion chromatograms for **46** $[M+H]^+$ *m/z* 1624 (yellow), $[M+2H]^{2+}$ *m/z* 812 (green), $[M+H]^+$ oxidized *m/z* 1640 (black). (**B**) MS spectrum for the peak of compound **46** tR 4.0-4.2 min.

6.1.3 **Bioactivity of FR-RR-BP**

To determine the properties of **46** to inhibit Gq-mediated signaling the IP1 accumulation assay could not be applied, because it is a fluorescence-based competitive immunoassay and the emission wavelength interferes with the emission of compound **46**. Hence, we applied dynamic mass redistribution (DMR) to measure signaling of G_qPCRs noninvasively in living cells (HEK293) as described by Schröder *et al.* (see also **Chapter** 3.7.5)[236].

The DMR measurements were performed by Tobias Benkel and Nina Heycke, Institute for Pharmaceutical Biology, Univ. of Bonn). Clearly, compound **46** was able to completely inhibit Gq-mediated signaling in a concentration-dependent manner, while the precursor compound **12** was inactive (**Figure 6-2A**). However, compound **46** was about 20 times less active when compared to FR. Similarly, competitive radioligand binding assays revealed low-affinity binding of compound **46** to Gq(**Figure 6-2B**).

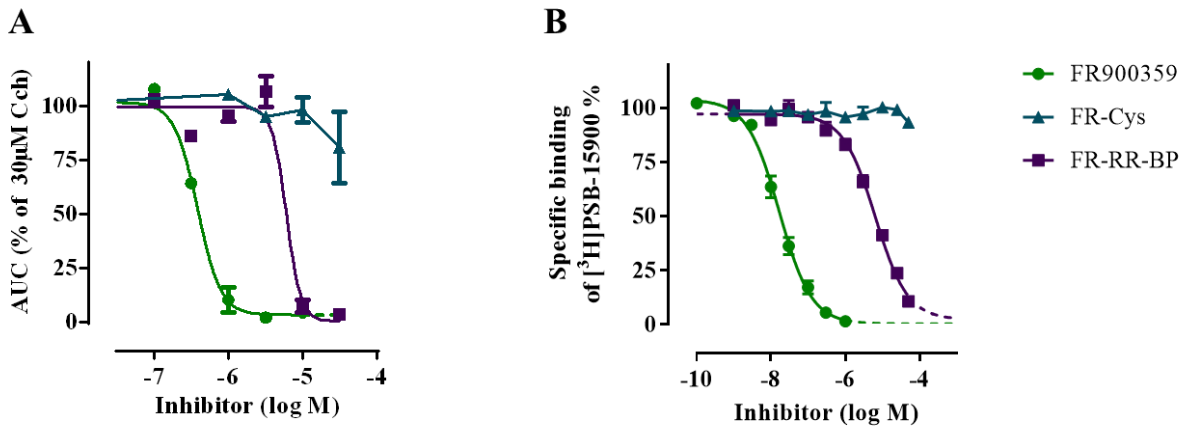

Figure 6-2: (**A**) DMR biosensing in HEK293 cells expressing endogenous Gq-coupled M3 receptors, preincubated with (potential) Gq inhibitors FR, **12**, **46** normalized to 30 µM carbachol. Experiments were performed by performed by Tobias Benkel and N. Heycke, Institute for Pharmaceutical Biology, Univ. of Bonn. (**B**) Competition binding study of FR, **12**, **46** versus [^{3}H]PSB-15900 (5 nM), the tritiated derivative of FR, at cell membrane preparations of platelets. Values represent means ± SEM of three independent experiments. Experiments were performed by performed by Markus Kuschak, Institute for Pharmaceutical Chemistry I, Univ. of Bonn.

6.1.3.1 Molecular modelling studies of compounds **12** and **46**

It was considered, whether the inactivity of **12** could be explained by the positive charge of the primary amine, which is masked upon conjugation with the BODIPY dye. This would be a possible explanation for the recovered activity. This assumption was investigated via *in-silico* binding studies, performed by Dr. Daniel Tietze, TU Darmstadt. The results suggest that **12** cannot bind to Gq due to repulsing effects of positively charged arginine residue R202 in Gq (**Figure 6-3**).

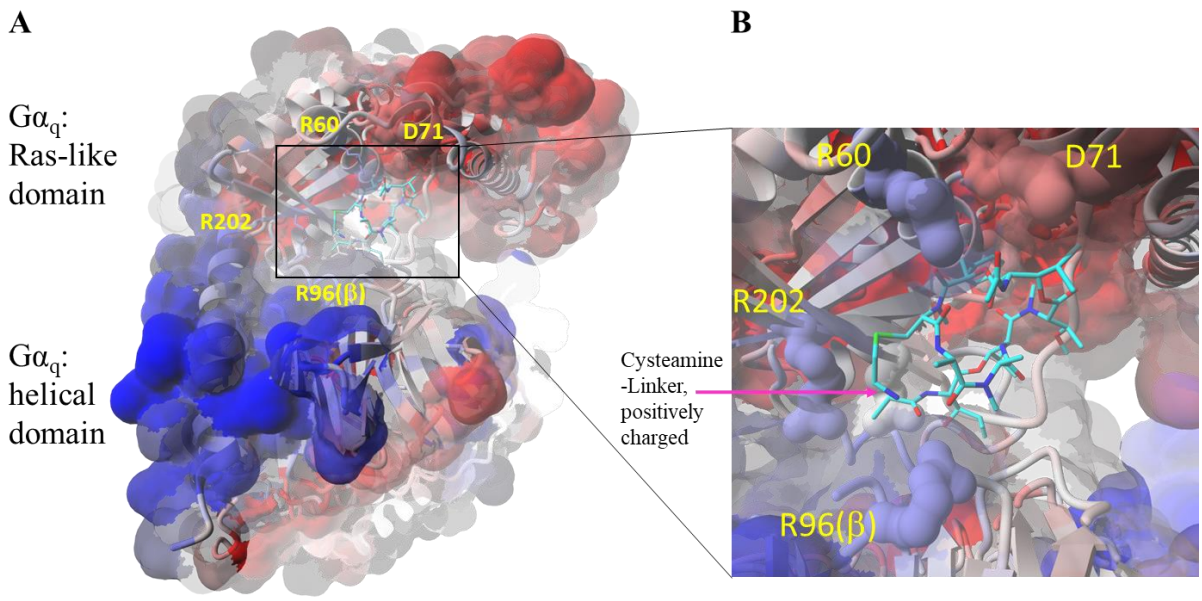

Figure 6-3: (**A**) Schematic representation of the $G\alpha_q$ subunit "bound" to **12** derived from docking by Dr. Daniel Tietze, TU Darmstadt. Surface charge distribution (red, negative; gray, neutral; blue, positive). (**B**) Zoomed-in view of (**A**).

In order to understand the significantly different binding affinities of FR-Cys (**12**) and FR-RR-BP (**46**) with respect to Gq, Dr. Tietze performed docking and molecular dynamics simulations (see **Chapter 3.6.4.** for detailed descriptions of methodology). For a holistic approach, he had to take into consideration D/L-epimers of both compounds (**12** and **46**), because the absolute configuration of the modified alanine residue is not known. Gq-bound conformations of FR-(D/L)-Cys and FR-(D/L)-RR-BP were derived from molecular docking employing a flexible docking protocol using VINA. The best scoring complex conformations (**Figure 6-4A and 6-5A**) showing the FR core structure in a similar conformation as found for YM in pdb3ah8 (taken from[53]) were subjected to further analysis and all-atom MD and steered MD simulations. Binding energies calculated from the docking (Appendix **Table 10-5**) runs unveiled the lowest binding affinities for the D-isomers of FR-Cys and BODIPY-functionalized FR (33.8 kJ/mol and 31.6 KJ/mol). In contrast, binding energies for the L-isomers of FR-Cys and FR-BODIPY were about 6 kJ/mol higher (40.3 kJ/mol and 37.3 kJ/mol) whereas the binding energy of FR-L-Cys was almost at the level of FR and YM (40.8 kJ/mol and 41.2 kJ/mol, Appendix **Figure 10-41**). With respect to the slightly different orientation of the FR-L-Cys and FR-D-Cys (I) we re-scored the high affinity FR-L-Cys complex conformation inverting the respective stereo center (FR-D-Cys (II), Appendix **Table 10-6**) in order to test if the low FR-D-Cys affinity against Gq would be artificial. Remarkably, the resulting binding energy for FR-D-Cys (II) (33.4 kJ/mol) derived from the VINA re-scoring was almost at the same level as for FR-D-Cys (I) (33.8 kJ/mol). Despite this small difference, both FR-D-Cys complex conformations were

further analyzed through regular and steered MD simulations. Interestingly, ligand un-binding was observed for both FR-D-Cys conformations within less than 20 ns during all-atom MD simulations which were run for up to 500 ns on the best scoring complex conformations from the VINA dockings (**Figure 6-4B**). Again, FR-L-Cys was much stronger bound to Gq starting to un-bind at 420 ns which confirmed the higher receptor affinity predicted from the docking results (**Figure 6-4B**).

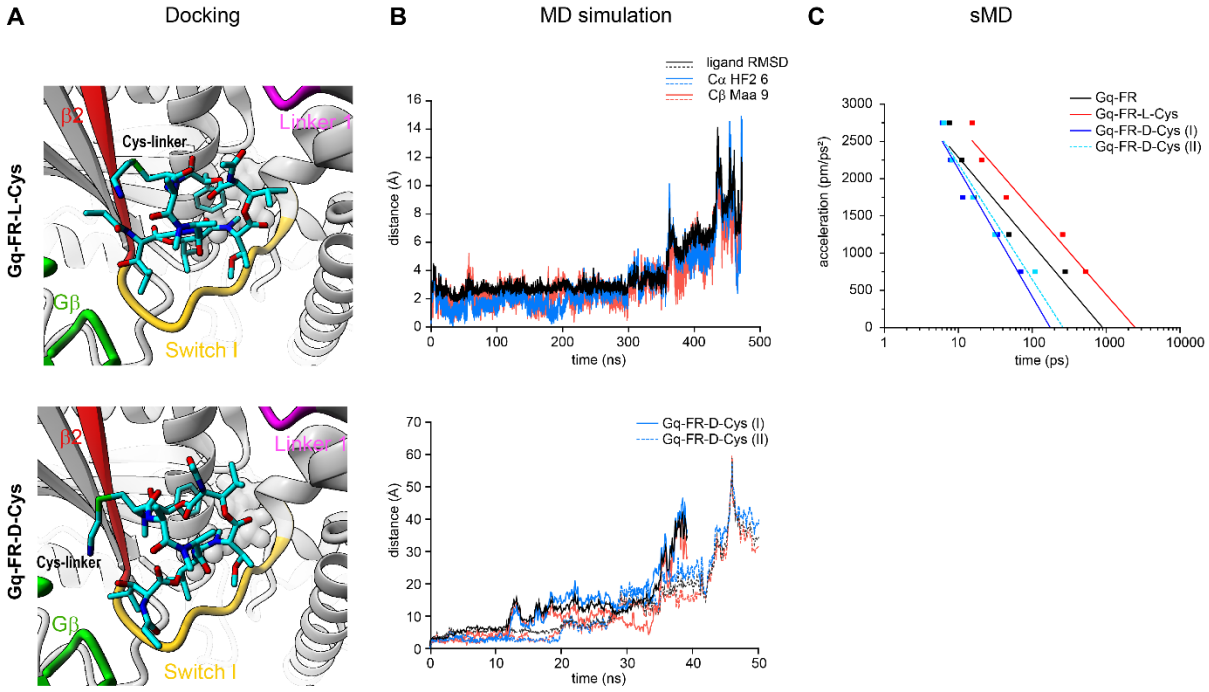

Figure 6-4: (**A**) Gq-bound FR-(D/L)-Cys (**12**) derived from molecular docking with the switch I (yellow), linker 1 (magenta) and β2 (red) region of the Gαq subunit. Gβ of the helical domain is indicated in green. **12** (I and II, see below) are shown as stick models (color code: carbon – cyan, nitrogen – blue, oxygen – red, sulfur – green) (**B**) ligand RMSD (root mean square deviation – black trace) and relative distance of two ligand atoms (Cα HF6 – blue trace, Cβ Maa9 – red trace) with respect to their starting (bound) position during all-atom MD simulation. (**C**) Steered MD profiles of ligand unbinding showing the time required to separate FR (black trace and squares), FR-L-Cys (red trace and squares) and FR-D-Cys (light and dark blue traces and squares) from the protein. Two alternative Gq bound conformations for FR-D-Cys were simulated whereas I. was derived from docking and II. (dotted lines) was derived from the docked conformation of FR-L-Cys by interconversion of the respective stereo center. Experiments performed by Dr. Daniel Tietze, TU Darmstadt.

However, FR-(D/L)-RR-BP as well as FR and YM did not show any ligand un-binding during the regular MD simulation (**Figure 6-5B**) resulting into stable complex conformations with Gq after 5 to 10 ns (40 and 100 ns for FR-L-Cys and FR-D-RR-BP). In order to have an additional estimate on the binding affinities of the FR derivatives presented in this study, steered MD simulations at various accelerations were conducted enforcing ligand un-binding by pulling the complex apart measuring the time (t_{diss}), which is needed to separate the ligand from the complex as a direct measure for the ligand binding affinity. Therefore, steered MD was performed starting from an equilibrated complex conformation taken from the regular MD runs

(Appendix **Table 10-5**). During the steered MD simulations a nearly linear dependence of t_{diss} on the acceleration was observed for all tested ligands (**Figure 6-4C and 6-5C**, Appendix **Figure 10-41**). Extrapolated complex dissociation times at zero acceleration t_{diss}^{0} (Appendix **Table 10-6**) of FR-D-Cys (~0.2 ns) confirmed its very low Gq binding affinity. Again, FR-L-Cys and FR-L-RR-BP revealed much longer t_{diss}^{0} times (~ 2.3 ns and ~ 1.8 ns, Appendix **Table 10-5**) compared to the D-isomers being even longer than for FR and YM (~ 0.9 ns and ~ 1.1 ns, Appendix **Table 10-6**) thus suggesting a significantly higher Gq affinity. Moreover, ligand binding affinities estimated from the sMD results also agree well with the ligand binding energies calculated from additional 10 ns MD simulations (Appendix **Table 10-5**) which were performed at a higher level of precision than the afore mentioned regular MD runs.

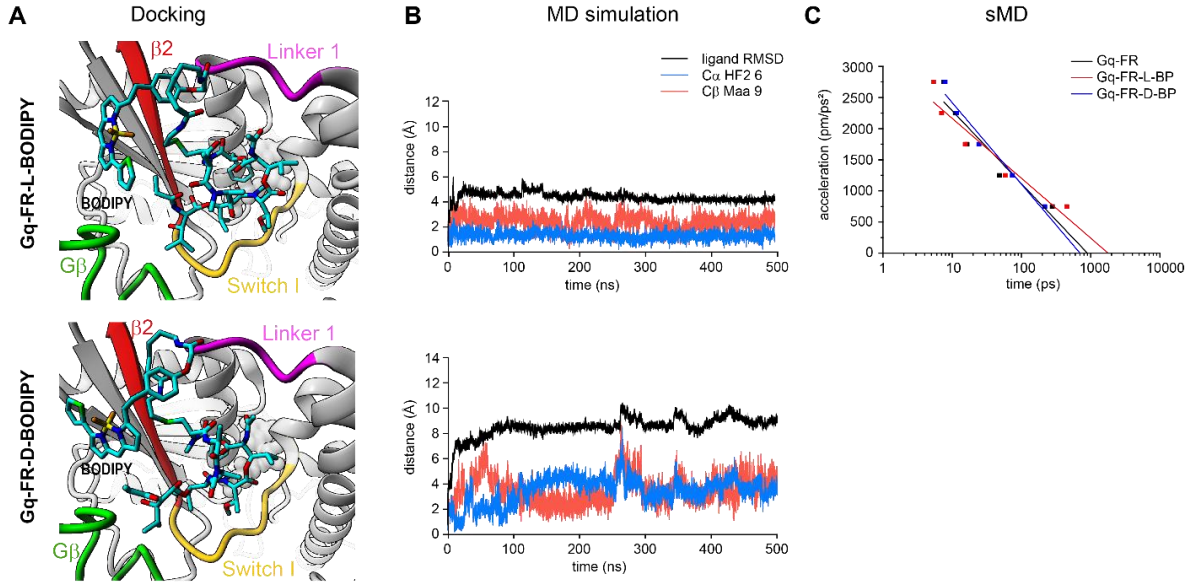

Figure 6-5: (**A**) Gq-bound FR-(D/L)-BODIPY (**46**) derived from molecular docking with the switch I (yellow), linker 1 (magenta) and β2 (red) region of the Gαq subunit. Gβ subunit is indicated in green. FR-(D/L)-BODIPY (**46**) are shown as stick models (color code: carbon – cyan, nitrogen – blue, oxygen – red, sulfur – green, fluorine – orange, boron - yellow) (**B**) ligand RMSD (root mean square deviation – black trace) and relative distance of two ligand atoms (Cα HF6 – blue trace, Cβ Maa9 – red trace) with respect to their starting (bound) position during all-atom MD simulation. (**C**) Steered MD profiles of ligand unbinding showing the time required to separate FR (black trace and squares), FR-L-BP (red trace and squares) and FR-D-BP (blue trace and squares) from the protein. Experiments performed by Dr. Daniel Tietze, TU Darmstadt.

From the molecular docking and dynamic simulations we concluded that (i) FR-L-Cys and FR-L-RR-BP should be highly bioactive or at least should strongly bind to Gq, (ii) FR-D-Cys shows much lower affinity for Gq than all other compounds, which might agree with inactivity. Therefore most likely compound **12** is FR-D-Cys (= S-epimer) as also discussed in **Chapter 5.2**, (iii) FR-D-RR-BP revealed an intermediate Gq affinity, which might agree with low experimentally found activity. Therefore most likely compound **46** is FR-D-RR-BP.

6.1.3.2 Synthesis of FR-Cys-Boc (**47**)

In **Chapter 6.1.3.1** we tried to explain the complete loss of activity of compound **12** with repulsing effects from neighboring arginine residues of Gq via molecular modelling. To verify this hypothesis we intended to create a FR derivative where the positive charge of compound **12** was masked. Hence, we coupled FR to an *N*-Boc-protected cysteamine. In general we applied the protocol from the synthesis of compound **12** (see **Chapter 6.2**) with small changes. We reacted 35 mg of FR with 20 eq *N*-Boc-cysteamine in methanol. The crude product was purified by liquid-liquid separation, flash chromatography and HPLC to yield 27 mg of compound **47** (FR-Cys-Boc) again as mixture of oxidized and unoxidized product (**Scheme 6-2**).

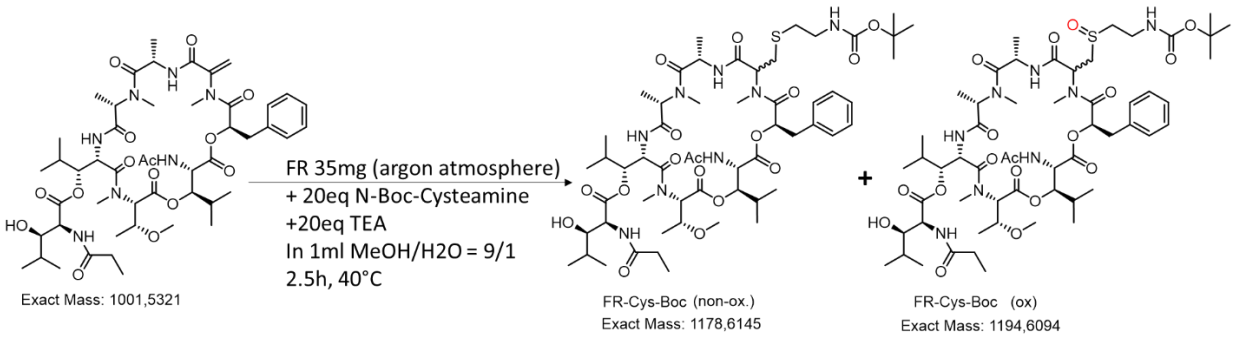

Scheme 6-2: Reaction scheme of FR-Cys-Boc (47) synthesis.

The molecular formula of the unoxidized compound **47** was determined to be $C_{56}H_{90}N_8O_{17}S$ (calcd. 1179.6217; obsd. 1179.6187) for $[M+H]^+$. This result from an accurate mass measurement suggests the successful conjugation between FR-Cys-Boc and FR (**Figure 6-6**).

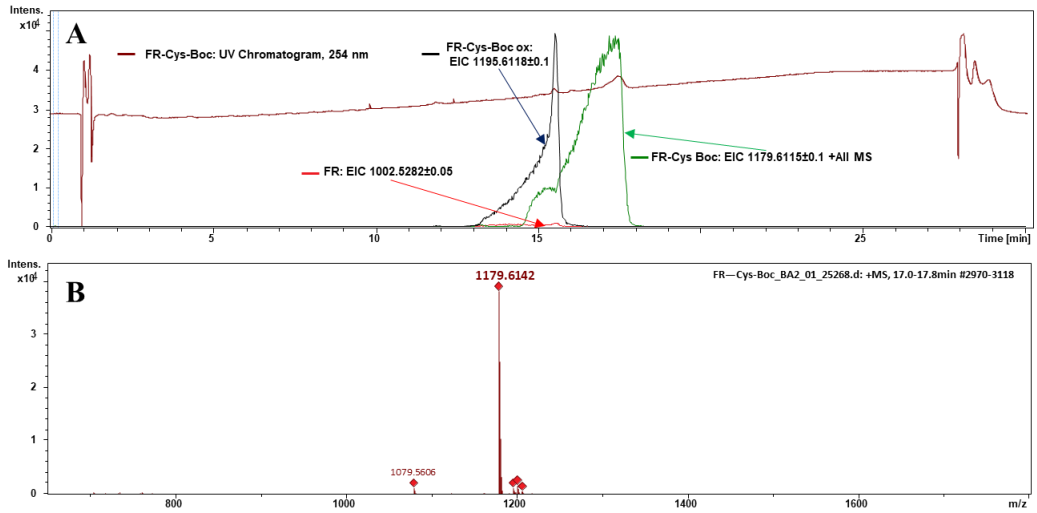

Figure 6-6: LCMS measurement of FR-Cys-Boc (47) product after Flash purification. (**A**) UV Chanel at 254 nm shows only one broad product peak. (**B**) Mass spectrum from tR 17-17.8 min. *m/z* range 650-1800 shows that the dominant signals of the sample are$[M+H]^+$ ions of unoxidized compound **47** (*m/z* 1179.61).

First bioactivity measurement show that it is completely inactive regarding Gq inhibition up to 100 µM (n = 2, personal communication, Nina Heycke). This result is surprising and would contradict our former assumption that compound **12** is most likely inactive due to its positive charge (**Chapter 6.1.3.1**). Another explanation was that there is no space for the bulky Boc group close to the FR backbone. A long flexible linker as applied in the active fluorescent FR analogs **46**, **48**, and **49** might not have these spatial demands and the bulky fluorogenic groups are possibly sufficient apart from the Gq protein. However, these results have to be confirmed before drawing final conclusions.

6.1.4 Application of FR-RR-BP (46)

After demonstrating Gq-inhibiting properties of the first reported fluorescent FR analog compound **46** we tried to visualize its interaction with Gq via fluorescence correlation spectroscopy (FCS). FCS, developed *inter alia* by Elliot Elson,[237] is widely applied to study membrane and protein dynamics, intracellular transport and cellular uptake,[238] protein-protein and ligand–receptor interaction.[239] FCS experiments were performed by Dr. Thomas Sorkalla, Dr. Stefan Franken, Stefan Aatz, Häberlein lab, Institute for Biochemistry and Molecularbiology, Univ. of Bonn on either HEK293 wildtype (wt) or HEK293 Gq/knockout (Ko) cells. First, HEK293 wt cells were incubated with compound **46**, then pictures were taken after 1 min, 15 min, and 30 min (**Figure 6-7A**). Afterwards the outcome was compared with the same setting, but using HEK293 cell where Gq proteins had been genetically depleted via CRISPR/Cas9[240] (**Figure 6-7B**). No significant differences between both cell lines could be observed, so it was concluded that compound **46** is unspecifically distributed and that direct specific binding to Gq could not be visualized. To examine whether the staining pattern observed in **Figure 6-7A+B** was due to solely the fluorescent dye or to FR coupled to the dye we repeated the experiment with BODIPY-630/650 conjugated with tris (hydroxymethyl)aminomethane (Tris), a common buffer component. Interestingly, while compound **46** entered cell membranes immediately after 1 min, it took the BODIPY-Tris conjugate about 30 min to be present in the cell membranes for both HEK wt cells and Gq/Ko cells (**Figure 6-7C+D**).

We concluded from these experiments that compound **46** is unspecifically distributed in HEK293 wt as well as HEK293 Gq/Ko cell lines and further that **46** rapidly binds to cell membranes and that the FR-part of **46** is responsible for cellular uptake.

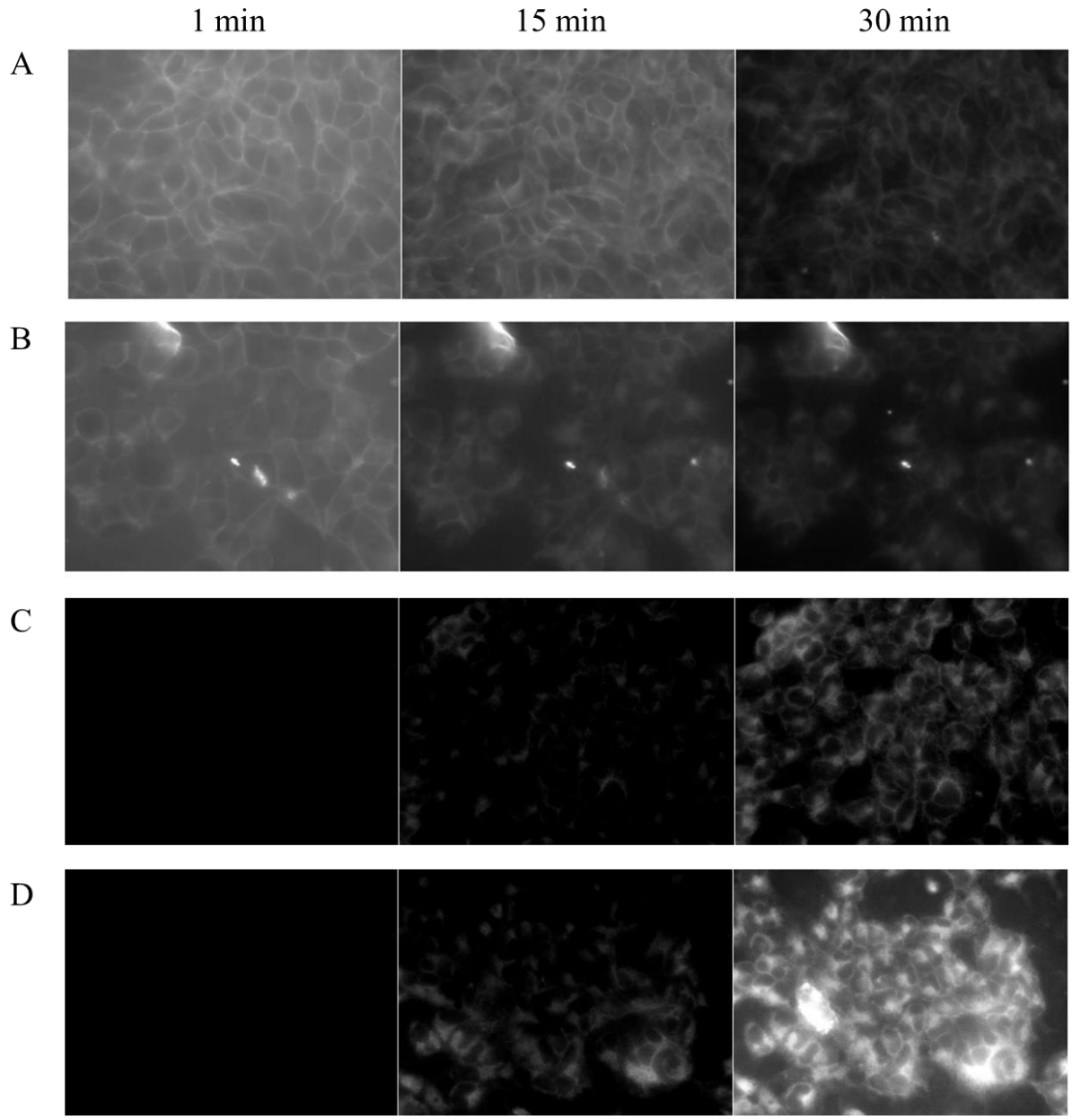

Figure 6-7: Comparative Life Cell imaging of FR-RR-BP in HEK293 wt and HEK293 Gq/Ko cells. (**A**) 50nM FR-RR-BP, HEK293 wt cells, (**B**) 50 nM FR-RR-BP, HEK293 Gq/Ko cells (**C**) 50 nM BP-TRIS, HEK293 wt cells, (**D**) 50nM BP-TRIS, HEK293 Gq/Ko cells. Exposure time = 300 ms. Experiments performed by Dr. Thomas Sorkalla, Dr. Stefan Franken, Stefan Aatz, Häberlein lab, Institute for Biochemistry and Molecularbiology, Univ. of Bonn.

A similar result could be observed by fluorescence microscopy (experiments performed by Belma Hot, Schulte lab, Karolinska Institute). We tried to show co-localization of FR-RR-BP with $G\alpha_q$-Venus (labeled Gq) and wanted to compare it to cells expressing $G\alpha_i$-GFP, but there were not observable differences (data not shown.). However, when treating the cells with compound **46** and Rab5-GFP, a marker of early endosomes[241] there was a clear indication of vesicle formation, implying endocytic uptake of compound **46** (**Figure 6-8**).

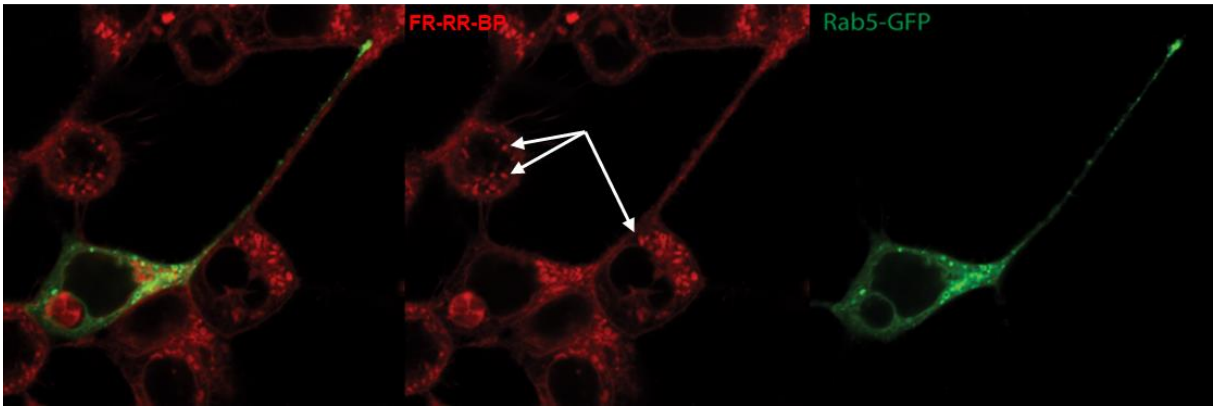

Figure 6-8: Fluorescence microscopy imaging of FR-RR-BP (46) in HEK293 cells. Rab5-GFP was used as endosomal marker. Compound **46** was found in vesicles, highlighted by white arrows. Experiments performed by Belma Hot, Schulte lab, Karolinska Institute.

Conclusions

We concluded that FR-RR-BP (**46**) is the first fluorescent selective Gq-signaling inhibitor. Applications like fluorescence microscopy & FCS measurements are at present unsuccessful due to lost specify. Compound **46** rapidly binds to cell membranes and enters cells most likely via endocytic uptake.

6.2 Development of a fluorescent FR probe with reduced hydrophobicity

FR analog **46** was determined to be a selective Gq-signaling inhibitor, though with moderate activity, and FCS experiments demonstrated that **46** unspecifically accumulates and sticks to biomembranes. To prevent the interaction with membranes and at the same time localize the fluorophore far away from the FR core structure we planned the synthesis of a fluorescent FR analog containing a prolonged and more hydrophilic linker. Dr. Daniel Tietze did *in silico* binding studies for the so far developed fluorescent FR analog **46** and also for an putative fluorescent probe containing an optimized linker (FR-JK-BP, **49**) towards Gq, Gq- NanoLuc® and Gq-RLuc (**Figure 6-9**). According to his calculations compound **49** should be suitable for bioluminescence resonance energy transfer (BRET) studies with Gq- NanoLuc®, because the NanoLuc® moiety and the BODIPY moiety are only 6-8 Å apart from each other (RET is detectable < 10 Å between donor and acceptor).

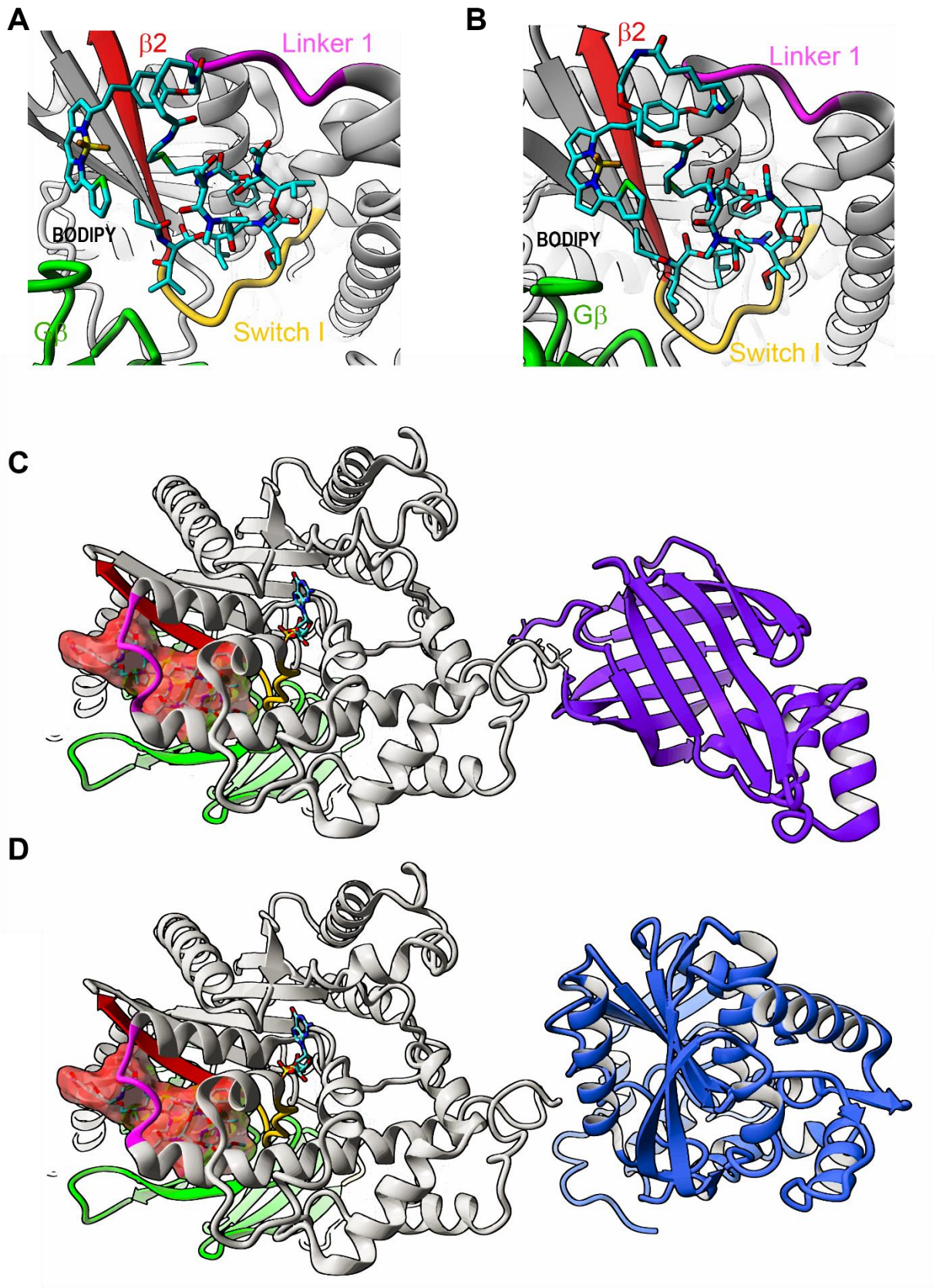

Figure 6-9: Structures of (**A**) FR-RR-BP (**46**) docked to Gq, (**B**) FR-JK-BP (**49**) with hydrophilic linker docked to Gq, (**C**) Gq-**49**- NanoLuc®, the NanoLuc® unit is shown in purple (D) Gq-**49**-RLuc8, the RLuc8 unit is shown in blue, structures of **46** and **49** (plus molecular surface colored in red for (C) and (D) are given in stick representation (atom color scheme: carbon – cyan, nitrogen – blue, oxygen – red, sulfur – green, fluorine – brown, boron – yellow). *In silico* binding experiments were performed by Dr. Daniel Tietze, TU Darmstadt.

The main reason for establishing a BRET assay was to characterize (binding kinetics) of cold, *i.e.* non-fluorescent, ligands. Firstly, for detectable RET to occur, the BRET luciferase/substrate combination needs to emit with sufficient intensity within the excitation wavelength range of the chosen fluorophore. As red fluorophores such as BODIPY 630/650 can be distinguished most readily from cellular autofluorescence and are therefore generally considered most desirable for binding assays, this was potentially a problem as luciferases emit largely at blue wavelengths that are sub-optimal for exciting red fluorophores.[242] Secondly, a BRET ligand binding assay requires extracellular fusion of the BRET donor luciferase to the receptor of interest.[242] Unfortunately, as G proteins are synthesized inside the cell and need to be trafficked and inserted into the plasma membrane, appropriate expression of such a fusion protein is not trivial. Both of these issues have been addressed by utilizing NanoLuc®. As a consequence of its very high luminescence intensity, NanoLuc®, although having an emission peak at 460 nm, has sufficient emission at longer wavelengths to enable transfer of resonance energy to red fluorophores such as BODIPY 630/650 to be readily detected.[228] The native luciferase from which NanoLuc® is derived is secreted by the shrimp in bright luminescence bursts as a defense mechanism to deter predators.[243–245] The fused Gq- NanoLuc® construct was kindly provided by Celine Galés, French Institute of Health and Medical Research, Paris.

6.2.1 **Syntheses of FR-JK-Boc (48) and FR-JK-BP (49)**

The proposed linker from Dr. Daniel Tietze was synthesized and provided by Jim Küppers (Gütschow lab, Institute for Pharmaceutical Chemistry I, Univ. of Bonn) and contained two ethyleneglycol units with a terminal tert-butyloxycarbonyl (=Boc)-protected amine on the one side and a free terminal thiol group on the other side (**Scheme 6-3**). The Boc-protecting group was used to prevent by-products in which the amino group attacked the Michael acceptor of FR.

In general we applied the synthesis protocol of compound **12** (see **Chapter 5.2**) with small changes. As LinkerJK was soluble in methanol we waived the micellar media and performed the reaction with 40 mg of FR (about 40 µM) and 120 mg LinkerJK (370 µM) under argon atmosphere in 1 mL hypergrade methanol containing 10 % milli-Q water (for details see **Chapter 3.5.4**). The crude reaction mixture was processed via liquid-liquid separation with butanol and flash chromatography (Appendix **Figure 10-1**) to yield 15 mg of the desired FR-Linker conjugate (FR-JK-Boc, **48**). Flash fractions 32-38 was controlled via $LCMS^2$ and afterwards in the second step, the acid-labile Boc group of compound **48** was cleaved with a

mixture of DCM/TFA = 5/1, controlled by TLC sprayed with ninhydrin, to obtain FR-JK-NH_2 intermediate product, which was not isolated, but directly further reacted. After removal of residual TFA, BODIPY630/650-X-NHS ester was coupled to the primary amine of FR-JK-NH_2 in DMSO and trimethylamine as catalyst. The reaction was stirred over night at room temperature and protected from light.

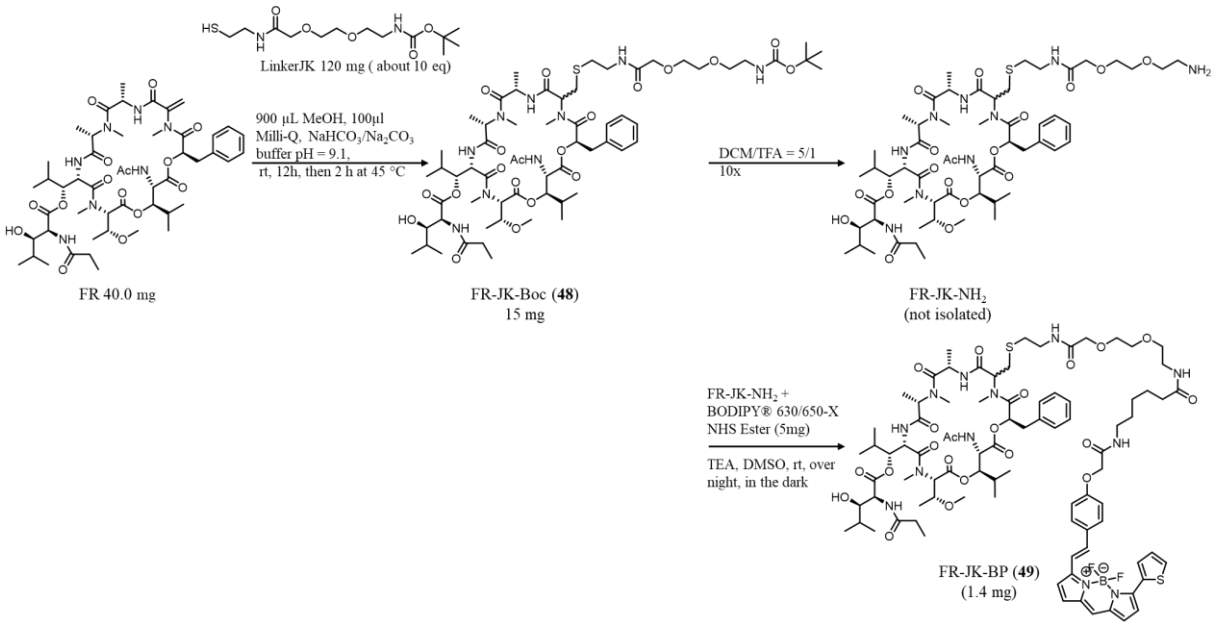

Scheme 6-3: Reaction scheme of FR-JK-BP (**49**) synthesis.

After HPLC purification of 10 mg reaction mixture, we finally obtained merely 1.4 mg of the desired product FR-JK-BP (**49**).

6.2.2 **Analysis of FR-JK-BP (49)**

The molecular formula of **49** was determined to be $C_{86}H_{119}BF_2N_{12}O_{21}S_2$ (calcd. 1769.8188; obsd. 1769.8254) for $[M+H]^+$. This result from an accurate mass measurement suggests the successful conjugation between BODIPY630/650-X and compound **48** (**Figure 6-10**). Mass spectrometric analysis. As observed earlier for compound **46**, a molecular ion + *m/z* 16 Da was also abundant for compound **49** (*m/z* 1785.82), pointing to an oxidation of the thioether to the corresponding sulfoxide, also supported by the slightly lower retention time for the oxidized product (**Figure 6-10**). That is why we exposed **49** to air until complete conversion.

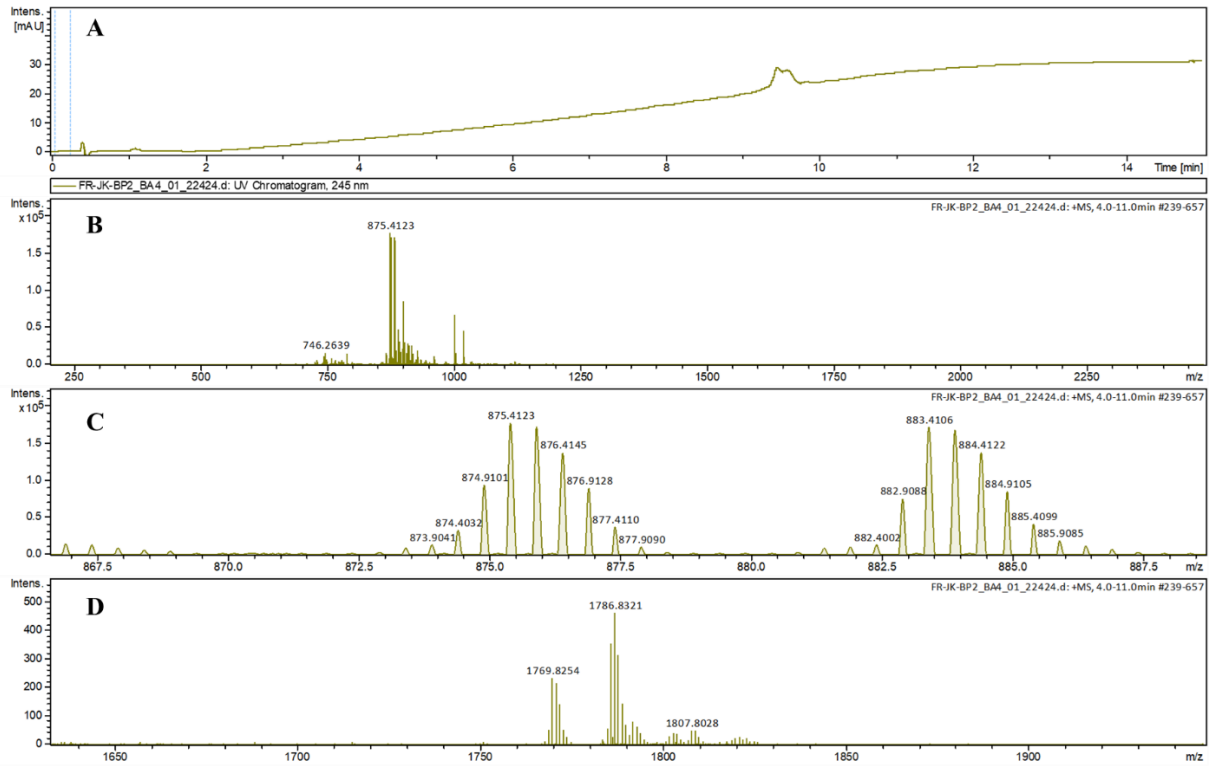

Figure 6-10: LCMS measurement of FR-JK-BP (49) product after HPLC purification. (**A**) UV Chanel at 254 nm shows only one broad product peak. (**B**) Mass spectrum from tR 4-11 min. (**C**) Mass spectrum *m/z* 865-890 shows that the dominant signals of the sample are $[M+2H]^{2+}$ ions of **49** (*m/z* 875.41)and oxidized **49** (*m/z* 883.41). (D) Mass spectrum *m/z* 1630-1950 shows the $[M+H]^{+}$ ions of **49** (*m/z* 1769.82) and oxidized **49** (*m/z* 1785.82).

6.2.3 Application of FR-JK-BP (49)

Unfortunately, when we tested compound **49** no change in BRET signal was detectable and therefore, the elongated linker might still be too short to render the fluorophore out of the binding pocket, not allowing for resonance energy transfer (personal communication with Tobias Benkel, Institute for Pharmaceutical Biology, Univ. of Bonn).

6.3 Development of FR probes with different fluorophores

The current developed fluorescent FR analogs **46** and **49** were demonstrated to be selective Gq-signaling inhibitors, though with moderate activity. Unfortunately, they seem to unspecifically accumulate in biomembranes. Further, establishment of BRET assays failed with both compounds. Therefore we intended to change the fluorophore to TAMRA, because this dye was also demonstrated to work well in BRET studies of GPCR-related research.[228]

In general, we applied the synthesis protocol of compound **47** (see **Chapter 6.2**) with small changes. We reacted 25 mg of FR with 25 mg TAMRA-thiol (2 eq) under argon atmosphere in

1 mL hypergrade methanol containing 10 % milli-Q water; deprotonation of the thiol was achieved by addition of 2 eq TEA. The reaction was stirred vigorously for 2.5 h at 40 °C, protected from light. Next, we added 10 ml milli-Q water and extracted three times with 15 mL butanol each. Afterwards the raw product was purified by flash chromatography and HPLC to yield 1.1 mg of compound **50** (FR-TAMRA, **Scheme 6-4**).

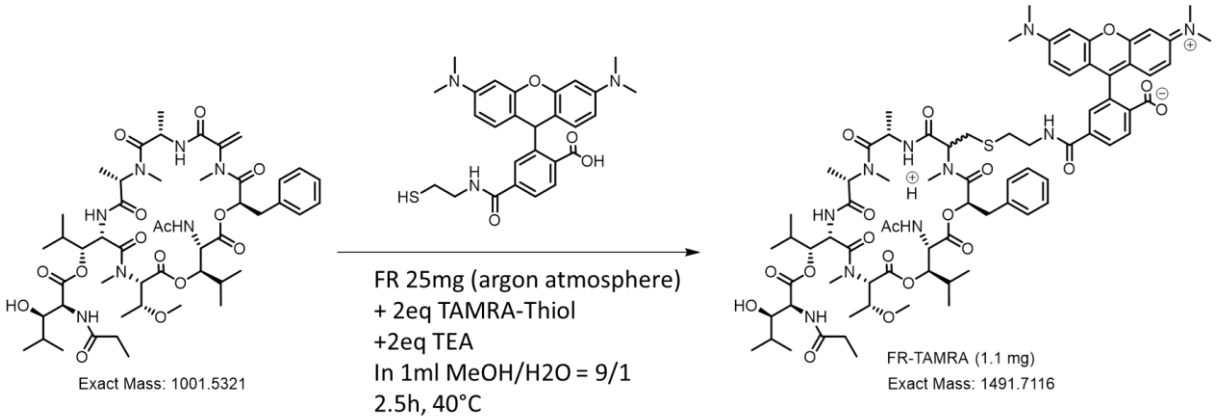

Scheme 6-4: Reaction scheme of FR-TAMRA (**50**) synthesis.

6.3.1 **Analysis of FR-TAMRA (50)**

The molecular formula of **50** was determined to be $C_{76}H_{102}N_{10}O_{19}S$ (calcd. 1491.7116; obsd. 1491.9372) for $[M+H]^+$. This result from an accurate mass measurement suggests the successful conjugation between TAMRA-thiol and FR (**Figure 6-11**).

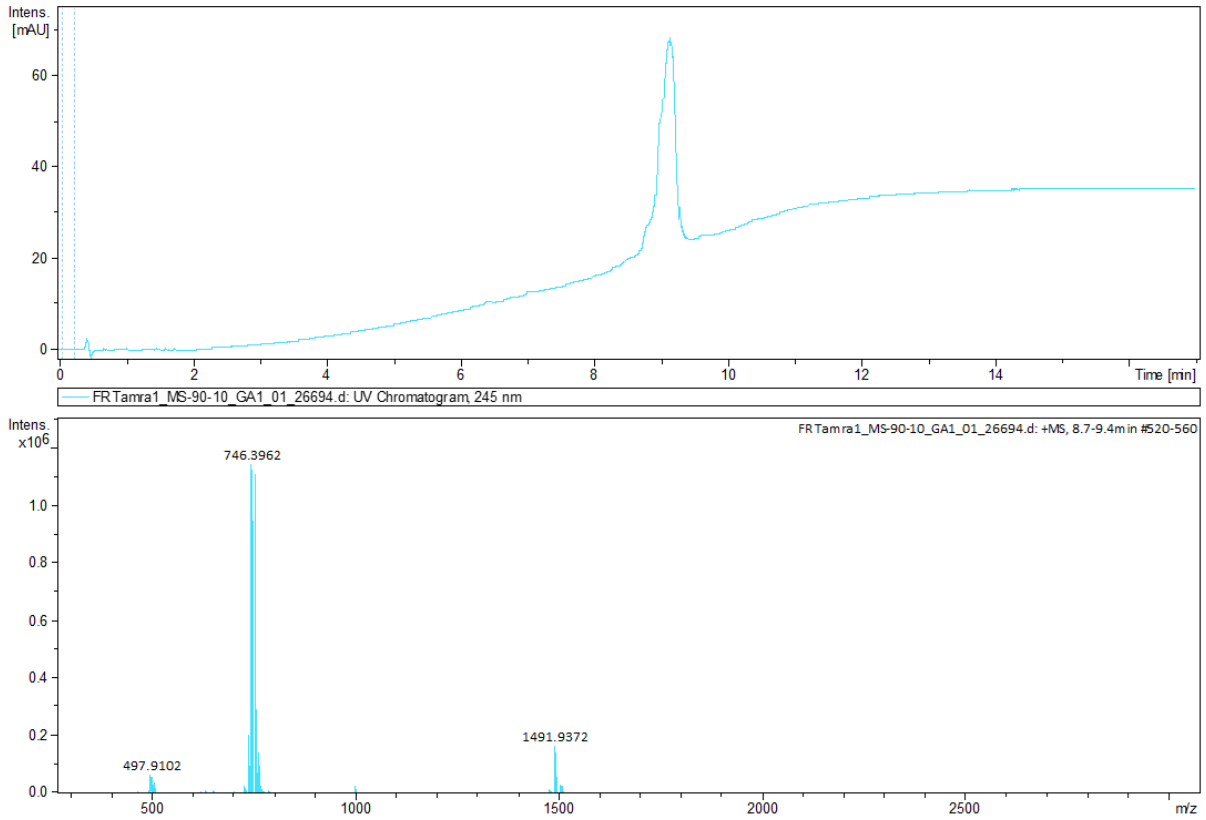

Figure 6-11: LCMS measurement of FR-TAMRA (50) product after HPLC purification. (**A**) UV Chanel at 245 nm shows only one broad product peak. (**B**) Mass spectrum from tR 4-11 min. (**C**) Mass spectrum *m/z* 300-3000 shows that the dominant signals of the sample are $[M+2H]^{2+}$ ions of **50** (*m/z* 746.40) and the $[M+H]^{+}$ ions of **50** (*m/z* 1491.94).

BRET assays with FR-TAMRA (**50**) are in progress.

6.3.2 Semisynthetic approach towards a coumarin-containing fluorophore

Besides the already used BODIPY and TAMRA fluorophores, we further intended to test the influence of the fluorophore moiety on the Gq activity. That is why we also tried to couple FR to a coumarin343-thiol derivative, synthesized and provided by Jim Küppers, Gütschow lab, Univ. of Bonn (**Scheme 6-5**).[246] Unfortunately, the coumarin-thiol was difficult to dissolve in micellar media as well as in methanol and after 24 hours only trace amounts of the desired compound could be detected via LCMS measurements. Hence, we were not able to isolate the product in quantities sufficient for further testing.

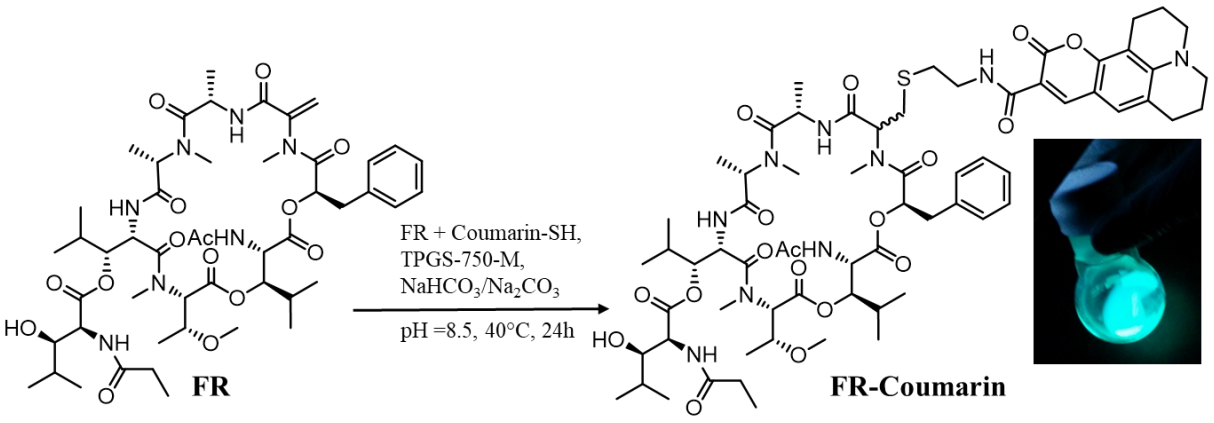

Scheme 6-5: Reaction Scheme of FR-Coumarin synthesis. Coumarin-SH was synthesized by Jim Küppers (Gütschow lab, Univ. of Bonn).

6.4 Alternative synthetic approach towards a fluorescent FR probe

Evaluation of compounds **12**, **46-50** showed that alteration of the planar sp²-hybridized (Michael acceptor of the dehydroalanine moiety) to a sp³-hybridized system was demonstrated to impede with biological effect. Thus, to keep the sp²-hybridized methylene group unchanged, a cross-metathesis reaction was conceived applying a 2nd generation catalyst developed by Nobel prize awardee Robert Grubbs[247] and a BODIPY derivative containing a terminal alkene, synthesized in the lab of Prof. Christa Müller, Univ. of Bonn (**Scheme 6-6**). The advantages of such a compound would be numerous; (i) the stereochemistry and conformation of the peptide backbone would remain intact, including the sp² hybridized exomethylene group (ii) the coupling product would have a relatively low molecular weight (iii) one-step synthesis. In natural product chemistry cross-metathesis is commonly used for ring-closing reactions.[248,249] However, there are also examples for late stage modifications of cyclic peptides via cross metathesis, and also reactions where BODIPY dyes were coupled to the molecule of interest via this type of reaction and reactions in micellar media were reported.[250–254]

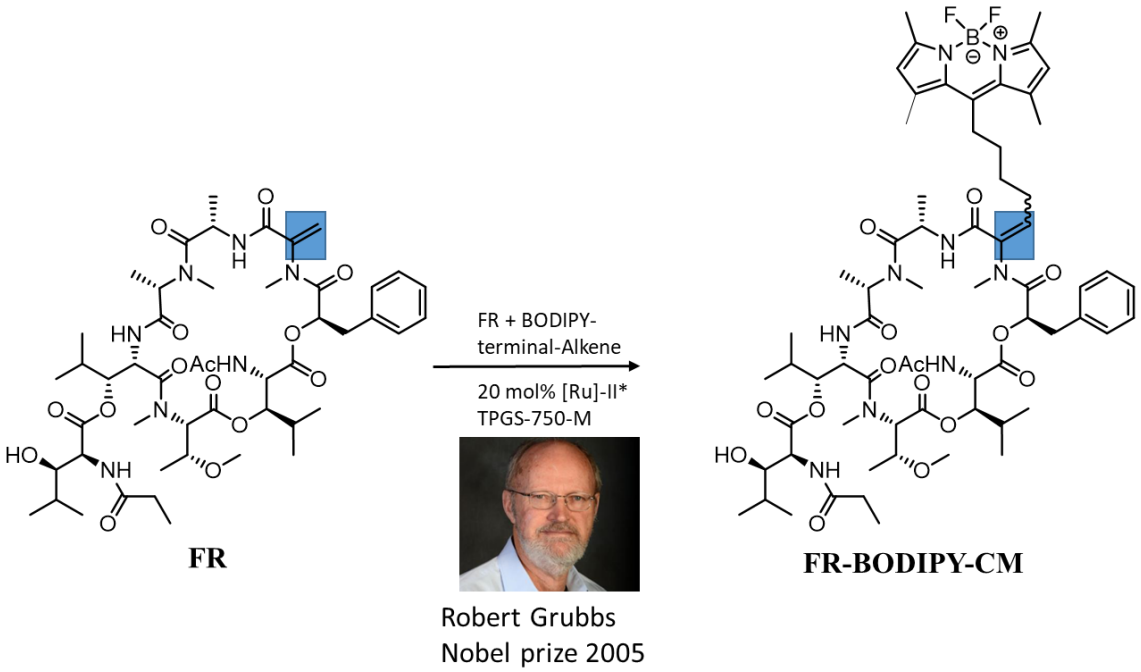

Scheme 6-6: Reaction Scheme of putative FR-BODIPY-CM synthesis. Terminal-Alkene was synthesized in the Müller lab (Univ. of Bonn).

Regrettably, pretesting with simplified structures, (performed by Jim Küppers, Gütschow lab, Univ. of Bonn) failed. That is why we did not follow this reaction type further.

Conclusions Section III

The so far developed fluorescent FR probes **46**, **49**, and **50** turned out to still inhibit Gq-mediated signaling. However, unspecific binding to biomembranes so far prevent their application as tools in fluorescence-based assays. Nevertheless, together with the failed reactions (**Chapter 6.3.2, 6.4**) compounds **46**, **49**, and **50** build a solid foundation for development of fluorescent FR analogs with improved applicabilities.

7 Discussion

7.1 Ecological considerations concerning the leaf nodule symbiosis and FR900359

It is assumed that symbiotic microbes of plants often function as biological defense for the host to combat phytopathogens. The protective functions of such endophytes are exerted often directly by releasing metabolites suitable to attack any antagonists, or indirectly by, either inducing host defense mechanisms or promoting growth.[11,12] We examined ecological aspects for the specialized leaf nodule symbiosis, occurring between bacteria of the genus *Burkholderia* and plants of Primulaceae, especially *A. crenata* as described in **Chapters 1.1** and **4.1**.

7.1.1 Burkholderia symbioses with plants and insects: Considerations about the origin of the leaf nodule symbiosis

The genus *Burkholderia*, proposed by Yabuuchi et al.,[255] is an ecologically very diverse bacterial group. To date, the ever-growing genus *Burkholderia* comprises over 100 species.[256] The genus *Burkholderia* occupies diverse ecological niches as there are several human, animal and plantpathogenetic species, including members of the *Burkholderia cepacia* complex (BCC)[257] and the *B. pseudomallei* group[258]. Some *Burkholderia* strains are, on the other hand, beneficially associated with their host organisms. These include nodule symbionts of leguminous plants, endophytic bacteria of diverse crops, mycelium and spore symbionts of fungal species, symbionts in the farming symbiosis of slime molds and gut symbionts of heteropteran insects.[256] Based on molecular phylogeny, the genus *Burkholderia* is grouped into three distinct clades (Appendix **Figure 10-42**). The first clade consists of many human, animal and plant pathogens, including *B. cepacia, B. pseudomallei, B. mallei* and their allied species, designated as the "*Burkholderia cepacia* complex and *Burkholderia pseudomallei* (BCC&P)" clade.[257] The second includes a number of plant growth-promoting rhizobacteria and nodule symbionts, assigned as the "plant-associated beneficial and environmental (PBE)" clade, *i.e*. *Ca*. B. crenata belongs to this clade. The third clade mainly consists of environmental species and gut symbionts of stink bugs, referred to as the "stinkbug-associated beneficial and environmental group (SBE)" or the *Burkholderia glathei* clade (BGC).[257] Although the *Burkholderia* symbionts of stink bugs in the SBE/BGC are genetically diverse (Appendix **Figure 10-42**), recent deep sequencing analyses revealed that the gut microbiota of each bean bug (*Riptortus pedestris*) individual was remarkably simple and consisted of one or a few SBE/BGC taxa.[257] Kikuchi *et al*. found the *Riptortus-Burkholderia* gut symbiosis to be an ideal

model system as the symbiont is easily culturable, genetically manipulatable, and the host can be reared free of symbionts.[256,259,260] Although the *Burkholderia* symbiont of *R. pedestris* is not essential for the host's survival, aposymbiotic insects exhibit retarded growth, smaller body size and weight and lower fecundity.[256] Unlike typical insect-microbe symbioses, rearing experiments have demonstrated that the bean bug does not vertically transmit the symbiont. Instead, the *Burkholderia* symbiont inhabits the ambient soil on which the host insect lives and *Riptortus* acquires the symbiont from the environment at every generation. The specific acquisition of the *Burkholderia* symbiont is speculated to occur via a specialized intestinal organ for sorting the symbiont from various non-symbiotic microorganisms.[256] Interestingly, many phytophagous insects are consistently associated with the "plant-associated beneficial and environmental (PBE)" group of *Burkholderia* and the symbiotic association with *Burkholderia* is speculated to be evolved at the common ancestor of at least the three superfamilies *Coreoidea*, *Lygaeoidea*, and *Pyrrhocoroidea*.[260,261]

7.1.1.1 Endosymbiotic *Burkholderia* – double agents, switching hosts between plants and insects and *vice versa*?

Development of insecticide resistance has become a serious concern worldwide. The resistance mechanisms have been attributed to evolutionary changes in pest insect genomes such as alteration of drug target sites, up-regulation of degrading enzymes, and enhancement of drug excretion. Recently, Kikuchi *et al*. reported an interesting new mechanism of insecticide resistance that is selection and cultivation of insecticide-degrading strains of *Burkholderia* by the bean bug *R. pedestris,* conferring insecticide resistance to the latter.[262–265] Further, they found evidence for a quick establishment of resistance within a single insect generation, and they assume that resistance moves around horizontally between different pest insects and other organisms.

A hint toward the mechanism of symbiont transmission between plants and insects comes from the nested clade of the plant endosymbionts *Ca*. B. punctata, *Ca*. B. kirkii and *Ca*. B. schumanniana, which form a sister group with stinkbug *R. pedestris* symbiont (*B*. sp. RPE64).[185] The same sister group also contains soil *Burkholderia* isolates with pesticide-degrading capabilites.[185] *B*. sp. RPE64 has been isolated from stinkbugs.[266] This group of *Burkholderia* species, to which the leaf nodule symbionts of *Rubiaceae* belong, live freely in soil or are associated with plants and insects. Hence, one can envision that the ancestor of the leaf nodule symbionts was a *Burkholderia* species with a remarkably broad host range.[185] It is therefore conceivable that some of the leaf nodule species have retained the ability for transient

association with insects, which could act as potential vectors (whereas non-vector insects may be targets of the insecticidal activity of kirkamide[7] or FR[7,10], respectively).[185]

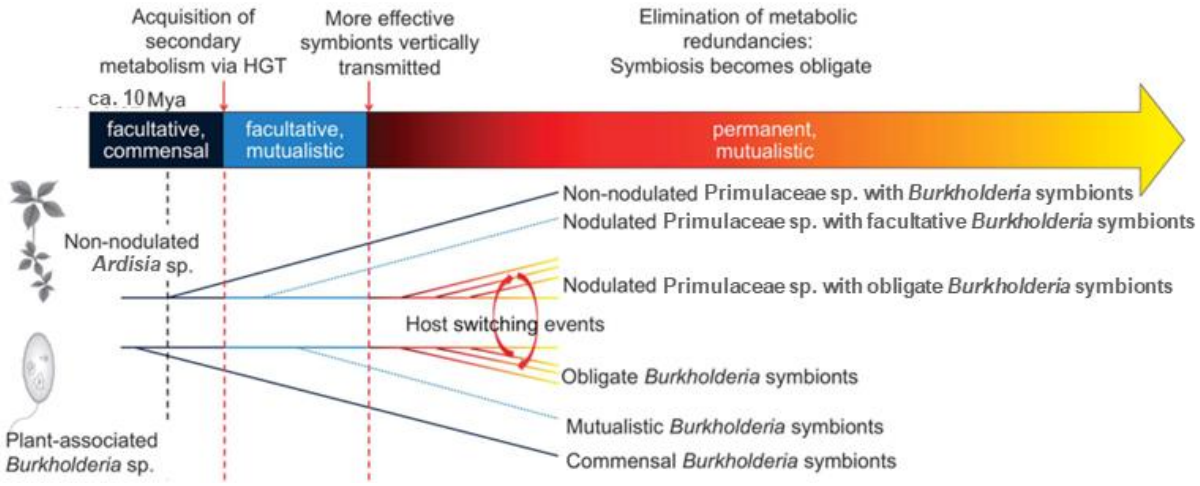

Figure 7-1: Figure modified after Pinto-Carbo *et al.*[185] Evolutionary history hypothesis for the leaf nodule symbiosis. Ancestors of modern *Ardisia* sp. were probably in transient association with endophytic, or possibly epiphytic commensal bacteria. About 10 Mya, the bacteria acquired genes for the production of protective secondary metabolites such as FR, thereby giving a net fitness benefit to the association. As more effective symbionts were selected, the symbiotic bacteria became vertically transmitted, making the symbiosis permanent. A consequence of this permanent association is the increased dependency of the host on the leaf nodule bacteria, possibly through the loss of redundant metabolic pathways. All described modern nodulated *Ardisia* species are locked in the relationship with the leaf nodule bacteria, regardless of the production of protective metabolites. Intermediate stages shown in dashed lines (mutualistic *Burkholderia* symbionts, nodulated Primulaceae with facultative symbionts) are hypothetical.

The obligate interaction between leaf nodule symbionts and their host plant (*Ardisia* sp.) could have evolved from an initial facultative and commensal association (**Figure 7-1**). The acquisition of secondary metabolite synthesis by the symbiotic bacteria via horizontal gene transfer is likely due to the flanking transposable elements in case of FR and kirkamide, respectively. This may likely have been essential for the transition to a mutualistic interaction and the establishment of the leaf nodule symbiosis. Subsequently, the association became permanent and the bacterial genomes started to erode.[185]

7.1.1.2 *Burkholderia-Ardisia lucida*: A pre-form of leaf nodule symbiosis?

The *Burkholderia-Crispardisia* leaf nodule symbiosis is considered to be obligate,[139] because neither the host nor the endosymbiont can survive outside the symbiotic interaction.[15,140–142] Seeds cured of the symbionts by antibiotic or heat treatment do germinate ordinary, but the resulting bacteria-free plants fail to reach maturity and die within two years.[17,146] We tried to replicate these results, however, our antibiotic treatment was unsuccessful (see **Chapter 4.1.1**).

In contrast, Nakahashi *et al.* clipped the nodules from mature seedlings of *A. crenata*, which had no detrimental effects on the plants.[143] One could hypothesize that the benefit, provided by the bacteria could be limited to another life stage of the plant. Considerations that the *Burkholderia* profits from nutrients and vitamins provided by the plant in return, turned out as possible, because *Ca*. B. crenata seems to possess a very eroded genome lacking of some necessary genes for the biosynthesis of its cellular components.[22] In this point it differs from closely related *Psychotria*-symbiont *Ca*. B. kirkii, which seems to be particularly self-sufficient for amino acids, nucleotides and vitamins, despite the younger age of the *Ardisia* leaf nodule symbiosis compared with the *Psychotria*-symbiosis (approximately 5 Mya versus 10 Mya).[146]

In **Chapter 5.1** we reported on the surprising occurrence of FR in the non-nodulated plant *A. lucida*. When investigating the leaves of *A. lucida*, modified stomata can be observed that we suspected to be a "pre-form" of the above mentioned leaf nodule symbiosis (**Figure 7-2**, pictures provided by Dr. Aurelièn Bailly, Eberl lab, Univ. of Zurich). Interestingly, these structures that resemble to nodules display heterogeneity in their color. Some nodules are black whereas others are green (**Figure 7-2C**). The structures are highly autofluorescent in areas that could describe cell wall (see **Figure 7-2D**), which could be indicative of the presence of lignin.

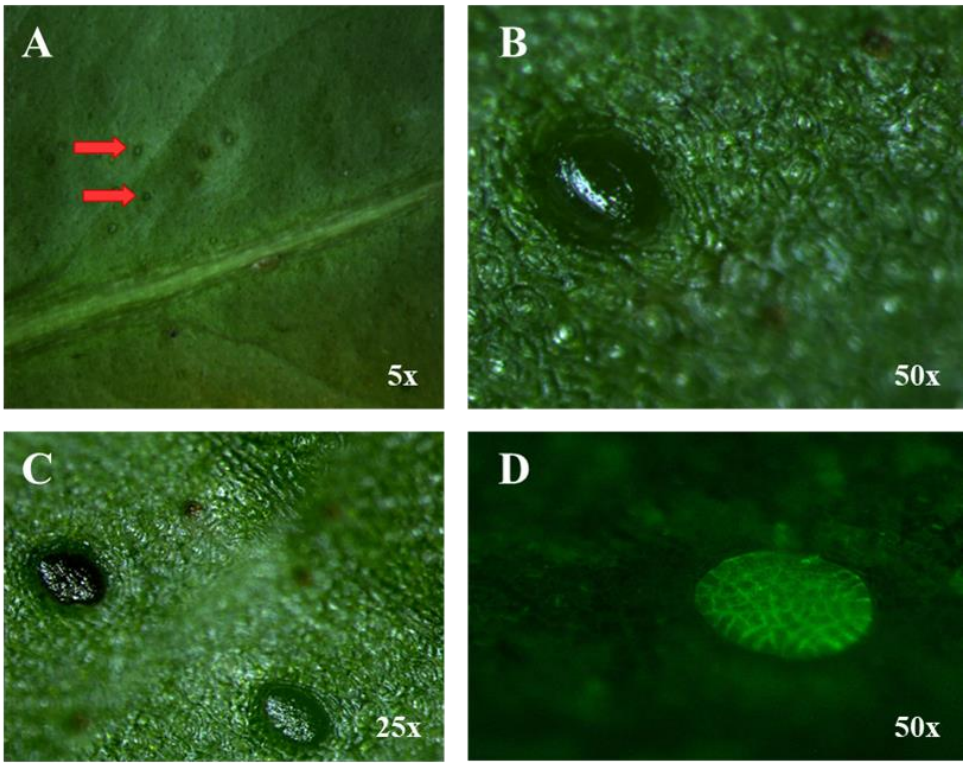

Figure 7-2: (**A**) *Ardisia lucida* leaf. The arrows are pointing on potential nodule structures. (**B**, **C**) Close-up picture on modified stomata similar to the ones observed in *Psychotria kirkii*, displaying heterogeneity in their color. (**D**) Close-up picture with eGFP-filter, highlighting autofluorescence in areas that could describe cell wall. Pictures were taken and provided by Dr. Aurelièn Bailly, Eberl lab, Univ. of Zurich.

In order to determine the location of the bacteria, Marta Pinto-Carbo (Eberl lab, Univ. of Zurich) performed a PCR in two different locations of the leaf, *i.e*. part of the leaf close to the main vein where the "nodules" are located, and of the margin of the leaf. Indeed, bacterial endophytes were detected within *A. lucida* leaves. In contrast to *A. crenata*, where the endosymbionts were concentrated in the nodules at the leaf rim, the endosymbiotic *Burkholderia* of *A. lucida* seem to be equally distributed around the whole leaf. Further PCR results indicated that there is more than one endophytic bacterium and a PCR product for the *frs* gene cluster was found. (Appendix **Table 10-8**).

These preliminary results may indicate a pre-form of the leaf nodule symbiosis, where host and endophytic *Burkholderia* are not in an obligate relationship, yet. Thus, cultivation and sequencing of the endosymbiotic bacteria could be considered to get deeper insights in the development of symbioses. Further, MALDI imaging of leaves, berries, and seeds could be performed in comparison to *A. crenata* to track FR as indirect marker for the bacteria.

7.1.2 Ecological function of leaf nodule symbiosis

Heritable symbiosis may have long-term consequences for the fitness of the host. It is predicted that co-dependence between host and symbionts may evolve over evolutionary time beyond the initial benefits of the symbiosis, *e.g*. through streamlining of redundant pathways or immunological susceptibilities. Some possible functions of the leaf nodule symbiosis are depicted in **Figure 7-3**.

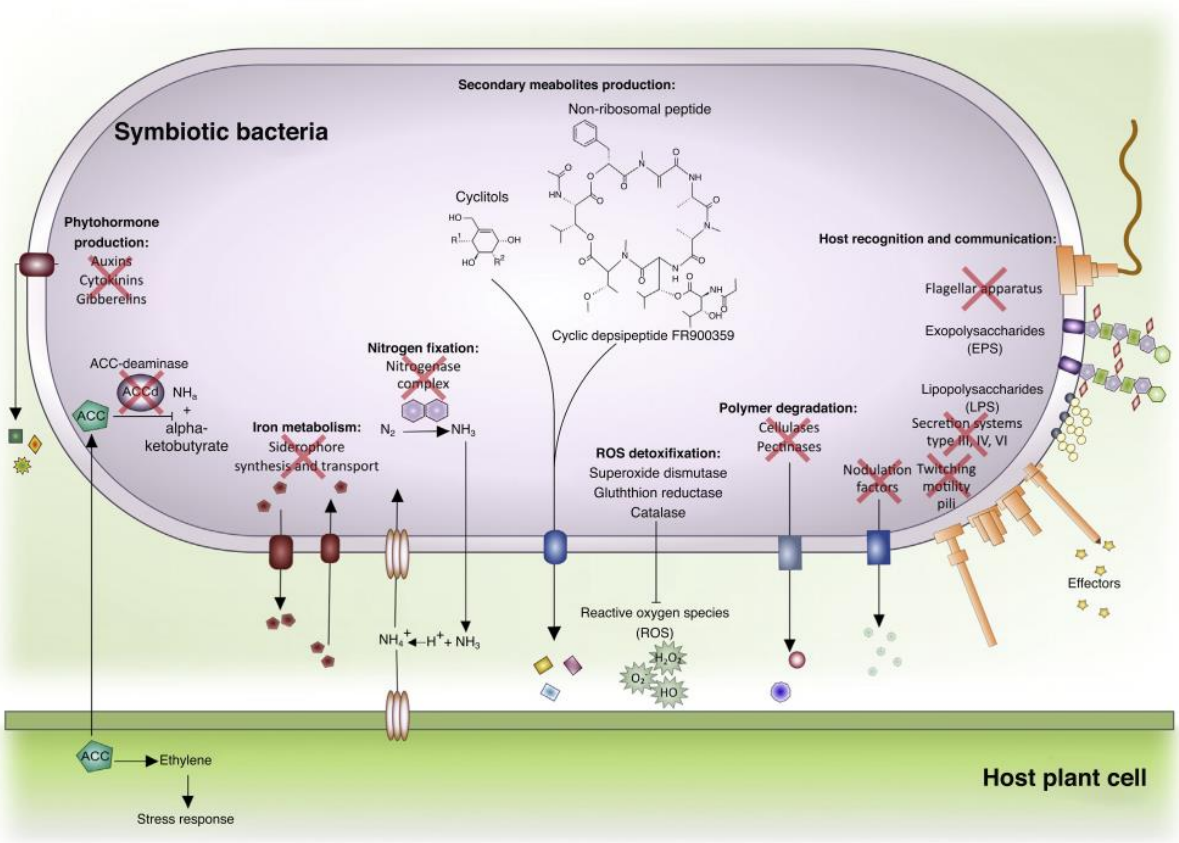

Figure 7-3: Figure taken from Pinto-Carbo *et al.*[7] Reduced set of plant-endophyte interaction pathways in leaf nodule symbionts. Items barred with red crosses indicate functions important for plant colonization of facultative endophytic bacteria, which are not conserved in leaf nodule symbionts. A general host-symbiont recognition mechanism not relying on protein secretion systems could be based on surface components such as lipopolysaccharides or exopolysaccharides. Secondary metabolites production is a common feature of all leaf nodule symbioses characterized so far and appears to provide the basis of the symbiotic alliances. The structure of the FR produced by the symbiont of *A. crenata* is shown, as well as the structure of cyclitols found in Rubiaceae species. For kirkamide, R1 = OH and R2 = *N*-Acetyl. ROS detoxification mechanisms are also conserved and likely represent adaptation to oxidative conditions in the leaf or provide resistance to host defenses. A putative ammonium transporter is conserved in the genomes of all leaf nodule symbionts and putative efflux transporters of secondary metabolites are associated with their respective biosynthetic clusters.

FR, known for inhibiting $G\alpha_q$-signalling in mammalian cells, is produced by *Ca*. B. crenata living in symbiosis with *A. crenata* as we demonstrated in **Chapters 4.2, 4.3**. Hence, we wondered whether *A. crenata* utilizes this molecule to regulate their own G signalling. This idea is supported by the structural similarity of mammalian G proteins to the plant G protein AtGPA1.[148–150] Plant G proteins differ from mammalian G proteins in that they are self-activating, which means that they do not G protein-coupled receptors to promote GDP-GTP need exchange. Therefore, regulation of G protein activation in plants occurs at the deactivation step.[149,150] Plants may also utilize a GDP dissociation inhibitor (GDI) like FR, which slows down nucleotide exchange. However, FR was not able to interfere with AtGPA1 (**Chapter 4.1.2**), but it could still be possible that FR plays a role in host-symbiont communication.

FR is found in all parts of *A. crenata*, but in different concentrations, thus *vice versa*, the bacterium could use FR to regulate primary metabolism of the plant according to the demands of the bacterium via plant G protein signaling. In this regard, it is noteworthy that the cyanobacterium *Nostoc punctiforme*, known to live in symbioses with plants, produces the cyclodepsipeptide nostopeptolide, which excerts vastly different effects on cellular differentiation and the direction of motility of *N. punctiforme*, depending on its concentration.[267] Furthermore, this peptide is down-regulated in symbiosis or altered by plant cells in the direct proximity to the bacterium, while it is expressed under all conditions in the free-living state of the cyanobacterium.[267] Maybe the nostopeptolide-signaling cascade is mediated via plant G proteins (other than AtGPA1). This would be in accordance with Urano & Jones *et al.*, who declared the primary function of G signaling in plants to be nutrient sensing, and this information impacts signaling by several plant hormones, light, pathogen-associated molecular patterns, and probably other signals.[150]

7.1.2.1 Insecticidal properties of FR via inhibition of insect GqPCR signaling

We provided first evidence for FR as a chemical protective agent for its host plant (**Chapter 4.1.5**). The interaction of FR with its molecular target, *i.e.* Gq proteins has been demonstrated to be very selective.[54,55,58,62] The resulting biological effect in cells, however, is pleiotropic due to the ubiquitous presence of GPCR signaling cascades. In essence, signal transmission by a huge number of GqPCRs is blocked. These features make FR a unique defense chemical with an unprecedented mode of action. As we have shown in this study[10], FR is, unexpectedly, orally bioavailable and causes a drastic physiological effect in mammals. Insects, however are probably the biggest threat for plants, and are likewise affected (all tested *R. pedestri*s individuals died after a delay of several days). Furthermore, molting of the *R. pedestris* nymphs was completely prevented in the two highest concentrations applied.

Most intriguing in this context is that $G\alpha_q$ was proven to be essentially important for molting and metamorphosis in a lepidopteran insect, *Helicoverpa armigera* via an insect steroid hormone (20-hydroxyecdysone).[168,268] Moreover, the 20-hydroxyecdysone-signaling pathway, including $G\alpha_q$, is highly conserved among different insects, such as *D. melanogaster*, *B. mori*, and *Culex quinquefasciatus*. These data suggest a possible explanation of the observed molting-inhibiting effect of FR towards *R. pedestris* (**Chapter 4.1.5**).

7.1.2.2 Potential of FR as crop protection chemical

Another studied insect GqPCR is the diapause hormone receptor (DHR) of *Bombyx mori*. Diapause is a delay in development with minimizes metabolic activity adopted by insects to survive regularly and recurring periods of adverse environmental conditions.[269] This unique process is regulated by diapause hormone (DH), which is a neuropeptide hormone that induces egg diapause in *B. mori* and is involved in terminating pupal diapause in heliothis moths.[163,270] Jiang *et al*. figured out that FR was able to completely inhibit DH-signaling. Thus, FR has great potential as crop protection chemical, as it is able to inhibit both initiation and termination of diapause in different stages (egg and pupal), an essential strategy of insects to survive and develop. As there are most likely many further insect G_qPCRs, obligate for many insects, resistance development can be suspected as difficult.[271] First evidence that diapause of *Helicoverpa zea* and likely many other pest insects is indeed susceptible to manipulation was provided by Zhang *et al*., who used a synthetic DHR-antagonist to significantly reduce diapause termination.[272,273] However, the currently applied antagonists suffer from poor cell-permeability.[272] FR has besides its capabilities of cell-penetration, other superior properties such as high potencies and affinities to different insect Gq proteins and a broad spectrum of effects due to its unique mechanism of action. Interestingly, the DH receptor (DHR) exhibits a high level of similarity to the receptors of mammalian neuromedin U. For the latter, application of FR helped to discover participation of neuromedin U receptors in innate immune responses of mammals.[55] A drawback, however is the toxicity of FR to mammalians.

7.1.2.3 Discovery of putatively FR-resistant scale insects on *A. crenata*

For the supply of FR to members of the Research Unit FOR2373 we cultivate several hundred *A. crenata* plants in the green house of the Botanical Garden, Bonn. While they are robust to most plant pathogens, our gardener Dirk Schmitz found some plants, heavily infected with scale insects (**Figure 7-4**). Most scale insects are parasites of plants, feeding on sap drawn directly from the plant's vascular system. Other scale insect species evolved symbiotically with some ant species.[274] Dr. Danièle Matile-Ferrero, an entomologist from the Muséum National d'Histoire Naturelle in Paris, determined the species attacking our *Ardisia* plant to be *Saissetia coffeae*, belonging to the family of soft scales (Coccidae). Interestingly, the colony of scale insects theirself were heavily attacked by a Hymenoptera parasite (parasitoid wasp), which is a natural enemies of *S. coffeae*.

In future efforts we want to investigate the resistance mechanism of *S. coffeae* towards FR. One possibility would be the selective uptake of insecticide-degrading *Burkholderia* from the soil

(see **Chapter 7.1.1.1**). Intriguingly, again obligatory *Burkholderia* have been described from species of the superfamily Coccidea to be transovarially, thus vertically, transmitted from the mother to offspring.[275] The complete genome sequencing of several obligatory symbionts of sap-feeding insects showed that their genomes are much smaller than the ones in their free living relatives, *e.g.* they lost mobile elements, most of the regulatory genes and pseudogenes, as we also observed for *Ca*. Burkholderia crenata.[22] These endosymbionts could also provide mechanism to escape FR exposure. It would be interesting to see whether the endosymbionts of the scale insects are closely related to *Ca*. Burkholderia crenata, because it is possible that *Crispardisia* sp. gained their endosymbionts by scale insects infecting them with their own *Burkholderia*. Another possibility would be that the scale insects lack or have mutated $G\alpha_q$ proteins and thus they are not affected by FR.

Figure 7-4: *Ardisia crenata*, infected with scale insects (*Saissetia coffeae*). (**A**) Non-infected leaf (8 cm) of *A. crenata*. (**B**) Picture of infected *A. crenata* plant. (**C**) Zoomed view of infected *A. crenata* plant. Red circle highlights transparent immobile female 2nd instar nymphs of *S. coffeae*. (**D**) Zoomed view of infected *A. crenata* plant. Blue circle highlights mobile, white female 1st instar nymphs (crawlers). Red circle highlights immobile female adult scale insect with a brown waxy shield. Dimensions of berries are 1 cm in diameter.

7.1.2.4 General considerations about symbiotic relationships between bacteria of the genus *Burkholderia*, - plants, - and insects

It is becoming plausible that the long-term persistence of symbiotic relationships such as *Burkholderia-Ardisia*, *Burkholderia-Psychotria*, *Burkholderia-Riptortus*, and *Burkholderia*-Coccidea could be prevalent not only in two-party interactions, but also in more complex systems comprising three or more associates. The common ancestor of *Burkholderia* symbionts is suspected to have had a notable broad host range from plants to insects, and its descendants served as a kind of double agents, sometimes killing former host insects and then defecting back to the insect, degrading the same insecticides for its former enemy. Thus, the complex relationship could be imagined as war between plants and insects in favor of the best *Burkholderia* endosymbionts for their purposes. In that way the bacteria always benefit unless they develop to close relationships to one host, as *e.g*. described for *Ca*. B. crenata. This endosymbiont has lost its independency due to ongoing genome erosion and needs its host plant *A. crenata* to survive.

An alternative option is that insects and plants are not necessarily enemies using bacteria as weapons, but they are all part of a bigger symbiotic network. A frequently encountered phenomenon in tropical forests is the association between ants (*Crematogaster*), plants (*Macaranga* trees) and *Coccus* scale insects.[276] The plants are protected against lianas and herbivores by the ants that in turn gain residence in domatia created by hollow stems and food bodies secreted by the plants. In addition, the ants are able to further extract nutrients from the plants indirectly via the exudates of *Coccus* scale insects feeding on *Macaranga* sap and cohabiting with the ants in the confines of the *Macaranga* stem domatia.

Concluding, the plant *A. crenata* and its obligate symbiotic bacterium *Ca*. B. crenata are a fabulous ecological system, where the host plant is protected from a big range of enemies and the metabolically very limited bacterium profits from primary metabolites of the plant. Further work is required to decipher the mutual benefits, possible biased effects depending on the concentration of signaling molecules and further molecular mechanisms underlying these benefits of this captivating type of symbiosis.

7.2 Biosynthetic considerations concerning FR and its analogs

Cyclic depsipeptides like FR are usually produced by fungal or bacterial microorganisms.[23,277] In this study we could prove via in-depth biosynthetic analysis and heterologous expression that FR is made by NRPSs encoded by the *frs* gene cluster of *Ca*. B. crenata, the endosymbiont of the vascular plant *A. crenata* (**Chapters 4.2, 4.3**).

The structure of FR is unusual in that it contains hydroxylated amino acids, allowing for the construction of two adjacent ester bonds, which is rarely observed among natural products. The cyclodepsipeptide skyllamycin derived from *Streptomyces* sp. Acta 2897 contains, like FR three β-hydroxylated amino acids, serving as a further example for the complex nature of NRPS-related biosynthesis.[278] Thus a few features of skyllamycin biosynthesis are noteworthy to mention. The hydroxylations in this case and supposedly also in FR biosynthesis are catalyzed by a single cytochrome P450 monooxygenase ($P450_{sky}$), which selectively accepts substrates bound to a peptidyl carrier protein (PCP) domain. Furthermore, the enzymatic system is able to distinguish between those PCPs on which the respective building blocks are hydroxylated in skyllamycin biosynthesis, and those PCPs where even the same amino acid building block is not hydroxylated. This reveals a new route of precursor production in NRPS biosynthesis, one which works in parallel with peptide synthesis.[279] Through modification of precursors and their supply *in vivo*, novel peptides could be generated that possess alternate properties to the unmodified skyllamycin.

7.2.1 Generation of new FR analogs via molecular biology-based approaches

7.2.1.1 Generation of new FR analogs by genetic engineering – a glimpse to future studies

The cyclodepsipeptide synthetases show a relatively broad tolerance for α-hydroxy acids and have been applied for *in vitro* syntheses of new cyclodepsipeptides, simply by adding synthetic α-hydroxy acids to those enzymes.[280] Maybe this lack of absolute substrate specifity of the synthetases is also the reason for the appearance of newly described compounds **1-4** in this study (**Chapter 5.1**) and also the reported YM analogs, most of which are NH-acylation products of β-Hle moieties.

After confirmation that the *frs* gene cluster is sufficient for FR production (**Chapters 4.2, 4.3**), now new FR analogs derived by targeted manipulation of the *frs* gene cluster are envisioned. Currently, we are exploring other hosts such as the cultivable endosymbiont of *R. pedestris* (*Burkholderia* RP64) that is closely related to leaf nodule symbionts (see **Chapter 7.1.1.1**).

Further, investigations of other expression plasmids to increase heterologous production yields of FR are planned. Finally, FR analogs with altered amino acids by genetic engineering of the A domains should be obtained. These derivatives will reveal new structure-activity relationships regarding the Gq binding pockets and may lead to development of at time unknown and urgently needed inhibitors of Gs or G12/13 proteins, that harbor a similar binding pocket.

Phenyllactate is a relatively rare, but prominent acid building block in depsipeptides. PF1022A, a cyclooctadepsipeptide possessing strong anthelmintic properties and being produced by the filamentous fungus *Rosellinia* sp. PF1022 contains *inter alia* two D-phenyllactate building blocks (FR contains one D-phenyllactate).[281] Yanai *et al*. produced unnatural PF1022A derivatives in which the two benzene rings were modified specifically at the para-position with amino and nitro groups by metabolic engineering. This approach is not limited to amino- and nitro-derivatives, and might be also transferred to approximately 100 secondary metabolites that may be biosynthesized via phenylpyruvate or p-hydroxyphenylpyruvate.[282]

In the case of FR the introduced amino group would be apart from the cyclic backbone and thus may not interfere with its conformation. Most strikingly, the phenyllactate moiety is thought to be responsible for the extreme selective inhibition of $G\alpha_q$ subunits. Via subsequent modification of the para-amino group, susceptible to a vast number of reactions, new FR analogs with altered Gα-subunit profile could be obtained.

7.2.1.2 Optimization of FR production in *Chromobacterium vaccinii*

As described in **Chapter 5.1.5**, FR was isolated from extracts of the cultivable bacterium *C. vaccinii*. In future, we plan to upscale the cultivation of *C. vaccinii*, and optimize the strain for FR production (by varying temperature, media, and genetic engineering). Further, we intend to diminish the violacein production, because this purple pigment impedes the purification process of FR. Khan *et al*. reported that clove oil (essential oil from *Syzigium aromaticum*) is a potent inhibitor of violacein in *C. violaceum*.[283] Indeed, we were able to completely prevent violacein production when treating the *C. vaccinii* cultures with glove oil (0.01% - 1% v/v). While in higher concentrations from 0.25%-1% glove oil FR could no longer be detected via LCMS measurements, lower concentrations (0.1% and less) retained FR and FR-2 (**2**) production. The glove oil experiments were performed by the Master student Wiebke Hanke, Pharmaceutical Biology, Univ. of Bonn.

7.2.1.3 Generation of new FR analogs by feeding experiments of *Chromobacterium vaccinii*

In parallel to optimization of FR production we plan feeding experiments with altered (and also with ^{13}C-labeled) precursors that may lead to novel derivatives of FR and novel insights into the biosynthesis of FR, respectively. First experiments were done with different carboxylic acids, because the starter-C domains of FR have demonstrated broader substrate specifity, proven by the existence of FR analogs such as FR-1 (**1**), FR-2 (**2**), and FR-3 (**3**).

We are especially interested in the production of compound **1**, because (i) it is originally not produced by *C. vaccinii* and (ii) its primary alcohol function may be the ideal anchor for derivatization with fluorescent dyes. Feeding of azido amino acids could also be envisaged. They can be subsequently coupled to alkyne-containing fluorophores via "Click-Chemistry".[284,285] Docking experiments revealed much more space around the primary alcohol for a fluorophore, when bound to Gq. Further, succinic acid was proposed for feeding studies by Dr. Daniel Tietze, because according to *in-silico* modelling the new acidic moiety could a form salt bridge with the neighboring arginine R202 residue (**Figure 7-5**).

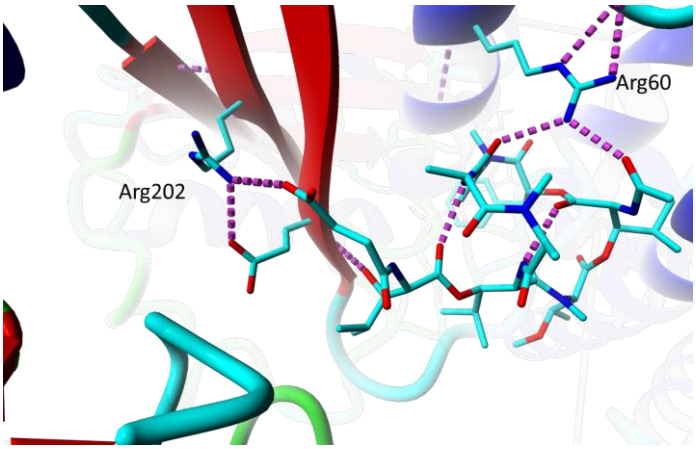

Figure 7-5: In-silico modelling of a putative FR analog, containing a succinate in place of a propionate residue to Gq. Hydrogen bonds and salt bridges are labeled in pink dashed lines. Experiment was performed by Dr. Daniel Tietze, TU Darmstadt.

Unfortunately, LCMS measurements indicated that none of the used substrates (3-OH-propionate, succinic acid, glutaric acid, β-alanine, γ-aminobutyric acid, D-tyrosine added after 1 week of cultivation) were incorporated into the FR molecule (Appendix **Figure 10-43**). But regarding the growth curve of *C. vaccinii* (**Chapter 5.1.5**) the bacterium reaches the stationary phase after two days. Therefore the experiments should be repeated with earlier addition of the substrates.

7.2.1.4 Generation of new FR analogs by chemoenzymatic assays

Chemoenzymatic methods offer additional approaches towards new FR derivatives. The *Actinoplanes utahensis*-assay gained our attraction, because it was applied to deacylate secondary amide residues of daptomycin and echinocandin B, two approved antiinfective and cyclic depsipeptide drugs.[204,286–289] The resulting amino functionalities offer new SAR insights and more importantly can be easily further derivatized or functionalized towards *e.g.* fluorescent dyes.

7.3 Structure-activity considerations of FR and analogs

A main goal of the study was the in-depth chemical examination of FR and structurally related cyclic depsipeptides provided by the plant *A. crenata*. Therefore, the isolation and identification of such peptides from the plant extract was optimized.

FR and its new discovered analogs **1-4** isolated from *A. crenata* are structurally closely related cyclic depsipeptides. Such peptides are not easily analyzed by NMR and MS due to different conformations and - concerning MS - their cyclic nature. This project, especially **Chapter 5** revealed that a combination of mass spectrometric approaches, including MS^2, Tandem-MS, and GNPS analyses of FR and analogs is a suitable, fast, sensitive, and specific method for analyzing amino-acid composition of FR and related compounds.

Conformational aspects seem to play an important role for the biological activity of FR. Several *N*-methylations reduce the number of possible hydrogen bonds and force the peptide into a certain conformation. This conformation also allows for the existence of peptide bonds in the generally unfavored *cis*-conformation.

7.3.1 Conformational analysis of FR with emphasis on the influence of *N*-methylation and *cis*-*trans* isomerization

In **Chapter 1.3**, the unusual structural features of FR were described, *inter alia*, the multiple *N*-methylations, offering several advantages regarding pharmacodynamic and pharmacokinetic parameters. Thus, structural modification of the peptide backbone via *N*-methylation is a powerful tool to modulate the pharmacokinetic profile and biological activity of peptides. Wang *et al.*[290] used temperature coefficients measured by NMR to identify and specifically *N*-methylate those amides being exposed to solvent. These capped amides resulted in a higher membrane permeability and consequenced in a distinctly increased oral bioavailability. Wang

et al further concluded that *N*-methylations of cyclic peptides improve their oral bioavailability without significantly modifying their biological activity and selectivity.

In my opinion, these considerations might be true for some compounds, but should not be generalized. Including the fact that FR already obtains several methylations, we think that its methylation pattern affects and determines its conformation and hydrogen bonding potential. X-Ray analysis of Myamae *et al.*[30] and our 2D-NMR experiments, especially ROESY measurements suggest that all free amide and hydroxyl protons of FR are involved in hydrogen bonds. NOE correlations (see **Figure 7-6,** Appendix **Figure 10-11,** and **Table 10-8**) add further evidence for the observation of Myamae[30] that the side-chain seems to be tightly bound to the cyclic backbone by these hydrogen bonds. Furthermore, the hydroxyl group at C-43 seems to play a key function in the hydrogen network.

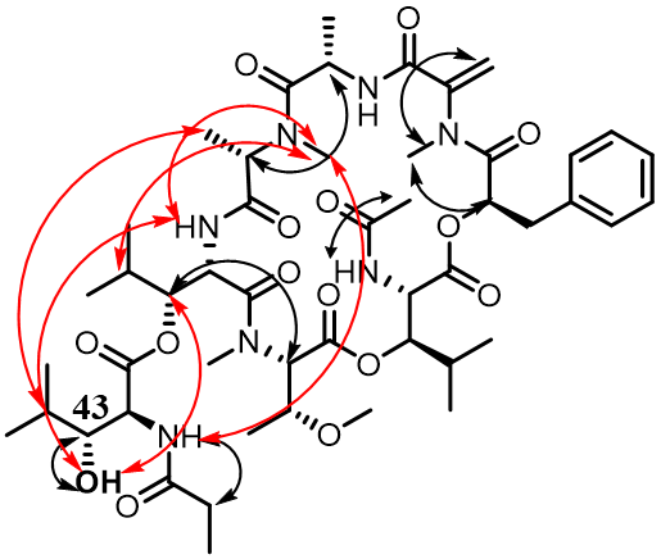

Figure 7-6: Key NOE correlations of FR derived from ROESY measurements: Red arrows highlight multiple long-range NOE correlations between protons of the side-chain and the peptide backbone deduced from ROESY experiments. This indicates that the side-chain is bound close to the backbone via hydrogen bonds. Black arrows show NOE correlations important for structure elucidation.

It is probable that the biological effect of FR will be substantially decreased by altering the number of *N*-methylations. An increased number of *N*-methylations would destroy the hydrogen bonds directing the side-chain and backbone spatially close together. The side-chain would point away from the backbone and possibly disturb target interactions. Decreasing the number of *N*-methylations would enhance the flexibility and hydrophilicity of the molecule. In accordance with these assumptions, the dramatic effect resulting from alterations of the *N*-methylation pattern of YM was demonstrated by Xiong *et al.*[26] They synthesized three compounds in which backbone modifications of *N*-Me amides were introduced. YM-2, where

N-Me-Dha was replaced for Dha, a 630-fold decrease in potency was observed. Similarly, for YM-5 (*N*,*O*-Me_2-Thr was replaced for *O*Me-Thr) a 465-fold decreased potency was displayed. YM-1 (*N*-Me-Ala was replaced for Ala), however, was nearly equipotent when compared to YM, indicating that effects due to altered methylations are hard to predict and cannot be generalized. Further, these analogs underline that not the number of *N*-methylations is important, but the specific pattern, contributing to a bioactive folding of the molecule.

In this regard, the dramatic effects upon alteration of the *N*-methylation pattern could be due to a completely altered H-bonding network and thus an altered global conformation, when introducing additional NH groups. Thereby many additional conformations regarding the side-chain and the backbone, *e.g*. the *cis*-peptide bonds could be changed to their *trans* counterparts. The *cis*-conformation, which occurs in nature very rarely, except on proline or tyrosine residues, can occur in FR, because the complex hydrogen bond network contributes to its overall stability. Furthermore, it is commonly known that *N*-methylation promotes *trans–cis* isomerization of amide bonds.[291,292] Thus, *N*-methylation affects not only the conformation of the modified amino acid but also of the preceding residue.[293] In addition, the α,β-double bond of *N*-Me-Dha has a profound effect on the conformational properties of the dehydroamino acid residue and, in consequence, on the conformation of the whole peptide molecule.[294] Altogether, loss of these features by destroying its unique conformation would possibly lead to a decreased selectivity and efficacy of FR for its target as observed for *e.g*. Michael addition conjugates **12**, and **46** - **50** (**Chapter 5.2**).

Considering application of FR as drug lead, it remains debatable if the conformational analysis by NMR measurements, recorded in unnatural media, like $CDCl_3$, can be transferred one-to-one to physiological milieus. To date, the transferability of the reported conformation of YM by Taniguchi *et al.*[28] is supported by the study of Nishimura *et al.*[53] who did a biochemical characterization of YM using purified G proteins *in vitro* and determined the X-ray crystal structure of the heterotrimeric G_q protein complexed with YM. They found that YM in this complex exhibits a combination of *cis*-and *trans*-amide bond conformations identical to the major conformer suggested by a previous NMR analysis in solution of Taniguchi.[28] Taniguchi *et al.*[28] proposed the occurrence of two conformers for YM. The same phenomenon was observed for FR in the present work. Comparing the chemical shifts and NOE correlations, it attracts attention that the same NOE correlations were noticed in the minor conformer, except that no NOE correlation between the α-proton of Pla and the *N*-methyl protons of *N*-Me-Dha was observed. This indicated that the distinction between major and minor conformers may lie

in the geometry of the amide bond between Pla and *N*-Me-Dha. The chemical shift of β-carbon of *N*-Me-Dha 6-CH_2 (major: δ_C 106.9; minor: δ_C 121.8) was much different between both conformers, implying that it was influenced by the steric hindrance caused by the geometry of the amide bond. In the minor conformer, the high-field chemical shift (d, δ_H 3.73) of 6b-H of *N*-Me-Dha, compared to (d, δ_H 5.07) in the major conformer, suggested that the proton of the minor conformer might sit just above or below the plane of the benzene ring of Pla and be affected by an anisotropic shielding effect (for NMR spectroscopic data see **Table 5-5**).

7.3.1.1 FR and analogs adopt different conformations in aqueous medium compared to $CDCl_3$

In contrast to the above mentioned assumption of Nishimura *et al*. that YM (and FR) will adopt the same conformation as measured in $CDCl_3$ upon Gq binding[53], we observed strikingly different conformations for FR, YM, and compound **1** when recording NMR spectra in more physiological media (H_2O/D_2O = 9/1) (Appendix **Figures 10-44 to 10-55**). The major conformer in water of all three compounds contains a single *cis* amide bound between *N*-Me-Dha/Pla. This conformation fits much better in the Gq binding pocket than the previously published crystal structure.[53] Further it can better explain why the *N*-Me-Dha residue does not tolerate any modifications. When the major conformer of the NMR structure measured in water is docked to Gq, the *N*-Me of Dha residue strongly interacts with Tyr192, Arg60, and K57.

Interestingly, the ratio between major and minor conformers for YM (obtained in H_2O/D_2O = 9/1) was 3:1, while the ratio for FR and compound **1** was 10:1. The increased conformational flexibility of YM could be an explanation for its much higher off-rate kinetics, observed in radioligand binding assays (PhD thesis Markus Kuschak, Univ of Bonn, manuscript in preparation). If our proposed structure for FR is indeed the biological active conformation this would force us to revise all so far drawn SAR insights and would also have huge impact on mutational studies towards other Gα subunits. That is why in-depth NMR studies with labeled Gq protein in physiological medium are urgently needed for verification or falsification of these assumptions.

7.3.2 Implications of the *N*-methyldehydroalanine moiety of FR

Another interesting feature of FR is the unusual amino acid *N*-Me-Dha, which besides in FR and BE-22179[207,208] only occurs in microcystins that are, like FR, cyclic heptadepsipeptides, in this case produced by cyanobacteria. It is known that nucleophiles may attack α,β-unsaturated carbonyl groups (occurring in *N*-Me-Dha) via Michael addition, and indeed we successfully applied this reaction for semisynthetic modifications of FR as described in Chapters **5.2** and

6.1, **6.2**, **6.3**. For microcystins, mechanistic studies by Craig and co-workers[212] revealed a two-step mechanism for irreversible inhibition of target proteins under physiological conditions. In the first step, the rapid non-covalent binding and inhibition occurs, and then the slower covalent modification of a cysteine residue takes place over the course of hours.

Thus, in analogy, the mechanism behind the biological activity of FR could be assumed as rapid non-covalent interaction, which is sufficient to block GDP release and simultaneously direct the dehydroalanine moiety towards a cysteine residue nearby, followed by a thereby possible slowly occurring covalent modification afterwards. This two-step-mechanism could explain both, the remaining activity of the hydrogenated YM-385780 and the irreversible, covalent binding mode of FR to the $G\alpha_{q/11}$ protein.

In a previous study Schrage *et al*. performed wash-out experiments in both *ex vivo* (mouse tail arteries) and *in vitro* (HEK-293 cells expressing Gq-sensitive muscarinic M3 receptors).[54] They observed in both systems retained Gq inhibition after washout, indicating the formation of a covalent complex or, alternatively, very tight association of FR with Gq. As also a hydrogenated FR derivative displayed potent Gq inhibition and this effect remained after washout Schrage *et al*. concluded that the α,β-unsaturated carbonyl group within FR is not crucial for Gq/11 inhibition and that FR and Gq do not interact in a covalent way.[54]

These experiments were repeated in CHO-M1 cells, incubated with FR or compound **1** (FR-1) for 1 h, followed by extensive washing, before activation of Gq-sensitive muscarinic M1 receptors with carbachol (CCh) (**Figure 7-7**). The experiments were performed by Tobias Benkel and Nina Heycke (Institute for Pharmaceutical Biology, Kostenis lab, Univ. of Bonn). In all four trials the inhibitory effect of compound **1** could not be reversed through Cch after washing. In contrast to the former published data (Schrage *et al.*[54]) the effect of FR seems to be compromised to about half of the initial value after washing and exaggerated stimulation of 1 mM Cch. Regarding the putative discrepancies compared to the former published data, one has to keep in mind that we achieved a shift in the x-axis of about 1.5. This might be due to the cellular background. Instead of HEK293 M3 cells, we used CHO M1 cells. As seen below, adjusting the x-axis by 1.5, leads to a quite similar result, indicating that the former data achieved for FR, could be confirmed for compound **1**. This data is congruent with our assumption that FR and **1** adopt similar conformations (**Chapter 7.3.1.1**). In this context, it would be interesting to repeat the wash-out experiments with YM to see whether it is easier to remove.

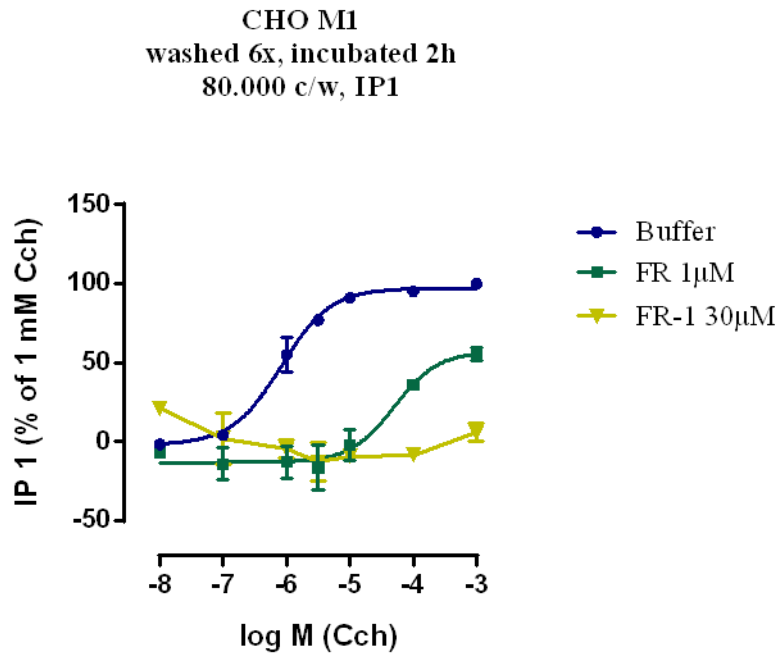

Figure 7-7: Muscarinic M1 receptor-mediated production of IP1 induced by Cch in CHO cells in presence and absence of FR and FR-1, with or without wash-out.

We posit that a slow off-rate may contribute significantly to the high affinity of FR to Gq, accounting for both pseudo-irreversible inhibition and resistance to washout in *ex vivo* vessel preparations as well as in intact cells in culture. An experimental set-up that could be used to confirm the slow off-rate kinetics of FR and analogs compared to YM and analogs was reported by Deng *et al.*, using label-free whole cell dynamic mass redistribution (DMR) assays under both persistent and duration-controlled stimulation conditions.[295] Furthermore, the implication that the non-covalent interactions are essential for a successful secondary covalent conjugation is a possible explanation for the selectivity of FR. Otherwise, if the *N*-Me-Dha moiety was freely accessible and solvent exposed, it would react in an unspecific way with many proteins.

As consequence, one could postulate that the *N*-Me-Dha moiety is either not reactive enough or sterically hampered for covalent binding to cysteine residues under physiological conditions. Nevertheless, this residue is important for the global conformation of FR, which is closely connected to the biological activity as most modifications in this residue led to dramatic loss in potency (*e.g.* YM-2, FR-Cys, FR-RR-BP, FR-JK-BP, and FR-TAMRA).

7.4 Application of FR and its derivatives as tools to study Gq-signaling and as therapeutic agents

7.4.1 Application of FR as tool to study Gq-signaling

Schrage *et al*. pointed out the value of FR towards the scientific community for the investigation of numerous physiological processes.[54] The data from Klepac *et al*. indicate that Gq signaling regulates brown/beige adipocytes and that inhibition of Gq signaling might be a novel therapeutic approach to combat obesity.[55] Klose *et al*. demonstrated the participation of neuromedin U in immune response and inflammation via its Gq-coupled neuromedin U receptor 1.[55]

Application of FR has not only become diagnostic of the involvement of Gq proteins in biological processes, but has the potential for initiating paradigm shifts as lately outlined by Grundmann *et al*.[299] G protein-independent, arrestin-dependent signaling has been such a paradigm that broadened the signaling scope of G protein-coupled receptors (GPCRs) beyond G proteins for numerous biological processes.[300,301] Only recently, Grundmann *et al*. provided evidence that arrestin signaling in the collective absence of functional G proteins does not occur, but that arrestins were essential mediators of internalization when G protein activation was inhibited. This highlights and expands the role of arrestins from desensitizers of G protein-dependent signaling to regulators of GPCR surface abundance under conditions when receptors are active but G proteins are not.[299]

To improve the tool box we lately developed fluorescent FR probes **46**, **49**, **50** that should have served to get deeper insights into the interaction of FR and Gq on a molecular basis and to enlighten the mechanism of action by real-time imaging of $G\alpha_q$ family members in living cells. Apart from being useful for SAR studies, the semisynthetically derived FR analogs FR-RR-BP (**46**), FR-JK-BP (**49**), FR-TAMRA (**50**) are the first fluorescent selective Gq-inhibitors and display increasing potencies concerning Gq-inhibition from **46** to **50** (**Chapter 6**). They also serve as basis for further investigations on the mechanism of cellular uptake of FR.

Further we wanted to establish a BRET assay between fluorescent compounds **46**, and **49** and Gq protein coupled to NanoLuc® for the characterization (binding kinetics) of cold ligands at physiological conditions. However, no BRET signal was detected for compound **46** and also no change in BRET signal was detectable for compound **49** and therefore, the elongated linker

might still be too short to render the fluorophore out of the binding pocket, not allowing for resonance energy transfer.[302]

The pharmacology of the developed fluorescent ligands was influenced by both the linker (prolonged hydrophilic linker of compound **49** resulted in higher Gq activity) and the associated fluorophore. Furthermore, it can be assumed that the physicochemical properties of the fluorophore/linker pairing determine where in the environment of the target protein the fluorophore is placed, and this, together with the environmental sensitivity of the resulting fluorescence, may finally decide its utility as a fluorescent probe.[242] A possible explanation for the finding that all fluorescent probes are still active Gq protein inhibitors, but do not display RET signals could be that the fluorescent moieties point away from the NanoLuc® part of Gq or are hidden behind secondary structural elements of the Gq protein. That is why in future efforts the following concepts are proposed to obtain fluorescent FR analogs with superior properties, applicable for use in fluorescence-based assays.

7.4.1.1 Application of different attachment points of the fluorophore (fluorescent analogs of FR-1)

The so far developed fluorescent FR analogs **46**, **49**, and **50** are all Michael adduct products coupled to FR via a thioether. This thioether might me partially cleaved under physiological conditions to FR, which would explain their residual activity on the one hand and the non-applicability as fluorescent probes on the other hand. Further, the conformation of the FR peptidic backbone is altered by Michael additions, because the sp^2 hybridized exomethylene group is reacted to a sp^3 hybridized system, generating diastereomers (epimers). Deduced from the results of this study it is highly recommended to have an intact *N*-Me-Dha residue. As the other functionality of FR that can be chemically modified (secondary alcohol of the side chain), has also been demonstrated to be crucial for biological activity, it is planned to modify the primary alcohol of compound **1** (FR-1). Altering this moiety would remain the stereochemistry and keep an intact conformation of the backbone. Further, the point of modification is the optimal derivatization side as predicted by molecular modelling (personal communication Dr. Daniel Tietze). However, only few milligrams of compound **1** have been isolated after four years, limiting the number of attempts. The idea is to first selectively oxidize the primary alcohol of compound **1** to the corresponding carboxylic acid derivative catalyzed by 2,2,6,6-Tetramethylpiperidin-1-yl)oxyl (TEMPO) under mild conditions.[303,304] In a second step the FR-

1-COOH should then be activated by EDC/DMAP and coupled to an amine-containing fluorophore (**Scheme 7-2**).

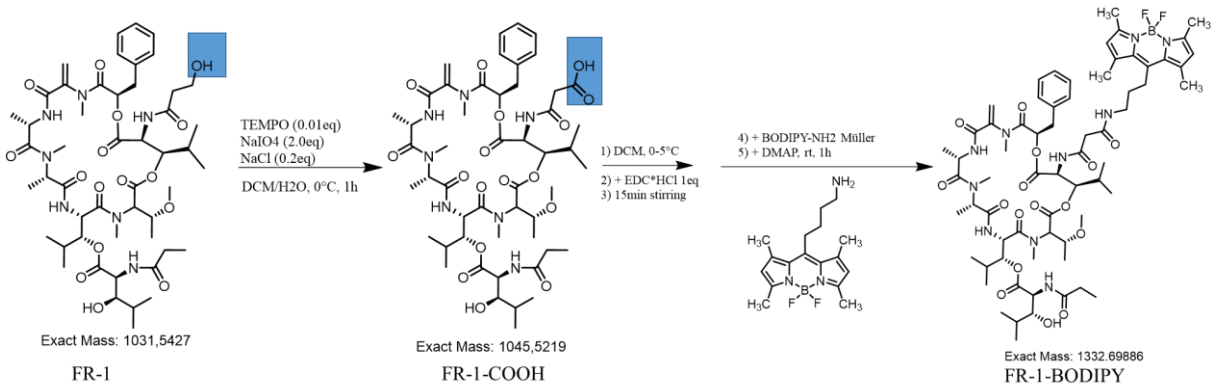

Scheme 7-1: Reaction scheme of FR-1-BODIPY synthesis.

The intermediate product FR-1-COOH can also be used for SAR studies. It could be a first step in the direction of a $G\alpha_s$ inhibitor, due to a possible interaction of the carboxylic acid with a lysine residue in Gs (the corresponding residue in Gq is F75).

7.4.1.2 Application of regioselective reactions followed by Click-Chemistry

An interesting approach to obtain regioselective precursors from *N*-Me-Dha residues, which could be reacted in a second step with a fluorescent dye was proposed by Zemskov *et al.*[219] In a first step they reacted microcystins with a nucleophile (glutathione) in a similar way as it was described in **Chapter 5.2** for compound **12**. They obtained a single diastereomer with high selectivity as Michael addition product. To drive the cleavage to completion they added propargylamine to trap the Michael acceptor. In that way they observed the formation of two diastereomeric forms of propargylamine conjugates. Further, the formed propargylamine conjugates had improved stability relative to the thioether and *N*-Me-Dha derivatives under basic conditions.

The great advantage of this approach is that two diastereomeric propargylamine-containing FR derivatives can be obtained and subsequently coupled to azide-containing fluorophores or photoswitches[305–308] via click chemistry, which are chemical reactions that are rapid, selective and high-yielding.[284,309–311] Click reactions are biorthogonal, that is, non-interacting with biological functionality while proceeding under physiological conditions *in vivo*.[310]

7.4.1.3 Application of click chemistry as proof of principle for BRET assays between Gq-NanoLuc® and FR-binding pocket

More recently, novel methods have been used to incorporate click reaction partners onto and into biomolecules, including the incorporation of unnatural amino acids containing reactive groups into proteins and the modification of nucleotides.[312–316] These techniques represent a part of the field of chemical biology, in which click chemistry plays a fundamental role by intentionally and specifically coupling modular units to various end. Therefore we could apply click-chemistry to examine, whether the applied Gq- NanoLuc® is generally suitable for BRET assays with fluorescent FR probes being located in their Gq binding pocket. To achieve that a single mutation in (or next to) the Gq binding pocket alanine to an fluorescent azido amino acid has to be introduced into the Gq- NanoLuc® as described before in other contexts.[316] BRET assays could be used to determine the best location of the fluorogenic amino acid and luminous Gq proteins would be generated. Thus also insights are gained about the preferred position of fluorophore coupled to FR. The in **Chapter 7.4.1.2** described FR-propargylamine diastereomers could then be applied separately. First they should be tested for Gq activity and their conformations determined by NMR spectroscopy to see whether in the former approaches (compounds **12**, **46**, **47**, **48**, **49**, **50**) always the unfavorable diastereomer was generated as anticipated, which would explain their decreased activity as well their non-suitable application in FCS and BRET studies. The superior diastereomer should then be applied to Gq- NanoLuc®-containing cells, harboring the fluorescent azido amino acid. In that way, the Gq proteins should be coupled to FR in a covalent manner. Afterwards, covalently inhibited and not-inhibited luminous Gq proteins could be compared via fluorescence microscopy and FCS, shedding light on the life cycle G proteins in active and inactive states.

7.4.2 **Applications of FR as potential drug lead**

Great therapeutic interest exists for modulation of GPCR-promoted signal transduction. Although most current therapies utilize receptor agonists or antagonists, manipulation of GPCR signaling at steps distal to receptors, such as on the level of heterotrimeric G proteins, is an attractive alternative, particularly for diseases with complex pathologies, involving multiple receptors and signaling pathways.[127] FR is an inhibitor of $G\alpha_{q/11/14}$-mediated signaling. Therefore, it is well suited to investigate contribution of Gq-input in complex biological processes *in vitro* and *ex vivo*. Remarkable, thermal and chemical stability of the peptide FR,

are extraordinary properties for a peptide. The activity remained for at least 8 days proven by Ca^{2+} mobilization assay[54] and no degradation was observed after stirring for 24h in a water bath of 60°C, followed by HPLC and NMR analysis.

7.4.2.1 Targeted inhibition of Gq with FR for the treatment of pulmonary diseases

Because a tremendous number of physiological processes are controlled and regulated by Gq signaling and the resulting pleiotropic effects, it is consistent that application of FR cannot occur systemically. In contrast, the local treatment of FR against pulmonary diseases is conceivable. Matthey *et al*. demonstrated that FR specifically inhibited Gq-dependent signaling in airway smooth muscle cells and that this compound strongly reduced airway tone in rodent, pig, and human airways *ex vivo*.[62] In addition, inhalation of FR effectively and persistently prevented airway constriction in both healthy and allergen-sensitized mice without causing acute cardiovascular side effects.[62] Despite the fact that effective medicinal therapy with low rates and weak adverse effects for diseases like asthma and COPD are available, additional benefit provided by FR can be anticipated, because of (i) the superior bronchiorelaxing activity when compared with the gold standard salbutamol, (ii) a single drug relieves several symptoms simultaneously and (iii) long-lasting effects. Furthermore, for incurable diseases with presently inadequate treatments, like pulmonary hypertension, FR could offer significant relief of symptoms. The new mechanism of action could cause vasodilatation of the constricted pulmonary arteries, independently of nitrogen monoxide (NO), whose production is disturbed at persons suffering from pulmonary hypertension.

7.4.2.2 FR has potential as first-in-class agent treatment of GNAQ/11-driven cancers

The notion that numerous GqPCRs regulate cell proliferation, but also motility and thereby invasive potential of cancer cells led us (Schrage *et al*.[54]) to posit that inhibition of Gq proteins rather than their linked receptors may be an efficient molecular intervention to target oncogenic signaling on the level of a postreceptor signaling hub where all cellular GqPCR input converges to eventually produce additive effects on cell behavior.[54]

In uveal melanoma, the most common ocular cancer of the adult eye, about 85% of patients carry mutations in their heterotrimeric $G\alpha_{q/11}$ proteins. Precision molecular therapies to target the oncogenes behind these mutations directly are lacking at present and current treatment options rely on radiation or surgery. First experiments indicate that FR potently silences mitogenic over canonical phospholipase Cβ (*PLCB*) signaling driven by these oncogene and

thus has potential as first-in-class agent to treat GNAQ/11-driven cancers in patients harboring Q209 pathway mutations (personal communication Suvi Annala).[317–319]

Concluding, FR has been demonstrated to be a fascinating molecule not only as selective pharmacological tool and potential drug lead candidate, but also in a biochemical point of view. Its suggested ecological role as chemical defense compound offers an answer to the question, how first beneficial bacterial-plant associations may have developed to obligate leaf nodule symbioses. Future interdisciplinary research of the FOR2372 and others will certainly expand our knowledge of human GqPCR-signaling in physiological and pathophysiological contexts as well as Gq-contribution to ecological aspects among different kingdoms of life.

8 Summary

Plant-derived natural products possess an astonishing diversity of structures and bioactivities. Such compounds play a prominent role, not only as drugs for a wide array of therapeutic indications, but also as pharmacological tools to unravel fundamental biological processes.

The DFG-funded research unit FOR2372 uses the cyclic depsipeptide FR900359 (FR) from *Ardisia crenata* as a molecular tool for investigations of $G\alpha_q$-mediated signaling of G protein-coupled receptors (G_qPCRs). Additionally, FR has potential as a lead structure for the development of novel therapeutics to treat conditions, in which multiple G_qPCRs contribute to pathology such as asthma, COPD or at present "undruggable" uveal melanoma.

A majority of *Ardisia* species harbor bacteria of the genus *Burkholderia* within specialized leaf nodules. We sequenced for the first time the genome of *Candidatus* Burkholderia crenata (*Ca*. B. crenata), the uncultured leaf nodule symbiont of *A. crenata*. The genome of *Ca*. B. crenata is the second smallest *Burkholderia* genome to date (2.85 Mb). We identified unique genes with a predicted role in secondary metabolism in the genome of *Ca*. B. crenata. Specifically, evidence is provided for the FR nonribosomal peptide synthetase (*frs*) gene cluster. To confirm the link between FR and the symbiotic bacteria, we quantified FR in the leaf nodules versus the leaf lamina and visualized the result via MALDI imaging. This gives a clear indication that synthesis of FR is concentrated in the leaf nodules (**Figure 8-1A**). Further, an in-depth investigation of the *frs* biosynthetic gene cluster and the successful heterologous expression now provides the basis for future biotechnological FR production, as well as engineering experiments.

The current project discovered FR as the first defense chemical applying inhibition of Gq proteins, a most effective and unique mode of action, that is suspected to act on a multitude of organisms based on the fact, that G proteins are highly conserved in the evolution of metazoans. FR is, unexpectedly, orally bioavailable and causes a drastic physiological effect in mammals. Insects, probably the biggest threat for plants, were likewise affected and all investigated bean bugs died when FR-concentrations of 40µM and higher were applied (**Figure 8-1B-D**). The plant *A. crenata* and its obligate symbiotic bacterium *Ca*. B. crenata are thus a fabulous ecological system, where the host plant is protected from a large range of enemies, and the metabolically very limited bacterium profits from primary metabolites of the plant.

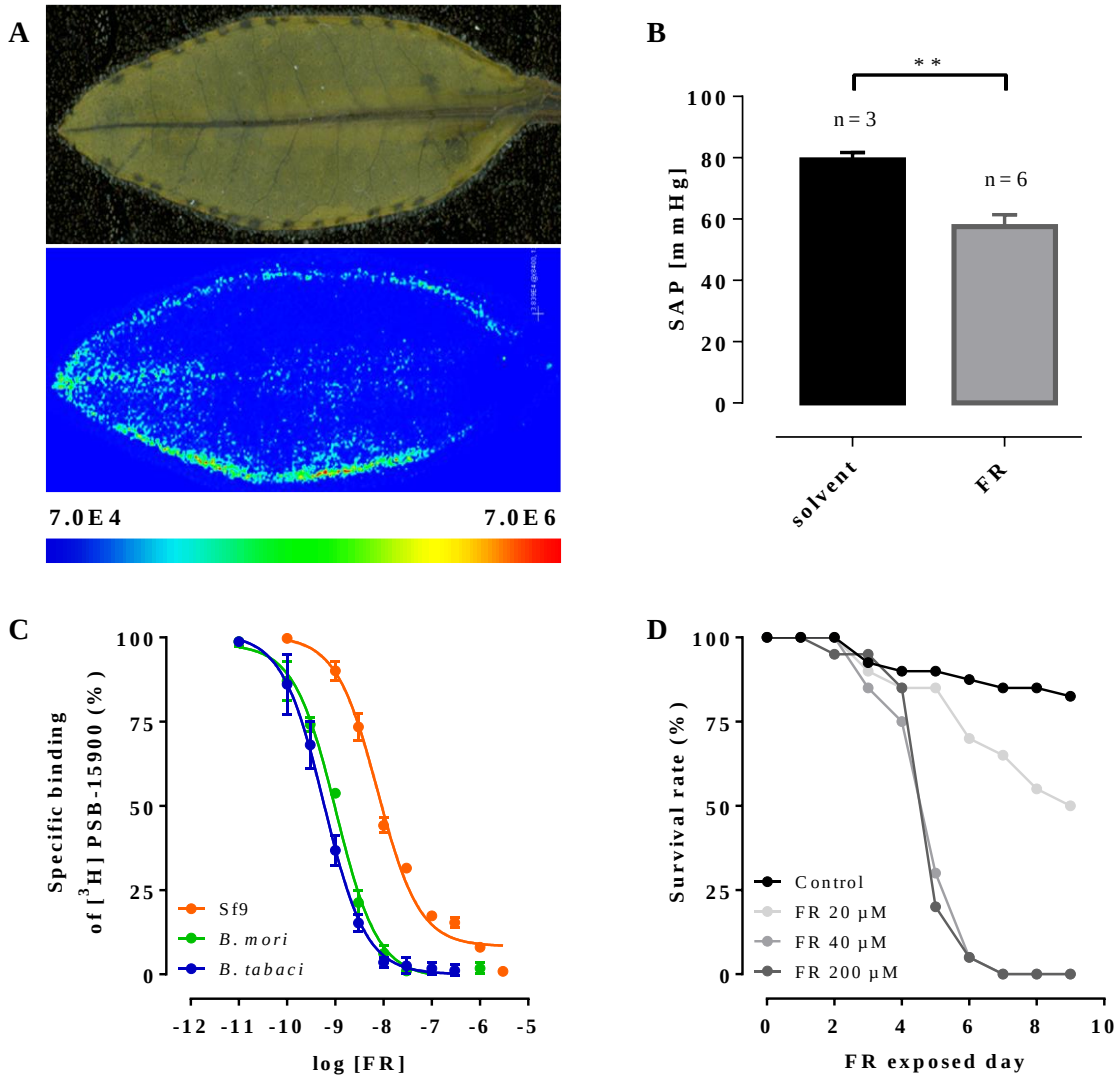

Figure 8-1: Evaluating the ecological function of FR. (**A**) MALDI imaging mass spectrometry of an *Ardisia crenata* leaf. The potassium adduct of the molecular ion of FR (*m/z* 1040.49) is highlighted according to intensity. (**B**) Statistical analysis of in vivo blood pressure recordings in mice revealed a strong reduction of systolic arterial pressure (SAP) in the aorta one hour after oral FR application. (**C**) Competition binding study of FR versus [^{3}H]PSB-15900 (5 nm), the tritiated derivative of FR, at Sf9 insect cell membranes, and at Gq proteins of *Bombyx mori* and *Bemisia tabaci* expressed in Gq-knockout HEK cell membrane preparations. Values represent means: SEM of three independent experiments. pIC_{50} values of 8.13–9.27 were determined. (**D**) Exposure of nymphs of a bean bug (*Riptortus pedestris*) to different concentrations of FR; the survival rate was measured.

Additionally, we were able to find new FR producers, namely the nodulated *A. crispa*, *A. hanceana*, *A. mamillata* and *A. villosa*, and unexpectedly also the non-nodulated *A. lucida*. Only recently, we were successful in isolating FR from a cultivable bacterium. These findings together with reports on the FR related compounds YM-254890 (YM) and sameuramide found in soil bacteria and a marine tunicate respectively, suggest a very broad distribution of the FR molecular family in nature and supports an important ecological role for this natural product and its congeners.

The mechanism of action of FR on the molecular level was investigated by examining the structural elements of the depsipeptide, responsible for biological activity. In that way information concerning the FR pharmacophore was gained. Structure activity relationship studies (SAR) of FR analogs were conducted using semisynthetically modified FR and natural variants, the latter obtained by in-depth investigation of *A. crenata*. For the latter project part, the usefulness of Global Natural Product Social (GNPS) molecular networking for the detection of a family of FR derivatives in the TCM plant *A. crenata* could be demonstrated. The new cyclic depsipeptides FR-1 (**1**), FR-2 (**2**), FR-3 (**3**), and FR-4 (**4**), all of them structurally closely related to FR (**Scheme 8-1**) were isolated and elucidated.

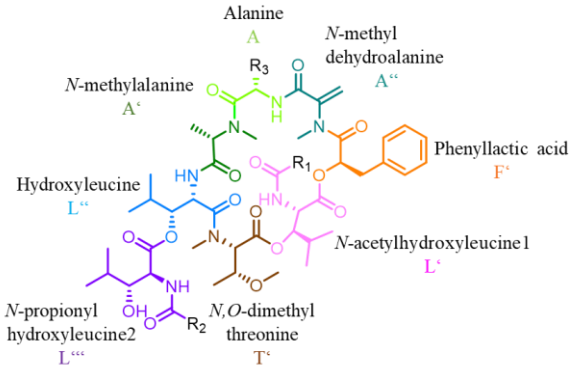

FR900359	$R_1 = CH_3$	$R_2 = CH_2CH_3$	$R_3 = CH_3$
FR-1 (**1**)	$R_1 = CH_2CH_2OH$	$R_2 = CH_2CH_3$	$R_3 = CH_3$
FR-2 (**2**)	$R_1 = CH_3$	$R_2 = CH_3$	$R_3 = CH_3$
FR-3 (**3**)	$R_1 = CH_2CH_3$	$R_2 = CH_2CH_3$	$R_3 = CH_3$
FR-4 (**4**)	$R_1 = CH_3$	$R_2 = CH_2CH_3$	$R_3 = CH_2CH_3$

Scheme 8-1: Structures of FR900359 and isolated “natural” FR analogs FR-1 to FR-4 (1-4). Scheme was taken from Reher *et al.*, submitted.

Isolation was guided by bioactivity and GNPS molecular networking. Structure elucidation was done by extensive 1D- and 2D-NMR analyses in combination with Tandem MS analysis. Evaluation of biological activities of the FR analogs **1-4** showed high affinities to the $G\alpha_q$ protein with IC_{50} values in the low nanomolar range, even exceeding the affinity of the parent compound FR (16.8 ± 3.20 to 2.3 ± 0.12 nM for **1**, **2**, **3**, **and 4** compared to 18.5 ± 4.55 for FR). Similarly, downstream effects mediated by Gq proteins were equipotent inhibited by **1-4** as compared to FR (**Figure 8-2**).

In contrast, FR analogs obtained by semisynthetic modification of the secondary alcohol of FR (FR-Hex, **11**) or of the exomethylene group, respectively (**12**, **46**, **47**, **48**, **49**, **50**), as well as most of the literature known YM analogs derived by total synthesis (Zhang, Xiong *et al.*), displayed a dramatic loss of efficacies, or were even found to be inactive (**Scheme 8-2, Figure 8-2**).

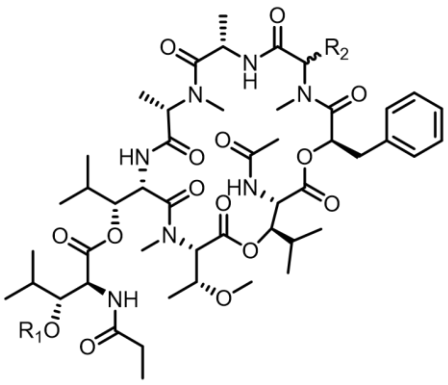

FR900359	R_1 = H	R_2 = CH_2
FR-Hex (**11**)	R_1 = $CO[CH_2]_4CH_3$	R_2 = CH_2
FR-Cys (**12**)	R_1 = H	R_2 = $CH_2S[CH_2]_2NH_2$
FR-Cys-Boc (**47**)	R_1 = H	R_2 = $CH_2S[CH_2]_2NHCO_2C(CH3)_3$
FR-JK-Boc (**48**)	R_1 = H	R_2 = $CH_2S[CH_2]_2NHCOCH_2O[CH_2]_2O[CH_2]_2$-$NHCO_2C(CH3)_3$
FR-RR-BP (**46**)	R_1 = H	R_2 = $CH_2S[CH_2]_2NH$-X-BODIPY630/650®
FR-JK-BP (**49**)	R_1 = H	R_2 = $CH_2S[CH_2]_2NHCOCH_2O[CH_2]_2O[CH_2]_2$-NH-X-BODIPY630/650®
FR-TAMRA (**50**)	R_1 = H	R_2 = $CH_2S[CH_2]_2NH$-TAMRA

Scheme 8-2: Structures of FR900359 and semisynthetically derived FR analogs.

Apart from being useful for SAR studies, the semisynthetically derived FR analogs FR-RR-BP, FR-JK-BP, FR-TAMRA are the first fluorescent selective Gq-inhibitors and display increasing potencies concerning Gq-inhibition. Thus they serve as basis for further investigations on the mechanism of cellular uptake of FR and characterization of unlabeled FR analogs via BRET assays.

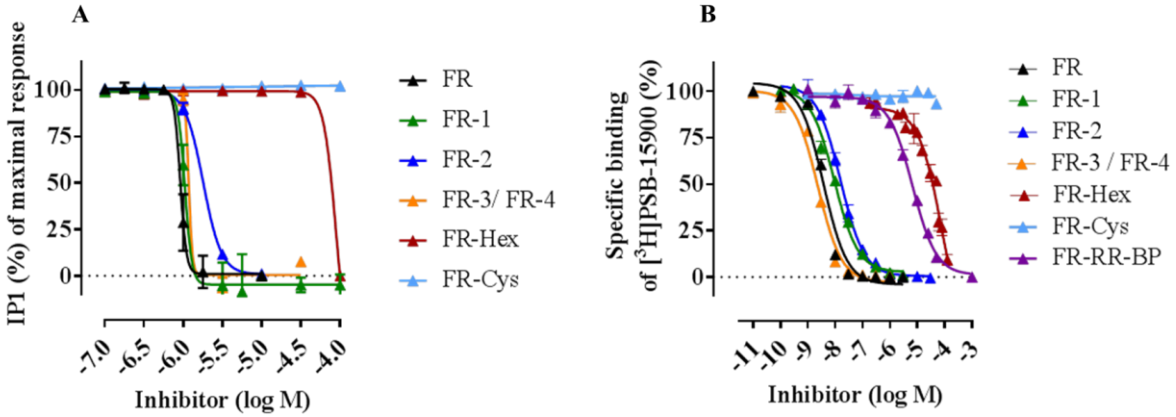

Figure 8-2: SAR studies of FR and analogs. FR-3/FR-4 was tested in a 3/1 mixture. (**A**) IP_1 accumulation assay of FR and analogs. Untransfected cell lines (CHO-M1R) were analyzed in the IP_1 accumulation assay. All data are means of three experiments performed in triplicates and were performed by Suvi Annala, Nina Heycke, and Tobias Benkel (Kostenis lab, Institute for Pharmaceutical Biology, Univ. of Bonn). (**B**) Radioligand binding assay of FR and analogs, performed at human platelet membranes at 37 °C. All data are means of three experiments and were performed by Markus Kuschak (Müller lab, Institute for Pharmaceutical Chemistry, Univ. of Bonn).

Concluding from this in-depth SAR study of the currently isolated and synthesized FR and YM analogs by us and others, it can be suggested that nature has optimized FR and YM for the specific inhibition of $G\alpha_q$ in a long-term co-evolutionary process.

9 References

(1) Jun, W.; Nian-He, X. Ardisia Crenata Complex (Primulaceae) Studies Using Morphological and Molecular Data. In *Botany*; InTech, 2012.

(2) Byng, J. W.; Chase, M. W.; Christenhusz, M. J.; Fay, M. F.; Judd, W. S.; Mabberley, D. J.; Sennikov, A. N.; Soltis, D. E.; Soltis, P. S.; Stevens, P. F. An Update of the Angiosperm Phylogeny Group Classification for the Orders and Families of Flowering Plants: APG IV. *Bot. J. Linn. Soc.* **2016**, *181* (1), 1–20.

(3) Ku, C.; Hu, J.-M. Phylogenetic and Cophylogenetic Analyses of the Leaf-Nodule Symbiosis in *Ardisia* Subgenus *Crispardisia* (Myrsinaceae): Evidence from Nuclear and Chloroplast Markers and Bacterial *Rrn* Operons. *Int. J. Plant Sci.* **2014**, *175* (1), 92–109.

(4) Kitajima, K.; Fox, A. M.; Sato, T.; Nagamatsu, D. Cultivar Selection Prior to Introduction May Increase Invasiveness: Evidence from Ardisia Crenata. *Biol. Invasions* **2006**, *8* (7), 1471–1482.

(5) Ma, L.; Li, W.; Wang, H.; Kuang, X.; Li, Q.; Wang, Y.; Xie, P.; Koike, K. A Simple and Rapid Method to Identify and Quantitatively Analyze Triterpenoid Saponins in Ardisia Crenata Using Ultrafast Liquid Chromatography Coupled with Electrospray Ionization Quadrupole Mass Spectrometry. *J. Pharm. Biomed. Anal.* **2015**, *102*, 400–408.

(6) Jia, Z.; Koike, K.; Ohmoto, T.; Ni, M. Triterpenoid Saponins from Ardisia Crenata. *Phytochemistry* **1994**, *37* (5), 1389–1396.

(7) Pinto-Carbó, M.; Gademann, K.; Eberl, L.; Carlier, A. Leaf Nodule Symbiosis: Function and Transmission of Obligate Bacterial Endophytes. *Curr. Opin. Plant Biol.* **2018**, *44*, 23–31.

(8) Abdalla, M. A.; Matasyoh, J. C. Endophytes as Producers of Peptides: An Overview About the Recently Discovered Peptides from Endophytic Microbes. *Nat. Prod. Bioprospecting* **2014**, *4* (5), 257–270.

(9) Strobel, G.; Daisy, B. Bioprospecting for Microbial Endophytes and Their Natural Products. *Microbiol. Mol. Biol. Rev.* **2003**, *67* (4), 491–502.

(10) Crüsemann, M.; Reher, R.; Schamari, I.; Brachmann, A. O.; Ohbayashi, T.; Kuschak, M.; Malfacini, D.; Seidinger, A.; Pinto-Carbó, M.; Richarz, R.; et al. Heterologous Expression, Biosynthetic Studies, and Ecological Function of the Selective Gq-Signaling Inhibitor FR900359. *Angew. Chem. Int. Ed.* **2018**, *57* (3), 836–840.

(11) Yu, H.; Zhang, L.; Li, L.; Zheng, C.; Guo, L.; Li, W.; Sun, P.; Qin, L. Recent Developments and Future Prospects of Antimicrobial Metabolites Produced by Endophytes. *Microbiol. Res.* **2010**, *165* (6), 437–449.

(12) Strobel, G.; Daisy, B.; Castillo, U.; Harper, J. Natural Products from Endophytic Microorganisms ┴. *J. Nat. Prod.* **2004**, *67* (2), 257–268.

(13) HORNER JR, H. T.; LERSTEN, N. R. Nomenclature of Bacteria in Leaf Nodules of the Families Myrsinaceae and Rubiaceae. *Int. J. Syst. Evol. Microbiol.* **1972**, *22* (2), 117–122.

(14) MILLER, I. M.; Gardner, I. C.; Scott, A. The Development of Marginal Leaf Nodules in Ardisia Crispa (Thunb.) A. DC.(Myrsinaceae). *Bot. J. Linn. Soc.* **1983**, *86* (3), 237–252.

(15) Lemaire, B.; Smets, E.; Dessein, S. Bacterial Leaf Symbiosis in Ardisia (Myrsinoideae, Primulaceae): Molecular Evidence for Host Specificity. *Res. Microbiol.* **2011**, *162* (5), 528–534.

(16) Lemaire, B.; Vandamme, P.; Merckx, V.; Smets, E.; Dessein, S. Bacterial Leaf Symbiosis in Angiosperms: Host Specificity without Co-Speciation. *PLoS ONE* **2011**, *6* (9), e24430.

(17) Miller, I. M. Bacterial Leaf Nodule Symbiosis. In *Advances in botanical research*; Elsevier, 1990; Vol. 17, pp 163–234.

(18) Compant, S.; Nowak, J.; Coenye, T.; Clément, C.; Ait Barka, E. Diversity and Occurrence of *Burkholderia* Spp. in the Natural Environment. *FEMS Microbiol. Rev.* **2008**, *32* (4), 607–626.
(19) Coenye, T.; Vandamme, P. Diversity and Significance of Burkholderia Species Occupying Diverse Ecological Niches. *Environ. Microbiol.* **2003**, *5* (9), 719–729.
(20) Chen, W.-M.; de Faria, S. M.; Straliotto, R.; Pitard, R. M.; Simoes-Araujo, J. L.; Chou, J.-H.; Chou, Y.-J.; Barrios, E.; Prescott, A. R.; Elliott, G. N.; et al. Proof That Burkholderia Strains Form Effective Symbioses with Legumes: A Study of Novel Mimosa-Nodulating Strains from South America. *Appl. Environ. Microbiol.* **2005**, *71* (11), 7461–7471.
(21) de Souza, J. T.; Raaijmakers, J. M. Polymorphisms within the PrnD and PltC Genes from Pyrrolnitrin and Pyoluteorin-Producing Pseudomonas and Burkholderia Spp. *FEMS Microbiol. Ecol.* **2003**, *43* (1), 21–34.
(22) Carlier, A.; Fehr, L.; Pinto-Carbó, M.; Schäberle, T.; Reher, R.; Dessein, S.; König, G.; Eberl, L. The Genome Analysis of *C Andidatus* Burkholderia Crenata Reveals That Secondary Metabolism May Be a Key Function of the *A Rdisia Crenata* Leaf Nodule Symbiosis: *Ca* . B. Crenata Genome. *Environ. Microbiol.* **2016**, *18* (8), 2507–2522.
(23) Sivanathan, S.; Scherkenbeck, J. Cyclodepsipeptides: A Rich Source of Biologically Active Compounds for Drug Research. *Molecules* **2014**, *19* (12), 12368–12420.
(24) Mootz, H. D.; Schwarzer, D.; Marahiel, M. A. Ways of Assembling Complex Natural Products on Modular Nonribosomal Peptide Synthetases. *ChemBioChem* **2002**, *3* (6), 490–504.
(25) Kopp, F.; Marahiel, M. A. Macrocyclization Strategies in Polyketide and Nonribosomal Peptide Biosynthesis. *Nat. Prod. Rep.* **2007**, *24* (4), 735.
(26) Xiong, X.-F.; Zhang, H.; Underwood, C. R.; Harpsøe, K.; Gardella, T. J.; Wöldike, M. F.; Mannstadt, M.; Gloriam, D. E.; Bräuner-Osborne, H.; Strømgaard, K. Total Synthesis and Structure–activity Relationship Studies of a Series of Selective G Protein Inhibitors. *Nat. Chem.* **2016**, *8* (11), 1035–1041.
(27) Fujioka, M.; Koda, S.; Morimoto, Y.; Biemann, K. Structure of FR900359, a Cyclic Depsipeptide from Ardisia Crenata Sims. *J. Org. Chem.* **1988**, *53* (12), 2820–2825.
(28) Taniguchi, M.; Suzumura, K.; Nagai, K.; Kawasaki, T.; Saito, T.; Takasaki, J.; Suzuki, K.; Fujita, S.; Tsukamoto, S. Structure of YM-254890, a Novel Gq/11 Inhibitor from Chromobacterium Sp. QS3666. *Tetrahedron* **2003**, *59* (25), 4533–4538.
(29) Yamashita, J.; Nakao, Y.; Katsumata, R. Novel Cyclic Peptide and the Use Thereof. Patent No.: WO 2011/142485 A1. WO 2011/142485 A1, November 17, 2011.
(30) Miyamae, A.; Fujioka, M.; Koda, S.; Morimoto, Y. Structural Studies of FR900359, a Novel Cyclic Depsipeptide from Ardisia Crenata Sims (Myrsinaceae). *J. Chem. Soc. [Perkin 1]* **1989**, *5*, 873–878.
(31) Lipinski, C. A.; Lombardo, F.; Dominy, B. W.; Feeney, P. J. Experimental and Computational Approaches to Estimate Solubility and Permeability in Drug Discovery and Development Settings1. *Adv. Drug Deliv. Rev.* **2001**, *46* (1–3), 3–26.
(32) Lipinski, C. A. Lead- and Drug-like Compounds: The Rule-of-Five Revolution. *Drug Discov. Today Technol.* **2004**, *1* (4), 337–341.
(33) Zhang, M.-Q.; Wilkinson, B. Drug Discovery beyond the 'Rule-of-Five.' *Curr. Opin. Biotechnol.* **2007**, *18* (6), 478–488.
(34) Lipinski, C. A. Rule of Five in 2015 and beyond: Target and Ligand Structural Limitations, Ligand Chemistry Structure and Drug Discovery Project Decisions. *Adv. Drug Deliv. Rev.* **2016**, *101*, 34–41.
(35) Haviv, F.; Fitzpatrick, T. D.; Swenson, R. E.; Nichols, C. J.; Mort, N. A.; Bush, E. N.; Diaz, G.; Bammert, G.; Nguyen, A. Effect of N-Methyl Substitution of the Peptide Bonds

in Luteinizing Hormone-Releasing Hormone Agonists. *J. Med. Chem.* **1993**, *36* (3), 363–369.

(36) Barker, P. L.; Bullens, S.; Bunting, S.; Burdick, D. J.; Chan, K. S.; Deisher, T.; Eigenbrot, C.; Gadek, T. R.; Gantzos, R. Cyclic RGD Peptide Analogs as Antiplatelet Antithrombotics. *J. Med. Chem.* **1992**, *35* (11), 2040–2048.

(37) Hewitt, W. M.; Leung, S. S. F.; Pye, C. R.; Ponkey, A. R.; Bednarek, M.; Jacobson, M. P.; Lokey, R. S. Cell-Permeable Cyclic Peptides from Synthetic Libraries Inspired by Natural Products. *J. Am. Chem. Soc.* **2015**, *137* (2), 715–721.

(38) Rajeswaran, W. G.; Hocart, S. J.; Murphy, W. A.; Taylor, J. E.; Coy, D. H. Highly Potent and Subtype Selective Ligands Derived by *N* -Methyl Scan of a Somatostatin Antagonist. *J. Med. Chem.* **2001**, *44* (8), 1305–1311.

(39) Bockus, A. T.; Lexa, K. W.; Pye, C. R.; Kalgutkar, A. S.; Gardner, J. W.; Hund, K. C. R.; Hewitt, W. M.; Schwochert, J. A.; Glassey, E.; Price, D. A.; et al. Probing the Physicochemical Boundaries of Cell Permeability and Oral Bioavailability in Lipophilic Macrocycles Inspired by Natural Products. *J. Med. Chem.* **2015**, *58* (11), 4581–4589.

(40) Bennett, R. N.; Wallsgrove, R. M. Secondary Metabolites in Plant Defence Mechanisms. *New Phytol.* **1994**, *127* (4), 617–633.

(41) Hartmann, T. Plant-Derived Secondary Metabolites as Defensive Chemicals in Herbivorous Insects: A Case Study in Chemical Ecology. *Planta* **2004**, *219* (1), 1–4.

(42) Iriti, M.; Faoro, F. Chemical Diversity and Defence Metabolism: How Plants Cope with Pathogens and Ozone Pollution. *Int. J. Mol. Sci.* **2009**, *10* (12), 3371–3399.

(43) Trzaskowski, B.; Latek, D.; Yuan, S.; Ghoshdastider, U.; Debinski, A.; Filipek, S. Action of Molecular Switches in GPCRs-Theoretical and Experimental Studies. *Curr. Med. Chem.* **2012**, *19* (8), 1090–1109.

(44) Rask-Andersen, M.; Almén, M. S.; Schiöth, H. B. Trends in the Exploitation of Novel Drug Targets. *Nat. Rev. Drug Discov.* **2011**, *10* (8), 579–590.

(45) Offermanns, S.; Wieland, T.; Homann, D.; Sandmann, J.; Bombien, E.; Spicher, K.; Schultz, G.; Jakobs, K. H. Transfected Muscarinic Acetylcholine Receptors Selectively Couple to Gi-Type G Proteins and Gq/11. *Mol. Pharmacol.* **1994**, *45* (5), 890–898.

(46) Thomas, R. L.; Mistry, R.; Langmead, C. J.; Wood, M. D.; Challiss, R. A. J. G Protein Coupling and Signaling Pathway Activation by M1 Muscarinic Acetylcholine Receptor Orthosteric and Allosteric Agonists. *J. Pharmacol. Exp. Ther.* **2008**, *327* (2), 365–374.

(47) Burke, R. E. The Relative Selectivity of Anticholinergic Drugs for the M1 and M2 Muscarinic Receptor Subtypes. *Mov. Disord.* **1986**, *1* (2), 135–144.

(48) Ridley, R. M.; Bowes, P. M.; Baker, H. F.; Crow, T. J. An Involvement of Acetylcholine in Object Discrimination Learning and Memory in the Marmoset. *Neuropsychologia* **1984**, *22* (3), 253–263.

(49) Crow, T. J.; Grove-White, I. G. An Analysis of the Learning Deficit Following Hyoscine Administration to Man. *Br. J. Pharmacol.* **1973**, *49* (2), 322–327.

(50) Jaffe, R. J.; Novakovic, V.; Peselow, E. D. Scopolamine as an Antidepressant: A Systematic Review. *Clin. Neuropharmacol.* **2013**, *36* (1), 24–26.

(51) Digby, G. J.; Lober, R. M.; Sethi, P. R.; Lambert, N. A. Some G Protein Heterotrimers Physically Dissociate in Living Cells. *Proc. Natl. Acad. Sci.* **2006**, *103* (47), 17789.

(52) Taniguchi, M.; Suzumura, K.; Nagai, K.; Kawasaki, T.; Takasaki, J.; Sekiguchi, M.; Moritani, Y.; Saito, T.; Hayashi, K.; Fujita, S.; et al. YM-254890 Analogues, Novel Cyclic Depsipeptides with Gαq/11 Inhibitory Activity from Chromobacterium Sp. QS3666. *Bioorg. Med. Chem.* **2004**, *12* (12), 3125–3133.

(53) Nishimura, A.; Kitano, K.; Takasaki, J.; Taniguchi, M.; Mizuno, N.; Tago, K.; Hakoshima, T.; Itoh, H. Structural Basis for the Specific Inhibition of Heterotrimeric Gq Protein by a Small Molecule. *Proc. Natl. Acad. Sci.* **2010**, *107* (31), 13666–13671.

(54) Schrage, R.; Schmitz, A.-L.; Gaffal, E.; Annala, S.; Kehraus, S.; Wenzel, D.; Büllesbach, K. M.; Bald, T.; Inoue, A.; Shinjo, Y.; et al. The Experimental Power of FR900359 to Study Gq-Regulated Biological Processes. *Nat. Commun.* **2015**, *6* (1).

(55) Klose, C. S. N.; Mahlakõiv, T.; Moeller, J. B.; Rankin, L. C.; Flamar, A.-L.; Kabata, H.; Monticelli, L. A.; Moriyama, S.; Putzel, G. G.; Rakhilin, N.; et al. The Neuropeptide Neuromedin U Stimulates Innate Lymphoid Cells and Type 2 Inflammation. *Nature* **2017**, *549* (7671), 282–286.

(56) Inamdar, V.; Patel, A.; Manne, B. K.; Dangelmaier, C.; Kunapuli, S. P. Characterization of UBO-QIC as a G $\boldsymbol{\alpha}_{q}$ Inhibitor in Platelets. *Platelets* **2015**, *26* (8), 771–778.

(57) Jacobsen, S. E.; Norskov-Lauritsen, L.; Thomsen, A. R. B.; Smajilovic, S.; Wellendorph, P.; Larsson, N. H. P.; Lehmann, A.; Bhatia, V. K.; Brauner-Osborne, H. Delineation of the GPRC6A Receptor Signaling Pathways Using a Mammalian Cell Line Stably Expressing the Receptor. *J. Pharmacol. Exp. Ther.* **2013**, *347* (2), 298–309.

(58) Klepac, K.; Kilić, A.; Gnad, T.; Brown, L. M.; Herrmann, B.; Wilderman, A.; Balkow, A.; Glöde, A.; Simon, K.; Lidell, M. E.; et al. The Gq Signalling Pathway Inhibits Brown and Beige Adipose Tissue. *Nat. Commun.* **2016**, *7*, 10895.

(59) Grace, M. S.; Lieu, T.; Darby, B.; Abogadie, F. C.; Veldhuis, N.; Bunnett, N. W.; McIntyre, P. The Tyrosine Kinase Inhibitor Bafetinib Inhibits PAR2-Induced Activation of TRPV4 Channels *in Vitro* and Pain *in Vivo*: Bafetinib Inhibits PAR2-TRPV4 Coupling. *Br. J. Pharmacol.* **2014**, *171* (16), 3881–3894.

(60) Link, A.; Müller, C. E. G-Protein-Coupled Receptors: Sustained Signaling via Intracellular Megaplexes and Pathway-Specific Drugs. *Angew. Chem. Int. Ed.* **2016**, *55* (52), 15962–15964.

(61) Smrcka, A. V. Molecular Targeting of Gα and Gβγ Subunits: A Potential Approach for Cancer Therapeutics. *Trends Pharmacol. Sci.* **2013**, *34* (5), 290–298.

(62) Matthey, M.; Roberts, R.; Seidinger, A.; Simon, A.; Schröder, R.; Kuschak, M.; Annala, S.; König, G. M.; Müller, C. E.; Hall, I. P. Targeted Inhibition of Gq Signaling Induces Airway Relaxation in Mouse Models of Asthma. *Sci. Transl. Med.* **2017**, *9* (407), eaag2288.

(63) Weiss, S. T. Emerging Mechanisms and Novel Targets in Allergic Inflammation and Asthma. *Genome Med.* **2017**, *9* (1).

(64) Matsuo, A.; Matsumoto, S.; Nagano, M.; Masumoto, K.; Takasaki, J.; Matsumoto, M.; Kobori, M.; Katoh, M.; Shigeyoshi, Y. Molecular Cloning and Characterization of a Novel Gq-Coupled Orphan Receptor GPRg1 Exclusively Expressed in the Central Nervous System. *Biochem. Biophys. Res. Commun.* **2005**, *331* (1), 363–369.

(65) Morishita, R.; Ueda, H.; Ito, H.; Takasaki, J.; Nagata, K.; Asano, T. Involvement of Gq/11 in Both Integrin Signal-Dependent and -Independent Pathways Regulating Endothelin-Induced Neural Progenitor Proliferation. *Neurosci. Res.* **2007**, *59* (2), 205–214.

(66) Uemura, T.; Takamatsu, H.; Kawasaki, T.; Taniguchi, M.; Yamamoto, E.; Tomura, Y.; Uchida, W.; Miyata, K. Effect of YM-254890, a Specific Gαq/11 Inhibitor, on Experimental Peripheral Arterial Disease in Rats. *Eur. J. Pharmacol.* **2006**, *536* (1–2), 154–161.

(67) Kawasaki, T.; Taniguchi, M.; Moritani, Y.; Uemura, T.; Shigenaga, T.; Takamatsu, H.; Hayashi, K.; Takasaki, J.; Saito, T.; Nagai, K. Pharmacological Properties of YM-254890, a Specific Gαq/11 Inhibitor, on Thrombosis and Neointima Formation in Mice. *Thromb. Haemost.* **2005**.

(68) Bleasdale, J. E.; Thakur, N. R.; Gremban, R. S.; Bundy, G. L.; Fitzpatrick, F. A.; Smith, R. J.; Bunting, S. Selective Inhibition of Receptor-Coupled Phospholipase C-Dependent Processes in Human Platelets and Polymorphonuclear Neutrophils. *J. Pharmacol. Exp. Ther.* **1990**, *255* (2), 756–768.

(69) Smith, R. J.; Sam, L. M.; Justen, J. M.; Bundy, G. L.; Bala, G. A.; Bleasdale, J. E. Receptor-Coupled Signal Transduction in Human Polymorphonuclear Neutrophils: Effects of a Novel Inhibitor of Phospholipase C-Dependent Processes on Cell Responsiveness. *J. Pharmacol. Exp. Ther.* **1990**, *253* (2), 688–697.

(70) Eccles, R. Menthol and Related Cooling Compounds. *J. Pharm. Pharmacol.* **1994**, *46* (8), 618–630.

(71) Kim, K. Y.; Bang, S.; Han, S.; Nguyen, Y. H.; Kang, T. M.; Kang, K. W.; Hwang, S. W. TRP-Independent Inhibition of the Phospholipase C Pathway by Natural Sensory Ligands. *Biochem. Biophys. Res. Commun.* **2008**, *370* (2), 295–300.

(72) Treiman, M.; Caspersen, C.; Christensen, S. B. A Tool Coming of Age: Thapsigargin as an Inhibitor of Sarco-Endoplasmic Reticulum Ca 2+-ATPases. *Trends Pharmacol. Sci.* **1998**, *19* (4), 131–135.

(73) Doan, N. T. Q.; Paulsen, E. S.; Sehgal, P.; Møller, J. V.; Nissen, P.; Denmeade, S. R.; Isaacs, J. T.; Dionne, C. A.; Christensen, S. B. Targeting Thapsigargin towards Tumors. *Steroids* **2015**, *97*, 2–7.

(74) Mahalingam, D.; Wilding, G.; Denmeade, S.; Sarantopoulas, J.; Cosgrove, D.; Cetnar, J.; Azad, N.; Bruce, J.; Kurman, M.; Allgood, V. E.; et al. Mipsagargin, a Novel Thapsigargin-Based PSMA-Activated Prodrug: Results of a First-in-Man Phase I Clinical Trial in Patients with Refractory, Advanced or Metastatic Solid Tumours. *Br. J. Cancer* **2016**, *114* (9), 986–994.

(75) Hakii, H.; Fujiki, H.; Suganuma, M.; Nakayasu, M.; Tahira, T.; Sugimura, T.; Scheuer, P. J.; Christensen, S. B. Thapsigargin, a Histamine Secretagogue, Is a Non-12-O-Tetradecanolphorbol-13-Acetate (TPA) Type Tumor Promoter in Two-Stage Mouse Skin Carcinogenesis. *J. Cancer Res. Clin. Oncol.* **1986**, *111* (3), 177–181.

(76) Ganley, I. G.; Wong, P.-M.; Gammoh, N.; Jiang, X. Distinct Autophagosomal-Lysosomal Fusion Mechanism Revealed by Thapsigargin-Induced Autophagy Arrest. *Mol. Cell* **2011**, *42* (6), 731–743.

(77) Hishinuma, S.; Saito, M. DIFFERENTIAL ROLES OF RYANODINE- AND THAPSIGARGIN-SENSITIVE INTRACELLULAR Ca $^{2+}$ STORES IN EXCITATION?CONTRACTION COUPLING IN SMOOTH MUSCLE OF GUINEA-PIG TAENIA CAECI. *Clin. Exp. Pharmacol. Physiol.* **2006**, *33* (12), 1138–1143.

(78) Feher, J. J.; Lee, K. N.; Wu, Q. Y. Ryanodine-Sensitive, Thapsigargin-Insensitive Calcium Uptake in Rat Ventricle Homogenates. *Mol. Cell. Biochem.* **1998**, *189* (1–2), 9–17.

(79) Stutzmann, G. E.; Mattson, M. P. Endoplasmic Reticulum Ca2+ Handling in Excitable Cells in Health and Disease. *Pharmacol. Rev.* **2011**, *63* (3), 700–727.

(80) Wilson, C. H.; Ali, E. S.; Scrimgeour, N.; Martin, A. M.; Hua, J.; Tallis, G. A.; Rychkov, G. Y.; Barritt, G. J. Steatosis Inhibits Liver Cell Store-Operated Ca2+ Entry and Reduces ER Ca2+ through a Protein Kinase C-Dependent Mechanism. *Biochem. J.* **2015**, *466* (2), 379–390.

(81) Marston, A. Natural Products as a Source of Protein Kinase Activators and Inhibitors. *Curr. Top. Med. Chem.* **2011**, *11* (11), 1333–1339.

(82) Wu-zhang, A. X.; Newton, A. C. Protein Kinase C Pharmacology: Refining the Toolbox. *Biochem. J.* **2013**, *452* (2), 195–209.

(83) Zhao, J.; Zhou, C. Virtual Screening of Protein Kinase C Inhibitors from Natural Product Library to Modulate General Anaesthetic Effects. *Nat. Prod. Res.* **2015**, *29* (6), 589–591.

(84) Shi, B. X.; Chen, F. R.; Sun, X. Structure-Based Modelling, Scoring, Screening, and *in Vitro* Kinase Assay of Anesthetic Pkc Inhibitors against a Natural Medicine Library. *SAR QSAR Environ. Res.* **2017**, *28* (2), 151–163.

(85) Castagna, M.; Takai, Y.; Kaibuchi, K.; Sano, K.; Kikkawa, U.; Nishizuka, Y. Direct Activation of Calcium-Activated, Phospholipid-Dependent Protein Kinase by Tumor-Promoting Phorbol Esters. *J. Biol. Chem.* **1982**, *257* (13), 7847–7851.
(86) Emerit, I.; Cerutti, P. A. Tumour Promoter Phorbol-12-Myristate-13-Acetate Induces Chromosomal Damage via Indirect Action. *Nature* **1981**, *293* (5828), 144–146.
(87) Lebwohl, M.; Swanson, N.; Anderson, L. L.; Melgaard, A.; Xu, Z.; Berman, B. Ingenol Mebutate Gel for Actinic Keratosis. *N. Engl. J. Med.* **2012**, *366* (11), 1010–1019.
(88) Jiang, G.; Mendes, E. A.; Kaiser, P.; Wong, D. P.; Tang, Y.; Cai, I.; Fenton, A.; Melcher, G. P.; Hildreth, J. E. K.; Thompson, G. R.; et al. Synergistic Reactivation of Latent HIV Expression by Ingenol-3-Angelate, PEP005, Targeted NF-KB Signaling in Combination with JQ1 Induced p-TEFb Activation. *PLOS Pathog.* **2015**, *11* (7), e1005066.
(89) Mangmool, S.; Kurose, H. Gi/o Protein-Dependent and -Independent Actions of Pertussis Toxin (PTX). *Toxins* **2011**, *3* (12), 884–899.
(90) Carbonetti, N. H. Pertussis Toxin and Adenylate Cyclase Toxin: Key Virulence Factors of *Bordetella Pertussis* and Cell Biology Tools. *Future Microbiol.* **2010**, *5* (3), 455–469.
(91) Dolphin, A. C.; Prestwich, S. A. Pertussis Toxin Reverses Adenosine Inhibition of Neuronal Glutamate Release. *Nature* **1985**, *316* (6024), 148–150.
(92) Stein, P. E.; Boodhoo, A.; Armstrong, G. D.; Heerze, L. D.; Cockle, S. A.; Klein, M. H.; Read, R. J. Structure of a Pertussis Toxin–sugar Complex as a Model for Receptor Binding. *Nat. Struct. Mol. Biol.* **1994**, *1* (9), 591–596.
(93) Gupta, S.; Samanta, M. K.; Raichur, A. M. Dual-Drug Delivery System Based on In Situ Gel-Forming Nanosuspension of Forskolin to Enhance Antiglaucoma Efficacy. *AAPS PharmSciTech* **2010**, *11* (1), 322–335.
(94) Wagh, V. D.; Patil, P. N.; Surana, S. J.; Wagh, K. V. Forskolin: Upcoming Antiglaucoma Molecule. *J. Postgrad. Med.* **2012**, *58* (3), 199.
(95) Newman, D. J.; Cragg, G. M. Natural Products as Sources of New Drugs from 1981 to 2014. *J. Nat. Prod.* **2016**, *79* (3), 629–661.
(96) Atanasov, A. G.; Waltenberger, B.; Pferschy-Wenzig, E.-M.; Linder, T.; Wawrosch, C.; Uhrin, P.; Temml, V.; Wang, L.; Schwaiger, S.; Heiss, E. H.; et al. Discovery and Resupply of Pharmacologically Active Plant-Derived Natural Products: A Review. *Biotechnol. Adv.* **2015**, *33* (8), 1582–1614.
(97) Coll, J. C.; Bowden, B. F. The Application of Vacuum Liquid Chromatography to the Separation of Terpene Mixtures. *J. Nat. Prod.* **1986**, *49* (5), 934–936.
(98) Targett, N. M.; Kilcoyne, J. P.; Green, B. Vacuum Liquid Chromatography: An Alternative to Common Chromatographic Methods. *J. Org. Chem.* **1979**, *44* (26), 4962–4964.
(99) Rücker, G.; Neugebauer, M.; Willems, G. G. *Instrumentelle pharmazeutische Analytik*, 4.; Wissenschaftliche Verlagsgesellschaft mbH Stuttgart: Stuttgart, 2008.
(100) McLafferty, F. W. Tandem Mass Spectrometry. *Science* **1981**, *214* (4518), 280–287.
(101) Ngoka, L. C.; Gross, M. L. A Nomenclature System for Labeling Cyclic Peptide Fragments. *J. Am. Soc. Mass Spectrom.* **1999**, *10* (4), 360–363.
(102) Biemann, K. Mass Spectrometry of Peptides and Proteins. *Annu. Rev. Biochem.* **1992**, *61* (1), 977–1010.
(103) Roepstorff, P.; Fohlmann, J. Proposal for a Common Nomenclature for Sequence Ions in Mass Spectra of Peptides. *Biomed. Mass Spectrom.* **1984**, *11* (11), 601.
(104) Johnson, R. S.; Martin, S. A.; Biemann, K. Collision-Induced Fragmentation of (M + H)+. *Int. J. Mass Spectrom. Ion Process.* **1988**, *86*, 137–154.
(105) Schmelzer, H. D.-I. F. C. *Massenspektrometrische Charakterisierung von Proteinhydrolysaten: Verdaustudien an β-Casein Und Strukturuntersuchungen an Elastin*; Dissertation. Martin–Luther–Universität Halle–Wittenberg, 2007.

(106) Mitchell Wells, J.; McLuckey, S. A. Collision-Induced Dissociation (CID) of Peptides and Proteins. In *Methods in Enzymology*; Elsevier, 2005; Vol. 402, pp 148–185.
(107) Marshall, A. G.; Hendrickson, C. L. Fourier Transform Ion Cyclotron Resonance Detection: Principles and Experimental Configurations. *Int. J. Mass Spectrom.* **2002**, *215* (1), 59–75.
(108) Liu, W.-T.; Ng, J.; Meluzzi, D.; Bandeira, N.; Gutierrez, M.; Simmons, T. L.; Schultz, A. W.; Linington, R. G.; Moore, B. S.; Gerwick, W. H.; et al. Interpretation of Tandem Mass Spectra Obtained from Cyclic Nonribosomal Peptides. *Anal. Chem.* **2009**, *81* (11), 4200–4209.
(109) Ngoka, L. C.; Gross, M. L. Multistep Tandem Mass Spectrometry for Sequencing Cyclic Peptides in an Ion-Trap Mass Spectrometer. *J. Am. Soc. Mass Spectrom.* **1999**, *10* (8), 732–746.
(110) Karas, M.; Krüger, R. Ion Formation in MALDI: The Cluster Ionization Mechanism. *Chem. Rev.* **2003**, *103* (2), 427–440.
(111) Cha, S.; Zhang, H.; Ilarslan, H. I.; Wurtele, E. S.; Brachova, L.; Nikolau, B. J.; Yeung, E. S. Direct Profiling and Imaging of Plant Metabolites in Intact Tissues by Using Colloidal Graphite-Assisted Laser Desorption Ionization Mass Spectrometry. *Plant J.* **2008**, *55* (2), 348–360.
(112) Vranken, W. F.; Boucher, W.; Stevens, T. J.; Fogh, R. H.; Pajon, A.; Llinas, M.; Ulrich, E. L.; Markley, J. L.; Ionides, J.; Laue, E. D. The CCPN Data Model for NMR Spectroscopy: Development of a Software Pipeline. *Proteins Struct. Funct. Bioinforma.* **2005**, *59* (4), 687–696.
(113) Cheung, M.-S.; Maguire, M. L.; Stevens, T. J.; Broadhurst, R. W. DANGLE: A Bayesian Inferential Method for Predicting Protein Backbone Dihedral Angles and Secondary Structure. *J. Magn. Reson.* **2010**, *202* (2), 223–233.
(114) Krieger, E.; Vriend, G. YASARA View—molecular Graphics for All Devices—from Smartphones to Workstations. *Bioinformatics* **2014**, *30* (20), 2981–2982.
(115) Krieger, E.; Vriend, G. New Ways to Boost Molecular Dynamics Simulations. *J. Comput. Chem.* **2015**, *36* (13), 996–1007.
(116) Harjes, E.; Harjes, S.; Wohlgemuth, S.; Müller, K.-H.; Krieger, E.; Herrmann, C.; Bayer, P. GTP-Ras Disrupts the Intramolecular Complex of C1 and RA Domains of Nore1. *Structure* **2006**, *14* (5), 881–888.
(117) Essmann, U.; Perera, L.; Berkowitz, M. L.; Darden, T.; Lee, H.; Pedersen, L. G. A Smooth Particle Mesh Ewald Method. *J. Chem. Phys.* **1995**, *103* (19), 8577–8593.
(118) Krieger, E.; Joo, K.; Lee, J.; Lee, J.; Raman, S.; Thompson, J.; Tyka, M.; Baker, D.; Karplus, K. Improving Physical Realism, Stereochemistry, and Side-chain Accuracy in Homology Modeling: Four Approaches That Performed Well in CASP8. *Proteins Struct. Funct. Bioinforma.* **2009**, *77* (S9), 114–122.
(119) Krieger, E.; Nielsen, J. E.; Spronk, C. A. E. M.; Vriend, G. Fast Empirical PKa Prediction by Ewald Summation. *J. Mol. Graph. Model.* **2006**, *25* (4), 481–486.
(120) Trott, O.; Olson, A. J. AutoDock Vina: Improving the Speed and Accuracy of Docking with a New Scoring Function, Efficient Optimization, and Multithreading. *J. Comput. Chem.* **2009**, NA-NA.
(121) Wang, J.; Wolf, R. M.; Caldwell, J. W.; Kollman, P. A.; Case, D. A. Development and Testing of a General Amber Force Field. *J. Comput. Chem.* **2004**, *25* (9), 1157–1174.
(122) Jakalian, A.; Jack, D. B.; Bayly, C. I. Fast, Efficient Generation of High-Quality Atomic Charges. AM1-BCC Model: II. Parameterization and Validation. *J. Comput. Chem.* **2002**, *23* (16), 1623–1641.
(123) Grubmüller, H.; Tavan, P. Multiple Time Step Algorithms for Molecular Dynamics Simulations of Proteins: How Good Are They? *J. Comput. Chem.* **1998**, *19* (13), 1534–1552.

(124) Maier, J. A.; Martinez, C.; Kasavajhala, K.; Wickstrom, L.; Hauser, K. E.; Simmerling, C. Ff14SB: Improving the Accuracy of Protein Side Chain and Backbone Parameters from Ff99SB. *J. Chem. Theory Comput.* **2015**, *11* (8), 3696–3713.
(125) Comparison of multiple Amber force fields and development of improved protein backbone parameters - Hornak - 2006 - Proteins: Structure, Function, and Bioinformatics - Wiley Online Library https://onlinelibrary.wiley.com/doi/pdf/10.1002/prot.21123 (accessed Mar 19, 2018).
(126) Schulz, B.; Sucker, J.; Aust, H. J.; Krohn, K.; Ludewig, K.; Jones, P. G.; Döring, D. Biologically Active Secondary Metabolites of Endophytic Pezicula Species. *Mycol. Res.* **1995**, *99* (8), 1007–1015.
(127) Schmitz, A.-L.; Schrage, R.; Gaffal, E.; Charpentier, T. H.; Wiest, J.; Hiltensperger, G.; Morschel, J.; Hennen, S.; Häußler, D.; Horn, V.; et al. A Cell-Permeable Inhibitor to Trap Gαq Proteins in the Empty Pocket Conformation. *Chem. Biol.* **2014**, *21* (7), 890–902.
(128) Ge, L.; Ly, Y.; Hollenberg, M.; DeFea, K. A β-Arrestin-Dependent Scaffold Is Associated with Prolonged MAPK Activation in Pseudopodia during Protease-Activated Receptor-2-Induced Chemotaxis. *J. Biol. Chem.* **2003**, *278* (36), 34418–34426.
(129) Alnouri, M. W.; Jepards, S.; Casari, A.; Schiedel, A. C.; Hinz, S.; Müller, C. E. Selectivity Is Species-Dependent: Characterization of Standard Agonists and Antagonists at Human, Rat, and Mouse Adenosine Receptors. *Purinergic Signal.* **2015**, *11* (3), 389–407.
(130) Thimm, D.; Knospe, M.; Abdelrahman, A.; Moutinho, M.; Alsdorf, B. B. A.; von Kügelgen, I.; Schiedel, A. C.; Müller, C. E. Characterization of New G Protein-Coupled Adenine Receptors in Mouse and Hamster. *Purinergic Signal.* **2013**, *9* (3), 415–426.
(131) Matthey, M.; Roberts, R.; Seidinger, A.; Simon, A.; Schröder, R.; Kuschak, M.; Annala, S.; König, G. M.; Müller, C. E.; Hall, I. P. Targeted Inhibition of Gq Signaling Induces Airway Relaxation in Mouse Models of Asthma. *Sci. Transl. Med.* **2017**, *9* (407), eaag2288.
(132) Wenzel, D.; Knies, R.; Matthey, M.; Klein, A. M.; Welschoff, J.; Stolle, V.; Sasse, P.; Roll, W.; Breuer, J.; Fleischmann, B. K. 2-Adrenoceptor Antagonist ICI 118,551 Decreases Pulmonary Vascular Tone in Mice via a Gi/o Protein/Nitric Oxide-Coupled Pathway. *Hypertension* **2009**, *54* (1), 157–163.
(133) Rosen, V. M.; Guerra, I.; McCormack, M.; Nogueira-Rodrigues, A.; Sasse, A.; Munk, V. C.; Shang, A. Systematic Review and Network Meta-Analysis of Bevacizumab Plus First-Line Topotecan-Paclitaxel or Cisplatin-Paclitaxel Versus Non–Bevacizumab-Containing Therapies in Persistent, Recurrent, or Metastatic Cervical Cancer: *Int. J. Gynecol. Cancer* **2017**, *27* (6), 1237–1246.
(134) Noble, R. L. The Discovery of the Vinca Alkaloids—chemotherapeutic Agents against Cancer. *Biochem. Cell Biol.* **1990**, *68* (12), 1344–1351.
(135) Taher, M. A.; Nyeem, M. A. B.; Billah, M. M.; Ahammed, M. M. Vinca Alkaloid-the Second Most Used Alkaloid for Cancer Treatment-A Review. **2017**.
(136) Manju, K.; Jat, R. K.; Anju, G. A Review on Medicinal Plants Used as a Source of Anticancer Agents. *Int. J. Drug Res. Technol.* **2017**, *2* (2), 6.
(137) Tan, R. X.; Zou, W. X. Endophytes: A Rich Source of Functional Metabolites. *Nat. Prod. Rep.* **2001**, *18* (4), 448–459.
(138) Li, J.; Zhao, G.-Z.; Varma, A.; Qin, S.; Xiong, Z.; Huang, H.-Y.; Zhu, W.-Y.; Zhao, L.-X.; Xu, L.-H.; Zhang, S.; et al. An Endophytic Pseudonocardia Species Induces the Production of Artemisinin in Artemisia Annua. *PLoS ONE* **2012**, *7* (12), e51410.
(139) Carlier, A. L.; Omasits, U.; Ahrens, C. H.; Eberl, L. Proteomics Analysis of *Psychotria* Leaf Nodule Symbiosis: Improved Genome Annotation and Metabolic Predictions. *Mol. Plant. Microbe Interact.* **2013**, *26* (11), 1325–1333.

(140) Lemaire, B.; Vandamme, P.; Merckx, V.; Smets, E.; Dessein, S. Bacterial Leaf Symbiosis in Angiosperms: Host Specificity without Co-Speciation. *PLoS ONE* **2011**, *6* (9), e24430.
(141) Miller, I. M. Bacterial Leaf Nodule Symbiosis. *Adv. Bot. Res. Inc. Adv. Plant Pathol.* **1990**, *17*, 163–234.
(142) Lemaire, B.; Van Oevelen, S.; De Block, P.; Verstraete, B.; Smets, E.; Prinsen, E.; Dessein, S. Identification of the Bacterial Endosymbionts in Leaf Nodules of Pavetta (Rubiaceae). *Int. J. Syst. Evol. Microbiol.* **2012**, *62* (1), 202–209.
(143) Nakahashi, C. D.; Frole, K.; Sack, L. Bacterial Leaf Nodule Symbiosis in Ardisia (Myrsinaceae): Does It Contribute to Seedling Growth Capacity? *Plant Biol.* **2005**, *7* (5), 495–500.
(144) 山田保. 抗生物質による葉瘤植物の瘤の形成. 植物学雑誌 **1955**, *68* (808), 267–273.
(145) Sieber, S.; Carlier, A.; Neuburger, M.; Grabenweger, G.; Eberl, L.; Gademann, K. Isolation and Total Synthesis of Kirkamide, an Aminocyclitol from an Obligate Leaf Nodule Symbiont. *Angew. Chem. Int. Ed.* **2015**, *54* (27), 7968–7970.
(146) Carlier, A. L.; Eberl, L. The Eroded Genome of a *Psychotria* Leaf Symbiont: Hypotheses about Lifestyle and Interactions with Its Plant Host: *Psychotria Kirkii* Symbiont Genome. *Environ. Microbiol.* **2012**, *14* (10), 2757–2769.
(147) Brader, G.; Compant, S.; Mitter, B.; Trognitz, F.; Sessitsch, A. Metabolic Potential of Endophytic Bacteria. *Curr. Opin. Biotechnol.* **2014**, *27*, 30–37.
(148) Jones, J. C.; Duffy, D. W.; Machius, M.; Temple, B. R. S.; Dohlman, H. G.; Jones, A. M. The Crystal Structure of a Self-Activating G Protein Alpha Subunit Reveals Its Distinct Mechanism of Signal Initiation. *Sci. Signal.* **2011**, *4* (159), ra8.
(149) Urano, D.; Chen, J.-G.; Botella, J. R.; Jones, A. M. Heterotrimeric G Protein Signalling in the Plant Kingdom. *Open Biol.* **2013**, *3* (3), 120186–120186.
(150) Urano, D.; Jones, A. M. Heterotrimeric G Protein–Coupled Signaling in Plants. *Annu. Rev. Plant Biol.* **2014**, *65* (1), 365–384.
(151) Li, L.; Wright, S. J.; Krystofova, S.; Park, G.; Borkovich, K. A. Heterotrimeric G Protein Signaling in Filamentous Fungi. *Annu Rev Microbiol* **2007**, *61*, 423–452.
(152) Segers, G. C.; Nuss, D. L. Constitutively Activated Gα Negatively Regulates Virulence, Reproduction and Hydrophobin Gene Expression in the Chestnut Blight Fungus Cryphonectria Parasitica. *Fungal Genet. Biol.* **2003**, *38* (2), 198–208.
(153) Gao, S.; Nuss, D. L. Distinct Roles for Two G Protein α Subunits in Fungal Virulence, Morphology, and Reproduction Revealed by Targeted Gene Disruption. *Proc. Natl. Acad. Sci.* **1996**, *93* (24), 14122–14127.
(154) Görcsös, G.; Irinyi, L.; Radócz, L.; Tarcali, G.; Sándor, E. Diversity of *Cryphonectria Parasitica* Populations from the Carpathian Basin. *Acta Microbiol. Immunol. Hung.* **2015**, *62* (3), 247–266.
(155) Segers, G. C.; Regier, J. C.; Nuss, D. L. Evidence for a Role of the Regulator of G-Protein Signaling Protein CPRGS-1 in G Subunit CPG-1-Mediated Regulation of Fungal Virulence, Conidiation, and Hydrophobin Synthesis in the Chestnut Blight Fungus Cryphonectria Parasitica. *Eukaryot. Cell* **2004**, *3* (6), 1454–1463.
(156) Turina, M.; Rostagno, L. Virus-Induced Hypovirulence in Cryphonectria Parasitica: Still an Unresolved Conundrum. *J. Plant Pathol.* **2007**, 165–178.
(157) Bosch, D. E.; Willard, F. S.; Ramanujam, R.; Kimple, A. J.; Willard, M. D.; Naqvi, N. I.; Siderovski, D. P. A P-Loop Mutation in Gα Subunits Prevents Transition to the Active State: Implications for G-Protein Signaling in Fungal Pathogenesis. *PLoS Pathog.* **2012**, *8* (2), e1002553.
(158) Degani, O.; Lev, S.; Ronen, M. Hydrophobin Gene Expression in the Maize Pathogen Cochliobolus Heterostrophus. *Physiol. Mol. Plant Pathol.* **2013**, *83*, 25–34.

(159) Solomon, P. S.; Tan, K.-C.; Sanchez, P.; Cooper, R. M.; Oliver, R. P. The Disruption of a Gα Subunit Sheds New Light on the Pathogenicity of Stagonospora Nodorum on Wheat. *Mol. Plant. Microbe Interact.* **2004**, *17* (5), 456–466.
(160) García-Rico, R. O.; Martín, J. F.; Fierro, F. Heterotrimeric Gα Protein Pga1 from Penicillium Chrysogenum Triggers Germination in Response to Carbon Sources and Affects Negatively Resistance to Different Stress Conditions. *Fungal Genet. Biol.* **2011**, *48* (6), 641–649.
(161) Krishnan, A.; Mustafa, A.; Almén, M. S.; Fredriksson, R.; Williams, M. J.; Schiöth, H. B. Evolutionary Hierarchy of Vertebrate-like Heterotrimeric G Protein Families. *Mol. Phylogenet. Evol.* **2015**, *91*, 27–40.
(162) Sandoval-Mojica, A. F.; Capinera, J. L. Antifeedant Effect of Commercial Chemicals and Plant Extracts against Schistocerca Americana (Orthoptera: Acrididae) and Diaprepes Abbreviatus (Coleoptera: Curculionidae). *Pest Manag. Sci.* **2011**, *67* (7), 860–868.
(163) Miura, N.; Atsumi, S.; Tabunoki, H.; Sato, R. Expression and Localization of Three G Protein ? Subunits, Go, Gq, and Gs, in Adult Antennae of the Silkmoth (Bombyx Mori). *J. Comp. Neurol.* **2005**, *485* (2), 143–152.
(164) Seno, K.; Fujikawa, K.; Nakamura, T.; Ozaki, M. Gqα Subunit Mediates Receptor Site-Specific Adaptation in the Sugar Taste Receptor Cell of the Blowfly, Phormia Regina. *Neurosci. Lett.* **2005**, *377* (3), 200–205.
(165) Kain, P.; Chakraborty, T. S.; Sundaram, S.; Siddiqi, O.; Rodrigues, V.; Hasan, G. Reduced Odor Responses from Antennal Neurons of Gq , Phospholipase C , and RdgA Mutants in Drosophila Support a Role for a Phospholipid Intermediate in Insect Olfactory Transduction. *J. Neurosci.* **2008**, *28* (18), 4745–4755.
(166) Yao, C. A.; Carlson, J. R. Role of G-Proteins in Odor-Sensing and CO2-Sensing Neurons in Drosophila. *J. Neurosci.* **2010**, *30* (13), 4562–4572.
(167) Deng, Y.; Zhang, W.; Farhat, K.; Oberland, S.; Gisselmann, G.; Neuhaus, E. M. The Stimulatory Gαs Protein Is Involved in Olfactory Signal Transduction in Drosophila. *PLoS ONE* **2011**, *6* (4), e18605.
(168) Ren, J.; Li, X.-R.; Liu, P.-C.; Cai, M.-J.; Liu, W.; Wang, J.-X.; Zhao, X.-F. G-Protein Aq Participates in the Steroid Hormone 20-Hydroxyecdysone Nongenomic Signal Transduction. *J. Steroid Biochem. Mol. Biol.* **2014**, *144*, 313–323.
(169) Jia, Z.; Koike, K.; Ohmoto, T.; Ni, M. Triterpenoid Saponins from Ardisia Crenata. *Phytochemistry* **1994**, *37* (5), 1389–1396.
(170) Rahman, M. M.; Lim, U. T. Evaluation of Mature Soybean Pods as a Food Source for Two Pod-Sucking Bugs, Riptortus Pedestris (Hemiptera: Alydidae) and Halyomorpha Halys (Hemiptera: Pentatomidae). *PLOS ONE* **2017**, *12* (4), e0176187.
(171) Rausch, C.; Hoof, I.; Weber, T.; Wohlleben, W.; Huson, D. H. Phylogenetic Analysis of Condensation Domains in NRPS Sheds Light on Their Functional Evolution. *BMC Evol. Biol.* **2007**, *7* (1), 78.
(172) Ziemert, N.; Podell, S.; Penn, K.; Badger, J. H.; Allen, E.; Jensen, P. R. The Natural Product Domain Seeker NaPDoS: A Phylogeny Based Bioinformatic Tool to Classify Secondary Metabolite Gene Diversity. *PLoS ONE* **2012**, *7* (3), e34064.
(173) Ray, L.; Yamanaka, K.; Moore, B. S. A Peptidyl-Transesterifying Type I Thioesterase in Salinamide Biosynthesis. *Angew. Chem. Int. Ed.* **2016**, *55* (1), 364–367.
(174) Wang, M.; Carver, J. J.; Phelan, V. V.; Sanchez, L. M.; Garg, N.; Peng, Y.; Nguyen, D. D.; Watrous, J.; Kapono, C. A.; Luzzatto-Knaan, T.; et al. Sharing and Community Curation of Mass Spectrometry Data with Global Natural Products Social Molecular Networking. *Nat. Biotechnol.* **2016**, *34* (8), 828–837.

(175) Wright, S. K.; Viola, R. E. Alteration of the Specificity of Malate Dehydrogenase by Chemical Modulation of an Active Site Arginine. *J. Biol. Chem.* **2001**, *276* (33), 31151–31155.
(176) Minarik, P.; Tomaskova, N.; Kollarova, M.; Antalik, M. Malate Dehydrogenases-Structure and Function. *Gen. Physiol. Biophys.* **2002**, *21* (3), 257–266.
(177) Makris, T. M.; Chakrabarti, M.; Münck, E.; Lipscomb, J. D. A Family of Diiron Monooxygenases Catalyzing Amino Acid Beta-Hydroxylation in Antibiotic Biosynthesis. *Proc. Natl. Acad. Sci.* **2010**, *107* (35), 15391–15396.
(178) Makris, T. M.; Knoot, C. J.; Wilmot, C. M.; Lipscomb, J. D. Structure of a Dinuclear Iron Cluster-Containing β-Hydroxylase Active in Antibiotic Biosynthesis. *Biochemistry (Mosc.)* **2013**, *52* (38), 6662–6671.
(179) Roy, A.; Kucukural, A.; Zhang, Y. I-TASSER: A Unified Platform for Automated Protein Structure and Function Prediction. *Nat. Protoc.* **2010**, *5* (4), 725–738.
(180) Herbst, D. A.; Boll, B.; Zocher, G.; Stehle, T.; Heide, L. Structural Basis of the Interaction of MbtH-like Proteins, Putative Regulators of Nonribosomal Peptide Biosynthesis, with Adenylating Enzymes. *J. Biol. Chem.* **2013**, *288* (3), 1991–2003.
(181) Phelan, V. V.; Du, Y.; McLean, J. A.; Bachmann, B. O. Adenylation Enzyme Characterization Using γ -18O4-ATP Pyrophosphate Exchange. *Chem. Biol.* **2009**, *16* (5), 473–478.
(182) Tillett, D.; Dittmann, E.; Erhard, M.; von Döhren, H.; Börner, T.; Neilan, B. A. Structural Organization of Microcystin Biosynthesis in Microcystis Aeruginosa PCC7806: An Integrated Peptide–polyketide Synthetase System. *Chem. Biol.* **2000**, *7* (10), 753–764.
(183) Lefebre, M. D.; Valvano, M. A. Construction and Evaluation of Plasmid Vectors Optimized for Constitutive and Regulated Gene Expression in Burkholderia Cepacia Complex Isolates. *Appl. Environ. Microbiol.* **2002**, *68* (12), 5956–5964.
(184) Huang, C.-Y.; Lee, C.-Y.; Wu, H.-C.; Kuo, M.-H.; Lai, C.-Y. Interactions of Chaperonin with a Weakly Active Anthranilate Synthase from the Aphid Endosymbiont Buchnera Aphidicola. *Microb. Ecol.* **2008**, *56* (4), 696–703.
(185) Pinto-Carbó, M.; Sieber, S.; Dessein, S.; Wicker, T.; Verstraete, B.; Gademann, K.; Eberl, L.; Carlier, A. Evidence of Horizontal Gene Transfer between Obligate Leaf Nodule Symbionts. *ISME J.* **2016**, *10* (9), 2092.
(186) Rath, C. M.; Janto, B.; Earl, J.; Ahmed, A.; Hu, F. Z.; Hiller, L.; Dahlgren, M.; Kreft, R.; Yu, F.; Wolff, J. J.; et al. Meta-Omic Characterization of the Marine Invertebrate Microbial Consortium That Produces the Chemotherapeutic Natural Product ET-743. *ACS Chem. Biol.* **2011**, *6* (11), 1244–1256.
(187) Schmidt, E. W.; Nelson, J. T.; Rasko, D. A.; Sudek, S.; Eisen, J. A.; Haygood, M. G.; Ravel, J. Patellamide A and C Biosynthesis by a Microcin-like Pathway in Prochloron Didemni, the Cyanobacterial Symbiont of Lissoclinum Patella. *Proc. Natl. Acad. Sci. U. S. A.* **2005**, *102* (20), 7315–7320.
(188) Süssmuth, R. D.; Mainz, A. Nonribosomal Peptide Synthesis-Principles and Prospects. *Angew. Chem. Int. Ed.* **2017**, *56* (14), 3770–3821.
(189) Yang, J. Y.; Sanchez, L. M.; Rath, C. M.; Liu, X.; Boudreau, P. D.; Bruns, N.; Glukhov, E.; Wodtke, A.; de Felicio, R.; Fenner, A.; et al. Molecular Networking as a Dereplication Strategy. *J. Nat. Prod.* **2013**, *76* (9), 1686–1699.
(190) Crüsemann, M.; O'Neill, E. C.; Larson, C. B.; Melnik, A. V.; Floros, D. J.; da Silva, R. R.; Jensen, P. R.; Dorrestein, P. C.; Moore, B. S. Prioritizing Natural Product Diversity in a Collection of 146 Bacterial Strains Based on Growth and Extraction Protocols. *J. Nat. Prod.* **2017**, *80* (3), 588–597.
(191) Nothias, L.-F.; Nothias-Esposito, M.; da Silva, R.; Wang, M.; Protsyuk, I.; Zhang, Z.; Sarvepalli, A.; Leyssen, P.; Touboul, D.; Costa, J.; et al. Bioactivity-Based Molecular

Networking for the Discovery of Drug Leads in Natural Product Bioassay-Guided Fractionation. *J. Nat. Prod.* **2018**.

(192) Kleigrewe, K.; Almaliti, J.; Tian, I. Y.; Kinnel, R. B.; Korobeynikov, A.; Monroe, E. A.; Duggan, B. M.; Di Marzo, V.; Sherman, D. H.; Dorrestein, P. C.; et al. Combining Mass Spectrometric Metabolic Profiling with Genomic Analysis: A Powerful Approach for Discovering Natural Products from Cyanobacteria. *J. Nat. Prod.* **2015**, *78* (7), 1671–1682.

(193) Boudreau, P. D.; Monroe, E. A.; Mehrotra, S.; Desfor, S.; Korobeynikov, A.; Sherman, D. H.; Murray, T. F.; Gerwick, L.; Dorrestein, P. C.; Gerwick, W. H. Expanding the Described Metabolome of the Marine Cyanobacterium Moorea Producens JHB through Orthogonal Natural Products Workflows. *PLOS ONE* **2015**, *10* (7), e0133297.

(194) Naman, C. B.; Rattan, R.; Nikoulina, S. E.; Lee, J.; Miller, B. W.; Moss, N. A.; Armstrong, L.; Boudreau, P. D.; Debonsi, H. M.; Valeriote, F. A.; et al. Integrating Molecular Networking and Biological Assays To Target the Isolation of a Cytotoxic Cyclic Octapeptide, Samoamide A, from an American Samoan Marine Cyanobacterium. *J. Nat. Prod.* **2017**, *80* (3), 625–633.

(195) Paizs, B.; Suhai, S. Fragmentation Pathways of Protonated Peptides. *Mass Spectrom. Rev.* **2005**, *24* (4), 508–548.

(196) Kaur, H.; Harris, P. W. R.; Little, P. J.; Brimble, M. A. Total Synthesis of the Cyclic Depsipeptide YM-280193, a Platelet Aggregation Inhibitor. *Org. Lett.* **2015**, *17* (3), 492–495.

(197) de Mejía, E. G.; Ramírez-Mares, M. V. *Ardisia* : Health-Promoting Properties and Toxicity of Phytochemicals and Extracts. *Toxicol. Mech. Methods* **2011**, *21* (9), 667–674.

(198) Pearson, W. R. An Introduction to Sequence Similarity ("Homology") Searching. In *Current Protocols in Bioinformatics*; Baxevanis, A. D., Petsko, G. A., Stein, L. D., Stormo, G. D., Eds.; John Wiley & Sons, Inc.: Hoboken, NJ, USA, 2013.

(199) Vöing, K.; Harrison, A.; Soby, S. D. Draft Genome Sequence of *Chromobacterium Vaccinii* , a Potential Biocontrol Agent against Mosquito (*Aedes Aegypti*) Larvae. *Genome Announc.* **2015**, *3* (3), e00477-15.

(200) Soby, S. D.; Gadagkar, S. R.; Contreras, C.; Caruso, F. L. Chromobacterium Vaccinii Sp. Nov., Isolated from Native and Cultivated Cranberry (Vaccinium Macrocarpon Ait.) Bogs and Irrigation Ponds. *Int. J. Syst. Evol. Microbiol.* **2013**, *63* (Pt 5), 1840–1846.

(201) Zhang, H.; Xiong, X.-F.; Boesgaard, M. W.; Underwood, C. R.; Bräuner-Osborne, H.; Strømgaard, K. Structure-Activity Relationship Studies of the Cyclic Depsipeptide Natural Product YM-254890, Targeting the G_q Protein. *ChemMedChem* **2017**, *12* (11), 830–834.

(202) Neises, B.; Steglich, W. Simple Method for the Esterification of Carboxylic Acids. *Angew. Chem. Int. Ed.* **1978**, *17* (7), 522–524.

(203) Tsakos, M.; Schaffert, E. S.; Clement, L. L.; Villadsen, N. L.; Poulsen, T. B. Ester Coupling Reactions – an Enduring Challenge in the Chemical Synthesis of Bioactive Natural Products. *Nat. Prod. Rep.* **2015**, *32* (4), 605–632.

(204) Baltz, R. H.; Miao, V.; Wrigley, S. K. Natural Products to Drugs: Daptomycin and Related Lipopeptide Antibiotics. *Nat. Prod. Rep.* **2005**, *22* (6), 717.

(205) Müller, A.; Wenzel, M.; Strahl, H.; Grein, F.; Saaki, T. N.; Kohl, B.; Siersma, T.; Bandow, J. E.; Sahl, H.-G.; Schneider, T. Daptomycin Inhibits Cell Envelope Synthesis by Interfering with Fluid Membrane Microdomains. *Proc. Natl. Acad. Sci.* **2016**, *113* (45), E7077–E7086.

(206) Chatterjee, C.; Paul, M.; Xie, L.; van der Donk, W. A. Biosynthesis and Mode of Action of Lantibiotics. *Chem. Rev.* **2005**, *105* (2), 633–684.

(207) OKADA, H.; SUZUKI, H.; YOSHINARI, T.; ARAKAWA, H.; OKURA, A.; SUDA, H.; YAMADA, A.; UEMURA, D. A NEW TOPOISOMERASE II INHIBITOR, BE-22179, PRODUCED BY A STREPTOMYCETE. *J. Antibiot. (Tokyo)* **1994**, *47* (2), 129–135.
(208) Boger, D. L.; Ichikawa, S. Total Syntheses of Thiocoraline and BE-22179: Establishment of Relative and Absolute Stereochemistry. *J. Am. Chem. Soc.* **2000**, *122* (12), 2956–2957.
(209) Puddick, J.; Prinsep, M.; Wood, S.; Kaufononga, S.; Cary, S.; Hamilton, D. High Levels of Structural Diversity Observed in Microcystins from Microcystis CAWBG11 and Characterization of Six New Microcystin Congeners. *Mar. Drugs* **2014**, *12* (12), 5372–5395.
(210) MacKintosh, R. W.; Dalby, K. N.; Campbell, D. G.; Cohen, P. T.; Cohen, P.; MacKintosh, C. The Cyanobacterial Toxin Microcystin Binds Covalently to Cysteine-273 on Protein Phosphatase 1. *FEBS Lett.* **1995**, *371* (3), 236–240.
(211) Drahl, C.; Cravatt, B. F.; Sorensen, E. J. Protein-Reactive Natural Products. *Angew. Chem. Int. Ed.* **2005**, *44* (36), 5788–5809.
(212) Craig, M.; Luu, H. A.; McCready, T. L.; Holmes, C. F. B.; Williams, D.; Andersen, R. J. Molecular Mechanisms Underlying the Interaction of Motuporin and Microcystins with Type-1 and Type-2A Protein Phosphatases. *Biochem. Cell Biol.* **1996**, *74* (4), 569–578.
(213) Pereira, S. R.; Vasconcelos, V. M.; Antunes, A. Computational Study of the Covalent Bonding of Microcystins to Cysteine Residues - a Reaction Involved in the Inhibition of the PPP Family of Protein Phosphatases: Covalent Bonding of MCs to Cysteine Residues. *FEBS J.* **2013**, *280* (2), 674–680.
(214) Movassagh, B.; Shaygan, P. Michael Addition of Thiols to α, β-Unsaturated Carbonyl Compounds under Solvent-Free Conditions. *Arkivoc* **2006**, *12*, 130–137.
(215) Ferreira, P. M. T.; Maia, H. L. S.; Monteiro, L. S.; Sacramento, J. Michael Addition of Thiols, Carbon Nucleophiles and Amines to Dehydroamino Acid and Dehydropeptide DerivativesElectronic Supplementary Information (ESI) Available: Experimental Data for Compounds 1–15. See Http://Www.Rsc.Org/Suppdata/P1/B1/B106487h/. *J. Chem. Soc. [Perkin 1]* **2001**, No. 23, 3167–3173.
(216) Kondo, F.; Ikai, Y.; Oka, H.; Okumura, M.; Ishikawa, N.; Harada, K.; Matsuura, K.; Murata, H.; Suzuki, M. Formation, Characterization, and Toxicity of the Glutathione and Cysteine Conjugates of Toxic Heptapeptide Microcystins. *Chem. Res. Toxicol.* **1992**, *5* (5), 591–596.
(217) Naidu, B. N.; Sorenson, M. E.; Connolly, T. P.; Ueda, Y. Michael Addition of Amines and Thiols to Dehydroalanine Amides: A Remarkable Rate Acceleration in Water. *J. Org. Chem.* **2003**, *68* (26), 10098–10102.
(218) Firouzabadi, H.; Iranpoor, N.; Jafari, A. ?A. Micellar Solution of Sodium Dodecyl Sulfate (SDS) Catalyzes Facile Michael Addition of Amines and Thiols to ?,?-Unsaturated Ketones in Water under Neutral Conditions. *Adv. Synth. Catal.* **2005**, *347* (5), 655–661.
(219) Zemskov, I.; Kropp, H. M.; Wittmann, V. Regioselective Cleavage of Thioether Linkages in Microcystin Conjugates. *Chem. - Eur. J.* **2016**, *22* (31), 10990–10997.
(220) Miles, C. O.; Sandvik, M.; Nonga, H. E.; Rundberget, T.; Wilkins, A. L.; Rise, F.; Ballot, A. Thiol Derivatization for LC-MS Identification of Microcystins in Complex Matrices. *Environ. Sci. Technol.* **2012**, *46* (16), 8937–8944.
(221) Rensing, D. T.; Uppal, S.; Blumer, K. J.; Moeller, K. D. Toward the Selective Inhibition of G Proteins: Total Synthesis of a Simplified YM-254890 Analog. *Org. Lett.* **2015**, *17* (9), 2270–2273.

(222) Maharani, R.; Ammatillah, N.; Muhammad, G.; Hidayat, A. T.; Zainuddin, A.; Al-Anshori, J.; Subroto, T. Good Coupling Performance of PyBOP in the Solid-Phase Synthesis of Tetrapeptide, OH-Pro-Leu-Ala-Ileu-NH2; 2017; p 030006.
(223) Bazin, H.; Preaudat, M.; Trinquet, E.; Mathis, G. Homogeneous Time Resolved Fluorescence Resonance Energy Transfer Using Rare Earth Cryptates as a Tool for Probing Molecular Interactions in Biology. *Spectrochim. Acta. A. Mol. Biomol. Spectrosc.* **2001**, *57* (11), 2197–2211.
(224) Lambright, D. G.; Sondek, J.; Bohm, A.; Skiba, N. P.; Hamm, H. E.; Sigler, P. B. The 2.0 Å Crystal Structure of a Heterotrimeric G Protein. *Nature* **1996**, *379* (6563), 311–319.
(225) Ji, H.-F.; Li, X.-J.; Zhang, H.-Y. Natural Products and Drug Discovery: Can Thousands of Years of Ancient Medical Knowledge Lead Us to New and Powerful Drug Combinations in the Fight against Cancer and Dementia? *EMBO Rep.* **2009**, *10* (3), 194–200.
(226) Koehn, F. E.; Carter, G. T. The Evolving Role of Natural Products in Drug Discovery. *Nat. Rev. Drug Discov.* **2005**, *4* (3), 206–220.
(227) Harvey, A. L.; Edrada-Ebel, R.; Quinn, R. J. The Re-Emergence of Natural Products for Drug Discovery in the Genomics Era. *Nat. Rev. Drug Discov.* **2015**, *14* (2), 111–129.
(228) Stoddart, L. A.; Johnstone, E. K. M.; Wheal, A. J.; Goulding, J.; Robers, M. B.; Machleidt, T.; Wood, K. V.; Hill, S. J.; Pfleger, K. D. G. Application of BRET to Monitor Ligand Binding to GPCRs. *Nat. Methods* **2015**, *12* (7), 661–663.
(229) Sadik, O. A.; Yan, F. Novel Fluorescent Biosensor for Pathogenic Toxins Using Cyclic Polypeptide ConjugatesElectronic Supplementary Information (ESI) Available: Synthetic Approach for Microcystin Conjugates. See Http://Www.Rsc.Org/Suppdata/Cc/B3/B316057b/. *Chem. Commun.* **2004**, No. 9, 1136.
(230) Stoddart, L. A.; White, C. W.; Nguyen, K.; Hill, S. J.; Pfleger, K. D. G. Fluorescence- and Bioluminescence-Based Approaches to Study GPCR Ligand Binding: Fluorescence and Bioluminescence in Ligand Binding. *Br. J. Pharmacol.* **2016**, *173* (20), 3028–3037.
(231) Lipshutz, B. H.; Gallou, F.; Handa, S. Evolution of Solvents in Organic Chemistry. *ACS Sustain. Chem. Eng.* **2016**, *4* (11), 5838–5849.
(232) Vogt, W. Oxidation of Methionyl Residues in Proteins: Tools, Targets, and Reversal. *Free Radic. Biol. Med.* **1994**, *18* (1), 93–105.
(233) Shechter, Y. Selective Oxidation and Reduction of Methionine Residues in Peptides and Proteins by Oxygen Exchange between Sulfoxide and Sulfide. *J. Biol. Chem.* **1986**, *261* (1), 66–70.
(234) Brot, N.; Weissbach, H. Biochemistry and Physiological Role of Methionine Sulfoxide Residues in Proteins. *Arch. Biochem. Biophys.* **1983**, *223* (1), 271–281.
(235) Lushington, G. H.; Cowley, A. B.; Silchenko, S.; Lukat-Rodgers, G. S.; Rodgers, K. R.; Benson, D. R. Comparison of Thioethers and Sulfoxides as Axial Ligands for *N* -Acetylmicroperoxidase-8: Implications for Oxidation of Methionine-80 in Cytochrome *C*. *Inorg. Chem.* **2003**, *42* (23), 7550–7559.
(236) Schröder, R.; Schmidt, J.; Blättermann, S.; Peters, L.; Janssen, N.; Grundmann, M.; Seemann, W.; Kaufel, D.; Merten, N.; Drewke, C.; et al. Applying Label-Free Dynamic Mass Redistribution Technology to Frame Signaling of G Protein–coupled Receptors Noninvasively in Living Cells. *Nat. Protoc.* **2011**, *6* (11), 1748–1760.
(237) Elson, E. L. Fluorescence Correlation Spectroscopy: Past, Present, Future. *Biophys. J.* **2011**, *101* (12), 2855–2870.
(238) Singh, A. P.; Wohland, T. Applications of Imaging Fluorescence Correlation Spectroscopy. *Curr. Opin. Chem. Biol.* **2014**, *20*, 29–35.

(239) Kilpatrick, L. E.; Hill, S. J. The Use of Fluorescence Correlation Spectroscopy to Characterize the Molecular Mobility of Fluorescently Labelled G Protein-Coupled Receptors. *Biochem. Soc. Trans.* **2016**, *44* (2), 624–629.
(240) Jinek, M.; Chylinski, K.; Fonfara, I.; Hauer, M.; Doudna, J. A.; Charpentier, E. A Programmable Dual-RNA–Guided DNA Endonuclease in Adaptive Bacterial Immunity. *Science* **2012**, *337* (6096), 816–821.
(241) Zeigerer, A.; Gilleron, J.; Bogorad, R. L.; Marsico, G.; Nonaka, H.; Seifert, S.; Epstein-Barash, H.; Kuchimanchi, S.; Peng, C. G.; Ruda, V. M.; et al. Rab5 Is Necessary for the Biogenesis of the Endolysosomal System in Vivo. *Nature* **2012**, *485* (7399), 465–470.
(242) Baker, J. G.; Middleton, R.; Adams, L.; May, L. T.; Briddon, S. J.; Kellam, B.; Hill, S. J. Influence of Fluorophore and Linker Composition on the Pharmacology of Fluorescent Adenosine A1 Receptor Ligands. *Br. J. Pharmacol.* **2010**, *159* (4), 772–786.
(243) Hall, M. P.; Unch, J.; Binkowski, B. F.; Valley, M. P.; Butler, B. L.; Wood, M. G.; Otto, P.; Zimmerman, K.; Vidugiris, G.; Machleidt, T.; et al. Engineered Luciferase Reporter from a Deep Sea Shrimp Utilizing a Novel Imidazopyrazinone Substrate. *ACS Chem. Biol.* **2012**, *7* (11), 1848–1857.
(244) Machleidt, T.; Woodroofe, C. C.; Schwinn, M. K.; Méndez, J.; Robers, M. B.; Zimmerman, K.; Otto, P.; Daniels, D. L.; Kirkland, T. A.; Wood, K. V. NanoBRET—A Novel BRET Platform for the Analysis of Protein–Protein Interactions. *ACS Chem. Biol.* **2015**, *10* (8), 1797–1804.
(245) Soave, M.; Stoddart, L. A.; Brown, A.; Woolard, J.; Hill, S. J. Use of a New Proximity Assay (NanoBRET) to Investigate the Ligand-Binding Characteristics of Three Fluorescent Ligands to the Human β_1 -Adrenoceptor Expressed in HEK-293 Cells. *Pharmacol. Res. Perspect.* **2016**, *4* (5), e00250.
(246) Küppers, J.; Schulz-Fincke, A.; Palus, J.; Giurg, M.; Skarżewski, J.; Gütschow, M. Convergent Synthesis of Two Fluorescent Ebselen-Coumarin Heterodimers. *Pharmaceuticals* **2016**, *9* (3), 43.
(247) Trnka, T. M.; Grubbs, R. H. The Development of L2X2RuCHR Olefin Metathesis Catalysts: An Organometallic Success Story. *Acc. Chem. Res.* **2001**, *34* (1), 18–29.
(248) Chatterjee, A. K.; Morgan, J. P.; Scholl, M.; Grubbs, R. H. Synthesis of Functionalized Olefins by Cross and Ring-Closing Metatheses. *J. Am. Chem. Soc.* **2000**, *122* (15), 3783–3784.
(249) Marx, V. M.; Herbert, M. B.; Keitz, B. K.; Grubbs, R. H. Stereoselective Access to *Z* and *E* Macrocycles by Ruthenium-Catalyzed *Z* -Selective Ring-Closing Metathesis and Ethenolysis. *J. Am. Chem. Soc.* **2013**, *135* (1), 94–97.
(250) Klumphu, P.; Lipshutz, B. H. "Nok": A Phytosterol-Based Amphiphile Enabling Transition-Metal-Catalyzed Couplings in Water at Room Temperature. *J. Org. Chem.* **2014**, *79* (3), 888–900.
(251) Mukherjee, J. P.; Sil, S.; Pahari, A. K.; Chattopadhyay, S. K. A Modular Synthesis of Some Biologically Relevant Cyclic Peptides through Late-Stage Functionalization. *Synthesis* **2016**, *48* (08), 1181–1190.
(252) Wallace, S.; Balskus, E. P. Designer Micelles Accelerate Flux Through Engineered Metabolism in *E. Coli* and Support Biocompatible Chemistry. *Angew. Chem. Int. Ed.* **2016**, *55* (20), 6023–6027.
(253) Lin, Y. A.; Chalker, J. M.; Davis, B. G. Olefin Metathesis for Site-Selective Protein Modification. *ChemBioChem* **2009**, *10* (6), 959–969.
(254) Peters, C.; Billich, A.; Ghobrial, M.; Högenauer, K.; Ullrich, T.; Nussbaumer, P. Synthesis of Borondipyrromethene (BODIPY)-Labeled Sphingosine Derivatives by Cross-Metathesis Reaction. *J. Org. Chem.* **2007**, *72* (5), 1842–1845.
(255) Yabuuchi, E.; Kosako, Y.; Oyaizu, H.; Yano, I.; Hotta, H.; Hashimoto, Y.; Ezaki, T.; Arakawa, M. Proposal of Burkholderia Gen. Nov. and Transfer of Seven Species of the

Genus Pseudomonas Homology Group II to the New Genus, with the Type Species Burkholderia Cepacia (Palleroni and Holmes 1981) Comb. Nov. *Microbiol. Immunol.* **1992**, *36* (12), 1251–1275.

(256) Takeshita, K.; Kikuchi, Y. Riptortus Pedestris and Burkholderia Symbiont: An Ideal Model System for Insect–microbe Symbiotic Associations. *Res. Microbiol.* **2017**, *168* (3), 175–187.

(257) Coenye, T.; Vandamme, P.; Govan, J. R. W.; LiPuma, J. J. Taxonomy and Identification of the Burkholderia Cepacia Complex. *J. Clin. Microbiol.* **2001**, *39* (10), 3427–3436.

(258) Galyov, E. E.; Brett, P. J.; DeShazer, D. Molecular Insights into Burkholderia Pseudomallei and Burkholderia Mallei Pathogenesis. *Annu. Rev. Microbiol.* **2010**, *64* (1), 495–517.

(259) Kikuchi, Y.; Yumoto, I. Efficient Colonization of the Bean Bug Riptortus Pedestris by an Environmentally Transmitted Burkholderia Symbiont. *Appl. Environ. Microbiol.* **2013**, *79* (6), 2088–2091.

(260) Takeshita, K.; Matsuura, Y.; Itoh, H.; Navarro, R.; Hori, T.; Sone, T.; Kamagata, Y.; Mergaert, P.; Kikuchi, Y. *Burkholderia* of Plant-Beneficial Group Are Symbiotically Associated with Bordered Plant Bugs (Heteroptera: Pyrrhocoroidea: Largidae). *Microbes Environ.* **2015**, *30* (4), 321–329.

(261) Kikuchi, Y.; Hosokawa, T.; Fukatsu, T. An Ancient but Promiscuous Host–symbiont Association between Burkholderia Gut Symbionts and Their Heteropteran Hosts. *ISME J.* **2011**, *5* (3), 446.

(262) Kikuchi, Y.; Hayatsu, M.; Hosokawa, T.; Nagayama, A.; Tago, K.; Fukatsu, T. Symbiont-Mediated Insecticide Resistance. *Proc. Natl. Acad. Sci.* **2012**, *109* (22), 8618–8622.

(263) Tago, K.; Okubo, T.; Itoh, H.; Kikuchi, Y.; Hori, T.; Sato, Y.; Nagayama, A.; Hayashi, K.; Ikeda, S.; Hayatsu, M. Insecticide-Degrading *Burkholderia* Symbionts of the Stinkbug Naturally Occupy Various Environments of Sugarcane Fields in a Southeast Island of Japan. *Microbes Environ.* **2015**, *30* (1), 29–36.

(264) Itoh, H.; Hori, T.; Sato, Y.; Nagayama, A.; Tago, K.; Hayatsu, M.; Kikuchi, Y. Infection Dynamics of Insecticide-Degrading Symbionts from Soil to Insects in Response to Insecticide Spraying. *ISME J.* **2018**, *12* (3), 909–920.

(265) Tago, K.; Kikuchi, Y.; Nakaoka, S.; Katsuyama, C.; Hayatsu, M. Insecticide Applications to Soil Contribute to the Development of *Burkholderia* Mediating Insecticide Resistance in Stinkbugs. *Mol. Ecol.* **2015**, *24* (14), 3766–3778.

(266) Kikuchi, Y.; Hayatsu, M.; Hosokawa, T.; Nagayama, A.; Tago, K.; Fukatsu, T. Symbiont-Mediated Insecticide Resistance. *Proc. Natl. Acad. Sci.* **2012**, *109* (22), 8618–8622.

(267) Liaimer, A.; Helfrich, E. J. N.; Hinrichs, K.; Guljamow, A.; Ishida, K.; Hertweck, C.; Dittmann, E. Nostopeptolide Plays a Governing Role during Cellular Differentiation of the Symbiotic Cyanobacterium *Nostoc Punctiforme*. *Proc. Natl. Acad. Sci.* **2015**, *112* (6), 1862–1867.

(268) Jing, Y.-P.; Liu, W.; Wang, J.-X.; Zhao, X.-F. The Steroid Hormone 20-Hydroxyecdysone via Nongenomic Pathway Activates Ca^{2+} /Calmodulin-Dependent Protein Kinase II to Regulate Gene Expression. *J. Biol. Chem.* **2015**, *290* (13), 8469–8481.

(269) Tauber, M. J.; Tauber, C. A.; Masaki, S. *Seasonal Adaptations of Insects*; New York : Oxford University Press, 1986.

(270) Jiang, X.; Yang, J.; Shen, Z.; Chen, Y.; Shi, L.; Zhou, N. Agonist-Mediated Activation of Bombyx Mori Diapause Hormone Receptor Signals to Extracellular Signal-Regulated Kinases 1 and 2 through Gq-PLC-PKC-Dependent Cascade. *Insect Biochem. Mol. Biol.* **2016**, *75*, 78–88.

(271) Dhadialla, T. S.; Carlson, G. R.; Le, D. P. New Insecticides with Ecdysteroidal and Juvenile Hormone Activity. *Annu. Rev. Entomol.* **1998**, *43* (1), 545–569.
(272) Zhang, Q.; Nachman, R. J.; Denlinger, D. L. Diapause Hormone in the Helicoverpa/Heliothis Complex: A Review of Gene Expression, Peptide Structure and Activity, Analog and Antagonist Development, and the Receptor. *Peptides* **2015**, *72*, 196–201.
(273) Zhang, Q.; Nachman, R. J.; Kaczmarek, K.; Zabrocki, J.; Denlinger, D. L. Disruption of Insect Diapause Using Agonists and an Antagonist of Diapause Hormone. *Proc. Natl. Acad. Sci.* **2011**, *108* (41), 16922–16926.
(274) Peeters, C.; Foldi, I.; Matile-Ferrero, D.; Fisher, B. L. A Mutualism without Honeydew: What Benefits for *Melissotarsus Emeryi* Ants and Armored Scale Insects (Diaspididae)? *PeerJ* **2017**, *5*, e3599.
(275) Michalik, K.; Szklarzewicz, T.; Kalandyk-Kołodziejczyk, M.; Jankowska, W.; Michalik, A. Bacteria Belonging to the Genus Burkholderia Are Obligatory Symbionts of the Eriococcids Acanthococcus Aceris Signoret, 1875 and Gossyparia Spuria (Modeer, 1778) (Insecta, Hemiptera, Coccoidea). *Arthropod Struct. Dev.* **2016**, *45* (3), 265–272.
(276) Ueda, S.; Quek, S.-P.; Itioka, T.; Inamori, K.; Sato, Y.; Murase, K.; Itino, T. An Ancient Tripartite Symbiosis of Plants, Ants and Scale Insects. *Proc. R. Soc. B Biol. Sci.* **2008**, *275* (1649), 2319–2326.
(277) Boudreau, P. D.; Byrum, T.; Liu, W.-T.; Dorrestein, P. C.; Gerwick, W. H. Viequeamide A, a Cytotoxic Member of the Kulolide Superfamily of Cyclic Depsipeptides from a Marine Button Cyanobacterium. *J. Nat. Prod.* **2012**, *75* (9), 1560–1570.
(278) Pohle, S.; Appelt, C.; Roux, M.; Fiedler, H.-P.; Süssmuth, R. D. Biosynthetic Gene Cluster of the Non-Ribosomally Synthesized Cyclodepsipeptide Skyllamycin: Deciphering Unprecedented Ways of Unusual Hydroxylation Reactions. *J. Am. Chem. Soc.* **2011**, *133* (16), 6194–6205.
(279) Uhlmann, S.; Süssmuth, R. D.; Cryle, M. J. Cytochrome P450 $_{Sky}$ Interacts Directly with the Nonribosomal Peptide Synthetase to Generate Three Amino Acid Precursors in Skyllamycin Biosynthesis. *ACS Chem. Biol.* **2013**, *8* (11), 2586–2596.
(280) Süssmuth, R.; Müller, J.; von Döhren, H.; Molnár, I. Fungal Cyclooligomerdepsipeptides: From Classical Biochemistry to Combinatorial Biosynthesis. *Nat Prod Rep* **2011**, *28* (1), 99–124.
(281) Yanai, K.; Sumida, N.; Okakura, K.; Moriya, T.; Watanabe, M.; Murakami, T. Para-Position Derivatives of Fungal Anthelmintic Cyclodepsipeptides Engineered with Streptomyces Venezuelae Antibiotic Biosynthetic Genes. *Nat. Biotechnol.* **2004**, *22* (7), 848–855.
(282) Yanai, K.; Okakura, K.; Yasuda, S.; Watanabe, M.; Miyamoto, K.; Midoh, N.; Murakami, T. Transformant Producing Secondary Metabolite Modified with Functional Group and Novel Biosynthesis Genes. US7109018B1, September 19, 2006.
(283) Khan, M. S. A.; Zahin, M.; Hasan, S.; Husain, F. M.; Ahmad, I. Inhibition of Quorum Sensing Regulated Bacterial Functions by Plant Essential Oils with Special Reference to Clove Oil. *Lett. Appl. Microbiol.* **2009**, *49* (3), 354–360.
(284) Kolb, H. C.; Sharpless, K. B. The Growing Impact of Click Chemistry on Drug Discovery. *Drug Discov. Today* **2003**, *8* (24), 1128–1137.
(285) Zhu, X.; Zhang, W. Tagging Polyketides/Non-Ribosomal Peptides with a Clickable Functionality and Applications. *Front. Chem.* **2015**, *3*.
(286) Takeshima, H.; Inokoshi, J.; Takada, Y.; Tanaka, H.; Ōmura, S. A Deacylation Enzyme for Aculeacin A, a Neutral Lipopeptide Antibiotic, from Actinoplanes Utahensis: Purification and Characterization. *J. Biochem. (Tokyo)* **1989**, *105* (4), 606–610.
(287) BOECK, L. V. D.; FUKUDA, D. S.; ABBOTT, B. J.; DEBONO, M. Deacylation of Echinocandin B by Actinoplanes Utahensis. *J. Antibiot. (Tokyo)* **1989**, *42* (3), 382–388.

(288) Kreuzman, A. J.; Hodges, R. L.; Swartling, J. R.; Pohl, T. E.; Ghag, S. K.; Baker, P. J.; McGilvray, D.; Yeh, W. K. Membrane-Associated Echinocandin B Deacylase of Actinoplanes Utahensis: Purification, Characterization, Heterologous Cloning and Enzymatic Deacylation Reaction. *J. Ind. Microbiol. Biotechnol.* **2000**, *24* (3), 173–180.
(289) Torres-Bacete, J.; Hormigo, D.; Stuart, M.; Arroyo, M.; Torres, P.; Castillon, M. P.; Acebal, C.; Garcia, J. L.; de la Mata, I. Newly Discovered Penicillin Acylase Activity of Aculeacin A Acylase from Actinoplanes Utahensis. *Appl. Environ. Microbiol.* **2007**, *73* (16), 5378–5381.
(290) Wang, C. K.; Northfield, S. E.; Colless, B.; Chaousis, S.; Hamernig, I.; Lohman, R.-J.; Nielsen, D. S.; Schroeder, C. I.; Liras, S.; Price, D. A.; et al. Rational Design and Synthesis of an Orally Bioavailable Peptide Guided by NMR Amide Temperature Coefficients. *Proc. Natl. Acad. Sci.* **2014**, *111* (49), 17504–17509.
(291) Siodłak, D.; Gajewska, M.; Macedowska, A.; Rzeszotarska, B. Conformational Studies into N-Methylation of Alanine Diamide Models: A Quantitative Approach. *J. Mol. Struct. THEOCHEM* **2006**, *775* (1–3), 47–59.
(292) Piriou, F.; Lintner, K.; Fermandjian, S.; Fromageot, P.; Khosla, M. C.; Smeby, R. R.; Bumpus, F. M. Amino Acid Side Chain Conformation in Angiotensin II and Analogs: Correlated Results of Circular Dichroism and 1H Nuclear Magnetic Resonance. *Proc. Natl. Acad. Sci.* **1980**, *77* (1), 82–86.
(293) Kessler, H. Detection of Hindered Rotation and Inversion by NMR Spectroscopy. *Angew. Chem. Int. Ed. Engl.* **1970**, *9* (3), 219–235.
(294) Siodłak, D. α,β-Dehydroamino Acids in Naturally Occurring Peptides. *Amino Acids* **2015**, *47* (1), 1–17.
(295) Deng, H.; Wang, C.; Su, M.; Fang, Y. Probing Biochemical Mechanisms of Action of Muscarinic M3 Receptor Antagonists with Label-Free Whole Cell Assays. *Anal. Chem.* **2012**, *84* (19), 8232–8239.
(296) Hohenegger, M.; Waldhoer, M.; Beindl, W.; Böing, B.; Kreimeyer, A.; Nickel, P.; Nanoff, C.; Freissmuth, M. Gsα-Selective G Protein Antagonists. *Proc. Natl. Acad. Sci.* **1998**, *95* (1), 346–351.
(297) Ullmann, H.; Meis, S.; Hongwiset, D.; Marzian, C.; Wiese, M.; Nickel, P.; Communi, D.; Boeynaems, J.-M.; Wolf, C.; Hausmann, R.; et al. Synthesis and Structure−Activity Relationships of Suramin-Derived P2Y $_{11}$ Receptor Antagonists with Nanomolar Potency. *J. Med. Chem.* **2005**, *48* (22), 7040–7048.
(298) Amatruda, T. T.; Steele, D. A.; Slepak, V. Z.; Simon, M. I. G Alpha 16, a G Protein Alpha Subunit Specifically Expressed in Hematopoietic Cells. *Proc. Natl. Acad. Sci.* **1991**, *88* (13), 5587–5591.
(299) Grundmann, M.; Merten, N.; Malfacini, D.; Inoue, A.; Preis, P.; Simon, K.; Rüttiger, N.; Ziegler, N.; Benkel, T.; Schmitt, N. K.; et al. Lack of Beta-Arrestin Signaling in the Absence of Active G Proteins. *Nat. Commun.* **2018**, *9* (1).
(300) Luttrell, L. M.; Ferguson, S. S. G.; Daaka, Y.; Miller, W. E.; Maudsley, S.; Della Rocca, G. J.; Lin, F. T.; Kawakatsu, H.; Owada, K.; Luttrell, D. K. Receptor–Src Protein Kinase Complexes.
(301) Rajagopal, S.; Rajagopal, K.; Lefkowitz, R. J. Teaching Old Receptors New Tricks: Biasing Seven-Transmembrane Receptors. *Nat. Rev. Drug Discov.* **2010**, *9* (5), 373–386.
(302) Weinstain, R.; Kanter, J.; Friedman, B.; Ellies, L. G.; Baker, M. E.; Tsien, R. Y. Fluorescent Ligand for Human Progesterone Receptor Imaging in Live Cells. *Bioconjug. Chem.* **2013**, *24* (5), 766–771.
(303) Kammili, V. R.; Reddy, G. M.; Mukkanti, K. Oxidation of Alcohol to Carboxylic Acid under Mild Acidic Condition and Followed by Synthesis of Ester Analogues of Corey's Lactone.

(304) Tojo, G.; Fernández, M. TEMPO-Mediated Oxidations. In *Oxidation of Primary Alcohols to Carboxylic Acids*; Springer, 2007; pp 79–103.
(305) Mart, R. J.; Allemann, R. K. Azobenzene Photocontrol of Peptides and Proteins. *Chem. Commun.* **2016**, *52* (83), 12262–12277.
(306) Wiedbrauk, S.; Dube, H. Hemithioindigo—an Emerging Photoswitch. *Tetrahedron Lett.* **2015**, *56* (29), 4266–4274.
(307) Szymański, W.; Beierle, J. M.; Kistemaker, H. A. V.; Velema, W. A.; Feringa, B. L. Reversible Photocontrol of Biological Systems by the Incorporation of Molecular Photoswitches. *Chem. Rev.* **2013**, *113* (8), 6114–6178.
(308) Cordes, T.; Elsner, C.; Herzog, T. T.; Hoppmann, C.; Schadendorf, T.; Summerer, W.; Rück-Braun, K.; Zinth, W. Ultrafast Hemithioindigo-Based Peptide-Switches. *Chem. Phys.* **2009**, *358* (1–2), 103–110.
(309) Nair, D. P.; Podgórski, M.; Chatani, S.; Gong, T.; Xi, W.; Fenoli, C. R.; Bowman, C. N. The Thiol-Michael Addition Click Reaction: A Powerful and Widely Used Tool in Materials Chemistry. *Chem. Mater.* **2014**, *26* (1), 724–744.
(310) Baskin, J. M.; Bertozzi, C. R. Bioorthogonal Click Chemistry: Covalent Labeling in Living Systems. *QSAR Comb. Sci.* **2007**, *26* (11–12), 1211–1219.
(311) Shih, H.-W.; Kamber, D. N.; Prescher, J. A. Building Better Bioorthogonal Reactions. *Curr. Opin. Chem. Biol.* **2014**, *21*, 103–111.
(312) Lee, Y.-J.; Wu, B.; Raymond, J. E.; Zeng, Y.; Fang, X.; Wooley, K. L.; Liu, W. R. A Genetically Encoded Acrylamide Functionality. *ACS Chem. Biol.* **2013**, *8* (8), 1664–1670.
(313) Kaya, E.; Vrabel, M.; Deiml, C.; Prill, S.; Fluxa, V. S.; Carell, T. A Genetically Encoded Norbornene Amino Acid for the Mild and Selective Modification of Proteins in a Copper-Free Click Reaction. *Angew. Chem. Int. Ed.* **2012**, *51* (18), 4466–4469.
(314) Hong, V.; Presolski, S.; Ma, C.; Finn, M. â€ …G. Analysis and Optimization of Copper-Catalyzed Azide–Alkyne Cycloaddition for Bioconjugation. *Angew. Chem. Int. Ed.* **2009**, *48* (52), 9879–9883.
(315) Li, F.; Zhang, H.; Sun, Y.; Pan, Y.; Zhou, J.; Wang, J. Expanding the Genetic Code for Photoclick Chemistry in *E. Coli* , Mammalian Cells, and *A. Thaliana*. *Angew. Chem. Int. Ed.* **2013**, *52* (37), 9700–9704.
(316) Dieterich, D. C.; Lee, J. J.; Link, A. J.; Graumann, J.; Tirrell, D. A.; Schuman, E. M. Labeling, Detection and Identification of Newly Synthesized Proteomes with Bioorthogonal Non-Canonical Amino-Acid Tagging. *Nat. Protoc.* **2007**, *2* (3), 532–540.
(317) Urtatiz, O.; Van Raamsdonk, C. D. Gnaq and Gna11 in the Endothelin Signaling Pathway and Melanoma. *Front. Genet.* **2016**, *7*.
(318) Mouti, M. A.; Dee, C.; Coupland, S. E.; Hurlstone, A. F. Minimal Contribution of ERK1/2-MAPK Signalling towards the Maintenance of Oncogenic GNAQQ209P-Driven Uveal Melanomas in Zebrafish. *Oncotarget* **2016**, *7* (26), 39654.
(319) Krantz, B. A.; Dave, N.; Komatsubara, K. M.; Marr, B. P.; Carvajal, R. D. Uveal Melanoma: Epidemiology, Etiology, and Treatment of Primary Disease. *Clin. Ophthalmol.* **2017**, *Volume 11*, 279–289.

10 Appendix

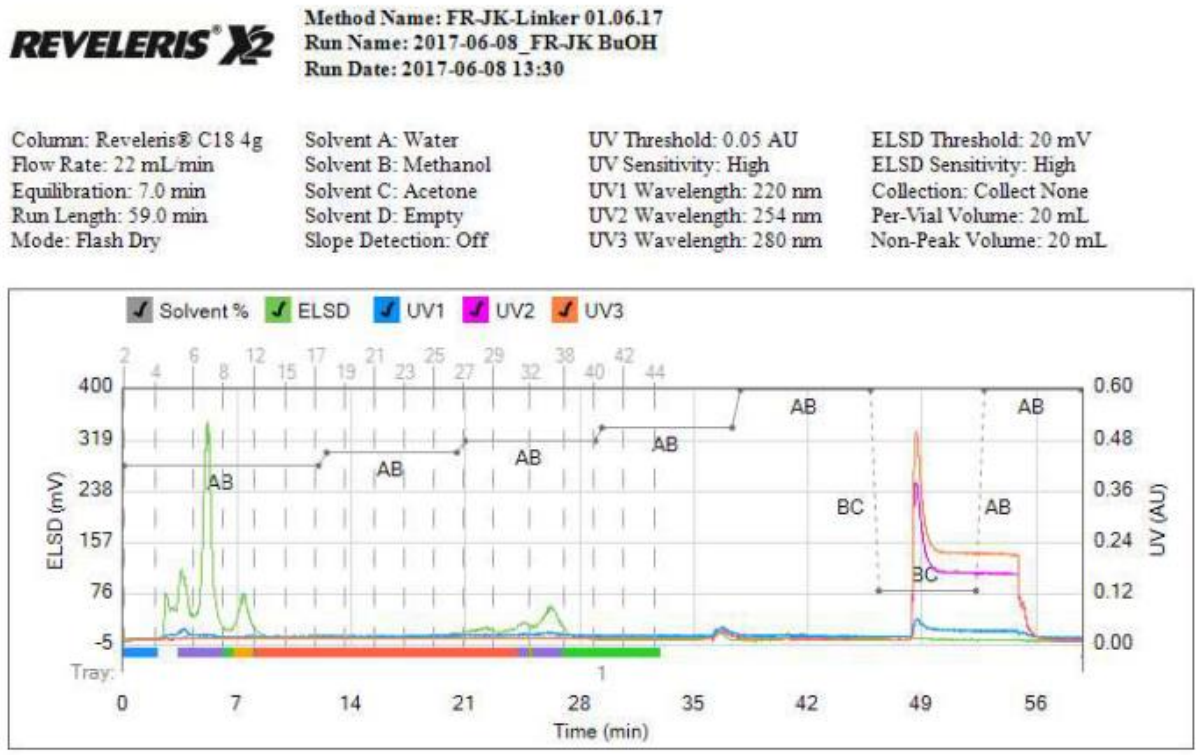

Figure 10-1: Flash chromatography of FR-JK-Boc crude product. 15 mg pure FR-JK-Boc (47) was obtained from fractions 32-38.

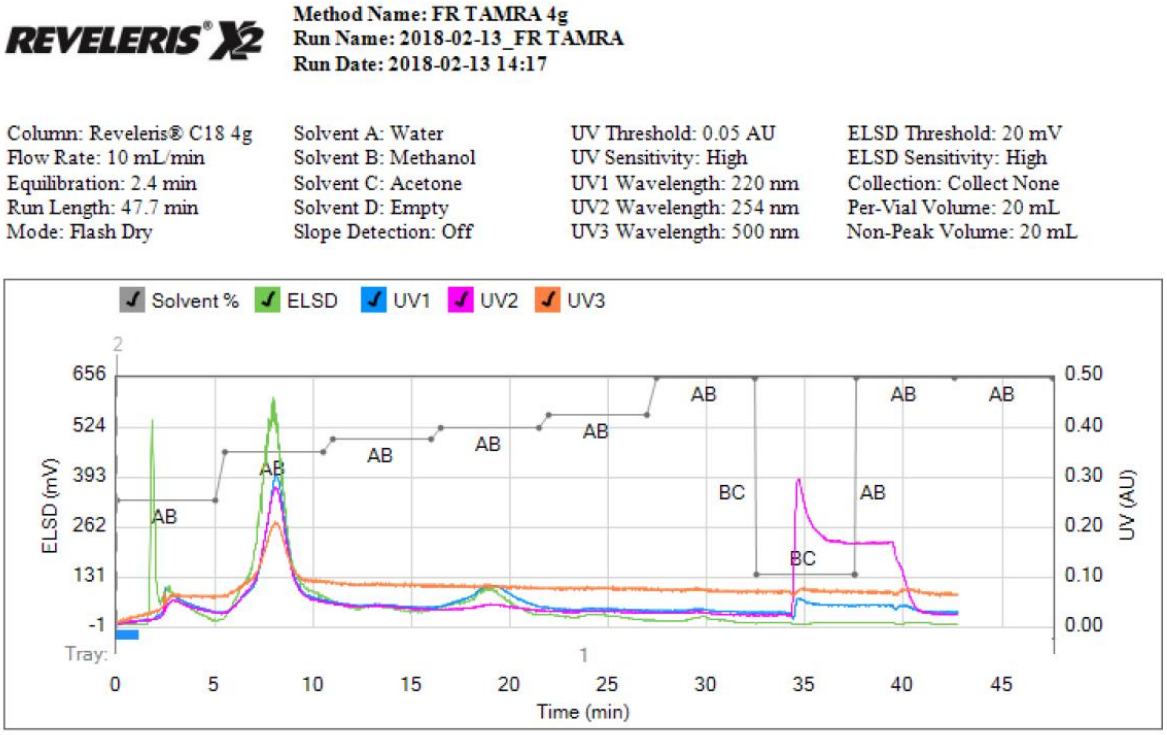

Figure 10-2: Flash chromatography of FR-TAMRA (49) crude product. 4 mg FR-TAMRA was obtained from tR 17-27 and further purified by HPLC.

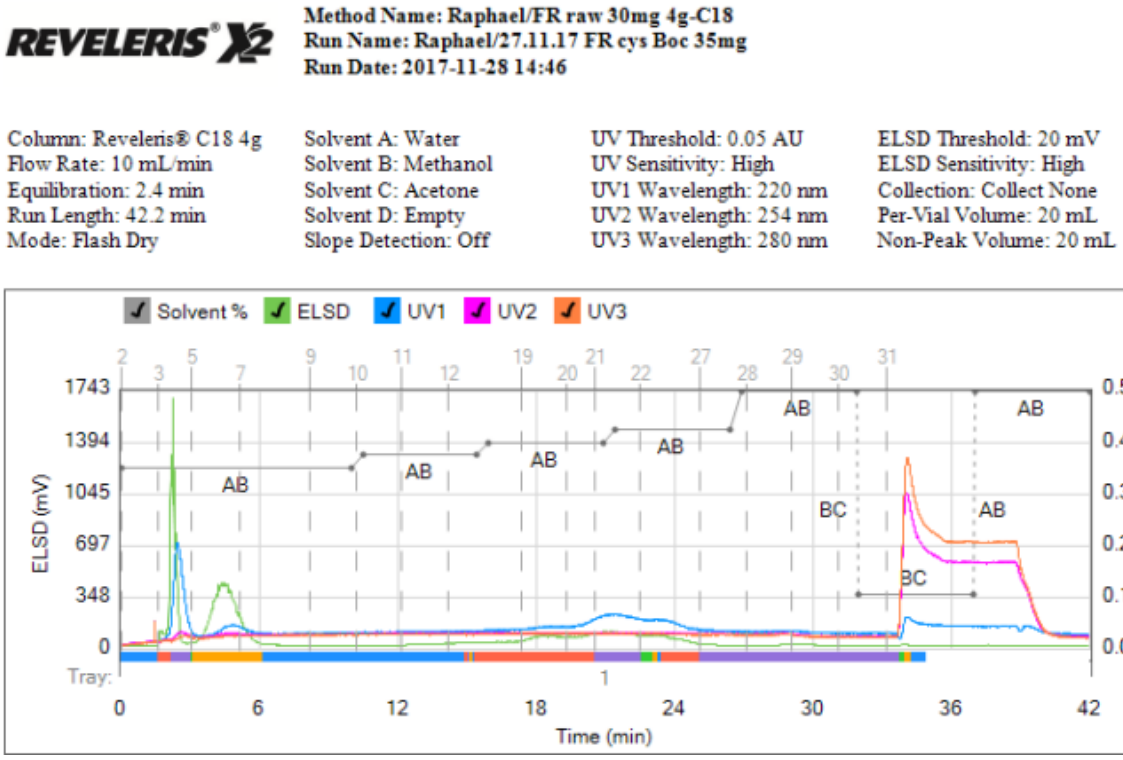

Figure 10-3: Flash chromatography of FR-Cys-Boc (50) crude product. 32 mg compound 50 was obtained from fractions 19-28 and further purified by HPLC.

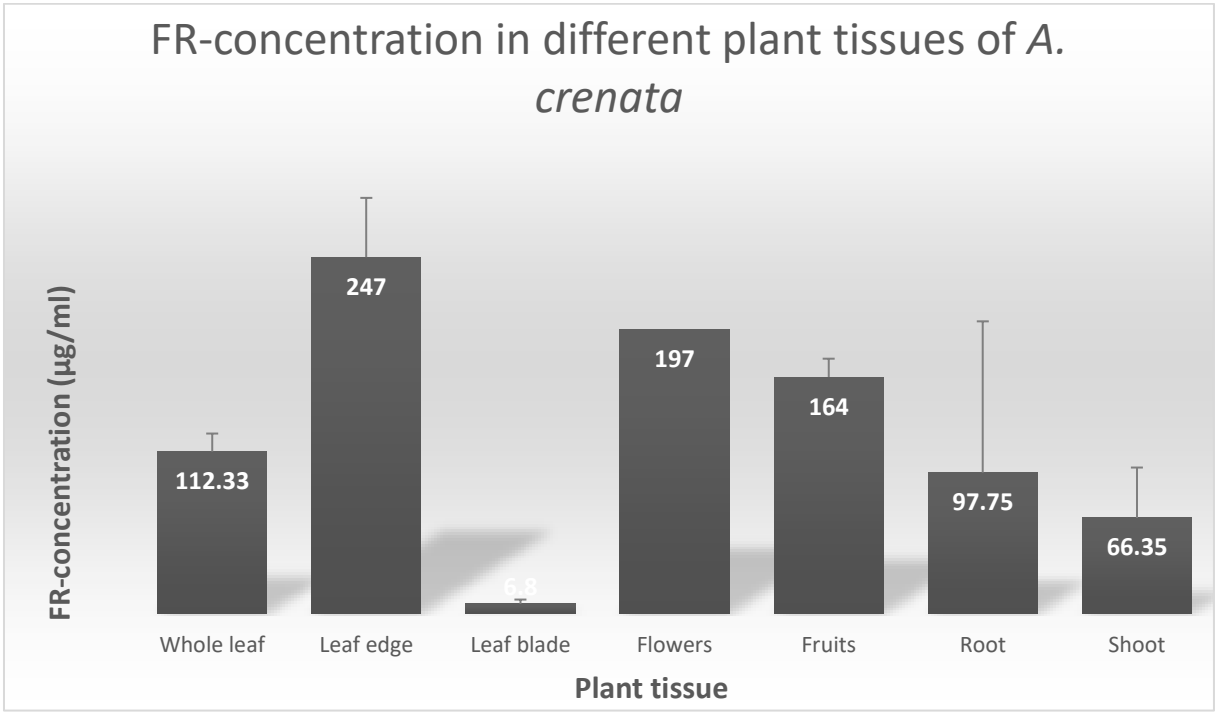

Figure 10-4: FR-concentration (µg/ml) in different plant tissues of *A. crenata* determined by LCMS measurements. Calibration curve with 4 different concentration (1 µg/ml, 10 µg/ml, 100 µg/ml, 1 mg/ml),of standard FR was applied.

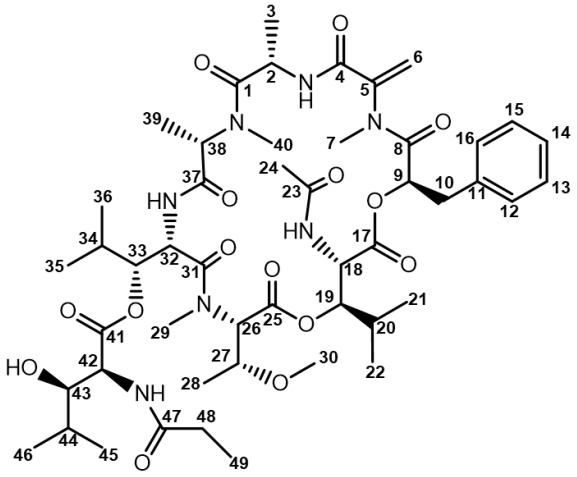

Scheme 10-1: Structure and numbering of C-atoms of FR900359 (FR).

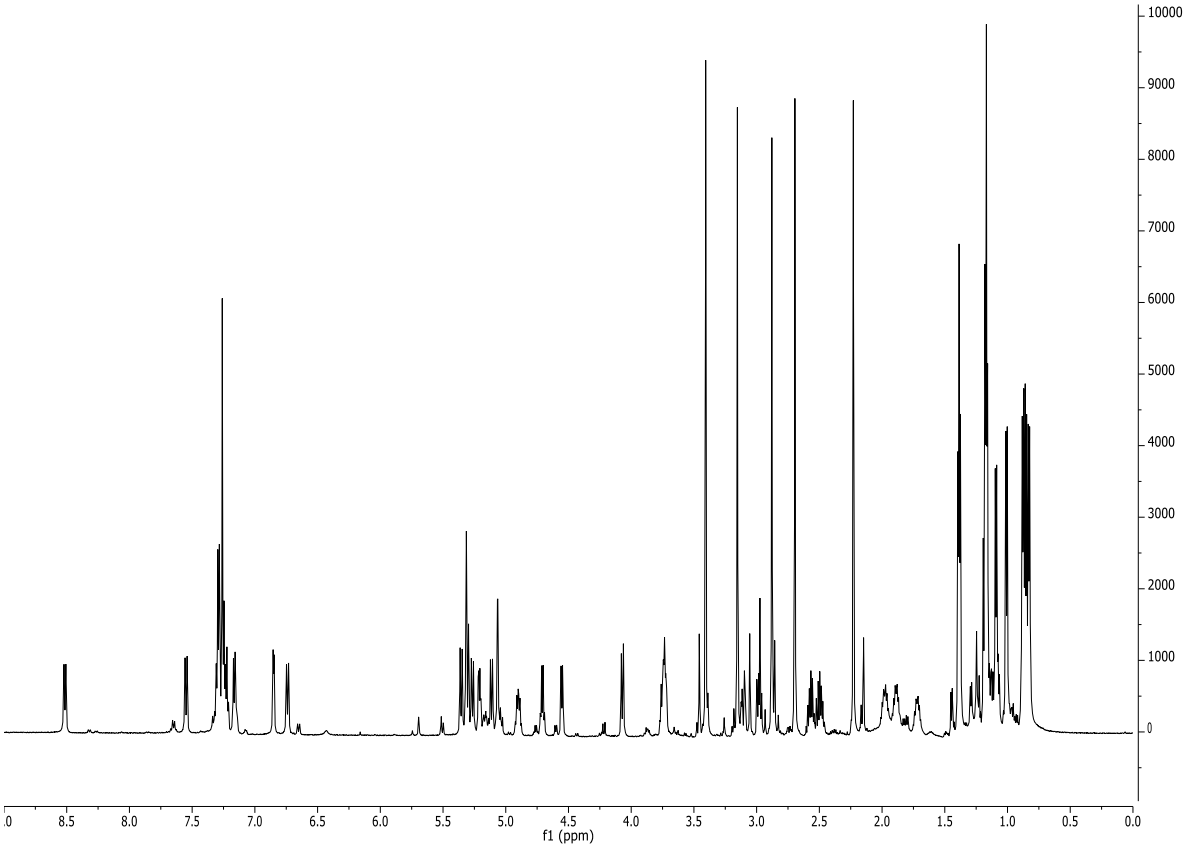

Figure 10-5: ^{1}H NMR spectrum (600 MHz $CDCl_3$) of FR900359 (FR). Assignments see **Table 10-1**.

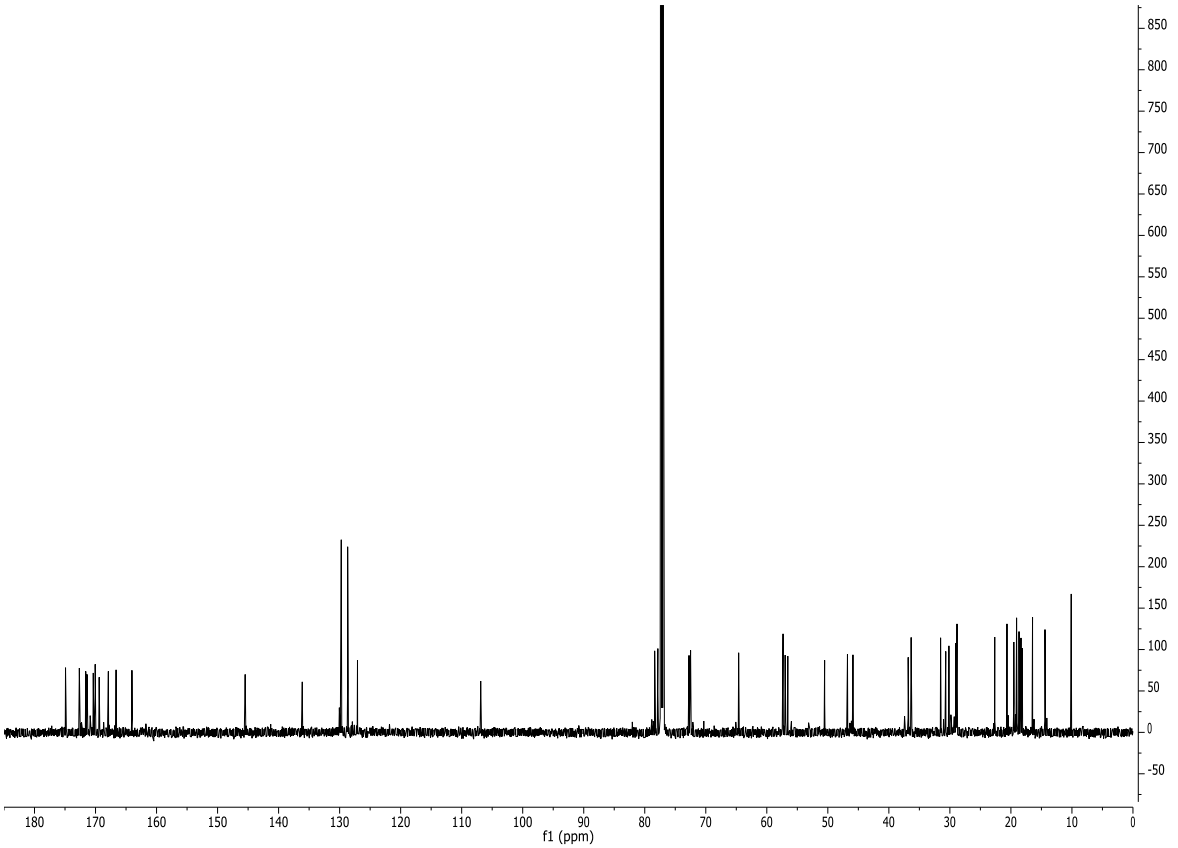

Figure 10-6: ^{13}C NMR spectrum (150 MHz $CDCl_3$) of FR900359 (FR). Assignments see **Table 10-1**.

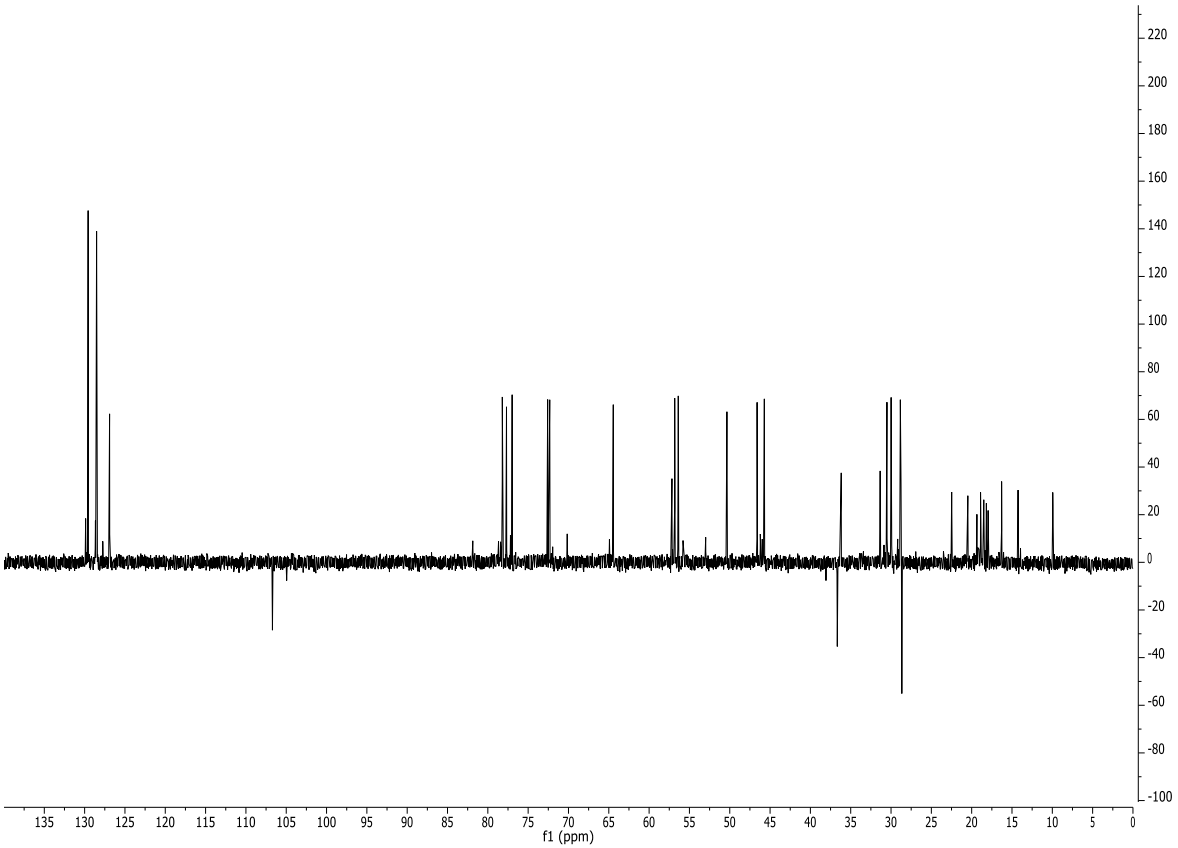

Figure 10-7: DEPT-135 NMR spectrum (150 MHz $CDCl_3$) of FR900359 (FR). Assignments see **Table 10-1**.

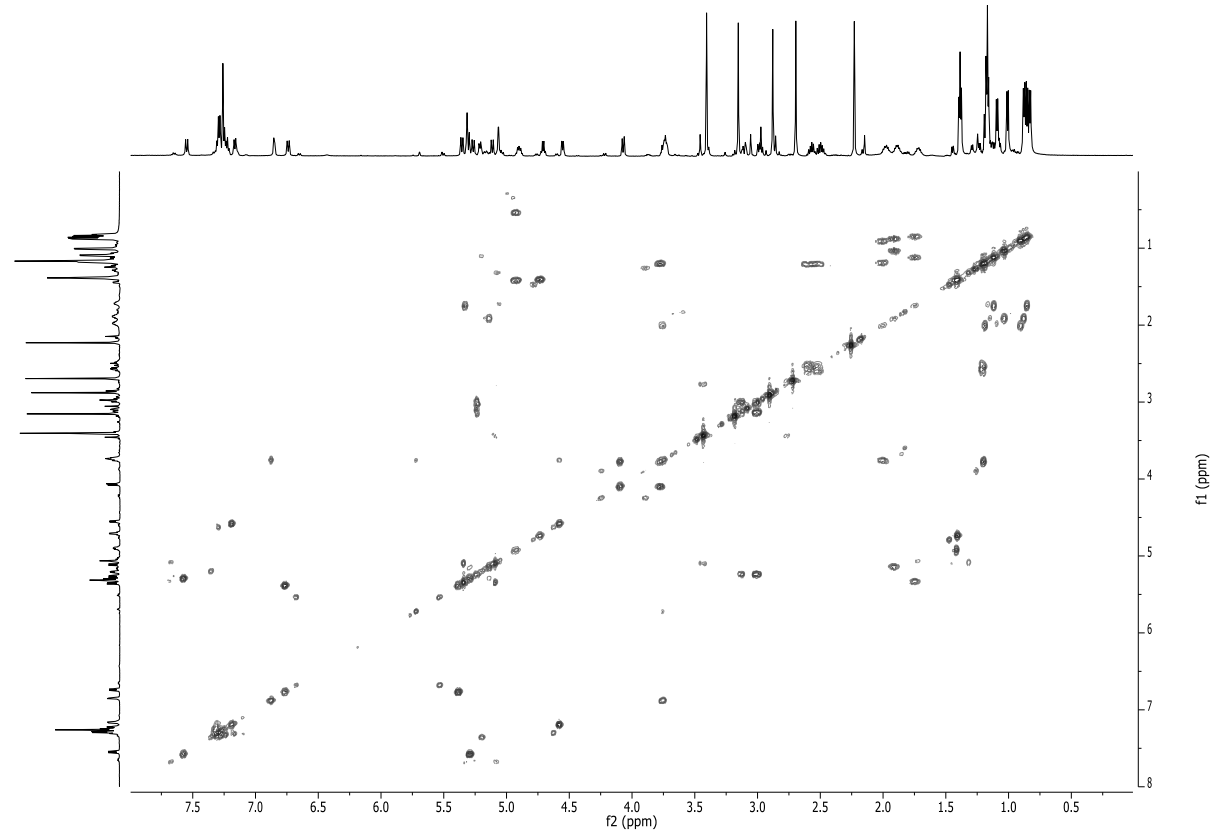

Figure 10-8: ^{1}H-^{1}H-COSY NMR spectrum (600 MHz $CDCl_3$) of FR900359 (FR).

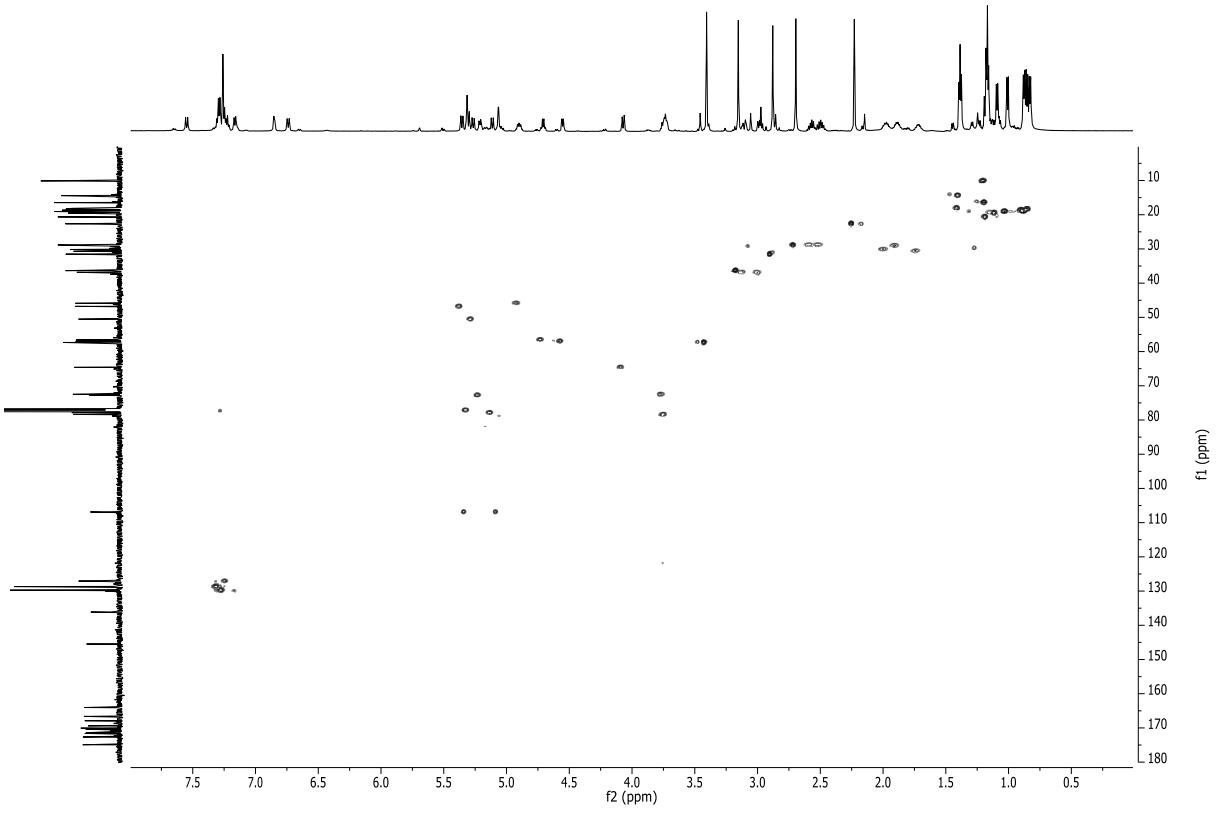

Figure 10-9: ^{1}H-^{13}C HSQC NMR spectrum (600 MHz $CDCl_3$) of FR900359 (FR).

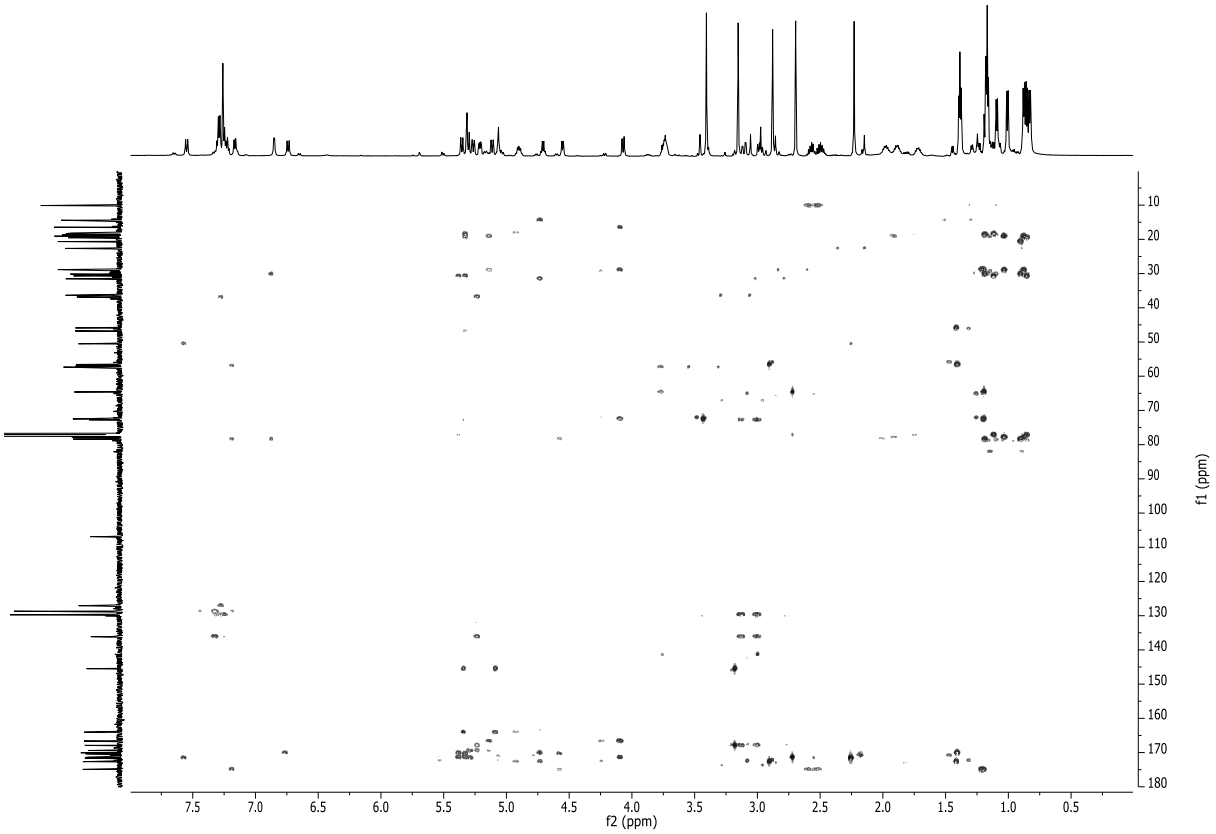

Figure 10-10: ^{1}H-^{13}C HMBC NMR spectrum (600 MHz $CDCl_3$) of FR900359 (FR).

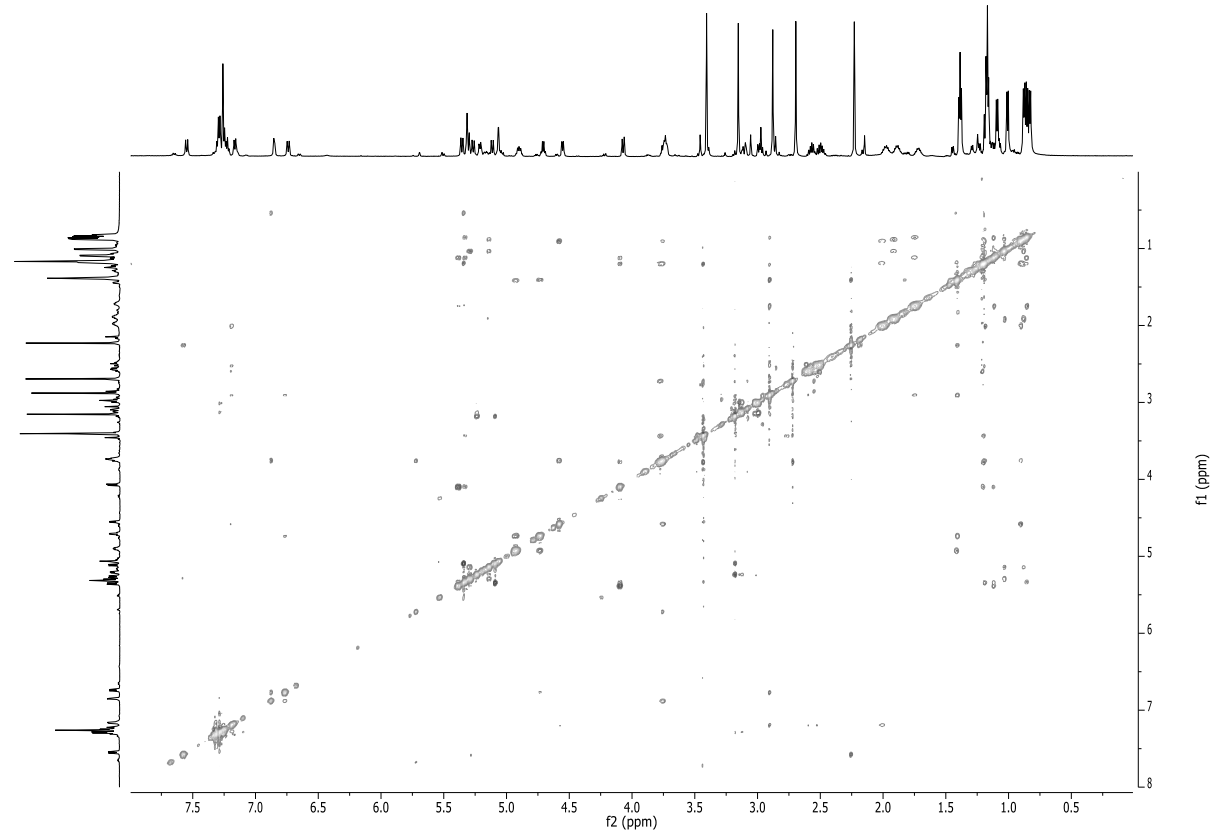

Figure 10-11: ROESY NMR spectrum (600 MHz $CDCl_3$) of FR900359 (FR).

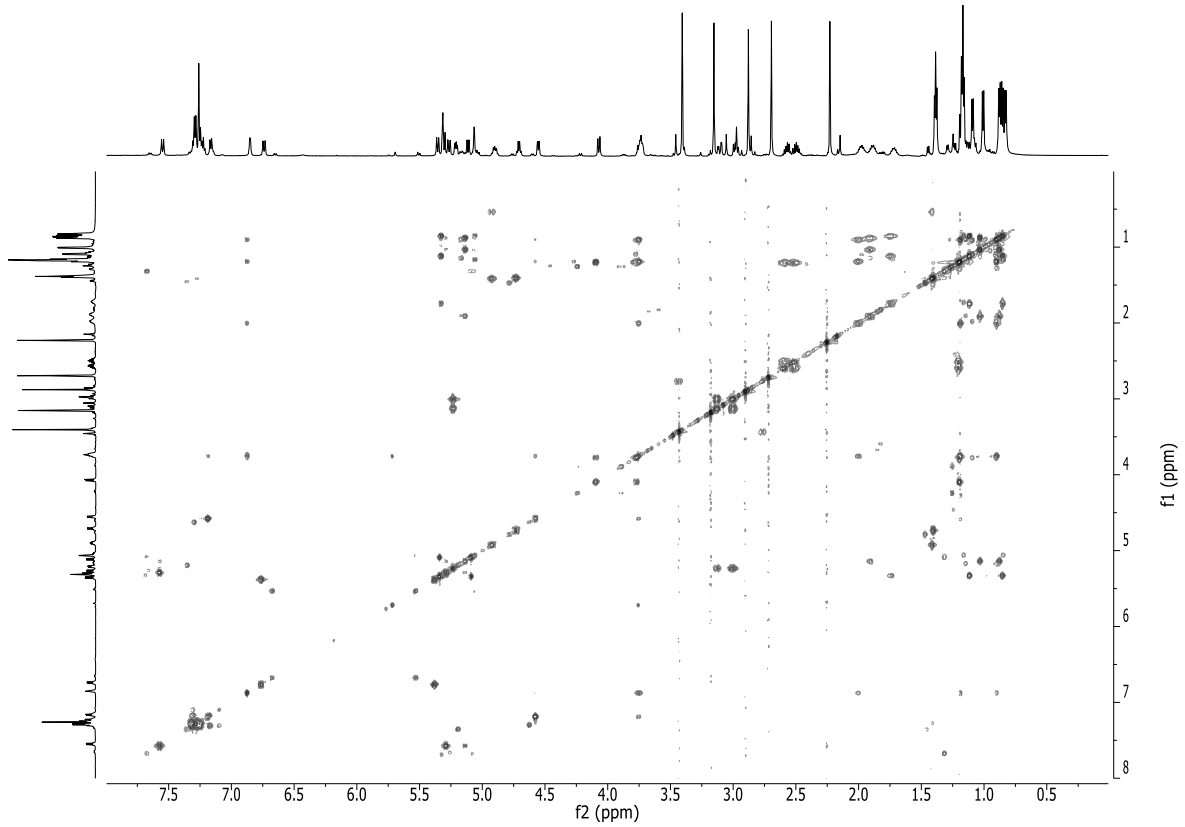

Figure 10-12: TOCSY NMR spectrum (600 MHz CDCl3) of FR900359 (FR).

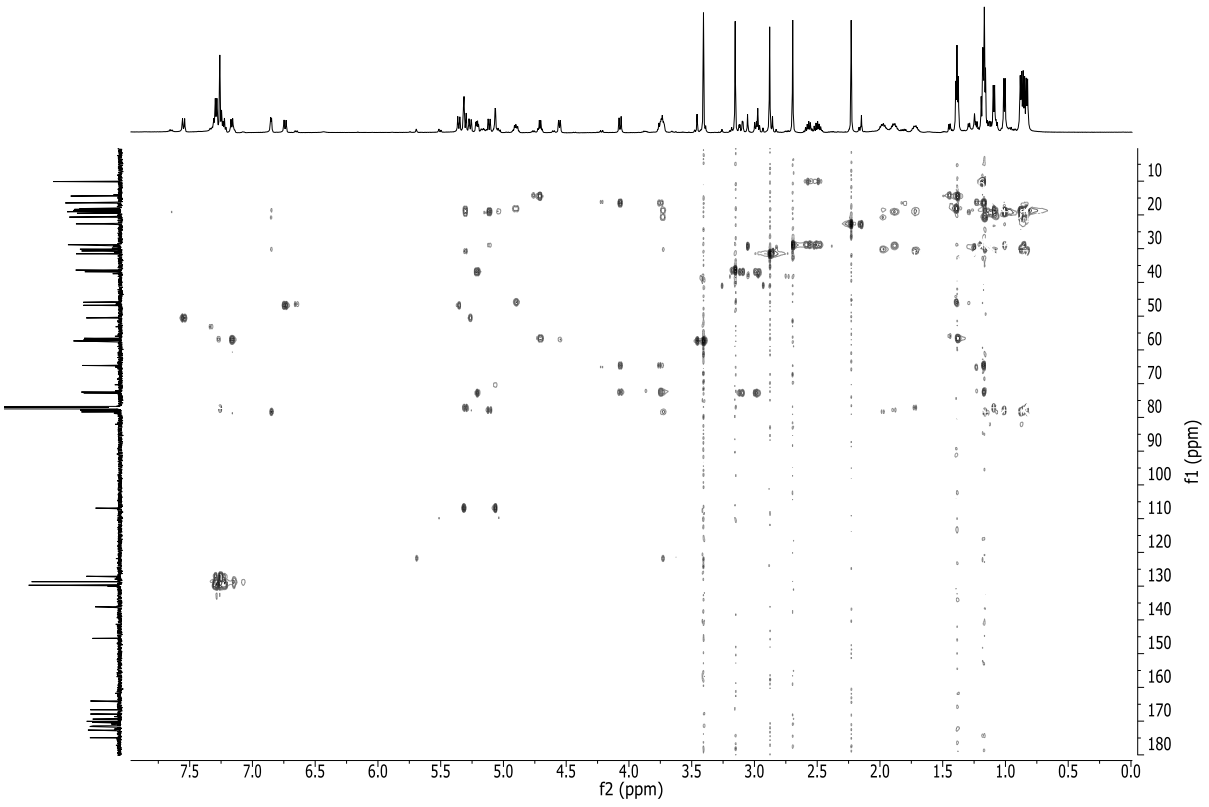

Figure 10-13: HSQC-TOCSY NMR spectrum (600 MHz CDCl3) of FR900359 (FR).

Table 10-1: ^{1}H and ^{13}C NMR spectroscopic data of FR900359 (FR) in $CDCl_3$ (^{1}H: 600 MHz; ^{13}C: 150 MHz).

Residue[c]	**No C/H[b]**	**δ_C[a], mult**	**δ_H[a] (mult, J in Hz)**
Ala	1	172.6, C	–
	2	45.9, CH	4.90 (m)
	2-NH	–	8.51 (d, 9.1)
	3	18.1, CH_3	1.39 (d, 6.7)
N-Me-Dha	4	164.0, C	–
	5	145.5, C	–
	6a	106.9, CH_2	a 5.32 (d, 2.2)
	6b	–	b 5.07 (d, 2.2)
	7	36.3, CH_3	3.15 (s)
Pla	8	167.9, C	–
	9	72.7, CH	5.21 (dd, 4.1, 8.3)
	10a	36.8, CH_2	a 3.11 (dd, 4.1, 14.8)
	10b	–	b 2.98 (dd, 8.3, 14.8)
	11	136.1, C	–
	12/16	129.7, CH	7.26[d]
	13/15	128.7, CH	7.29[d]
	14	127.1, CH	7.23[d]
N-Ac-*β*-HyLeu-1	17	169.4, C	–
	18	50.5, CH	5.27 (dd, 1.3, 10.0)
	18-NH	–	7.55, (d, 10,0)
	19	77.8, CH	5.12 (dd, 1.3, 10.0)
	20	29.0, CH	1.89 (m)
	21	19.1, CH_3	1.01 (d, 6.8)
	22	19.0, CH_3	0.85 (d, 6.8)
	23	171.6, C	–
	24	22.6, CH_3	2.23 (s)
N,*O*-Me_2-Thr	25	166.6, C	–
	26	64.6, CH	4.07 (d, 9.8)
	27	72.5, CH	3.76 (m)
	28	16.5, CH_3	1.18 (d, 5.8)
	29	28.9, CH_3	2.70 (s)
	30	57.3, CH_3	3.41 (s)
β-HyLeu	31	171.4, C	–
	32	46.8, CH	5.36 (d, 9.9)
	32-NH		6.74, (d, 9.9)
	33	77.1, CH	5.31
	34	30.7, CH	1.72 (m)
	35	19.5, CH_3	1.09 (d, 6.7)
	36	18.3, CH_3	0.83 (d, 6.7)
N-Me-Ala	37	170.1, C	–

	38	56.6, CH	4.71 (q, 6.8)
	39	14.4, CH_3	1.38 (d, 6.8)
	40	31.5, CH_3	2.88 (s)
N-Pr-*β*-HyLeu-2	41	170.4, C	–
	42	57.0, CH	4.55 (dd, 1.4, 7.8)
	42-NH	–	7.17 (d, 7.8)
	43	78.4, CH	3.73 (m)
	43-OH	–	6.85 (d, 4.2)
	44	30.1, CH	1.98 (m)
	45	20.6, CH_3	1.17 (6.7)
	46	18.7, CH_3	0.88 (6.7)
	47	174.9, C	–
	48a	28.8, CH_2	2.57 (dq, 14.9, 7.5)
	48b		2.50 (dq, 14.9, 7.5)
	49	10.1, CH_3	1.19 (t, 7.5)

[**a**] Assignments are based on extensive 1D and 2D NMR measurements (HMBC, HSQC, COSY). ^{13}C-NMR spectra were recorded at 150 MHz. [**b**] Numbers according to Scheme S1. [**c**] Residues: Ala = alanine, *N*-Me-Dha = *N*-methyldehydroalanine, Pla = 3-phenyllactic acid, *N*-Ac-*β*-HyLeu= *N*-acetylhydroxyleucine-1, *N*,*O*-Me2-Thr = *N*,*O*-dimethylthreonine, *β*-HyLeu = hydroxyleucine, *N*-Me-Ala = *N*-methylalanine, *N*-Pr-*β*-HyLeu = *N*-propionylhydroxyleucine-2.[d] overlaying resonances.

Compound FR900359 (FR), 50mg/kg dried *A. crenata* leaves (all spectroscopic data as reported in Fujioka et al[1], Crüsemann and Reher et al.[10]).

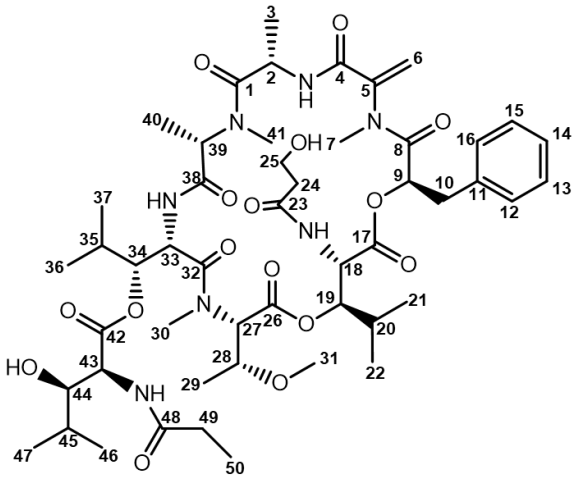

Scheme 10-2: Structure and numbering of C-atoms of **1** (FR-1).

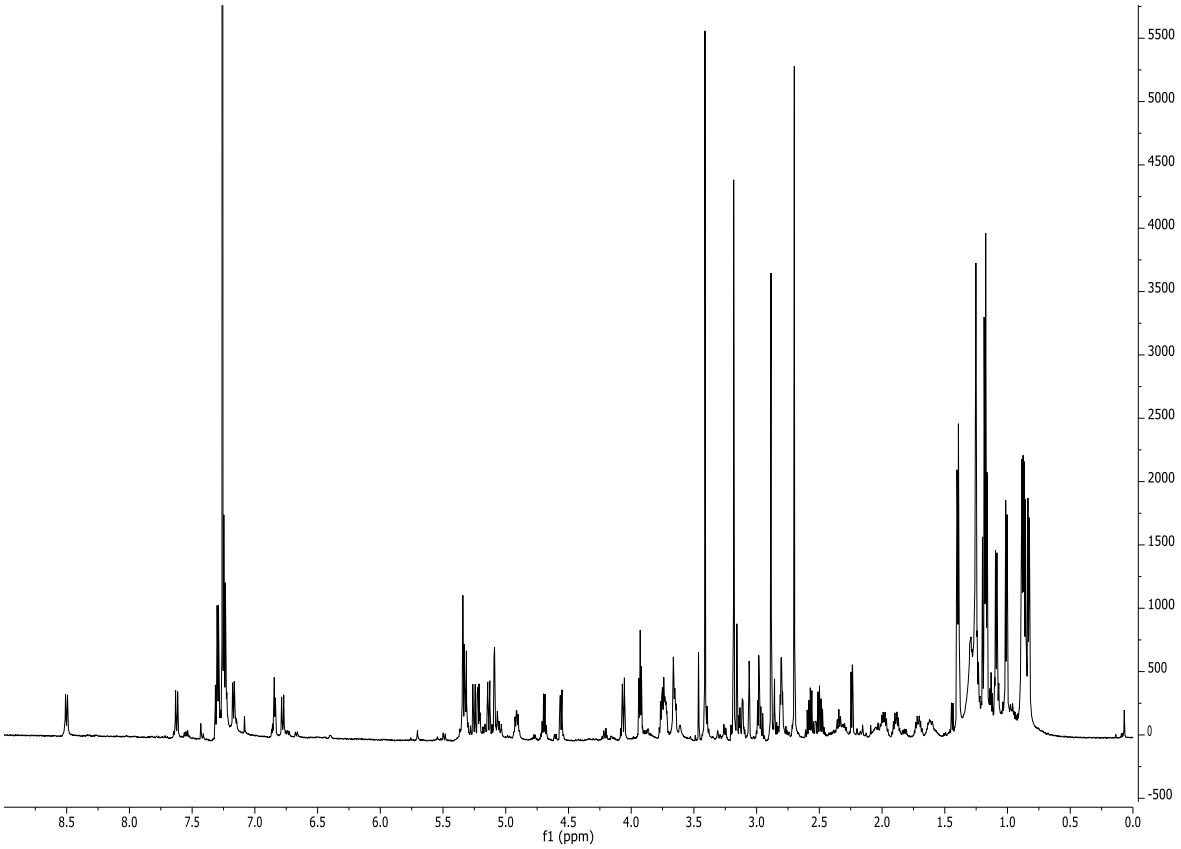

Figure 10-14: Structure and ^{1}H NMR spectrum (600 MHz, $CDCl_3$) of **1** (FR-1). Assignments see **Table 10-2**.

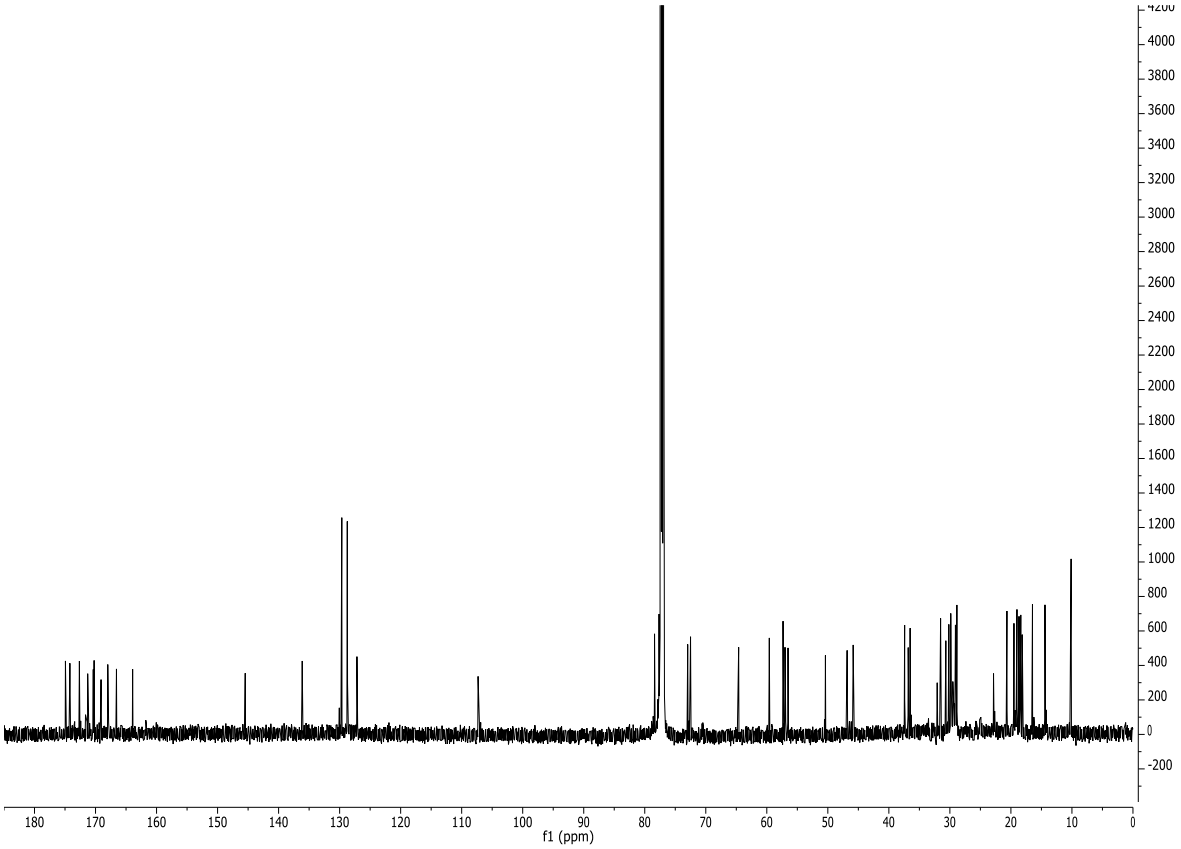

Figure 10-15: ^{13}C NMR spectrum (150 MHz $CDCl_3$) of **1** (FR-1). Assignments see **Table 10-2**.

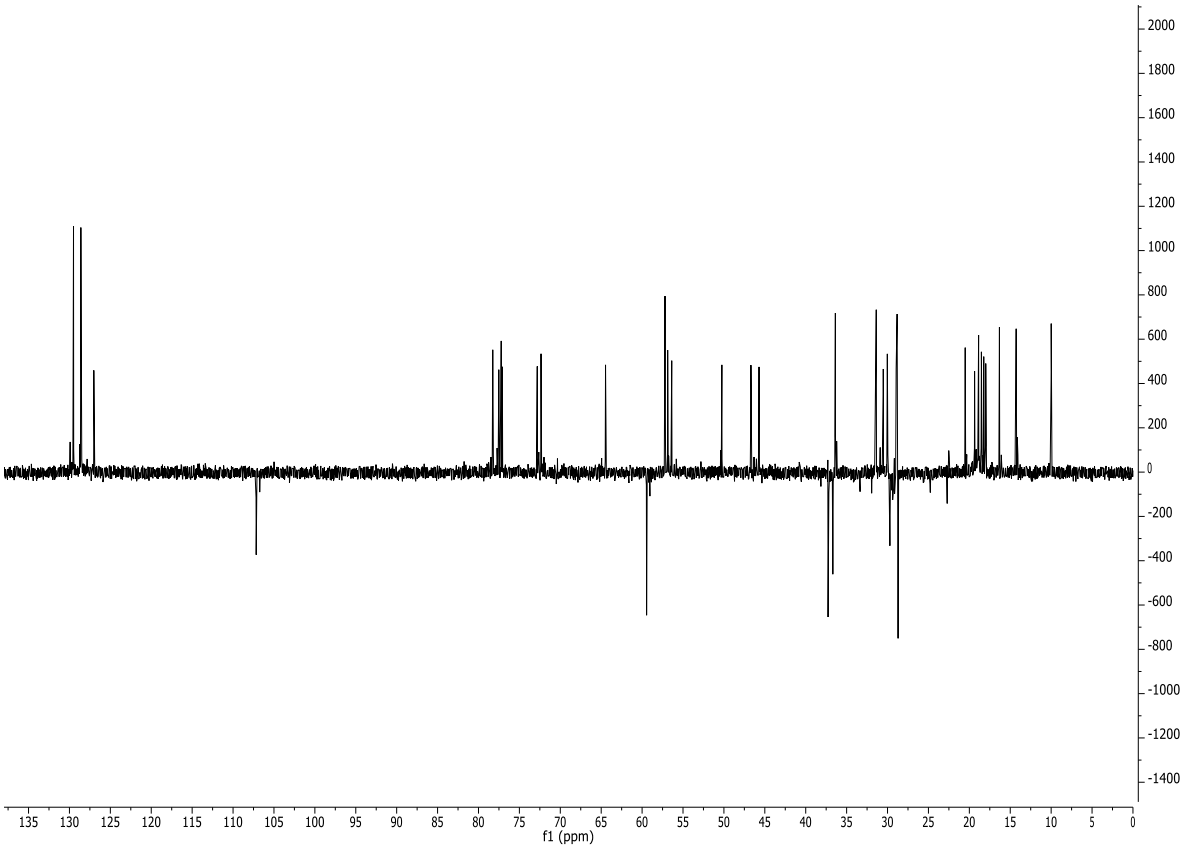

Figure 10-16: DEPT-135 NMR spectrum (150 MHz $CDCl_3$) of **1** (FR-1). Assignments see **Table 10-2**.

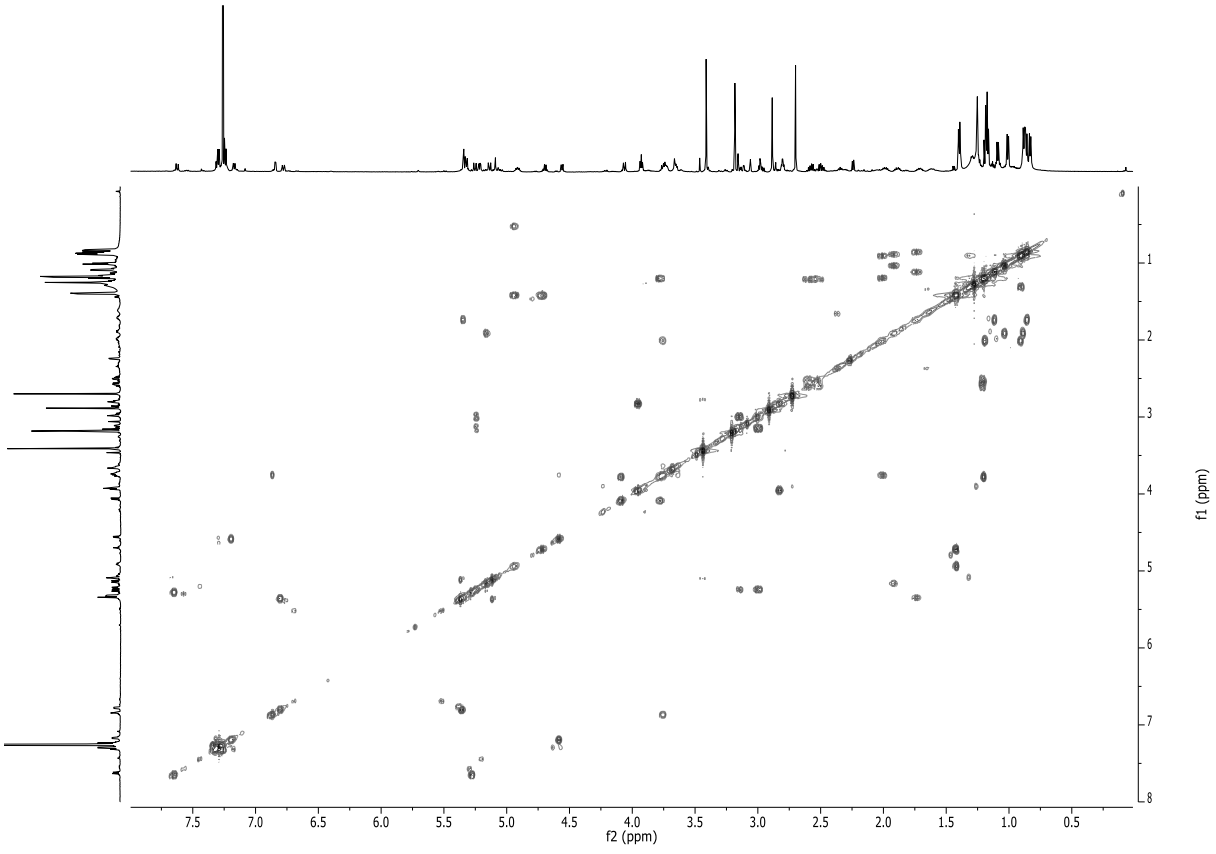

Figure 10-17: ^{1}H-^{1}H-COSY NMR spectrum (600 MHz $CDCl_3$) of **1** (FR-1).

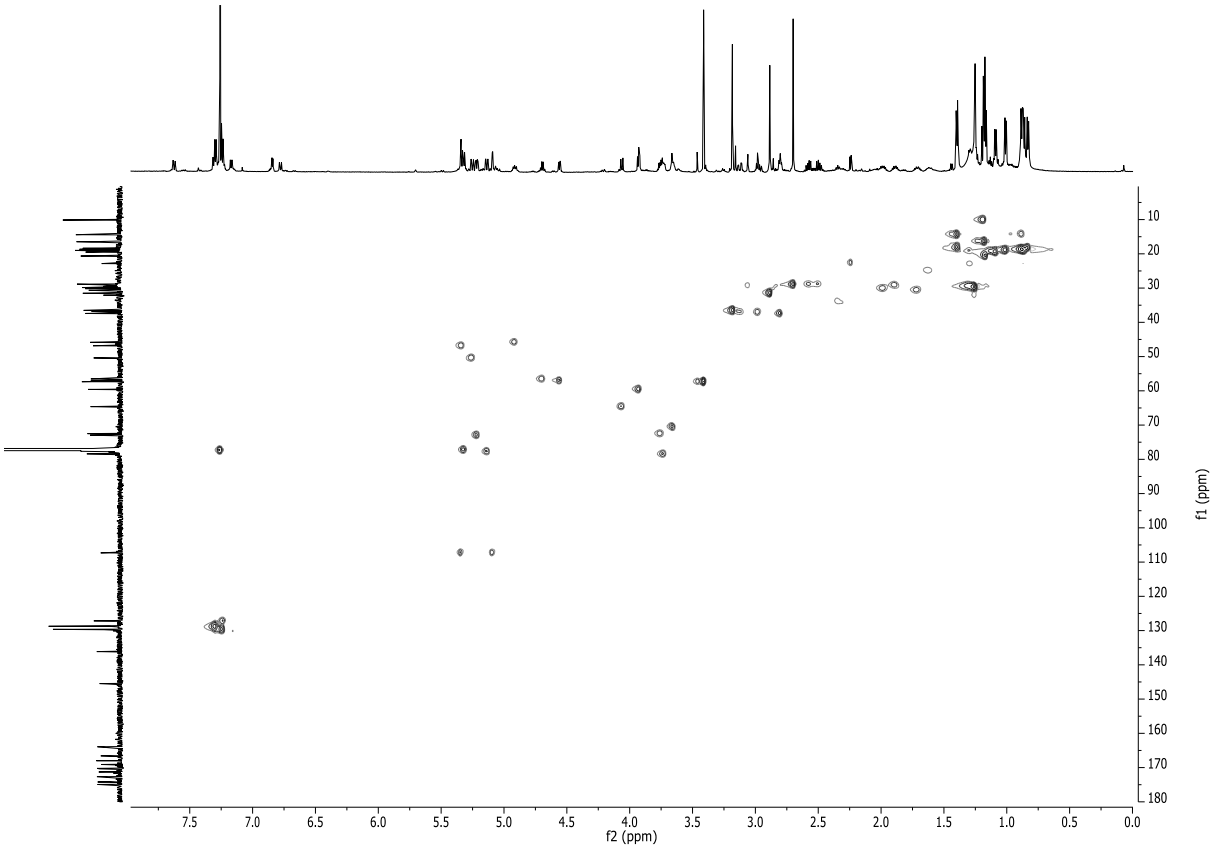

Figure 10-18: ^{1}H-^{13}C HSQC NMR spectrum (600 MHz $CDCl_3$) of **1** (FR-1).

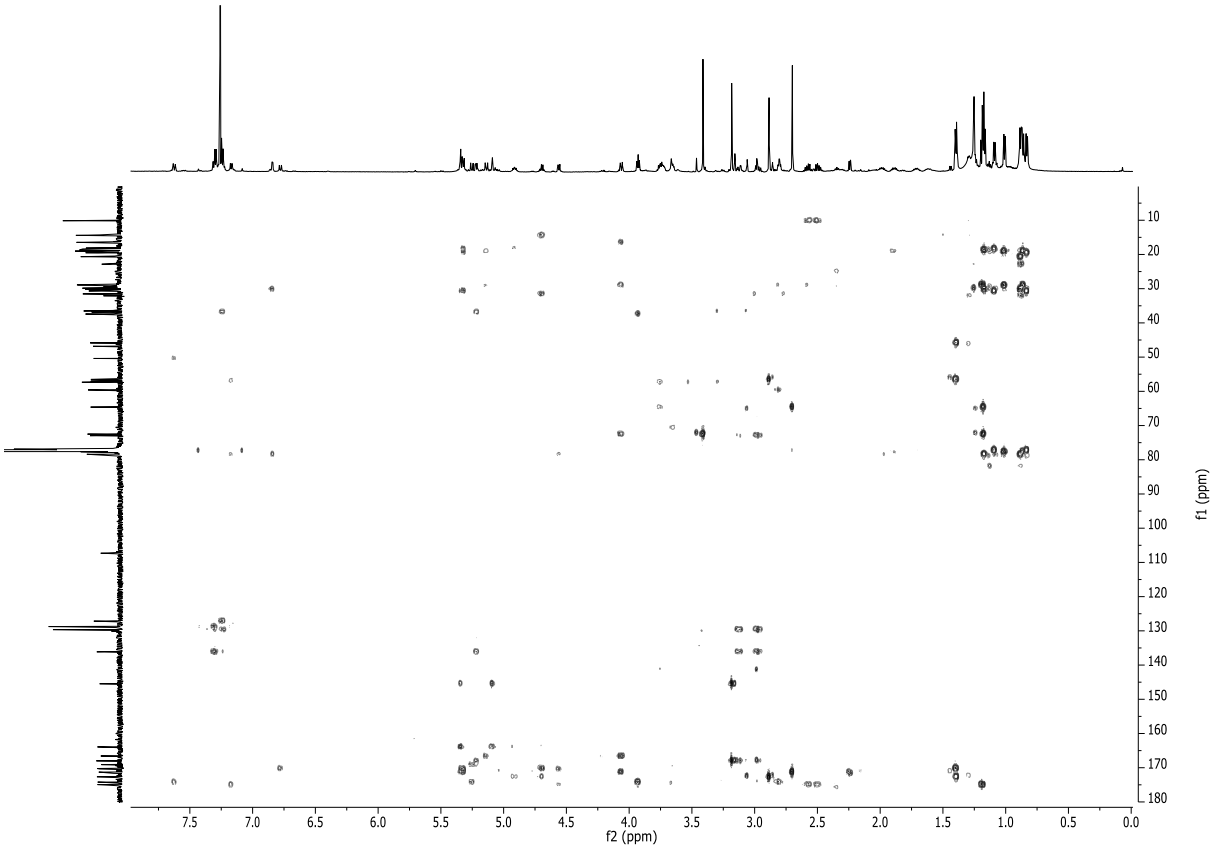

Figure 10-19: ^{1}H-^{13}C HMBC NMR spectrum (600 MHz $CDCl_3$) of **1** (FR-1).

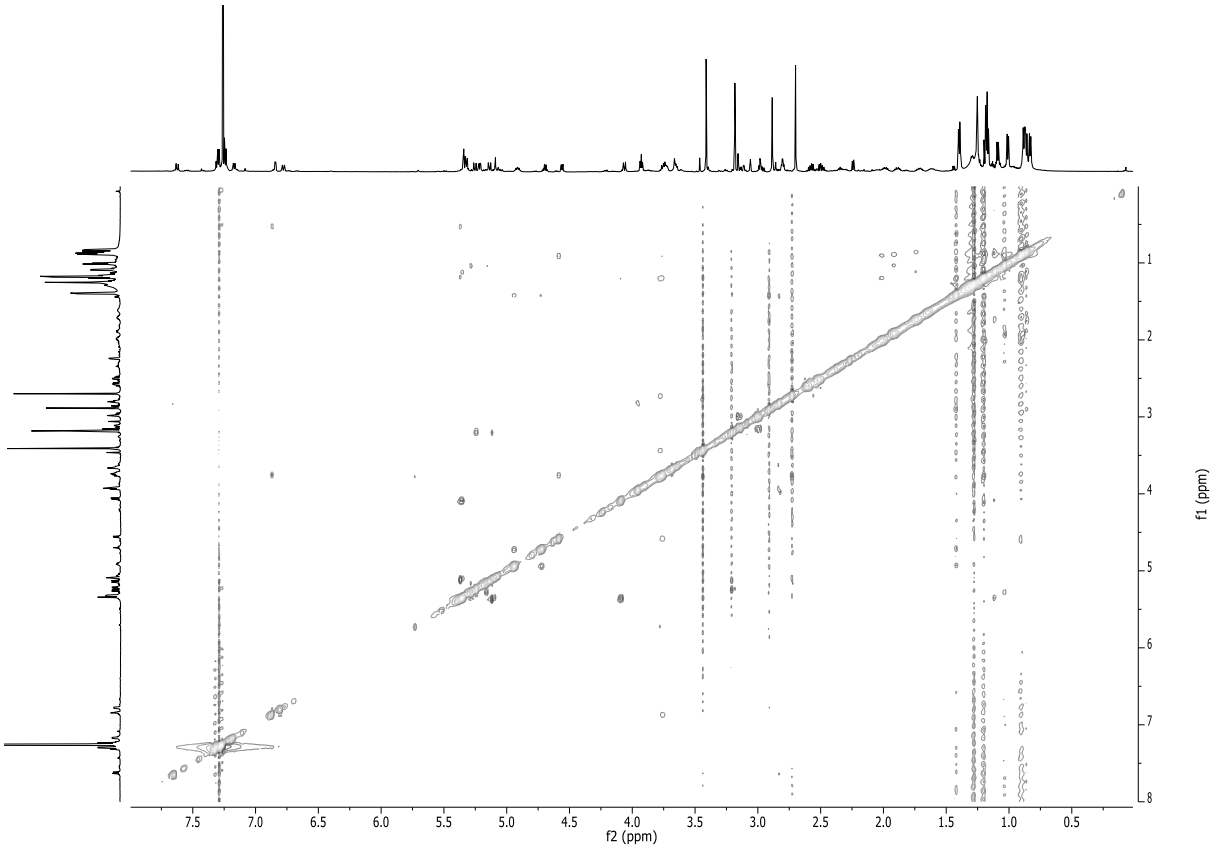

Figure 10-20: ROESY NMR spectrum (600 MHz $CDCl_3$) of **1** (FR-1).

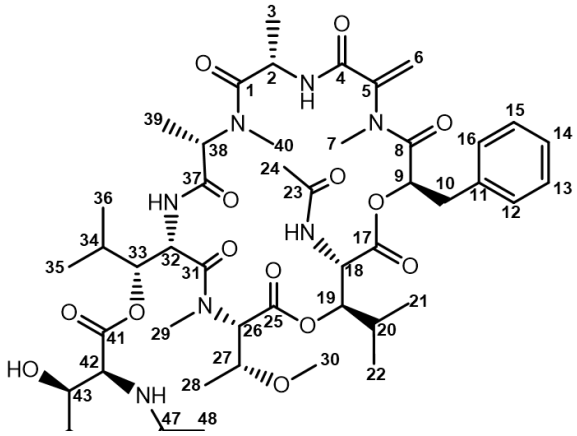

Scheme 10-3: Structure and numbering of C-atoms of **2** (FR-2).

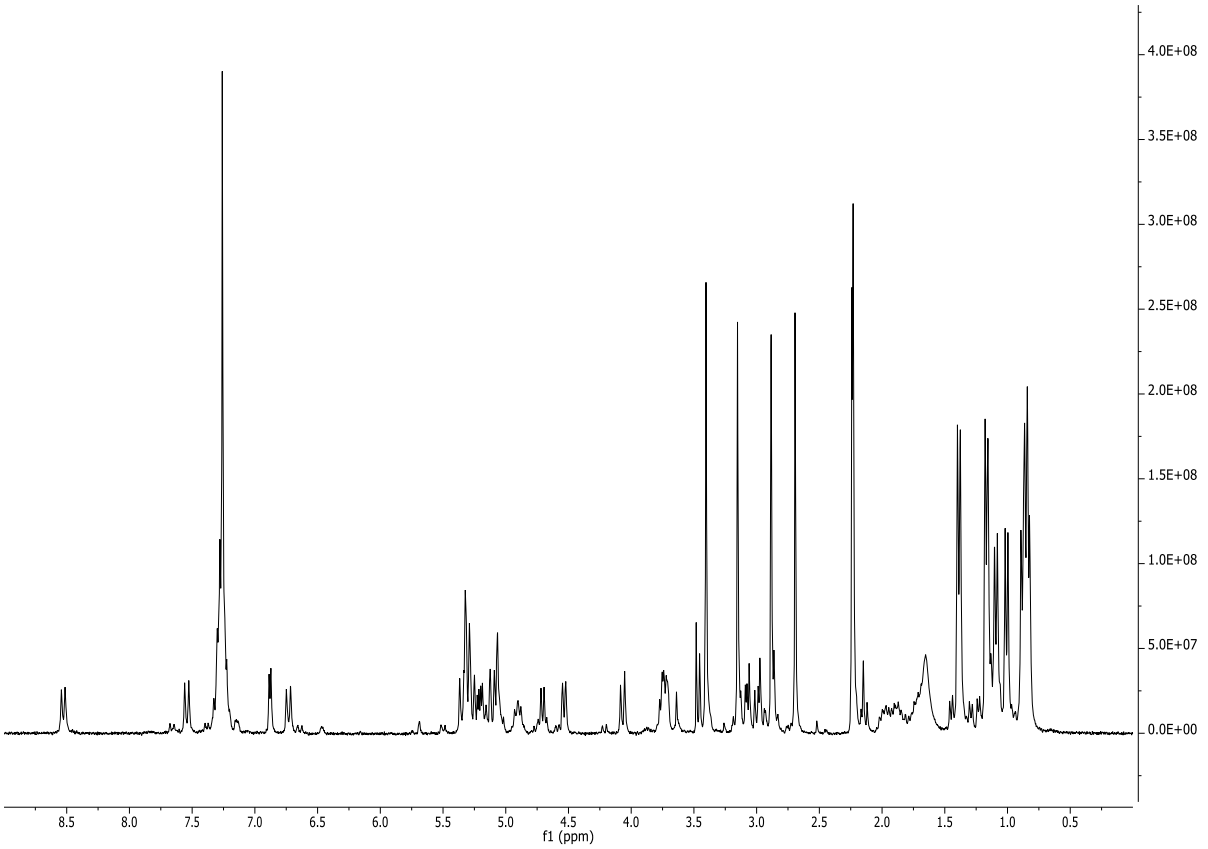

Figure 10-21: ^{1}H NMR spectrum (300 MHz $CDCl_3$) of **2** (FR-2).Assignments see **Table 10-3**.

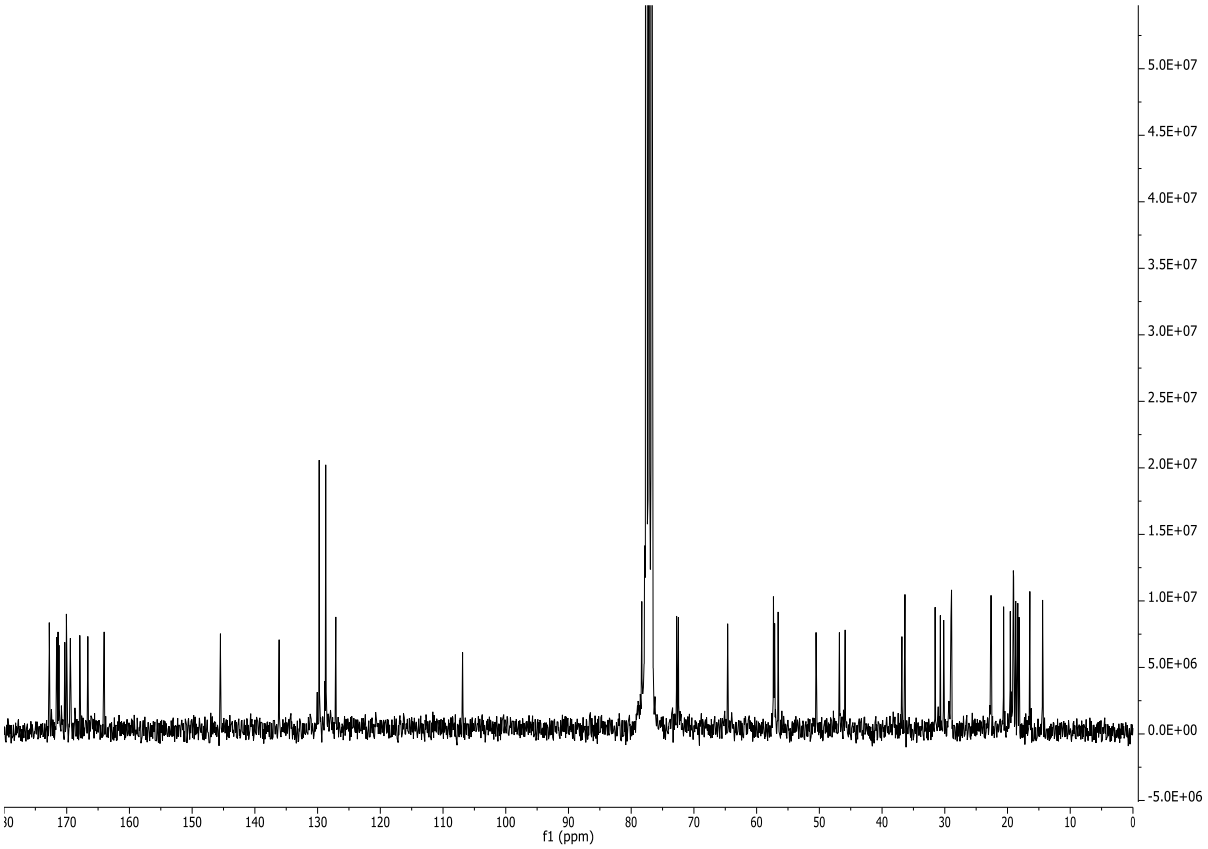

Figure 10-22: ^{13}C NMR spectrum (75 MHz $CDCl_3$) of **2** (FR-2). Assignments see **Table 10-3**.

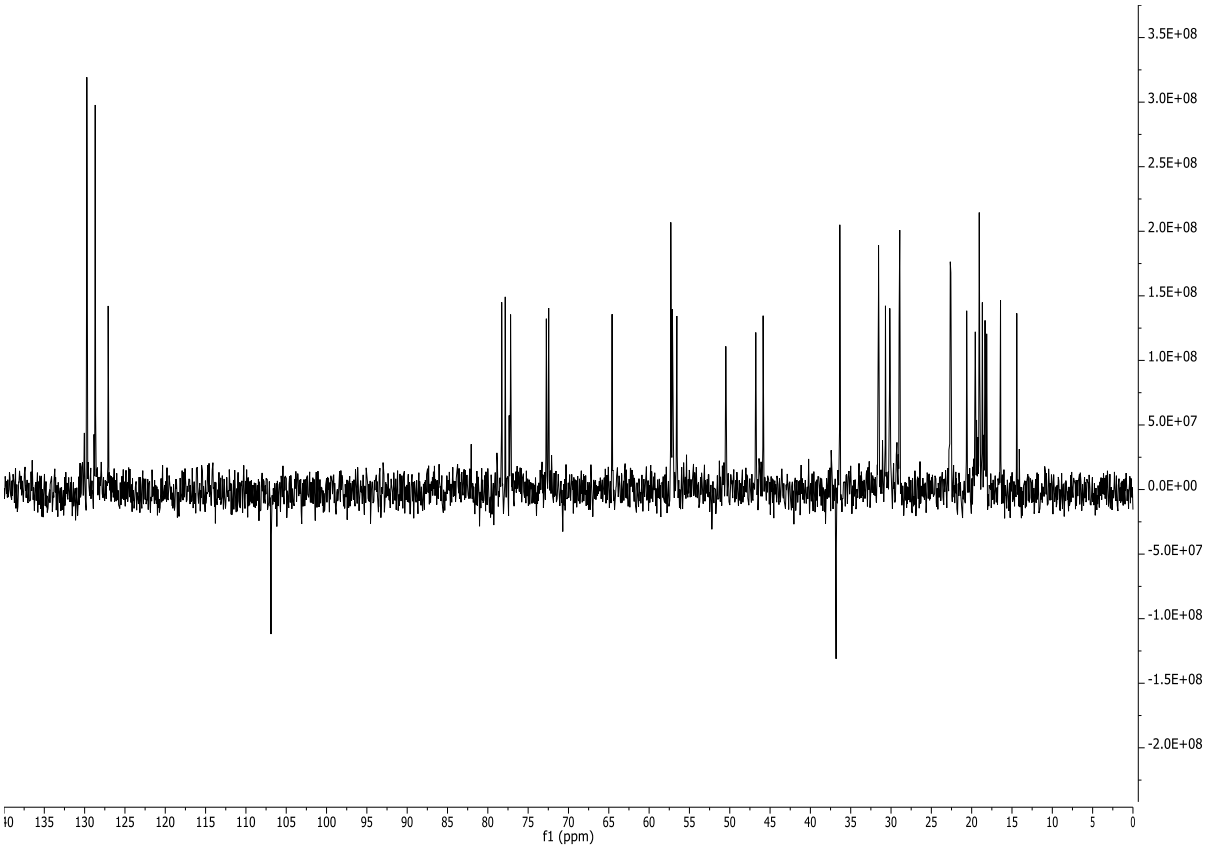

Figure 10-23: DEPT-135 NMR spectrum (75 MHz $CDCl_3$) of **2** (FR-2). Assignments see **Table 10-3**.

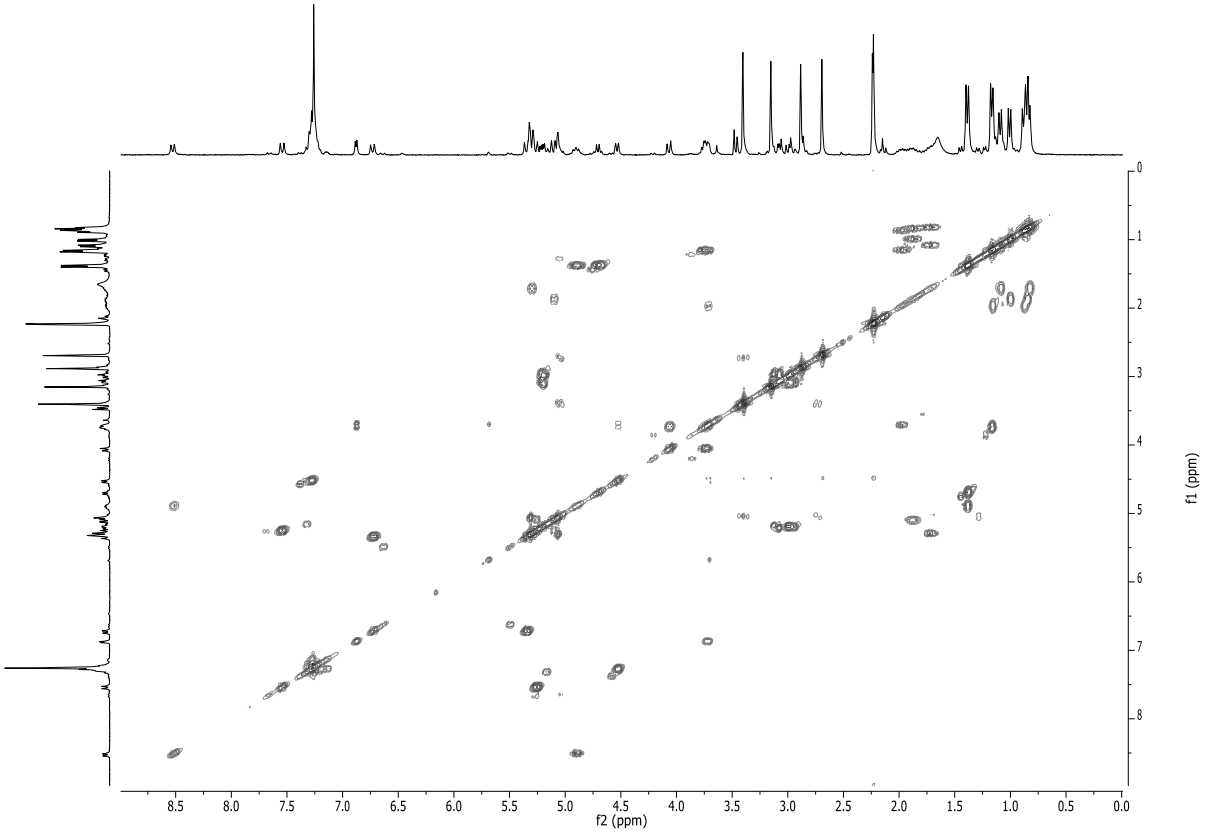

Figure 10-24: ^{1}H-^{1}H-COSY NMR spectrum (300 MHz $CDCl_3$) of **2** (FR-0).

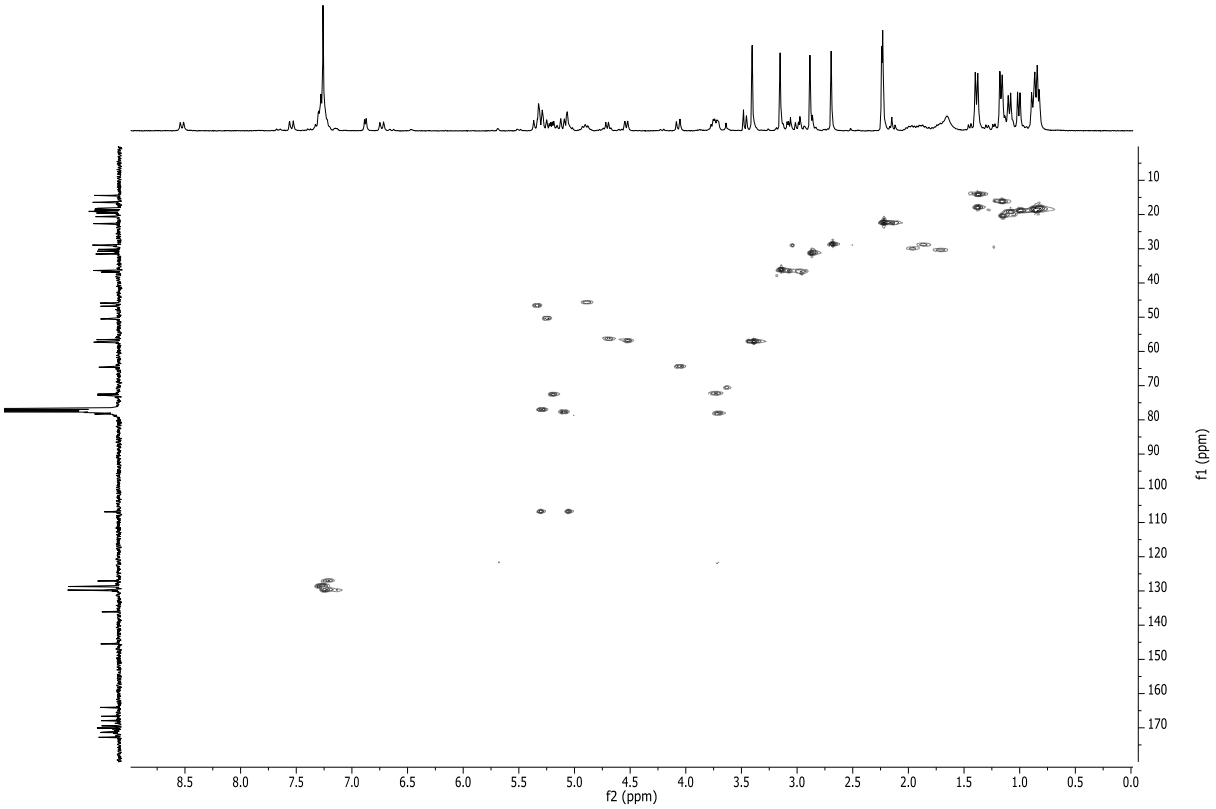

Figure 10-25: ^{1}H-^{13}C HSQC NMR spectrum (300 MHz $CDCl_3$) of **2** (FR-2).

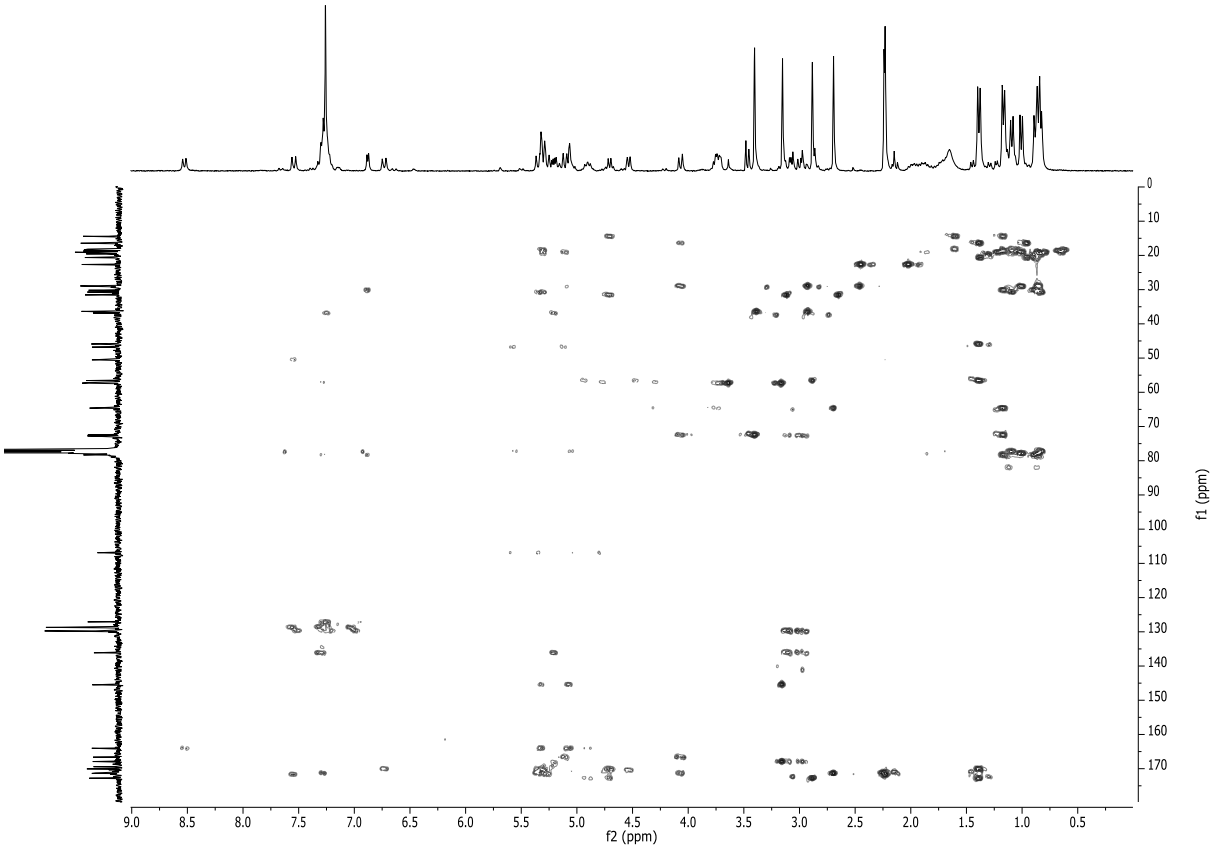

Figure 10-26: ^{1}H-^{13}C HMBC NMR spectrum (300 MHz $CDCl_3$) of **2** (FR-2).

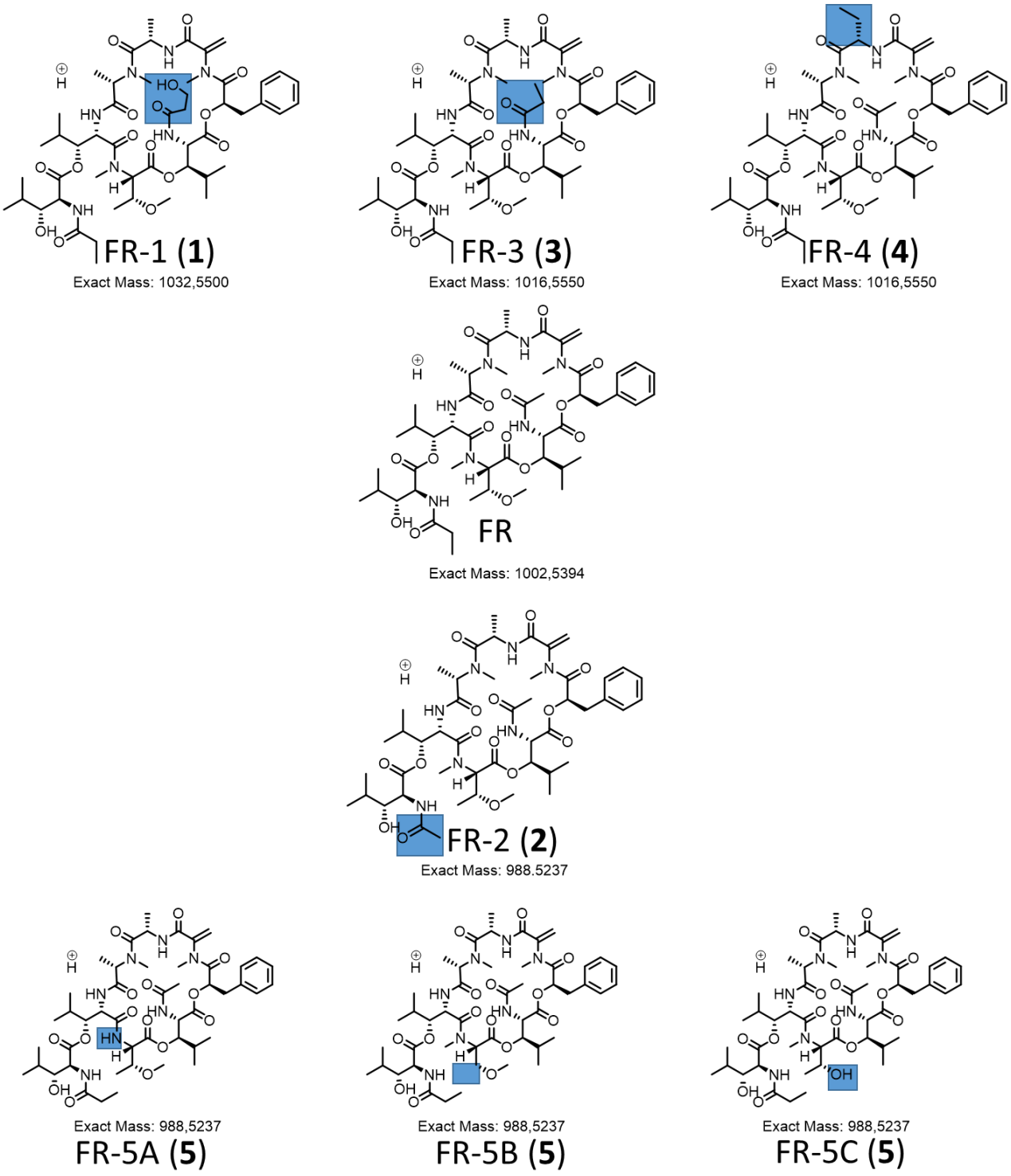

Scheme 10-4: Structures of FR900359 (FR), FR-1 (**1**), FR-2 (**2**), FR-3 (**3**), and FR-4 (**4**); putative structures of FR-5 (**5**), isomeric to **2**. (Putative) differences are highlighted (blue box). For **2** complete 1D and 2D NMR data exist, but are in submission process of another manuscript. Due to the limitations of LCMS² analysis for **5** we can only determine the residue *N*,*O*-dimethylthreonine to be modified by one missing methyl group. Hence, three chemically and biosynthetically reasonable structures remain.

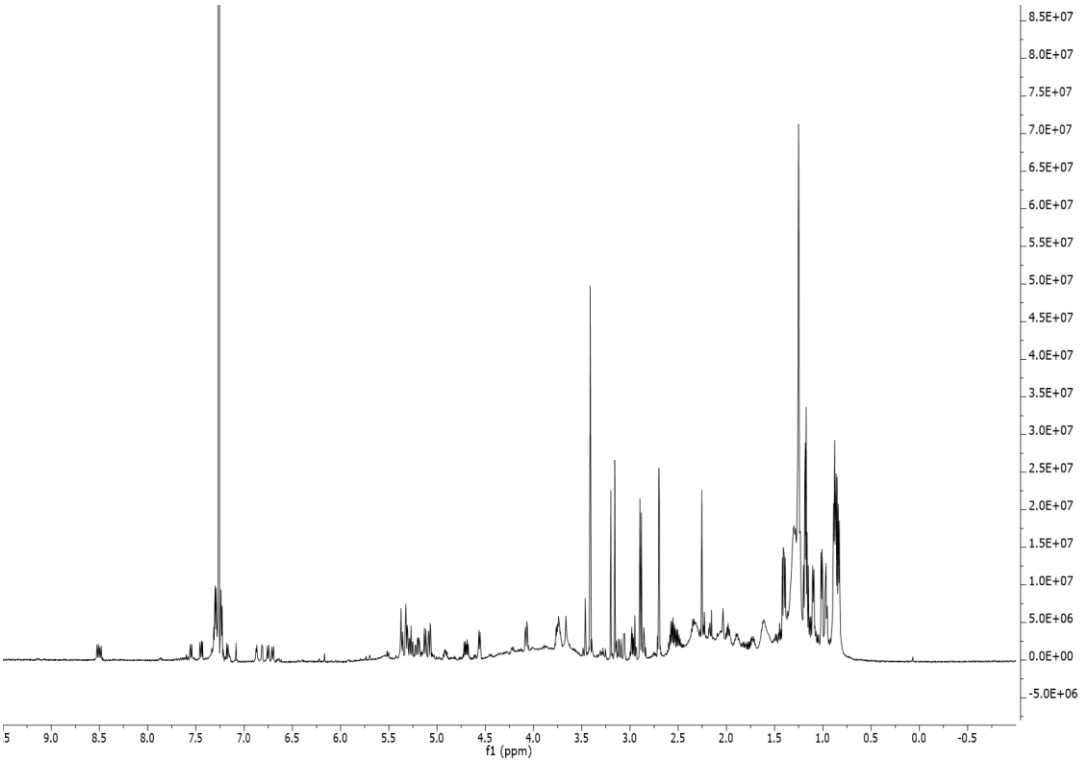

Figure 10-27: ^{1}H NMR spectrum (600 MHz $CDCl_3$) of FR-3 (**3**) and FR-4 (**4**), 1:1 mixture.

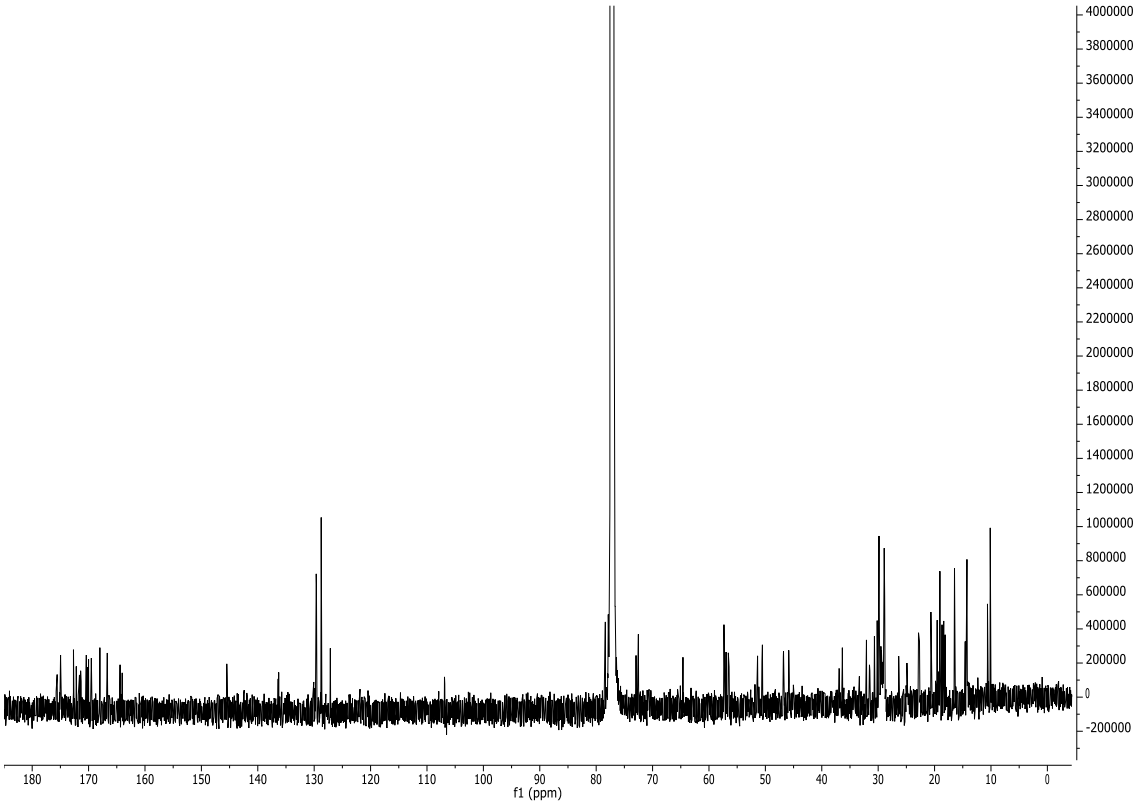

Figure 10-28: ^{13}C NMR spectrum (150 MHz $CDCl_3$) of FR-3 (**3**), and FR-4 (**4**), 1:1 mixture.

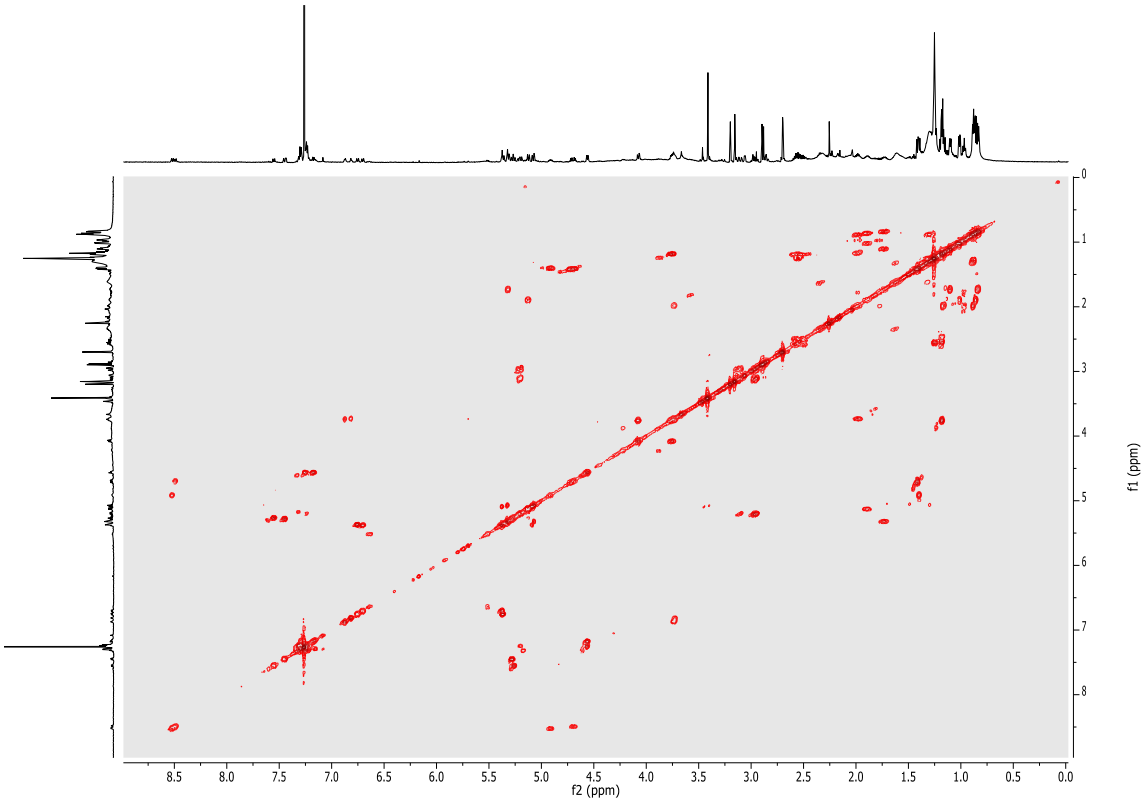

Figure 10-29: ^{1}H-^{1}H-COSY NMR spectrum (600 MHz $CDCl_3$) of FR-3 (**3**) and FR-4 (**4**), 1:1 mixture.

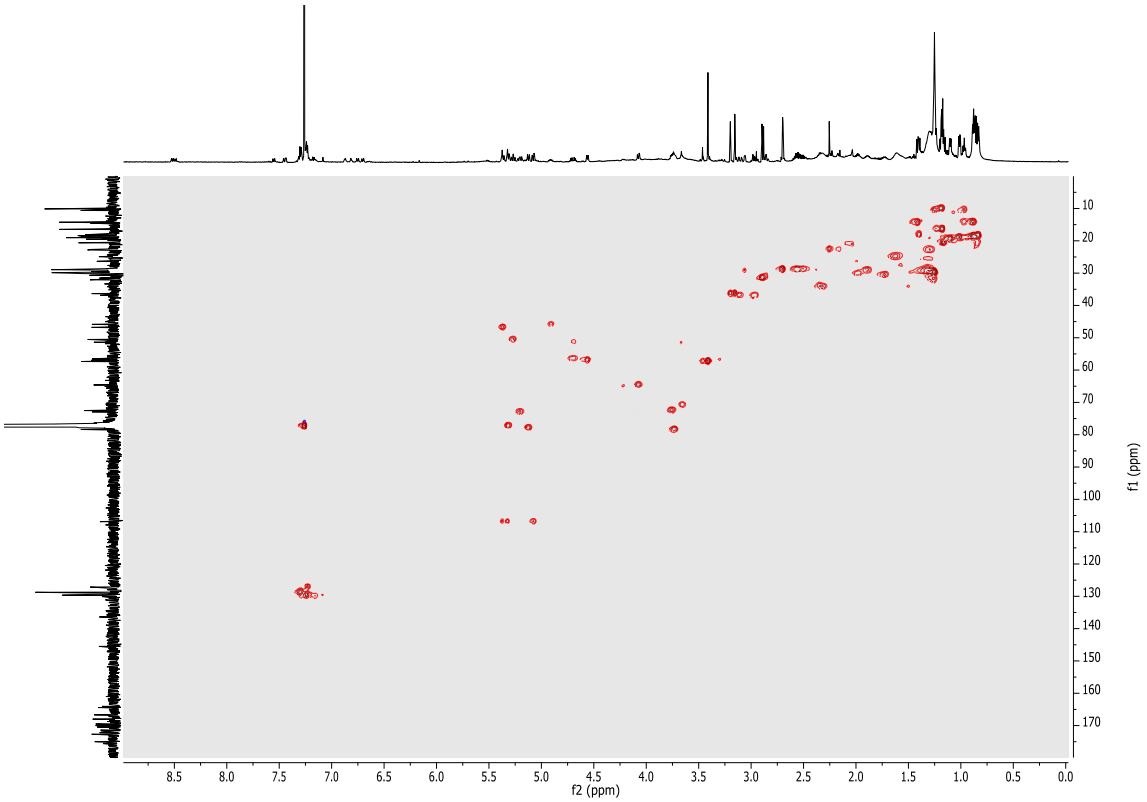

Figure 10-30: ^{1}H-^{13}C HSQC NMR spectrum (600 MHz $CDCl_3$) of FR-3 (**3**) and FR-4 (**4**), 1:1 mixture.

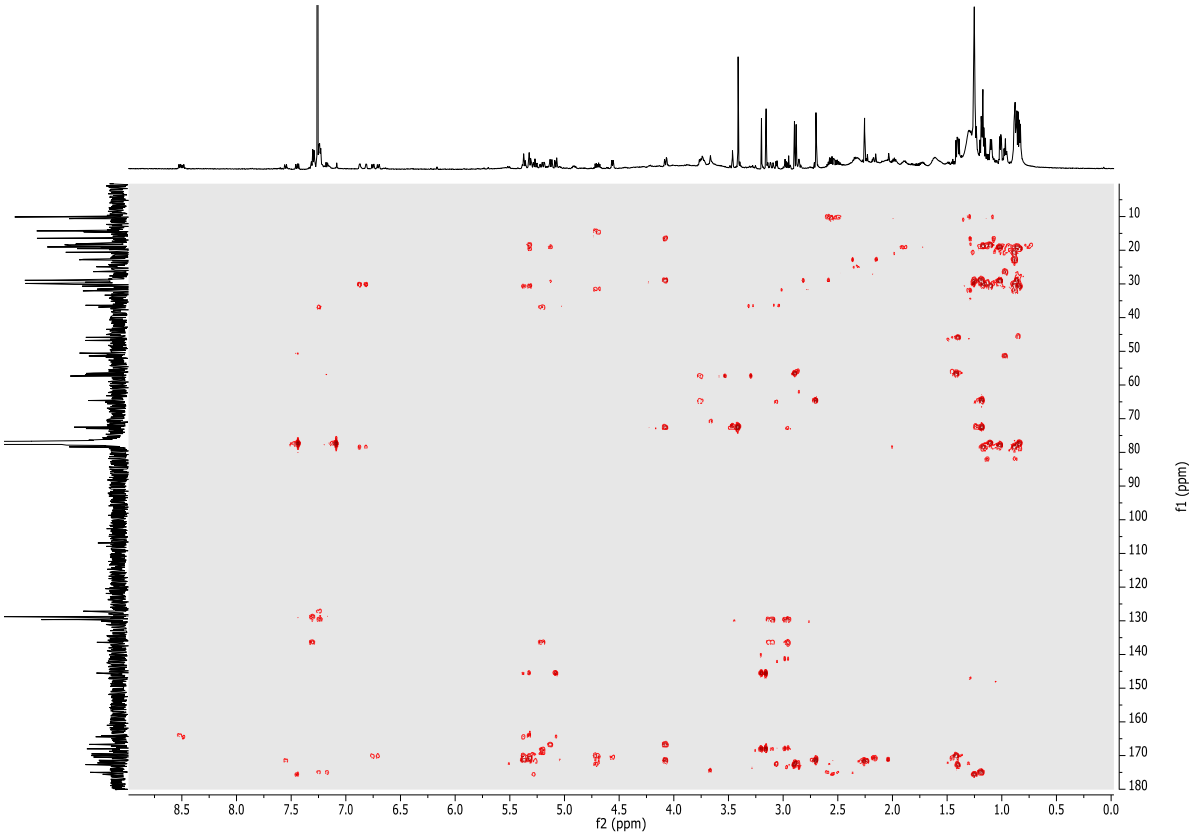

Figure 10-31: ^{1}H-^{13}C HMBC NMR spectrum (600 MHz $CDCl_3$) of FR-03 (**3**) and FR-4 (**4**), 1:1 mixture.

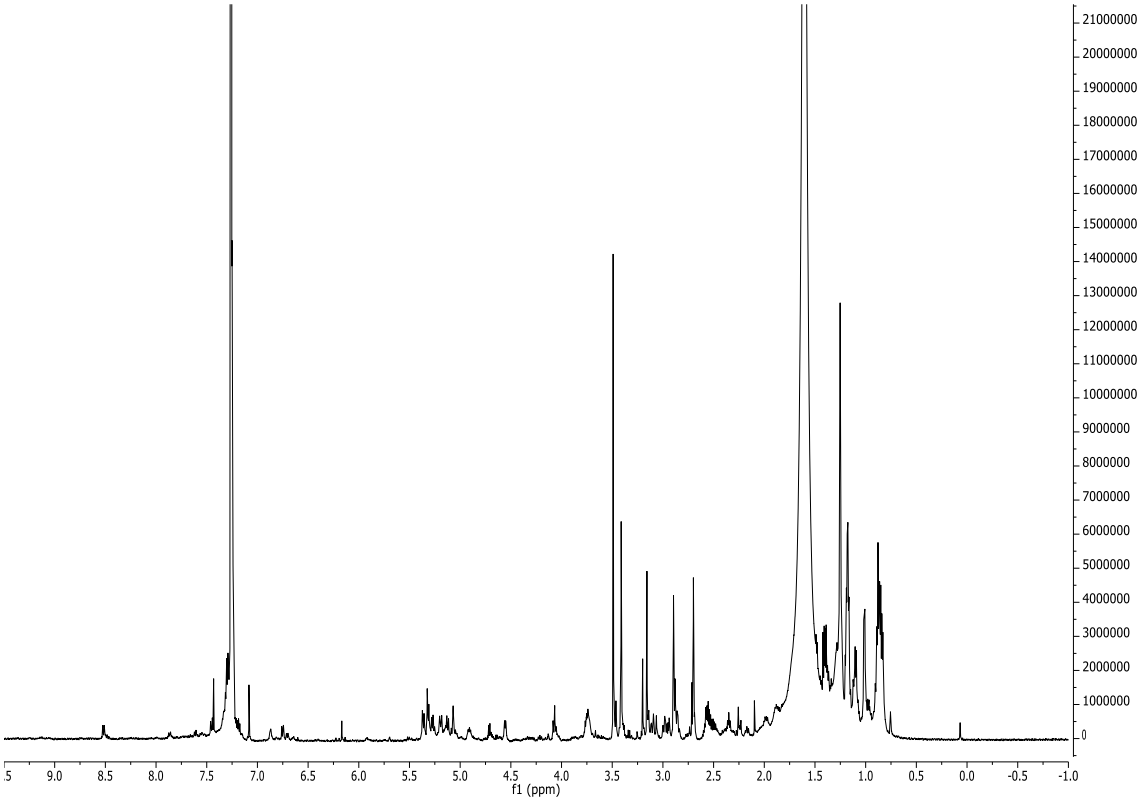

Figure 10-32: ^{1}H NMR spectrum (600 MHz $CDCl_3$) of FR-3 (**3**) and FR-4 (**4**), 3:1 mixture.

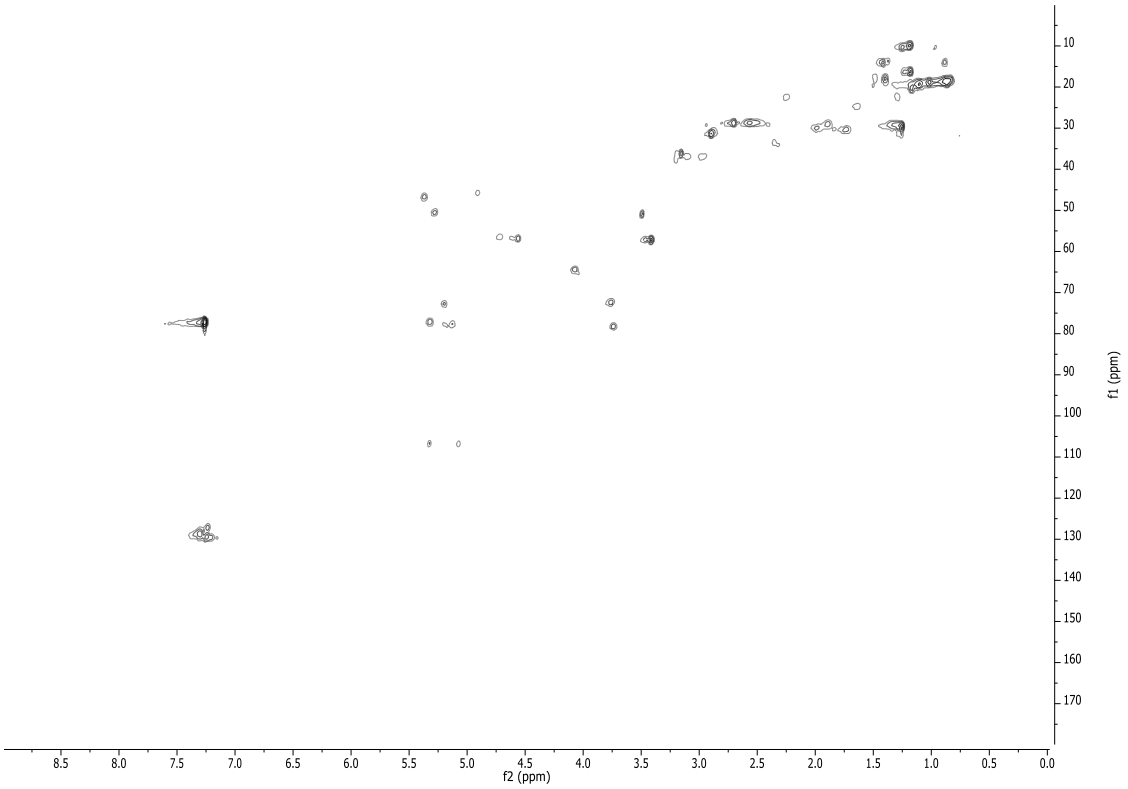

Figure 10-33: ^{1}H-^{13}C HSQC NMR spectrum (600 MHz $CDCl_3$) of FR-3 (**3**) and FR-4 (**4**), 3:1 mixture.

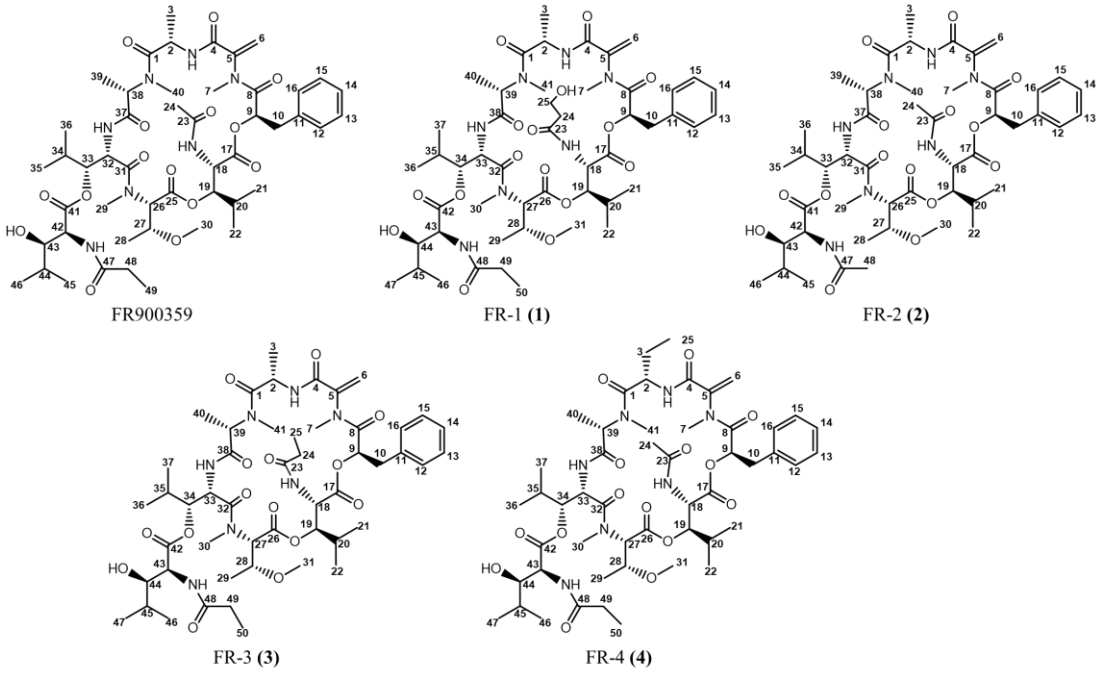

Scheme 10-5: Structures and numbering of FR900359 (FR), FR-1 (**1**), FR-2 (**2**), FR-3 (**3**), and FR-4 (**4**).

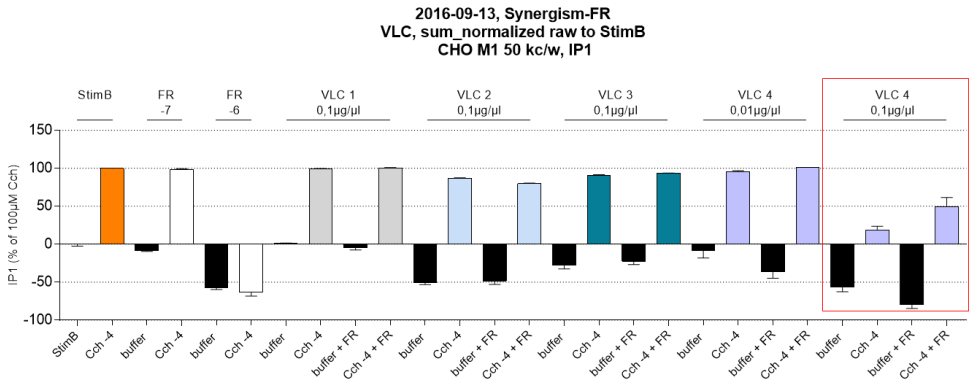

Figure 10-34: Results of the second messenger assays. Agonist induced IP1 production of CHO M1 cells after pretreatment with either vacuum liquid chromatography fractions VLC1 to VLC4 alone or in combination with a subliminal concentration of FR900359. Mean values ± s.e.m. of up to two independent experiments. Experiments performed by Tobias Benkel, Kostenis lab, Institute for Pharmaceutical Biology, Univ. of Bonn.

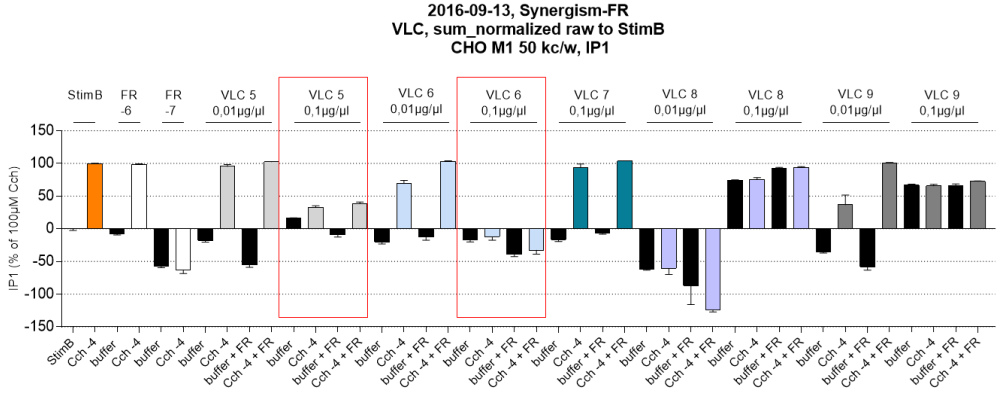

Figure 10-35: Results of the second messenger assays. Agonist induced IP1 production of CHO M1 cells after pretreatment with either vacuum liquid chromatography fractions VLC5 to VLC9 alone or in combination with a subliminal concentration of FR900359. Mean values ± s.e.m. of up to two independent experiments. Experiments performed by Tobias Benkel, Kostenis lab, Institute for Pharmaceutical Biology, Univ. of Bonn.

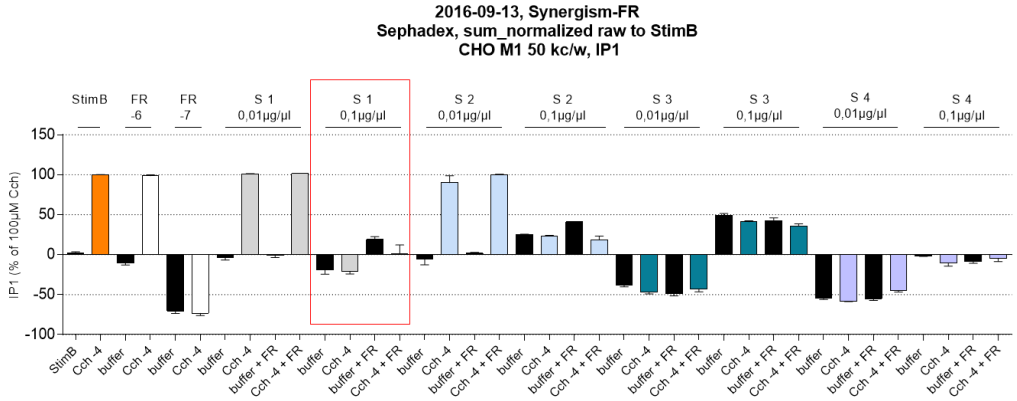

Figure 10-36: Results of the second messenger assays. Agonist induced IP1 production of CHO M1 cells after pretreatment with either Sephadex fractions S1 to S4 alone or in combination with a subliminal concentration of FR900359. Mean values ± s.e.m. of up to two independent experiments. Experiments performed by Tobias Benkel, Kostenis lab, Institute for Pharmaceutical Biology, Univ. of Bonn.

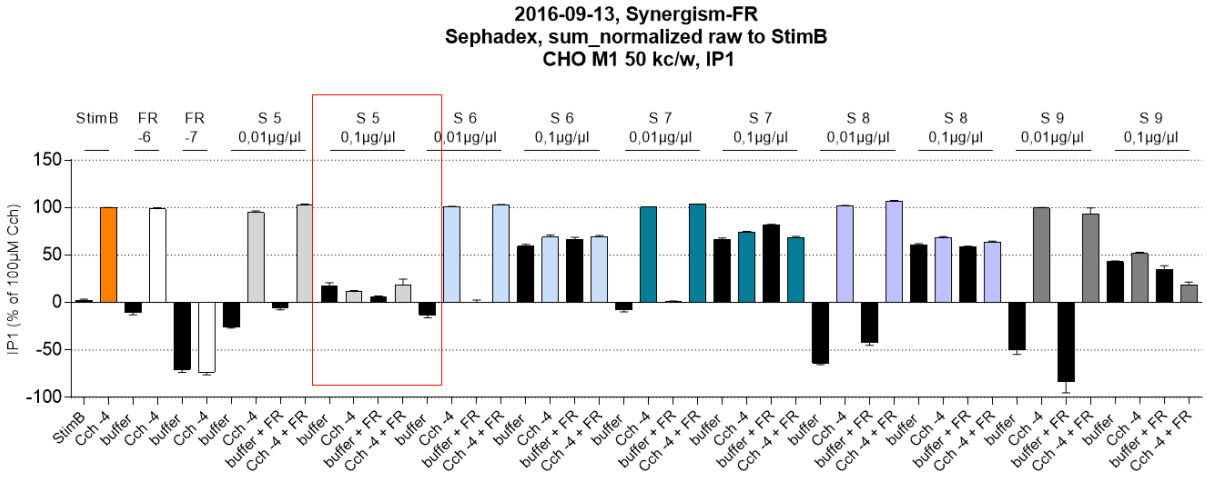

Figure 10-37: Results of the second messenger assays. Agonist induced IP1 production of CHO M1 cells after pretreatment with either Sephadex fractions S5 to S9 alone or in combination with a subliminal concentration of FR900359. Mean values ± s.e.m. of up to two independent experiments. Experiments performed by Tobias Benkel, Kostenis lab, Institute for Pharmaceutical Biology, Univ. of Bonn.

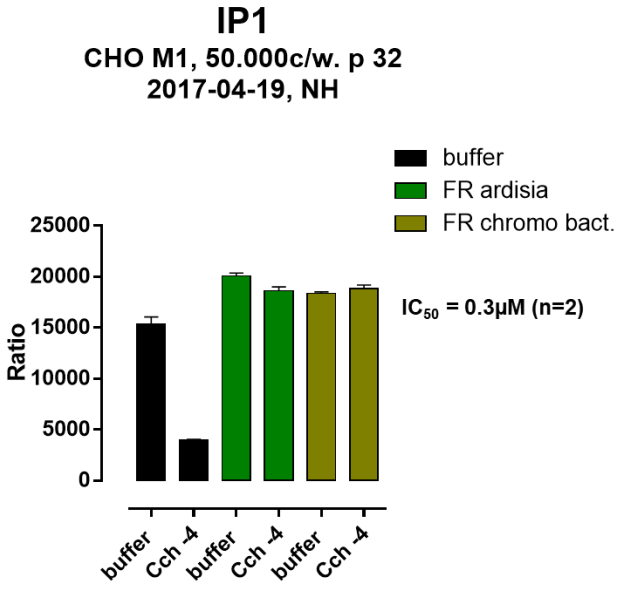

Figure 10-38: Results of the second messenger assays. Agonist induced IP1 production of CHO M1 cells after pretreatment with FR either isolated from *A. crenata* or *C. vaccinii*. Mean values ± s.e.m. of two independent experiments. Experiments performed by Nina Heycke, Kostenis lab, Institute for Pharmaceutical Biology, Univ. of Bonn.

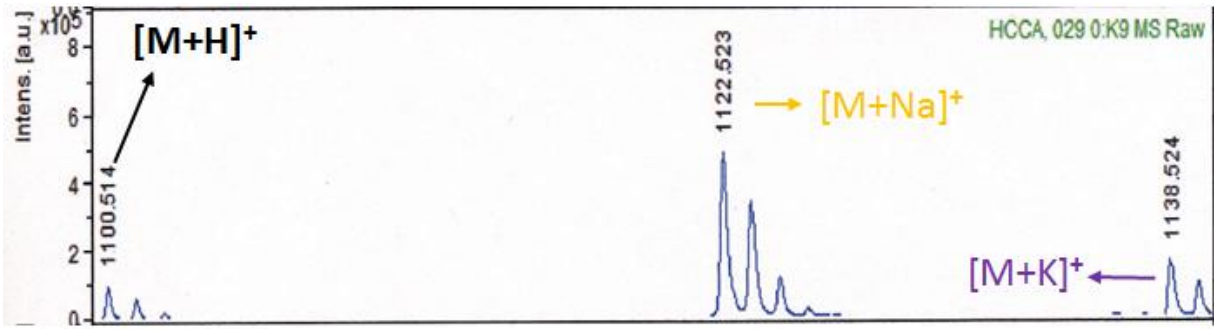

Figure 10-39: MALDI-TOF measurement of FR-Hex (11). α-cyano-4-hydroxycinnamic acid (HCCA) was used as matrix material.

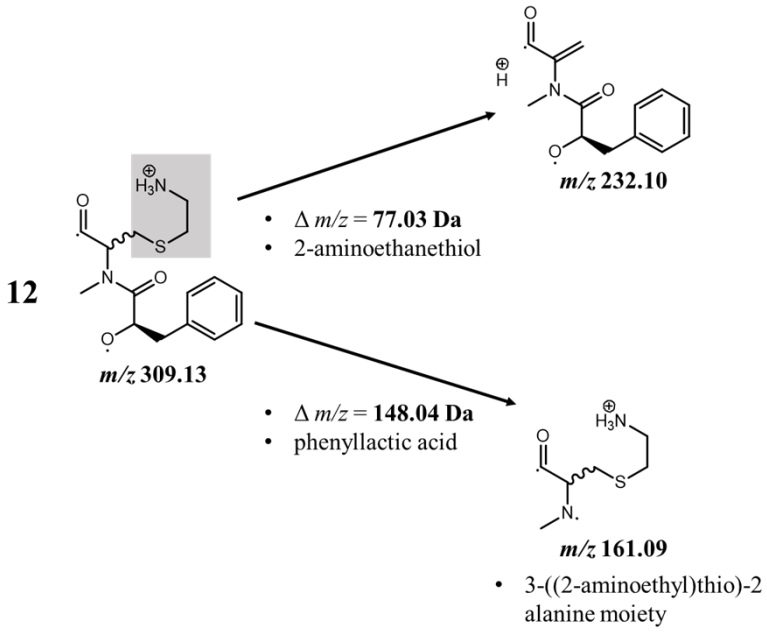

Scheme 10-6: Fragmentation pathways of first-generation (MS^2) product ions obtained from **12**. The modified *m/z* 309.13 (**12**) loses phenyllactic acid *Δm/z* 148.04 Da or only the modified 2-aminoethanethiol residue *Δm/z* 77.03 Da, resulting in the single modified amino acid *N*-methyl-((2-aminoethyl)thio)-2-alanine *m/z* 161.09 only occurring in **12** (not in FR) or A''-F' dipeptide residue, *m/z* 232.10, respectively.

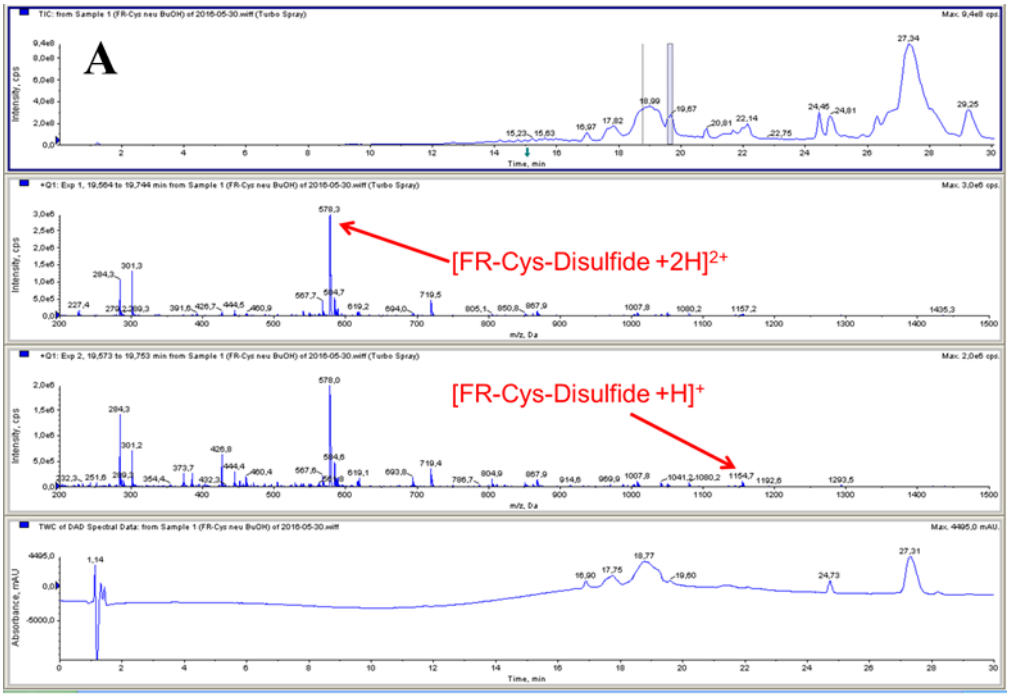

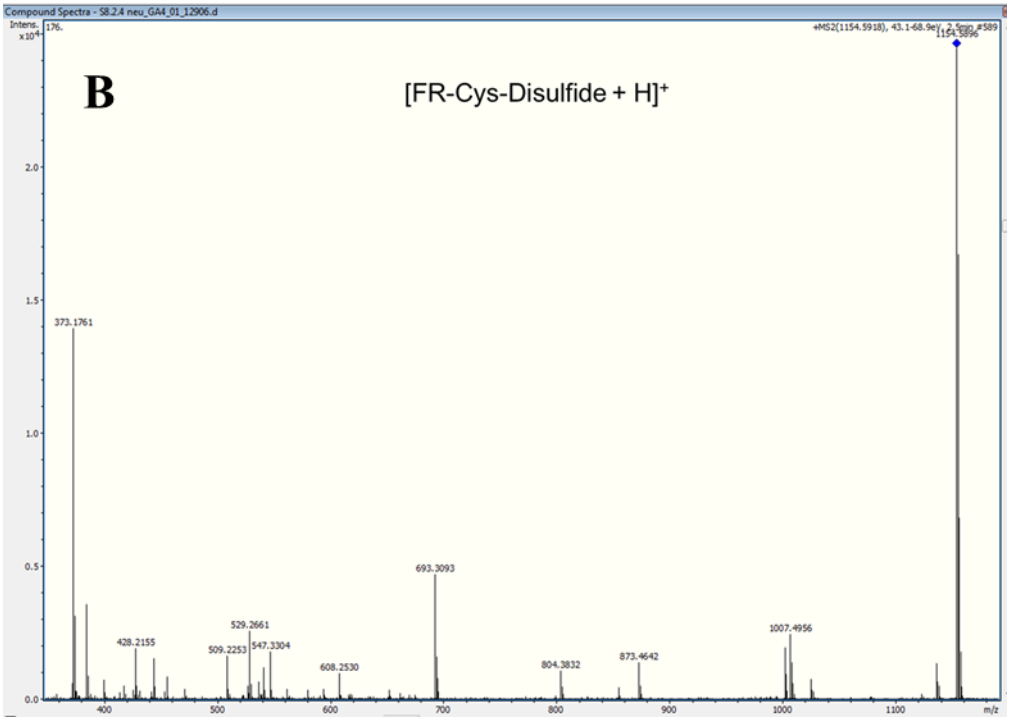

Figure 10-40: FR-Cys-Disulfide Michael addition product indicated by mass spectrometry. (**A**) LCMS measurement of compound **12** crude reaction mixture. (B) MS^2 spectrum of *m/z* 1154.58 = putative $[M+H]^+$ ion of FR-Cys-Disulfide.

Table 10-2: Analytical data of depsipeptides and peptides used in this study.

Peptide No.	Peptide sequence	M_w / (M_w calc.) [g/mol]	preparative HPLC t_r [min]	analytical HPLC t_r [min]*	TLC R_f
1	cyclo-[OHCH$_2$CH$_2$CO-β-HyLeu-D-Pla-*N*-MeDha-Ala-*N*-MeAla-β-HyLeu(Pr-β-HyLeu)-*N*-MeThr(*O*Me)]	1032.54[a] (1031.54)	23.73[d]	58.16[k]	0.80[o] 0.87[p]
2	cyclo-[Ac-β-HyLeu-D-Pla-*N*-MeDha-Ala-*N*-MeAla-β-HyLeu(Ac-β-HyLeu)-*N*-MeThr(*O*Me)]	988.51[a] (987.52)	23.01[d]	60.01[k]	0.78[o] 0.89[p]
11	cyclo-[Ac-β-HyLeu-D-Pla-*N*-MeDha-Ala-*N*-MeAla-β-HyLeu(Pr-β-HyLeu(*O*CO(CH$_2$)$_4$CH$_3$))-*N*-MeThr(*O*Me)]	1120.60[b] (1090.61)	13.12[e]	62.25[k]	0.87[o] 0.87[p]
12	cyclo-[Ac-β-HyLeu-D-Pla-*N*-Me-D/L-(C$_\alpha$CH$_2$S(CH$_2$)$_2$NH$_2$)-Gly-Ala-*N*-MeAla-β-HyLeu(Pr-β-HyLeu)-*N*-MeThr(*O*Me)]	1079.57[a] (1078.56)	27.21[f]	49.34[l]	0.82[o]
13	cyclo-[Ala-*N*-MeAla-Lys(Ac)-Thr(*O*Me)-Thr(*O*Me)-D-Phe-*N*-MeAla]	789.44[a] (788.44)	71.56[g]	14.11[l]	0.58[o] 0.77[p]
14	cyclo-[Ala-*N*-MeAla-Lys(Ac)-Thr(*O*Me)-Thr(*O*Me)-Phe-*N*-MeAla]	789.45[a] (788.44)	81.59[h]	16.54[l]	0.59[o] 0.79[p]
15	cyclo-[Ala-Ala-Lys(Ac)-Thr(*O*Me)-Thr(*O*Me)-D-Phe-Ala]	761.42[a] (760.41)	93.79[i]	12.46[l]	0.55[o] 0.75[p]
17	cyclo-[Ala-Ala-Lys(Ac)-Thr(*O*Me)-Thr(*O*Me)-Phe-Ala]	761.44[a] (760.41)	73.67[h]	15.32[l]	0.55[o] 0.72[p]
18	cyclo-[Ala-*N*-MeAla-Leu-Thr(*O*Me)-Thr(*O*Me)-D-Phe-*N*-MeAla]	732.44[a] (731.42)	78.56[i]	24.28[l]	0.68[o] 0.76[p]
19	cyclo-[Ala-*N*-MeAla-Leu-Thr(*O*Me)-Thr(*O*Me)-Phe-*N*-MeAla]	732.43[a] (731.42)	87.16[h]	24.19[l]	0.54[o] 0.75[p]
20	cyclo-[Ala-Ala-Leu-Thr(*O*Me)-Thr(*O*Me)-D-Phe-Ala]	704.40[a] (703.39)	88.69[h]	19.40[l]	0.55[o] 0.76[p]
21	cyclo-[Ala-Ala-Leu-Thr(*O*Me)-Thr(*O*Me)-Phe-Ala]	704.39[a] (703.39)	98.96[h]	42.8[m]	0.55[o] 0.76[p]
22	cyclo-[Ahx-*N*-Me-D-Phe-Ado-Dap(Ac-Thr)]	647.32[c] (648.35)	65.15[g]	20.67[m]	0.64[o] 0.75[p]
23	cyclo-[Ahx-*N*-Me-D-Phe-Ado-β-HyLeu]	549.32[a] (548.32)	71.16[j]	36.04[n]	0.73[o] 0.63[p]

MS-peaks were detected as [a][M+H]$^+$, [b][M+Na]$^+$, or [c][M-H]$^-$. Peptides were detected with LC-ESI-MS. Purification was performed using semipreparative RP-HPLC: [d]75% eluent D isocratic for 20 min, then 75-100% in 15 min, [e]70-100% eluentF in 30 min, [f]57% eluent D isocratic for 35 min, [g]10–60 % eluent B in 120 min, [h]0–50 % eluent B in 120 min, [i]20–70 % eluent B in 120 min, and [j]15–65 % eluent B in 120 min. For analytical RP-HPLC the following gradients were used: [k]0–80 % eluent B in 80 min, [l]0–60 % eluent B in 60 min, [m]10–50 % eluent B in 40 min, and [n]0–50 % eluent B in 60 min. TLC was performed with systems containing: [o]*n*-butanol/acetic acid/water (48:18:24, v/v) and [p]*n*-propanol/25% NH3 (7:3). *All peptides were >95 % HPLC pure.

Table 10-3: Energy and structural statistics of the NMR ensembles of FR900359, **13**, and **22** (10 lowest energy structures). Maximum distance restraints violations were < 0.026 Å for **13**, < 0.043 Å for **22** and < 0.07 Å for FR.

Peptide	**FR900359**	**5**	**13**
Distance restraints	100	40	38
Dihedral angle restraints	11	9	3
Structure statistics			
Violations	in kJ/mol		
Total restraint violation energy	1.266	0.439	0.411
Distance restraints	1.266	0.080	0.411

Dihedral angle restraints	0	0.360	0
Total Force field energy (Yasara)	-51	-904	-938
Internal solute energy	574	-209	-290
Electrostatic solv. energy	-415	-511	-518
Van der Waals solv. energy	-212	-184	-131
Mean RMSD (Å)	Mean (s.d.)		
Backbone global	0.18 (± 0.10)	0.74 (± 0.25)	
Heavy atoms	0.48 (± 0.14)	0.83 (± 0.20)	0.71 (± 0.18)

Table 10-4: Temperature coefficients for FR900359 in MeOH/H2O/D2O (v:v:v/ 1:1:0.2, 1H: 500 MHz).

NH of residue	**Temperature coefficient** **Δδ/ΔT** (-ppb/K)
N-Ac-β-HyLeu-1	12.31
N-Pr-β-HyLeu-2	7.62
β-HyLeu	-0.003

Table 10-5: Overview of inhibitor binding energies and inhibitor dissociation times tdiss calculated from docking, regular MD and steered MD (n.o. – not observed)

	E_{bind} (kJ/mol) Vina	$E_{binding}$ (kJ/mol) MD	t_{diss} (ns) MD	t_{diss}^0 (ns) at 0 acceleration sMD
FR	40.8	135	n.o.	0.9
YM	41.2	142	n.o.	1.1
FR-L-Cys	40.3	174	425	2.3
FR-D-Cys (I)	33.8	98	12	0.17
FR-D-Cys (II)	33.4	61	20	0.23
FR-L-BP	37.3	189	n.o.	1.8
FR-D-BP	31.6	330	n.o.	0.7

Binding energies were calculated with Yasara from a separate 10 ns molecular dynamics simulation using the following formula:

$$E_{binding} = \left(E_{internal}^{protein} + E_{internal}^{inhibitor} + E_{solvation}^{protein} + E_{solvation}^{inhibitor}\right) - \left(E_{internal}^{complex} + E_{solvation}^{complex} + E_{surface}^{accessible} \times 0.65\right)$$

where E – energy, A – area in Å^2, and 0.65 is a guestimate of the entropic cost of exposing one Å^2 to the solvent. E_{bind} was calculated as an average value derived from the individual simulation snapshot. Each individual simulation snapshot was energy minimized before the E_{bind} calculation using the Amber14 force field parameters. Starting structures were the same as for the sMD simulations. Integration time steps for intra-molecular and inter-molecular forces were 1.25 fs and 2.5 fs, respectively. All other parameters were identical with the simulations described above.

Table 10-6: Overview of simulation times of the regular MD runs used to generate the starting structures for sMD simulations

	time
FR	5 ns
YM	5 ns
FR-L-Cys	40 ns
FR-D-Cys (I)	5ns
FR-D-Cys (II)	5ns
FR-L-BP	10 ns
FR-D-BP	100 ns

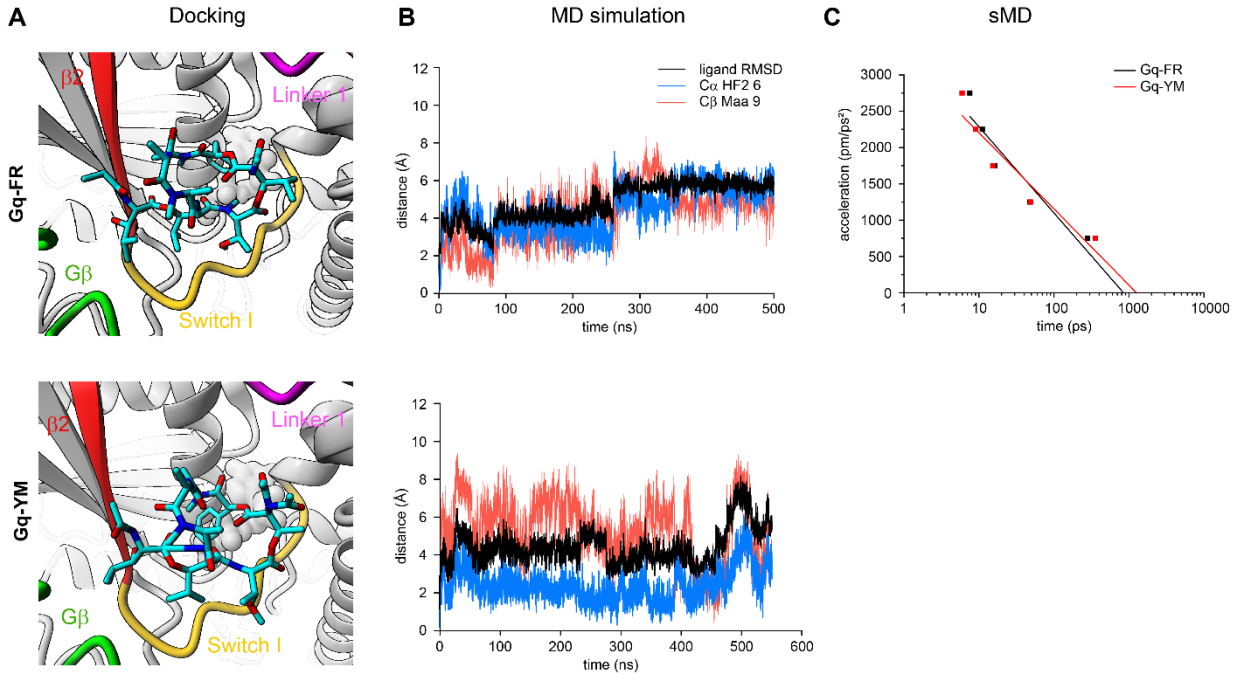

Figure 10-41: (A) Gq-bound FR and YM (pdb 3ah8) derived from molecular docking with the switch I (yellow), linker 1 (magenta) and β2 (red) region of the Gαq subunit. Gβ subunit is indicated in green. FR and YM are shown as stick model (color code: carbon – cyan, nitrogen – blue, oxygen – red, sulfur – green) (**B**) ligand RMSD (root mean square deviation – black trace) and relative distance of two ligand atoms (Cα HF6 – blue trace, Cβ Maa9 – red trace) with respect to their starting (bound) position during all-atom MD simulation. (**C**) steered MD profiles of ligand unbinding showing the time required to separate FR (black trace and squares) and YM (red trace and squares) from the protein.

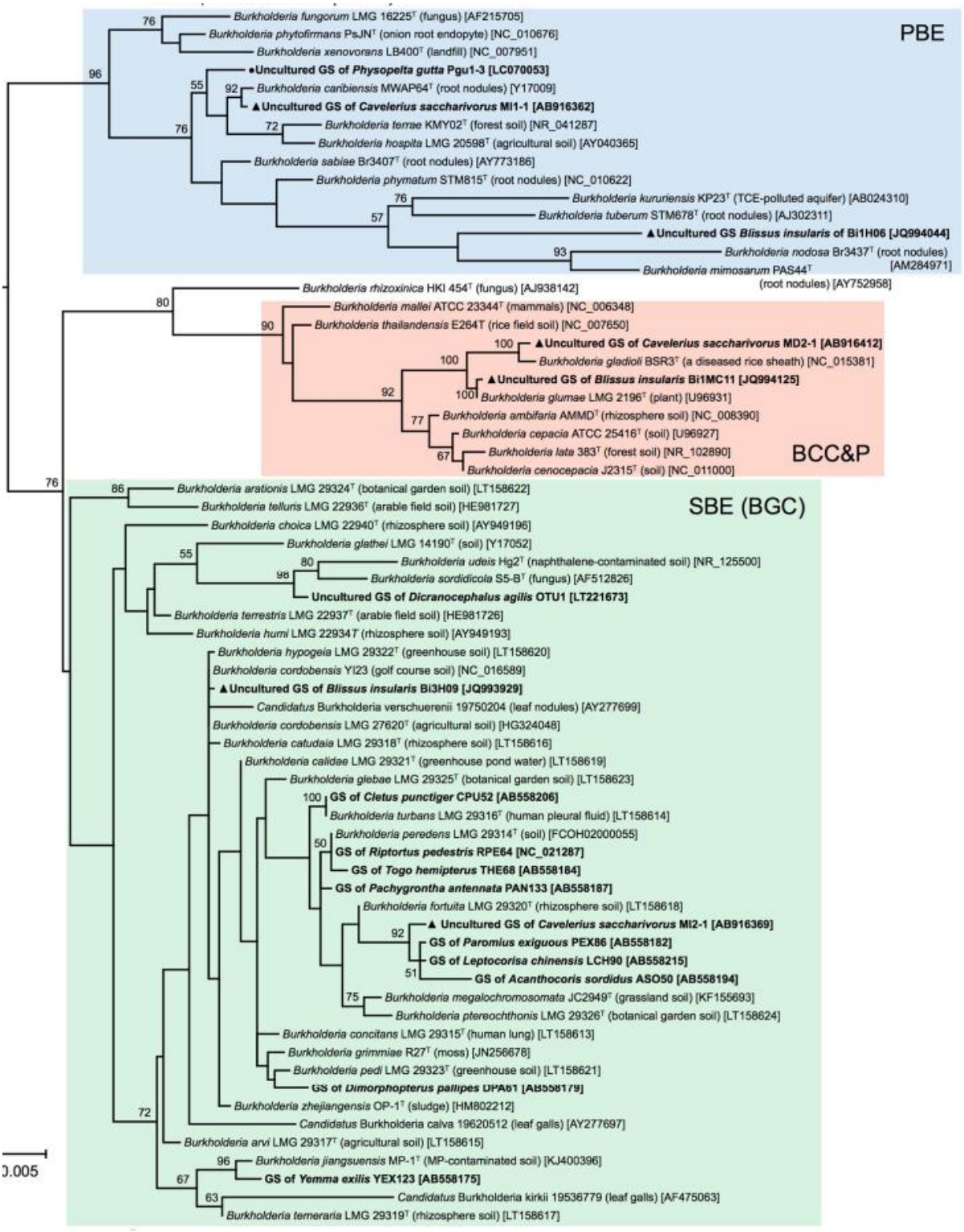

Figure 10-42: Figure taken from Takeshita *et al*.[244] 16S rRNA gene sequences of selected *Burkholderia* species/strains and *Pandoraea pulmonicola* LMG 18106T as outgroup were aligned by using MAFFT v7.273 (L-INS-i)[245]. Gap-including and ambiguous sites in the alignments were then removed, resulting in the final alignment data with 1,317 nucleotide sites. Phylogenetic relationships were reconstructed with RAxML v8.2.3[246] using the GTR+Γ model of nucleotide protein substitution and maximum likelihood method. The bootstrap support values of 1,000 replicates were calculated and values higher than 50% are depicted at the nodes. The main *Burkholderia* clades, BCC&P, PBE and SBE/BGC, are respectively shown in red, blue and green. The gut symbionts of stink bugs are shown in bold, and those of *Largidae* and *Bllisidae* are indicated by a circle and triangle, respectively. The isolation sources of the *Burkholderia* and accession numbers in the DNA database (DDBJ/EMBL/GenBank) are represented in parentheses and square brackets, respectively. GS: gut symbiont.

Table 10-7: PCR results of endosymbiotic bacteria of *A. lucida* equally distributed over the whole leaf.

Sequencing results:

Primers tested	Amplification	Blast result	Comments
16S_27F 16S_1492R	Positive	Ardisia polysticta chloroplast Identity 99% Accession KC465962.	
16S_BurkF 16S_BurkR	Positive	Burkholderia sp. DHC34 16S Identity 96% Accession KP938219.1	The sequence has indeterminations. Needs to be confirmed after clonning the product.
16S_BurkF_seq 16S_BurkR_seq	Negative		
gyrBF gyrBR	Positive	Agromyces flavus strain CPCC 202695 Identity 80% Accession LT629755.1	The sequence has indeterminations. Needs to be confirmed after clonning the product.
RecAF RecAR	Negative		

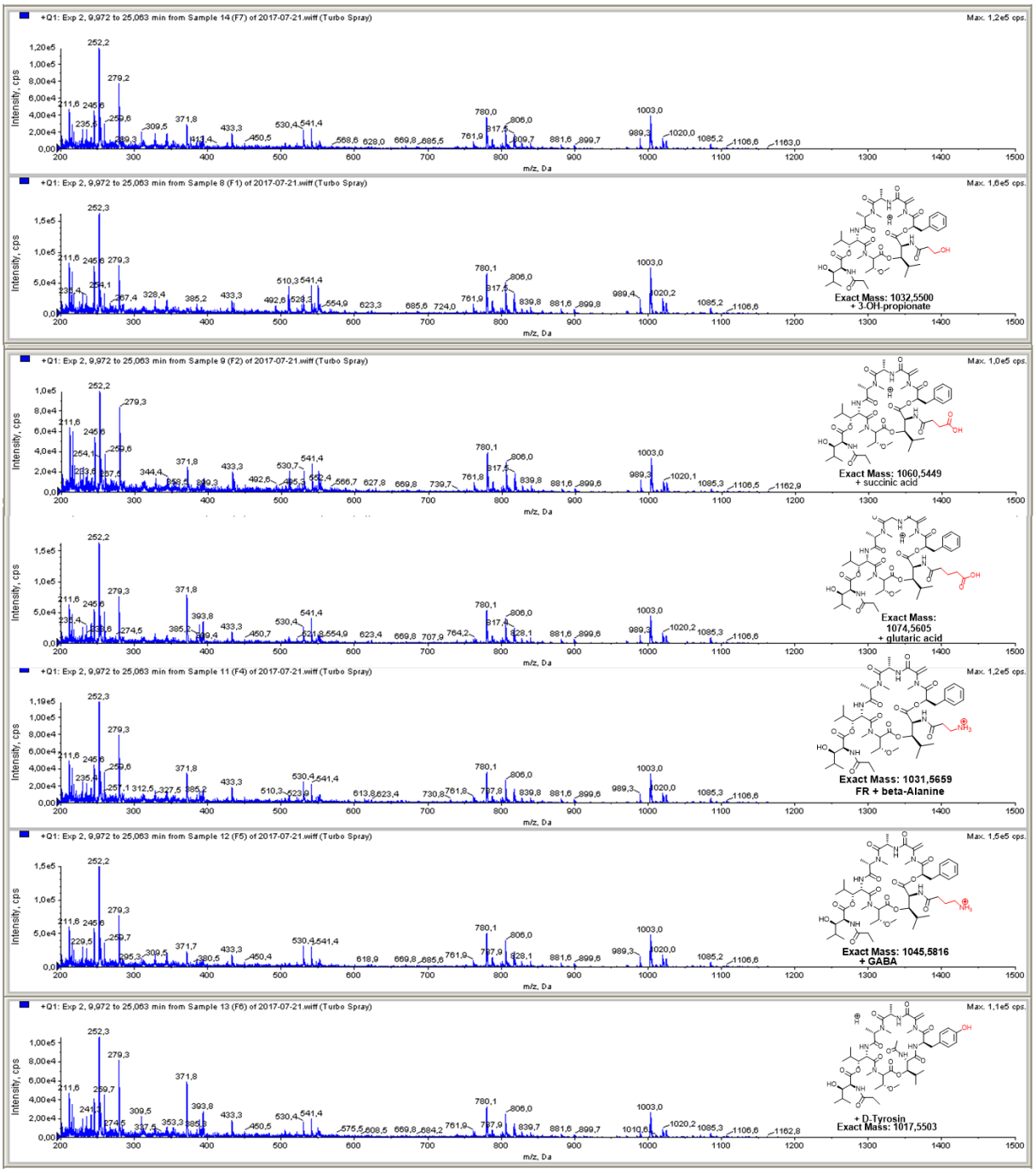

Figure 10-43: Feeding experiments with *C. vaccinii* and several carboxylic acid substrates monitored by LCMS measurements.

Table 10-8: ^{1}H-^{1}H-COSY, ^{1}H-^{13}C-HMBC and ^{1}H-^{1}H-ROESY spectroscopic data for FR900359 ($CDCl_3$, 293K).

Residue[c]	No C/H[b]	^{1}H-^{1}H-COSY	^{1}H-^{13}C-HMBC[a]	^{1}H-^{1}H-ROESY (selected)
Ala	1	–		
	2	3	1, 3, 4, 5(w)	H-3, H-38
	2-NH	–		
	3	2	1, 2, 4(w)	
N-Me-Dha	4	–		
	5	–		
	6a	b	4, 5	H-6b
	6b	a	4, 5	H-7, H-6a
N-Me	7	–	8, 5, 6(w)	H-6b, H-9
Pla	8	–		
	9	10a	6, 8, 10, 11, 17	H-10a/b
	10a	10b	8, 9, 11, 12/16	H-9, H-12/16
	10b	9	8, 9, 11, 12/16	H-9
	11	9		
	12/16		14, 10	
	13/15		11	
	14		12/16	
N-Ac-Hle-1	17			
	18	NH-18	23, 17	H-19, H-20, H-21, H-24 (w)
	18-NH	18	23, 18, 17	H-24, H-18, H-20, H-38 (w)
	19	20	25, 20, 22	H-18, H-20, H-21, H-22
	20	19, 21 22	18, 19, 22	H-19, H-21, H-22, H-24,
	21	20	19, 20, 22	H-22 (w), H-20, H-18, H-19
	22	20	19, 20, 21	H-20
N-Ac	23	–	24	
	24	–	18	H-39 (w), NH-18
N,*O*-Me_2Thr	25	–		
	26	27	25, 27, 28, 29, 31	H-32, H-33, H-28, H-29 (w), H-30 (w)
	27	28, 26	26, 28, 30	H-29, H-30
	28	27	27, 29	H-26, H-30
N-Me	29	–	26, 31	H-30 (w), H-7 (w) H-43, H-27
O-Me	30	–	27	H-27
Hle	31	–		
	32	NH-32	26, 31, 33, 34, 37	H-34, H-36
	32-NH	32	32, 33, 37	H-40, H-38, H-32
	33	34	32, 36, 41	H-30, H-33, H-34, H-35
	34	33, 35, 36	32, 33, 34, 36	H-35, H-36, H-40
	35	34	33, 34, 36	H-34, H-36, H-26
	36	34	33, 34, 35	H-34, H-35

N-Me-Ala	37	–		
	38	39	1, 37, 39, 40	H-39
	39	38	37, 38	H-40
N-Me	40	–	1, 38	NH-32, NH-42(w), H-34, H-39
N-Pr-Hle-2	41	–		
	42	43	47, 41, 43	NH-42, H-43, H-45, H-39(w)
	42-NH	42	47, 43, 42	H-44, H-48, H-40, H-42
	43	OH-43	41, 44, 45	H-42 bis 46, H-26
β-OH	43-OH	43, 45	43, 44, 46	H-43, NH-32, H-33
	44	43, 46	42, 43, 45, 46	H-45, H-39, 42-NH, H-42
	45	44	43, 46	
	46	44	43, 44, 45	H-43, H-44
N-Pr	47	–		
	48a	49	47, 49	H-49 (w), NH-42
	48b			
	49	48	47	

[a] Numbers refer to carbon resonances. (w): weak. [b] Numbers according to Figure 4-1. **[c]** Residues: Ala = alanine, N-Me-Dha = *N*-methyldehydroalanine, Pla = 3-phenyllactic acid, *N*-Ac-Hle = *N*-acetylhydroxyleucine-1, *N*,*O*-Me_2-Thr = *N*,*O*-dimethylthreonine, Hle = hydroxyleucine, N-Me-Ala = *N*-methylalanine, *N*-Pr-Hle = *N*-propionylhydroxyleucine-2.

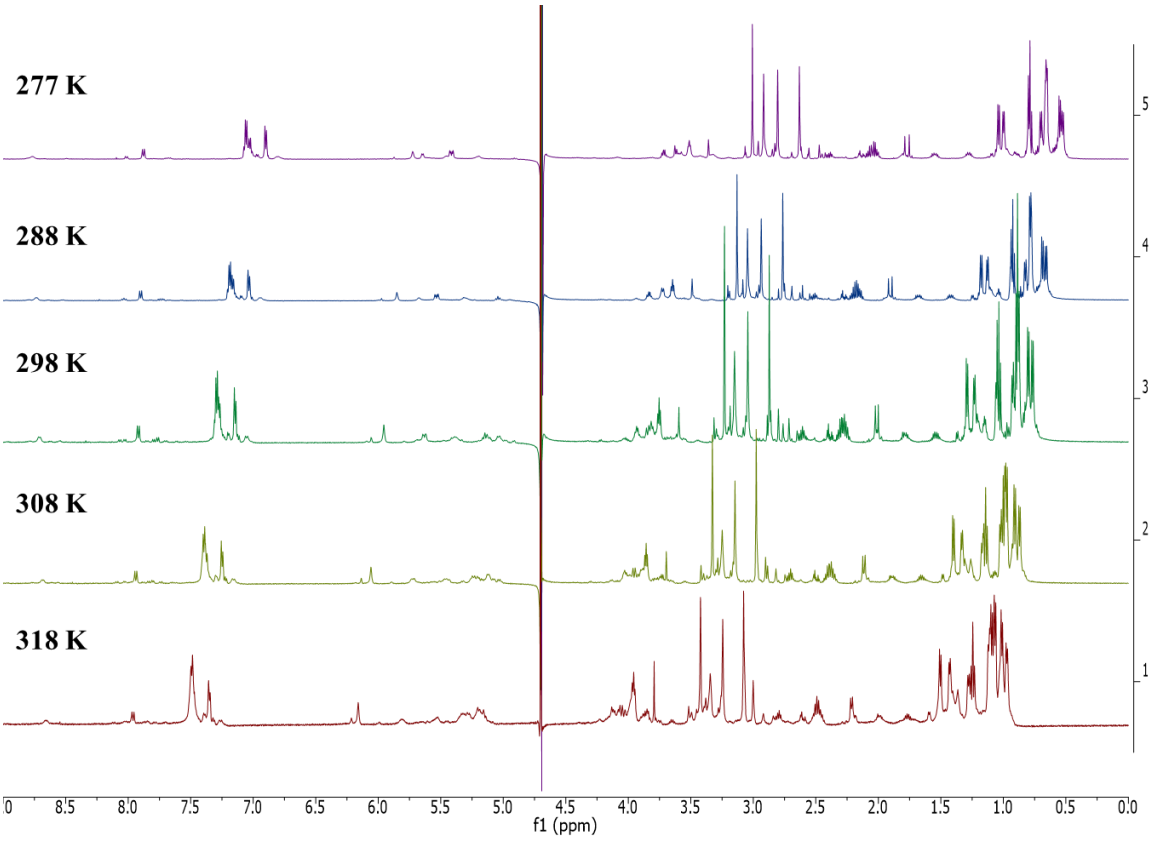

Figure 10-44: ^{1}H NMR spectrum of compound **1** (FR-1, 600 MHz H2O/D2O = 9:1, v/v, at 277-318K).

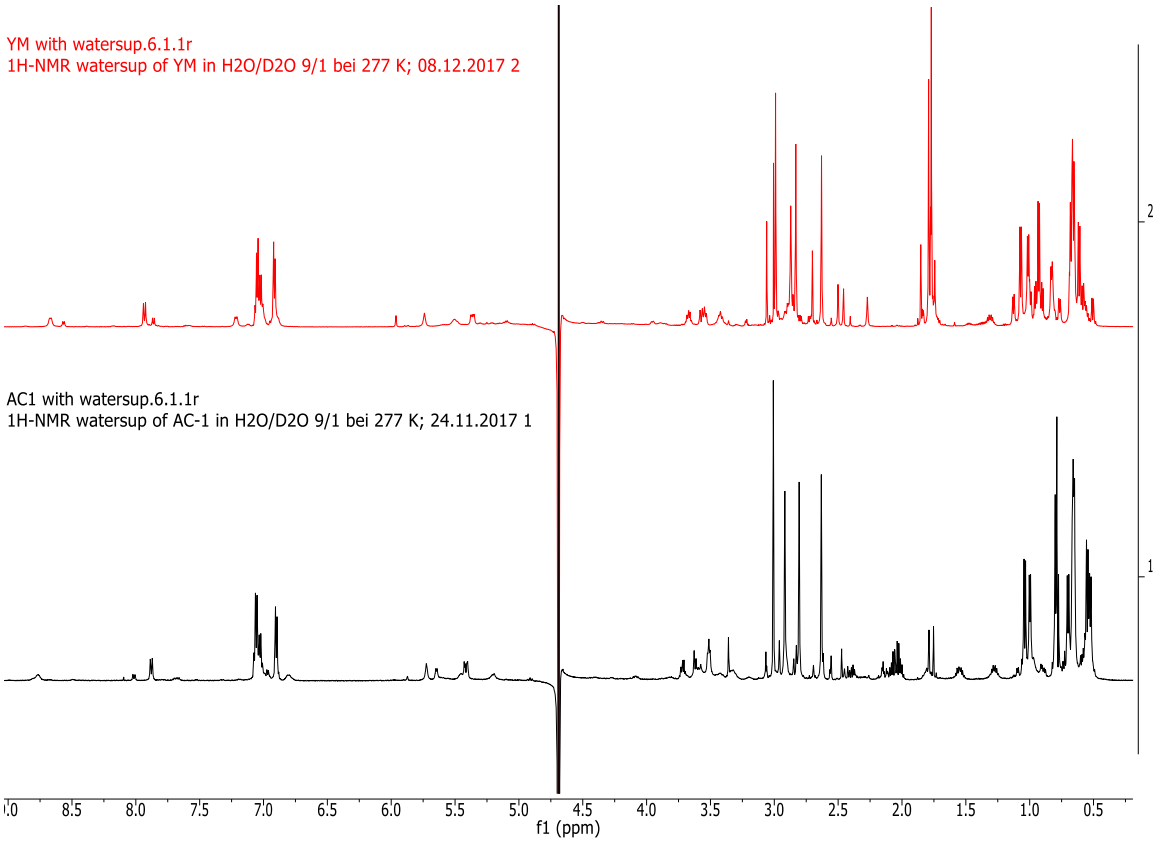

Figure 10-45: ^{1}H-NMR spectrum of YM and compound **1** (600 MHz H2O/D2O = 9:1, v/v, at 277K).

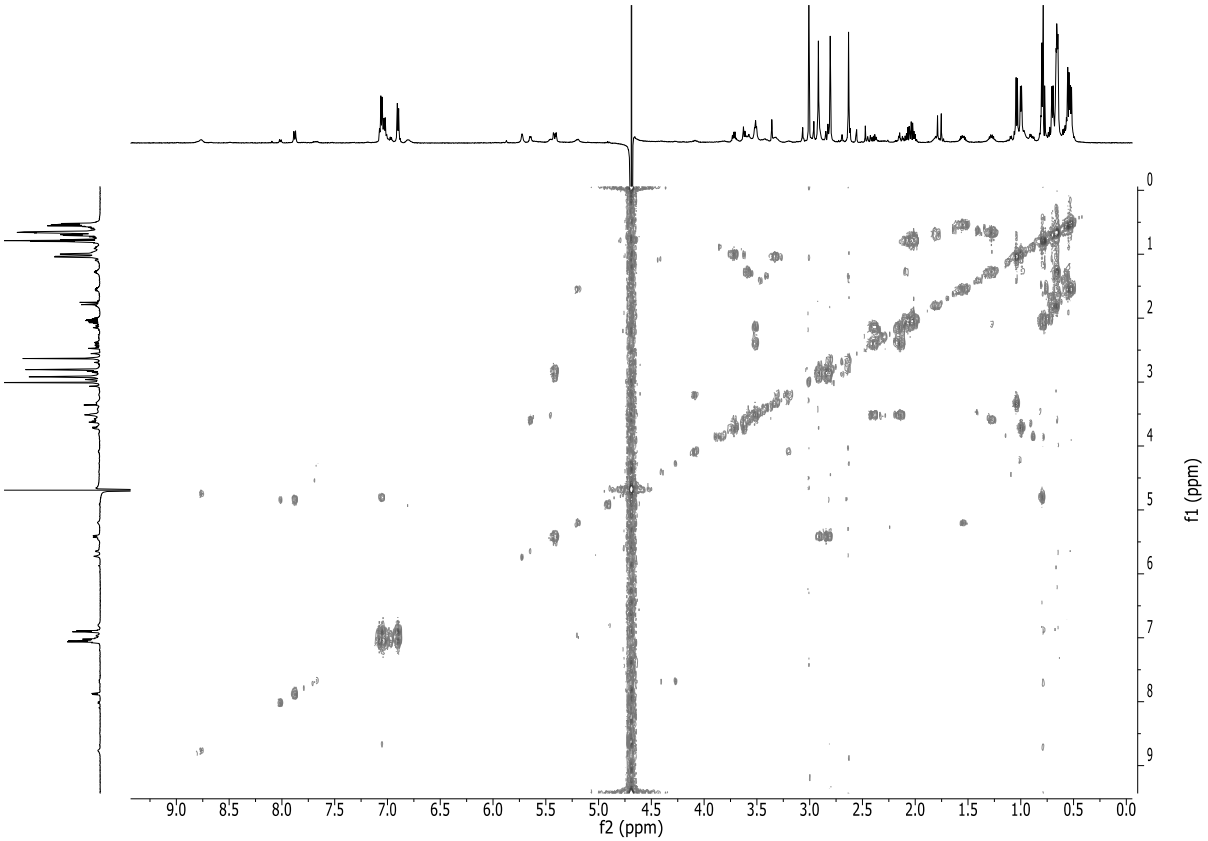

Figure 10-46: ^{1}H-^{1}H COSY NMR spectrum of compound **1** (FR-1, 600 MHz H2O/D2O = 9:1, v/v, at 277K).

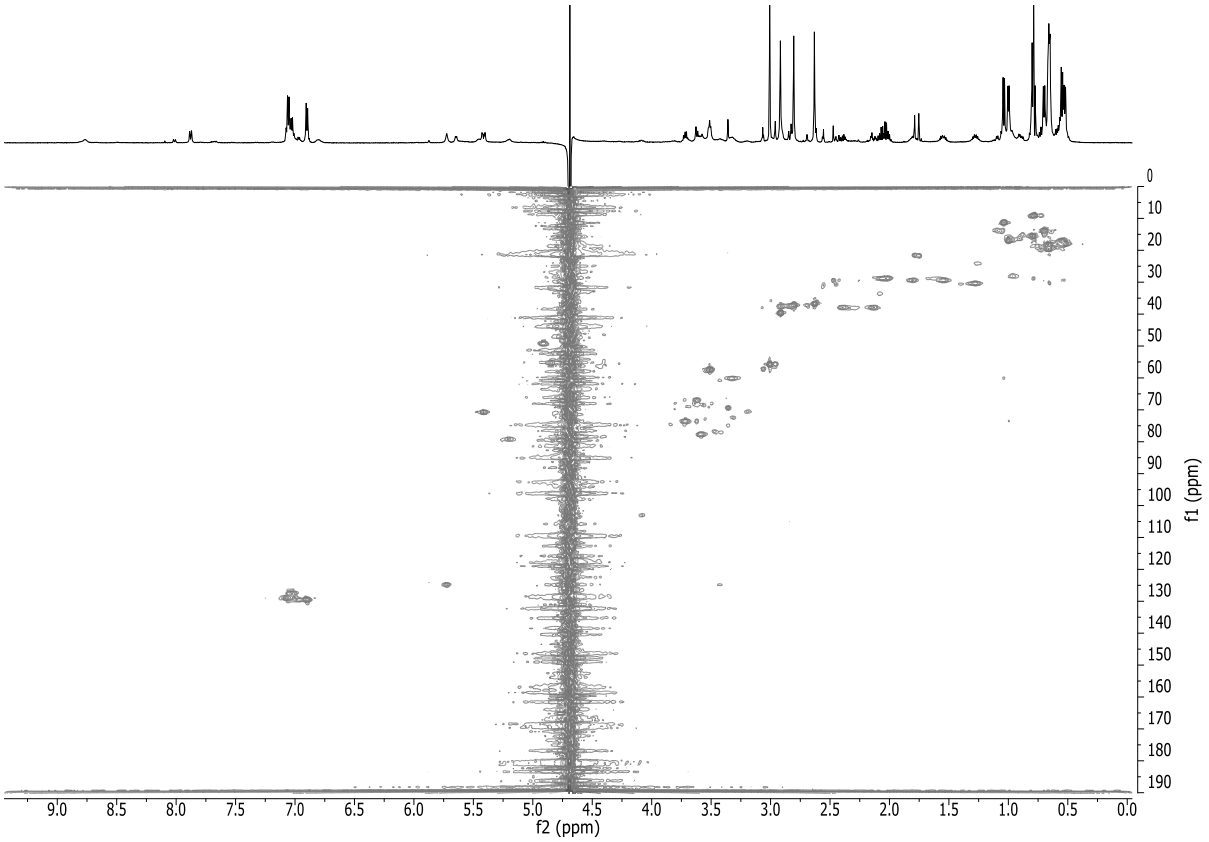

Figure 10-47: ^{1}H-^{13}C HSQC NMR spectrum spectrum of compound **1** (FR-1, 600 MHz H2O/D2O = 9:1, v/v).

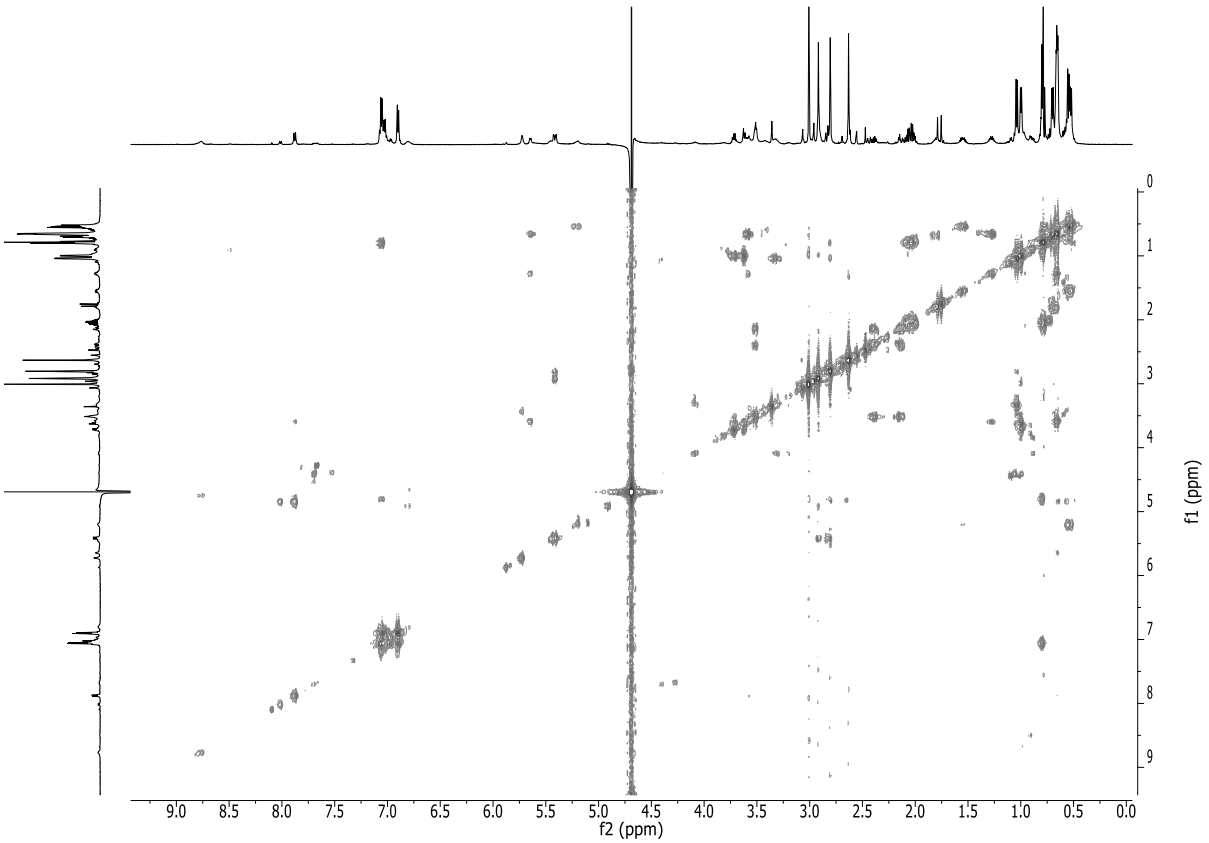

Figure 10-48: ^{1}H-^{1}H TOCSY NMR spectrum of compound **1** (FR-1, 600 MHz H2O/D2O = 9:1, v/v, at 277K).

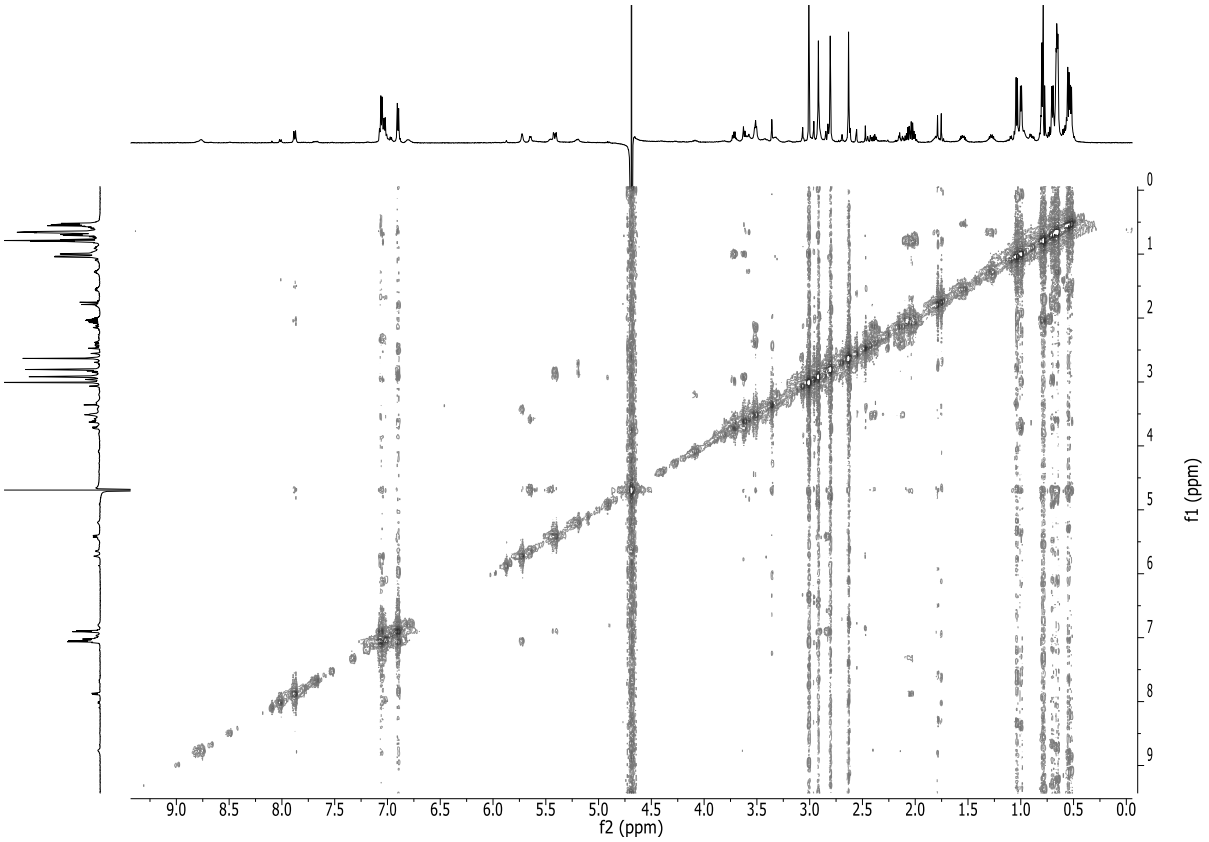

Figure 10-49: ^{1}H-^{1}H NOESY NMR spectrum of compound **1** (FR-1, 600 MHz H2O/D2O = 9:1, v/v, at 277K).

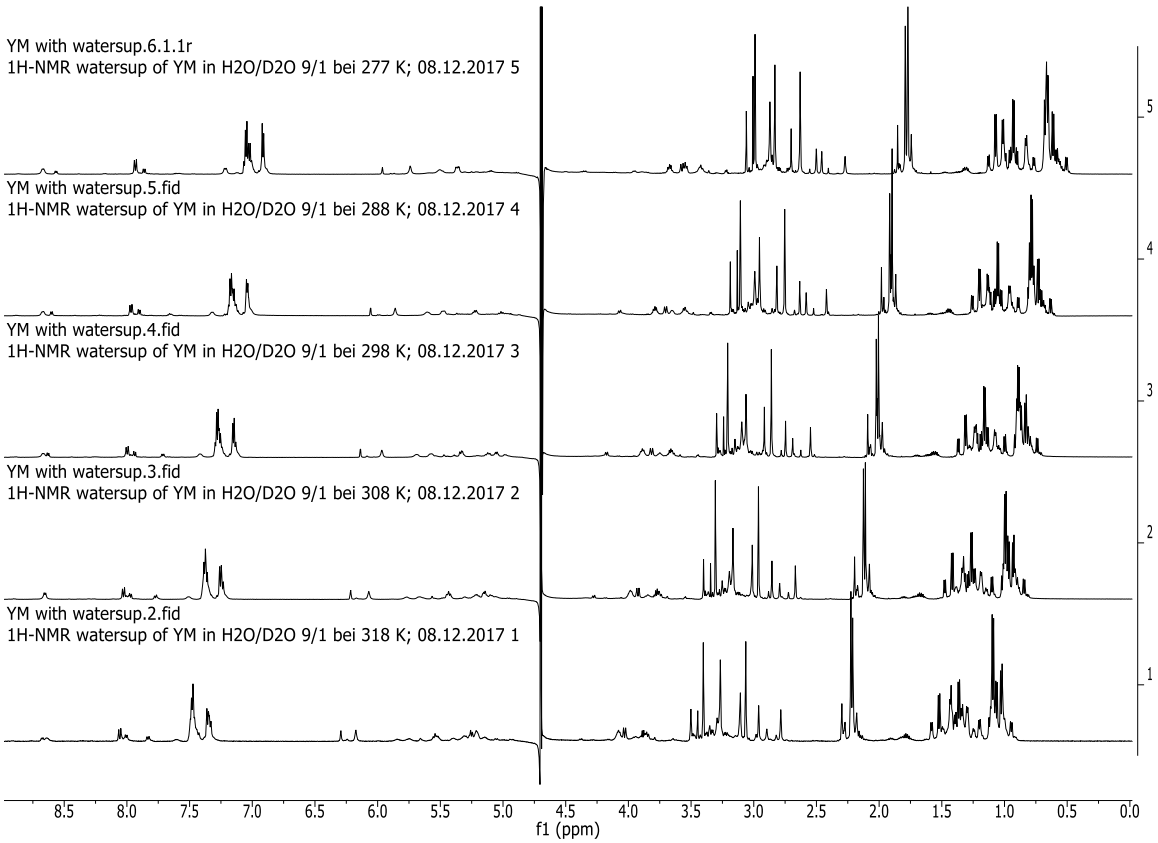

Figure 10-50: ^{1}H NMR spectrum of YM-254890 (600 MHz H2O/D2O = 9:1, v/v, at 277-318K).

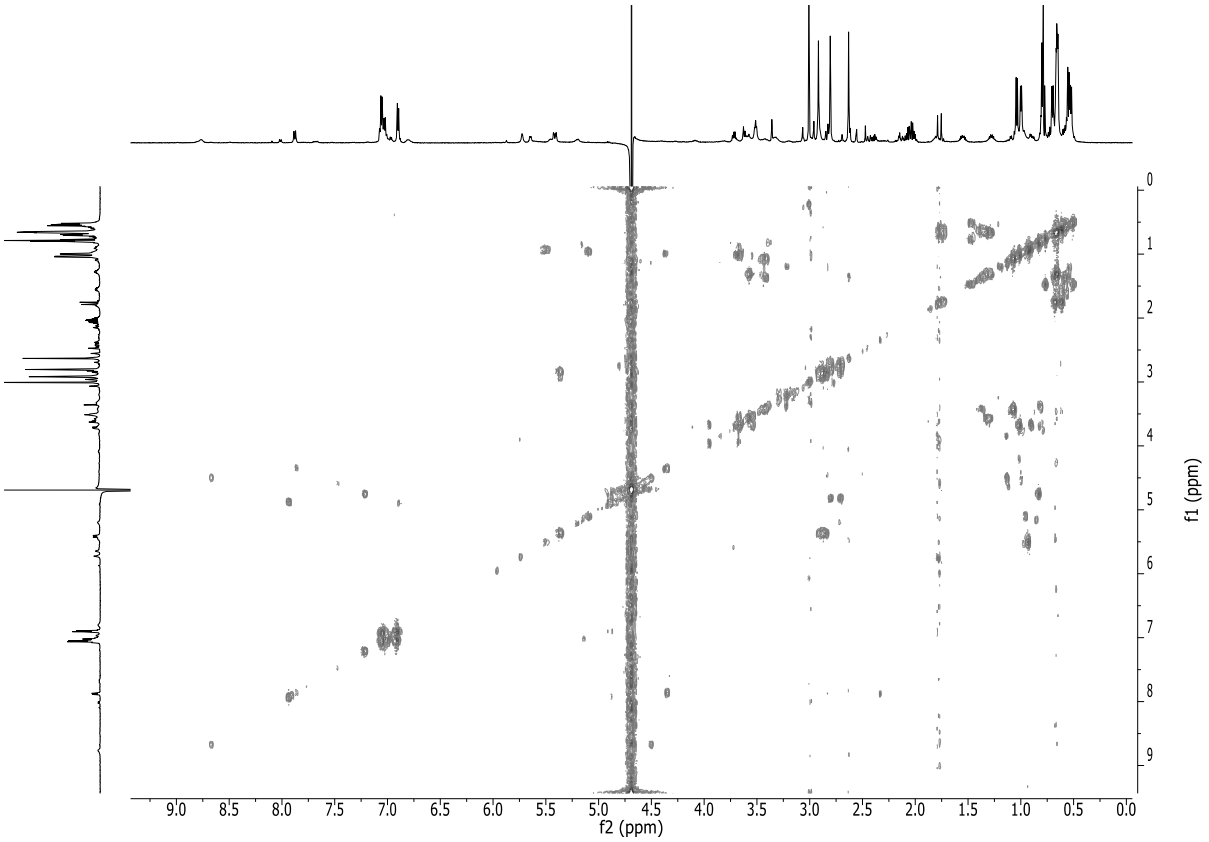

Figure 10-51: ^{1}H-^{1}H COSY NMR spectrum of YM-254890 (600 MHz H2O/D2O = 9:1, v/v, at 277K).

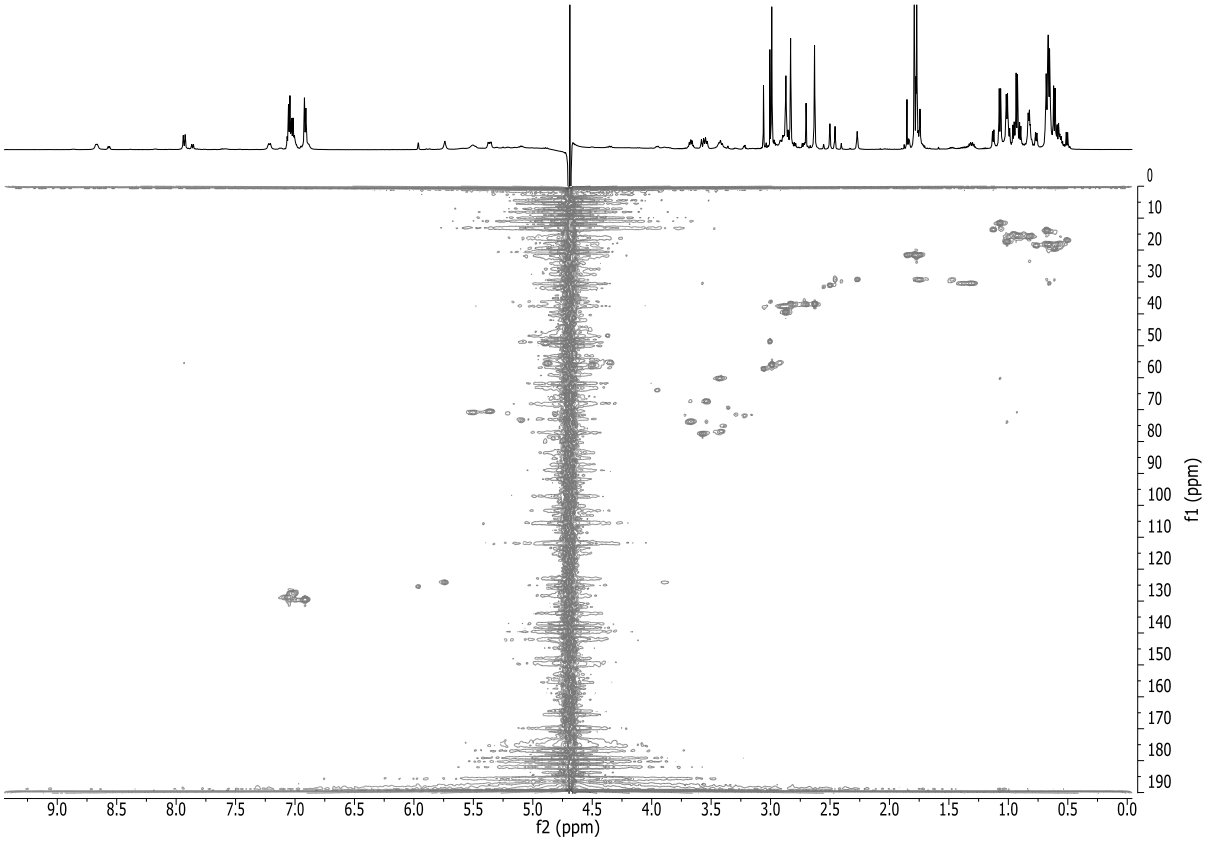

Figure 10-52: ^{1}H-^{13}C HSQC NMR spectrum of YM-254890 (600 MHz H2O/D2O = 9:1, v/v, at 277K).

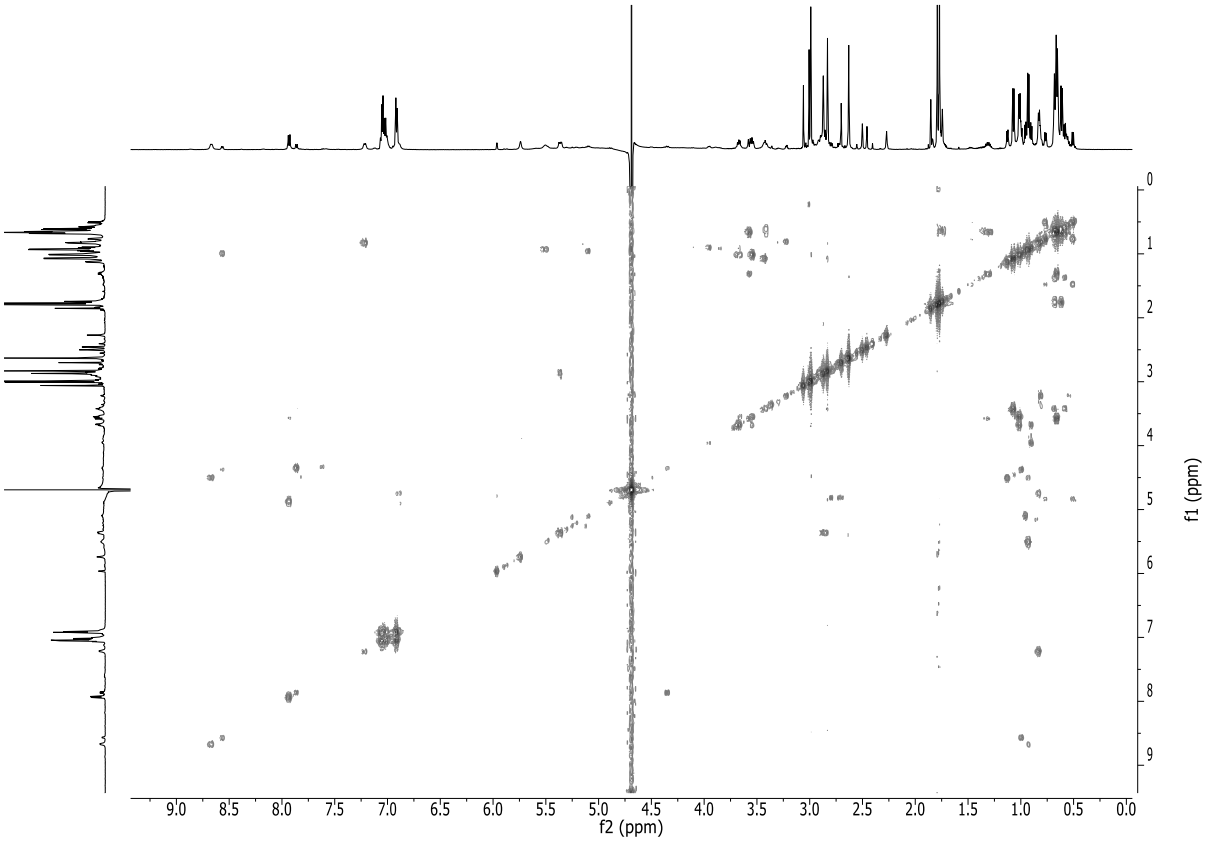

Figure 10-53: ^{1}H-^{1}H TOCSY NMR spectrum of YM-254890 (600 MHz H2O/D2O = 9:1, v/v, at 277K).

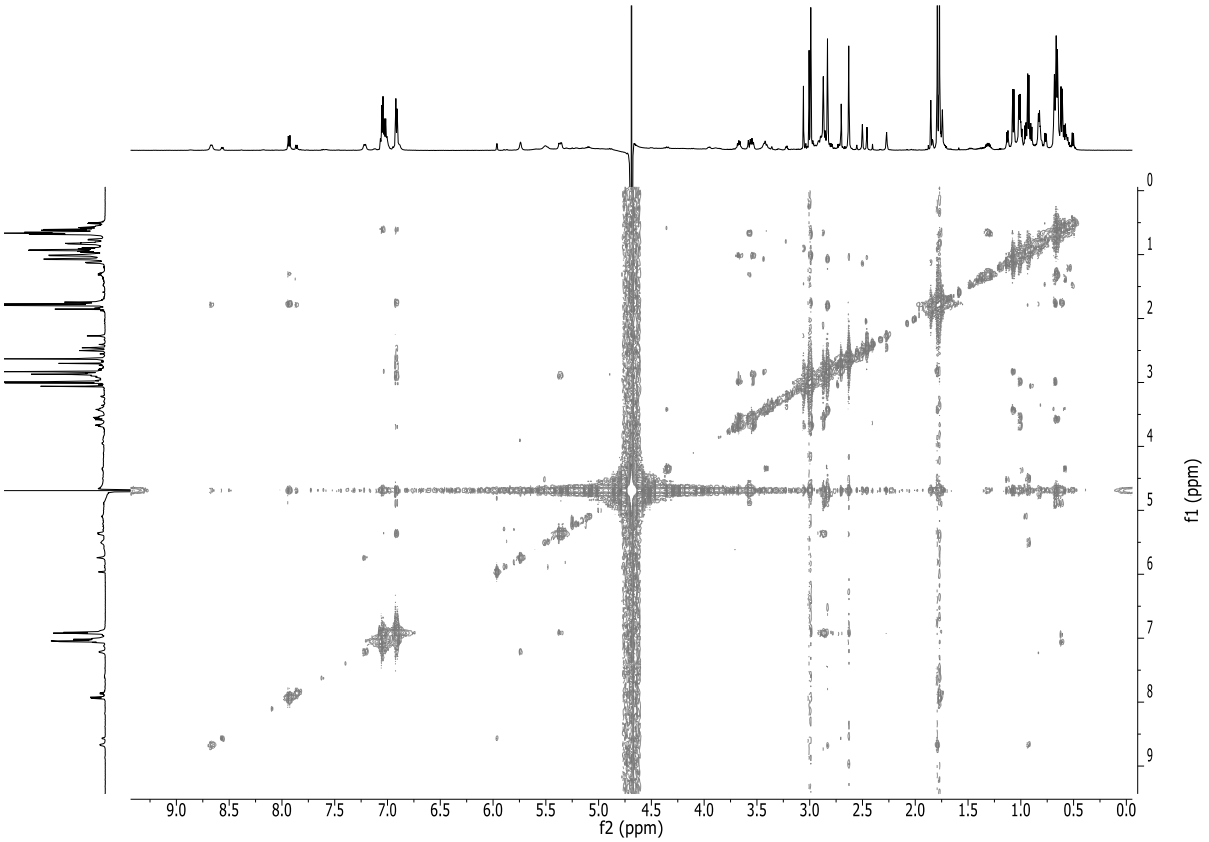

Figure 10-54: ^{1}H-^{1}H ROESY NMR spectrum of YM-254890 (600 MHz H2O/D2O = 9:1, v/v, at 277K).

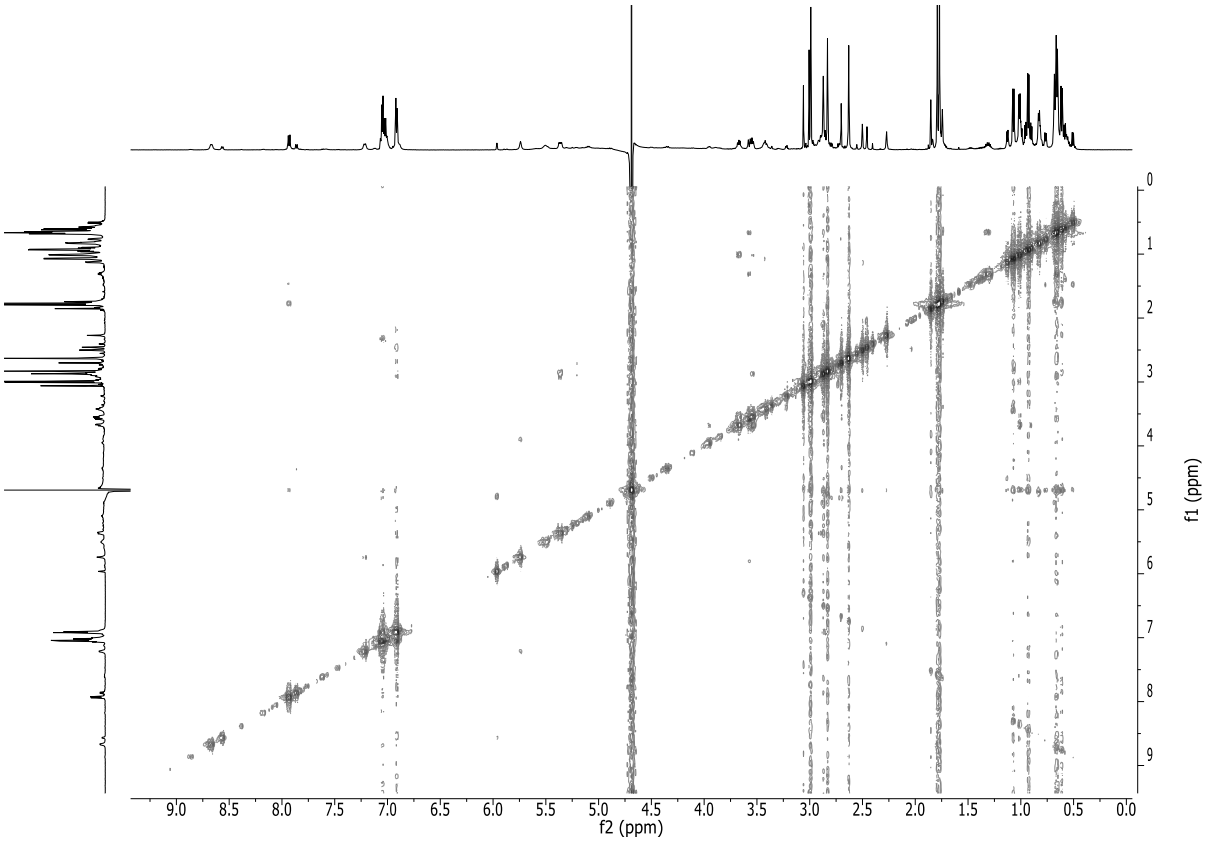

Figure 10-55: ^{1}H-^{1}H ROESY NMR spectrum of YM-254890 (600 MHz H2O/D2O = 9:1, v/v, at 277K).

11 Abbreviations and Units

°C	Degrees Celsius
α	optical rotation
$[\alpha]^{T}_{D}$	specific optical rotation, sodium D-line (589 nm); T: temperature
δ	NMR chemical shift [ppm]
ε	Extinction coefficient (UV/VIS spectroscopy)
λ	Wavelength [nm]
µ	micro (10^{-6})
µg	microgram (10^{-6} gram)
µl	microliter (10^{-6} liter)
µm	Micrometer
µM	10^{-6} molar, micromolar (= 10^{-6} mol/L)
ν	wave number [cm^{-1}]
1D	One-dimensional
2D	Two-dimensional
A	Absorption
AAA	Amino acid analysis
A-domain	Adenylation-domain
Ab	Antibody
Ac	Acetyl
ACN	Acetonitrile
ACP	Acyl carrier protein
approx.	Approximately
c	Concentration
C_{18}	C-18 modified silica gel

C -domain	Condensation-domain
C_T-domain	Condensation-like domain
calcd	Calculated
$CDCl_3$	chloroform-*d*
CD_3CN	acetonitrile-d_3
CD_3OD	methanol-d_4
CH_2Cl_2	dichloromethane (DCM)
CH_3CN	acetonitrile
cm	10^{-2} meter
CoA	Coenzyme A
conc.	concentration
COSY	Correlation spectroscopy
d	Doublet (in connection with NMR data)
Da	Dalton
DAD	Diode array detector
DCM	Dichlormethane
DEPT	Distortionless enhancement by polarization transfer
DH	Dehydratase
DMAP	4-Dimethylaminopyridine
E-domain	Epimerization-domain
EC_{50}	half maximal effective concentration (drug concentration causing 50% of maximal effect)
EDC	*N*-ethyl-*N*'-(3-dimethylaminopropyl)carbodiimide
e.g.	Latin "exempli gratia"; for example
et al.	Latin "*et alii*"; and others
ESI	electron spray ionization

EtOH	ethanol
Fmoc	9-Fluorenymethyloxycarbonyl
FR	FR900359
g	Gram
GPCRs	G protein-coupled receptors
G protein	heterotrimeric guanine nucleotide-binding protein
GTP	guanosine-5′-triphosphate
$G\alpha_i$	adenylate cyclase inhibitory G protein subunit
$G\alpha_q$	phospholipase C activating G protein subunit
$G\alpha_s$	adenylate cyclase stimulating G protein subunit
h	Hour
HCl	Hydrochloric acid
HMBC	Heteronuclear multiple-bond correlation
HPLC	High-performance liquid chromatography
HSQC	Heteronuclear single quantum correlation
Hz	Hertz
i.e.	id est (Latin for “that is”)
IP1	Inositol-1-phosphate
J	Spin-spin coupling constant [Hz]
K_D	Dissociation constant
L	Litre
LC-ESI-MS	Liquid chromatography Electrospray-ionization mass spectrometry
m	Multiplet (in connection with NMR data)
M	Molar [mol/l]
M-domain	Methylation-domain
M_r	Molecular Mass

MALDI-ToF	Matrix-assisted laser desorption/ionization - time of flight
Me	methyl
MeOH	Methanol
MeOD	methanol-d_4
mg	milligram (10^{-3} gram)
MHz	Megahertz
min	Minute
mL	milliliter (10^{-3} liter)
mm	millimeter (10^{-3} meter)
mM	millimolar (10^{-3} molar, = 10^{-3} mol/L)
mult	Multiplicity
nM	nanomolar (10^{-9} molar, = 10^{-9} mol/L)
NMR	Nuclear magnetic resonance
No	Number
NRPS	Nonribosomal peptide synthetase
obsd	Observed
PCP	Peptidyl carrier protein
ppm	Parts per million
q	Quartet (in connection with NMR data)
ref.	Reference
RP	Raw product
rpm	Rounds per minute
RP	Reverse-phase RT
rt	room temperature
s	singlet (in connection with NMR data)
SDS	sodium dodecyl sulfate

sec	Second
sp.	Species
t	Triplet (in connection with NMR data)
T (-domain)	Thiolation-domain
t_R	Retention time
TE	Thioesterase
TE-domain	Thioesterase-domain
TFA	Trifluoroacetic acid
V	Volume
VLC	Vacuum liquid chromatography
wt%	percentage by mass (m/m)
YM	YM-254890

Abbreviations for amino acids

Ala	alanine	A
β-HyLeu	hydroxyleucine	L''
N-Me-Ala	*N*-methylalanine	A'
N-Me-Dha	*N*-methyldehydroalanine	A''
N-Ac-*β*-HyLeu1	*N*-acetylhydroxyleucine1	L'
N,O-Me_2-Thr	*N,O*-dimethylthreonine	T'
N-Pr-*β*-HyLeu2	*N*-propionylhydroxyleucine2	L'''
Phe	Phenylalanine	F
Pla	Phenyllactic acid	F'
Ser	Serine	S
Thr	Threonine	T

12 Acknowledgements

I wish to express my sincere and cordial gratitude to my supervisor Prof. Dr. G. M. König for the expert guidance, encouragement and kind support during my PhD thesis program. In particular, I want to thank her to entrust me this intriguing project and let me be a part of an interdisciplinary team (FOR 2372). I would like to thank her that she provided constructive freedom on the one hand while at the same time always had an open door for dialogue and advice. The friendly atmosphere within in the working group made the work very motivating and pleasant.

Special thanks go to Prof. Dr. E. Kostenis (Institute for Pharmaceutical Biology, University of Bonn, Germany) for officiating as second referee and most importantly offering me her great expertise, idealism, and advice in both, science what it is supposed to be, but also science, what it can be in reality (politics and begging for money).

I thank:

Especially Dirk Schmitz (Botanical Garden Bonn) for planting and providing me with *Ardisia crenata* (dried and fresh material). I thank Dr. Wolfram Lobin, Dr. Claudia Löhne and Bernhard Reinken for providing me leaves of *A. lucida*.

Especially Prof. Dr. Leo Eberl, Marta Pinto-Carbo (Univ. of Zurich) for introducing me into the fascinating Leaf Nodule Symbiosis and Prof. Dr. Aurelièn Carlier (Univ. of Ghent) for providing the BAC library containing the *frs* gene cluster.

Especially Prof. Dr. Piel, and Dr. Alexander Brachmann (ETH Zurich) for supervision and guidance during my research stay to perform MALDI imagin of a young *A. crenata* leaf.

Prof. Dr. C. E. Müller and Markus Kuschak (Institute for Pharmaceutical Chemistry, University of Bonn, Germany) for Gq-affinity testing isolated and synthesized FR analogs in competitive binding studies against triatiated FR-Radioligand ^{3}[H]PSB-15900.

Prof. Dr. Diana Imhof, Dr. Daniel Tietze (also for my research stay at TU Darmstadt) and Dr. Toni Kühl for the collobrative work on SAR insights of FR.

Prof. Dr. Michael Gütschow and Jim Küppers for the collaborative work and synthetic expertise towards superior fluorescent FR analogs.

Acknowledgements

Jun-Prof. Daniela Wenzel + Alexander Seidinger (Univ. of Bonn), Prof. Dr. Till Schäberle (Univ. of Giessen), Timo Hartmann (Museuem König Bonn), Prof. Y. Kikuchi (Univ of), Dr. O. Tsubasa + Prof. Dr. P. Mergaert (CNRS Paris), for the collaborative work on the ecological function of FR.

Prof. Dr. Häberlein, Dr. Thomas Sorkalla, Dr. Sebastian Franken, and Stefan Aatz for performing FCS studies on FR-RR-BP (compound **46**).

Dr. Marc Sylvester (Institute for Biochemistry and Molecularbiology, University of Bonn, Germany) for performing Tandem MS and Bernd Gehrig for MALDI-TOF MS measurements.

Many specific tasks involved in this study were performed in cooperation with other members of the Institute for Pharmaceutical Biology, University of Bonn. For this work cordial thanks go to:

Dr. S. Kehraus for providing professional laboratory support during all phases of this study, for proofreading manuscripts and for indispensable help concerning the implementation and interpretation of NMR experiments, for which he has my great admiration and gratitude.

Dr. Max Crüsemann for measurement and analysis of HR-LC-MS and Tandem-MS measurements. He also introduced and trained us to apply LC-MS²-based GNPS molecular networking and guided about biosynthetic investigations.

Nina Heycke, Suvi Annala, Tobias Benkel, Dr. Davide Malfacini for performing the IP1 accumulation and DMR assays most important for all parts of this thesis.

Ekaterina Egereva for recording LC-MS spectra and Marion Schneider for measurement and analysis of HR-LC-MS measurements.

Dr. M. Koch and Dr. Ralf Schröder for their help in administrative questions.

Thomas Koegler for his support in all technical matters, regarding computer, software and equipment.

Drs. Till, Katharina, Frieda and Max, for mediating excellent teaching skills in the supervision of students.

Special thanks go to my office colleagues and close friends, especially Jan Schroer (teaching a lot of Ruhrpott-vocab and always having at least a klitzekleinen, kühlen Hobel to offer), Henrik

Harms (teaching me lab work and “Rheinische Lebensart” en detail) and Alexander Bogdanov (teaching me maximal criticism towards anything and anybody as well as a vast number of valuable and just as much pointless advisory about science and life itself). The discussions with you during and after work made the laboratory work much easier.

Further I thank Paul Barac, Emilie Goralski for the fun trip to Transylvania and lots of coffee I owe them, and Nils Böhringer for his great parties. I thank Ben Libor, Cora Hertzer and all the other nerds introducing me to weird games and the world apart from the lab.

I would like to thank especially Henrik Harms, Max Crüsemann, Jan Schroer and Paul Barac for proofreading parts of this thesis.

I would like to thank also all other members of the Institute for Pharmaceutical Biology, University of Bonn, as well as all SS08 members of the University of Münster, especially Dome, Nikita, Jochen, and Stephi, present or past for cooperation and friendship.

I would like to express my deepest gratitude to my family, in particular my mother and stepfather, who have always supported me and enabled this study by their limitless love, trust and encouragement. The latter also applies for my siblings, father, and friends Daniel Vey, Marius Staggenborg, Christina Hoegen-Leist, Oliver Bestmann and last but not least Ines Bresler.